Hudson Bay Systems Study (BaySys)

Phase 2 Report: Results, Integration, and Project Conclusions

Project Managers:
Dr. David Barber and Mr. Kevin Sydor

This document is a draft and should not be cited.

This report can be downloaded through:
http://lwbin-datahub.ad.umanitoba.ca/dataset/baysys-project-reports-phase-1-2

Team Leads of the BaySys Project

Principle Investigator: David Barber (UManitoba)
Manitoba Hydro Lead and Project Manager: Kevin Sydor (Manitoba Hydro)
Academic Project Manager: Lauren Candlish (UManitoba)
Project Coordinators: David Landry (UManitoba) and Karen Wong (Manitoba Hydro)
Team 1: Jens Ehn (UManitoba), Kevin Sydor and Karen Wong (Manitoba Hydro)
Team 2: Tricia Stadnyk (UCalgary) and Kristina Koenig (Manitoba Hydro)
Team 3: Jean-Éric Tremblay (ULaval), Gary Swanson (Manitoba Hydro), and Marilynn Kullman (Manitoba Hydro)
Team 4: Tim Papakyriakou (UManitoba) and Bob Gill (Manitoba Hydro)
Team 5: Feiyue Wang (UManitoba), Sarah Wakelin (Manitoba Hydro), and Allison Zacharias (Manitoba Hydro)
Team 6: Jennifer Lukovich (UManitoba), Paul Myers (UAlberta), and Karen Wong

Editorial Team

Editors: David Landry, Lauren Candlish, Karen Wong
Final Review: Kevin Sydor, David Barber

Research Advisory Committee

Funding and Support

This project is part of the NSERC-Manitoba Hydro-funded Collaborative Research and Development (CRD) program. Primary data collection for this research would not have been possible without the support and hospitality of the CCGS Amundsen crew during the 2018 field season, along with Amundsen Science. Much of the HQP and graduate student research has been supported by the University of Manitoba Graduate Fellowship (UMGF), the Northern Scientific Training Program (NSTP), and NSERC Masters and Doctoral Awards. This work is a contribution to the ArcticNet Networks of Centres of Excellence and the Arctic Science Partnership (ASP, asp-net.org).

CHAPTER 1 INTRODUCTION

The Hudson Bay System Study (BaySys) was designed by the University of Manitoba and Manitoba Hydro, collaboratively with several other academic intuitions, government departments, and several industry partners. These collaborators met in May 2012 to participate in a two-day workshop looking at the state of knowledge for Hudson Bay, with a focus on the freshwater and marine systems (for further information see Sydor, 2012). During the workshop significant gaps in the current research, datasets, and analyses were highlighted, showcasing the need for a large-scale collaborative multidisciplinary study such as represented by the Hudson Bay System Study (BaySys).

The BaySys project was initiated in 2015 as an NSERC Collaborative Research and Development CRD Grant. Through this grant, the University of Manitoba and Manitoba Hydro partnered with Hydro Québec, Ouranos, Environment and Climate Change Canada, as well as seven other academic institutions across Canada (University of Northern British Columbia, University of Alberta, University of Calgary, University of Guelph, Université de Sherbrooke, Université de Laval, and Université de Québec à Rimouski). The overall objective of BaySys is to separate the effects of climate change from those of regulation of freshwater on the physical, biological and biogeochemical processes operating within the Hudson Bay Complex (HBC). Addressing this central objective required a better understanding of physical, biological, and biogeochemical processes operating within the HBC. This included the collection and analysis of new datasets for sea ice, river and bay water, the atmosphere, and the hydrological system, along with large-scale hydrological modelling and oceanographic modelling. The Phase 1 Report (Barber & Sydor, 2019) describes in detail the field campaigns, data collection methods, and processes. (Link to the Phase 1 report).

This Phase 2 report addresses the research questions outlined by the BaySys project proposal (Barber & Sydor, 2014) and discusses how the project evolved to address the overall objective from a systems perspective. This report begins with a brief background on research done prior to the BaySys study. Chapter 2 provides the project framework, including details regarding fieldwork, data collection, and methods for integrating results. In Chapter 3, each Team – 3.1 through 3.6 – provides an introduction, background into their study area, detailed description of their data analysis, and results addressing individual Team tasks and overall objectives. The integration of the results is presented and discussed in Chapter 4. In Chapter 5, research gaps and recommendations for future work are discussed, along with proposed improvements to datasets and models. The final chapter summarizes the project outcomes and suggests directions for future research.

1.1 An Overview of the Hudson Bay Complex

The HBC (Hudson Bay, James Bay, Foxe Basin, Hudson Strait, and Ungava Bay) occupies an area of 1.3 million km^2 (Kuzyk & Candlish 2019). The Complex represents one of the largest inland seas in the world. Its nearly complete ice cover during the winter and nearly ice-free condition in summer make it unusual among the world's oceans. It is also defined by the large volume of freshwater runoff it receives. The total drainage basin, 3.8 million km^2 is the largest watershed in Canada, extending over five Canadian provinces (Alberta, Saskatchewan, Manitoba, Ontario, Québec) and into the Northwest Territories and Nunavut. The terrestrial catchment is larger than the combined St. Lawrence and Mackenzie River watersheds and represents an area of about four times the size of Hudson Bay. From this extensive catchment area, approximately 960 km^3 of freshwater drains into the Marine Region annually (Stadnyk et al., 2019). The importance of freshwater in the HBC ecosystem cannot be overstated. The HBC functions like a vast estuary, inputs of freshwater dominate the physical processes of vertical and horizontal mixing of its waters, which strongly influences the supply and recycling of nutrients that support all biological life in the system (McCullough et al., 2019). Throughout the year, rivers and precipitation together supply the HBC with the equivalent of about 1 m of water (if it were spread uniformly over its entire surface) and freezing withdraws almost as much from circulation in the water column each fall, only to release it at the surface when it melts the following spring. Winds and tides mix this freshwater with the saltier marine water below, but even so, the layer of reduced salinity reaches only a few tens of meters deep by the end of each open water season. Deeper, more saline layers are supplied by the flow of Arctic water into the region, while entrained river water provides additional salt and constituents by the sinking of brine during the process of sea ice formation. The sources of fresh and marine water to the region are generally known, but most pathways were poorly defined, and rates of key processes were also not well quantified.

Before the launch of the BaySys project (pre-2015), there were limited large-scale studies focusing on the HBC as a whole. A multi-year program conducted by the Groupe interuniversitaire de recherches océanographiques du Québec (GIROQ) studied hydrodynamic control of primary and secondary productivity of Hudson Bay estuaries. The GIROQ program, held from spring to summer 1988-1990, was based in La Grande Rivière and provided a fundamental understanding of plume dynamics, ice algae, and primary production in sub-ice environments. In 2003, DFO (Quebec Region) had a program called MERICA-Nord (études des MERs Intérieures du Canada, Hudson Bay northern component) to improve the understanding of climate change in the HBC. The MERICA Nord field program focused on moorings and physical and biological sampling across the centre of the bay in Hudson Strait and into Foxe Basin (Harvey et al., 2006). Starting in 2005, ArcticNet deployed several moorings in Hudson Bay with limited surveys of the bay during the summer period. Utilizing the CCGS Amundsen, or the CCGS Pierre Radisson, ArcticNet continued to do short summer field campaigns in the HBC during the years 2009, 2010, 2011, and 2013. During a 2009 University of Manitoba and Manitoba Hydro study, a winter field program focused on the characterization of ocean–sea ice–atmosphere coupling and sedimentary processes in the Nelson River estuary. In 2011, the Journal of Marine Sciences published a special issue focusing on the HBC (Macdonald & Kuzyk, 2011). The special issue featured some of the findings from the ArcticNet and MERICA programs as well as results from researchers who are a part of the BaySys project (i.e., Drs. Kuzyk, MacDonald, Mundy, Déry, Barber, Lukovich, and Fortier).

Numerical modelling of the HBC began in the 1990s (e.g., Wang et al., 1994a, 1994b; Saucier & Dionne, 1998; Gough, 1998). Increased resolution and better representation of mixing allowed later modelling studies to reproduce many features of the seasonal circulation and hydrography (Saucier et al., 2004), begin to understand the freshwater budget (St. Laurent et al., 2011) as well as carry out some simple climate studies (e.g., Joly et al., 2011) albeit without considering changes in the hydrological forcing.

As a joint initiative between ArcticNet and the University of Manitoba, the Hudson Bay Integrated Regional Impact Study (IRIS) was undertaken to summarize the state of knowledge for the Greater Hudson Bay Marine Region (geographically the same area as the HBC) (Kuzyk & Candlish, 2019). The Hudson Bay IRIS report was divided into three themes (Physical Environment, Ecosystems and Wildlife, Modernization and Development) with 16 topical chapters. Of the 16 chapters, 13 were lead or supported by BaySys researchers. We direct the reader to the Hudson Bay IRIS report for a comprehensive review of the state of knowledge, prior to the results of BaySys.

The BaySys project was designed to fill in some of the gaps in knowledge and to focus on collecting data from a large spatial area during the spring melt season. 'Estuary' work was to focus on contrasting the Churchill (low) and Nelson (high) outflows into estuaries. These data collection components were to be supported by remotely sensed data and modelling studies. Manitoba Hydro has a vested interest in research on impacts and adaptation strategies for climate change on northern ecosystems as it may affect system operations and future generation developments. This project was designed to help Manitoba Hydro investigate ways to enhance the quality and capacity of environmental science in the regions in which it operates, produce reliable assessments of impacts of climate change on water supply, and increase our understanding of the effects of climate change on northern ecosystems. More broadly, we designed BaySys to provide a better understanding of how seasonal shifts in freshwater, sediment, and nutrient delivery and climate change may affect primary and fisheries productivity, and transportation in Hudson Bay and how this may change in the future climate.

1.2 Project Objectives

The BaySys project was a comprehensive study that examined the influence of freshwater on Hudson Bay marine and coastal systems through the integration of field-based experimentation with coupled climatic-hydrological-oceanographic-biogeochemical modelling. It posited that factors that can be primarily attributed to climate change, such as a long-term change in temperature, atmospheric circulation, sea ice, and supply of freshwater have a different impact on Hudson Bay than factors that can be primarily attributed to regulation, such as seasonal shifts in the hydrograph. Specifically, BaySys provided a scientific basis to separate climate change effects from those of hydroelectric regulation of freshwater on physical, biological, and biogeochemical conditions in Hudson Bay. This overall project objective was addressed through a “systems” perspective, by which examining climate, marine, freshwater, carbon, contaminants, and marine ecosystems, and fully integrated modelling program incorporating historical, modelling, analysis, and satellite remote sensing were considered.

1.3 Team Overview and Objectives

BaySys is a collaborative project led by the partnership of the University of Manitoba and Manitoba Hydro, with participants from Hydro Québec, Ouranos, and seven academic institutions including the Universities of Alberta, Calgary, Northern British Columbia, Laval, Québec à Rimouski, Sherbrooke, Guelph, and Trent. Additional contributions to the project came from Amundsen Science, ArcticNet, the Canadian Coast Guard, and Environment and Climate Change Canada (ECCC). The members of BaySys combine to make up six academic research Teams with co-leading industry members from Manitoba Hydro. Each Team, investigating an inter-connected Hudson Bay system, with their objectives and research goals (Figure 1.1).

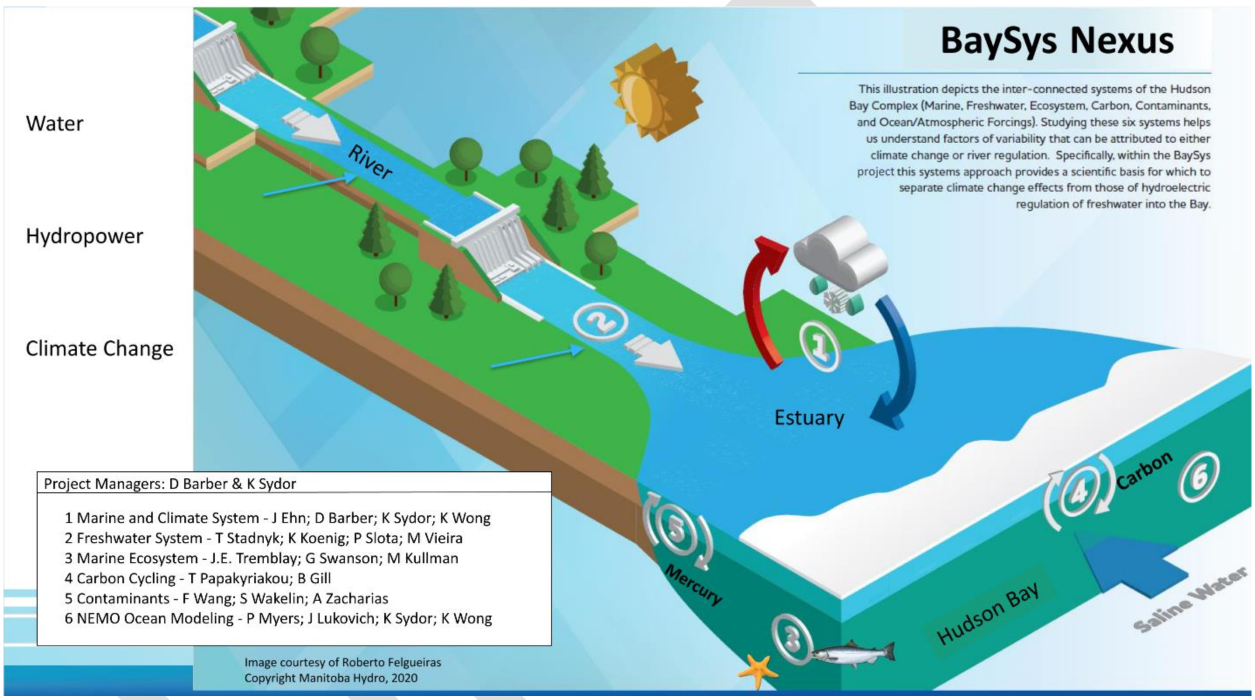

FIGURE 1.1 Graphic schematic view showing the conceptual relationship of the BaySys project sub-systems with the legend showing academic and industry co-leads.

The objectives for each BaySys Team were outlined to answer specific questions within their research area while helping to address the overall project objective through assessment and integration of results. To address the overall objective, Team 1 worked to understand how changes in climate variability and hydroelectric regulation affected processes related to mass and energy exchange between the freshwater, marine, sea ice, and atmospheric systems, and how these processes have manifested changes in the physical properties and distribution of water masses in Hudson Bay. Team 2 investigated the role of freshwater timing and magnitude on contemporary and future projections of freshwater-marine coupling in Hudson Bay as a means of understanding the relative contributions of regulation and climate change to the system. This was done through the development of continental-scale modelling of the entire Hudson Bay watershed, conducting uncertainty assessments on the model and projecting net changes to runoff under climate, regulation, and naturalized conditions. Results from this Team were integral to the ability of other Teams to evaluate the impacts of climate change and hydroelectric regulation on the physical, biological, and biogeochemical processes in the bay.

The Team 3 objectives were to assess how different drivers collectively affect biological productivity and the diversity and interaction of water column organisms (microbes, algae, and consumers) and the benthos, with an aim to identify the pathway of nutrients entering Hudson Bay through marine gateways and regulated versus unregulated rivers. For Team 4, the role of freshwater in moderating the carbon system of Hudson Bay was the focus, ultimately increasing our understanding of carbon cycling and Hudson Bays' current and future role as a CO_2 source/sink, derived from multi-season analysis. Mercury is one of the primary contaminants of concern associated with hydroelectric regulation due to enhanced mercury methylation in flooded reservoirs and wetlands, therefore the objective of Team 5 was to examine how contaminant transport and transformation in the Hudson Bay ecosystem responded to regulation and a changing climate.

Team 6 became its own Team during the second year of the project to ensure that the large-scale ocean modelling component could be completed and integrated into the rest of the Teams. Team 6 objectives were to investigate the relative impacts of climate change and regulation on freshwater-marine coupling within the Hudson Bay System from a modelling perspective coupling a freshwater hydrological model (HYPE) with the Nucleus for European Modelling of the Ocean (NEMO) model. Their goal was to provide an integrated observational-modelling freshwater/marine framework for model-data comparison, to improve our understanding of physical mechanisms responsible for observed phenomena based on observations and historical simulations, and to improve representation in future simulations. NEMO climate modelling initiatives were to enabled investigation and improvement in our understanding of freshwater dynamics, as well as momentum, and mass and heat flux in response to climate change and regulation.

1.4 Project Partnerships

BaySys was proposed as a comprehensive study that would integrate field-based experimentation with coupled climatic-hydrological-oceanographic-biogeochemical modelling. The study was carried out by research Teams from nine academic institutions in close cooperation with Manitoba Hydro and its subcontractors. Research Teams were organized to investigate six inter-connected subsystems with continuous consultation, integration, and feedback from Manitoba Hydro and other project participants.

The University of Manitoba and Manitoba Hydro have had a long history of collaboration, including programs in the Nelson River estuary (2005 and 2010), and a winter field program focusing on the characterization of ocean-sea ice-atmosphere coupling and sedimentary processes in 2009. These research programs fed into the development of the Hudson Bay IRIS Report, and a series of presentations and workshops throughout ArcticNet conferences. Manitoba Hydro has a vested interest in the results of this project and specific research on the impacts and adaptation strategies for climate change on northern ecosystems, as it may affect system operations and future generation developments. Results and publications from this project help Manitoba Hydro investigate ways to enhance the quality and capacity of environmental science in the operating regions, produce reliable assessments of impacts of climate change on water supply, and increase our understanding of the effects of the flow regulation and climate change on northern ecosystems. They also help to enhance Manitoba Hydro's environmental assessment program and have led to the development of new greenhouse gas (GHG) monitoring technologies.

The outcomes of this study (i.e., datasets, model development, and publications/analysis reports) provide Manitoba Hydro with access to unique knowledge, expertise, and experience in the Arctic system of Hudson Bay, and provide a scientific basis to allow us to distinguish between hydrological (seasonality and volume of discharge as affected by the operating regime) and climate (changing runoff and sea ice forcing) effects on estuarine processes and sea ice formation and decay in Hudson Bay, and the interplay between these processes. This project provides for a better understanding of how seasonal trends and variability in freshwater, sediment, and nutrient delivery affect Hudson Bay and how this may change under a future climate for Manitoba, Nunavut, Northern Ontario, and Quebec.

For the University of Manitoba, this partnership with Manitoba Hydro allowed researchers to have a much more extensive marine sampling program than would have otherwise been possible. Past surveys co-funded by Manitoba Hydro guided the strategic placement of the BaySys moorings, locations of bay-wide and estuary sampling transect, and provided ocean and freshwater state variables at various locations and times of the year.

Throughout this project, Manitoba Hydro provided historical data through their environmental monitoring program, such as the Coordinated Aquatic Monitoring Program (CAMP), in addition to extensive logistical and in-kind support for the sampling of on- and off-system water bodies for mercury and organic matter. In addition, they provided hundreds of hours of staff time for Team collaboration, meetings, conferences, and manuscript reviewing. Their in-kind contributions extended to other in-field activities throughout the project, including covering helicopter costs, equipment donations, purchases, repairs and calibrations, and some necessary mooring anchors. In addition, vital contributions from Manitoba Hydro allowed the project to hire the *RV William Kennedy* for recovery of the James Bay mooring in 2018, and also to cover conference fees for many BaySys HQPs over the final two years of the project.

Manitoba Hydro integrated the Nelson River Basin's regulation rules into the HYPE hydrologic model, which allowed the project to output regulated and unregulated river discharges for various climate scenarios. In addition, providing unregulated weir flow equations and information on land covers.

HQPs across BaySys published results of the BaySys project in high-impact journals and at international conferences. Throughout the project, BaySys members have participated in numerous national and international conferences exceeding 70 oral and poster presentations, as well as chairing several topical sessions on our research in Hudson Bay. In addition, BaySys management organized a special issue for the project in the open access journal, *Elementa: Science of the Anthropocene,* providing an accessible, and integrated space for academic readership and referencing of the BaySys project (Link to collection).

Throughout the BaySys project, hundreds of datasets have been collected, with thousands of associated resources (individual files). As per the project mandate, they are stored, along with their metadata, in the University of Manitoba's data repository. The value in these datasets is immense, not only will our partners at Manitoba Hydro and Hydro Quebec benefit from these environmental datasets, but the project will also significantly contribute to the scientific literature in a region that has been traditionally understudied. The wealth of knowledge and data generated from the BaySys program is publicly available through the University of Manitoba's CanWIN datahub (Link to DataHub).

By sharing data in an integrated and open manner we have provided our partners, the public, and other researchers with the ability to accelerate data discovery, visualization, analysis, and interconnections between datasets. This transformed our ability to address critical scientific questions in the future and to meet unaddressed researchers, Inuit, First Nation, government, operational service provider, and private sector needs for data-driven knowledge. Providing data in the open platform format increased the visual impact of industry and other partners' contributions to addressing concerns surrounding the impacts of climate change in the arctic and the freshwater-marine interface.

Hydro-Québec's vital contribution to this project includes the production and distribution of regulated system modelling controlling discharge from the eastern side of Hudson Bay and providing pre-regulation land cover data. These include historical data of both regulated and unregulated flow for the eastern part of Hudson Bay, including James Bay. Pre- and post-regulation land cover for the La Grand basin area was also provided to the BaySys project.

Hydro-Québec performed hydrological simulations under climate change with the HSAMI hydrological model for rivers on the eastern part of Hudson Bay. They then performed regulated system modelling controlling discharge from the eastern side of Hudson Bay. Hydro-Québec has also participated in the redaction and revision of scientific publications and collaborated with students and scientists working in Team 2 of BaySys.

Ouranos – a consortium on regional climatology and adaptation to climate change – has contributed to the BaySys project since 2014. BaySys researchers within this consortium, have worked to create extensive circulation and climate models that have contributed to the Team 2 and Team 6 HYPE and NEMO models, respectively. Ouranos focussed on providing upstream Climate Model Intercomparison Project-5 (CMIP5) general circulation model (GCM) simulation data appropriate for the regional context of the Hudson Bay watershed. In addition, in-kind contributions from Ouranos to the BaySys project focussed on the identification, extraction, post-processing, and transfer of suitable reference climate and climate change projection data. This included the support and the associated expertise for the ingestion of climate scenarios into the hydrological model and their analyses.

1.5 References Cited

Barber, D.G., Sydor, K. (2020). *Hudson Bay Systems Study (BaySys) Phase 1 Report: Campaign Reports and Data Collection*. (Eds.) Landry, D.L., Candlish L. Unpublished Project Report. University of Manitoba, Winnipeg, MB. Canada.

Barber, D.G., Sydor, K. (2014). *BaySys – Contributions of climate change and hydroelectric regulation to the variability and change of freshwater-marine coupling in the Hudson Bay System* – NSERC CRD.

Gough, W.A. (1998). Projections of sea-level change in Hudson and James Bays, Canada due to global warming. *Arctic and Alpine Research*, 30(1), 84–88. 10.1080/00040851.1998.12002878

Joly, S., Senneville, S., Caya, D., Saucier, F. (2011). Sensitivity of Hudson Bay sea ice and ocean climate to atmospheric temperature forcing. *Climate Dynamics*, 36, 1835–1849. 10.1007/s00382-009-0731-4

Kuzyk, Z.A., and Candlish, L.M. (2019). *From Science to Policy in the Greater Hudson Bay Marine Region: An Integrated Regional Impact Study (IRIS) of Climate Change and Modernization*. ArcticNet, Québec City, 424 pp.

Harvey, M., Starr, M., Therriault, J-C., Saucier, F., Gosselin, M. (2006). MERICA-Nord Program: Monitoring and research in the Hudson Bay complex. *AZMP Bulletin PMZA*, 5 27–32.

Macdonald, R.W., and Kuzyk, Z.A. (2011). The Hudson Bay System: A northern inland sea in transition. *Journal of Marine Systems*, 88(3), 337-488. 10.1016/j.jmarsys.2011.06.003

McCullough, G., Kuzyk, Z.A., Ehn, J., Babb, D G., Ridenour, N., Myers, P.G., Wong, K., Koenig, K., Sydor, K., Barber, D. (2019). ‘Freshwater Marine Coupling in the Greater Hudson Bay Marine Region’ Chapter I.v in *From Science to Policy in the Greater Hudson Bay Marine Region: An Integrated Regional Impact Study (IRIS) of Climate Change and Modernization*. (Eds.) Kuzyk, ZZA and Candlish, LM. ArcticNet, Quebec City.

Saucier, F., Senneville, S., Prinsenberg, S., Roy, F., Smith, G., Gachon, P., Caya, D., Laprise, R. (2004). Modelling the sea ice-ocean seasonal cycle in Hudson Bay, Foxe Basin and Hudson Strait, Canada. *Climate Dynamics*, 23, 303–326. 10.1007/s00382-004-0445-6

Saucier, F., Dionne, J. (1998). A 3-D coupled ice-ocean model applied to Hudson 978 Bay, Canada: The seasonal cycle and time-dependent climate response to at atmospheric forcing and runoff. *Journal of Geophysical Research*, 103, 27689– 27705.

St-Laurent, P., Straneo, F., Dumais, J., Barber, D. (2011). What is the fate of the river waters of Hudson Bay? *Journal of Marine Sciences*, 88, 352–361. 10.1016/j.jmarsys.2011. 998 02.004.

Stadnyk, T., Déry, S., MacDonald, M., Koenig, K. (2019). ‘The Freshwater System’ Chapter I.iv in *From Science to Policy in the Greater Hudson Bay Marine Region: An Integrated Regional Impact Study (IRIS) of Climate Change and Modernization*. (Eds.) Kuzyk, ZZA and Candlish, LM. ArcticNet, Quebec City.

Sydor, K. (2012). *ArcticNet-Manitoba Hydro: Cold-Region Estuaries Workshop*. Workshop hosted at ArcticNet 2012. May 28-29, 2012.

Wang, J., Mysak, L., Ingram, R. (1994a). A numerical simulation of sea ice cover in Hudson Bay. *Journal of Physical Oceanography*, 24, 2515–2533. https://doi.org/10.1175/1520-0485(1994)024<2515:ANSOSI>2.0.CO;2

Wang, J., Mysak, L., Ingram, R. (1994b). A three-dimensional numerical simulation of Hudson Bay summer ocean circulation: topographic gyres, separations, and coastal jets. *Journal of Physical Oceanography*, 24, 2496–2514. https://doi.org/10.1175/1520-0485(1994)024<2496:ATDNSO>2.0.CO;2

CHAPTER 2 GENERAL PROJECT FRAMEWORK AND METHODOLOGY

2.1 Project Framework

BaySys became an official NSERC CRD project after management and Team leads successfully defended their proposal in November of 2014. The multi-year planned partnership and research agreement between the University of Manitoba and Manitoba Hydro was signed on December 15, of that same year, while a project timeline was developed to track the progress of the research. A team of central project coordinators served as the primary link between the university and industry partners, ensuring the sharing of information between the two parties was consistent and effective. This Team was responsible for organizing and leading the annual research and science steering committee meetings throughout the project and played an integral role in coordinating all integrated field campaigns.

Teams 2 and 6 used existing data, modelling, and analysis, not previously used, to attribute causality for observed and projected climate change to the marine and freshwater physical systems. The research conducted by Teams 1, 3-5 collected and analyzed data and applied newly developed and innovative techniques to better understand the fundamental processes of the respective marine, biological, carbon and contaminant systems. The objectives of this study, however, could only be achieved using a 'systems' approach, drawing expertise from and integrating across all science Teams. This approach not only called for a thorough investigation of each major component of the natural system and their integration but also the design and implementation of a coordinated field program and a fully integrated modelling program run in both 'upstream and downstream' modes.

2.2 Observational Fieldwork and Satellite Remote Sensing Data

At the onset of the BaySys project, contemporary fieldwork needed to play a significant role in the data-driven analysis of the bay. Specifically, the observational data were used to enhance knowledge of processes and inform the ocean modelling and integrated observational-modelling framework. Therefore, over the multi-year BaySys program, seven campaigns were conducted, including winter and fall surveys, and the first bay-wide survey conducted during the spring freshet in the Hudson Bay.

The BaySys project included the largest ever conducted simultaneous measurements of physical, biological, and biogeochemical processes of freshwater marine coupling in Hudson Bay during the winter to summer transition (Figures 2.1, 2.2, 2.3, 2.4). The field programs noted below, coupled with historical analysis, re-evaluation of previously collected data, and modelling activities provided an interdisciplinary foundation for innovative research contrasting impacts of freshwater regulation and climate change on Hudson Bay. These data are centrally stored in the CanWin data system as described in section 2.7.

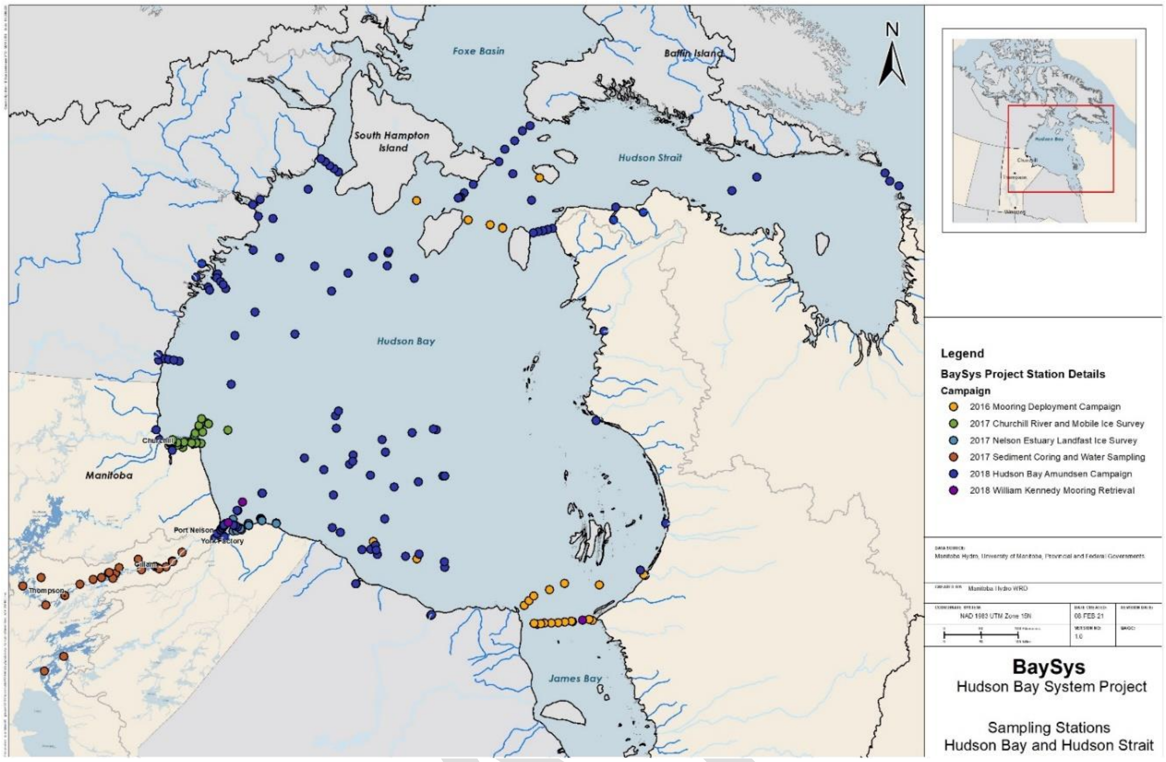

FIGURE 2.1 Complete BaySys station map including all campaigns conducted between 2016 and 2018.

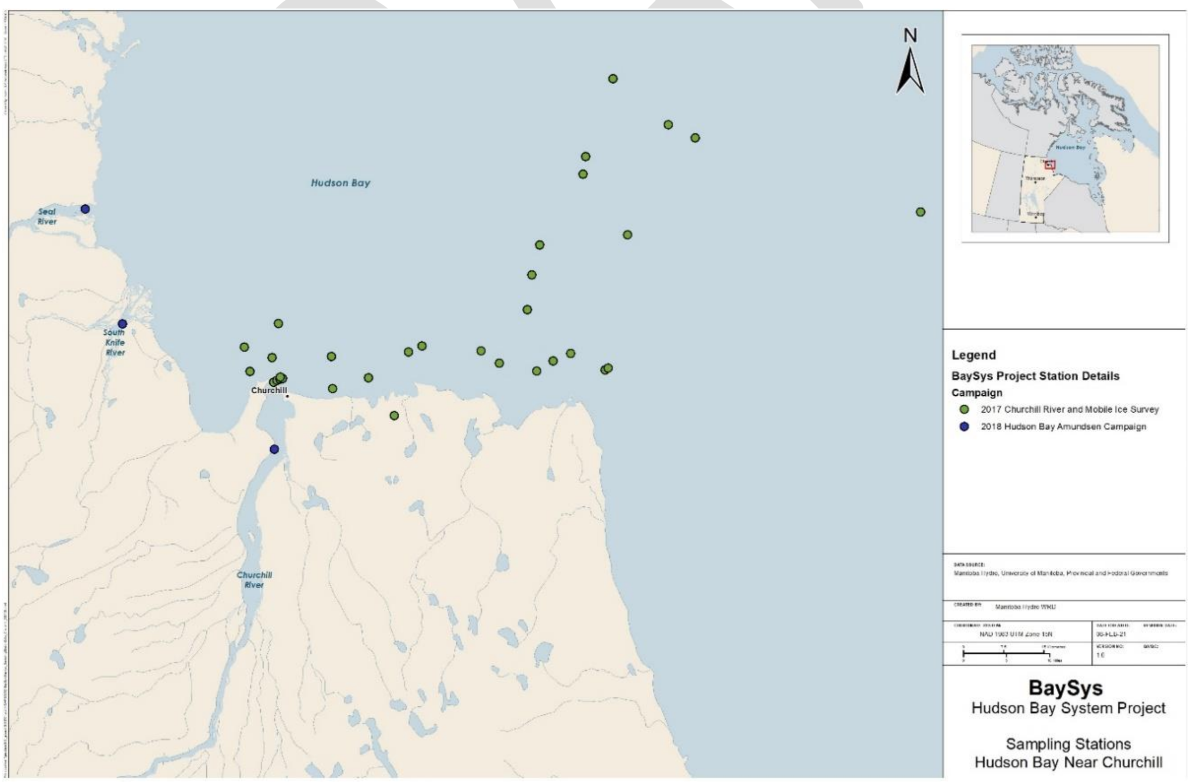

FIGURE 2.2 BaySys station map from the Churchill region. This map includes station locations from the 2017 Churchill River and Mobile Ice survey and the 2018 Amundsen Campaign.

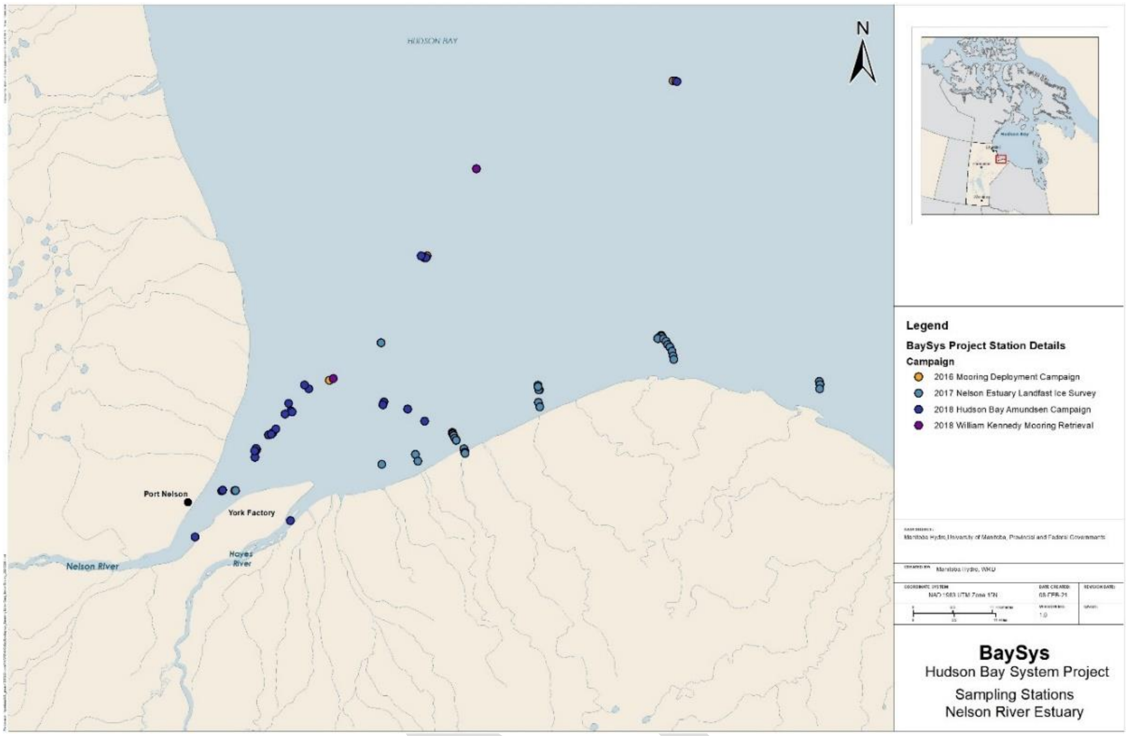

FIGURE 2.3 BaySys station map from the Nelson Estuary region. This map includes station locations from the 2016 and 2018 Mooring programs, along with the Nelson Estuary Landfast Ice survey and the 2018 Hudson Bay Amundsen Campaign.

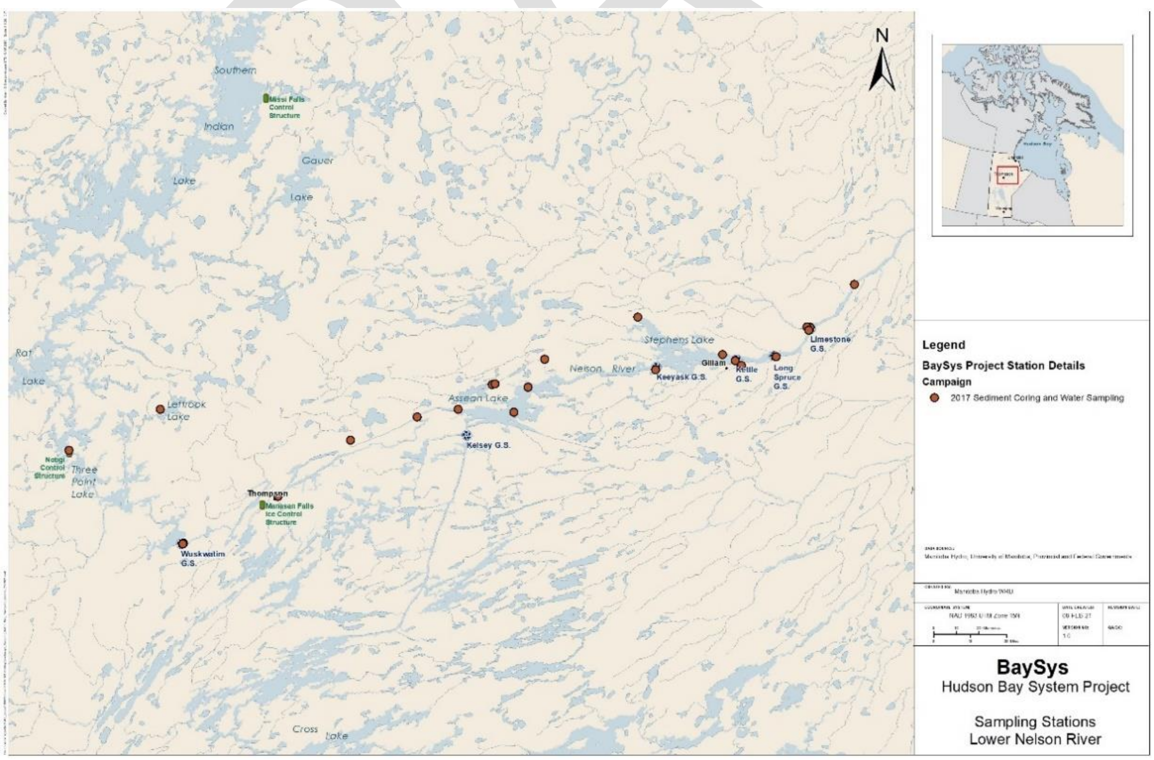

FIGURE 2.4 BaySys station map from the Nelson River and Northern Manitoba region. This map includes station locations from the 2017 Sediment Coring and Water Sampling campaigns.

In the fall of 2016, ship-based mooring deployments began off the *CCGS Des Groseilliers*. These moorings were later recovered over the following two years onboard the *CCGS Henry Larson* (2017) and the *CCGS Amundsen* and *RV William Kennedy* (2018). The moorings provided long-term temporal, in-situ measurements for temperature, salinity, water currents, ice draft and wave characterization, conductivity, turbidity, chlorophyll-a fluorescence, CDOM fluorescence, and sediments. Extensive water and biological sampling operations were conducted during all the vessel-based campaigns. During the 2017 winter and spring seasons, on-ice field camps were deployed on the Churchill River and Nelson River estuaries to survey the land fast and near-shore ice through ice coring and water sampling operations. These campaigns aimed to provide information on the freshwater-marine conditions prior to the key biologic and geochemical processes which occur during the spring melt. Sediment, soil, and water quality surveying continued throughout the summer and fall of 2017, with Teams conducting fieldwork throughout the southwestern shores and estuaries of the bay.

From May to July 2018, the Amundsen BaySys cruise completed the first-ever bay-wide survey of the marine ecosystem at the time when the freshet was at maximum and the ice cover was still in place. This field campaign was an enormous success with an unprecedented 122 sampling stations completed, making use of the Amundsen, helicopter, barge, and zodiac. These are categorized as 45 stations on board the vessel, 53 stations via helicopter, and 24 stations via a combination of zodiac and barge operations. This resulted in thousands of water, sea ice, sediment, and biological samples being collected. Many of our objectives for the cruise and BaySys project were achieved during this campaign, bearing a few locations in the bay in which we were not able to access due to ice and weather conditions. Overall, data collection and sampling went exceptionally well throughout the program, including all onboard, on-ice, terrestrial, and remote sensing-based operations. Combined, these field efforts provide the first comprehensive physical, biological and biogeochemical status of Hudson Bay. For more detail on the observational fieldwork conducted during the BaySys project please refer to the Phase 1 BaySys project report.

This combination of sampling campaigns was integral to addressing the overall objective and integration into the observational-modelling framework. Almost all Teams used an approach combining *in situ* (ship-based sampling, shore-based winter operations, and Bay-wide sampling, moorings for project duration, historical data), remote-sensing, and coupled numerical modelling. Discrete data were used to define the current state in the bay and, where possible, they provided reference points by which to assess prior and future change (with respect to less comprehensive historical data). These data were also used to refine algorithms for remote sensing, as well as the parameterization and initialization of the numerical models. Remote sensing images and modelling were used to fill spatial and temporal gaps in discrete sampling and to identify drivers of variability and change across the bay.

2.3 Fresh Water Modelling Component

A robust climatic input ensemble was determined for BaySys based on rigorous analysis of 12 hydrologic variables over the Hudson Bay Drainage Basin (HBDB) domain. The ensemble includes 14 General Circulation Models (GCMs) across two Representative Concentration

Pathways (RCPs) 4.5 and 8.5 for a total of 19 climate simulations that represent 87% of the variability from a total of 154 IPCC climate simulations. A smaller subset of five climate models was selected to drive Nucleus for European Modelling of the Ocean (NEMO) over the open ocean, and across the larger ANHA4 domain. A pan-Arctic domain version of the HYPE hydrologic model (A-HYPE) was set up and driven using Hydro-GFD historic reanalysis data, which was consistent with the ERA forcing for NEMO. The H-HYPE model was then truncated from this larger domain, recalibrated, and additional functionality for frozen soils, diversions and regulation, non-contributing area runoff and lake parameterizations added (Stadnyk et al., 2020). A hydrologic analysis across the pan-Arctic domain was conducted, including trend analysis; trend analyses of historic discharge records across the HBDB was conducted on gap-filled records generated by (Déry et al., 2016), and a subsequent comparison of the regulated and unregulated systems within the HBDB (Déry et al., 2018). Team 2's (MacDonald & Kuzyk, 2018) assessed hydroclimatic change within the HBDB under 1.5oC and 2.0oC warming.

2.4 Ocean Modelling Component

NEMO is a fully integrated modelling program that incorporated historical, modelling, reanalysis, and satellite remote sensing data as a means of up-scaling process studies in both space and time. Details regarding the development, setup, and analysis of the model can be found in Chapter 10 of the Phase 1 report and Section 3.6 of this Phase 2 report. The coupled atmosphere/sea ice/ocean model was optimized and used in direct support of the over-arching goal to distinguish climate change from regulation. Team 1 and Team 6 worked together to analyze differences between observed and modeled timing of ice cover formation and decay (statistical and numerical models) both regionally and Bay-wide in terms of seasonal and annual freshwater loading from the watershed. Then, through apportioning variability and trends in seasonal and inter-annual runoff volumes between climate forcing and regulation by Team 2, the remaining Teams tested for distinct and/or interlinked forcing by each as they affect ecosystem functioning on Hudson Bay (Teams 3-5). Watershed models and coupled physical-biogeochemical models of the marine environment were informed by the field observations and were used to project conditions for the 2030s and 2050s. The models were forced with scenarios of climate change and regulation, allowing for the separation of those two impacts on the Hudson Bay system.

As part of the BaySys project, the Nucleus for European Modelling of the Ocean (NEMO) model was optimized for Hudson Bay and includes the integration of the watershed data from the HYPE model. The NEMO ANHA configuration developed and run by Dr. Paul Myers and his Team shows new features in Hudson Bay that were undetected by previous models such as the Saucier model (2004). The Saucier model is still referenced in current literature (see examples such as Kuzyk & Candlish 2019, in the Hudson Bay IRIS report), as there have been no updated ocean-sea ice models for Hudson Bay since 2004 that have gone through the peer-reviewed process. This issue has now been addressed throughout the BaySys project with several publications from HQPs specifically detailing the use of NEMO in the bay, including our new understanding of the circulation features in Hudson Bay (Ridenour et al., 2018).

2.5 Data Analysis

Following the numerous fieldwork campaigns conducted during this BaySys project, extensive data processing and analysis occurred. The campaign reports are featured in the BaySys Phase 1 report, where fieldwork data collection and methods are outlined and discussed in detail. The data processing and analysis results are found throughout Chapter 3 of this Phase 2 report. The analysis included both in-house and remote sample preparation, processing, and analysis for hundreds of variables within thousands of samples across all four observational data Teams (Team 1, 3, 4, and 5). Samples included physical sea ice cores, CTDs, marine, river, and melt pond water. In addition, thousands of benthic, sediment, fish, and nutrient samples were processed and analyzed. Lastly, intensive post-processing and analysis were conducted on remote sensing datasets, including satellite, and drone images and surveys.

2.6 Integrated Observational-Modelling Framework

The combined research efforts of the six science Teams represented an **unprecedented and innovative** effort to provide a scientific basis to separate climate change effects from those of regulation of freshwater on physical, biological, and biogeochemical conditions in Hudson Bay. However, these Teams did not complete their work in isolation from each other. Each Team collected data and/or provided model outputs that were crucial to the success of other Teams. Following the field programs, they fully integrated through annual workshops and integration groups to provide project updates and coordinate their analysis, modelling, and preparation of results.

Mooring and observational data from team 1 were used to evaluate the accuracy of the models (see Section 3.6.3) while Teams 2 and 6 provided outputs to workgroups within Teams 1, 3, and 4 (see Sections 3.1.3; 3.2.3; 3.3.3). These modelling outputs were used to support the results of the observational Teams and specifically used to evaluate their data with future outputs to assess the condition within which regulation and climate change have affected any significant change.

2.7 Data Archival and Management

Through the BaySys project, hundreds of datasets have been collected, with thousands of associated resources (individual data files). After being quality assured and quality controlled, the data are being stored, along with their metadata, into the University's data repository. The value in these datasets is immeasurable, as not only will our partners at Manitoba Hydro and Hydro Quebec benefit from these environmental datasets, it also significantly contributes to a sizable research gap in a region that has been traditionally understudied. The wealth of knowledge and data generated from the BaySys program is readily available and where data licenses allow, publicly available with assigned DOIs. Working with the UofM Data Manager and data Team, all QA/QC data were input into CanWIN (project datahub). Datasets are listed in the datahub and are available for download at the link provided: CanWIN Data HUB – BaySys Organization (link).

By sharing data in an integrated and open manner, the public, industry, and other researchers are provided with the ability to accelerate data discovery, visualization, analysis, and interconnections between datasets. This transforms our society's ability to address critical scientific questions and to meet unaddressed researchers, Inuit, First Nation, government, operational service providers, and private sector needs for data-driven knowledge. Providing data in an open platform format increases the visual impact of industry and other partners' contributions to addressing concerns surrounding the impacts of climate change in the arctic and the freshwater-marine interface.

As the data archival is fully implemented, our researchers and industry partners can use traditional (i.e., number of publications), and Altmetric reporting systems. Altmetrics allows data publishers to demonstrate more fully the impact of their research by tracking not only citation information, but hundreds of other sources including social media mentions (e.g. Twitter, Facebook), news outlets, video, Wikipedia, and other information outlets mentions.

2.8 References Cited

Déry, S.J., Stadnyk, T.A., MacDonald, M.K., Gauli-Sharma, B. (2016). Recent trends and variability in river discharge across northern Canada. *Hydrology and Earth System Sciences,* 20(12), 4801-4818.

Déry, S.J., Stadnyk, T.A., MacDonald, M.K., Koenig, K.A. (2018). Flow alteration impacts on Hudson Bay river discharge. *Hydrological Processes*, 32(24), 3576-3587.

Kuzyk, Z.A. and Candlish, L.M. (2019). *From Science to Policy in the Greater Hudson Bay Marine Region: An Integrated Regional Impact Study (IRIS) of Climate Change and Modernization*. ArcticNet, Québec City, 424 pp.

Macdonald, R.W., and Kuzyk, Z.A. (2011). The Hudson Bay System: A northern inland sea in transition. Special Issue in *Journal of Marine Systems,* 88(3), 337-488. 10.1016/j.jmarsys.2011.06.003

Saucier, F., Senneville, S., Prinsenberg, S., Roy, F., Smith, G., Gachon, P., Caya, D., Laprise, R. (2004). Modelling the sea ice-ocean seasonal cycle in Hudson Bay, Foxe Basin and Hudson Strait, Canada. *Climate Dynamics,* 23, 303–326. 10.1007/s00382-004-0445-6.

Stadnyk, T. A., MacDonald, M. K., Tefs, A., Awoye, O. H. R., Déry, S. J., Gustafsson, D., Isberg, K., and Arheimer, B. (2020). Hydrological modelling of freshwater discharge into Hudson Bay using HYPE. Special Feature in *Elementa: Science of the Anthropocene,* 8 ,43. https://doi.org/10.1525/elementa.439

Ridenour, N. A., Hu, X., Jafarikhasragh, S., Landy, J. C., Lukovich, J. V., Stadnyk, T. A., Sydor, K., Myers, P. G., Barber, D. G. (2019). Sensitivity of freshwater dynamics to ocean model resolution and river discharge forcing in the Hudson Bay Complex. *Journal of Marine Systems,* 196, 48-64. https://doi.org/10.1016/j.jmarsys.2019.04.002

CHAPTER 3 BAYSYS TEAM RESULTS

Chapter 3 is an essential deliverable of the BaySys project. Throughout this chapter, each Team presents an introduction to their research - and in turn to a specific Hudson Bay system - and states their overall Team objectives. A description of their analytical and interpretive methods is then provided, followed by a detailed presentation and discussion of results, specifically relating to each of their specific tasks. In the conclusions, Teams address each of their project hypotheses and discuss their results in the context of the overall project objective. Lastly, each science Team ends their section with a description of research gaps and future recommendations.

3.1 Marine and Climate System (Team 1)

Team Member	Affiliation	Tasks contributed to				Role
Jens Ehn	*a*	*1.1*	*1.2*	*1.3*	*1.4*	*Science Lead*
David Barber	*a*	*1.1*	*1.2*	*1.3*	*1.4*	*Contributor*
Kevin Sydor	*b*	*1.1*	*1.2*	*1.3*	*1.4*	*Hydro Lead*
Karen Wong	*b*	*1.1*	*1.2*	*1.3*	*1.4*	*Hydro Lead*
David Babb	*a*	*1.1*	*1.2*	*1.3*	*1.4*	*Contributor*
Jennifer Lukovich	*a*	*1.1*	*1.2*	*1.3*	*1.4*	*Contributor*
Sergei Kirilov	*a*	*1.1*	*1.2*	*1.3*	*1.4*	*Contributor*
Greg McCullough	*a*	*1.1*	*1.2*	*1.3*	*1.4*	*Contributor*
Igor Dmitrenko	*a*	*1.1*	*1.2*	*1.3*	*1.4*	*Contributor*
Simon Belanger	*c*	*1.1*	*1.2*	*1.3*	*1.4*	*Contributor*
Jennifer Bruneau	*a*	*1.1*	*1.2*	*1.3*	*1.4*	*Contributor*
Madison Harasyn	*a*	*1.1*	*1.2*	*1.3*	*1.4*	*Contributor*
Anirban Mukhopadhyay	*a*	*1.1*	*1.2*	*1.3*	*1.4*	*Contributor*
Wayne Chan	*a*	*1.1*	*1.2*	*1.3*	*1.4*	*Contributor*
Atreya Basu	*a*	*1.1*	*1.2*	*1.3*	*1.4*	*Contributor*
Kaushik Gupta	*a*	*1.1*	*1.2*	*1.3*	*1.4*	*Contributor*
Vladislav Petrusevich	*a*	*1.1*	*1.2*	*1.3*	*1.4*	*Contributor*
Yanique Campbell	*a*	*1.1*	*1.2*	*1.3*	*1.4*	*Contributor*
Christopher Peck	*a*	*1.1*	*1.2*	*1.3*	*1.4*	*Contributor*
Nathalie Theriault	*a*	*1.1*	*1.2*	*1.3*	*1.4*	*Contributor*
Masayo Ogi	*a*	*1.1*	*1.2*	*1.3*	*1.4*	*Contributor*
Jack Landy	*a*	*1.1*	*1.2*	*1.3*	*1.4*	*Contributor*

a) Centre for Earth Observation Science, University of Manitoba, Winnipeg, Manitoba, Canada.
b) Manitoba Hydro, Winnipeg, Manitoba, Canada
c) Université Quebec à Rimouski, Québec, Canada

3.1.1 Introduction and Objectives

The objective of Team 1 is to advance the understanding of the baseline oceanographic conditions (primarily temperature, salinity, $\delta^{18}O$, CDOM, snow, and ice thickness) and physical processes (related to mass and energy exchange between the land, ocean, and atmosphere) that control the input and distribution of freshwater in the marine system of Hudson Bay. The main tasks 1.1-1.4 associated with Team 1 involved the collection of new data and the use of available observational records (such as remote sensing products, climate reanalysis products, oceanographic mooring and survey data, weather station data) to characterize changes and variability in the Hudson Bay climate, marine, and sea ice systems. Team 1 contributes new data and process understanding to help the Nucleus for European Modelling of the Ocean (NEMO) ocean modelling efforts (lead by Team 6), which addresses questions related to past and projected interannual and long-term changes caused by climate variability, trends, and hydroelectric development. Initially, the NEMO ocean modelling was included as a task within Team 1 (previously Task 1.5). However, in 2017, it was decided to separate Task 1.5 from Team 1 and create Team 6 to focus on ocean modelling. An additional objective of Team 1 is furthermore to contribute baseline oceanographic data for the science teams, in particular, Teams 3 to 6.

Observations across the Arctic oceans reveal that the seasonal timing and volumes of freshwater inputs through both sea ice melt and river runoff have been affected by the changing climate (e.g., Haine et al., 2015). In the Hudson Bay marine system, both the timing and local magnitudes of runoff have additionally been affected by river diversions and seasonal storage for hydroelectric purposes. The BaySys project was motivated by the lack of understanding of how the Hudson Bay marine systems might change in response to these Arctic-wide and local changes. An overarching focus for Team 1 on freshwater was justified by the fact that the input of freshwater has a controlling influence on the physical (and also biological and chemical) oceanography of the Arctic Ocean, including the Hudson Bay system, through its control of heat, light, and momentum exchange between the atmosphere and ocean.

Freshwater is present in the Hudson Bay marine system in both liquid (meltwater, land runoff) and solid (snow, sea ice) forms. Over 1.4 m of freshwater is supplied annually by melting sea ice and snow, and another 0.9 m by runoff from the bay's watershed (Granskog et al., 2011; Prinsenberg, 1988). Freshwater inventories are the highest in the southern half of the bay, because of the ice meltwater transport by southeastward wind-driven ice drift and the cyclonic ocean circulation and because over two-thirds of all terrestrial runoff to the bay debouches into southern Hudson Bay (e.g., Granskog et al., 2011). If the marine water end-member is taken as a typical North Atlantic value of 34.8 PSU (Straneo & Saucier, 2008) rather than the locally representative 33 PSU, about 1.6 times the local freshwater input (terrestrial, ice melt) is supplied by Arctic water inflow through Fury and Hecla Strait and Hudson Strait (Barber, 1967; Prinsenberg, 1977; Ridenour et al., 2019) revealing the close connection of the Hudson Bay system with the Arctic Ocean. However, if selecting the 33 PSU marine seawater end-member, then the marine sources of freshwater are a much more conservative 20% of the terrestrial runoff, with Fury and Hecla Strait being the only marine freshwater input source. This is the case from both *in situ* and mooring observations for salinity, and thus also reflected in modelling (Straneo & Saucier, 2008). As such, it depends on the reference point and scale of the study (local Hudson Bay vs. Arctic-wide). If the study is considered within the context of other Arctic FW flux studies, 34.8 PSU is used, however, when the freshwater distribution from local sources is to be delineated then 33 PSU is appropriate.

Past studies have shown that the strong vertical stratification imparted by the input of freshwater during the open water season has a controlling influence on the biogeochemical cycling in Hudson Bay and persistently lower nutrient levels. The measured low nutrient concentrations have been invoked to explain low biological productivity compared to other estuarine systems (e.g. Anderson & Roff, 1980; Ingram et al., 1996; Ferland, 2011; Sibert et al., 2011). However, these studies were limited to the navigable open water season and did not address the dichotomy between the seemingly low productivity and the large marine mammal stock. A goal of BaySys was to provide *in situ* observations during the previously poorly understood winter season and the late spring-early summer melt season to improve the understanding of the spring bloom preconditioning and onset. We found the northern part of the bay to be more biologically active than previously thought. This content is discussed in more detail in section 3.3.

The downward trend in Arctic sea ice extent and volume is one of the most prominent signals of environmental change on our planet. The Arctic ice extent displays negative trends for all months of the year (Stroeve et al., 2011), but the strongest decline in ice extent is seen for September (–13.1% loss per decade from 1980-2020) at the end of the melt season (NSIDC, 2020). By being a product of the thermodynamic and mechanical forces acting on the ocean surface, sea ice responds directly to changes in atmospheric, oceanic, and terrestrial influences on the system. Previous studies of the Hudson Bay sea ice climatology have reported quantitative relationships between timing of sea ice formation and decay, and seasonal temperature and wind patterns driven by hemisphere-scale atmospheric circulation (Hochheim & Barber, 2010, 2014; Hochheim et al., 2011). In Hudson Bay, the length of the ice-covered period was reported to have decreased by about 3 weeks on average between 1980-1995 and 1996-2010 (Hochheim & Barber, 2014). For offshore waters, the overall trend between 1980 to 2014 was towards a delay in freeze-up by +0.47 days year^{-1} and earlier break-up by –0.58 days year^{-1} (Andrews et al., 2018).

There is a complex interaction between the formation of under-ice plumes and the development of the bay-wide brackish surface layer created by mixing seawater with freshwater from river runoff and ice melt. In general, the presence of ice restricts deep mixing caused by tide, wave, and wind action, so that the fresher surface waters may spread more widely in winter (Ingram & Larouche, 1987). Through increased stratification of the water column, the spreading of freshwater promotes the onset ice formation, but the less saline surface waters result in less brine production associated with freezing of seawater (Anctil & Couture, 1994; Macdonald et al., 1995; Eastwood et al., 2020) thereby limiting thermohaline vertical convection and ventilation of deep waters. However, in well-mixed coastal zones where ice-deficit polynyas and flaw-leads form, the brine released from sea ice formation may find pathways to advect and sink below the halocline into Hudson Bay deep waters. The fact that these processes, that control water column stability and mixing, were not well quantified in the Hudson Bay system, where tidal forcing is a much more significant factor than in most of the shelf waters surrounding the Arctic Ocean (Padman & Erofeeva, 2004; Kleptsova & Pietrzak, 2018) was a motivation for the BaySys research program.

3.1.2 Analysis and Methods

Central to Team 1 is the study of Hudson Bay water's stratification and mixing patterns, water mass modification and displacement by tides, currents, air-sea interactions, and terrestrial freshwater, both in ice-covered and open water conditions in the Hudson Bay marine system using in-situ field observations and remote sensing observations. Despite recognizing that the Hudson Bay marine environment is an interconnected system, Team 1's research separates into the study of three regimes: i) estuarine and coastal hydrographic regime, ii) offshore bay-wide hydrographic regime, and iii) trends and properties of the sea ice cover, which each require separate methodological approached and techniques for observation.

Five team tasks were established at the onset of the project to address each objective of Team 1. These tasks are largely associated with the field campaigns that are described in detail in the BaySys Phase I report. However, here we will briefly describe the methods not covered in the Phase I report which are associated with laboratory analysis of ice and water samples, and particularly for remote sensing.

Ice thickness estimations from mooring ADCP data

To study the effect of atmospheric forcing on interannual spatial variability of sea ice thickness in the Hudson Bay, we used *in-situ* data obtained with upward-looking 5-beam Acoustic Doppler Current Profilers (ADCP, Nortek Signature500) at three BaySys moorings (AN01, NE03, and JB02) in 2016-2018. The ice thicknesses were estimated from the echo-ranging distance between ADCP and the submerged part of the ice floes drifted over the profiler during the ice-covered period (https://www.nortekgroup.com/assets/software/N3015-011-SignaturePrinciples.pdf). The 2-to-8-minute acoustic bursts were transmitted at 2 Hz every 1-to-3 hours during two consecutive winters 2016/17 and 2017/18. The acoustic-derived ice drafts were first corrected for ADCP tilt, water level, and atmospheric pressure (Krishfield et al., 2014). They were then corrected for the speed of sound by applying a semiautomated method of open water detection based on spectral analysis of burst data and identifying the spectral maximums within the wind-generated short-wave periods (3-8 seconds). Despite the reliability of this method, open water conditions were rarely observed during winter, introducing the largest error associated with sound speed due to the unknown seasonal and synoptic thermohaline changes in the surface layer. However, considering the shallow deployment depths of all used ADCPs (varying between 27 m and 37 m) and small variations of surface layer temperature and salinity during winter, the overall draft error was estimated as less than 5 cm (Kirillov et al., 2020). Within each burst, outliers beyond 2.5σ, where σ is the standard deviation of ice draft within the burst, were removed. Furthermore, only bursts with $\sigma < 0.5$ m and range < 1.0 m were used to determine a mean ice draft and calculate the mean ice thickness following Archimedes' principle. The densities of seawater and sea ice were taken as 1024 and 930 kg m^{-3}, respectively, and a no-snowpack assumption was applied. For context, assuming a snow depth of 15 cm, based on an estimate of the mean maximum end of winter (April) snow depth in Hudson Bay (Landy et al., 2017) and a snow density of 300 kg m^{-3}, reveals that ice thickness may be overestimated by only 5 cm, although typically this would be much less as less snow would have accumulated on thinner ice in December-March.

Water sampling and analysis

The *in-situ* ice and water sampling was a collaborative effort among teams, but Team 1's sampling focused on measuring four freshwater tracers: salinity, H_2O stable oxygen isotope ratio ($\delta^{18}O$), and spectral absorption by coloured (or chromophoric) dissolved organic matter (CDOM) (hereinafter $a_{cdom}(\lambda)$). The discrete water sampling was supplemented by continuous instrument profiles (salinity, temperature, Chl-*a* and CDOM fluorescence, beam attenuation at 660 nm and/or turbidity) which are described in detail in the Phase I report. Apparent optical properties were measured for radiative transfer information and satellite validation using Satlantic HyperSAS (surface reflectance) and a Satlantic HyperOCR and/or Biospherical Instruments C-OPS profiling spectroradiometer (open water conditions), and also TriOS Ramses irradiance sensors (under-ice observations).

The sampling was conducted using various methods outlined in respective cruise reports and the Phase 1 report. Salinity and $\delta^{18}O$ have previously been used to distinguish freshwater sources at the bay-wide scale (Granskog et al., 2011). CDOM is a semi-conservative freshwater tracer at the estuarine scale (Guéguen et al., 2011). CDOM has the advantage over the more conservative $\delta^{18}O$ in that continuous water column profiles can be obtained using fluorescence sensors, and over salinity and $\delta^{18}O$ in that CDOM surface concentrations can be estimated by satellite remote sensing of ocean colour. Water and ice samples for Salinity and $a_{cdom}(\lambda)$ were measured using a Guildline Autosal salinometer and a Perkin-Elmer Lambda 650 spectrophotometer, respectively. Samples for $\delta^{18}O$ (and deuterium composition for select samples) were either analyzed at the Centre for Earth Observation Science (U. Manitoba) using a Picarro isotope analyzer or sent to GEOTOP in Montreal, Hatch in Ottawa, or IsoLab at the University of Washington for analysis.

Additional water and ice samples were also collected for determination of total suspended solids (TSS) (GF/F filtration in the field) on estuarine and shore-perpendicular surveys, along with other optically active substances (i.e., $a_{cdom}(\lambda)$ and spectral particulate absorption, $a_p(\lambda)$) in coordination with Team 3. Although TSS (alternatively termed Suspended Particulate Material, SPM) is not expected to be an optimal freshwater tracer as particles may undergo settling and resuspension, it does play an important role in determining the optical properties of the water and ice and is a key indicator of estuarine and coastal dynamics in remote sensing.

In-situ CDOM and TSS measurements

For CDOM determination, water or ice melt samples were filtered through 0.2 mm 25 mm syringe filters (BaySys) or 0.7 mm 25 mm Whatman GF/F (earlier ArcticNet missions) filters, and stored in amber glass vials in the dark at +4 °C. Subsequently, aliquots of the CDOM samples were transferred to a 10-cm cuvette and tested for CDOM spectral absorbance (or optical density) using Perkin-Elmer Lambda 650 spectrophotometer at 275 – 800 nm. CDOM samples collected during the previous year's fieldwork were analyzed using different spectrophotometers (cf. Granskog et al., 2007) but following the same general method. After baseline correction (Babin, 2003), the raw absorbance (or optical density, $OD(\lambda)$) spectra were converted to CDOM spectral absorption coefficients, $a_{CDOM}(\lambda)$ (m^{-1}), using the following equation:

$$a_{CDOM}(\lambda) = 2.303\ \frac{OD(\lambda)}{d}$$

where, and d is the path length (m) of the cuvette (1, 5, or 10 cm) used for spectrophotometric measurement. Finally, the CDOM concentration was represented using the spectral absorption coefficient at a specific wavelength band of 412 nm as the reference value (Bricaud et al., 1981).

TSS concentration (g/L) was determined by filtering a known volume of water (or ice melt) sample through pre-weighed glass fiber filters: (a) in 2006: 0.7mm pore size and 47 mm diameter Whatman GF/F filters, and (b) in 2017: 1.5mm pore size and 47 mm diameter ProWeigh glass-fiber filters. The processed filters were oven-dried at 55 °C for 24 hrs and weighed. Triplicate measurements ensured a complete loss of moisture content on the filter paper and the filtrate. The difference in the weight of filters pre-weighed before filtering, and with dry particles after filtering, divided by the known filtered water volume, provided the TSS concentration (Van der Linde, 1998).

These in-situ CDOM and TSS concentration data were used to formulate empirical optical relationships enabling their satellite-based retrieval for plume extent characterization (Basu et al., in prep.).

Remote sensing data

CDOM and TSS: The goal of optical remote sensing was to study the dynamics of the Nelson River plume. This involves the estimation of freshwater dispersion and sediment transport. Coloured Dissolved Organic Matter (CDOM), the photoactive component of the dissolved organic carbon pool, has been used as an optical tracer of river plumes because its concentration correlates inversely with salinity. This correlation was established through in-situ field observation conducted as a part of Task 1.2, and from past observations in 2006 and 2010. The first step in CDOM retrieval involved the calculation of remote sensing reflectance (R_{rs}) from Moderate Resolution Imaging Spectrometer (MODIS, NASA) satellite imagery. The absorption coefficient of CDOM at 412 nm, a_{cdom}(412 nm) [m^{-1}], was then obtained using the following band ratio (Basu et al., in prep.):

$$a_{cdom}(412\text{ nm}) = 2.2105\left(\frac{R_{rs}\,(488\,nm)}{R_{rs}(667\,nm)}\right)^{-1.244}$$

Along with CDOM, total suspended sediment, TSS [g m^{-3}], concentration has been optically estimated using the optimized Nechad (2010) algorithm:

$$TSS = 5.49 \cdot\ exp\big(53.31\,R_{rs}(667\,nm)\big)$$

CDOM end-member values for Nelson River, Hayes River, and off-shore marine waters were then determined. Satellite imagery (29 images in total from 2000 to 2010) where acquired representing ebb- and flow tidal stages. Summer representing high and low river discharge years were compared.

Sea surface temperature (SST): The spatial-temporal variabilities of satellite-derived sea surface temperature (SST), sea ice concentration breakup, and freeze-up dates from 1982-2020 were analyzed to expand on the analysis provided by Galbraith & Larouche (2011) that covered the period 1985-2009 (Ehn et al., in prep). We used NOAA National Centers for Environmental Information (NCEI) Group for High-Resolution Sea Surface Temperature (GHRSST) Daily Level-4 Optimally Interpolated SST (OISST) in-situ and AVHRR Analysis, version 2.1 (NCEI, 2020; Reynolds et al., 2007) to obtain daily SST data on a 0.25-degree grid from January 1982 to December 2020. This data product (AVHRR_OI-NCEI-L4-GLOB-v2.1) incorporates satellite observations of SST from the Advanced Very High-Resolution Radiometer (AVHRR) and in-situ platforms. When sea ice concentration (SIC) in a grid point is higher than 30%, the freezing point of seawater is used to generate proxy SST (Reynolds et al., 2007; Banzon et al., 2020). The daily SST was further used to calculate weekly and monthly averages per grid point and for regions, and to estimate the annual maximum SST (SSTmax) and its day of the year, for each year between 1982 and 2020. The NOAA NCEI GHRSST data product also imbeds passive microwave SIC at the same 0.25-degree grid as the SST. This SIC, produced for the NOAA CRD program, is a combination of NASA Team algorithm (NSIDC-0051) and the Bootstrap algorithm (NSIDC-0079) as described in Meier (2012). For the Hudson Bay Complex (HBC), no discernible difference is seen to the NT SIC, however, the EUMETSAT OSI-SAF product produced unrealistically long persistence of sea ice for the shallow turbid waters of the southern James Bay. Hence, we have used the embedded CRD SIC when direct comparisons to SST were required.

<u>Remote sensing for sea ice type, concentration, and extent:</u> The historical record of Canadian Ice Service ice charts from 1971 to the present were used to provide context on mooring observations, characterize the regional landfast ice regime and examine the polynya in northwestern Hudson Bay. Ice charts are produced through expert manual interpretation of remote sensing imagery and observations from aircraft, coastal communities, and ships. Ice charts delineate different ice regimes with polygons that present sea ice concentration by stage of development using the World Meteorological Organizations Egg code. Ice charts are retrieved as E00 files from the CIS and converted to .shp files using ArcGIS.

Daily fields of sea ice concentration derived from spaceborne passive microwave radiometers were used to quantify sea ice concentration and key dates of breakup and freeze-up across HBC. Specifically, sea ice concentration products from the NSIDC (National Snow and Ice Data Centre) and OSI SAF (Ocean and Sea Ice Satellite Application Facility) were used. In these, sea ice concentration is presented as a gridded product and describes the percentage of the grid cell covered by sea ice. There is a well-known, but poorly quantified, bias towards underestimating sea ice concentration during the melt season when liquid water at the ice surface affects the signal. Typically, breakup and freeze-up were defined as the day that sea ice concentration passed the threshold of 15% (note that additional thresholds or other values may have been used depending on the case).

Daily optical images collected by Moderate Resolution Imaging Spectrometer (MODIS) of the Hudson Bay region were furthermore examined in the online NASA Worldview portal. Images are provided at 250 m resolution and provide a continuous time series since February 2000. However, the images are often by clouds, such that all or portions of the study areas may be obscured for several days or weeks at a time. Because of their higher spatial resolution compared to passive microwave products and optical wavebands, MODIS imagery was used to quantify the areal coverage of sediment-laden sea ice and the seasonal evolution of the landfast ice cover that forms around the periphery of the study region. Delineation of ice boundaries can often be performed even in the absence of optical atmospheric conditions.

<u>Satellite altimeter observations of sea ice freeboard and surface roughness</u>: A combination of ICESat (laser altimeter, 2003-2008), Cryosat-2 (Radar Altimeter, 2010-present), and ICESat-2 (multiple laser altimeter, 2018-present) were used to calculate mean fields of ice thickness in Hudson Bay (Landy et al., 2017) and provide observations of sea ice thickness and roughness around specific case studies (e.g., dirty ice in southern Hudson Bay, see Barber et al., 2021). All three altimeters measure the elevation of the sea ice or snow-covered sea ice relative to the surrounding sea surface height that is interpolated from observations of the sea surface in leads and areas of open water. ICESat and ICESat-2 are laser altimeters that are assumed to not penetrate the snow, while Cryosat-2 is a radar altimeter that is assumed to penetrate the snow and interact with the ice surface. The work of Landy et al. (2017) was the first spatially and temporally complete view of ice thickness within the HBC and provides a detailed list of methods used to estimate ice thickness. More recently, ICESat-2 provides higher resolution observations of sea ice freeboard along with three strong (15-m resolution) and weak (60-m resolution) beams that reveal added detail on sea ice roughness. ICESat-2 was used to examine the roughness and thickness of sediment-laden sea ice in southern Hudson Bay (Barber et al., 2021).

<u>Passive microwave thin ice algorithm for polynya identification</u>: Daily fields of surface brightness temperatures from AMSR-E (2003 – 2011) and –2 (2013 – present) (Advanced Microwave Scanning Radiometer-Emergency and –2) were used to determine the seasonal and interannual variability in the size and location of the polynya in northwestern Hudson Bay. Following previous studies, a thin ice algorithm was used to identify the polynya as the area of open water and new ice that was up to 10 cm thick. Once the polynya had been defined, atmospheric re-analysis from ERA-5 was used to model thermodynamic ice growth within the polynya and quantify ice production during winter from 2003 to 2020. Results were complimented the bay-wide observations of ice thickness and total regional ice volume presented by Landy et al. (2017).

<u>Passive microwave ice drift products:</u> Both the NSIDC Polar Pathfinder Daily 25 km EASE-Grid sea ice motion vectors (https://nsidc.org/data/NSIDC-0116 – 25 km) and OSI SAF Low-Resolution sea ice drift (http://osisaf.met.no/p/ice/index.html - 62.5 km) products were used to study sea ice motion in Hudson Bay. The datasets are derived from cross-correlation of sequential daily passive microwave fields and are available daily since 1979. Landy et al. (2017) used the NSIDC product to examine the mean fields of motion and dynamic kinematic properties (divergence, shear, and vorticity) of the ice pack, while Kirillov et al. (2020) used the OSI SAF product to track Lagrangian ice drift through winter. Kirillov et al. (2020) found that the NSIDC product underestimates ice drift speeds in Hudson Bay, although OSI SAF has a much lower spatial resolution.

In-situ passive microwave radiometry: A passive microwave radiometer with three frequencies (19, 37, and 89 GHz) was installed approximately 12 m above the sea surface height on the port side of the CCGS Amundsen during the 2017 and 2018 research programs. Scans were conducted across various incidence angles and ice types while the ship was stationary at ice stations. Radiometers measure the surface brightness temperature (T_B) and were compared against *in situ* observations of the thermophysical properties (temperatures, salinity, thickness, and wetness) of the ice within view of the radiometer's view. Additionally, ship-based observations were compared against satellite observations that are used to derived sea ice concentration datasets and are particularly uncertain during the spring melt period (Harasyn et al., 2019). Scans of the ice surface brightness temperatures (T_B) were conducted when the ship was immobile at ice stations. In-situ radiometer T_B data was compared to space-borne passive microwave data (Harasyn et al., 2019). Averaged *in situ* T_B for each incidence angle of measurement throughout the scan.

Local-scale remote sensing using Unmanned Aerial Vehicles (UAVs): Drone imagery was collected over study sites during the Amundsen (Task 1.2) and Nanuk (Task 1.1) programs to characterize the different ice types sampled. These images were stitched into true color mosaics and digital elevation models (DEM) through photogrammetric techniques. The mosaics were classified to determine the arieal coverage of melt ponds, sediment-laden ice, and the floe size distribution. The DEMs were used to calculate surface roughness statistics, and to estimate sea ice thickness based on the mean floe-scale freeboard.

Ancillary datasets

General Bathymetric Charts of the Ocean (GEBCO): GEBCO data was retrieved from https://download.gebco.net/ and used to examine the bathymetry along the landfast ice edge in Hudson Bay. Data is provided in Geo-Tiff format with a resolution of 15 arc-second.

Atmospheric observations from Environment Canada Weather stations: A collection of *in situ* observations from community-based weather stations distributed around the bay were used to examine atmospheric forcing and verify the results of the much broader reanalysis datasets used (described below).

Atmospheric reanalysis products: A combination of ERA5 (from ECMWF) and NCEP reanalysis 2 (from NOAA) were used to examine atmospheric conditions over the HBC. Variables such as air temperatures, surface winds, pressure patterns, solar irradiance, and longwave radiative fluxes were used to examine the seasonal changes and interannual variability across the atmosphere-ice-ocean system. Specifically, pressure patterns were used to identify storm events (Dmitrenko et al., 2020) and drive ice motion (Kirillov et al., 2020), calculate sea ice production within the NW polynya (hereafter known as the Kivalliq polynya) (Bruneau et al., 2021), drive sea ice surface melt (Barber et al., 2021) and many other processes within the marine environment.

3.1.3 Results and Discussion

Team 1 presents the results of their analyses following five team tasks that were established at the onset of the BaySys project and discusses them within the greater context of the team's objectives, and overarching project.

Task 1.1 Winter estuarine survey - To characterize the ice cover in the two estuaries, in general, and of the pack ice bordering the Nelson Estuary polynya, in particular, and to study sub-ice freshwater-marine mixing and circulation processes at the mouths of large (Nelson) and small (Churchill) sub-Arctic rivers.

Task 1.2 Spring/summer survey - To study processes governing the mixing of freshwater with seawater and the horizontal distribution of freshwater throughout Hudson Bay and Hudson Strait, and in greater detail in coastal waters near river estuaries surrounding the bay.

Task 1.3 Moorings - To complement and extend ice- and ship-based data collected during field campaigns and to assist in comparing fluvial-marine mixing and sediment transport processes in open water and sub-ice conditions.

Task 1.4 Remote Sensing - To conduct a Bay-wide survey of the timing (weekly time scale) of sea ice formation and decay (5 km spatial resolution) by analysis of remotely-sensed data following Hochheim & Barber (2014).

Task 1.5 Coupled sea ice/ocean model - Sea ice and oceanographic models will be used to further study the effects of freshwater loading and ice cover on the circulation of Hudson Bay. This task was led by Team 6 (see section 3.6.3)

Winter estuarine survey (Task 1.1)

The goal of the Team 1 winter sub-Arctic estuary surveys was to (i) characterize the ice cover in the Nelson and Churchill River estuaries, and (ii) characterize sub-ice freshwater-marine mixing and circulation processes at the mouths of the large Nelson River and the smaller Churchill River. Both locations are affected to varying degrees by riverine freshwater during the winter season, such that the studies were designed to provide in-situ data to assess the impact of riverine freshwater on sea ice growth (and its consequent structure and morphology) modulated by atmospheric (wind, temperature) and oceanic forcing (e.g., tides). The fieldwork and preliminary results for the winter surveys are presented in the Phase 1 report, Chapters 2-3.

Salinity profiles (Figure 3.1.1) of ice cores in the Nelson River estuary show similar or slightly higher values near the surface than what is typical for Arctic sea ice. This suggests that the freshwater from the Nelson River has little influence on the ice formation during the initial stages of ice growth. The high ice salinities indicate that the shallow water column likely maintains a high salinity (via strong tidal mixing) in the water column while water dynamics likely lead to a high fraction of frazil ice (rather than columnar ice) during the initial period of ice growth. Salinity values of 4-5 PSU and less are typical for the Arctic. At T1 and NRM, the ice cores show salinity values below 3 PSU. This is an indication of freshwater influence in the water column that is reflected in the low salinity captured within the ice matrix.

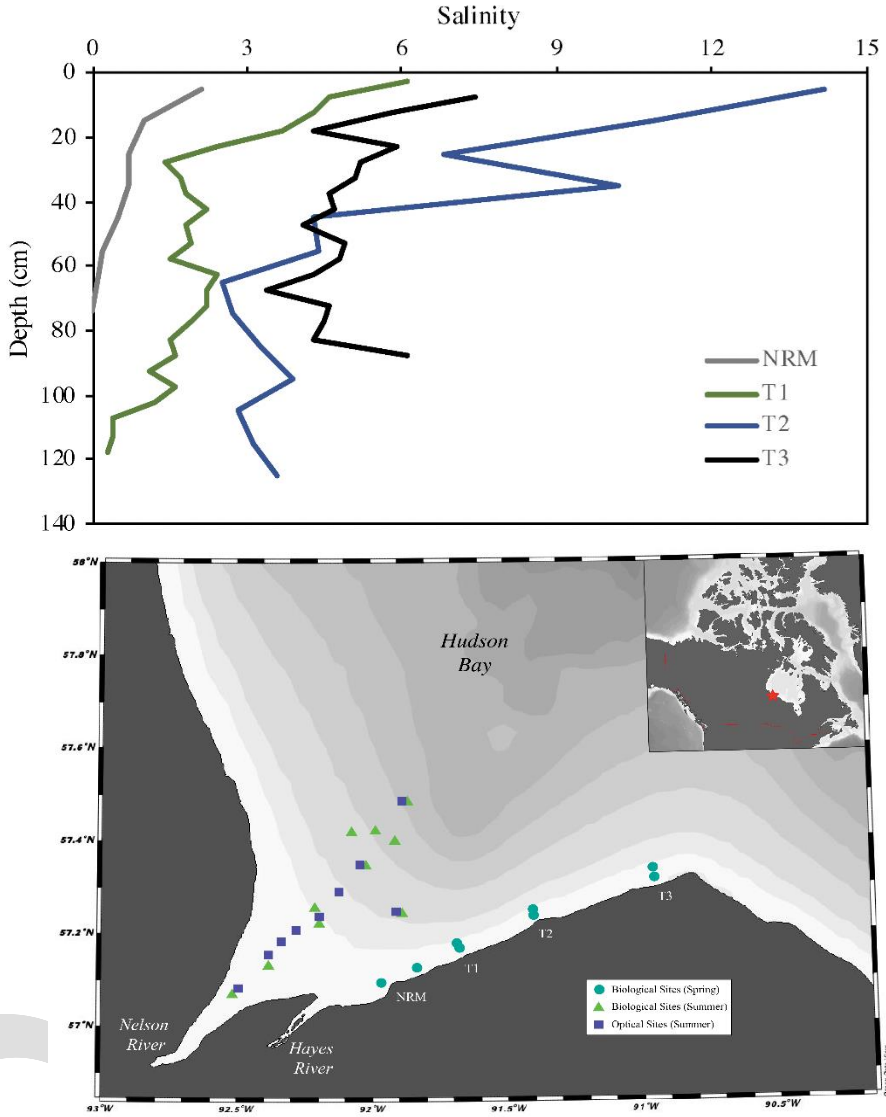

FIGURE 3.1.1 Top) Sea ice salinity profiles from 4 locations on the landfast ice cover collected during Leg 3 in April 2017. Bottom) Map of stations locations, including stations sampled during the summer cruise in 2018. NRM is the Nelson River Mouth. Samples were sectioned at 10 cm intervals.

The salinity variations seen in the upper portion of the ice cores during Leg 3 (with the unexpected higher salinity at T2 than T3) were also reflected in the CTD profiles collected during Leg 1 in February (Figure 3.1.2). There was an absence of vertical stratification beneath the sea ice with the water column well-mixed to the bottom. This is a consequence of mixing by the strong tidal currents. The transects across the landfast ice revealed that the freshwater distribution involved off-shore decreasing of salinity at the first two transects T1 and T2, whereas salinity increased off-coast at the easternmost transect near Cape Tatnam (T3). This implies that fresher river waters were directed toward the coast at some point between the T2 and T3 basic transects. The likely, but unconfirmable, explanation was the presence of thick or grounded sea ice along the coast that acted as a barrier that to some degree hindered the water exchange between the inshore and offshore environment.

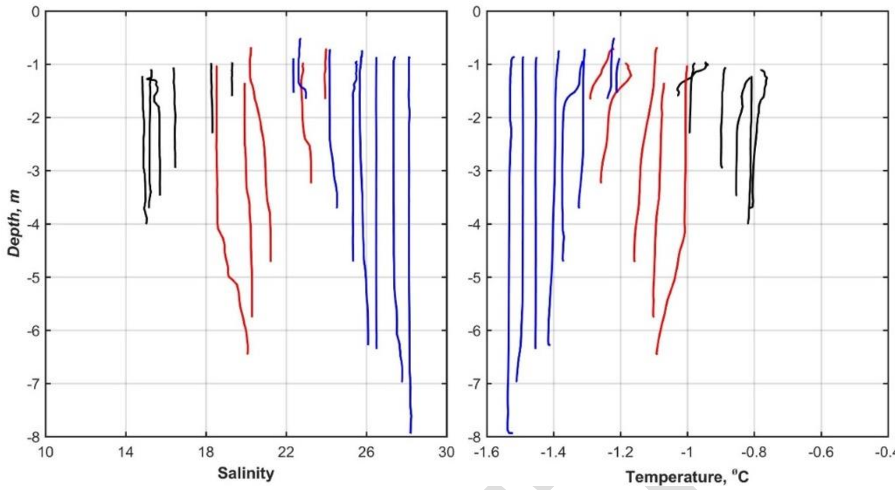

FIGURE 3.1.2 Salinity and temperature profiles were recorded at three CTD transects across landfast ice during the Nanuk campaign on 23-25 February 2017 (Leg 1). Black lines are associated with stations 1-6 near to T1; red lines – stations 15-19 by T3; and blue lines – stations 7-14 located near to T2 (see Phase 1 report for a map of locations).

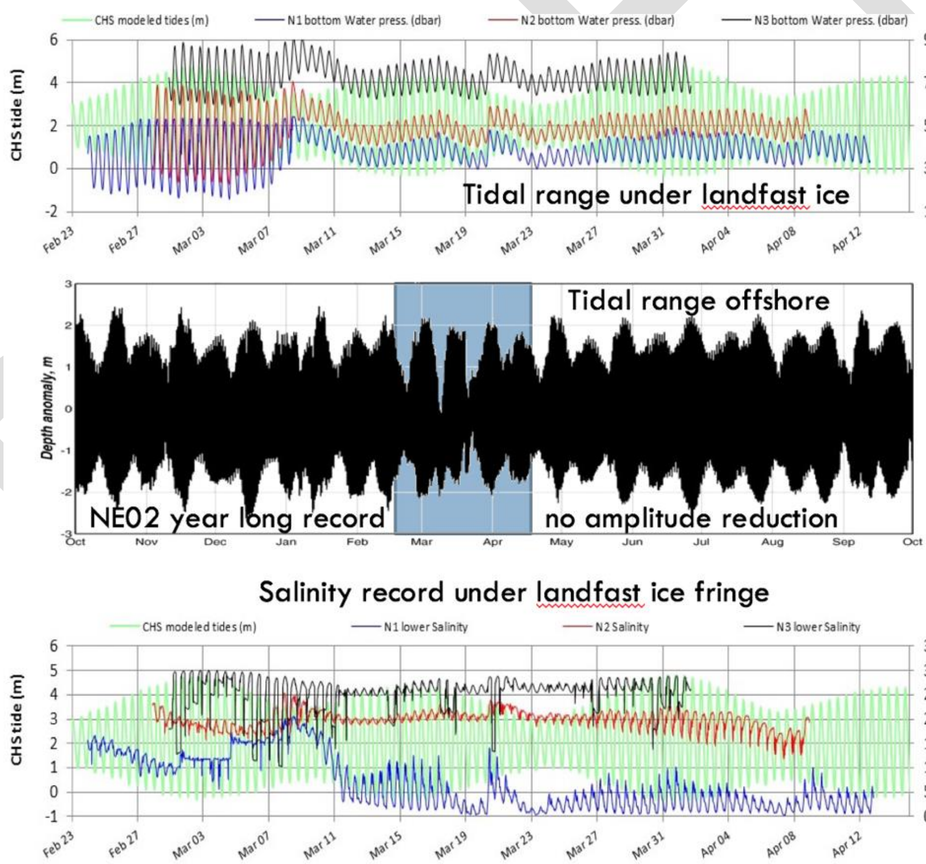

FIGURE 3.1.3 (upper and lower) Mooring record of water level and salinity at moorings N1 (blue), N2 (red), and N3 (black) (located along with transects T1, T2, and T3, respectively). (middle) Tidal record from mooring NE02 location offshore, with a blue shaded area corresponding to the period of the Nanuk ice-tethered mooring record. The locations of the moorings are displayed in Figure 3.1.1.

Initially, the ice-tethered moorings recorded tidal ranges comparable to those predicted by the Canadian Hydrological Service tidal predictions. However, following a storm on March 8, the tidal ranges reduced to a third of pre-storm levels (Figure 3.1.3). This was caused by the expansion of the landfast sea ice fringe by the accruement of mobile ice floes, and mechanical deformation by this convergence. The presence of the rough sea ice would cause the tidal current to slow due to increased frictional drag while also reducing the volume of water, and thus reduce the volume and speed of the water moved by the tide at the moorings (see Figure 3.1.4). The mooring record also revealed a reduction in salinity from pre-storm values generally > 10 PSU to post-storm values < 10 PSU at mooring N1. This is likely caused by the new rough ice hindering river water from dissipating further offshore and the reduction in tidal driven mixing thus promoting flow along the shoreline. The sea ice salinity profile at T1 (Figure 3.1.1) that shows low salinity near the bottom further indicates that the seawater it formed from had a relatively high freshwater content.

FIGURE 3.1.4 Example of the deformed landfast ice edge composed of newly formed thin ice during the Nanuk campaign in March 2017.

Data from mass balance stations, weather stations, and ice beacons, that were deployed on the mobile ice pack as part of the BaySys winter campaigns, have yet to be thoroughly analyzed. However, Lukovich et al. (2021b) used a portion of the ice beacon data to analyze drift patterns and deformation of the ice pack during the 8 March 2017 storm event. Specifically, they analysed single-particle dispersion characteristics before, during, and after the storm, finding that the storm led to a sub-diffusive regime compared to an advective regime prior to the storm. Following the storm, the beacons were trapped in the coastal area near Button Bay and showed super- and sub-diffusive regimes that indicate the increase in ice-ice and ice-coast interactions that limited ice drift. Deformation within the ice pack was also characterized by calculating the area within triplets of ice beacons and the differential kinematic parameters. This analysis reveals limited deformation during the storm, but this may have been due to coastal interactions rapid formation of new ice within leads, and cracks within the ice pack due to the cold air temperatures during the storm (~-30°C).

Other noteworthy winter campaigns in Hudson Bay linked to BaySys and involving BaySys researchers, includes community-based research conducted in collaboration with the Arctic Eider Society in the Belcher Islands (Petrusevich et al., 2018; Eastwood et al., 2020) and Northeastern James Bay within the coastal region influence by the La Grande River (Peck et al., in review). Results highlight the extent and structure of the La Grande River under-ice plume along the James Bay coast and the far-field effect of the wintertime river discharge on the stratification around the Belcher Islands.

Landfast ice extent, duration, and roughness have been observed to play an important role in freshwater dispersion and stratification in the nearshore zone. The stable and immobile ice cover isolates the underlying ocean from mixing under the action of wind also allowing a further export of river plume into the ocean compared to spring or fall months. As seen in some previous studies, during the winter months, a ridged outer boundary (“stamukhi”) of the landfast ice cover can prevent dispersion of the river plume that remains on the shelf in the winter and contributes to higher export of the river water out of the Arctic (Itken, 2014). Landfast ice cover also reduces tidal amplitudes and surface layer mixing by blocking air-water interaction (Proshutinsky, 2007). This was evident in the mooring records obtained during the BaySys winter campaign (Figure 3.1.3). Thus, the landfast ice cover also limits the areal extent of the highly buoyant under-ice river plume layer, because as the plume approaches or flows past the ice edge it is subject to strong mixing, as seen in the La Grande River estuary (Messier et al., 1989; Peck et al., in review). It was also observed, that landfast ice has an important contribution in controlling the overall freshwater cycle in the ocean by storing a substantial amount of terrestrial freshwater in the winter and releasing it during summer (Bareiss & Görgen, 2005; Eicken, 2005). Hence, the changing patterns of landfast ice duration as observed throughout the Hudson Bay System (Figure 3.1.20) will impact the freshwater dispersion and freshwater marine coupling in the region (Gupta et al., in review).

Spring/Summer survey (Task 1.2)

<u>Water mass distributions:</u> Results from the BaySys spring/summer survey (Ahmed et al., 2020) show minor contributions of freshwater within the NW Polynya during summer. However, river runoff contributes a significant freshwater fraction (>10%) close to the coast, while ice meltwater temporarily stratifies the water column in the vicinity and within the eastward retreating sea ice cover (Figures 3.1.5 and 3.1.6; Ahmed et al., 2020).

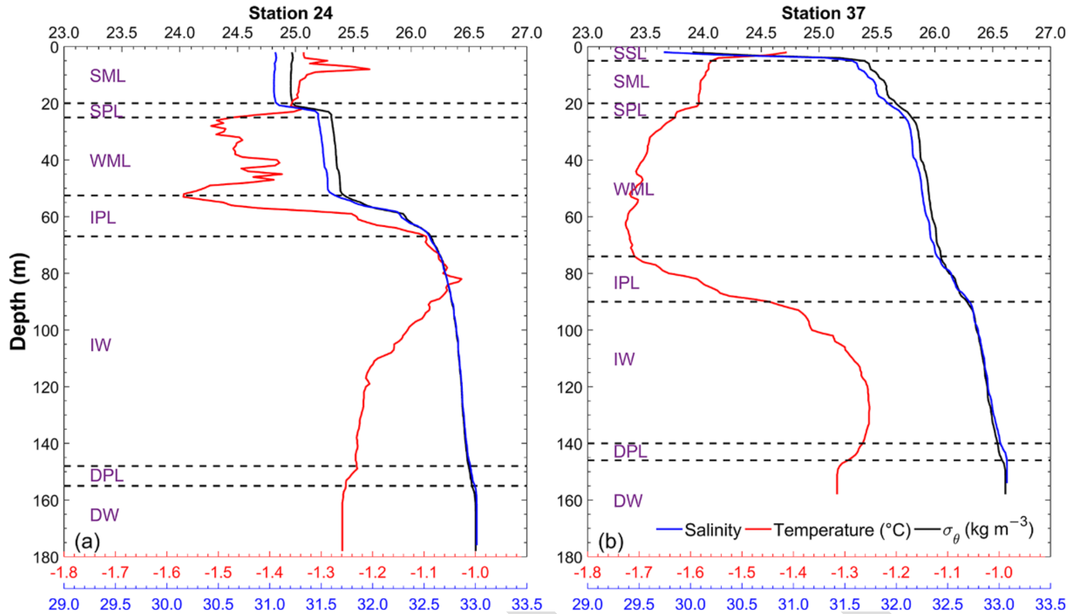

FIGURE 3.1.5 Water mass layers in Hudson Bay during the 2018 spring season (published in Ahmed et al., 2020). Temperature, salinity, and density (σθ) measured by the ship CTD, showing the vertical water mass structure at two contrasting stations, 24 and 37, in Hudson Bay: shallow stratified layer (SSL), spring mixed layer (SML), shallow pycnocline layer (SPL), winter mixed layer (WML), intermediate pycnocline layer (IPL), intermediate water (IW), deep pycnocline layer (DPL), and deep water (DW). https://doi.org/10.1525/elementa.084.f5

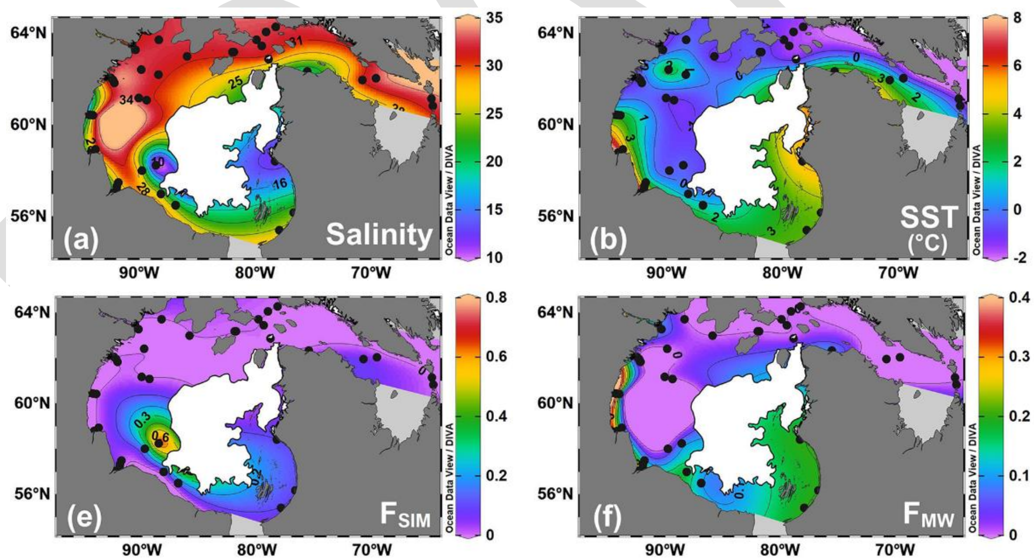

FIGURE 3.1.6 Surface water characteristics in Hudson Bay (published in Ahmed et al., 2020). Surface distributions of (a) salinity, (b) sea surface temperature (SST), (e) sea ice melt fraction (FSIM), and (f) meteoric water fraction (FMW). The white area represents sea ice cover (> 9/10) as of 9 July 2018, based on weekly ice charts provided by the Canadian Ice Service. https://doi.org/10.1525/elementa.084.f6

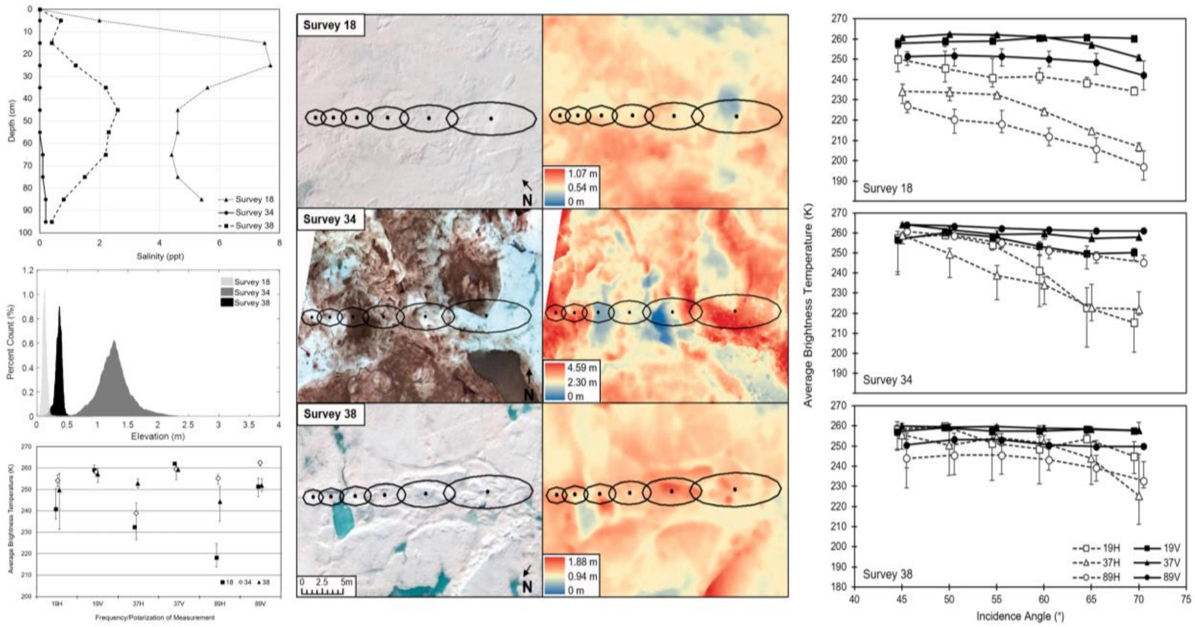

FIGURE 3.1.7 Summary of UAV and radiometer observations presented in Harasyn et al. (2019). See Fig. 3.1.8 for station locations). (Upper left) Salinity profiles for the top meter of sampled floes, with a depth of 0 cm representing ice/snow interface salinity. (Middle left) Histograms displaying percent count of elevation values for the whole survey area for each survey site. Surveys 18 and 38 have lower surface elevation means, with narrow distributions around the mean in comparison with survey 34. (Middle panels) *In situ* radiometer FOV area for all incidence angles (45°–70°) plotted across optical orthomosaic and DEM to display the approximate surficial features influencing measured T_B at each angle. (Right-hand side panels) T_B for all frequencies/polarizations between 45° and 70°, with vertical bars showing the maximum and minimum measured brightness temperatures. Values for 19 GHz and 89 GHz are offset along the x-axis by –0.5° and 0.5°, respectively, for better visualization of the data. (Lower left) Average T_B for the 55° incidence angle at each survey location, with vertical bars showing the maximum and minimum measured brightness temperatures. Values for 19 GHz and 89 GHz are offset along the x-axis for better visualization of the data.

<u>In-situ Passive Microwave Brightness Temperatures (T_B):</u> This research has considered the *in situ* and satellite-based passive microwave T_B collected within Hudson Bay at various sea ice thermophysical stages throughout the melt period. In particular, the effect of sediment on the ice surface was observed and found to affect T_B signals by enhancing surface melt rates and surface roughness (Figure 3.1.7; Harasyn et al., 2019). Stations showed surface thermophysical properties corresponding to late spring, early melt, and advanced melt, following the melt stage classification outlined in Onstott et al. (1987). The melt stage was determined through a combination of *in situ* thermophysical property sampling and UAV optical imagery collection, which was used to calculate ice surface elevations in relation to surface properties (Figure 3.1.7).

Analysis of *in situ* T_B in relation to sea ice thermophysical properties revealed a strong positive correlation between liquid water present in the snow matrix and *in situ* T_B for frequencies 37 and 89 GHz. *In situ* T_B for all stations agreed with PR(19) values for the NT2 clear sky FYI tie point (Figure 3.1.8). Stations, where liquid water was present in the snow pack, had GR(37/19V) values greater than the FYI tie point, whereas stations with a dry snow matrix were slightly lower than the NT2 FYI tie point. GR(89/19H) and GR(89/19V) were positively correlated with UAV-derived full floe melt pond coverage. Overall, liquid water present in the snowpack and melt ponds was shown to drive an increase in high-frequency T_B (37 and 89 GHz) and a decrease in lower frequency T_B (19 GHz).

Results from the comparison between *in situ* T_B and AMSR2-retrieved T_B (Figure 3.1.8), show that liquid water present in the snow matrix during early melt increase T_B in all frequencies. This increase agrees with the comparison between *in situ* T_B and thermophysical properties. In AMSR2 data, melt pond formation during advanced melt was shown to influence PR at lower frequencies (Harasyn et al., 2020). This phenomenon is similar to *in situ* data; however, thick ice cover on the melt pond surface masks the emission signature of liquid melt ponds, rendering a signature similar to early melt. Results reported in Harasyn et al. (2020) show that melt ponds increase GR(89/19V) and GR(89/19H), which agrees with both *in situ* T_B and AMSR2 T_B. Overall, relationships derived between sea ice thermophysical properties and *in situ* TB agree with AMSR2 T_B, suggesting that *in situ* studies of T_B signatures can be scaled up effectively to satellite-retrieved T_B signatures.

In situ T_B was plotted against coinciding AMSR2 T_B for direct comparison (Figure 3.1.8). Overall, V-pol T_B is clustered within the range of 200–260 K along both axes, whereas H-pol experiences more outliers, particularly along the AMSR-2 T_B axis. Values for 89 GHz V-pol and H-pol fall closest along the 1:1 slope, meaning that *in situ* T_B and AMSR2 T_B are most similar for measurements at 89 GHz. Values for 19 and 37 GHz H-pol have outliers with low AMSR2 T_B in comparison to *in situ* values. These three outliers correspond to stations 9, 18, and 34 (stations with the lowest AMSR2 T_B in Figure 3.1.8).

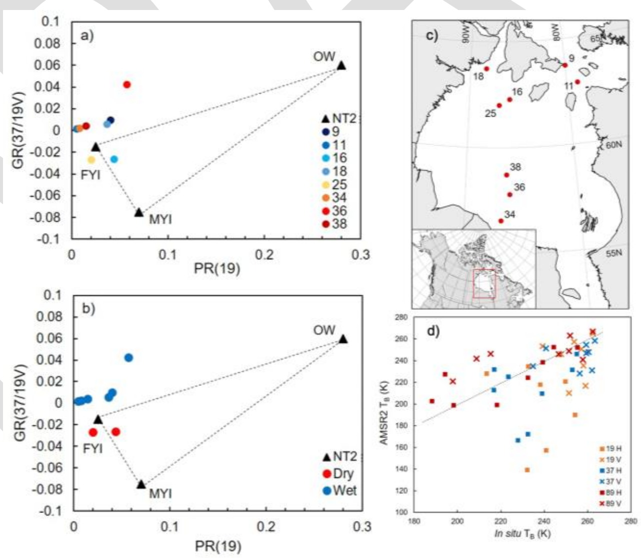

FIGURE 3.1.8 *In situ* T_B plotted in parameter space against tie points specified for the NASA Team2 (NT2) algorithm. Graphs represent GR(37/19V) vs PR(19) labeled by (a) station number and (b) based on the presence or absence of liquid water on the ice surface, in the form of liquid water in the snow matrix or melt ponds not impacted by surface. The location of stations is shown on the map in (c). (d) *In situ* gradient ratio versus melt pond coverage for surveys having a wet snow matrix. GR is shown for a) melt pond coverage within the FOV of the SBR, and (b) melt pond coverage for the full floe sampled. Strong statistical relationships are not evident between GR and melt pond coverage within the SBR FOV, but a strong positive linear relationship exists between GR(89/19H) and full floe melt pond coverage. Reproduced from Harasyn et al. (2020).

Within the dataset of this study, *in situ* T_B did not correlate with snow depth or snow temperature. Previous studies have shown a relationship between snow depth and passive microwave signature (Grenfell, 1986; Markus et al., 2006; Rostosky et al., 2018); however, that relationship is based on a winter snowpack. The absence of correlation between T_B and snow depth in the present dataset is a result of the influence of liquid water in the snowpack on the measured passive microwave signature (Ulaby & Long, 2014; Rostosky et al., 2018).

Liquid water presence in the snow matrix and T_B for 37 GHz and 89 GHz were positively correlated in both polarizations (Harasyn et al., 2020). Previous research has shown snow emissivity increases in all frequencies during melt onset when liquid water content in the snow matrix exceeds winter values (Grenfell, 1986; Eppler et al., 1992). The exclusion of 19 GHz in this correlation can be explained by the change in sea ice surface emissivity between late spring and early summer (Onstott et al., 1987). Results from Onstott et al. (1987) show surface emissivity increases at higher frequencies between late spring and early summer, while emissivity at lower frequencies remains relatively similar (Figure 7 in Onstott et al., 1987). Results from our data agree with this relationship: stations with a dry snow matrix are characteristic of the late spring microwave emission pattern, whereas those with a wet snow matrix are characteristic of the early to late summer emission pattern outlined in Onstott et al. (1987).

Satellite-based sea ice concentration retrievals during the summer melt period are notably inaccurate due to the evolution of sea ice thermophysical properties throughout this period (Rösel et al., 2012b; Ivanova et al., 2015). The spring and summer months are of particular importance for maritime activities in Hudson Bay, due to the transition from a fully ice-covered to ice-free sea surface in 3 months (Gagnon & Gough, 2005). The breakup of the ice pack allows for the opening of commercial shipping routes and ceases local hunting operations in offshore locations (Andrews et al., 2017). Predictions of the timing and rate of ice pack breakup within Hudson Bay can better inform future maritime operations, for which accurate sea ice concentration products are required.

This BaySys study contributes to this field by providing a comprehensive analysis of the co-evolution of *in situ* T_B and sea ice thermophysical properties throughout the melt period in Hudson Bay. Direct comparisons between *in situ* T_B and satellite-retrieved T_B throughout the sea ice melt period have not been reported, which limits our knowledge of the accuracy of SIC retrievals and detection of sea ice thermophysical properties. This study relates *in situ* T_B and AMSR2 T_B throughout the melt season, using SIC algorithm products and optical satellite imagery to facilitate the comparison. In this sense, it is the first study of its kind, and thus provides a basis for adopting data integration methods in future multi-scale passive microwave studies.

<u>Surface waves in partly ice-covered conditions:</u> During the 2018 summer cruise, a TRIAXYS wave buoy was deployed in NE02 position next to the temporal bottom-anchored mooring with a single ADCP instrument. Overall, the wave characteristics were recorded during one week and this period did include two rough weather events with relatively strong wind speeds (Figure 3.1 8). Results from these data show that the wave regime over this period was characterised by 3-6 sec period waves with significant wave heights up to 2 m. The vertical current velocities reached

0.3 m/s during periods with larger waves. At the moment of deployment, the NE02 position was mostly ice-free with the presence of the sparse remnant ice floes that can interpret this area as a marginal ice zone. The key output of this short-term experiment was a justification that bottom-anchored 5-beam ADCP may be used to record the wave characteristic including periods when the presence of ice cover does not allow for the use of surface buoys. The joint wave buoy and ADCP measurements confirmed excellent correspondence in wave period and significant height over both the calm and windy periods (Figure 3.1.7). However, the dominant wave direction estimated from ADCP velocity data demonstrated a fair correspondence with buoy records only during periods with a relatively high (>1 m) wave height (Figure 3.1.7). These periods were also characterized by the enhanced changeability of vertical current velocities. The size of the waves corresponded to the depth and strength of the vertical mixing in the water column. The horizon where these velocity fluctuations were still observed (i.e., wave base) can be interpreted as a wave mixing depth. This depth was approximately 15 m at the moment the maximum wave height reaches 2 m. A detailed analysis of wave data obtained from the BaySys (and also the Churchill Marine Observatory (CMO)) mooring records is yet to be completed. The good correspondence gives us confidence in the use of the ADCP on the BaySys (and CMO) moorings to study wave development and interactions across Hudson Bay over the annual cycle.

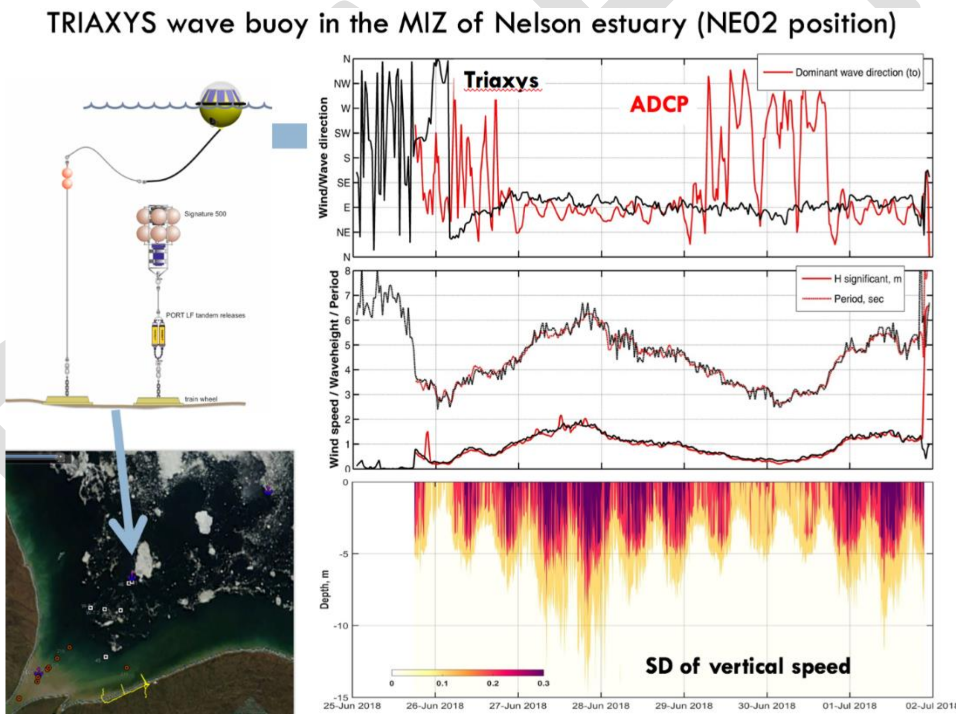

FIGURE 3.1.9 Buoy and mooring observations of surface waves, and standard deviation of vertical speed from ADCP as an indicator of surface layer mixing, in the Nelson Estuary in June 2018.

Analysis of how river runoff interplays with the Hudson Bay sea ice persistence has yet to be completed as part of the BaySys project. However, it is evident from satellite imagery, as well as observations during the spring/summer survey, that heat influx from river and coastal runoff play a significant role in the melt of coastal sea ice during spring and summer. Recently, Park et al. (2020) used model simulations to suggest that riverine heat influx contributed up to 10% of the sea ice reduction over the Arctic shelves, which are marine environments similar to Hudson Bay. The next step in understanding SST and ice break-up/freeze-up in the HBC will involve the investigation of the role of CDOM (mainly supplied via river runoff), TSS, and bathymetry in determining rates of change in SST in open waters over time.

Sediment-laden Sea ice in southern Hudson Bay: During the BaySys research expedition in spring/summer 2018, vast areas of heavily deformed sediment-laden ice were encountered in southern Hudson Bay and presented difficult navigation conditions for the CCGS Amundsen (Figure 3.1.10). The ship was forced to 'back and ram' several floes just to make forward progress. This was a completely unexpected ice type and was required to stop and investigate. One of the "dirty" ice floes sampled had a layer of sediment at the surface and bands of sediment within the vertical structure of the ice. An aerial drone survey revealed an average freeboard of 2.2 m corresponding to a total ice thickness of approximately 18 m (Barber et al., 2021) estimated based on Archimedes' principle, which is extremely thick for the seasonal ice cover in Hudson Bay and much thicker than the nearby clean level ice. A combination of fine-grained sediments and gravel (golf ball size) was observed at the surface and within the ice cores collected.

Because of its denseness and low salinity (Figure 3.1.10b), it was initially hypothesized that this ice was formed from freshwater or brackish water. The suspicion was that this ice floe could have formed in the highly dynamic Nelson River estuary, where large, deformed floes had been observed during the Nanuk campaign in winter 2017 (Barber et al., 2021). However, oxygen isotopic ratios of the sampled ice were found to be above –2‰ (Figure 3.1.11) revealing that the ice formed from Hudson Bay marine seawater with relatively little terrestrial or meteoric contribution of freshwater. This provides evidence of formation within the tidal flaw-leads forming along the coast.

Satellite imagery shows that sediment-laden ice is typical of southern Hudson Bay and varies in extent from 47 to 118 km2 during June when snow and surface melt makes the brown colour of the ice surface visible in optical satellite imagery (Figure 3.1.12; Barber et al., 2021). Previous studies from the Arctic Ocean have also traced the formation of sediment laden ice back to shallow coastal zones and polynyas that form when storms advect the mobile ice pack offshore, both exposing an area of open water for rapid new ice growth and increasing turbulent mixing down to the shallow seafloor, where sediment is resuspended and entrained in the new ice growth. However, we propose that this mechanism is intensified in Hudson Bay because of the strong tidal dynamics that can keep in suspension or resuspend sediment in shallow coastal areas, which then can be entrained in frazil ice or new ice formed during the semidiurnal flaw lead (Figure 3.1.13).

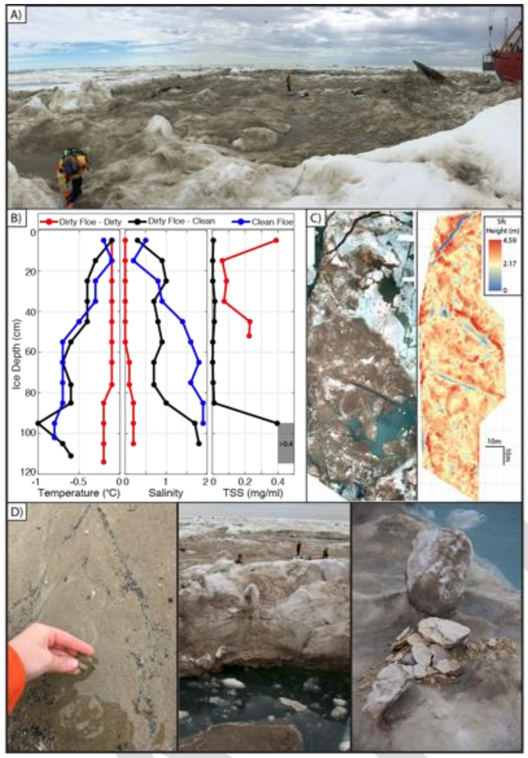

FIGURE 3.1.10 *In situ* observations of the sediment-laden ice. A) Panorama over a sediment-laden sea ice floe (station 34; Figure 2). B) Profiles of temperature, salinity, and total suspended sediments (TSS) from three ice cores: two from the sediment-laden sea ice floe (clean and sediment-laden area, station 34) and one from the clean ice floe (station 32). The grey box denotes ice sections with TSS > 0.4 mg ml^{-1}; TSS in the clean ice core was negligible. C) Mosaic of a sediment-laden sea ice floe derived from imagery using a remotely piloted airborne system and digital elevation model, indicating the location of the two ice cores (clean in red, sediment laden in blue; station 34). D) Examples of the sediment-laden sea ice conditions (station 34).

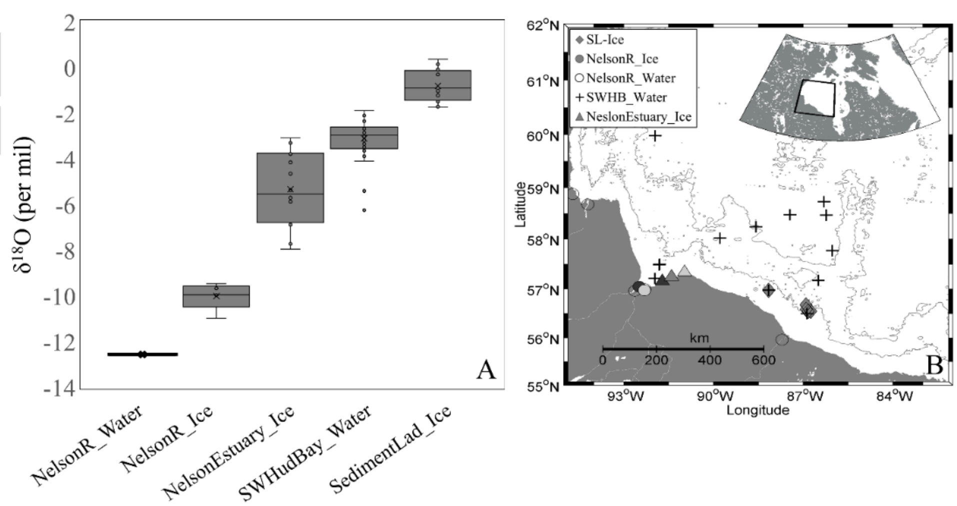

FIGURE 3.1.11 The $\delta^{18}O$ values for sea ice and water samples from Hudson Bay. The box and whisker plots in panel A show median δ18O values, showing median (horizontal line in box), interquartile ranges (upper and lower edge of each box), mean (x). Upper and lower whiskers denote the most positive and most negative isotope values that are within 1.5 times the interquartile range above the upper and lower quartiles, respectively. Outliers are denoted by dots outside the whiskers. Samples were collected during June 2018, except the Nelson Estuary ice samples which were collected during winter 2017 at sample locations shown in panel B.

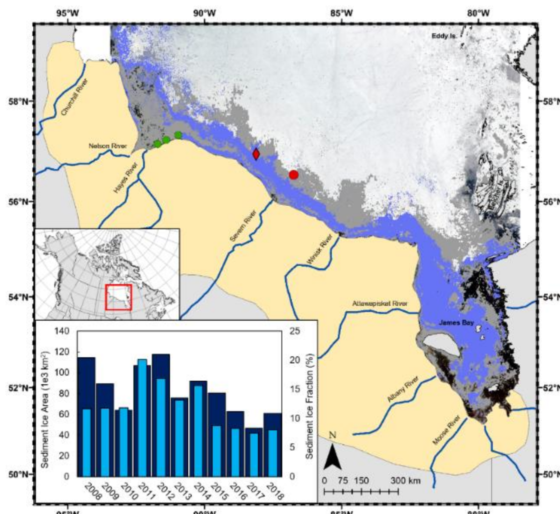

FIGURE 3.1.12 Spatial extent of sediment-laden sea ice in southern Hudson Bay and James Bay in early June 2018. MODIS imagery over southern Hudson Bay and James Bay from 10 June 2018 presenting areas classified as sediment-laden sea ice in 2018 (purple) and the cumulative spatial distribution of sediment-laden sea ice from 2008 – 2017 (grey) within the extent of displayed imagery. The inset graph shows the total area of sediment-laden sea ice (dark blue) and the fraction of the regional ice cover that is classified as sediment-laden sea ice (light blue) during June over the past decade. The location of ice sampling near station 34 is denoted by a red dot, station 32 by a red diamond, and ice sampling completed in winter 2017 by green dots (left to right; T1, T2, and T3). The extent of Hudson Bay lowlands shown in light yellow.

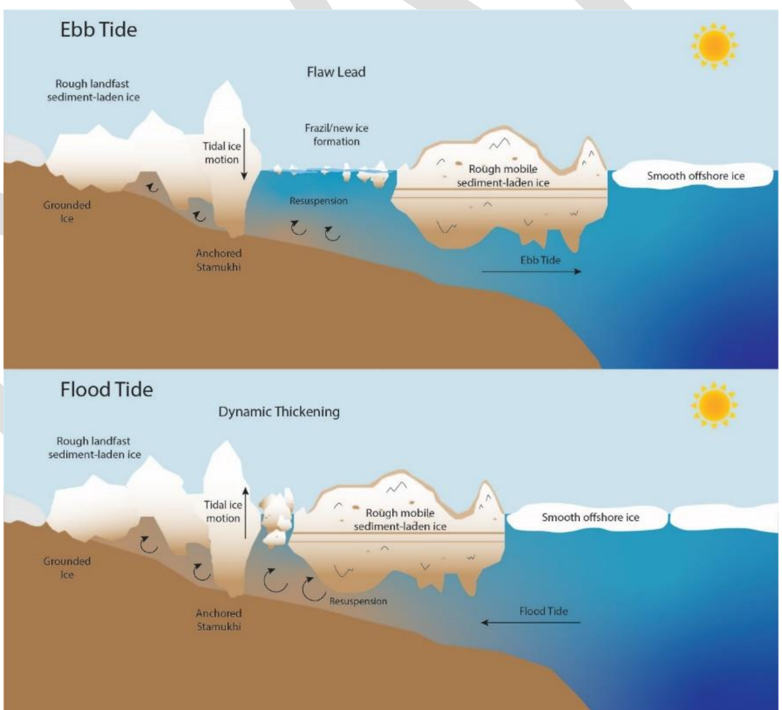

FIGURE 3.1.13 Conceptual diagram of the mechanisms of sediment-laden ice formation in a dynamic tidal flaw lead environment. Sediment becomes entrained during frazil/new ice formation when the flaw lead opens (top), and becomes incorporated into larger ice floes when the flaw lead closes (bottom). Thick ice floes become anchored in shallow coastal waters during high tide, allowing for the incorporation of larger sediment particles from the sea floor.

Sediment-laden sea ice has previously been observed in Foxe Basin and James Bay (Pelletier, 1986). However, during the spring/summer survey, the science team onboard the CCGS Amundsen collected a unique suite of in-situ samples on the physical and biogeochemical properties of this unique ice type that allowed us to determine the source waters and mechanism by which the heavily deformed dirty ice formed. These were the first detailed observations of this unique ice type in Hudson Bay, which highlighted additional questions for future research on dynamics in the coastal flaw lead environment (see gaps below). The presence of heavily deformed, thick pieces of ice within the seasonal ice cover of southern Hudson Bay presents a hazard for any vessels, including ice breakers, operating in the area, while it also exerts a considerable influence on biogeochemical cycles and geomorphodynamics of southern Hudson Bay, particularly in terms of the offshore transport of sediment and contaminants from coastal areas to greater distances offshore. Its presence is not a direct result of winter-time river discharge or a solid-ice contributor to riverine freshwater transport. However, its presence as a thick boundary and a marine freshwater source may influence dispersion and direction of flow of riverine freshwater in Hudson Bay. It likely plays a significant geomorphodynamic role in scouring the tidal flats and the accretion beach ridges that mark the southern Hudson Bay coastline. Remnants of these beach ridges, that were preserved by the post-glacial rebound of the land, testify to past operation of this ice-ocean-land interaction. The beach ridges play a key role in the formation of salt marches that support vibrant ecosystems and are important carbon sinks (peat lands).

Mooring program (Task 1.3)

<u>Temperature and salinity timeseries record:</u> Five moorings were deployed as a part of BaySys fall cruise in September 2016 (see Phase 1 report for locations and configurations). The Phase 1 report already showed preliminary temperature/salinity (TS) results from the moorings near the Nelson River estuary (Phase 1 report Figures 11-12, pp. 121-122). Here, we additionally show the TS results from moorings AN01 and JB02 (Figures 3.1.14 and 3.1.15). At AN01 (Figure 3.1.14), surface layer temperature reached the freezing point of about –1.7 °C by January in 2017, but already one month earlier in December in 2018. Further below, retained heat kept the temperature above freezing throughout winter. Minimum temperatures are reached no earlier than July. Maximum temperatures at 30-50 m depths occurred in November, which is months after solar insolation levels have begun to decline. These discrepancies in seasonal timing are explained by advection and mixing of water masses.

The salinity at AN01 ranges between 31.5 to 32.7 PSU at the 35-40 m depth horizon; and rises to a maximum of about 33 PSU at 100 m (Figures 3.1.14). The water column at AN01 remained stratified throughout the annual cycle, although brine input from sea ice formation is seen to gradually increase the salinity at the 30-50 m depth interval during the ice growth period in winter. This mooring record misses the near-surface layers; however, values are consistent with the profile and water masses depicted in Figure 3.1.8.

Conditions are much more dynamic at the JB-02 mooring site in James Bay compared to western Hudson Bay, as revealed by the high temporal variability in the temperature and salinity timeseries (Figure 3.1.15). The salinity at 35 m depth varied between about 27.5 to 30.5, which is > 2 PSU fresher than at AN01, and explained by the high riverine influx into James Bay. The water column remains stratified throughout the annual cycle; with a couple of exceptions: A notable mixing event of the water column occurred around 22 November 2016; and on 30 April 2017, there was a brief period when the water column was homogenous. Prior to this latter event, the salinity of the water column continued to increase from January through April due to sea ice brine inputs, despite the enhanced winter discharge from the La Grande River (but note that the uppermost record is at 35 m depth). The onset of sea ice melt in early May quickly re-established salinity stratification; and the water column structure remained fairly stable throughout the remained of summer and fall periods, even as temperatures continued to increase into October.

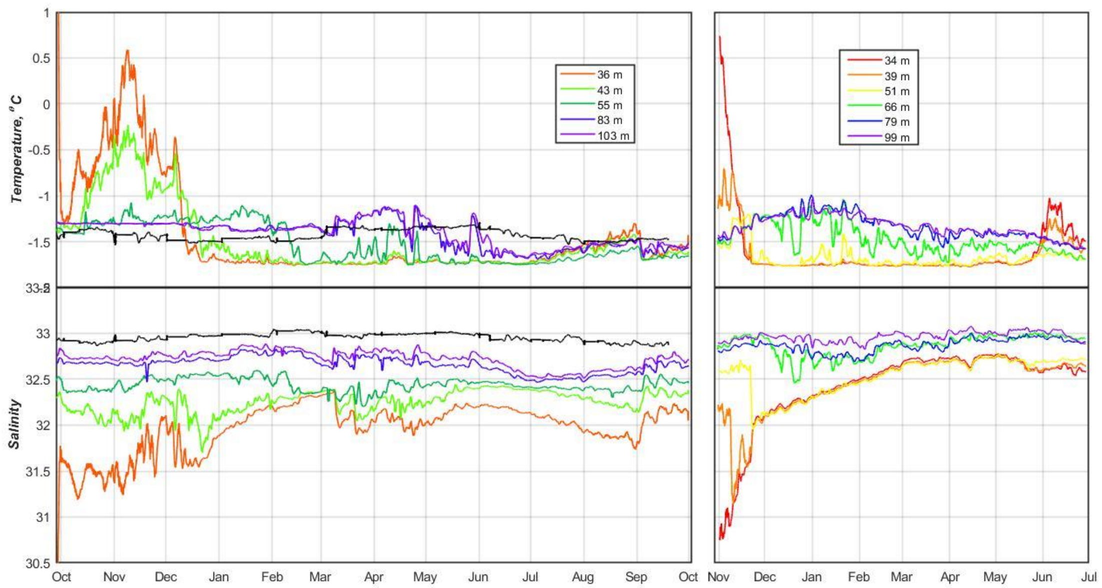

FIGURE 3.1.14 Temperature and salinity records from mooring AN01 for periods 2016-2017 (left) and 2017-2018 (right). The black lines in the left panels show the temperature and salinity records from 2007-2008 AN01 mooring measured at 77 m depth as a part of ArcticNet operations.

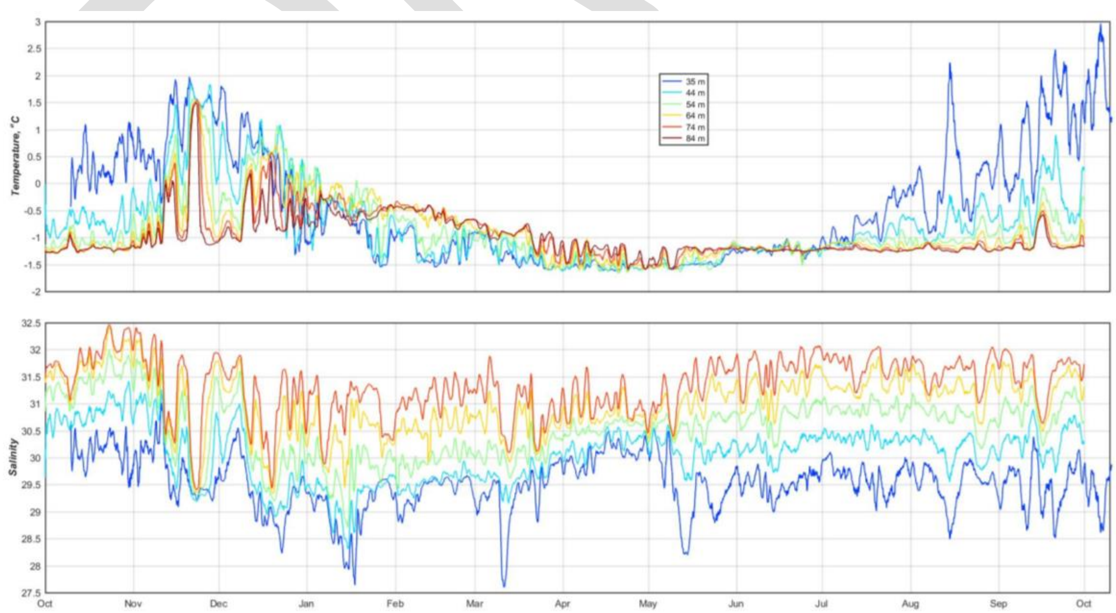

FIGURE 3.1.15. Temperature and salinity record from mooring JB02 for periods 2016-2017.

Atmosphere-Ocean coupling: The freshwater distribution in the Hudson Bay is mainly controlled by wind forcing with a prevailing cyclonic regime. Such forcing leads to both water and ice (in winter) circulating counterclockwise within the bay. The new hydrological data obtained with BaySys moorings in 2016-2018 allowed us to quantify the effect of wind forcing on both solid and liquid freshwater transport within the bay. The timeseries of ice drafts from the upward-looking ADCP from moorings AN01, NE03, and JB02 (Figure 3.1.16) revealed a distinct difference between ice growth during winter 2016/17 compared to 2017/18 that was attributed to an interannual difference in prevailing wind direction and speed. During the first winter, the average wind speed over the bay was less than 2 m/s with a prevailing north-northwesterly direction. The average wind speed during the second winter was about 3 m/s but with a more pronounced zonal component resulted in prevailing east-northeasterly wind direction (Table 3.1.1).

The impact of atmospheric forcing on the Hudson Bay basin-wide water dynamics and freshwater redistribution has been also considered based on the temperature, salinity, and current velocity data obtained at BaySys moorings AN01 and NE03 in 2016-2017 (Dmitrenko et al., 2020). It was found that altering atmospheric circulation affects the intensity of along-shore currents resulting in current amplification when low-pressure cyclones pass over the central Bay (Table 3.1.1; Figure 3.1.17). The process of cyclonic atmospheric forcing enhancing water circulation in western Hudson Bay can be applied to the entirety of Hudson Bay, as the spatial scales of cyclones during storms #1 and #3–7 roughly equalled the area of Hudson Bay (Figure 3.1.17; Dmitrenko et al., 2020).

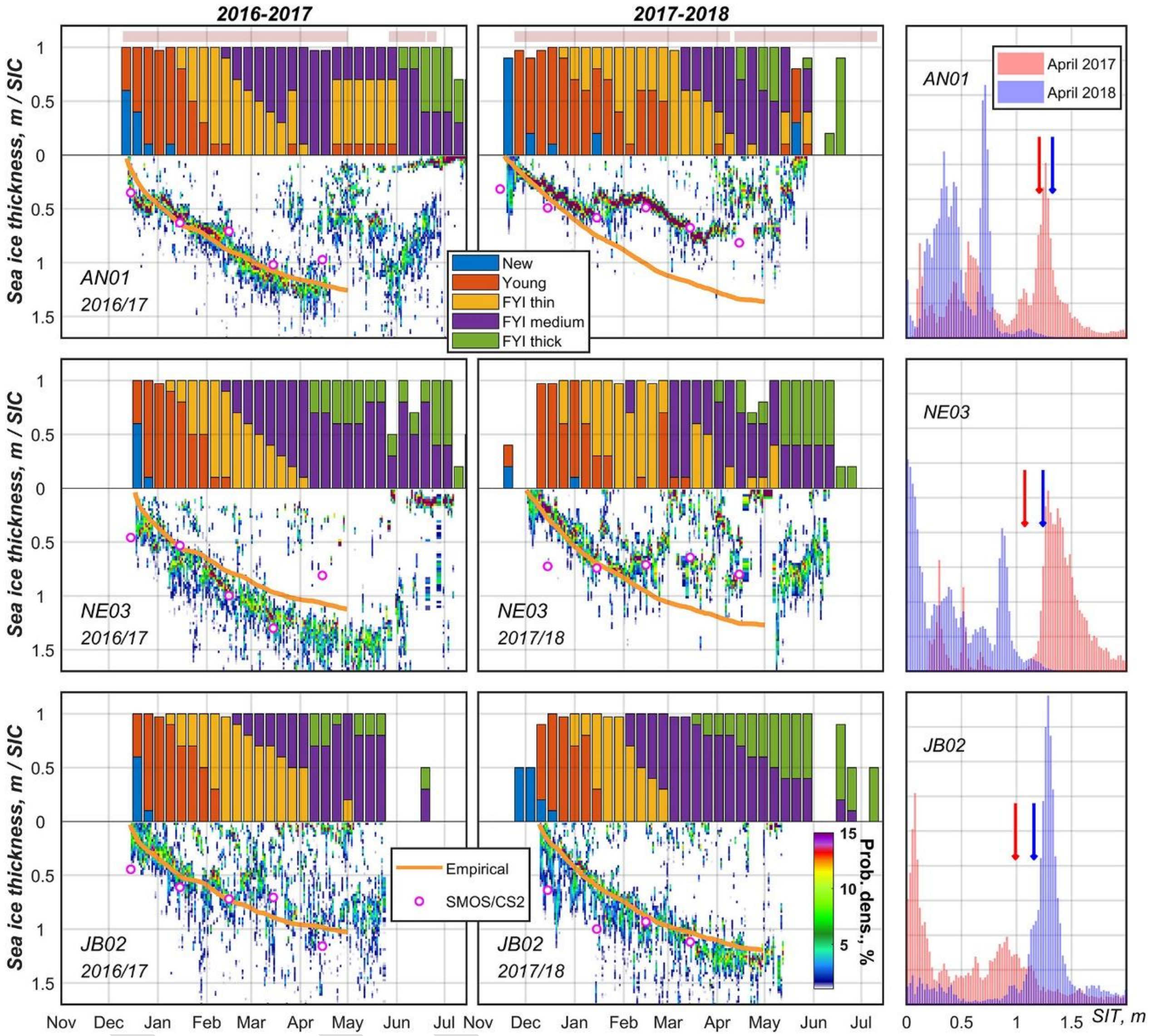

FIGURE 3.1.16 Evolution of sea ice thicknesses and ice types at AN01 (top), NE03 (middle), and JB02 (bottom) during winter 2017 and 2018. The measured ice thickness is shown as a percent occurrence, and those maxima (from green to red colors) correspond to the peak probability of daily ice thickness at 2-cm bin spacing. The monthly mean CS2/SMOS data are presented as magenta circles at the center of every month. Daily mean ice thickness estimated from empirical thermodynamic growth is shown with orange line. CIS data on partial concentration of different types of sea ice are shown with color bars (new < 10 cm, young < 10–30 cm, FYI thin 30–70 cm, FYI medium 70–120 cm, and FYI thick > 120 cm). Availability of OSI-405-c ice drift data is shown with pink horizontal bars at the top of the figure. The normalized frequency distributions of measured ice thickness at 2-cm bin spacing in April 2017 and 2018 are shown in the right panels together with arrows indicating the April-averaged empirical ice thicknesses. Taken from Kirillov et al. (2020).

TABLE 3.1.1 Correlations between atmospheric vorticity, along-shore wind, and sea level anomalies in western Hudson Bay for the full annual cycle and the ice-covered period. (a/b). Taken from Dmitrenko et al. (2020)

		Along-shore wind		Sea level anomaly (SLA)			
Parameter	**Vorticity**	**AN01**	**NE03**	**Churchill**	**AN01**	**NE02**	**NE03**
Vorticity	—	–0.65/–0.72	–0.56/–0.65	0.49/0.41	0.14[c]/0.19[c]	0.57/0.62	0.54/0.58
Wind AN01	–0.65/–0.72	—	0.90/0.91	–0.40/–0.33	–0.21/–0.26	–0.62/–0.67	–0.60/–0.62
Wind NE03	–0.56/–0.65	0.90/0/91	—	–0.23/–0.22	–0.23/–0.27	–0.60/–0.63	–0.58/–0.61
SLA Churchill	0.49/0.41	–0.40/–0.33	–0.23/–0.22	—	0.70/0.64	0.57/0.61	0.63/0.62
SLA AN01	0.14[c]/0.19[c]	–0.21/–0.26	–0.23/–0.27	0.70/0.64	—	0.60/0.72	0.70/0.79
SLA NE02	0.57/0.62	–0.62/–0.67	–0.60/–0.63	0.57/0.61	0.60/0.72	—	0.94/0.99
SLA NE03	0.54/0.58	–0.60/–0.63	–0.58/–0.61	0.63/0.62	0.70/0.79	0.94/0.99	—

[a]Correlation computed for the entire period of observations: left value (before slash).
[b]Correlation computed only for the ice-covered period: right value (after slash).
[c]Correlation not statistically significant at the 99% confidence level.

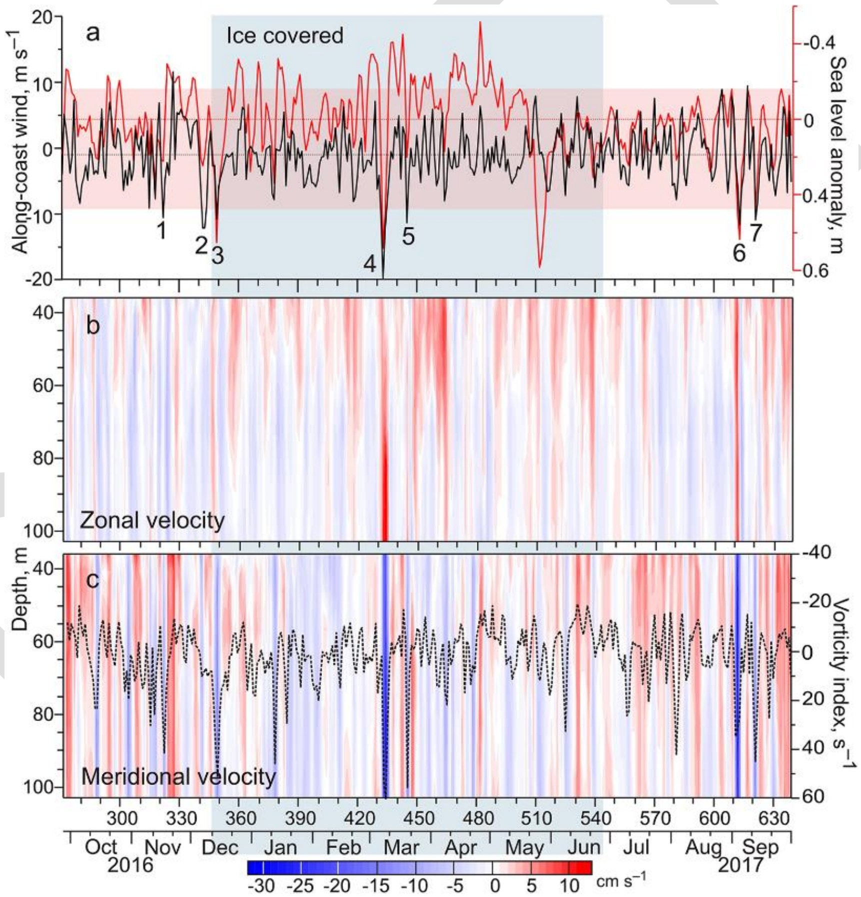

FIGURE 3.1.17 Time series of wind, sea level anomaly, and current velocity for AN01. The (a) 24-h mean sea level anomaly (m) measured at the tide gauge in Churchill (red) and meridional 10-m wind velocity (black, m s–1), and (b) zonal and (c) meridional current velocity (cm s–1) as a function of depth for AN01. Blue shading highlights the ice-covered period following Kirillov et al. (2020). Pink shading (a) shows ± two standard deviations of the mean meridional wind velocity. Numbers identify storm events with northerly wind exceeding two standard deviations. The dashed black line (c) depicts vorticity index (s–1), the finite-differenced numerator of the Laplacian of sea-level atmospheric pressure computed for 60°N, 85°W. Taken from Dmitrenko et al. (2020). The equivalent figure for NE03 at Nelson Estuary is found at https://doi.org/10.1525/elementa.049.f6.

The AN01 mooring was placed northwest of Churchill at or near the margin of the Kivalliq polynya. Because of the large amount of ice formed by latent heat from the polynya, brine production at the AN01 site is expected to be among the largest throughout Hudson Bay. However, AN01 mooring results indicate that insufficient brine was produced in winter 2017 to create overturning of the upper 100 m water column (isohalines remain separated in Figure 3.1.18). The only existing previous record from 1981-1982 revealed that overturning convection occurred during late April 1982, when the temperature and salinity isolines briefly intersect. A comparison between the two mooring records shows a significantly increased freshwater content throughout the water column in 2017 (Figure 3.1.18). This points to potentially significant hydrographic changes that may have occurred over the past 35 years, although it is necessary to keep in mind that very little is known about conditions in intervening years. The influence of tidal mixing in offshore waters was found not to be sufficient to cause deepening of surface layer, as also predicted by Kleptsova & Pietrzak (2018).

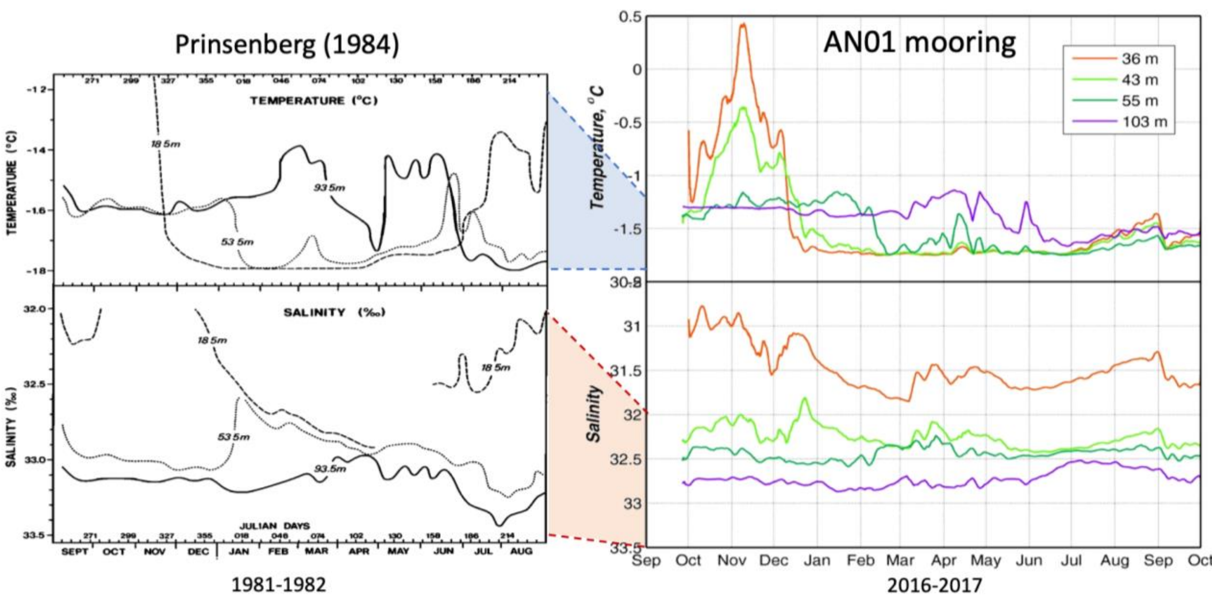

FIGURE 3.1.18 Annual development of seawater temperature and salinity over years 1981-82 (left; from Prinsenberg, 1984) and 2016-17 (right; BaySys project) at mooring location AN01.

Based on BaySys mooring data, Dmitrenko et al. (2020) showed that wind speed and vorticity strongly impact the intensity of ocean circulation in the Hudson Bay (Figure 3.1.17). It was found that the spatial scales of cyclones during storms #1 and #3–7 roughly equal the Hudson Bay area (see Figure 3.1.17). This scaling equivalency implies that cyclones passing over Hudson Bay cause on-shore Ekman transport and storm surges over the entire Hudson Bay coast as depicted schematically in Figure 3.1.19a. These effects produce a cross-shelf pressure gradient that drives alongshore geostrophic flow and favours the cyclonic circulation around Hudson Bay (Figure 3.1.19a). In contrast, a negative (anticyclonic) vorticity forces off-shore Ekman transport, which produces an opposite cross-slope pressure gradient and generates geostrophic flow in the opposite direction (Figure 3.1.19b). This flow diminishes or even reverses the Hudson Bay background thermohaline cyclonic circulation generated by coastal freshening.

The ocean circulation in the bay is strongly linked to an index of atmospheric vorticity that quantifies the strength and general direction of wind forcing. Altering water dynamics is associated with a wind-forced Ekman pumping in the central Bay (Figure 3.1.19). The cyclonic atmospheric circulation leads to on-shore Ekman transport and rise of sea level in the coastal regions that further results in enhancement of geostrophic currents coinciding with the wind direction. Therefore, recurring cyclonic wind forcing favors freshwater transport along the Hudson Bay coastline towards Hudson Strait. As a result, a significant reduction in the residence time of riverine water in Hudson Bay can be expected, with important implications for water column stability and thus primary production and support of the Hudson Bay ecosystem (see Ch. 3.3). During an anticyclonic wind forcing, the background thermohaline cyclonic circulation in Hudson Bay is expected to slow down or even reverse. This effect would likely result in a reduction of the freshwater transport to Hudson Strait and an increase of the riverine water residence time in the bay. Thus, the long-term trends in regional wind forcing may modify the pace of riverine freshwater removal from the Hadson Bay as well as stratification and vertical mixing in some regions, although the rate of these changes and their geography can only be estimated with numerical simulations.

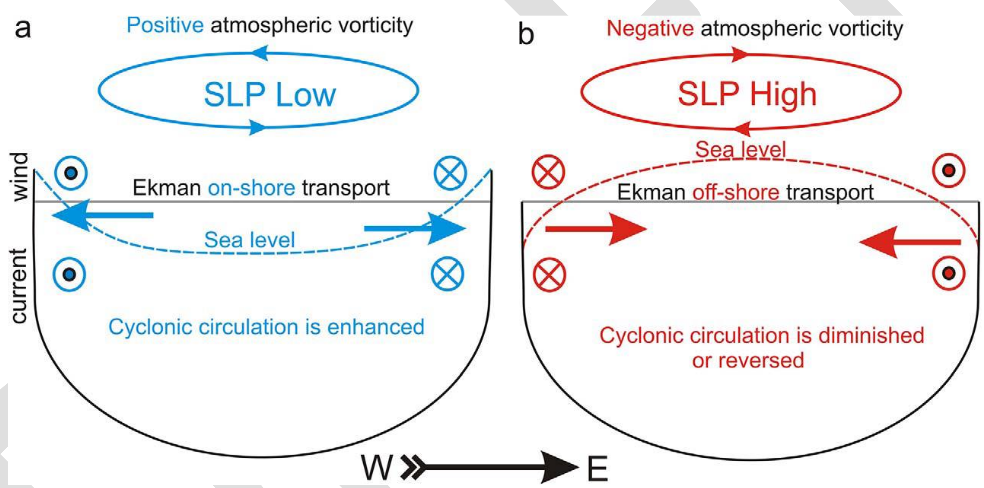

FIGURE 3.1.19 Diagram of the proposed impact of atmospheric vorticity on the Hudson Bay circulation. (a) Positive (cyclonic) vorticity causes onshore Ekman transport and storm surges over the coast, which produces a cross-slope pressure gradient that drives geostrophic flow favouring cyclonic circulation. (b) Negative (anticyclonic) vorticity forces offshore Ekman transport, which produces a cross-slope pressure gradient, generating geostrophic flow in the opposite direction and diminishing or reversing cyclonic circulation. Taken from Dmitrenko et al. (2020).

Offshore waters remain vertically stratified underneath the ice surface throughout winter by freshwater derived from both terrestrial and ice melt remaining within the bay. Ice production adds brine that decreases buoyancy, but (at least during BaySys) not sufficiently to cause loss of stability (Eastwood et al., 2020). This was the case even in the western parts that have less freshwater preconditioning and more ice production (as seen in the AN01 mooring record in Figure 3.1.14).

The mooring program demonstrated that wave mixing can be considered as an important factor in breaking down vertical stratification resulting in vertical redistribution of solar heat and riverine and ice melt freshwater within the water column. The BaySys program showed that upward-looking sonars provide reliable measurements of the surface wave parameters (Figure 3.1.9). This finding allows the measurement of surface waves within sea ice-infested waters. Within ice fields (even in heavily decayed, low concentration ice conditions) wave development was found to be fetch limited. The surface mixing depth of ~15 m observed within MIZ in the Nelson estuary in June 2018 was likely associated with the wind waves reaching 2 m height during strong wind events. More severe autumn storms over both coastal and less stratified central parts of Hudson Bay may lead to more efficient vertical mixing and penetration of the seasonal signal into the deeper layers. A more detailed investigation of this process is a subject of a future study (Campbell et al., in prep.) that might also help to adjust the parameterization of vertical mixing in the NEMO model at least at the regional scale.

In contrast to the offshore regime, tidal mixing is a dominant force in the coastal zone with the water column remaining fully mixed throughout November to March (Figure 3.1.14). However, freshwater inputs from ice melt and river runoff, and solar/atmospheric heating, create a stratified surface layer during summer. The Nelson estuary mooring records NE02 and NE03 demonstrate this seasonality: from December through February, the ~50 m deep water column displayed increasing salinity (from brine released by sea ice growth) and remained vertically fully mixed. Weaker stratification began to develop from March 2017 onwards presumably due to fluvial loading. Water temperatures, however, remained near their freezing point until July, after which they rapidly began heating up facilitated by the retreat of the sea ice. Thus, buoyancy inputs in spring, summer, and early fall overcame mixing forces at the 50 m deep water column offshore of Nelson River.

<u>Zooplankton diurnal vertical migration:</u> Finally, we note that ADCP acoustic backscatter data from mooring AN01 was also used by Petrusevich et al. (2020) to investigate how environmental factors (tide, wind, ice coverage) affected diel vertical migration (DVM) of zooplankton in Hudson Bay. Figure 3.1.20 shows that the DVM of zooplankton to the surface layer was more active during the open water period compared to the dark winter period, however, it persisted throughout the year. The major factors determining the observed DVM pattern were found to be the following (Petrusevich et al., 2020): (i) *Illuminance:* Unlike other ice-covered and ice-free Arctic and sub-Arctic locations such as Svalbard and north-east Greenland (Last et al., 2016; Petrusevich et al., 2016), DVM in Hudson Bay was found to be controlled by solar illumination throughout the whole year, and not by the moonlight cycle; (ii) *Tidal dynamics:* The tide in Hudson Bay is mostly lunar semidiurnal (M2) with an amplitude of a few meters. The area in the proximity of the AN01 mooring has variable bottom topography. The barotropic tide interacts with bottom topography, generating tidal flow diverging and converging vertically. It was found that zooplankton tended to avoid expending additional energy swimming against the vertical flow. This response of zooplankton was consistent with the zooplankton's tendency to stay away from layers with enhanced water dynamics and to adjust their DVM accordingly; (iii) *Storm-induced disruptions:* When daily mean wind speed exceeded 25 km h^{-1} during the ice-free period in the surface layer, there were observed irregular spots of higher VBS related to the bubbling generated by the wind forcing. The zooplankton tended to remain deeper in the water column during these periods with high wind speeds.

In addition, the ADCP backscattering record revealed the presence of sinking sediment particulates released from sediment-laden sea ice. The sediments were particularly noticeable in the upper layers of the water column (Figure 3.1.20d) during periods April-June 2017 when the mooring recorded decreasing ice thicknesses above (Figure 3.1.20b). However, evidence for sediment release was seen for the January-March winter period, as well as for July 2017 when sparse sediment-laden ice floes drifted over the AN01 location.

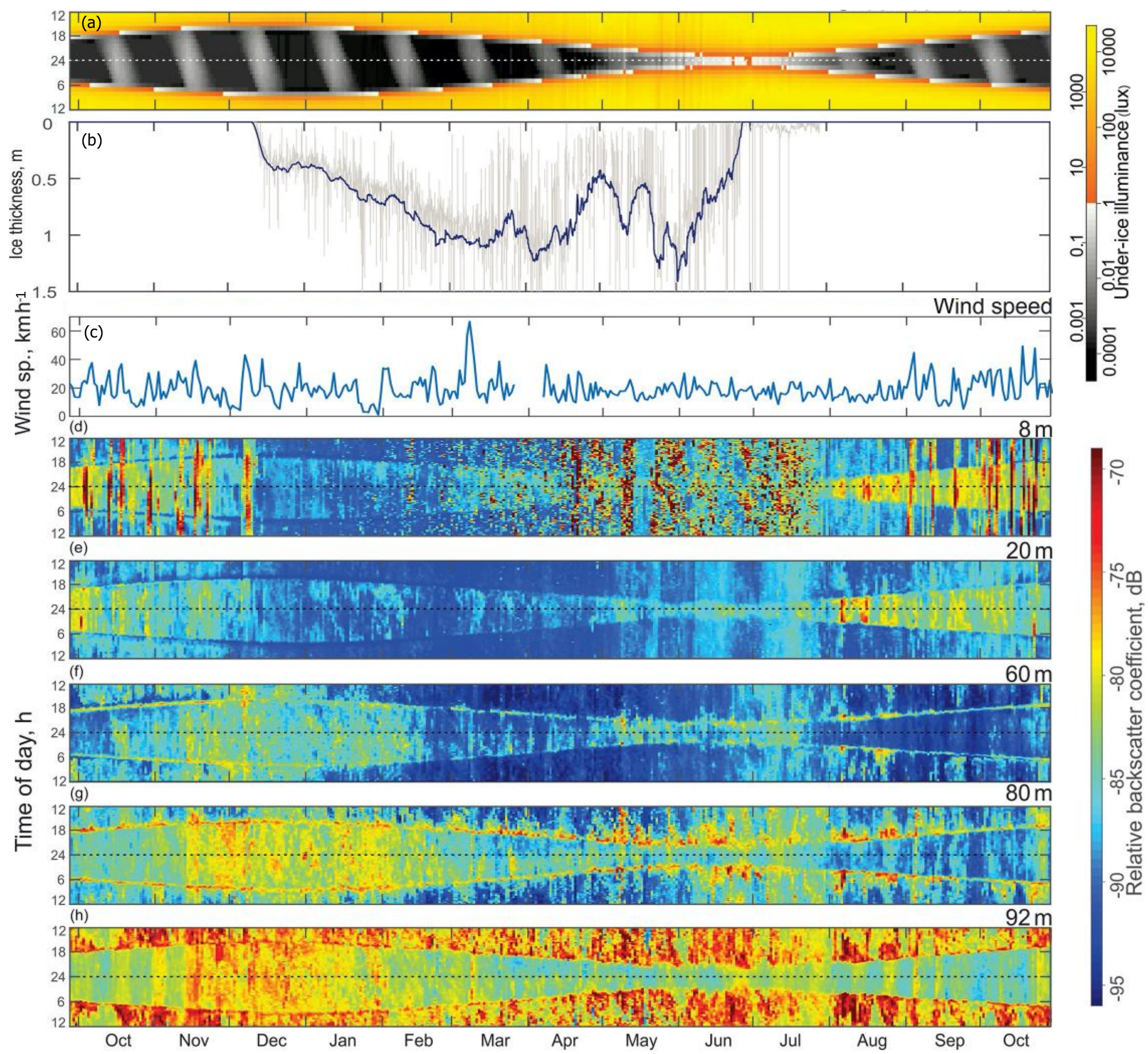

FIGURE 3.1.20 Time series (October 2016 to October 2017) of the AN01 mooring record showing (a) modelled under-ice illuminance, (b) ADCP measured ice thickness (with the blue line representing daily average values), (c) daily mean wind speed measured at Churchill airport (YYQ), and (d)–(h) actograms of ADCP acoustic backscatter at five depth levels: (d) 8 m, (e) 20 m, (f) 60 m, (g) 80 m, and (h) 92 m revealing diurnal vertical migration by zooplankton. Dashed horizontal lines represent astronomical midnight. The diurnal signal is presented at the vertical axis, while the long-term changes in diurnal behavior are presented along the horizontal axis. High backscattering seen in (d) are related to wind-driven mixing during open water periods (c), and the release of ice-rafted sediments during the sea ice melt period (April-July). Modified from Petrusevich et al. (2020).

Remote sensing (Task 1.4)

Sea ice thickness distribution from satellite altimetry and SMOS: The sea ice in the eastern side of the bay always grows thicker during the winter compared to the western part, despite the fact that the ice formation commences from the north-west and gradually progresses towards the south-east (Figure 3.1.21). This occurs because of overall west-south ice drift resulting in (i) persistent formation of new thinner ice within the northwestern polynya and (ii) dynamical thickening of pack ice while encountering the eastern coast (Landy et al., 2017). However, the seasonal measurements during two successive ice growth seasons (December-April) demonstrated that this normal asymmetry may be considerably altered by the direction and strength of prevailing winds during winter (Figure 3.1.22). The BaySys mooring record revealed that more meridional atmospheric circulation in 2016/17 led to 36-38 cm thicker ice in the west and 42-58 cm thinner in the south-east compared to 2017/18. On a broader bay-wide scale, remotely sensed (CryoSat-2 and SMOS) fields of ice thickness confirmed the difference in zonal sea ice thickness asymmetry between these two years. On average sea ice was 48 cm thinner in eastern Hudson Bay in April 2017 and 46 cm thinner in southern Hudson Bay in April 2018. Moreover, the anomalies formed by a reduction in eastward winds in 2016/17 created the inversion of the climatological west-east gradient of ice thickness. Conversely, in 2018, strong WNW winds led to enhanced cyclonic ice drift speeds and resulted in the formation of thicker ice in eastern Hudson Bay (56 cm above the 2003-2016 climatology), while divergence in western Hudson Bay created a thinner ice cover in the area of the northwestern polynya. These results highlight the influence of atmospherically driven sea ice dynamics on the state of the end of winter ice cover and its impact on breakup patterns across the bay (Kirillov et al., 2020). This impact was seen in the aerial distribution of remnant sea ice that persisted along the shores of southern and eastern Hudson Bay in summer 2017 and 2018, respectively. The persistence of sea ice has a direct impact on the development of sea surface temperatures of an area (see next section), the development of surface waves, water column stratification by introducing ice meltwater and restricting mixing, and thus also ocean circulation patterns. Sea ice breakup patterns may therefore majorly influence the patterns and variability of biochemical processes, dispersion of river runoff into the ocean, and biological productivity across Hudson Bay; however, these linkages with sea ice persistence have not yet been fully explored.

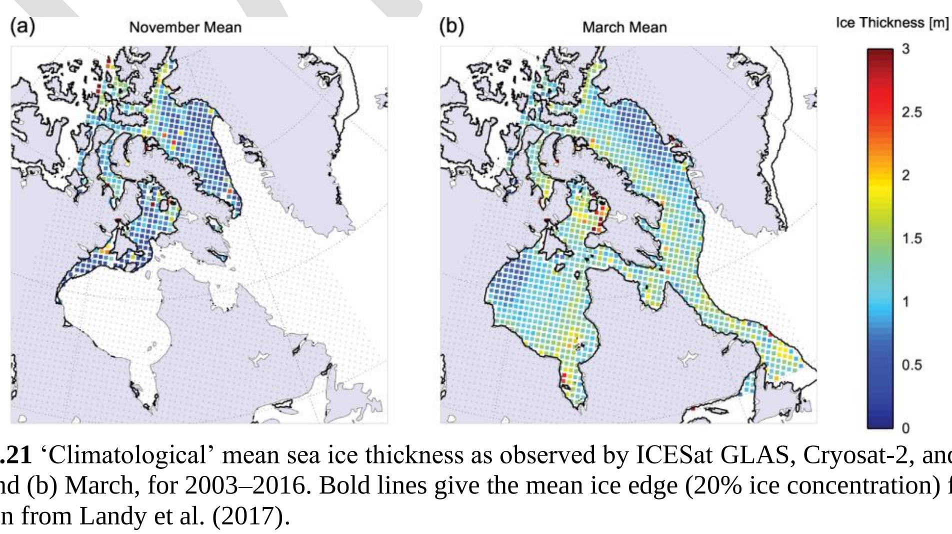

FIGURE 3.1.21 'Climatological' mean sea ice thickness as observed by ICESat GLAS, Cryosat-2, and SMOS in (a) November, and (b) March, for 2003–2016. Bold lines give the mean ice edge (20% ice concentration) for these periods. Taken from Landy et al. (2017).

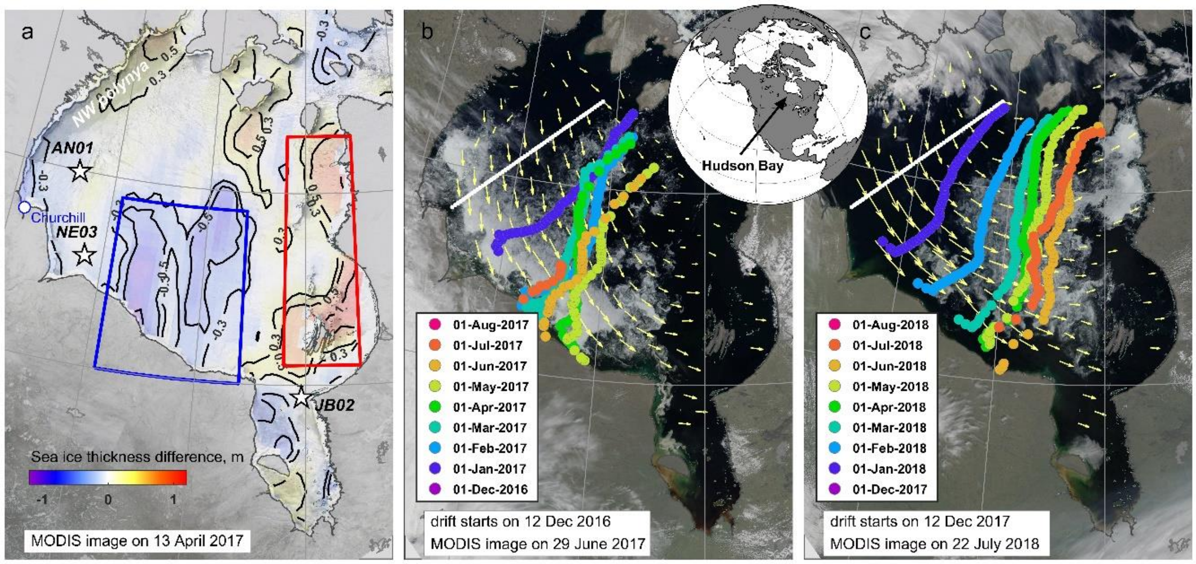

FIGURE 3.1.22 The sea ice thickness difference from satellite altimetry between April 2018 and April 2017 and the monthly projection of ice drift during two successive winters 2016/17 and 2017/18. Taken from Kirillov et al. (2020).

<u>Sea surface temperature (SST) trends and variability:</u> The goal of the SST investigation (Ehn et al., 2021, in prep.) was to update the Galbraith & Larouche (2011) study, which was limited to the period up to 2009, to cover the BaySys project timeframe. This BaySys study used satellite SST products by GHRSST (https://www.ghrsst.org), sea ice concentration information obtained with SSMI, and air temperatures from MERRA-2. Note that the SST measured by infrared detectors on satellites represents the skin temperature at the interface between the ocean surface layer and atmospheric boundary layer, and thus the SST is affected by both and may not fully correspond with the temperature of the ocean surface layer beneath. However, SST is consequently one of the most widely used climate variables for observing seasonal and interannual variations in the ocean surface.

The analysis of satellite data by Galbraith & Larouche (2011) revealed positive trends in both the length of the open water period and SST throughout the HBC over the 1985-2009 period. The positive (warming) trends were found to continue in the southwestern and southern coastal regions in Hudson Bay and James Bay over the 2008-2018 period with an increase in the annual mean open water SST of up to 0.32 °C/year. In Hudson Bay, an increasing trend of SST was observed in areas near Churchill River estuary, Nelson River and Hayes River estuary and along the Southern Hudson Bay Lowlands. In the case of James Bay, a similar pattern was observed with the largest increasing trend in SST along the western and southern nearshore regions. The observations outlined a positive trend near to the rivers with a comparatively higher terrestrial drainage into the bay system. Surprisingly, a reversal into a negative trend in annual mean open water SST of down to –0.23 °C/year over the 10 year period was observed along the south-western, central, and eastern Hudson Bay (Figure 3.1.23). This > 2 °C decrease in seawater surface temperature over the 10 years was centered on the Ottawa Islands in eastern Hudson Bay and explained by reductions to the length of the ice-free season caused by sea ice drift from the west.

The close association between the patterns for sea ice concentration (SIC) and open water SST was evident in our study (Figures 3.1.23A and 3.1.23B). The southwestern and southern regions experienced a trend towards longer open-water periods, with both earlier ice break-up and later freeze-up, exposing it to the longer solar insolation (Figure 3.1.24). Over the 10-year period, sea ice breakup (defined as a reduction below 15% sea ice concentration from passive microwave data) timing increased by > 3 days per year in the eastern Hudson Bay region, with a significant positive trend of delayed ice break-up of up to 4 days per year observed for NE Hudson Bay near the community of Puvirnituq in Nunavik.

Further analysis of the annual surface temperature maxima (SST_{max}) helps us to better interpret the spatial and temporal changes in SST over the HBC and allows comparisons with SST_{max} results by Galbraith & Larouche (2011). An average of the SST_{max} from the year 2008-2018 over HBC ranged from 1.1 to 15.1 °C (Figure 3.1.25). A higher range of SST_{max} was visible in the coastal margins of Hudson Bay and specifically south-western James Bay, with Central Hudson Bay being on a comparatively lower temperature than the surrounding coastal margin. The Foxe Basin, Narrows, and Hudson Strait were observed to have a comparably lower range of SST_{max} as compared to Hudson Bay and James Bay.

The yearly SST_{max} has also been observed to have changed over the last decade. There has been a considerable increase in the SST_{max} with a maximum of 0.59 °C per decade found in the western and southern James Bay, western coastal margins of Foxe Basin, and the south-western and southern Hudson Bay (Figure 3.1.25). Contrastingly, a notable decrease in the SST_{max} was found in the eastern coastal margin of Foxe Basin and Hudson Bay. The highest rate of decrease in SST_{max} was observed in the eastern offshore region surrounding the Ottawa Islands (nearly 0.63 °C per decade).

According to Galbraith & Larouche (2011), regional trends in the SST_{max} recorded each year are consistent across Hudson Bay and are lower in Hudson Strait from 1985 to 2009. However, during the last decade 2008 to 2018, the trend of mean SST_{max} showed a steady increase in South and Southwestern Hudson Bay and James Bay along with western Foxe Basin, while the Eastern Hudson Bay indicated a decrease in the SST_{max} (Figure 3.1.25).

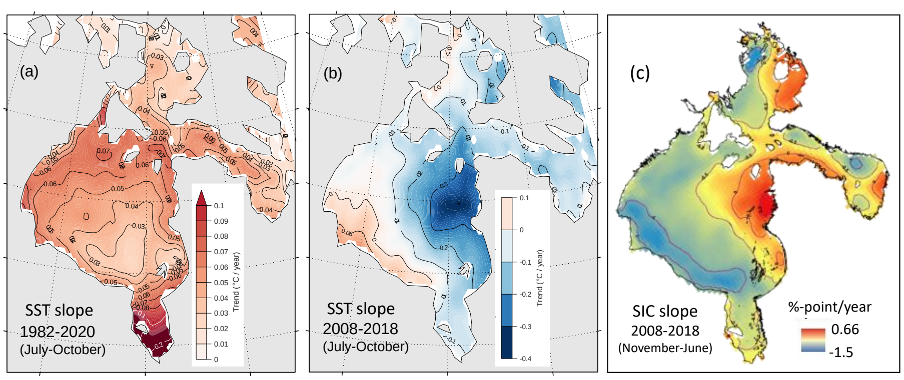

FIGURE 3.1.23 Trends in mean sea surface temperature (for open water period) for (a) 1982-2020 and (b) the 2008-2018 decade leading up to BaySys and Ice concentration from 2008 to 2018. (c) Interannual trends in seasonal (November-June) average sea ice concentration (SIC) over 2008-2018.

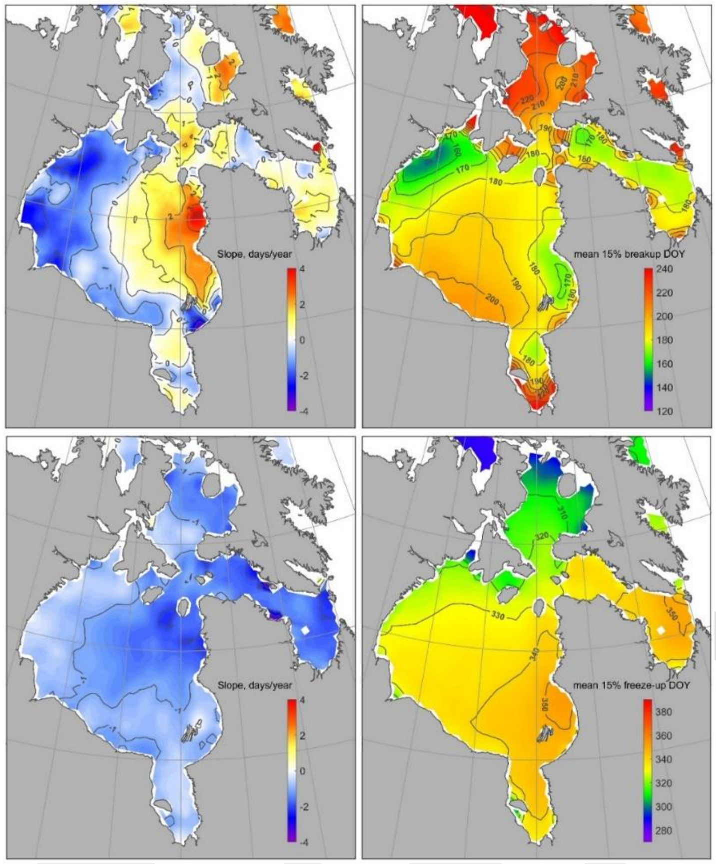

FIGURE 3.1.24 Trends in sea ice freeze-up and break-up for the 2008-2018 period calculated from the OSI-SAF sea ice concentration product. Note, and disregard, the erroneously late ice break-up DOY's shown for southern James Bay.

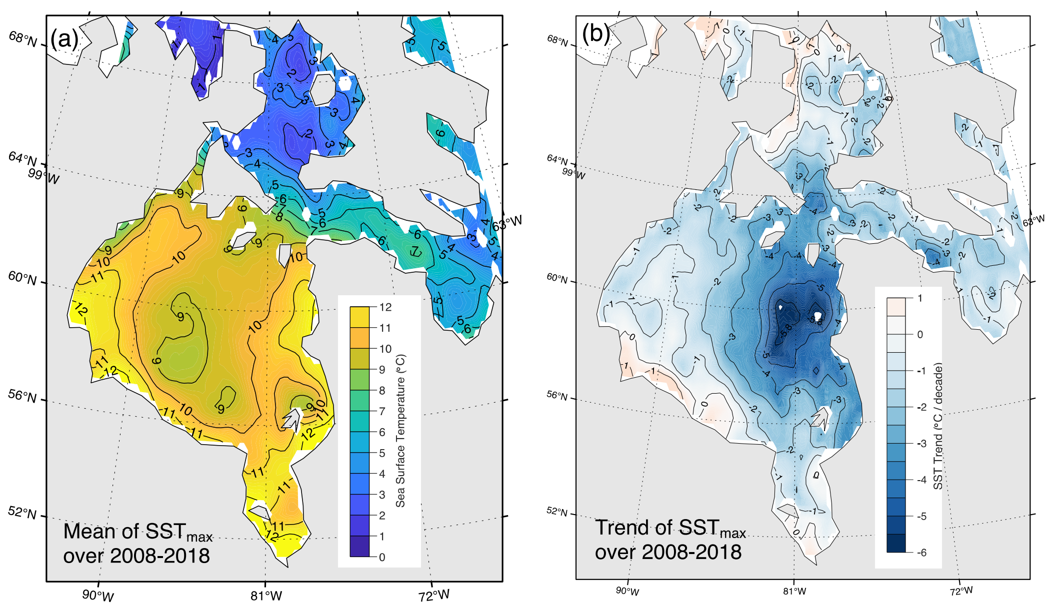

Figure 3.1.25 (a) Mean and (b) annual trend of SST_{max} over the 2008-2018 time period.

The relationship between ice break-up, SST, SIC, and ice freeze-up is evidence of the operation of a positive feedback mechanism within Hudson Bay. The earlier break-up and consequently longer ice-free period allow the water to warm up over a relatively extended time in the southern regions compared to the northern and eastern sectors of HBC. This trend pattern was also reflected in the ambient air temperature in this region, with areas of increased SST associated with higher air temperatures while the areas with increased SIC experienced a decrease in air temperature (Ehn et al., 2021, in prep.). One of the most interesting findings of this study was the increasing percentage of SIC over the eastern parts of Hudson Bay and the consequent decrease in SST during the open water period that followed. As air temperature continues to increase, we expect to see a decrease in thermodynamic ice growth, earlier ice break-up, and a consequent SST increase in Western and Southern Hudson Bay and Southern James Bay open water areas. Because of the combined effect of earlier break-up and delayed freeze-up, an earlier study by Hochheim and Barber (2014) found that the length of the open water period in Hudson Bay increased by ~3.1 weeks on average between 1980-1995 and 1996-2010, which was attributed to atmospheric forcing (i.e., increasing air temperatures).

Our results from BaySys suggest that this development has already created more mobile ice (i.e., sea ice that is more readily drifting), such that sea ice has accrued increasingly in eastern areas. Landy et al. (2017) showed that the seasonal ice cover of Hudson Bay is characterized by a pronounced east-west asymmetry in ice thickness that is created by the regional pattern of ice drift (Figure 3.1.21; Landy et al., 2017). More recently, Kirillov et al. (2020) used satellite altimetry and the upward-looking sonars on three BaySys moorings to examine the role of atmospherically driven ice dynamics in producing contrasting regional ice thickness patterns (Figure 3.1.16). They found that years with stronger westerly winds led to increased ice thickness in eastern Hudson Bay by as much as 50 cm at the end of winter, which in turn delayed the break-up of the ice cover in eastern Hudson Bay, allowing sea ice to persist longer into summer. An extended analysis in Kirillov et al. (2020) of the 40-year satellite and atmospheric reanalysis data revealed that a stronger zonal component of wind forcing may postpone the timing of breakup by 30 days in eastern Hudson Bay. This development has led to a prolonged ice melt season in eastern Hudson Bay and consequently more limited surface warming (Figures 3.1.24 and 3.1.25), with feedbacks onto regional air temperature and water column stratification. Although the fall ice freeze-up dates have trended towards later, this feedback associated with drifting ice has resulted in earlier ice formation (up to –2 days/year over 2008-2018) in eastern Hudson Bay regions (Figure 3.1.25b). This result may seem counterintuitive to the broader trends in climate warming.

<u>Interannual variations in landfast ice cover in Hudson Bay:</u> Remote sensing was used to characterize the changing annual cycle of the landfast sea ice for 19 ice seasons (2000-2019) environment (Gupta et al., in review) Datasets used for this study included Ice Charts from the Canadian Ice Service, satellite imagery (LANDSAT, Sentinel-1), and daily real-time viewing of MODIS imagery in the NASA Worldview platform.

Records of landfast ice freeze-up from the 14 study locations around Hudson Bay and James Bay indicate a northwest to east pattern of freeze-up across the bay (Figure 3.1.26a). Landfast ice freeze-up first occurred near Chesterfield Inlet, where the freeze-up typically began in early to mid-November. The freezing progressed gradually southwards along the shore, and by the end of

December, landfast ice formed in the north-eastern part of Hudson Bay in Ivujivik. In general, this timing is consistent with the bay-wide ice growth pattern in offshore waters (Stewart & Barber, 2010). The difference between the earliest and the last record of landfast ice freeze-up observed across Hudson Bay and James Bay was found to be 47 days over the 2000-2019 study period.

The progression of ice break-up events across the Hudson Bay and James Bay (Figure 3.1.26b) follows a south to north trend with landfast ice breaking up as early as mid-May in southern James Bay and gradually progressing northwards, with the final break-up events taking place in the north-western part of Hudson Bay around mid to late July. An approximately 50-day difference between the earliest (Southern James Bay) and latest (Northern Hudson Bay) break-up events was observed across the Hudson Bay and James Bay.

Hudson Bay and James Bay exhibited a stable mean landfast ice cover ranging from around 5 months in the southeast to around 6-7 months in the northwest (Figure 3.1.26c). The annual average of landfast ice duration across the Hudson Bay and James Bay was observed to be 185 ± 10 days. Following the initial formation of landfast ice, the ice edge expanded seaward, gradually reaching its maximum extent by April. The landfast ice cover remained immobile throughout April, and decay started by the beginning of May. By the middle of June, Southern and Eastern Hudson Bay and the entire James Bay reaches an ice-free condition, with some parts of the Northern and Western Hudson Bay still retaining landfast ice. We observed a minimum landfast ice duration of 143 days (about 4.7 months) at Moosonee in the southeast and a maximum duration of approximately 233 days (about 7.7 months) near Rankin Inlet in the west. Rankin Inlet is the location within the Hudson Bay and James Bay system where landfast ice generally appears first and its presence the most persistent.

The interannual trends in landfast ice duration over the 2000-2019 period (Figure 3.1.26f) show that the landfast ice duration along the west coast of Hudson Bay has been decreasing at a rate of 1-6 days per decade. All other locations across Hudson Bay and James Bay, except for Moosonee, have experienced increasing landfast ice duration. This increase has been particularly notable in Sanikiluaq and Chisasibi with +9 and +5.56 days per decade, respectively (Figure 3.1.26d). This pattern is generally consistent with bay-wide trends in sea ice concentration, sea ice break-up, and SST, and is likely a consequence of them. However, the timing of landfast ice break-up did not coincide with the bay-wide ice break-up pattern as determined by passive microwave-derived 15% sea ice concentration threshold. Along the western coast of Hudson Bay, landfast ice break-up trails the ice breakup by 10-20 days, while in the eastern Hudson Bay it precedes the ice breakup by more than a month at places. Along the Hudson Bay lowlands on the southern shores, where the offshore sea ice persists the longest, landfast ice breakup occurs 40-50 days earlier. This pattern can be explained by the differing thermodynamic and dynamic forcings acting upon the various ice types.

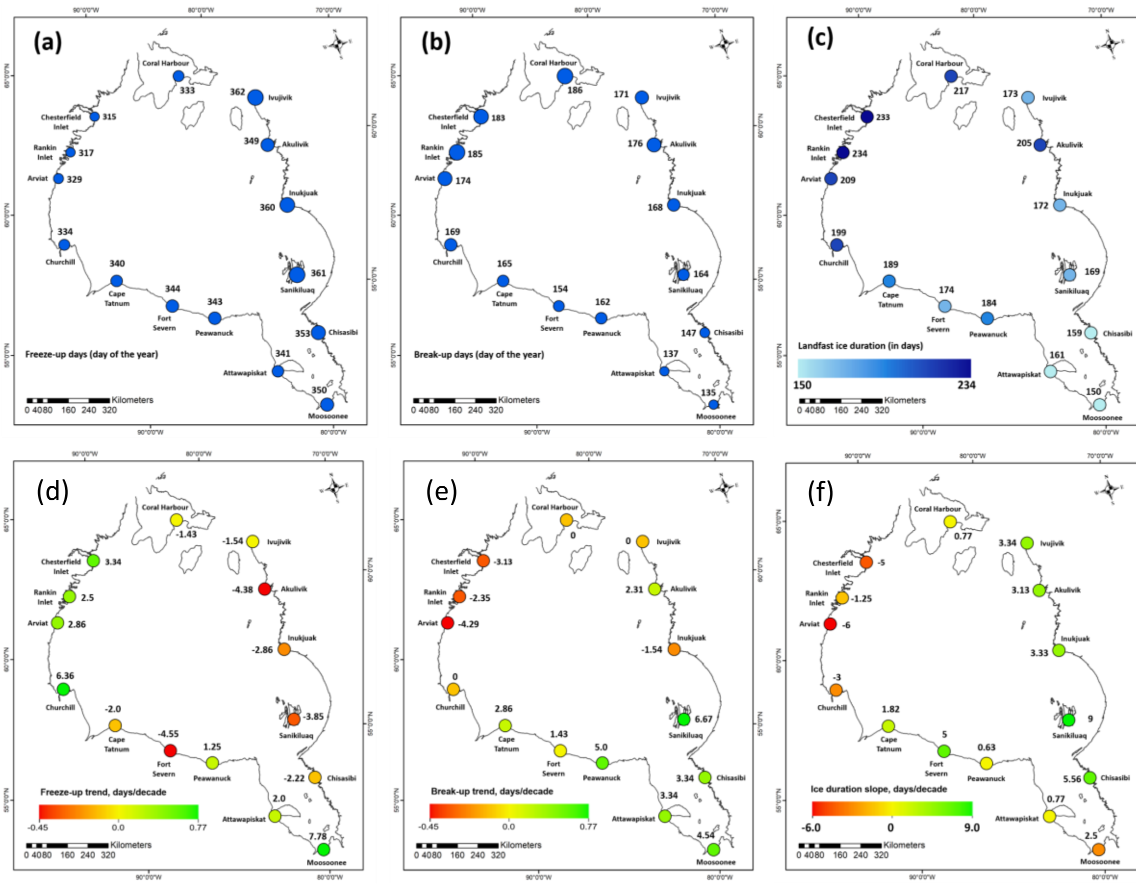

FIGURE 3.1.26 Landfast sea ice temporal variability and trends at 15 Hudson Bay and James Bay community locations over the 2000-2019 period. The average day of the year of freeze-up (a) and break-up (b), and average annual duration of landfast sea ice (c). Lower row provides trends (days/decade) for freeze-up (d), break-up (e) and annual duration (f).

The seasonal change in landfast ice area (in km^2) and its inter-annual variability from 2000-2001 to 2018-2019 was also investigated by Gupta et al. (in review). The 2014-15 ice season exhibited the highest landfast ice area of >140,000 km^2 in March. This large area is explained by the size of the 'ice-bridges' that formed between the mainland and Ottawa Islands, Belcher Island, and Charlton Island. By contrast, the lowest annual maximum landfast ice cover over the study period occurred in 2008 (~55,000 km^2). In Figure 3.1.27a, the annual maximum ice coverage is expressed within a 0-100% range, with the 0% being the seaward edge of the maximum limit of landfast ice recorded in the 2000-2019 period and 100% being the area that became landfast ice covered all 19 years. The 90% occurrence line is used to represent the safe and stable seaward landfast ice edge in Hudson Bay and James Bay. Note that this 90% limit does not cover the 'ice-bridges'; however, evidence suggests that they may have occurred much more frequently in the past (e.g., Flaherty, 1918). The relationships between depth and landfast ice extent are shown in Figures 3.1.27b and c; Even though the landfast ice edge during its annual maximum extent on average falls on the typical 20 m isobath (diamond in Figure 3.1.27b), much variability is seen spatially, temporally and interannually (Gupta et al., in review).

Climatic variations, like the increasing air temperature or precipitation changes, also impact the ice cycle by affecting the timing of freeze-up and break-up of the landfast ice. A reduction in the landfast ice duration means a longer open water condition prevalent in the coastal zone. This has implications on coastal erosion and sediment resuspension from the seafloor, and on how terrestrial freshwater enters the marine environment. Sediments entrained in sea ice, as seen across southern Hudson Bay, James Bay, and Foxe Basin will further enhance ice melt during spring and summer (Barber et al., 2021; Harasyn et al., 2019).

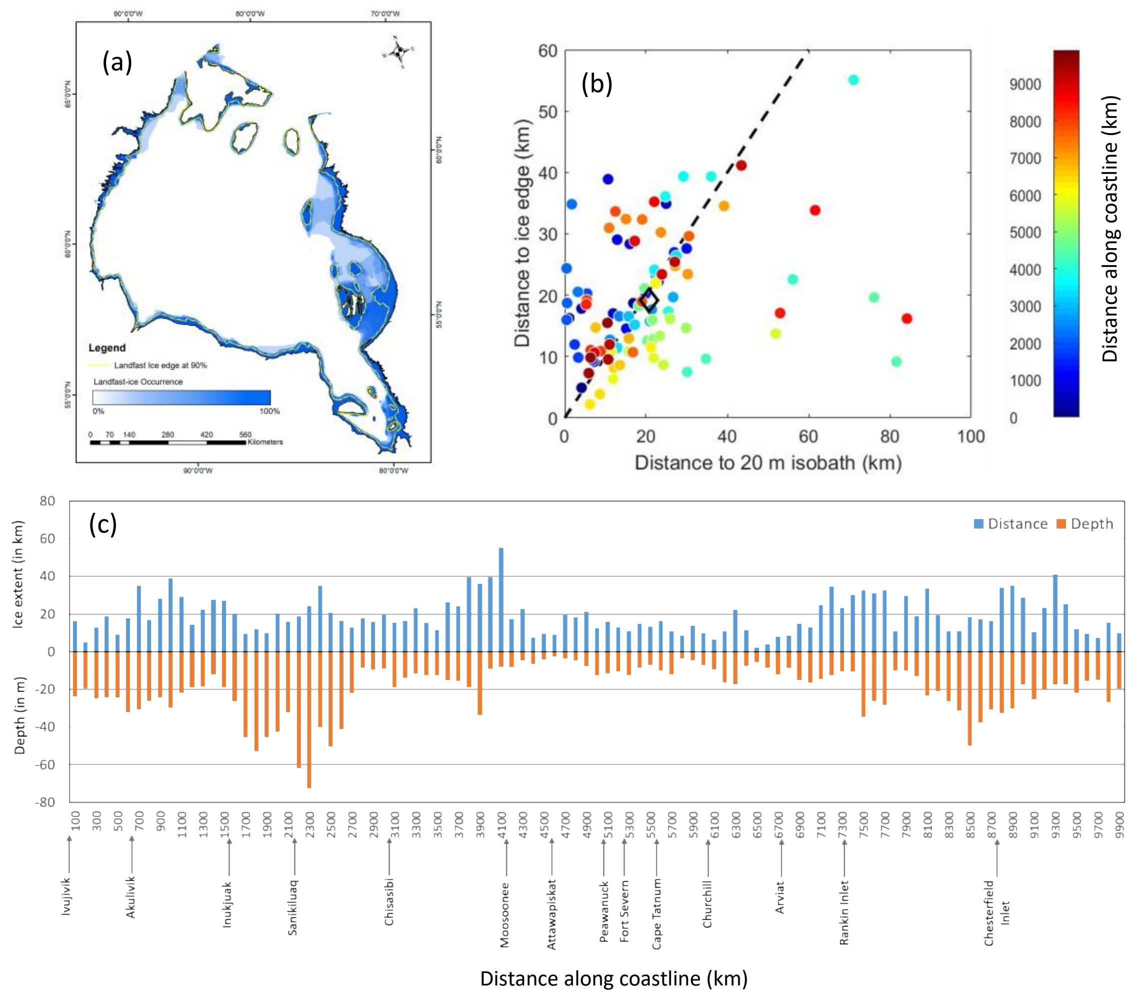

FIGURE 3.1.27 (a) Occurrence of landfast ice along the Hudson Bay and James Bay region (2000-2001 to 2018-2019). The scale in blue defines the occurrence of landfast ice cover forming along the coastline on a scale of 0% - 100% frequency of occurrence. The yellow line represents the zone where the landfast ice edge has a 90% occurrence level. (b) Relationship between fast-ice edge and distance from coastline to the 20 m isobath. Calculated at 100 points across the Hudson Bay and James Bay, each point represents the average distance of the fast-ice edge observed at each point from the 2000-2019 time period and the distance of the 20m isobaths from the coastline at that specific point. The diamond represents the mean of the distribution, signifying the average depth at which the fast-ice edge is limited to is 20.5 meters**.** (c) Variations in the width of the mean fast-ice edge, and the water depth at the mean edge, at 100 km intervals of the Hudson Bay and James Bay coastline. Locations of communities along the coastline are indicated in the colour bar in (b) and the horizontal axis in (c). Note that the distance between the locations may differ greatly from the shortest navigable distance as the data is based on the shape files of the coastline used by the Canadian Ice Service in their ice charts.

Interannual variability in polynya activity in NW Hudson Bay: A key component of the Hudson Bay marine system is the large latent heat polynya that forms throughout winter in northwestern Hudson Bay. The Kivalliq polynya forms as the prevailing northwesterly winds advect the mobile ice pack away from the landfast ice edge, revealing an area of open water surrounded by sea ice. The polynya maintains a thinner ice cover in western Hudson Bay (Landy et al., 2017; Kirillov et al., 2020), promotes new ice growth, and therefore enhances brine rejection into the surface waters of Hudson Bay (Dmitrenko et al., 2021), and promotes biological productivity in western Hudson Bay (Team 3; Matthes et al., 2021, Pierrejean et al., 2020, Barbedo et al., 2020). The polynya is a well-known feature with massive implications across the biogeophysical and human systems of Hudson Bay, yet a detailed study of the polynya had not been undertaken before BaySys.

As a part of BaySys, we used a thin ice algorithm for the AMSR-E and AMSR-2 (Advanced Microwave Scanning Radiometer – Emergency (2003 – 2011), and – 2 (2012 – present)) to detect the presence of open water or ice less than 10 cm thick at each 12.5 km pixel during winter (JFM) and then examined the interannual variability in the size and shape of the polynya. Between 2003 and 2019, the NW polynya was present every day during the winter record, although its size varied from only a few pixels (~10's of km^2) to a maximum size of 60,000 km^2 (Figure 3.1.28). The polynya was most commonly present in a narrow band along the seaward edge of the landfast ice, but during large opening events, it extended 100's of kilometers offshore. Over the 16-year record, there was no statistically significant trend observed in the size of the polynya (Figure 3.1.29).

With the thin ice algorithm, we not only identified the size of the polynya but were also able to estimate the heat flux and therefore ice growth within the polynya. On average 90 km^3 of new sea ice was produced within the polynya each winter (Figure 3.1.30), which was approximately 11% of the total end of winter ice volume reported by Landy et al. (2017). Furthermore, ice production within the polynya was found to be significantly correlated with offshore wind speed, which explained 63% of the interannual variability in ice production within the polynya. Ultimately, the highly variable yet persistent polynya in northwestern Hudson Bay is shown to be driven by offshore winds and to significantly contribute to the regional ice mass balance. From a salt balance perspective, the ice that forms in the polynya contributes salinity via brine rejection to the western Hudson Bay; however, since the ice is advected eastward where it melts, it represents a west-to-east freshwater transport. Results presented in Ahmed et al. (2020) indicate that very little freshwater (either from ice melt or river discharge) is retained within the polynya area during summer after sea ice had receded (Figure 3.1.7).

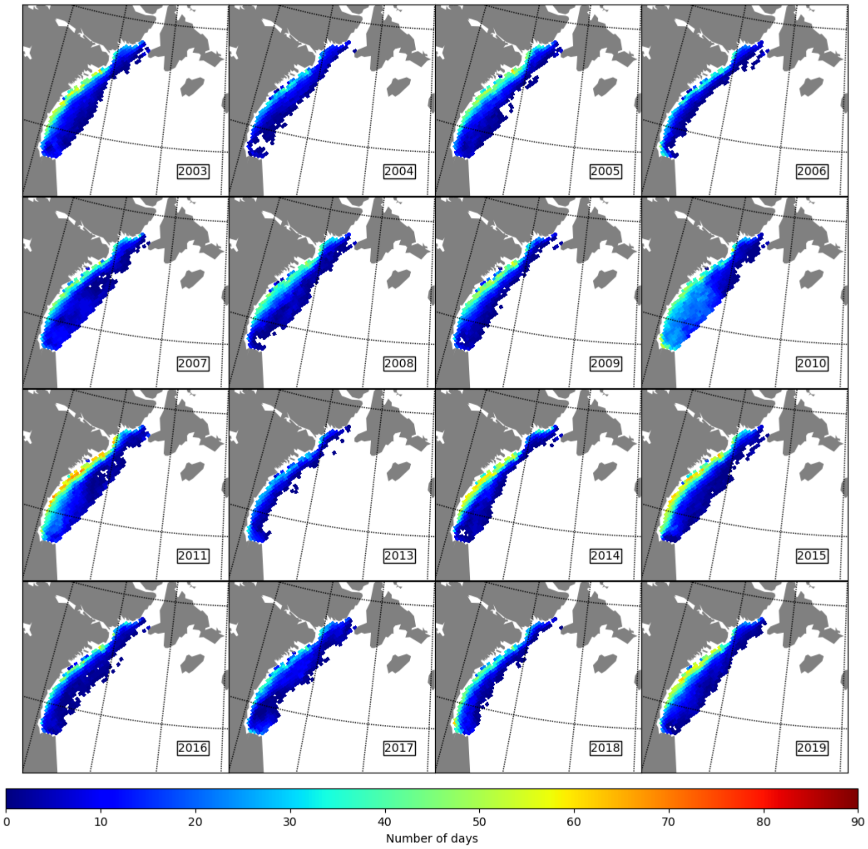

FIGURE 3.1.28 Polynya occurrence frequencies for winter 2003 to 2019. The number of days that the polynya (open water or ice thinner than 10 cm) was present in each grid cell during winter. Bruneau et al. (2021).

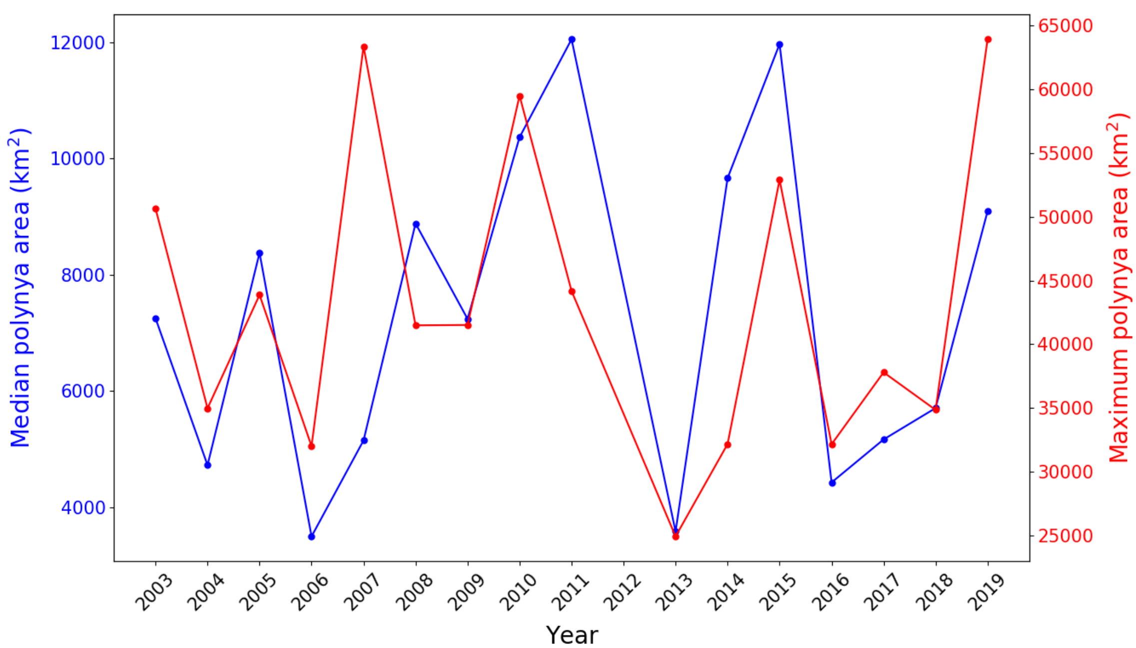

FIGURE 3.1.29 The median and maximum polynya area for 2003 to 2019. The annual median polynya area (km2) is represented in blue and the annual maximum polynya area (km2) is represented in red. Note the difference in scale. Bruneau et al. (2021).

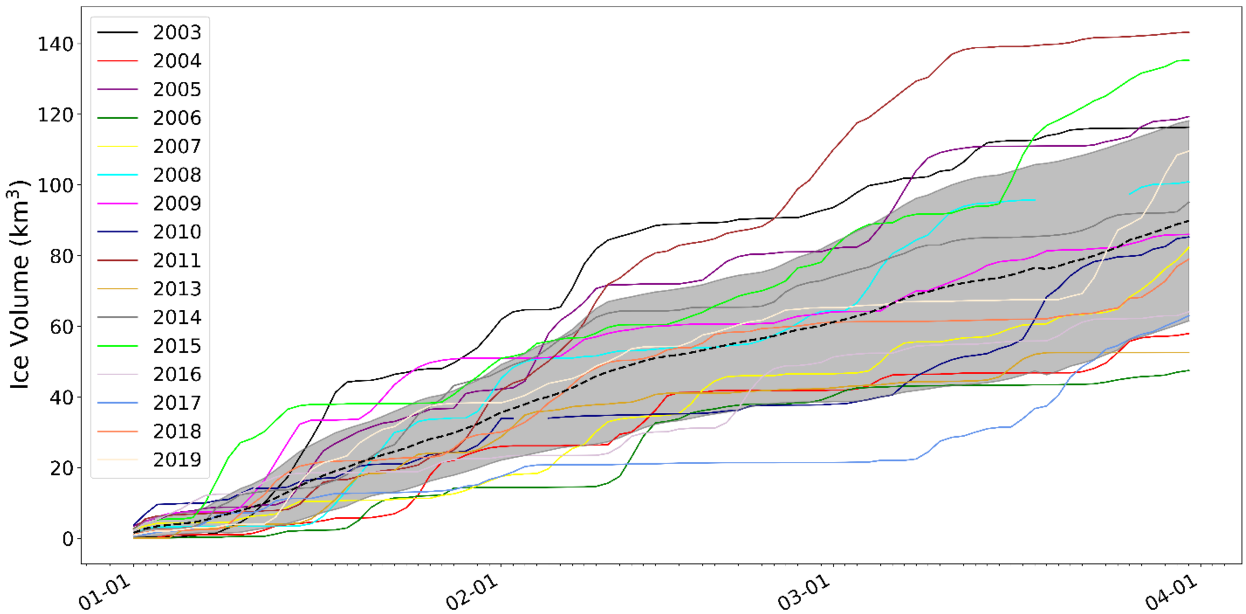

FIGURE 3.1.30 Daily cumulative ice production during winter (JFM) from 2003 to 2019. The dashed black line is the mean daily ice production while the grey area represents one standard deviation above and below the mean (Bruneau et al., 2021).

<u>In-situ CDOM and TSS distribution in the Nelson estuary:</u> The absorption coefficient for coloured dissolved organic matter at 412 nm, $a_{\mathrm{CDOM}}(412)$, and the concentration of total suspended solid, TSS, observed in the Nelson/Hayes River estuaries in 2006 reflected the contrasting characteristics of the two river sources (Figure 3.1.31). The Hayes River estuary had a higher $a_{\mathrm{CDOM}}(412)$ of 1.04-7.68 m^{-1} compared to the Nelson River estuary with 0.6-5.99 m^{-1}, which reflects the characteristics of the freshwater source in the wetlands of Northern Manitoba. However, the mean TSS concentration of the Nelson River (12.2 gL^{-1}) was found to be 1.55 times larger than the Hayes River (7.86 gL^{-1}) for the sampling period during August -September 2006. The range in TSS concentration varied significantly between the two rivers, with the Nelson River estuary having an observed TSS concentration maximum of 67 gL^{-1}, while the Hayes River estuary had a lower maximum concentration around 21 gL^{-1}. The observed TSS concentration minimum for Nelson River was close to zero for coastal waters adjacent to the Nelson River mouth. However, the Hayes River samples had a TSS concentration minima around 2 gL^{-1}.

Both CDOM and TSS showed a significant negative exponential relationship with the increase in salinity along the freshwater-marine salinity gradient in the estuary. The $a_{\mathrm{CDOM}}(412)$ versus salinity relationship of both the Nelson River and the Hayes River followed the theoretical mixing line explained by riverine CDOM dilution by salty marine waters with low CDOM concentration. The Hayes River had a sharper gradient of CDOM dilution relative to the Nelson River by a factor of 1.6, which is explained by the smaller size of the Hayes River. A peak of TSS concentration was observed in between around 5 PSU in the Nelson River estuary, beyond which the TSS concentration fell below the mixing line. These initial high TSS values reflect the processes of sediment resuspension and settling in the estuary, in addition to transport from the river source. This result complements the observed CTD-TSS data, where a well-mixed zone of

High TSS concentration persisted in the interior Nelson estuary. Beyond 20 PSU culmination of CDOM and TSS data of the NR and the HR indicated plume mixing of both rivers, which corresponds to the river mouth locations.

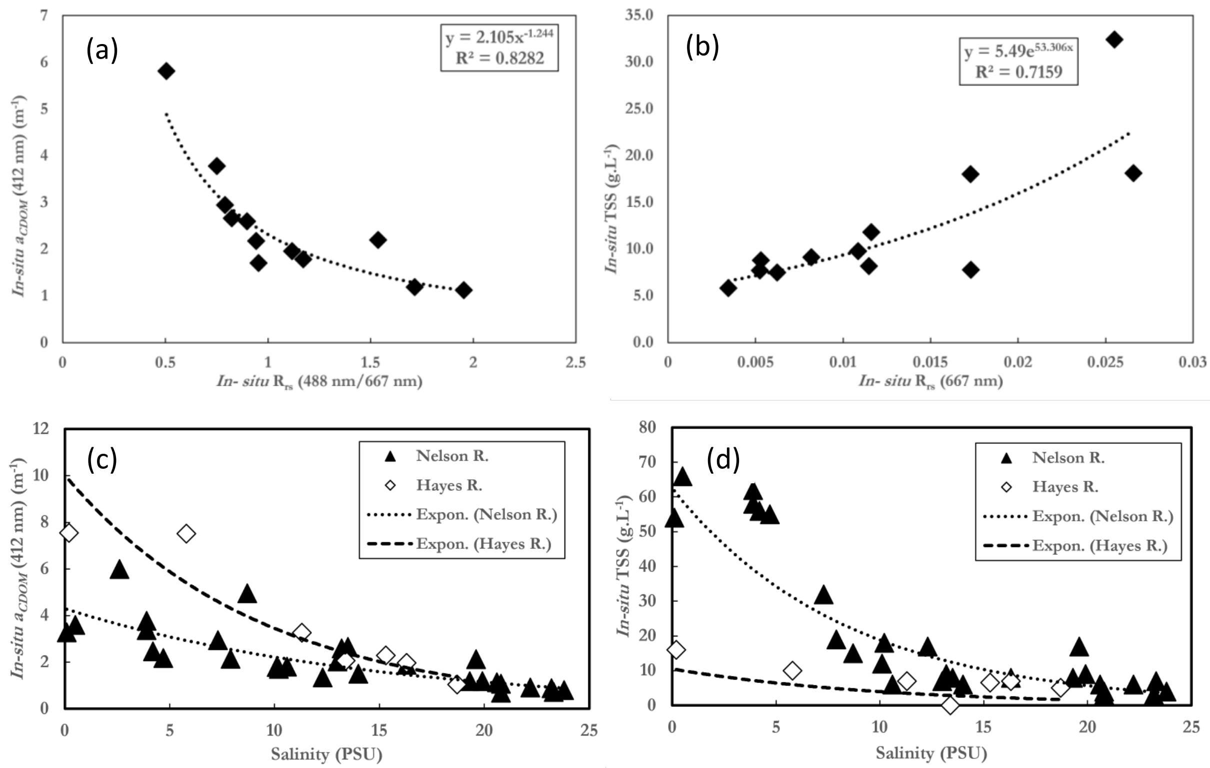

FIGURE 3.1.31 Empirical relationships between (a) a_{CDOM} (412 nm) and blue to red remote sensing reflectance bands, and (b) TSS and the red remote sensing reflectance band. Exponential distribution of (c) in-situ a_{CDOM} (412 nm) (d) TSS concentration along 0 - 25 PSU, salinity gradient in August-September 2006.

<u>Satellite determination of the extent of Nelson River and Hayes River influence:</u> Freshwater from the Nelson River is the major source of CDOM and a significant source of TSS in southwest Hudson Bay. The adjacent Hayes River is another source of CDOM. CDOM and TSS can be detected using optical remote sensing based on their impact on the ocean colour – and can thus be used to trace the dispersion of riverine freshwater into the marine environment. This remote sensing study was conducted to characterize the spatial variability of the influence of Nelson River / Hayes River water on surface layer optical properties during various stages of the tidal cycle (limited by ice-free and cloud-free conditions). This research, therefore, supports the addressing of hypotheses H1.2 and H1.3. The month of August was chosen for MODIS data procurement owing to the availability of match-ups, ice-free and clear-sky conditions, and the reliability of the optimized empirical algorithm. Since the river plume and river influenced surface mixed layer, does not disperse homogeneously as a function of distance from the river mouth, but rather its shape is affected by atmospheric and oceanic forcing factors, this study (using the equations presented in the Methods section) characterized the full distribution of CDOM and TSS concentrations as a function of distance from the river mouth. Quantiles were

calculated from these concentration distributions, and hence this novel method was termed "quantile-based partitioning".

Quantile-based partitioning of the satellite-retrieved river CDOM absorption at 412 nm, $a_{cdom, SAT}(412)$, and coastal total suspended solid concentrations, TSS_{SAT}, was conducted to reveal the dispersal patterns of the Nelson-Hayes River plumes/mixed layer into Hudson Bay (Basu et al., 2021, in prep.). Firstly, a higher discharge volume of the Nelson/Hayes Rivers was associated with a higher concentration of $CDOM_{SAT}$ within the estuary (Figures 3.1.32c and 3.1.33c). An equivalently strong relationship between discharge volume and coastal TSS concentration was not observed (Figure 3.1.33d). Apart from the riverine source, coastal TSS_{SAT} load could have contributions from nearshore mudflats and/or resuspended bottom sediments. While the dominant sources for CDOM are the rivers themselves, the additional sources for sediment within the estuary and along the coast are the likely reason for the poor relationship with Nelson/Hayes discharge. Though negatively correlated with discharge volume, TSS_{SAT} slopes (representing the exponential decrease in quantile concentrations with increasing area) were poorly correlated with discharge volume (Figure 3.1.33b). However, higher discharge volumes were strongly associated with a decrease in slope of river $CDOM_{SAT}$, which indicates a more significant offshore spread of river water (Figure 3.1.33a).

These relationships reveal that CDOM is an efficient optical tracer for assessing the extent of river runoff into Hudson Bay. The CDOM remote sensing reveals that the CDOM-rich surface waters from Nelson/Hayes Rivers typically spread along the eastern coast and then disperses offshore around Cape Tatnam (Figure 3.1.34). The 50% dilution (based on concentrations from Figure 3.1.32c) was mostly observed within 100 km from the river mouth (Figure 3.1.34a). The analysis of river water flow direction in relation to CDOM concentrations and oceanic- and atmospheric forcing is still underway; here, the preliminary results are provided for four clear-sky satellite images (Figure 3.1.34). A more encompassing analysis will be provided in Basu et al. (in prep.). However, the presented results show how the concentration-weighted mean direction of the river water-influenced surface layer is affected also by coastal geometry in addition to external forcings.

Even though terrestrial runoff is the major source of CDOM the HBC, the mooring records (Wetlabs ECO triplet CDOM fluorometers) and satellite remote sensing furthermore revealed that marine-derived CDOM has a noticeable contribution to the CDOM budget (Dmitrenko et al., 2021). High offshore CDOM concentrations were observed (Figure 3.1.35) following the spring phytoplankton bloom (Matthes et al., 2021).

Table 3.1.2: River discharge category, date, and time for the 30 clear-sky MODIS satellite images used in Basu et al. (2021, in prep.) to study the Nelson River plume dispersion along with corresponding tidal information.

	Date	*CDT*	*MODIS Satellite*	*Tidal Flow*	*Tidal Stage*	*Daily Tidal Range (m)*
	05-Aug-02	12:35	Terra	Ebb	Neap	0.9-3.2
	19-Aug-00	12:25	Terra	Flood	Spring	0.0-4.3
	18-Aug-00	13:20	Terra	Flood	Spring	0.0-4.3
Low Discharge (1000 - 4500 m^3s^{-1})	02-Aug-03	13:10	Terra	Flood	Spring	(-)0.01-4.4
	03-Aug-03	12:15	Terra	Flood	Spring	(-)0.01-4.4
	06-Aug-03	12:45	Terra	Ebb	Neap	0.02-3.9
	16-Aug-03	11:45	Terra	Flood	Spring	(-)0.02-4.2
	22-Aug-03	12:45	Terra	Ebb	Neap	0.9-3.1
	22-Aug-03	12:55	Aqua	Ebb	Neap	0.9-3.1
	14-Aug-01	13:05	Terra	Ebb	Neap	0.07-3.4
	23-Aug-01	13:00	Terra	Flood	Spring	(-)0.5 -4.6
	24-Aug-06	13:35	Aqua	Ebb	Spring	0.0-3.8
Moderate Discharge (4500 – 6500 m^3s^{-1})	05-Aug-06	13:05	Aqua	Ebb	Neap	0.09-3.1
	24-Aug-06	11:45	Terra	Flood	Spring	0.0-3.8
	09-Aug-07	12:00	Terra	Ebb	Neap	0.5-3.4
	10-Aug-07	12:40	Terra	Ebb	Neap	0.6-3.4
	10-Aug-07	14:30	Aqua	Ebb	Neap	0.6-3.4
	19-Aug-07	14:25	Aqua	Flood	Spring	0.02-3.9
	11-Aug-08	13:50	Aqua	Ebb	Neap	0.9-3.1
	10-Aug-10	11:50	Terra	Ebb	Spring	0.0-4.1
	18-Aug-05	13:00	Aqua	Ebb	Neap	0.05-3.8
	18-Aug-05	14:40	Aqua	Ebb	Neap	0.05-3.8
	21-Aug-05	13:30	Aqua	Ebb	Spring	(-)0.01-4.5
High Discharge (6500 – 9000 m^3s^{-1})	22-Aug-05	12:35	Aqua	Ebb	Spring	(-)0.04-4.5
	30-Aug-05	13:25	Aqua	Ebb	Neap	0.9-2.9
	30-Aug-05	11:40	Aqua	Ebb	Neap	0.9-2.9
	26-Aug-09	14:15	Aqua	Flood	Neap	(-)0.02-4.3
	27-Aug-09	13:20	Aqua	Flood	Neap	0.01-4
	28-Aug-09	12:10	Terra	Flood	Neap	0.3-3.7
	27-Aug-09	13:05	Terra	Flood	Neap	0.01-4

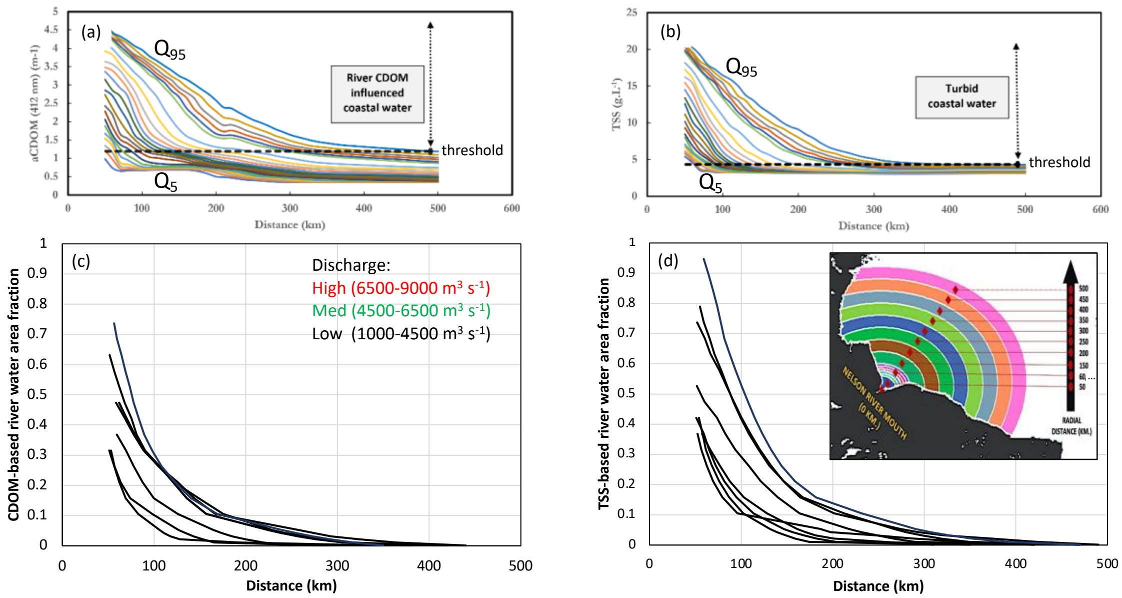

FIGURE 3.1.32 Quantile distribution (0.05 – 0.95) for (a) a_{CDOM} (412 nm) and (b) TSS within areas bounded by radial distance from the river mouth and the coastline (see inset in (d). The dashed line represents the "threshold" line separating the coastal and marine water types. The thresholds were taken as the 95^{th} quantile values with the lowest concentrations. Then, satellite-retrieved river-influenced water area fractions (RIAF) were determined based on (c) CDOM and (d) TSS as functions of the area within the radial distance from the Nelson River mouth. Three levels of discharge (see Table 3.1.2) are highlighted by colour.

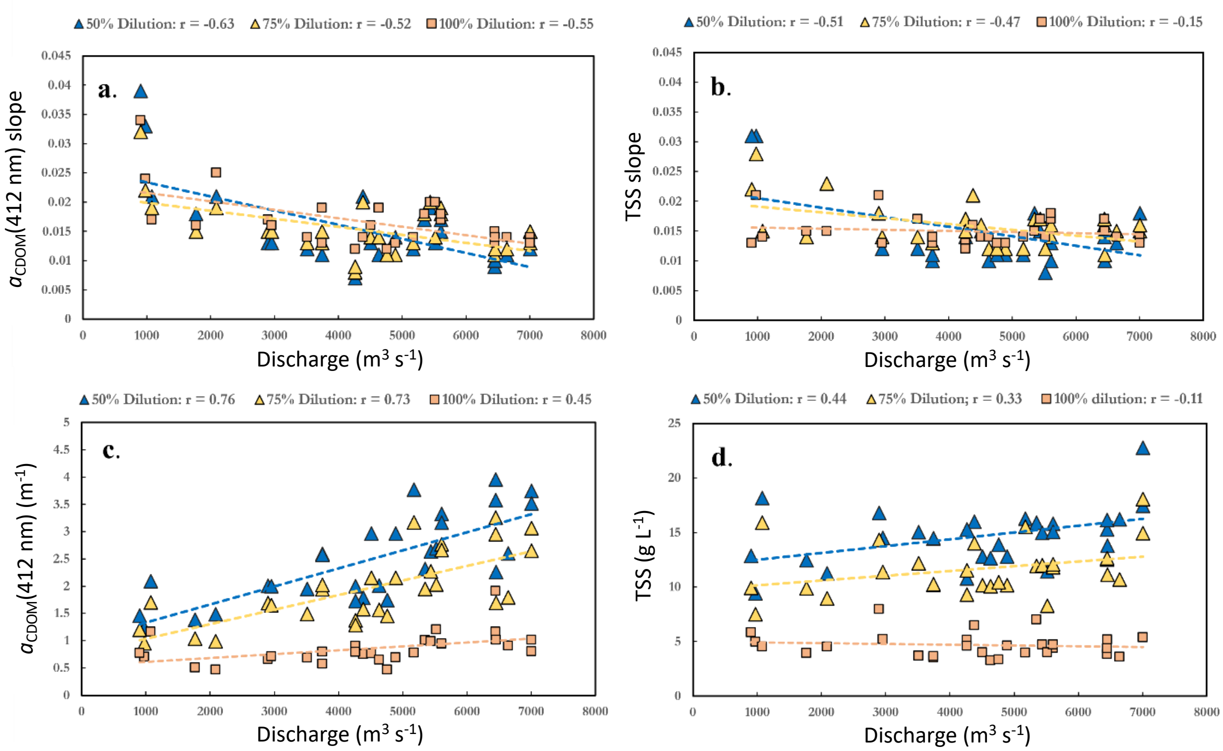

FIGURE 3.1.33 Variation of slope of (a) $a_{CDOM, SAT}$(412 nm), and (b) TSS_{SAT} within a low-high range of daily discharge volume of the Nelson River at three dilution limits: 50%, 75%, and 100%. Variation of (c) $a_{CDOM, SAT}$(412 nm) and (d) TSS_{SAT} concentration with increasing discharge volume, at 50%, 75% and 100% dilution limits.

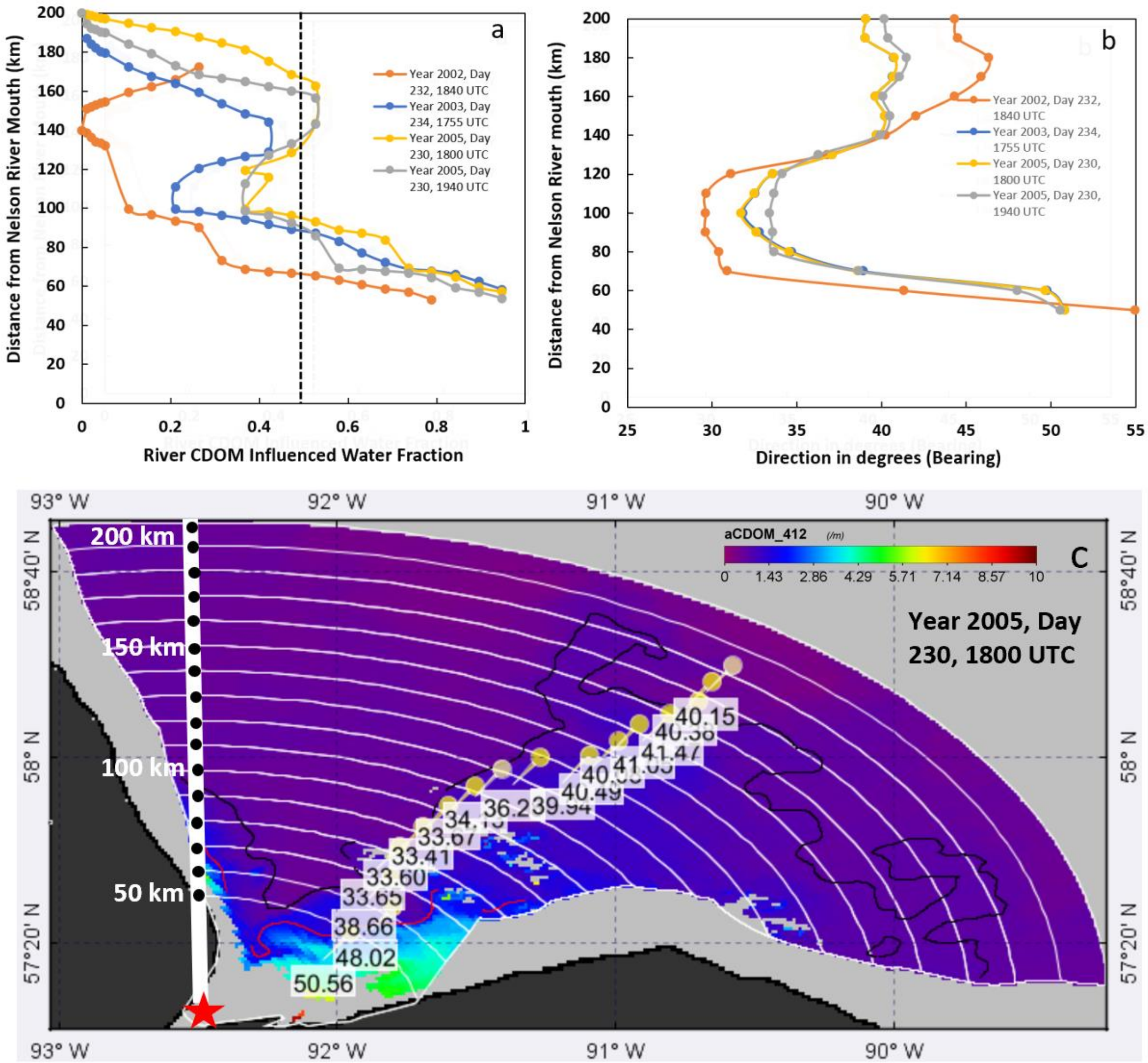

Figure 3.1.34 (a) Satellite-retrieved River a_{CDOM} (412 nm)-influenced water fraction (calculated per 5-km bands, not radial area) based on a function of distance from the Nelson River mouth for four MODIS- clear sky images. The dashed line represents 50% river influence fractions. (b) The concentration-weighted mean direction (bearing) of the Nelson River plume was obtained from four MODIS clear-sky satellite images. Calculations for the remaining 25 images and corresponding statistical analysis in under way. (c) Example of a^{sat}_{CDOM} (412 nm) map for southwestern Hudson Bay for the satellite image from year day 230 in 2005, showing contours of 50% dilution in red and 75% dilution in black, as representative of Nelson/Hayes River water dilution. The yellow pins represent the concentration-weighted mean direction from the river mouth represented by a star. This direction is also shown in (b) by the grey curve. The white bands represent the sections of quantile estimation, ranging from the river mouth to 200 km offshore.

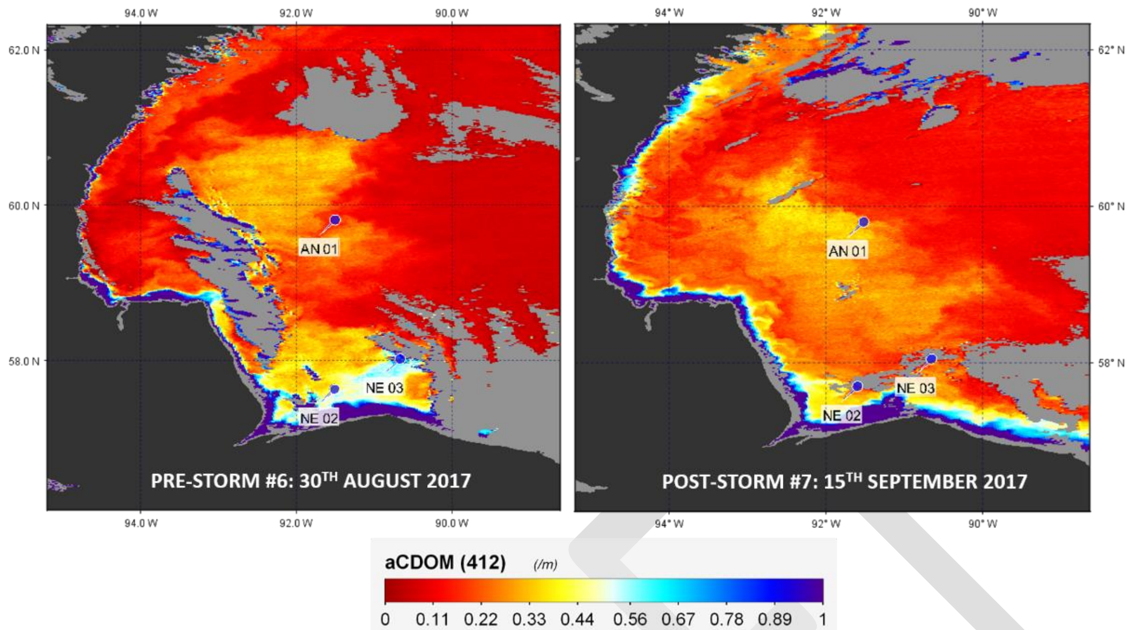

Figure 3.1.35 Normalized CDOM absorption at 412 nm in western Hudson Bay derived from MODIS at 1 km spatial resolution. (**a**) Data on 30 August 2017 before storms #6 and #7 shows CDOM maxima north of AN01. (**b**) On 15 September 2017 after storms #6 and #7, the on-shore displacement of CDOM maxima was observed in response to the northerly wind storms. The grey shadings denote no data due to cloud cover. Dmitrenko et al. (2021).

3.1.4 Conclusions

The BaySys proposal required Team 1 to address three highly integrated objectives through a combination of observational (Team 1) and modelling (Team 6) studies. We conclude this chapter by summarizing the results from our BaySys investigations as they pertain to each stated objective.

> **Hypothesis 1.1** – The spatial and temporal pattern of bay-wide sea ice growth and decay is a dominant factor forcing freshwater-marine coupling processes in Hudson Bay.
>
> **Hypothesis 1.2** – The seasonality and magnitude of river runoff is a dominant factor controlling freshwater-marine coupling processes in Hudson Bay.
>
> **Hypothesis 1.3** – Climate variability and change directly affect the vertical mixing and horizontal distribution of fresh and marine waters in Hudson Bay.

The Team 1 results highlight the importance of bay-wide sea ice growth and decay forcing freshwater-marine coupling processes in Hudson Bay (*Hypothesis 1.1*). They also indicate the important role of climate change and variability (specifically the roles of air temperature and wind) in setting the stage (thermodynamics) and controlling ice drift (*Hypothesis 1.3*). Furthermore, the findings demonstrate interlinking between hypothesis in that altering wind forcing during winter redistribute solid freshwater (i.e. in the form of ice) within the bay, modify the regional inputs of meltwater in summer and, therefore, may locally change stratification and vertical mixing with all related consequences for biological and chemical processes (*Hypotheses 1.1 and 1.3*).

The ocean circulation in the bay is strongly linked to an index of atmospheric vorticity that quantifies the strength and general direction of wind forcing. Altering water dynamics is associated with a wind-forced Ekman pumping in the central bay. The cyclonic atmospheric circulation leads to on-shore Ekman transport and rise of sea level in the coastal regions that further results in enhancement of geostrophic currents coinciding with the direction of the wind. Therefore, recurring cyclonic wind forcing favors freshwater transport along the Hudson Bay coastline towards Hudson Strait. As a result, a significant reduction in the residence time of riverine water in Hudson Bay can be expected, with important implications for water column stability and thus primary production and support of the Hudson Bay ecosystem. During an anticyclonic wind forcing, the background thermohaline cyclonic circulation in Hudson Bay is expected to slow down or even reverse. This effect would likely result in a reduction of the freshwater transport to Hudson Strait and an increase of the riverine water residence time in the bay. Thus, the long-term trends in regional wind forcing may modify the pace of riverine freshwater removal from the Hadson Bay as well as stratification and vertical mixing in some regions, although the rate of these changes and their geography can only be estimated with numerical simulations (*Hypothesis 1.1*).

Landfast ice extent, duration, and roughness have been observed to play an important role in freshwater dispersion and stratification in the nearshore zone. Climatic variations, like the increasing air temperature or precipitation changes, also impact the ice cycle by affecting the timing of freeze-up and break-up of the landfast ice. A reduction in the landfast ice duration means a longer open water condition prevalent in the coastal zone. This has implications on coastal erosion and sediment resuspension from the seafloor, and on how terrestrial freshwater enters the marine environment. Sediments entrained in sea ice, as seen across southern Hudson Bay, James Bay, and Foxe Basin will further enhance ice melt during spring and summer (Barber et al., 2021; Harasyn et al., 2019).

The stable and immobile ice cover isolates the underlying ocean from mixing under the action of wind also allowing a further export of river plume into the ocean compared to spring or fall months. As seen in some previous studies, during the winter months, a ridged outer boundary ("stamukhi") of the landfast ice cover can prevent dispersion of the river plume that remains on the shelf in the winter and contributes to higher export of the river water out of the Arctic (Itken, 2014). Landfast ice cover also reduces tidal amplitudes and surface layer mixing by blocking air-water interaction (Proshutinsky, 2007). Thus, the landfast ice cover also limits the areal extent of the highly buoyant under-ice river plume layer, because as the plume approaches or flows past the ice edge it is subject to strong mixing, as seen in the La Grande River estuary (Messier et al., 1989; Peck et al., submitted). It was also observed, that landfast ice has an important contribution in controlling the overall freshwater cycle in the ocean by storing a substantial amount of terrestrial freshwater in the winter and releasing it during summer (Bareiss & Görgen, 2005; Eicken, 2005). Hence, the changing patterns of landfast ice duration as observed throughout the Hudson Bay System will impact the freshwater dispersion and freshwater marine coupling in the region.

An extensive literature review by BaySys team members (McCullough et al., 2019) reported on the current state of knowledge of the freshwater budget and freshwater circulation through the Hudson Bay Marine Region. The fluvial inflow of 900 km3 dominates the total annual loading. An additional 330 and 90 km3 are supplied by net precipitation and freshwater inflow through Fury and Hecla Strait, respectively. There is a large inflow volume through Hudson Strait, but this does not include freshwater (with freshwater determined relative to a reference salinity of 33 PSU). Although there is large uncertainty in the estimates of both net precipitation and inputs through Fury and Hecla Strait, the total is balanced closely by the independent estimate of 1,300 km3 of net yearly freshwater export to the North Atlantic Ocean. Sea ice formation and melt contribute 1,200–1,300 km3 each year to the annual inventory of freshwater in the marine region—that is, very nearly as much as all other sources combined—but the process is cyclical and how it affects net freshwater export is not well understood.

The spatial distributions of the two major sources of freshwater differ markedly. Annual sea ice melt supplies over 60% of the seasonal freshwater load to Foxe Basin, but only about 20% to James Bay where fluvial discharge dominates the load. The two sources supply about equal parts of the freshwater in Hudson Strait, although almost all of the fluvial loading there is concentrated in Ungava Bay. Overall, sea ice melt supplies twice as much seasonal freshwater as does fluvial discharge to Hudson Bay itself, but neither source is evenly distributed. Seventy-five percent of the fluvial supply enters along the southwest coast or flows in through James Bay. The thickest sea ice is generated in northern Hudson Bay, but southward and eastward transport of ice causes the most melt to occur in the central to south-eastern half of the bay. Consequently, the freshwater inventory in the bay ranges from as little as 1.0 m in the northwest to 8–10 m in the southeast near the Belcher Islands. Most of this freshwater is contained within a surface mixed layer rarely greater than 100 m deep. (Although the mixed layer reaches more than 200 m depth in Hudson Strait, the 33 PSU halocline dips nearly to that depth only in the path of freshwater outflow along the Quebec shore.)

BaySys researchers described a more complex circulation of surface waters in Hudson Bay than had been previously understood. It was traditionally held that river discharge induces a cyclonic, relatively fresh coastal current. In the decade prior to BaySys, some complexity was introduced by Saucier et al. (2004) who used a numerical model to demonstrate a smaller, anticyclonic gyre in southeastern Hudson Bay, forced by freshwater accumulation from the spring freshet, and St. Laurent et al. (2011) who identified freshwater transport by Ekman transport from the coastal conduit to central Hudson Bay. BaySys investigators Ridenour et al. (2019) used the numerical model NEMO, together with GLORYS climate reanalysis data and AVISO satellite sea surface height data to show that seasonal variability in wind forcing alters circulation induced by spatiotemporal aspects of freshwater delivery to create more complex circulation than hitherto accepted. A bay-wide cyclonic circulation is limited to fall and winter conditions. From spring through summer, surface mixed layer circulation in Hudson Bay is marked by multiple small cyclonic and anticyclonic features, and the mean flow is directed towards the interior of the bay. However, the preponderance of freshwater delivery along the southern coast and via James Bay is reinforced by patterns of seawater accumulation forced by dominant wind circulation patterns.

The full power of NEMO to investigate the effects of climate and river regulation on freshwater distribution and circulation in the Hudson Bay Marine Region (HBC) continues to be accessed to address *Hypothesis 1.3*. For example, McCullough et al. (in prep.) use the modeled output for the historical period to describe responses in vertical mixing, circulation, and regional inventories to decadal variability in runoff from the watershed. NEMO runs using long term climate data sets with regulated and naturalized river discharge allow for the study of the interaction of climate (through impacts on river discharge, precipitation over the HBC, and winds) and river regulation (seasonal changes in discharge, and major water diversions) on the same variabilities. NEMO output using HYPE-modelled century-long watershed discharge forced by multiple future climate scenarios, and with regulated and naturalized flows, will allow further investigation and differentiation of climate and river regulation impacts.

Based on mooring data, it was shown that wind vorticity strongly impacts the intensity of ocean circulation in the Hudson Bay. A consideration of this impact on the freshwater system is difficult without numerical modelling. The first attempt of using NEMO to quantitatively estimate the relation between atmospheric vorticity over Hudson Bay and water transport through Hudson Strait showed no direct relationship, suggesting an integrative response to cyclonic wind forcing rather than a direct impact (Dmitrenko et al., 2020). However, the time frame of analysis limited by 2-year long mooring data did not allow us to quantify freshwater export and storage and to attribute them to the seasonal and interannual changes of wind forcing. Further numerical efforts are needed to investigate these freshwater cycle characteristics and relate them to the future projections of climate change at both regional and global scales.

Support hypothesis on the winter-time freshwater source – Eastwood et al. (2020) used NEMO results to support the hypothesis of circulation bringing freshwater from James Bay to Belchers Island during winter. Winter-time observations of circulation are difficult to obtain, so NEMO simulations were used to support the assumption of ocean circulation bringing riverine waters from James Bay. NEMO simulations thus supported the selection of the meteoric water end-member value that was most appropriate for the study period and location, which then allowed the calculation of brine inputs (–SIM) into the stratified surface layer (Figure 3.1.36c, d).

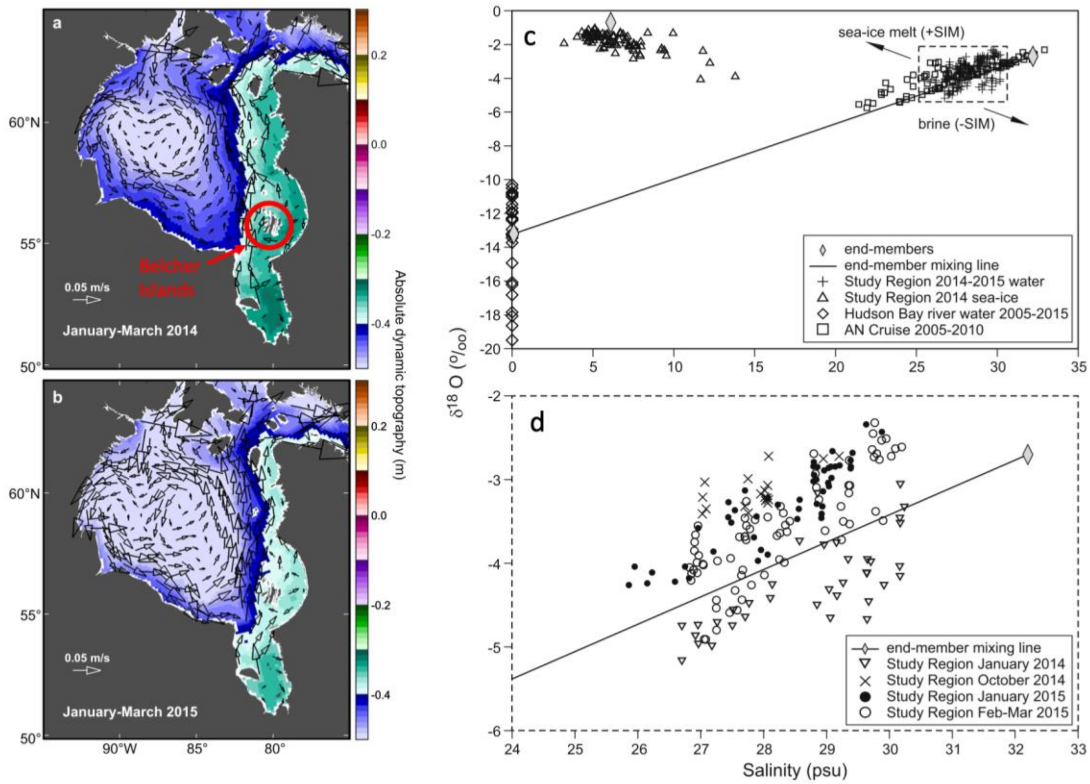

FIGURE 3.1.36 NEMO ocean model simulations of winter circulation in Hudson Bay and James Bay during January–March 2014 (a) and January–March 2015 (b). Arrows represent surface geostrophic current velocities and colors reflect sea surface height (absolute dynamic topography or height above the geoid). (c, d) δ18O versus salinity relationships for the Belcher Island region: Hudson Bay water (study region water samples (plus signs) and ArcticNet/Amundsen (AN) cruises 2005–2010 (empty squares)), river samples (empty diamonds), and melted sea ice samples (empty circles). End- members assigned for local seawater, river runoff, and sea ice are shown as filled diamonds. The lines indicate the mixing line between river runoff and seawater end-member values. (d) Seawater samples were replotted to highlight the changes in properties between January–February (plus sign), October 2014 (cross), January 2015 (filled circles), and February–March 2015 (empty square). Values above the mixing line indicate the presence of sea- ice melt (+SIM), while values below the mixing line indicate the presence of brine (–SIM). Taken and modified from Eastwood et al. (2020).

The sea ice and ocean systems are undergoing rapid change in response to climate change. The BaySys Team 1 has taken a comprehensive look at available past data set, including remote sensing products, hydrographic surveys, and mooring records, to provide a broad understanding of the Hudson Bay marine and climate systems, and their recent change. Changes to the persistence of sea ice and SST are indicated in the satellite record. Galbraith & Larouche (2011) found positive trends in both the length of the open water period and SST throughout the HBC over the 1985-2009 period. While these positive trends of warming SST continued over the 2008-2018 decade for the Southern and Southwestern portions of HBC and Western Foxe Basin, a reversal into a negative SST trend was found for the portions adjacent to Nunavik in the eastern HBC (Figure 3.1.23). The close association between the patterns for sea ice concentration (SIC) and open water SST was evident in our study (Figure 3.1.23). Comparison of the BaySys mooring record to the mooring record from 1981-1982 indicates that freshwater content has increased, and consequently the stratification of the water column has increased notably.

Between the campaigns in 1970's and 1980's and the recent ArcticNet and BaySys missions, there was a dearth of observations and a general lack of long-term monitoring of the marine system in Hudson Bay, such that many of the potential changes to the marine system will remain unknown. Moving forward: Some of the changes to the marine and coastal systems will need to be inferred through modelling efforts informed by a better process understanding and proxy records (such as sediment cores). By looking at seasonal changes using the mooring records, how the hydrography is affected by weather events, and how the sea ice patterns and characteristics evolve, Team 1 has contributed significant new process understanding that has been and will continue to be used to evaluate and improve the models. The BaySys oceanographic data and analysis methods will be used for years to come in these efforts, long after the project has ended.

Although BaySys researchers and others will continue to use models such as NEMO to test for long-term effects of regulation and climate change, The ongoing rapid changes to the climate system justify a sustained effort to monitor these Canadian inland waters. New technologies (remote sensing, moorings, AUVs) make such sustained observations much more logistically and economically feasible than ever before. CEOS researchers have continued to use the oceanographic equipment purchased with BaySys funding to monitor and record oceanographic processes in the Hudson Bay marine system. For example, BaySys moorings have been deployed in 2018-19 in Roes Welcome Sound as a part of CMO monitoring efforts and tethered from sea ice in 2019 in Belcher Islands with the help of local community members. CT and turbidity sensors have been installed in James Bay near Chisasibi to evaluate the spreading of the river plume. In August 2021, five moorings, composed of a combination of equipment purchased for BaySys, CMO, and from DFO, were deployed in James Bay using the R/V William Kennedy and ship time funding from NSERC. These moorings will be recovered in August 2022. In conclusion, research in the Hudson Bay marine system will continue and the BaySys data and equipment will continue to play a major role in it.

3.1.5 Gaps and Recommendations

An incredible amount of data was collected as part of BaySys Team 1, such that it will require significant time beyond the funded BaySys project to utilize its full capacity and to understand all ramifications of the counter-opposing forces of water regulation and climate change. We have addressed the deliverables of our objectives and uncovered new processes which have bearing on the overarching objectives of BaySys. We conclude by summarizing these gaps and making recommendations for further work from the perspective of Team 1:

a. To accurately estimate the sea ice transport within the Hudson Bay System (HBS), reliable data on ice thickness and drift is required. We have shown that ice thickness can be obtained from upward-looking sonars on moorings and satellite altimetry (Landy et al., 2017; Kirillov et al., 2020). However, the ice drift products in the Hudson Bay derived from satellite data need to be additionally qualified. We have found that NSIDC 25-km Polar Pathfinder sea ice motion vectors tend to underestimate the ice drift speeds, while the EUMETSAT Ocean and Sea Ice Satellite Application Facility OSI-405-c ice drift product has a relatively low spatial resolution of 62.5 km. Tidal circulation is a bigger factor in HBS than in the central Arctic Ocean; and thus time-series beacon data are needed to validate ice drift and to better understand divergence and convergence within the mobile ice field, which is important for the estimation of new ice growth and deformation. Mass balance stations, weather stations, and ice beacons were deployed as part of the BaySys winter campaigns. However, the data has yet to be thoroughly analyzed.

b. Ice production and deformation in coastal flaw leads around Hudson Bay – While the contribution of the northwest polynya to the regional ice mass balance has been evaluated during BaySys (Bruneau et al., 2021), the contribution of the tidal flaw-lead ice production has yet to be addressed and is an area of ongoing work. Specifically, ice beacon data from 2009 and 2017 fieldwork are being used to extract the tidal component of ice drift and therefore to determine the motion that reflects the opening and closing of the flaw lead on semidiurnal cycles. This tidal-driven process was observed in person during the Nanuk winter campaign and resulted in thin new ice heavily deforming along the landfast ice seaward edge (Figure 3.1.4). The recurrent growth and mechanical deformation of flaw-lead ice eventually result in the formation of very thick ice that may either become grounded onto the shallow mudflats or remain mobile and be advected offshore within the pack ice. The impact of ice formation in the flaw-leads on the Hudson Bay marine environment is currently not well understood. By quantifying the width of the flaw-lead and using in-situ observations of air temperature, we can estimate the growth of new ice within each flaw lead cycle, and extrapolate to the full coast of southern Hudson Bay, or other areas of the bay. Additional analysis will focus on the role of offshore and onshore winds in amplifying or limiting the flaw lead and distinguishing between the flaw lead and larger coastal polynyas that form during prolonged periods of offshore winds.

c. New opportunities from advances in satellite remote sensing – With the launch of the swath altimetry satellite SWOT and the current ICESat-2 mission, the advances in satellite altimetry will allow us to explore the estimation of ice roughness, ice volume as well as ocean dynamic topography and surface roughness (i.e., for retrieval of ocean circulation and wave development) with unprecedented accuracy. The increased temporal resolution provided by the new RadarSat Constellation Mission will allow for an improved understanding of ice processes such as break-up, ice-field convergence, and divergence, ice type classification. The use of NOAA’s geostationary satellite GOES-East is now also being investigated as an option for determining mean and tidally-driven ice drift within Hudson Bay. However, in-situ observations of ice thickness and drift are still a limitation in Hudson Bay and will be required for the validation of the remotely sensed data products.

d. Uncertainties remain in freshwater transport within and in/out of the HBC. The modelling of freshwater and salt transport in and out of the HBC relies on a very sparse set of *in-situ* observations. For example, currents observations in Fury and Hecla Strait are limited to the summer of 1960 and April-May 1976 (Barber, 1965; 1967; Sadler, 1982; Straneo & Saucier, 2008) which represent such brief periods before major evidence of Arctic wide freshening that the annual freshwater transport of today into HBC can hardly be assessed with confidence. Yet, model estimations (including those conducted with NEMO) of freshwater transport in and out of HBC must assume that net export though Hudson Strait must equal the input from rivers and Fury and Hecla Strait (Straneo & Saucier, 2008). Thus, new year-long mooring-based observations, using modern instrumentation, are needed in the flux gateways (Fury and Hecla Strait, the mouth of Hudson Strait, in the channels separating Hudson Bay, Foxe Basin, and Hudson Strait) to assess and accurately model the freshwater transport within and in/out of HBC. Within the HBC, Ridenour et al. (2019) used satellite altimetry and modelling to show a more complex circulation pattern of Hudson Bay driven by freshwater buoyancy effects. Petrusevich et al. (2018) observed wide-spread internal wave activity across much of the southeastern Hudson Bay. However, no in-situ observations were obtained during BaySys to support these findings such that vertical variations and relationships to water column stratification could not be made. The BaySys mooring program (Task 1.3) did attempt near-surface time-series observations using instrumented buoyant pipes; however, these were not successful as the pipes were lost. Thus, new strategies need to be employed in the future to assess the relationship between freshwater inputs, mixing, and stratification (and consequent biological production). This could involve autonomous glider transects to resolve spatial and temporal variations in pycnocline levels, geostrophic currents, and biogeochemical state (e.g., chl-a, CDOM, turbidity, nutrient concentrations).

e. Deep water properties and renewal – Even though it was planned, the BaySys field program did not provide us with the opportunity to deploy an oceanographic mooring and sample the deepest portion of the water column due to events out of our control. Past observations of deep waters are also extremely rare. The BaySys mooring AN01 was located adjacent to the large NW polynya and provided a two-year record. Despite the hydrography at AN01 being quite different during the two years (Figure 3.1.14), in neither year was the brine production sufficient to overcome the freshwater stratification. However, a longer record is required to better understand the variability in winter water modifications and possible modulations of deep waters within Hudson Bay. The continued observations with CMO moorings will improve our understanding of the deep water properties renewal and residence times; however, to date, there have been growing pains in CMO deployments that have resulted in limited data. A deeper understanding will furthermore require continuous water sampling to resolve variations throughout the annual cycle of water mass tracers and biogeochemical properties. This is now possible with automated water samplers that can be attached on moorings.

f. Optical remote sensing of freshwater-marine coupling – Satellite remote sensing estimates of freshwater-marine interactions in river estuaries and offshore are limited by few data points with coincident measurements of remote sensing reflectance, apparent optical properties, and the inherent optical properties of the optically active substances (CDOM, sediment, phytoplankton). The past field experiments have focused the collection on subsets of the required data, but not complete data sets. To achieve optical closure (i.e., a full understanding of how sunlight enters, propagates, and interacts in the water column), future fieldwork should emphasize the collection of complete optical datasets across the coastal continuum spanning the river mouth, across the estuary to the offshore marine waters. This will require a focused effort to study the optical properties of Nelson and Hayes River estuaries. It will allow the assessment of the role of CDOM, and TSS, in radiative heating of water column, and its effect on ice melt and the creation of subsurface warm water layers. It will also support studies of primary production. The next step in understanding SST and ice break-up/freeze-up in the HBC will involve the investigation of the roles of CDOM (mainly supplied via river runoff), TSS, and bathymetry in determining rates of change in SST in open waters over time.

g. Modelling of coastal processes – Due to a lack of match-ups between satellite imagery and in-situ observations (due to clouds and limited field work opportunities), future work would benefit from the development of a high-resolution numerical model for the Nelson-Hayes estuary. Manitoba Hydro has conducted such modelling using MIKE by DMI, however, open-source models such as Delft3D or FVCOM would promote broader scientific studies of, e.g., river plume spreading and dispersion during various conditions. The incorporation of sea ice coverage in these models is still in early development, with some models incorporating sea ice concentration but not thickness, and others simply assuming a thermodynamically grown smooth ice lid. However, the important role of sea ice and particularly landfast sea ice, in controlling freshwater-marine interactions during the ice-covered period was seen during BaySys (i.e., reductions in tidal mixing, control of river plume dispersion, etc.). The models also need to incorporate wind- and wave-driven mixing to better understand the development of surface stratification and mixed layers. BaySys mooring data (as well as more recent CMO mooring data) can be used to assess wave-driven mixing in partially ice-covered waters (Fig. 3.1.9), however, data analysis was not completed during the BaySys time frame. Thus, future efforts are needed to bring information of ice thickness distributions and wave characteristics into the coastal process models to assess freshwater-marine coupling processes. Such information is increasingly available from satellite remote sensing (see point c above).

h. A major hindrance to furthering our understanding and modelling of the circulation and mixing in the HBC is the lack of, or poor quality, of bathymetric information. Large areas remain uncharted, but where there are soundings we have found that the CHS bathymetric charts often underestimate the actual depth, often quite significantly. Efforts to map out the bathymetry of HBC should be put in place, which would not only significantly improve the oceanographic understanding of HBC but also improve the safety of shipping and travel in the region.

3.1.6 References Cited

The following is a list of publications produced and cited by Teams within the BaySys project.

Andrews, J.A., Babb, D.G., Barber, D.G. (2017). Climate change and sea ice: shipping accessibility on the marine transportation corridor through Hudson Bay and Hudson Strait (1980-2014). *Elementa: Science of the Anthropocene*, 5, 15. https://doi.org/10/1525/elementa.130

Andrews, J.A., Babb, D.G., Barber, D.G. (2018). Climate change and sea ice: shipping in Hudson Bay, James Bay, Hudson Strait, and Foxe Basin (1980-2016). *Elementa: Science of the Anthropocene*, 6, 19. 10.1525/elementa.281

Babb, D.G., Kirillov, S., Kuzyk, Z.A., Netser, T., Liesch, J., Kamula, C.M., Zagon, T., Barber, D.G., and Ehn, J.K. (in review). On the intermittent formation of an ice bridge (*Nunniq*) across Roes Welcome Sound, Northwestern Hudson Bay, and its use to local Inuit hunters. *Arctic*.

Babb et al. (in prep.). The dynamic ice cover of the Nelson Estuary.

Barbedo, L., Bélanger, S., Tremblay, J.-É. (2020). Climate control of sea ice edge phytoplankton blooms in the Hudson Bay system. *Elementa: Science of the Anthropocene*, 8(1), 039. https://doi.org/10.1525/elementa.039

Barber D.G., Harasyn, M.L., Babb, D.G., Capelle, D., McCullough, G., Dalman, L.A., Matthes, L.C., Ehn, J.K., Kirillov, S., Basu, A., Fayak, M., Schembri, S., Papkyriakou, T., Ahmed, M.M.M., Else, B., Guéguen, C., Meilleur, C., Dmitrenko, I., Mundy, C.J., Kuzyk, Z.A., Rysgaard, S., Stroeve, J., and Sydor, K. (2021). Sediment-laden sea ice in southern Hudson Bay: Entrainment, transport, and biogeochemical significance. *Elementa: Science of the Anthropocene*, 9(1), 00108. https://doi.org/10.1525/elementa.2020.00108

Basu, A., McCullough, G.K., Barber, D.G., Sydor, K., Mukhopadhyay, A., Doxaran, D., Bélanger, S., and Ehn, J.K. (in prep.). Characterizing the Nelson/Hayes River plume extent in Hudson Bay using remotely sensed CDOM and suspended sediment data. *Elementa: Science of the Anthropocene*.

Bruneau, J., Babb, D.G., Chan, W., Kirillov, S., Ehn, J.K., Hanesiak, J., Barber, D.G., (2021). The ice factory of Hudson Bay: Spatio-temporal variability of the polynya in northwestern Hudson Bay. *Elementa: Science of the Anthropocene*, 9(1), 00168. https://doi.org/10.1525/elementa.2020.00168

Campbell et al. (in prep.). Wave characteristics in partially ice-covered Hudson Bay waters.

Dmitrenko, I.A., Kirillov, S.A., Babb, D.G., Kuzyk, Z Z, A., Basu, A., Ehn, J.K., Sydor, K., Barber, D.G. (2021). Storm-driven hydrography of western Hudson Bay. *Continental Shelf Res*earch, 227, 104525. https://doi.org/10.1016/j.csr.2021.104525

Dmitrenko, I., Myers, P.G., Kirillov, S.A., Babb, D.G., Volkov, D.L., Lukovich, J.V., Tao, R., Ehn, J.K., Sydor, K., Barber, D.G. (2020). Atmospheric vorticity controls bay-scale circulation in Hudson Bay, *Elementa: Science of the Anthropocene*, 8(1). https://doi.org/10.1525/elementa.049

Eastwood, R.A., Macdonald, R.W., Ehn, J.K., Heath, J., Arragurtainaq, L., Myers, P.G., Barber, D.G., Kuzyk, Z.A., (2020). Role of River Runoff and sea Ice Brine Rejection in Controlling Stratification Throughout Winter in Southeast Hudson Bay. *Estuaries and Coasts*, 43, 756-786. https://doi.org/10.1007/s12237-020-00698-0)

Ehn, J.K., Mukhopadhyay, A., Kirillov, S., Gupta, K., Babb, D.G., Sydor, K., Barber, D.G. (in prep.). Sea Surface Temperature patterns and trends in relation to seasonal sea ice persistence in the Hudson Bay Complex, 2008-2018. *Elementa: Science of the Anthropocene*, manuscript in preparation.

Gupta, K., Mukopadhyay, A., Babb, D.G., Barber, D.G., Ehn, J.K. (submitted). Landfast sea ice in Hudson Bay and James Bay: Annual cycle, variability and trends, 2000-2019. *Elementa: Science of the Anthropocene*, manuscript submitted.

Harasyn, M.L., Isleifson, D., Chan, W., Barber, D.G., (2020). Multi-scale observations of the co-evolution of sea ice thermophysical properties and microwave brightness temperatures during the summer melt period in Hudson Bay. *Elementa: Science of the Anthropocene*, 8(1), 16. http://doi.org/10.1525/elementa.412

Harasyn, M.L., Isleifson, D., Barber, D.G. (2019). The influence of surface sediment presence on observed passive microwave brightness temperatures of first year sea ice during the summer melt period. *Canadian Journal of Remote Sensing*, 23(1), 1–17. 10.1080/07038992.2019.1625759

Kirillov, S., Babb, D.G., Dmitrenko, I., Landy, J., Lukovich, J., Ehn, J., Sydor, K., Barber, D., Stroeve, J. (2020). Atmospheric forcing drives the winter sea ice thickness asymmetry of Hudson Bay. *Journal of Geophysical Research: Oceans*, 125, e2019JC015756. https://doi.org/10.1029/2019JC015756

Landy, J.C., Ehn, J.K., Babb, D.G., Theriault, N., Barber, D.G. (2017). Sea ice thickness in the Eastern Canadian Arctic: Hudson Bay Complex and Baffin Bay. *Remote Sensing of the Environment*, 200, 281-294. 10.106/j.rse.2017.08.019

McCullough, G.K., Kuzyk, Z.A., Ehn, J.K., Babb, D.G., Ridenour, N., Myers, P.G., Wong, K., Koenig, K., Sydor, K., Barber, D.G. (2019). Freshwater-Marine Interactions in the Greater Hudson Bay Marine Region. P. 155–197 in Z.A. Kuzyk and L.M. Candlish, ed., *From Science to Policy in the Greater Hudson Bay Marine Region: An Integrated Regional Impact Study (IRIS) of Climate Change and Modernization.* ArcticNet, Québec City, 424 pp.

Peck et al. (submitted). Hydrography of the under-ice plume of the La Grande River, northeast James Bay, and implications for eelgrass habitat. submitted to *Journal of Geophysical Research*.

Petrusevich, V.Y., Dmitrenko, I., Niemi, A., Kirillov, S., Kamula, M., Kuzyk, Z-Z., Barber, D., Ehn, J.K. (2020). Impact of tidal dynamics on diel vertical migration of zooplankton in Hudson Bay. *Ocean Science*, 16, 337–353. https://doi.org/10.5194/os-16-337-2020

Petrusevich, V.Y., Dmitrenko, I.A., Kozlov, I.E., Kirillov, S.A., Kuzyk, Z.Z.A., Komarov, A.S., Heath, J.P., Barber, D.G., Ehn, J.K. (2018). Tidally-generated internal waves in Southeast Hudson Bay. *Continental Shelf Research*, 167, 65–76. 10.1016/j.csr.2018.08.002

Ridenour, N.A., Hu, X., Sydor, K., Myers, P.G., Barber, D.G. (2019). Revisiting the circulation of Hudson Bay: Evidence for a seasonal pattern. *Geophysical Research Letters*, 46. https://doi.org/10.1029/2019GL082344

Other Works Cited

Anctil, F. and Couture, R. (1994). Impacts cumulatifs du développement hydro-électrique sur le bilan d'eau douce de la baie d'Hudson. *Canadian Journal of Civil Engineering,* 21(2), 297-306. https://doi.org/10.1139/l94-031

Banzon, V., Smith, T.M., Steele, M., Huang, B., and Zhang, H. (2020). Improved Estimation of Proxy Sea Surface Temperature in the Arctic, *Journal of Atmospheric and Oceanic Technology, 37*(2), 341-349. 10.1175/JTECH-D-19-0177.1

Bareiss, J., and Görgen, K. (2005). Spatial and temporal variability of sea ice in the Laptev Sea: analyses and review of satellite passive-microwave data and model results, 1979 to 2002. *Global Planet Change,* 48, 28-54. http://dx.doi.org/10.1016/ j.gloplacha.2004.12.004

Barber, F.G. (1965). Current observations in Fury and Hecla Strait. *Journal of the Fisheries Research Board of Canada*, 22, 225–229.

Barber, F.G. (1967). A Contribution to the Oceanography of Hudson Bay. Department of Mines and Technical Surveys. *Marine Sciences Branch, Manuscript Report Series,* No. 4.

Carmack, E. (2007). The alpha/beta ocean distinction: A perspective on freshwater fluxes, convection, nutrients and productivity in high-latitude seas. *Deep-Sea Research II,* 54, 2578–2598. 10.1016/j.dsr2.2007.08.018.

Flaherty, R.J. (1918). The Belcher Islands of Hudson Bay: Their Discovery and Exploration. *Geographical Review*, 5(6), 433-458.

Hochheim, K. P. and Barber, D.G. (2014). An update on the ice climatology of the Hudson Bay System. *Arctic, Antarctic, and Alpine Research,* 46(1), 66–83.

Hochheim, K. P., and Barber, D.G. (2010). Atmospheric forcing of sea ice in Hudson Bay during the fall period, 1980–2005. *Journal of Geophysical Research*, 115, C05009. http://dx. doi. org/10. 1029/2009JC005334

Hochheim, K. P., Lukovich, J.V., and Barber, D.G. (2011). Atmospheric forcing of sea ice in Hudson Bay during the spring period, 1980–2005. *Journal of Marine Systems,* 88, 476–487. http://dx. doi. org/10. 1016/j. jmarsys.

Ingram, R.G., and Larouche P. (1987). Variability of an under-ice river plume in Hudson Bay. *Journal of Geophysical Research*, 92(C9), 9541-9547.

Kleptsova, O., and Pietrzak, J.D. (2018). High resolution tidal model of Canadian Arctic Archipelago, Baffin and Hudson Bay. *Ocean Modelling,* 128. 10.1016/j.ocemod.2018.06.001.

Krishfield R. A., Proshutinsky, A., Tateyama, K., Williams, W.J., Carmack, E.C., McLaughlin, F.A., and Timmermans, M-L. (2014). Deterioration of perennial sea ice in the Beaufort Gyre from 2003 to 2012 and its impact on the oceanic freshwater cycle. *Journal of Geophysical Research: Oceans,* 119, 1271-1305. 10.1002/2013JC008999.

Last, K. S., L. Hobbs, J. Berge, A. S. Brierley, and F. Cottier (2016). Moonlight drives ocean-scale mass vertical migration of zooplankton during the Arctic Winter. *Current Biology* 26(2) 244–251. 10.1016/j.cub.2015.11.038.

Meier, W.N., (2012). Climate algorithm theoretical basis document (C-ATBD). Passive microwave sea ice concentration. CDRP-ATBD-0107. Version 2, 29 May 2012. Asheville, NC: National Oceanic and Atmospheric Administration Climate Data Record (CDR) Program.

Messier, D., S. Lepage, and S. Margerie (1989). Influence du couvert de glace sur l'étendue du panache de La Grande Rivière (baie James). *Arctic* 42(3) 278–284.

Onstott, R. G., T. C. Grenfell, C. Matzler, C. A. Luther, E. A. Svendsen (1987). Evolution of microwave sea ice signatures during early summer and midsummer in the marginal ice zone. *Journal Geophysical Research: Ocean*. 92 6825–6835. https://doi.org/10.1029/JC092iC07p06825

Park, H., Watanabe, E., Kim, Y., Polyakov, I., Oshima, K., Zhang, X., Kimball, J.S., and Yang, D. (2020). Increasing riverine heat influx triggers Arctic sea ice decline and oceanic and atmospheric warming. *Science Advances*, 6(45), eabc4699. 10.1126/sciadv.abc4699.

Petrusevich, V., Dmitrenko, I.A., Kirillov, S.A., Rysgaard, S., Falk-Petersen, S., Barber, D.G., Boone, W., and Ehn, J.K. (2016). Wintertime water dynamics and moonlight disruption of the acoustic backscatter diurnal signal in an ice-covered Northeast Greenland fjord. *Journal of Geophysical Research: Oceans*, 121(7), 4804-4818.

Prinsenberg, S.J. (1977). Freshwater Budget of Hudson Bay. Canada Department of Fisheries and Oceans Manuscript Report Series No. 5.

Reynolds, R.W., Smith, T.M., Liu, C., Chelton, D.B., Casey, K.S., and Schlax, M.G. (2007). Daily High-resolution Blended Analyses for sea surface temperature. *Journal of Climate*, 20, 5473-5496.

Sadler, H.E. (1982). Water flow into Foxe Basin through Fury and Hecla Strait. *Le Naturaliste Canadien* 109, 701–707.

Saucier F.J., Senneville, S., Prinsenberg, S., Roy, F., Smith, G., Gachon, P., Caya, D., and Laprise, R. (2004). Modelling the sea ice-ocean seasonal cycle in Hudson Bay, Foxe Basin and Hudson Strait, Canada. *Climate Dynamic*, 23, 303–326.

Straneo, F., and Saucier, F.J. (2008). The Arctic–Subarctic exchange through Hudson Strait. Pp. 249–262 in *Arctic–Subarctic Ocean Fluxes: Defining the Role of the Northern Seas in Climate*., R. R. Dickson, J. Meincke and P. Rhines, Eds. Springer Science + Business Media.

St.-Laurent, P., Straneo, F., Dumais, J-F., and Barber, D.G. (2011). What is the fate of the river waters of Hudson Bay? *Journal of Marine Systems*. 88, 352–361.

Stroeve, J. C., Serreze, M.C., Holland, M.M., Kay, J.E., Malanik, J., and Barrett A.P. (2012). The Arctic's rapidly shrinking sea ice cover: a research synthesis. *Climatic Change*, 110, 1005–1027. https://doi.org/10.1007/s10584-011-0101-1

3.2 Freshwater System (Team 2)

Team Member	Affiliation	Tasks Contributed To				Role
Tricia A. Stadnyk	a, b, c	2.1	2.2	2.3	2.4	Science Lead
Kristina A. Koenig	d	2.1	2.2	2.3	2.4	Hydro Lead
Stephen J. Déry	c	2.1	2.2	2.3	2.4	Contributor
Genevieve A. Ali	e	2.1	2.2	2.3	2.4	Contributor
Matthew K. MacDonald	a	2.1	2.2	2.3	2.4	Contributor
Andrew A. G. Tefs	a, b	2.1	2.2	2.3	2.4	Contributor
Scott Pokorny	a	2.1	2.2	2.3	2.4	Contributor
Rajtantra Lilhare	c	2.1	2.2	2.3	2.4	Contributor
Bunu Gauli-Sharma	c	2.1	2.2	2.3	2.4	Contributor
Marie Broesky	a	2.1	2.2	2.3	2.4	Contributor
Matthew Hamilton	a	2.1	2.2	2.3	2.4	Contributor
Rodell Salonga	a	2.1	2.2	2.3	2.4	Contributor
Phil Slota	d	2.1	2.2	2.3	2.4	Collaborator
Michael Vieira	d	2.1	2.2	2.3	2.4	Collaborator
Shane Wruth	d	2.1	2.2	2.3	2.4	Collaborator
Mark Gervais	d	2.1	2.2	2.3	2.4	Collaborator
John Crawford	d	2.1	2.2	2.3	2.4	Collaborator
Catherine Guay	f	2.1	2.2	2.3	2.4	Contributor
Nathalie Thiemonge	g	2.1	2.2	2.3	2.4	Collaborator
Isabelle Chartier	f	2.1	2.2	2.3	2.4	Collaborator
Frédéric Guay	f	2.1	2.2	2.3	2.4	Collaborator
Vincent Fortin	f	2.1	2.2	2.3	2.4	Collaborator
Marco Braun	h	2.1	2.2	2.3	2.4	Contributor
David Gustafsson	i	2.1	2.2	2.3	2.4	Collaborator
Kristina Isberg	i	2.1	2.2	2.3	2.4	Collaborator
Berit Arheimer	i	2.1	2.2	2.3	2.4	Collaborator

a) Department of Civil Engineering, University of Manitoba, Winnipeg, Manitoba, Canada
b) Department of Geography, University of Calgary, Calgary, Alberta, Canada
c) Department of Civil and Environmental Engineering, University of Northern B.C., Prince George, B.C., Canada
d) Hydrologic and Hydroclimatic Studies Division, Manitoba Hydro, Winnipeg, Manitoba, Canada
e) Department of Geology, University of Manitoba, Winnipeg, Manitoba, Canada
f) Institut de recherche d'Hydro-Québec, Hydro-Québec, Varennes, Québec, Canada
g) Innovation, équipment, et services partagés d'Hydro-Québec, Hydro-Québec, Montréal, Canada
h) Groupe pour scénarios et services climatiques, Ouranos, Sherbrooke, Québec, Canada
i) Hydrologic Research Unit, Swedish Meteorological and Hydrological Institute, Norrköping, Östergötlands, Sweden

3.2.1 Introduction and Objectives

The timing and volume of freshwater delivered to Hudson Bay impacts the formation and dynamics of Hudson Bay sea ice and the bay's biogeochemical processes (Ingram et al., 1996; Eastwood et al., 2020). Terrestrial runoff of the Hudson Bay Drainage Basin (HBDB) is a major contributor of freshwater to Hudson Bay along with sea ice melt and precipitation (Granskog et al., 2011).

Over the previous five decades, major hydroelectric complexes in the La Grande Rivière Complex (LGRC) and the Nelson Churchill River Basin (NCRB), including the Lower Nelson River Basin (LNRB), have had effects not only on the timing of freshwater discharge but also on the volume by location (due to diversions), with both basins considered as "strongly affected" by river channel fragmentation and flow regulation (Dynesius & Nilsson, 1994). Changes to this water entering western Hudson Bay (from the NCRB) and eastern James Bay (from the LGRC) are a possible driver of changes to sea ice distribution and thickness (Anctil & Couture, 1994). This regulation aims to impound spring and summer flows to be used to generate power over the winter, when power-demand is highest, resulting in a "flattening" of the annual hydrograph (Déry et al., 2011).

Coinciding with an increased number of regulated reservoirs, freshwater runoff regimes of the HBDB are being affected by a changing climate. Shorter, warmer winters have increased winter runoff with a less significant spring freshet, seen in northwestern Canada (DeBeer et al., 2016), and the Arctic as a whole (Bring et al., 2017; Gelfan et al., 2017). The effect of this change on discharge is seen in interannual and interdecadal variability of freshwater discharge to Hudson Bay, both regulated and unregulated (Déry et al., 2018).

Distinguishing the effects of regulation and climate change on freshwater and predicting their long-term effects is a scientific priority among northern, hydroelectrically developed countries (Arheimer et al., 2017), but has yet to be attempted for Hudson Bay and other high-latitude Canadian basins due to data sparsity and difficulties associated with incorporating reservoir controls into continental-scale hydrologic models (Wada et al., 2017).

Beyond the challenges of accurate (or even sufficient) modelling in an environment as large and heterogeneous as the HBDB, uncertainty in long-term, large-scale climate studies is a pressing concern. This is particularly true when projecting results into the future (Beven, 2007). To quantify and allocate uncertainty to specific steps in the modelling process, multi-model studies (Chen et al., 2011; Clark et al., 2016) using climate-ensembles (Tebaldi & Knutti, 2007) and robust uncertainty analyses (Ajami et al., 2007) are necessary to report results with any confidence or authority. Not only is there a desire to quantify the total propagated uncertainty in a modelling study, but also to partition individual contributions from individual modelling steps towards the total uncertainty envelope. This information can guide water resource practitioners as to where it is most beneficial to invest their time and effort in the modelling process.

To address the challenges and opportunities discussed above, the overall goal of this work is to produce, (as much as is feasible) a complete dataset of terrestrial hydrology, discharge records, and discharge uncertainty bounds for the freshwater reaching the Hudson Bay Complex (HBC) (shown in Figure 3.2.1) from 1981 to 2070. These records will be used to complement historic fieldwork studying sea ice and biogeochemical processes in the HBC. They will further be used to analyse projected hydrologic change for the HBDB and will make up a portion of the input for oceanographic modelling describing circulation dynamics and sea ice formation in Hudson Bay. To achieve this, the work of the freshwater modelling group falls into four primary objectives (below) corresponding to (but with scope changes from) the four BaySys tasks assigned to Team 2 (Barber et al., 2014).

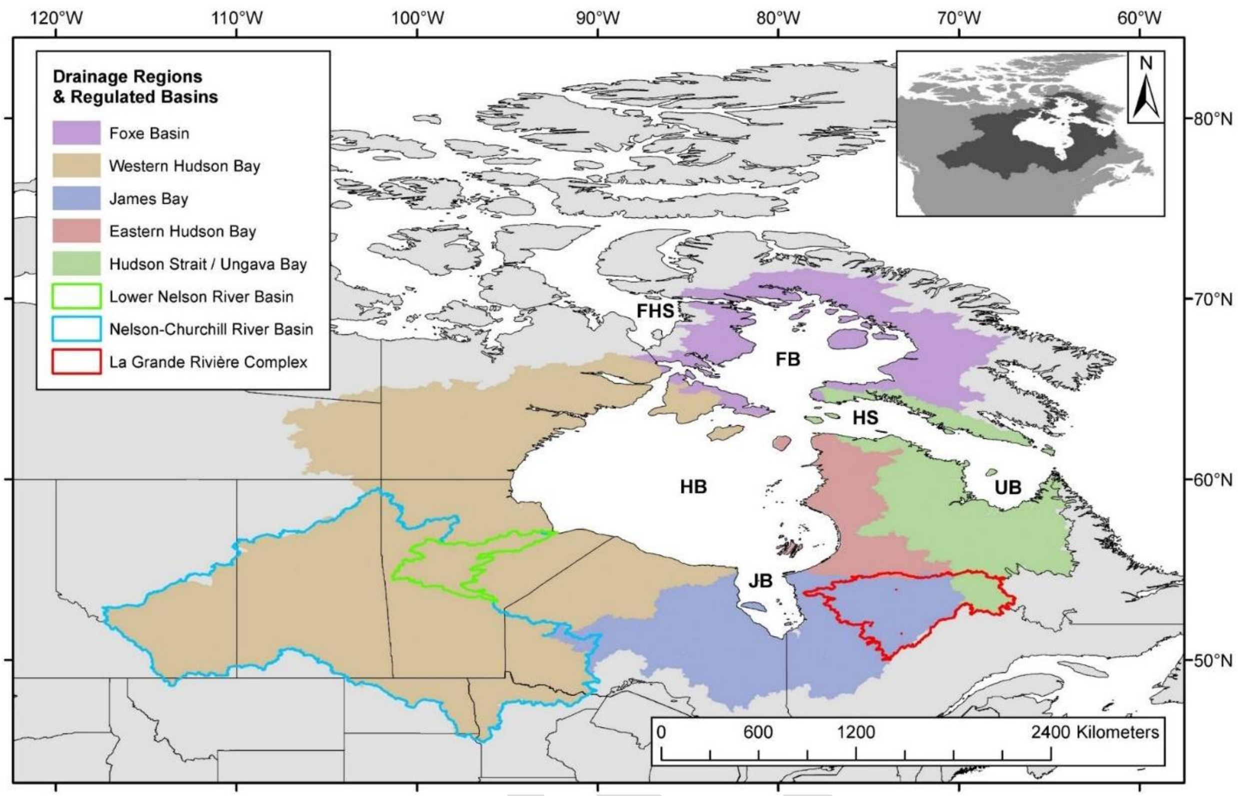

FIGURE 3.2.1 Major drainage regions of the HBDB contributing discharge to HBC regions: Hudson Bay (HB), James Bay (JB), Ungava Bay (UB), Hudson Strait (HS), Foxe Basin (FB), and Fury and Hecla Strait (FHS).

"The objective of Team 2 is to investigate the role of freshwater timing and magnitude on contemporary and future projections of freshwater-marine coupling in Hudson Bay as a means of understanding the relative contributions of regulation and climate change to the system. Results from this Team will be central to the ability of other Teams to evaluate the impacts of climate change and hydroelectric regulation on the physical, biological, and biogeochemical processes in Hudson Bay." The tasks associated with Team 2 are as follows:

2.1) Continental-scale HBDB hydrologic modelling
2.2) Uncertainty assessment of LNRB discharge
2.3) Regulated NCRB and LGRC modelling
2.4) Uncertainty assessment of HBDB discharge

These goals and the interconnected steps required to complete them are summarized in a workflow diagram (Phase 1 Report; Figure 9.2 and Table 9.1). The methods and processes used to generate the data are explained in Section 3.2.2, with a summary of results shown in Section 3.2.3. Each of these objectives contributes to a greater understanding of the changing face of freshwater as it reaches the HBC, the contributing influences of climate change and regulation, and understanding the uncertainties inherent in this modelling. Using these results as the terrestrial runoff in oceanographic modelling, BaySys will increase the understanding of sensitivities of oceanographic modelling to freshwater, as well as projecting an ensemble of possible futures for the physical, biological, and biogeochemical processes in Hudson Bay.

The structure of this chapter is the following: Section 3.2.1 introduces the background and goals of Team 2; Section 3.2.2 summarizes the literature review and describes the methods used or adapted; Section 3.2.3 summarizes the results of Team 2's analysis using methods from the previous section and discusses any uncertainty introduced by these methods and further discusses the larger implications of the results in the context of BaySys, and Section 3.2.4 explores remaining gaps and recommends future work in the domain of HBDB terrestrial freshwater systems.

3.2.2 Analysis and Methods

Continental-scale HBDB Hydrologic Modelling

A robust climatic input ensemble was selected prior to hydrologic modelling. This began with selecting a set of 14 General Circulation Models (GCMs) varyingly coupled with Representative Concentration Pathways (RCPs) 4.5 and 8.5 for a total of 19 climate simulations. These were selected from a larger ensemble of 154 HBDB-appropriate simulations available through the Coupled Model Intercomparison Project Phase 5 (CMIP-5; Taylor et al., 2012). The HydroGFD reanalysis climate product (Berg et al., 2018) was chosen as the primary reference dataset product (for bias correction) and hydroclimatic input (for model calibration) following consultation with Manitoba Hydro and Team 6 (oceanographic modelling). This product was chosen because it is: (1) near real-time and would provide overlapping "observed" data during the BaySys fieldwork cruise(s) ; (2) an ERA-based product, therefore consistent with forcing used in the oceanographic Nucleus for European Modelling of the Ocean (NEMO; Madec et al., 2008) model described in Chapter 3.6; (3) a high fidelity reanalysis product used by the Swedish Meteorological and Hydrological Institute (SMHI); and (4) globally available at a resolution consistent with continental-scale modelling (0.5° x 0.5° grid resolution).

Once bias-corrected (Chen et al., 2013), input was prepared for use in hydrologic models using two methods to assign gridded GCM data to sub-basin scale. A set of hydrologic input was developed first (called "version 2.0") using Inverse Distance Weighting (IDW; Lu & Wong, 2008) and a second (called "version 2.1") using the Nearest Neighbour (NN) method. IDW was selected and the optimal radius calibrated based on a sensitivity study of the Arctic domain. A large radius produced the smallest pan-Arctic RMSE but was found to create local errors in specific basins. Appendix B summarises those datasets and domains which use version 2.0 and 2.1.

These interpolation errors arose due to the interpolation radius exceeding the extents of the data frame (in the HBDB) in some watersheds and the watershed orientations. Those sub-basins with the largest errors were those closest to Hudson Bay itself and the borders of the data frame (nearer to bordering watersheds) for which no climatic data could be aggerated. Sub-basins in larger watersheds sample a larger number of grids within their watershed, and as such, local errors in individual sub-basins are more likely to be averaged out. These local errors were particularly noted in sub-basins where the climatic gradient was most pronounced from one watershed to the next, such as the LGRC.

For calibration of the hydrological models, observed discharge datasets were compiled. This included contributions from the Water Survey of Canada (WSC), Manitoba Hydro, Hydro-Québec, and Ontario Power Generation. Upstream nodes were calibrated using WSC gauges available publicly through their website. These include streamflow records for regulated (Tasks 2.1 and 2.3) and natural (Tasks 2.1 and 2.2) gauges. To quantify calibration performance at the outlets to the HBC, adjusted and gap-filled records were used, as developed for the 44 largest rivers draining Hudson Bay, James Bay, and Ungava Bay (Déry et al., 2005, Déry et al., 2016). Split-sample calibration and validation using these records were performed over the reference period 1981-2010, with the first five years of each decade included in the calibration record and the last five included in the validation record.

Task 2.1 also comprised the development of continental-scale runoff models of two domains. These models are used together to provide input (in the form of discharge at the river outlets) to the NEMO model. The hydrologic model selected was the HYdrological Predictions for the Environment (HYPE) model (Lindström et al., 2010) developed by the SMHI Hydrologic Research Unit. It was chosen for its strength in physically-based modelling, particularly in cold regions (i.e., snow accumulation, snow melt, frozen rivers) and continental-scale hydrologic modelling (Pechlivanidis & Arheimer, 2015). It was also preferred to other models because it is an open-source model onto which new processes have been added according to BaySys needs. Calibration within the HBDB was run using Markov Chain Differential Evolution (MCDE; Vrugt et al., 2009) for a robust calibration with built-in sensitivity analysis.

Hydrologic modelling of the Arctic domain was done using Arctic-HYPE (AHYPE) configuration (Andersson et al., 2015) of HYPE using BaySys climate forcing. The AHYPE model is an application of the HYPE model extending over the complete Arctic drainage basin (excluding Greenland), calibrated to Arctic-HYCOS and GRDC datasets. The gap-filled Dai & Trenberth (2002) dataset was also used to drive the NEMO model (oceanographic model developed by Team 6, Chapter 3.6) beyond the Arctic domain, extending globally to 20° south. The AHYPE model provides boundary discharge input at a monthly resolution at 3002 Arctic Ocean outlets beyond the HBC. This water mixes with that of the HBC domain through the Hudson Strait (eastern) and the Hecla and Fury Strait (northwestern) as shown in Figure 3.2.1. Reducing the AHYPE model to only the Hudson Bay domain and improving key functions (frozen soil infiltration, non-contributing areas, reservoir regulation), the Hudson HYPE (HHYPE) model was created, which is used to provide monthly data to NEMO at 398 HBC rivers. Greenland ice sheet runoff is provided to the oceanographic model from the Regional Atmospheric Climate MOdel dataset (RACMO; van Meijgaard et al., 2008)

The development of the new HYPE model processes and calibration strategies are detailed in Stadnyk et al. (2020). Two new model processes are added, first to simulate runoff from ephemerally disconnected drainage and prairie non-contributing areas (NCAs) and second to improve the representation of routines related to flow into and through frozen soils. A structural process was added by clustering physiographically similar lakes to bypass individual calibrations (there are 7600 lakes in the HBDB, with three parameters each). Calibration confidence was improved by clustering observation gauges according to groups of flow signatures and selecting a balanced number of gauges from each flow-signature cluster, for a total of 101 regulated and natural gauges. This method was compared against four sets of 101 random gauges, which were calibrated using the same calibration methodology. This finalized model is summarized in Appendix B, Table 2.1-2.

Monthly discharge from the Arctic Ocean outlets beyond the HBC has been generated using 5 members of the 19 BaySys climatic input ensemble (1981 to 2070) and the AHYPE model. As discussed in Chapter 6, only three of the selected BaySys GCM model simulations include sufficient variables to be used for NEMO modelling. Only these models (and their associated RCPs, for a total of five sets of input) were modelled in AHYPE. Spatial and temporal trends will be analysed from this model (Stadnyk et al., 2021). This sub-set of climatic inputs represent the greatest changes to runoff (MRI-CGCM3, RCP 4.5 and 8.5), changing runoff similar to the 19-member ensemble mean (GFDL-CM3, RCP 4.5), and runoff changes in the lower quartile of the ensemble (MIROC5, RCP 4.5 and 8.5), with the sub-set representation summarized in Braun et al. (2021).

Uncertainty Assessment of LNRB Discharge

The goal of Task 2.2 was a sensitivity study of the Lower Nelson River Basin (LNRB) and uncertainty study of the total discharge from the Nelson River. This was done by examining the sensitivity and associated uncertainty caused by input, model structure, model component selection, parameter optimization, and the output data used in the calibration process. In the LNRB itself, multiple historic reanalysis climatic data products are examined at a 10km grid resolution to establish basin and sub-basin uncertainty, as summarized in Appendix B, Table 2.2-1. Beyond the LNRB, the watersheds that drain this region (NCRB) are examined to establish their spatial and temporal correlation to observed data (Lespinas et al., 2015; Asong et al., 2017). For all simulations, the LNRB models were forced using observed records where upstream flows from the greater Nelson-Churchill watershed enter the LNRB.

The hydrologic sensitivity and associated discharge uncertainty of the LNRB in a semi-distributed model, the Variable Infiltration Capacity (VIC; Liang et al., 1994) model was examined. Using the 10km LNRB historic reanalysis datasets, a range of climatic input values were created for the LNRB. This range of input was fed to VIC and three other hydrologic models: Hydrologic Engineer Center – Hydrologic Modelling System (HEC-HMS; Charley et al., 1995); WATerloo FLOOD forecasting system (WATFLOOD; Kouwen, 1988); and a truncated version of the HHYPE model. A set of sensitive parameters and ranges for each model was developed using temporally variant Variogram Analysis of Response Surfaces (VARS; Razavi & Gupta, 2016), which produces information describing time-variant parameter sensitivity (Bajracharya et al., 2020). Following this, a Generalized Likelihood Uncertainty Estimate (GLUE; Beven & Binley, 1992) analysis was run to associate total uncertainty with input and parameter optimization. The parameter sets used in the GLUE analysis were selected using Orthogonal Latin Hypercube Sampling (OLHS: Gan et al., 2014) such that parameters had selection density proportional to their sensitivity.

Climatic studies include historical reanalysis dataset comparisons in the industrially significant and remote (data-sparse) LNRB (Lilhare et al., 2019) and input uncertainty estimates in the larger upstream basin of the NCRB (Pokorny et al., 2020 (a)). The VIC hydrologic model has been studied based on parameter optimization, optimization objective, model structure (using multiple combinations of optional model processes), and input (using multiple reanalysis datasets) in the LNRB, assessing sensitivity and associated uncertainty of projected discharges (Lilhare et al., 2019, 2020) using VARS. The addition of three other hydrologic models (HHYPE, HEC-HMS, WATFLOOD) and further uncertainty analysis using VARS, OLHS, and GLUE analyses have been used to develop daily probability curves (daily, 1981 to 2070) for the Nelson River discharge (Pokorny et al., 2020 (b)), with datasets used summarized in Appendix B, Table 2.2-2.

Regulated NCRB and LGRC Modelling

The effects of regulation (for hydroelectric power generation) on discharge volume and timing are well-noted in the HBDB as a major effect on freshwater discharge regimes in the last century (Anctil & Couture, 1994; Déry et al., 2011). The role of reservoir regulation in freshwater dynamics in HYPE is noted as a source of modelling error at the continental scale (Pechlivanidis & Arheimer, 2015). To confidently differentiate the effects of climate change and regulation on freshwater discharge, two versions of the HHYPE model were developed: one with improved regulation in the NCRB and LGRC ($HHYPE_{REG}$), one with all forms of regulation removed throughout the entire model, called the naturalized model (or $HHYPE_{NAT}$).

The NCRB and LGRC were selected due to their large effects on the outflow timing or volume (due to diversions) to Hudson Bay and James Bay, respectively. Other HBDB heavily fragmented river systems, such as Moose River (Dynesius & Nilsson, 1994), were excluded from this analysis. Although they feature regulation points, the regulation of Moose and Albany Rivers was not found to affect timing or volume of water to Hudson Bay significantly at the scale analysed (monthly to seasonal). Similarly, although many major river systems in the Arctic contain substantial regulation (i.e., the Ob River), significant barriers to data availability (regarding foreign observed datasets and regulation practices) prevented a full analysis at this time. HBC flow dynamics are also assumed to be insensitive to these effects at the monthly resolution over the Arctic Domain. Further analyses including the pan-Arctic Rivers have been conducted in Stadnyk et al. (2021) and on regulated rivers across North America (Déry et al., 2021).

Task 2.3 comprised the creation of regulated discharge predictions for the NCRB and LGRC basins. This was done by (1) embedding regulation directly into HHYPE in the NCRB (Tefs et al., in revision (a)) and (2) coordinating modelling efforts with Hydro-Québec for the LGRC. Together, these results are known as $HHYPE_{REG}$. The results of the $HHYPE_{REG}$ (Appendix B, Tables 2.3-2 and 2.3-3) model (forced using the climatic ensemble, daily 1981 to 2070 inclusive) have been distributed for Tasks 2.2 and 2.4 to help generate uncertainty results for the LNRB and HBDB, respectively. The naturalized HHYPE model ($HHYPE_{NAT}$; Appendix B, Table 2.3-1) with diversions, regulation, and land-cover changes removed has been analysed, comparing the climatic ensemble results of $HHYPE_{NAT}$ and $HHYPE_{REG}$ (Tefs et al., in revision (b)).

Uncertainty Assessment of HBDB Discharge

Hydrologic modelling involves numerous assumptions and processes, which introduce modelled uncertainty. We build on the analytical framework proposed for stochastic uncertainty (Montanari & Koutsoyiannis, 2012). For BaySys Task 2.4, this method was adapted to numerically incorporate cascading uncertainty, as has been applied to hydrologic ensembles in a practical manner (Chen et al., 2011; Her et al., 2016) and proposed conceptually (Figure 3.2.2;

Clark et al., 2016) as a critical step for accurately quantifying uncertainty in hydrology. This method includes downscaling, structure, parameter, and output uncertainty, making use of the more robust stochastic methods (Courbariaux et al., 2017). The modelled variance explained by climate input (Vehtari et al., 2017) selection is explained for BaySys (Stadnyk et al., 2019), but not included in this analysis.

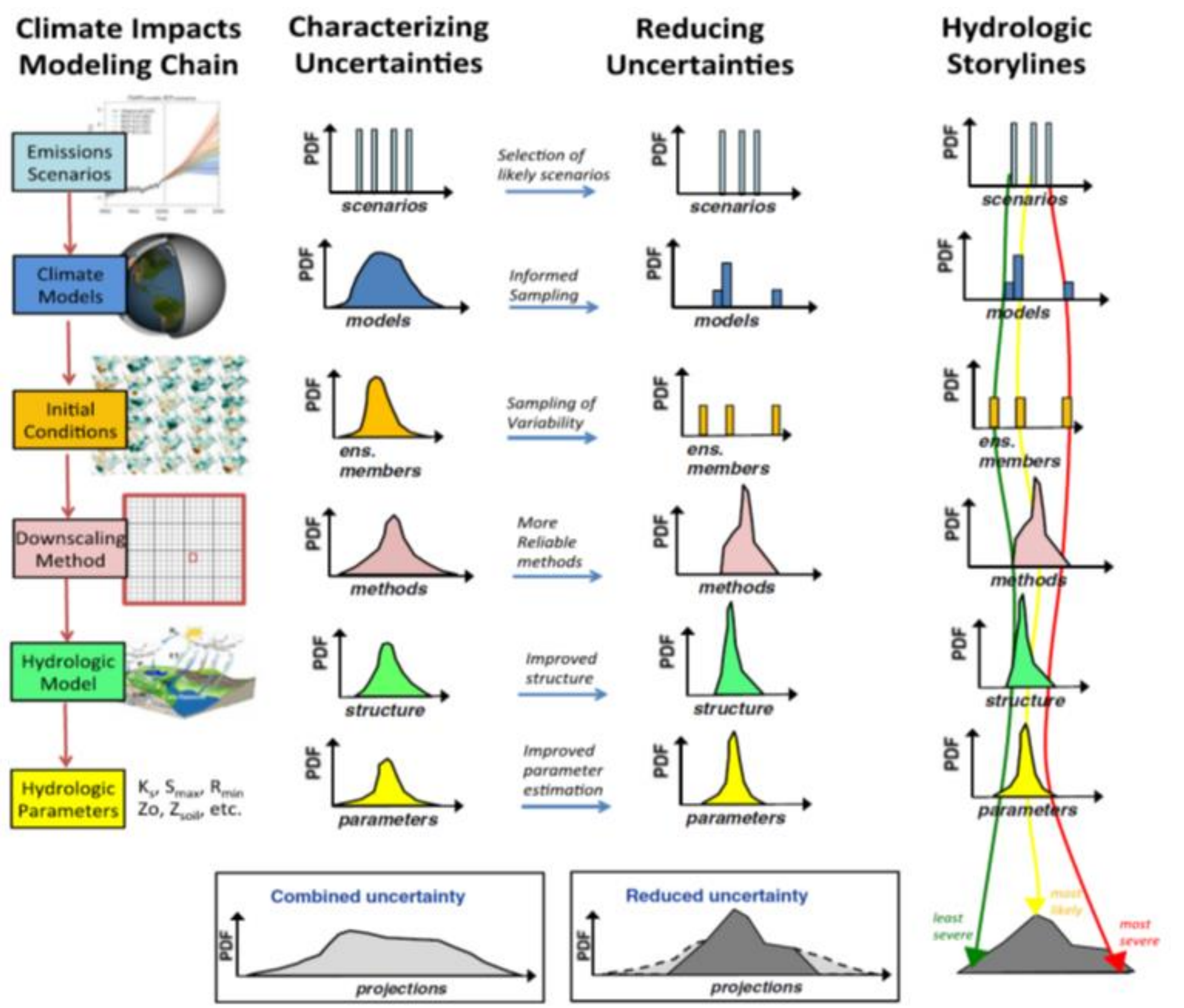

FIGURE 3.2.2 Cascading uncertainty framework (from Clark et al., 2016) to reduce overall uncertainty to hydrologic storylines.

The method develops multiple "hydrologic storylines" (Clark et al., 2016) which correspond to climate input used for NEMO oceanographic modelling. The selection of base-case hydrologic output used was similar to the original selection methodology for the BaySys climatologic ensemble (Casajus et al., 2016; Stadnyk et al., 2019).

Accounting for downscaling uncertainty was performed for the modelled error relative to HydroGFD simulation. We did so by creating a distribution of expected residuals (ensemble minus HydroGFD) for the equivalent historic quantile. By assessing the relative uncertainty (daily, by watershed) of the process of converting gridded data to sub-basin data, we examine the skill of downscaling. Ensemble downscaling uncertainty is assessed by modifying Normal Quantile Transformation (NQT; Krzysztofowicz & Kelly, 2000). NQT has been extensively used for predictive hydrologic forecasting (Weerts et al., 2011; Verkade et al., 2017), by developing ensemble predictions relative to residuals, adapting the Model Univariate Conditional Processor (MUCP; Coccia & Todini, 2011).

As parameter and structural uncertainty are only accounted for in 12 of the basins making up the LNRB (from Task 2.2), methods of Prediction in Ungauged Basins (PUB; Westerberg et al., 2016) were adapted by using basin flow signatures (Donnelly et al., 2016; Stadnyk et al., accepted), combined for a weighted average of multiple basins (de Levanne & Cudennec, 2019) accounting for the relative wetness and dryness of basins (Hong et al., 2006; Bourgin et al., 2015). Input data are analysed as a monthly antecedent precipitation record, where the number of antecedent months affecting output varies by month. This leverages the input record for the most efficient use of input data affecting that day's output, similar to "catchment memory" and input/output elasticity theory (Andréassian et al., 2016).

Overall, this method maximizes the use of available data (Tasks 2.1, 2.2, and 2.3) while returning probabilistic predictions of future uncertainty conditional on past observations and models (Koutsoyiannis, 2016). Using this analysis, quantification of the relative impacts of ensemble variability, inter-annual climatic variability, climatic ensemble sub-setting (such as those used as input to NEMO), and modelling uncertainty can be evaluated regionally and seasonally.

To apply the model structural and parametric uncertainty bounds calculated in Task 2.2, we have applied PUB methods to transfer uncertainty based on climatic conditions and dominant model processes. By computing quantile regressed limits of parametric and structural uncertainty, we can infer relative daily uncertainty of a watershed discharge for watersheds where we have not performed the (extremely computationally intensive) uncertainty study described in Task 2.2. This method makes use of the full limits of the input minimum/maximum structure and parameter assessment developed in Task 2.2 (Pokorny et al., 2019).

Selection of "most-change" discharge record used as the "seed" was justified using two metrics ($|\Delta\mu|$ and $\Delta\sigma$) of future change (2011 to 2040, 2041 to 2070) relative to historic (1981 to 2010) conditions. This method preserves the spatial and temporal coherence of individual climatic input while accounting for the potential uncertainty inherent in selection and hydrologic modelling. To link daily discharge values to downscaling uncertainty, precipitation is converted to antecedent precipitation. The result of this operation (for each river in the HBDB) is a monthly computation of the number of antecedent months affecting output optimized using least squares regression. This "most-change" seed will be used to model oceanographic sensitivity to freshwater uncertainty, being distributed to Team 6. Regional uncertainty of rivers has been assessed in the HBC and this uncertainty compared to inter-annual variability and intra-ensemble variability seasonally for 30-year climatic periods (Tefs et al., in preparation).

3.2.3 Results and Discussion

Team 2 presents the results of their analyses following four Team tasks that were established at the onset of the BaySys project and discusses them within the greater context of the Team's objectives, and overarching project.

> **Task 2.1 Continental-scale HBDB hydrologic modelling -** to quantify freshwater export into Hudson Bay under diverse projected future climate scenarios.

> **Task 2.2 Uncertainty assessment of LNRB discharge -** to quantify modelling and parameter uncertainty for future flow projections, and to provide higher-resolution hydrologic outputs for the LNRB.

> **Task 2.3 Regulated NCRB and LGRC modelling -** to incorporate regulation effects into projected freshwater exports for two major rivers in the Hudson Bay drainage system: the LNRB and La Grande Rivière.

> **Task 2.4 Uncertainty assessment of HBDB discharge -** to quantify the relative impacts of climate change from those caused by regulation on the timing and magnitude of freshwater export into Hudson Bay.

Continental-scale HBDB Hydrologic Modelling (Task 2.1)

Details of the study domain, the selected climatic ensemble, and the selection of HYPE as the primary hydrologic modelling system for the region have been compiled in the freshwater section of the Integrated Regional Impact Study (IRIS) for Hudson Bay (Chapter 3, Stadnyk et al., 2019). The gridded datasets which make up the climatic input ensemble (1981-2070) were bias-corrected by the Ouranos Consortium using quantile mapping referencing HydroGFD over the historic period 1981-2010, with their skill quantified (Braun et al., 2021).

Selection of climate models was done using cluster analysis on 10 metrics of climate change (between 1981-2010 and 2041-2070). This sub-set of 19 ensemble members was shown to express 87% of ensemble variability of the 154 CMIP-5 members compatible with the modelling done in BaySys (Stadnyk et al., 2019) metrics and sample variability shown in Figure 3.2.3. Using these climate models as input, HYPE projects overall seasonal discharge trends, shown to increase in all seasons in the past (significant using a 5% confidence Mann-Kendall test for winter-only; Figure 3.2.4a) and future (significant for same in all seasons; Figure 3.2.4b). Further analysis of the continental and regional changes in climate was performed in Braun et al. (2021).

Clustering Criteria	
Changes (Δ) to	annual mean temperature
	annual mean precipitation
	spring mean temperature
	summer mean temperature
	fall mean temperature
	winter mean temperature
	spring mean precipitation
	summer mean precipitation
	fall mean precipitation
	winter mean precipitation

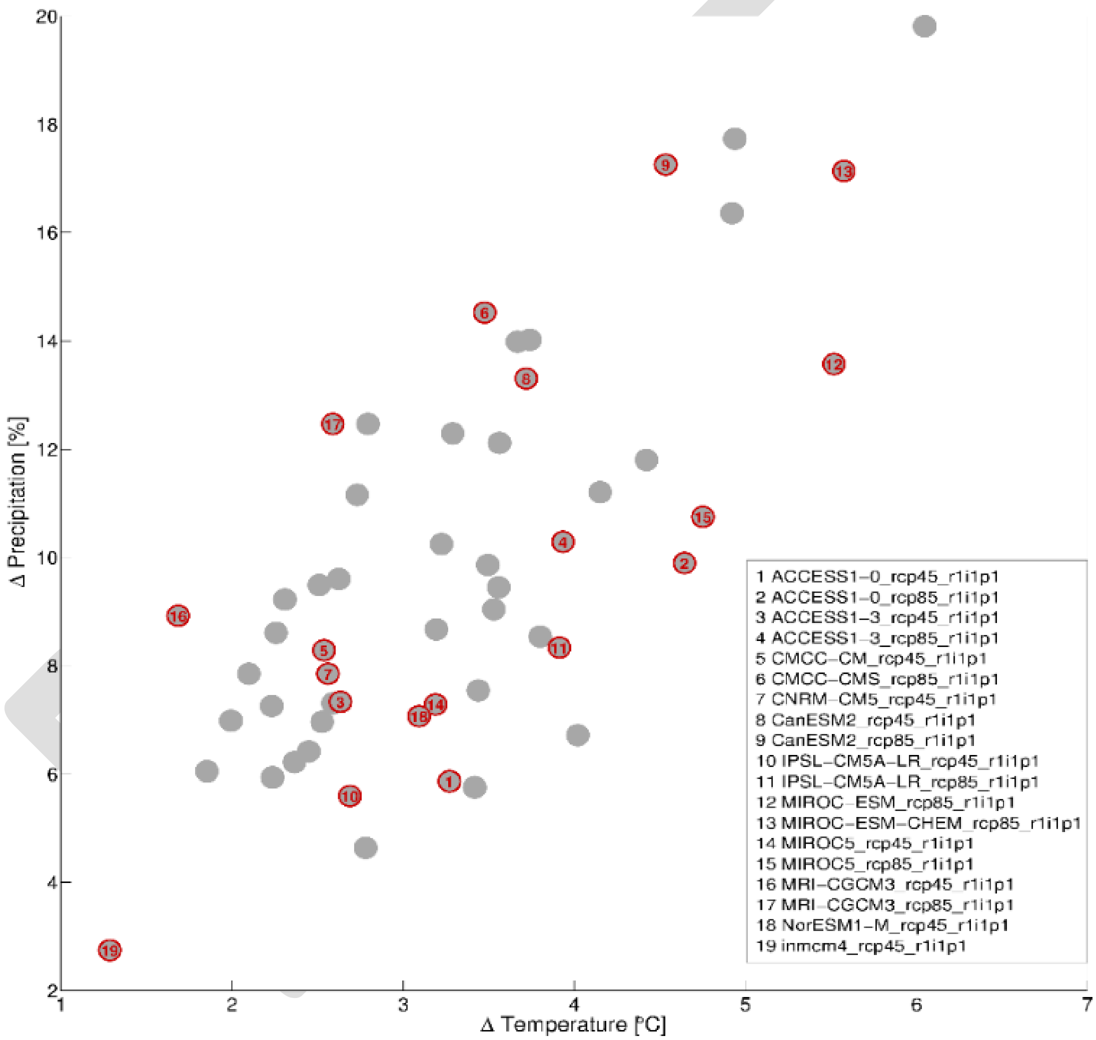

FIGURE 3.2.3 Climate model clustering criteria and model-ensemble selected for BaySys simulation (shown for two of ten criteria). Reproduced from: Stadnyk et al., 2019 (Table C-1, Figure C-2).

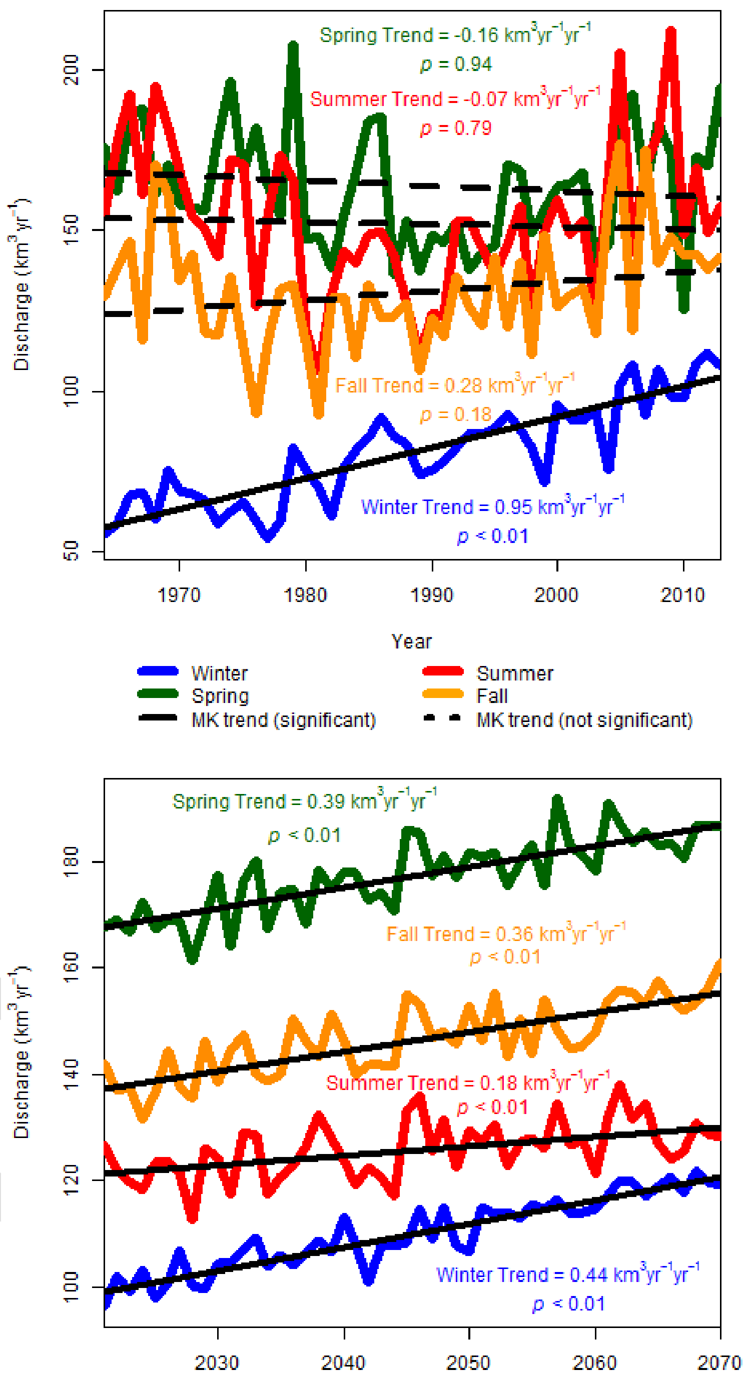

FIGURE 3.2.4 Seasonal trend analyses and significance of discharge for 21 gauged HBDB rivers for (a) observed, historical (1964-2013) period and (b) simulated, future (2021-2070) period where reservoirs are calibrated using default HYPE regulation. Reproduced from: Stadnyk et al., 2019 (Figures 13 and 17).

Analyzing 21 rivers draining to Hudson Bay against gauged records, distinct trends emerge between regulated and unregulated rivers (Déry et al., 2018), such as increasingly divergent interannual coefficients of variation (Figure 3.2.5). They further show increasingly flattened hydrographs in regulated and (less so) unregulated rivers from 1960 to 2016. This analysis shows the importance of weekly hydropeaking (reduced weekend flows coincident with lower energy demand) in rivers regulated for hydroelectric generation (Figure 3.2.6). Comparison of the spectral decomposition of the observed discharge shows the effect of regulation on sub-weekly discharge periodicity, with annual freshet periodicity still present, but weakened (Figure 3.2.7).

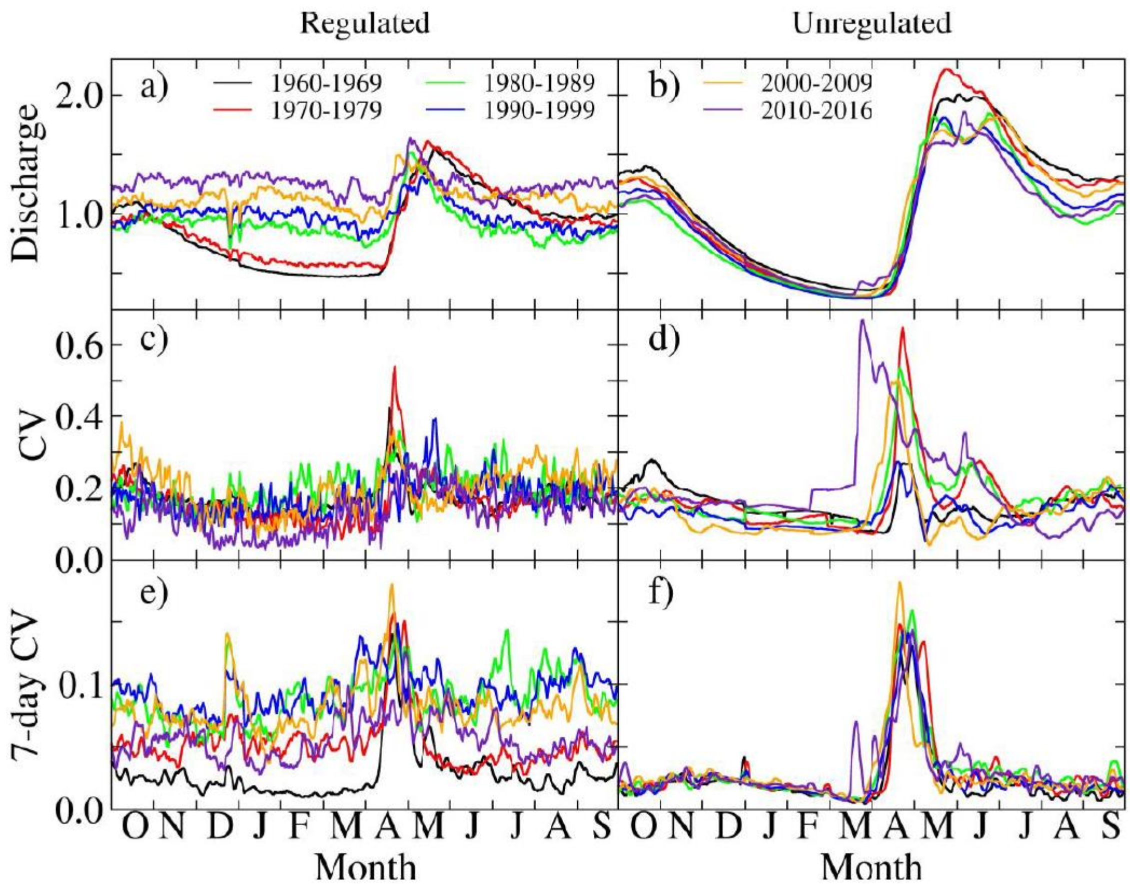

FIGURE 3.2.5 Decadal water year hydrographs for total outflow from the sum of 21 gauged HBDB rivers of the (a, b) normalized mean, (c, d) coefficient of variation, and (e, f) coefficient of variation in 7-day moving windows of daily discharge for regulated and unregulated rivers, 1960-2016. Reproduced from: Déry et al., 2018 (Figure 2).

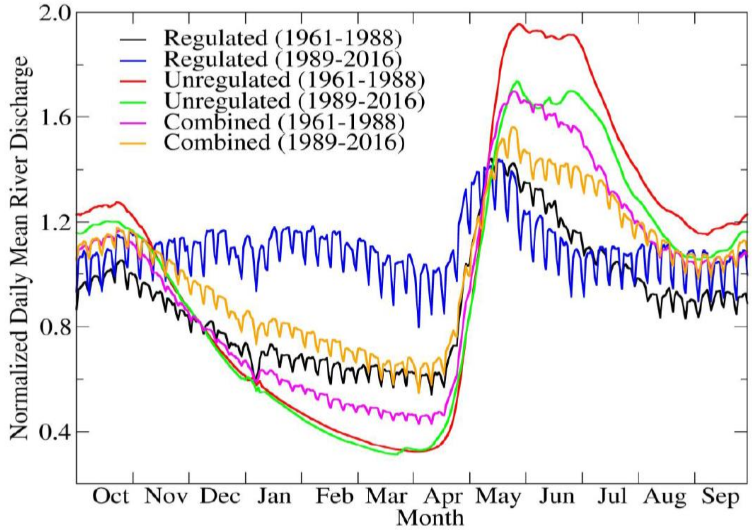

FIGURE 3.2.6 Water year hydrographs of the normalized mean daily discharge for regulated (sum of four rivers), unregulated (sum of 17 rivers), and combined rivers (sum of 21 gauged rivers) considering the day of the week during an early (1961-1988) and a late (1989-2016) period. Reproduced from: Déry et al., 2018 (Figure 3).

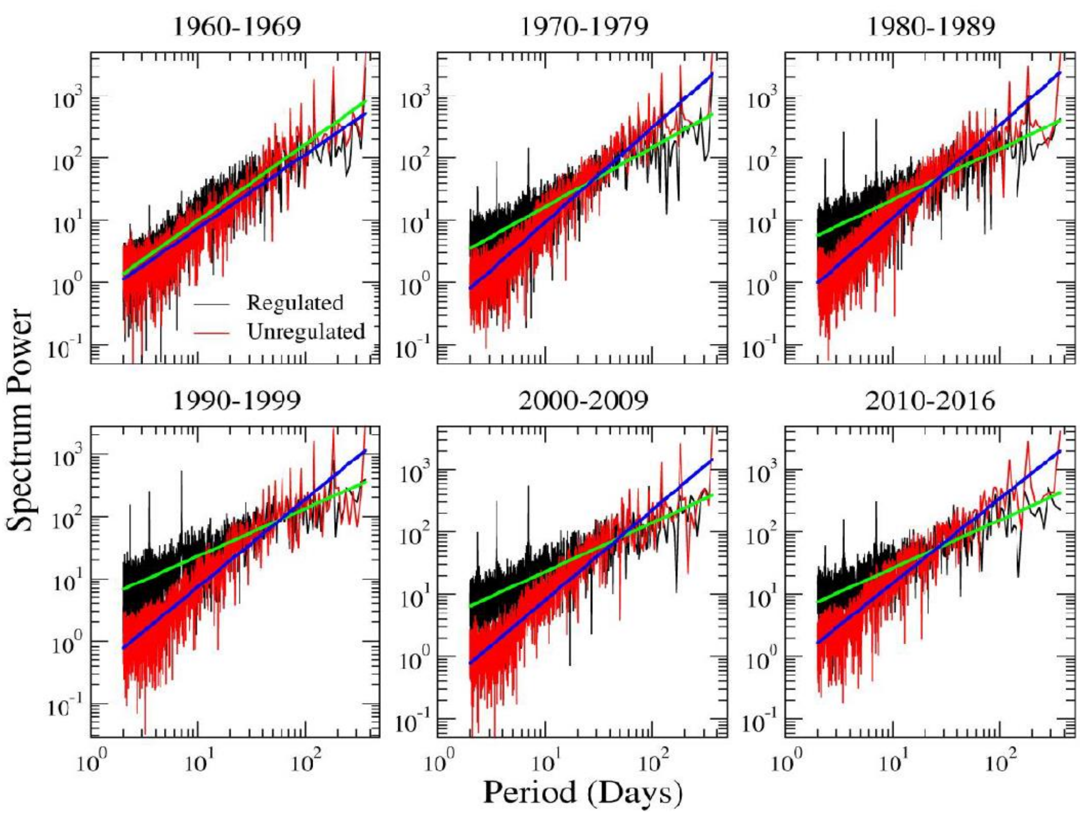

FIGURE 3.2.7 Decadal spectral analyses of daily discharge for regulated (sum of four rivers) and unregulated rivers (sum of 17 rivers), 1960-2016. Thick green and blue lines denote non-linear regressions performed on power spectra covering return periods of 2 to 365 days for the regulated and unregulated rivers, respectively. Reproduced from: Déry et al., 2018 (Figure 5).

To further aid in contextualizing observational studies, a baseline climatic study (HBDB HydroGFD precipitation and air temperature and regulated discharge) was conducted to establish average conditions over a historic climate-normal period (monthly, 1981 to 2010; Appendix B, Table 2.3-7). These averages were used to compute monthly anomalies and rankings for each year of observational field campaigns (summers 2015 to 2019; Lukovich et al., 2021). These results demonstrate that when considering total discharge emanating from the HBDB, the observation years (2016-2018) have been wetter than the reference mean February to April (mean and anomaly shown in Figures A1 to A3), exceeding the IQR of the reference period in 2016 and 2017 (monthly IQR and anomaly shown in Figures A4 to A6). These years are coincident with wetter (total precipitation) and cooler (air temperature) years, with rankings within their month of each year for the full HBDB shown in Figure A13. Regionally (except for summer 2017), the western HBDB has been drier (total precipitation, mean, and anomaly shown in Figures A7 and A8) than the reference period, where the eastern HBDB is wetter in all seasons 2016-2018. Except for local cool spots and autumn 2018, all seasons across the full HBDB domain have been warmer (air temperature, mean, and anomaly shown in Figures A9 and A10) than their reference period. Details are presented in Chapter 3.6.

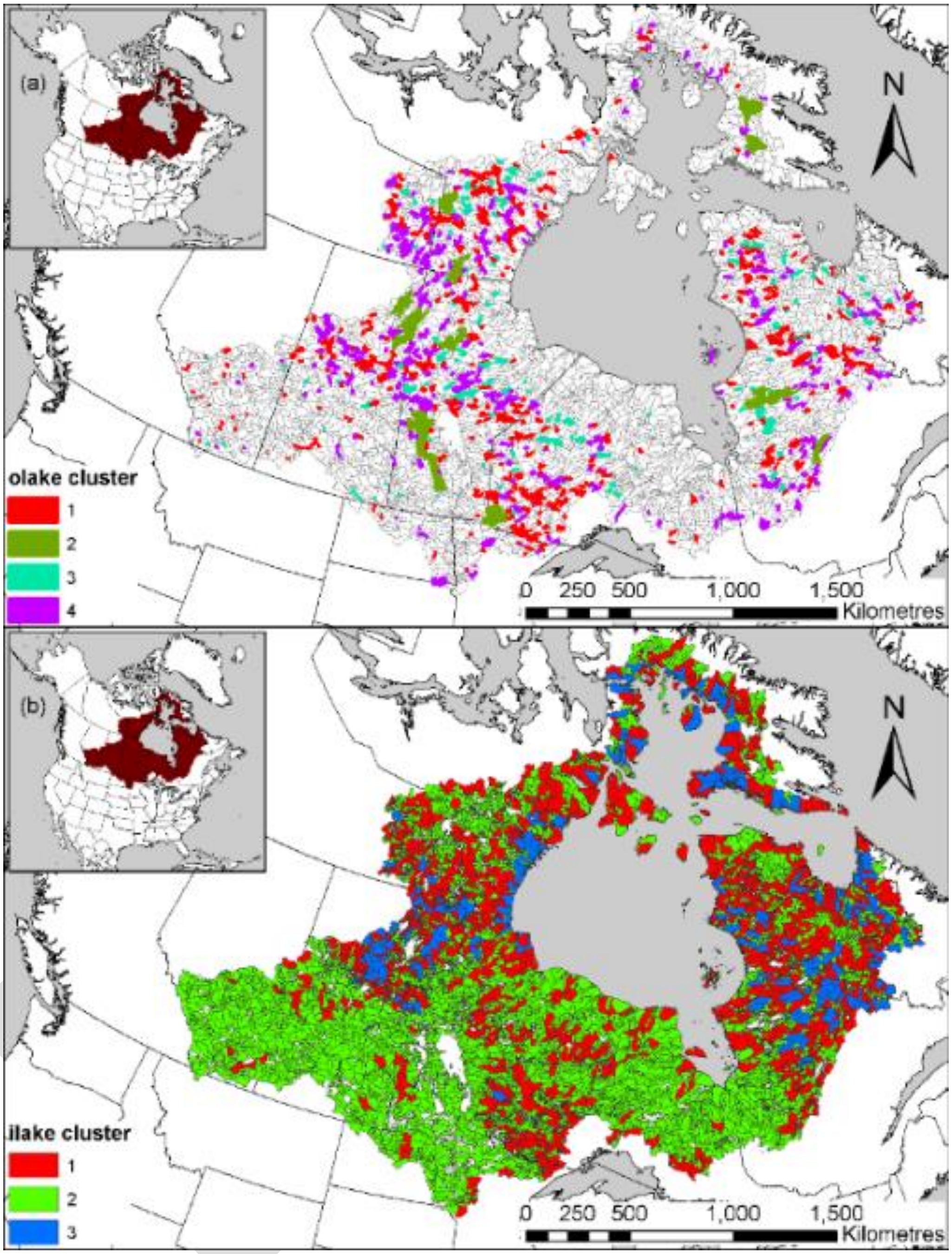

FIGURE 3.2.8 Maps showing locations of (a) olake clusters (sub-basin outlet lakes), and (b) ilake clusters (sub-basin internal lake) overlain on AHYPE sub-basins. Lake parameters are clustered by lake physiographic characteristics to facilitate simpler calibration. White sub-basins indicate no olakes or ilakes in the sub-basin. White sub-basins are not included in olakes because they are regulated and calibrated separately. Reproduced from: Stadnyk et al., 2020 (Figure S1)

The improved Hudson Bay HYPE (HHYPE; Stadnyk et al., 2020) model developed in Task 2.1 has been completed, with results passed to Tasks 2.2 and 2.3. New physical processes added to the existing AHYPE code were both shown to improve median Kling Gupta Efficiency (Figure 3.2.9b and 3.2.9c). Clustering of lakes improved calibration speed and was shown to contribute to overall calibration improvements (Figure 3.2.9a). The largest improvements between the original AHYPE parameter set and the HHYPE calibration are seen in the prairies (likely due to the addition of NCA processes), although improvement is seen in most regions (Figure 3.2.10). The default HHYPE configuration was used in this work (Appendix B, Table 2.1-2).

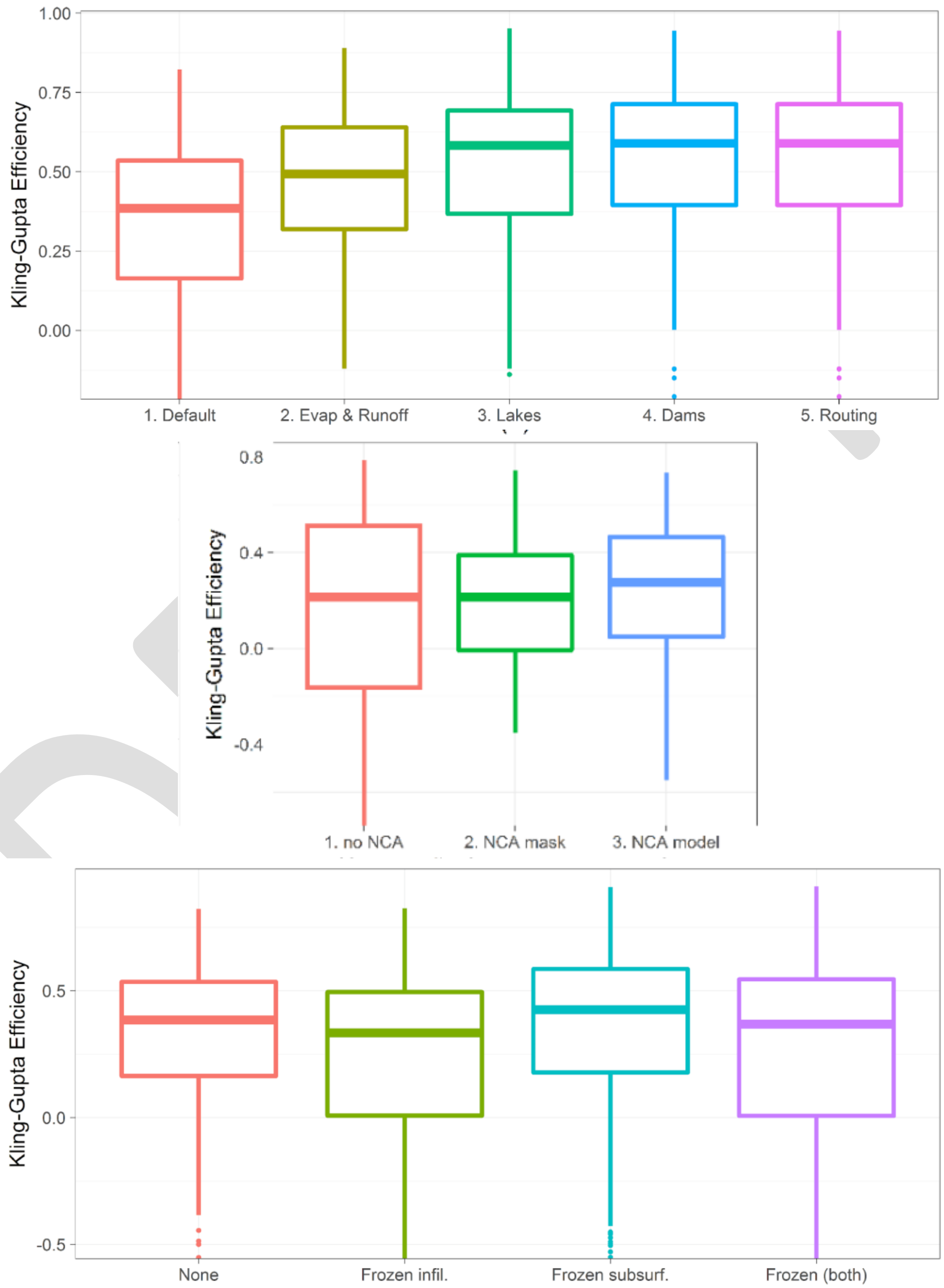

FIGURE 3.2.9 KGE results (daily discharge, 1971-2013) of model development by process for (a) stepwise calibration over 101 flow signature gauges, (b) NCA parameterizations for 10 gauges, and (c) frozen soil processes over 245 gauges. Reproduced from: Stadnyk et al., 2020 (Figures 8, 4b, and 6).

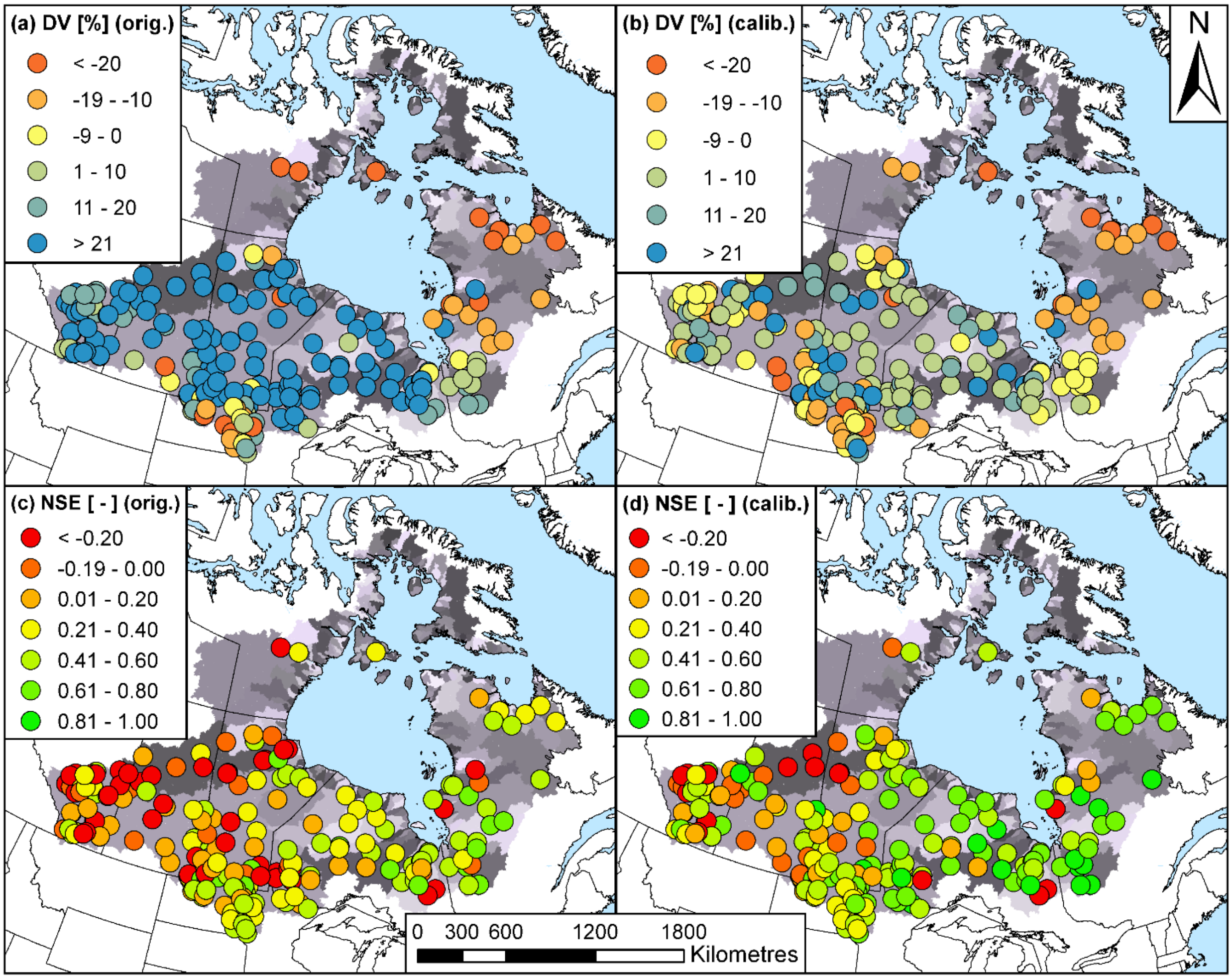

FIGURE 3.2.10 Spatial plots of model performance statistics: (a) Deviation of runoff volume (original parameters: Andersson et al., 2015), (b) Deviation of runoff volume (calibrated parameters), (c) Nash-Sutcliffe Efficiency (original parameters: Andersson et al., 2015), and (d) Nash-Sutcliffe Efficiency (calibrated parameters). Reproduced from: Stadnyk et al., 2020 (Figure 9).

An application of this model (Appendix B, Table 2.1-2) using the BaySys bias-corrected climate ensemble shows the non-linear impacts of 1.5 and 2.0 °C global warming on elements of the HBDB hydrologic cycle (MacDonald et al., 2018). This shows intensifying hydrologic cycles over the entire HBDB, including basin temperatures increasing one and a quarter to two times faster than the global mean (Figures 3.2.11 and 3.2.12). This intensification of the hydrology shows signs of increasing non-linearity between 1.5 and 2.0 degrees warming. This is particularly seen in the northern region (Foxe Basin). Western Hudson Bay shows the smallest increase and narrowest confidence intervals (Figure 3.2.12).

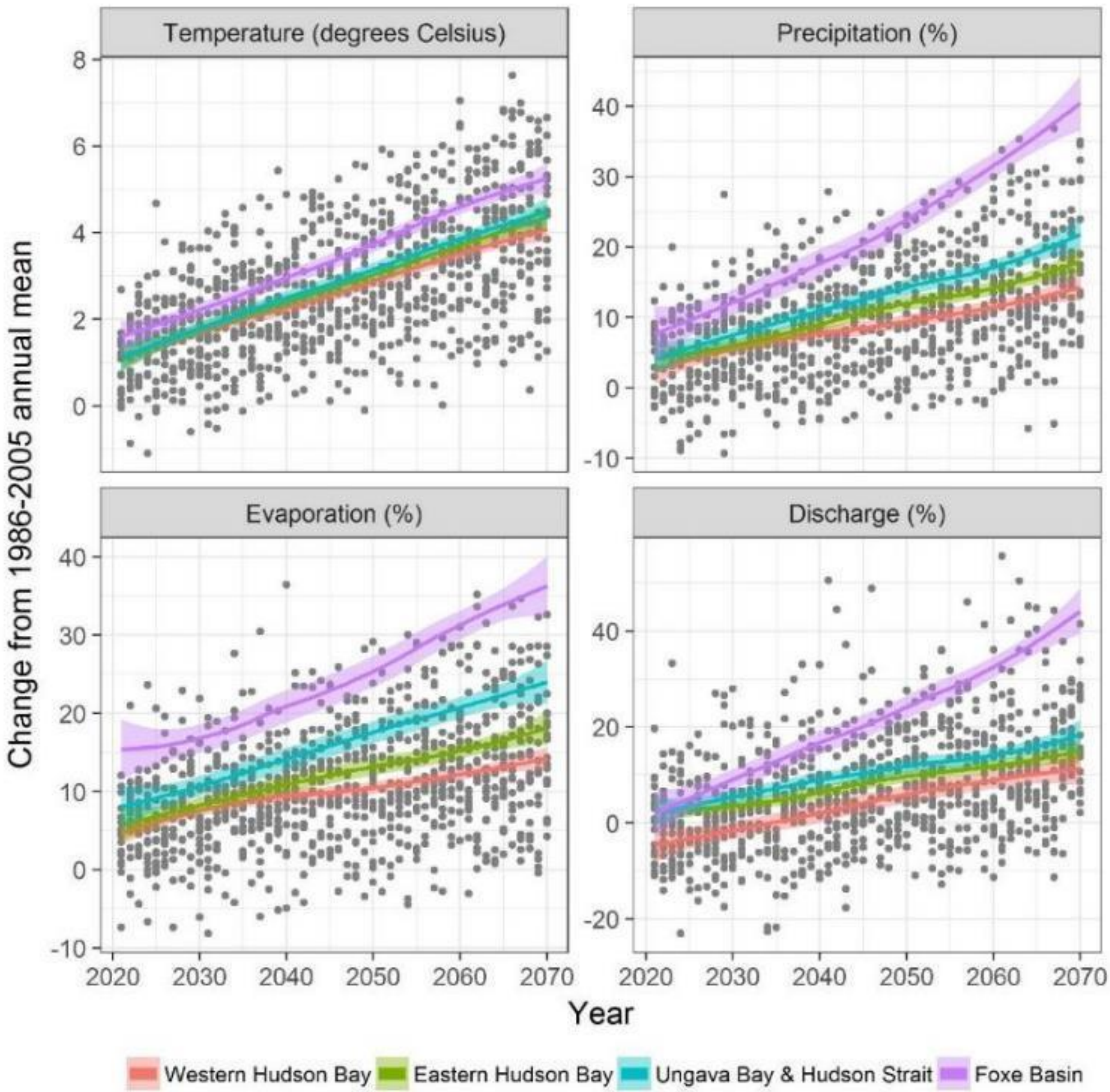

FIGURE 3.2.11 Projected changes in annual temperature, precipitation, evaporation, and discharge from 1986-2005 annual means using the 19 AHYPE-CMIP5 simulations. Black data points are for the entire HBDB. Coloured locally weighted scatterplot smooth curves are shown for the four regions (grey shading indicates 95% confidence intervals). Reproduced from: MacDonald et al., 2018 (Figure 2)

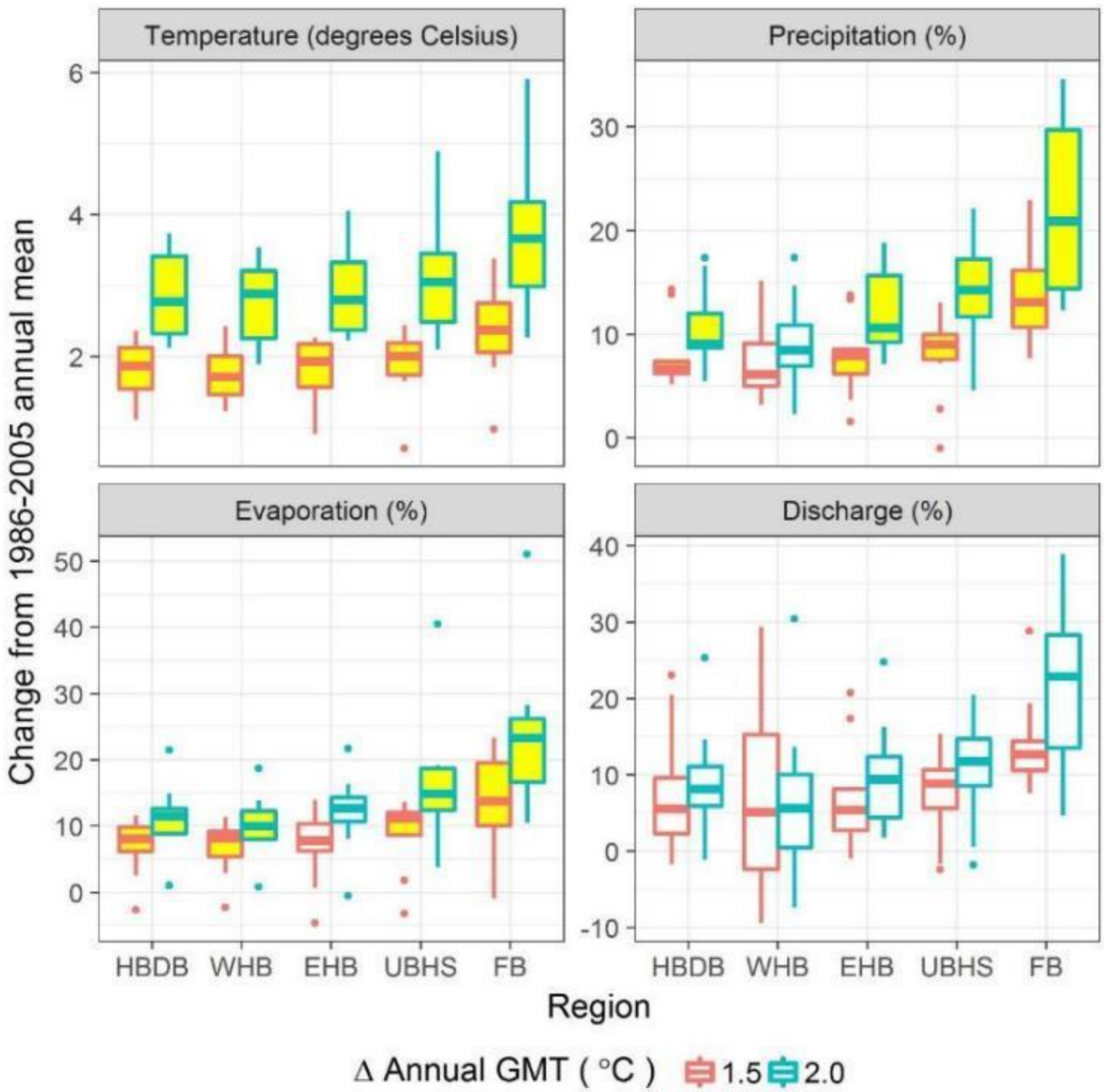

FIGURE 3.2.12 Projected changes in annual temperature, precipitation, evaporation, and discharge from 1986-2005 for 20-year time slices of GMT increases of 1.5°C and 2.0°C above pre-industrial level. Statistically significant differences resulting from 1.5°C versus 2.0°C GMT warming are highlighted in yellow. Boxplots show the median, 25th, and 75th percentiles at the hinges, and the whiskers extend to show a 95% confidence interval. Reproduced from: MacDonald et al., 2018 (Figure 3).

The discharge projections developed for this task (Appendix B, Table 2.1-3: monthly, 1981 to 2070 inclusive) have been distributed to Team 6 and published as part of a study detailing the calibration and sensitivity of the oceanographic model (Ridenour et al., 2019). A trend analysis of the HBC regulated, HBC unregulated, and Arctic Ocean rivers confirmed increasing freshwater discharge to the Arctic basin, with a projected 22% increase by the end of 2070 (Stadnyk et al., 2021). Discharge in all rivers entering the Arctic basin, including those in

Hudson Bay, is increasing from the historic period (1981-2010) into the future, statistically significant at 95% confidence level (Figure 3.2.13).

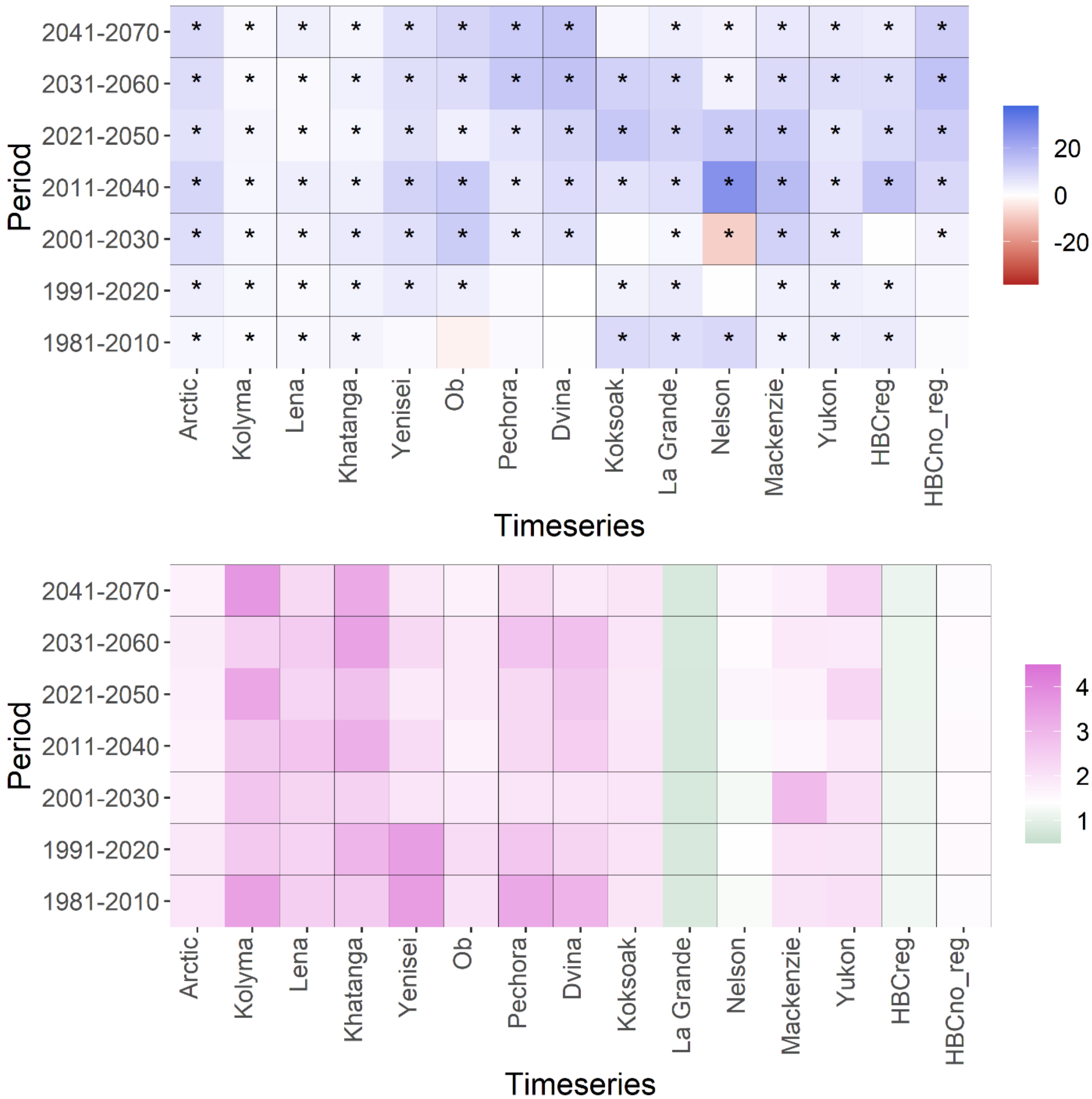

FIGURE 3.2.13 Decadal analysis by river and region using (top) Mann-Kendall normalized trend analysis (m^3s^{-1} per decade) and (bottom) spectral analysis power (B for $y = Ax^B$). Regional results for the HBC regulated and non-regulated rivers are shown to the far right. Asterisks indicate trends significant to 95%. Reproduced from Stadnyk et al., submitted (Figure 8) (Confidential pending publication).

Uncertainty Assessment of LNRB Discharge (Task 2.2)

The uncertainty study of the LNRB central to Task 2.2 has been completed. Elements of this study include climatic input sensitivity and analysis of uncertainty due to input, single-model uncertainty, multi-model sensitivity, and multi-model uncertainty results. These results, along with the discharge ensemble generated by Task 2.3 were used to develop bay-wide discharge probability curves in Task 2.4.

An assessment of six historic reanalysis climate products over the LNRB (Lilhare et al., 2019) shows the discontinuity of precipitation (Figure 3.2.14) and air temperature (Figure 3.2.15), even between high-quality reanalysis products and by extension, the value of using an ensemble (whether reanalysis or GCM) rather than any one product (Appendix B, Table 2.2-1).

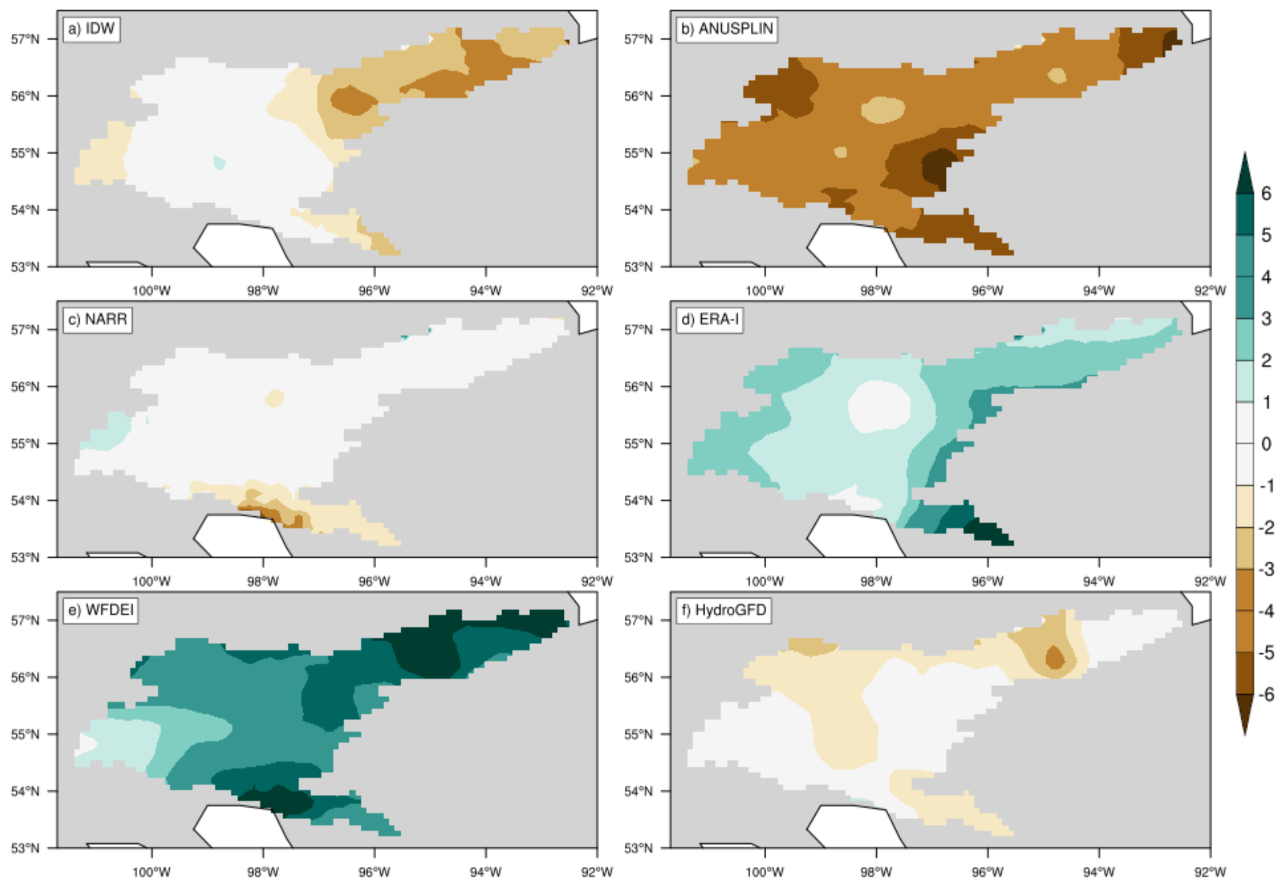

FIGURE 3.2.14 Bias as measured against the ENSEMBLE total annual precipitation (mm month^{-1}) for the (a) IDW, (b) ANUSPLIN, (c) NARR, (d) ERA-I, © WFDEI, and (f) HydroGFD datasets, 1981–2010. Reproduced from: Lilhare et al., 2019 (Supplementary Figure 3).

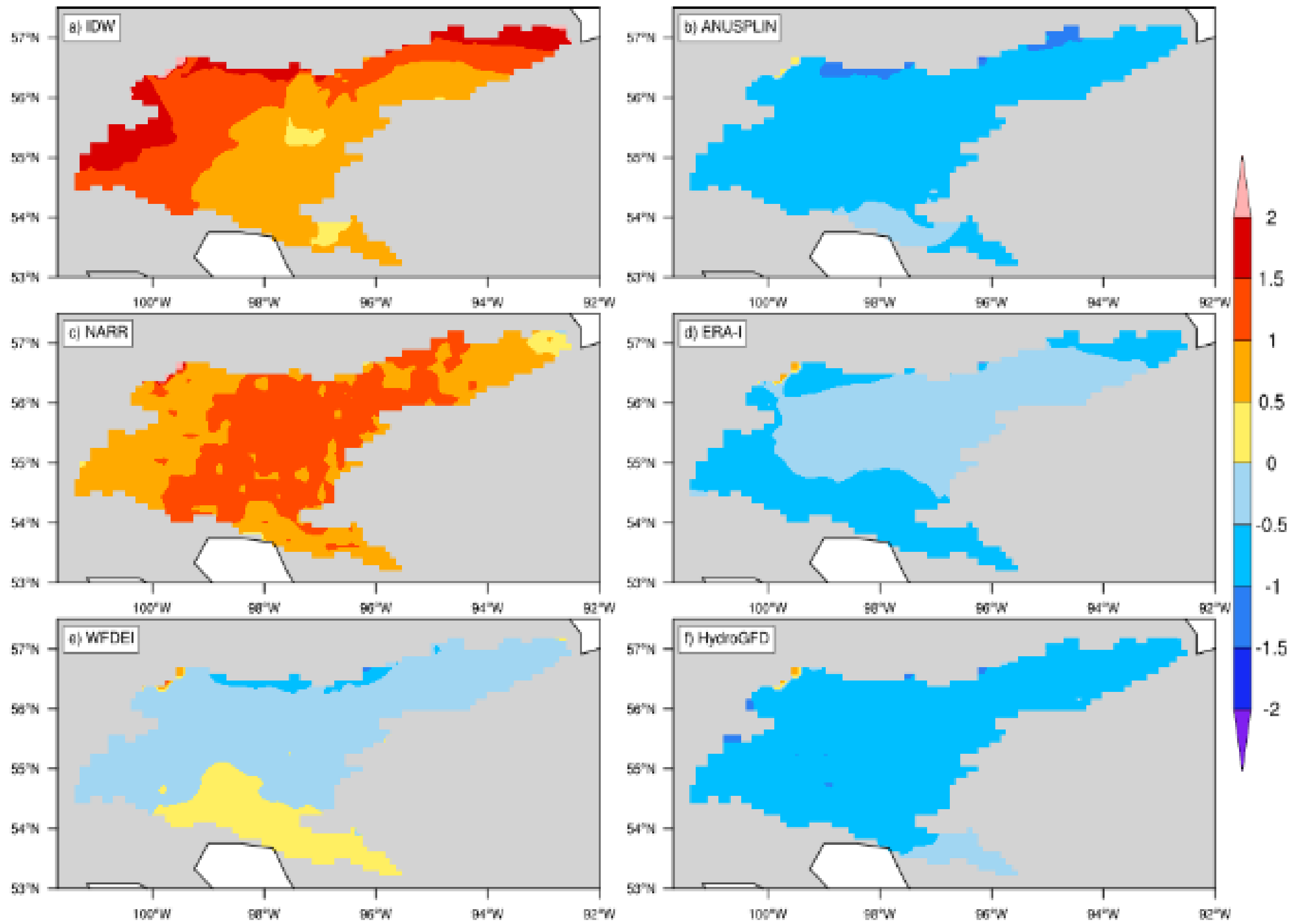

FIGURE 3.2.15 Bias as measured against the ENSEMBLE mean annual air temperature (°C) for the (a) IDW, (b) ANUSPLIN, (c) NARR, (d) ERA-I, © WFDEI, and (f) HydroGFD datasets, 1981–2010. Reproduced from: Lilhare et al., 2019 (Supplementary Figure 4).

A further sensitivity and uncertainty analysis of the LNRB using the VIC hydrological model (Lilhare et al., 2020) shows sensitivity of sub-basin discharge to the input products, the calibration metric used (Figure 3.2.16), and parameter calibration (Figure 3.2.17) using VARS and OLHS. These results reinforce the strength of climate ensembles of input, robust sensitivity analyses, and multi-model ensembles in quantifying uncertainty in discharge projections (Figure 3.2.18).

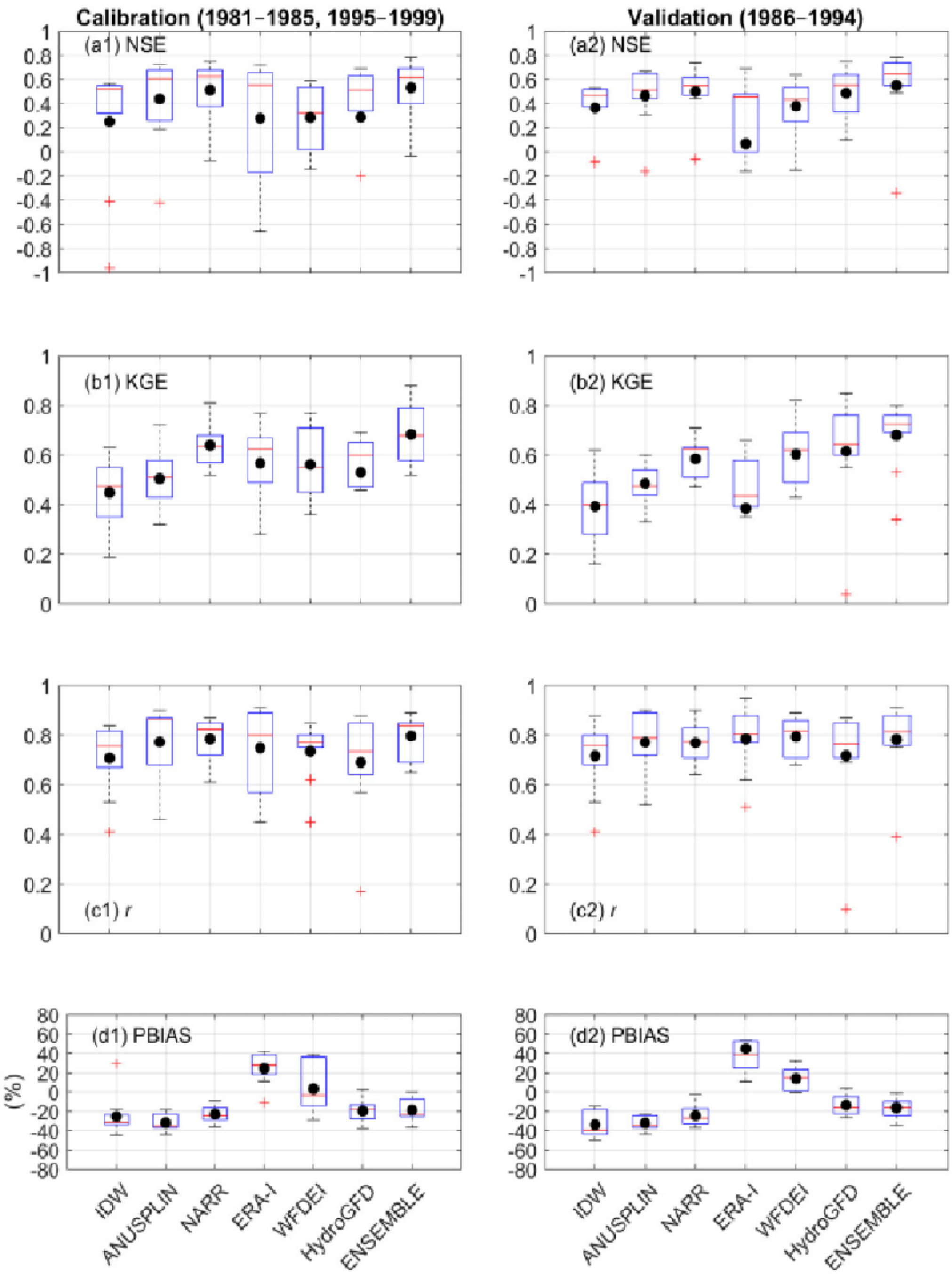

FIGURE 3.2.16 Boxplots for monthly calibration (a1-d1) and validation (a2-d2) performance metrics, NSE (a1-a2), KGE (b1-b2), r (p-value < 0.05 for all) (c1-c2) and PBIAS (d1-d2), for ten selected sub-watersheds within the LNRB based on IDW-VIC, ANUSPLIN-VIC, NARR-VIC, ERA-I-VIC, WFDEI-VIC, HydroGFD-VIC and ENSEMBLE-VIC simulations. The black dots within each box show the mean, the red lines show the median, the vertical black dotted lines show a range of minimum and maximum values excluding outliers, and the red + signs show the outliers defined as the values greater than 1.5 times the interquartile range of each metrics. Reproduced from: Lilhare et al., 2020 (Figure 3).

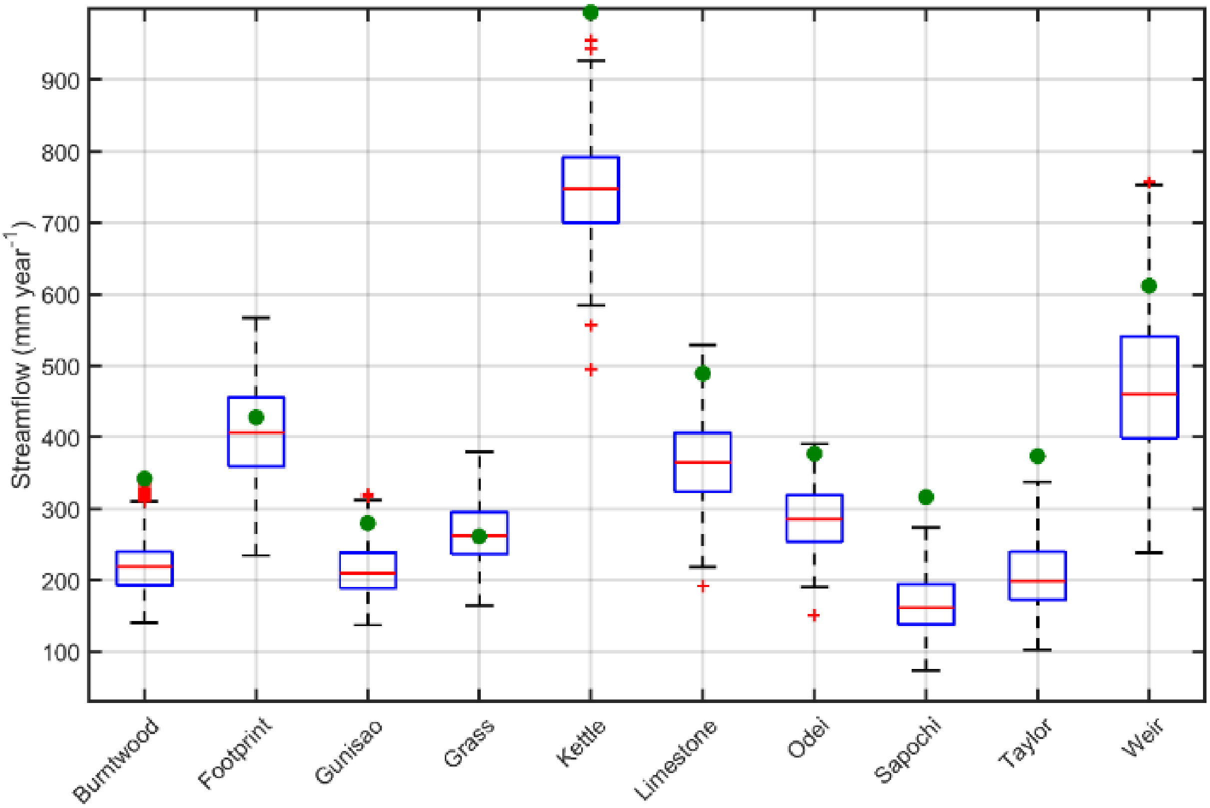

FIGURE 3.2.17 Annual streamflow sensitivity to parameter uncertainty for all LNRB's sub-watersheds. The green dots show streamflow associated with the control run (calibration), the red lines show the median, the vertical black dotted lines show a range of minimum and maximum values excluding outliers, and the red + signs show the outliers defined as the values greater than 1.5 times the interquartile range of annual streamflow. Reproduced from: Lilhare et al., 2020 (Figure 8).

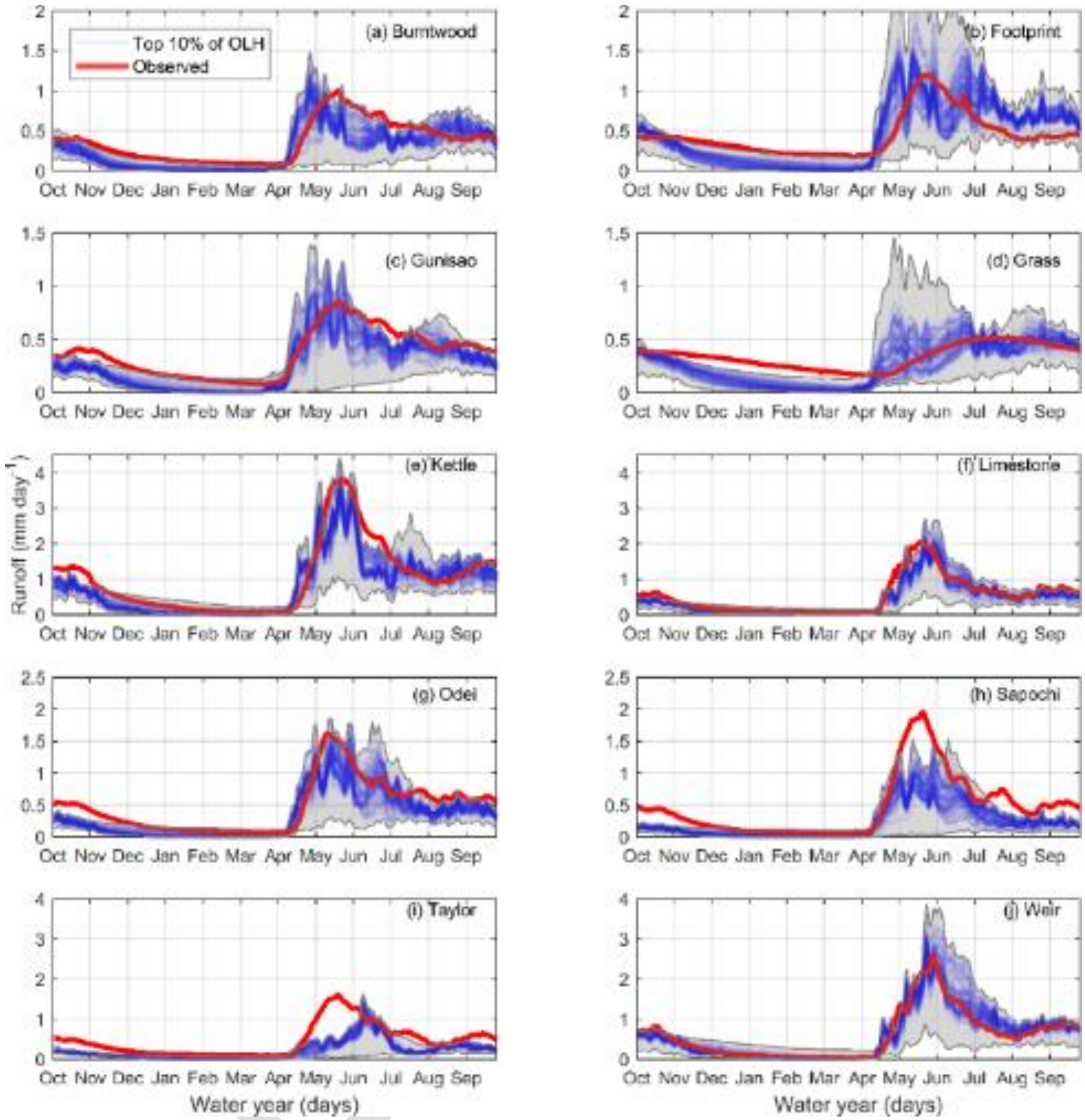

FIGURE 3.2.18 Streamflow prediction uncertainty associated with estimated parameters from the OLH. Top 10% (shown in blue color) of OLH samples, based on KGE, used for the prediction of (red) observed streamflow for all ten sub-watersheds, the water year 1981-2010. The shaded area (grey color) shows the envelope of VIC runs from 600 OLH samples. Reproduced from: Lilhare et al., 2020 (Figure 10).

An input study of the NCRB further shows the variability (spatially and temporally) between historic reanalysis climate products (Pokorny et al., in preparation (a)), especially in data-sparse regions (Figure 3.2.19). By comparing reanalysis products to the Adjusted and Homogenized Climate Change Data (AHCCD) for temporally continuous (Figure 3.2.20) and aggregated (Figure 3.2.21), the value is shown in studying not only ensemble-mean but extreme scenarios as well to account for input uncertainty (Appendix B, Table 2.2-1).

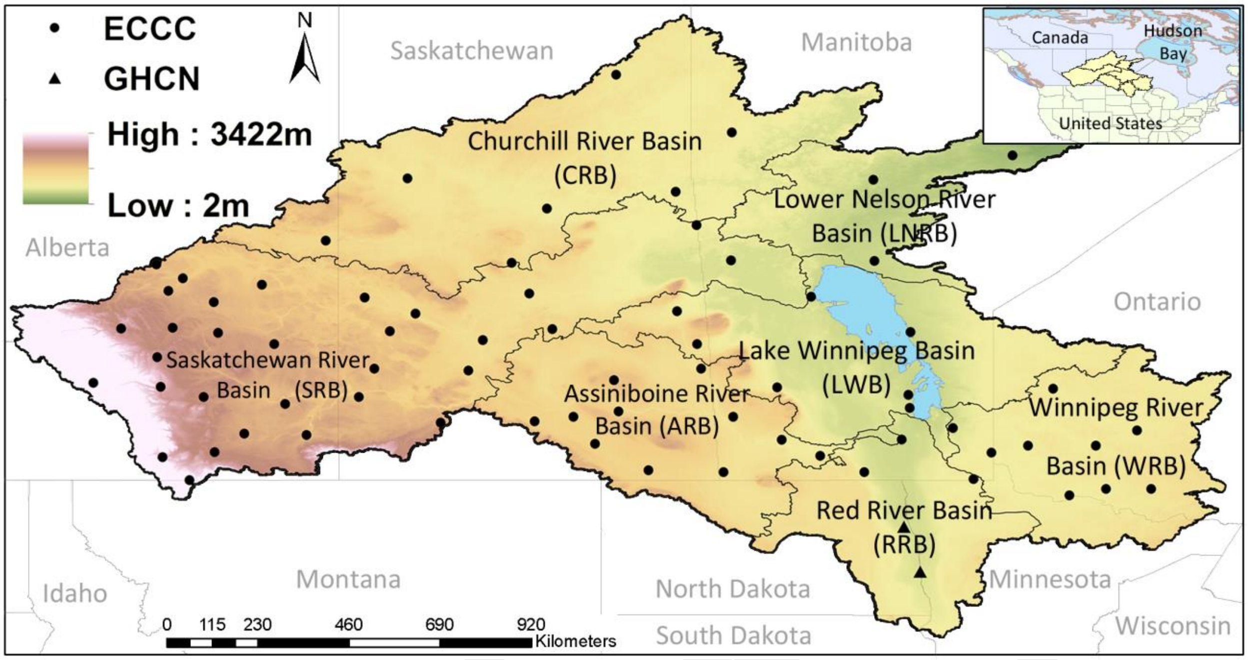

FIGURE 3.2.19 Map of the Nelson-Churchill Watershed including major basin delineations and 71 selected observed climate station locations. Reproduced from: Pokorny et al., 2020 (a) (Figure 1).

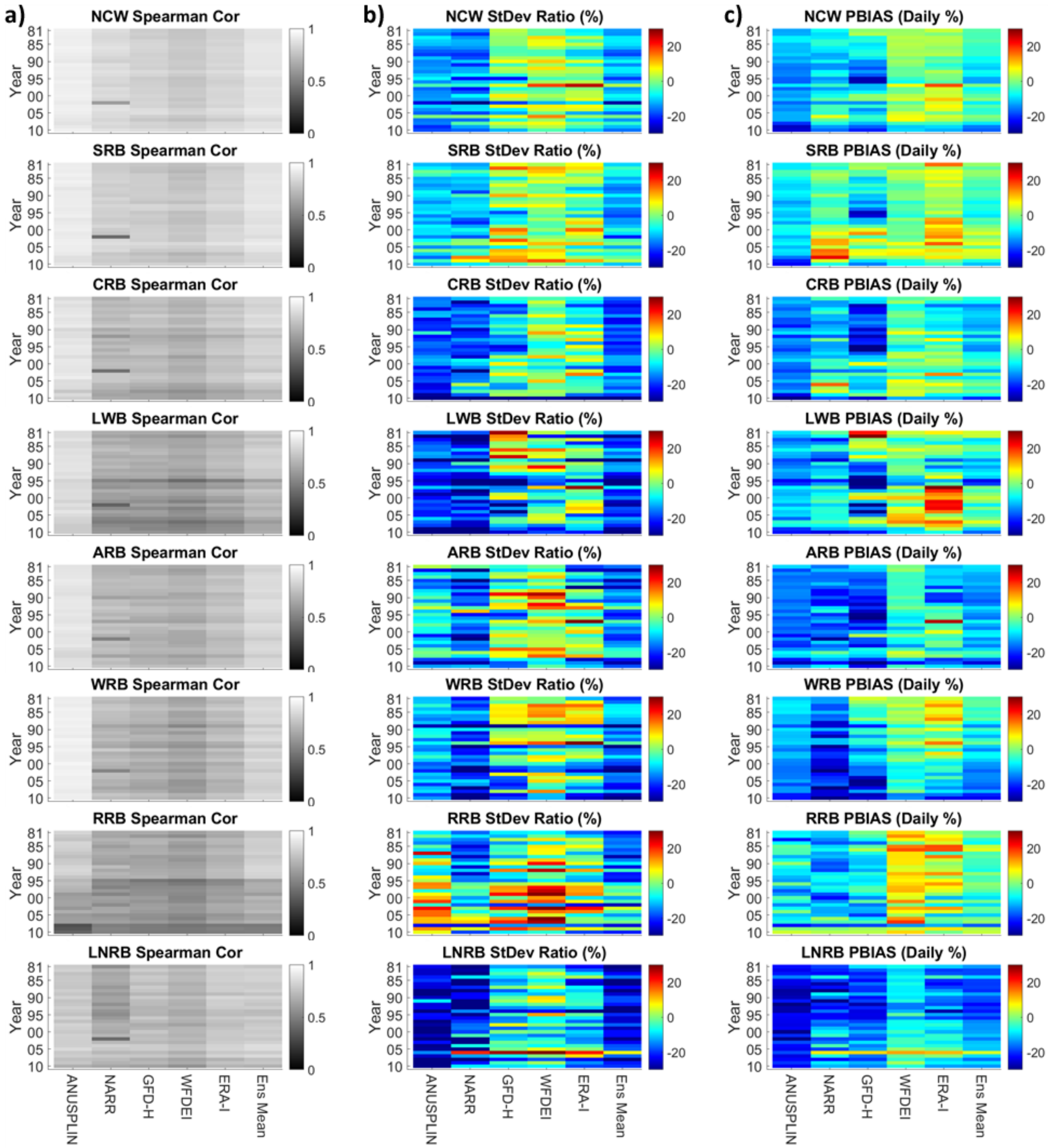

FIGURE 3.2.20 Daily precipitation spatially aggregated annual continuous statistics with reference to the AHCCD observed data set in each major basin. (a) daily Spearman correlation, (b) daily ratio of standard deviations, and (c) daily PBIAS. White is used to represent periods with no available data. Reproduced from: Pokorny et al., submitted (a) (Figure 3) (Confidential pending publication).

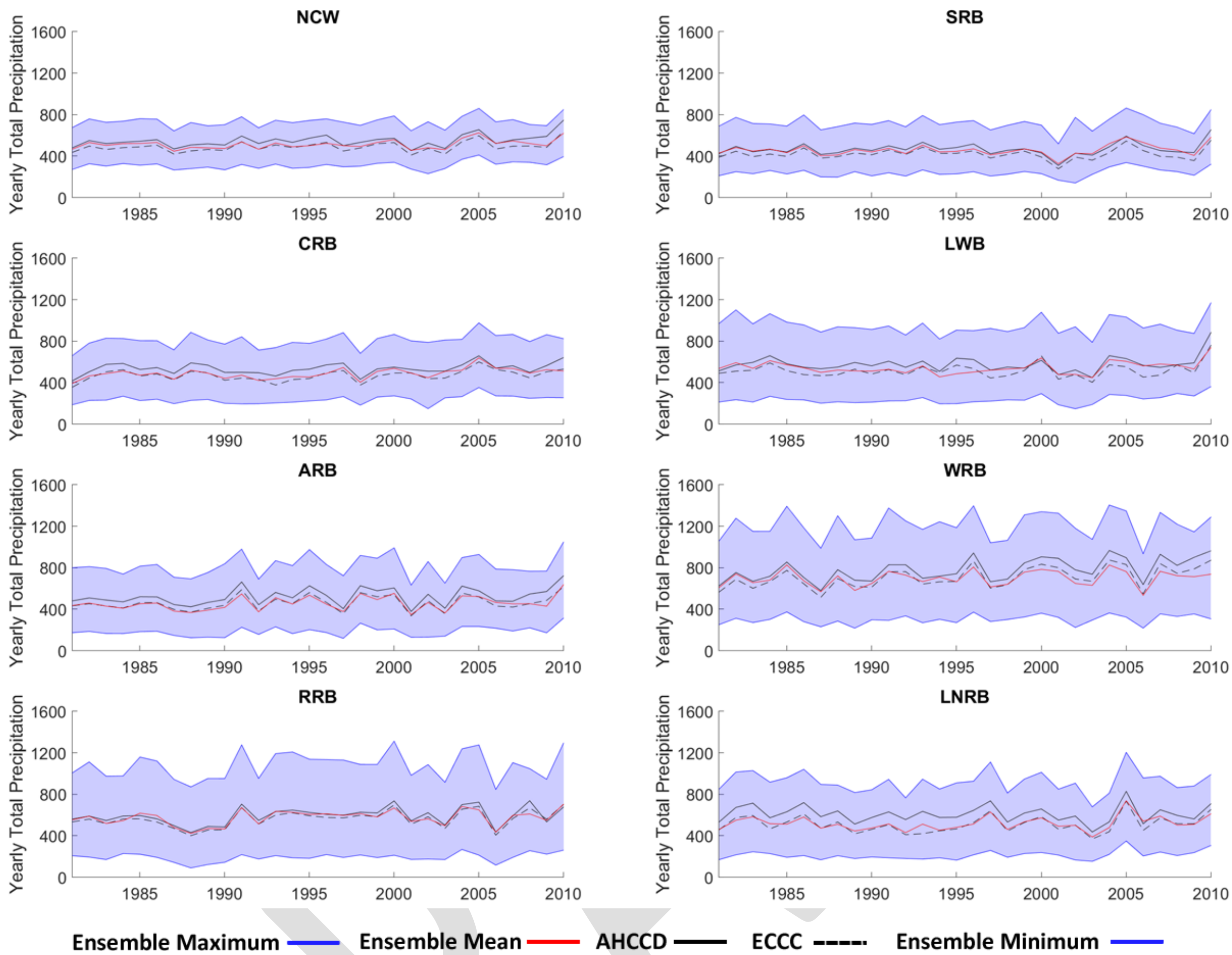

FIGURE 3.2.21 Basin-averaged daily precipitation continuous yearly statistics with reference to the AHCCD observed data set in each major basin for (a) daily Spearman correlation, (b) daily RMSE, and (c) daily PBIAS for the ensemble minimum, mean, and maximum. Reproduced from: Pokorny et al., submitted (a) (Figure 6) (Confidential pending publication).

By studying multiple historic, reanalysis input products, multiple hydrologic models, and a broad range of model parameters, sources of uncertainty in discharge projections of the Nelson River are evaluated and the associated probability of outflows for stations in the LNRB over the historical period 1981-2010 (Pokorny et al., submitted (b); Appendix B, Table 2.2-2). These results show the greater reliability (using VARS; Figure 3.2.22) over a greater range (from sensitive to insensitive) of parameters calibrated in gridded and semi-distributed models (WATFLOOD and HYPE, respectively) compared to lumped models (HEC-HMS). These results also show the multi-model results for any given input and climate ensemble for any given model return more robust distributions of discharge values than any single input product or hydrologic model (Figure 3.2.23).

FIGURE 3.2.22 VARS parameter sensitivity reliabilities were ordered from least (bottom) to most sensitive (top), based on the period sensitivity. Variables are color-coded to reflect their category within the hydrologic model. Reproduced from: Pokorny et al., submitted (b) (Figure 2) (Confidential pending publication).

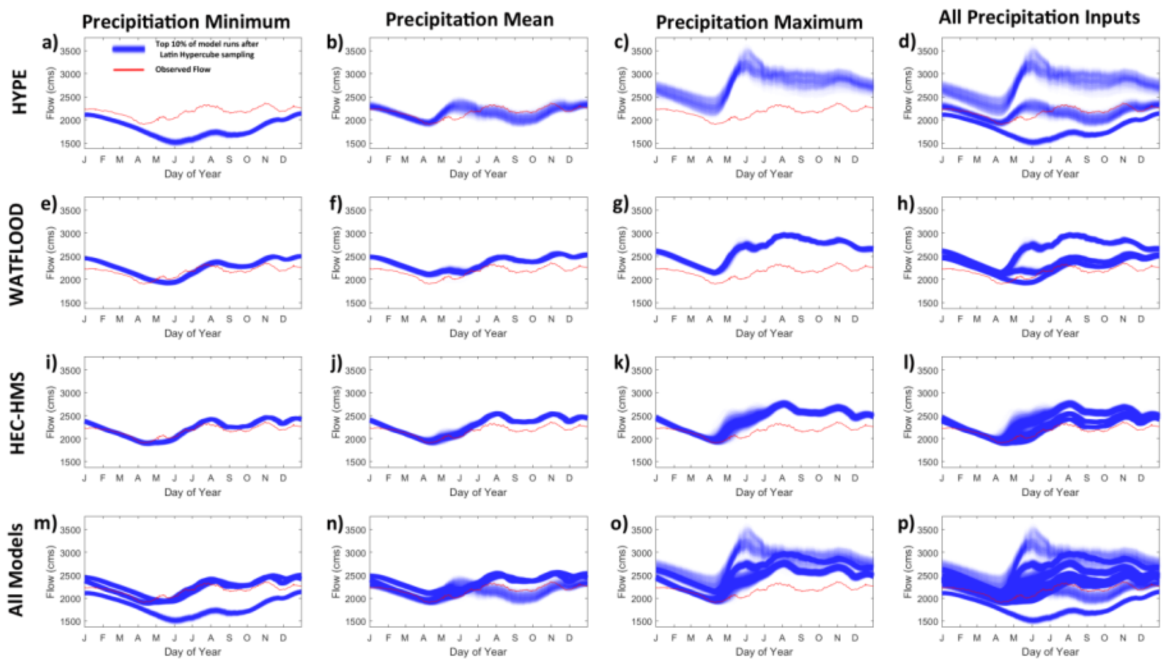

FIGURE 3.2.23 30-year average hydrographs for the Nelson River at Kelsey, generated by selecting the top 10% of orthogonal Latin Hypercube sampled runs for each hydrologic model and precipitation realization. Simulated hydrographs are darker blue when there was higher density of simulated flows. Reproduced from: Pokorny et al., submitted (b) (Supplementary Figure 27) (Confidential pending publication).

Regulated NCRB and LGRC Modelling (Task 2.3)

The HHYPE model is further improved for BaySys purposes by adding a generalized reservoir regulation scheme ($HHYPE_{REG}$; Tefs et al, in revision (a)). This regulation routine emphasizes maintenance of safe Water Surface Levels (WSLs) rather than the current HYPE regulation routine which is primarily calculated based on specified daily outflow. By increasing sensitivity to daily WSLs (Figures 3.2.24b and 3.2.24d) and developing an automated calibration procedure, the reservoir discharge results are improved for individual monthly and overall seasonal discharge time series (Figures 3.2.24a and 3.2.24c).

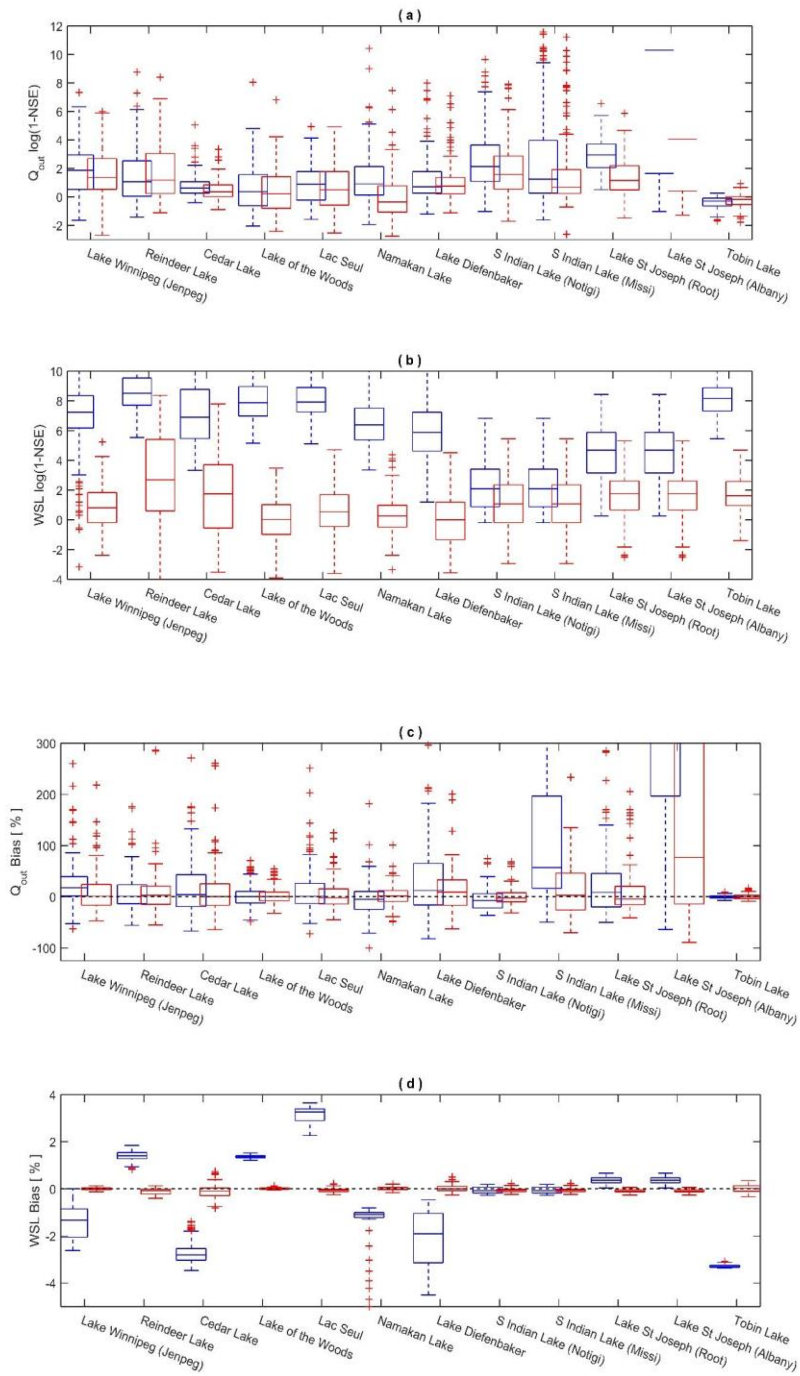

FIGURE 3.2.24 Distribution of 360 monthly evaluations (1981 to 2010) for (red) $HHYPE_{REG}$ and (blue) default AHYPE when measuring (a, c) daily outlet discharge and (b, d) daily water surface level (WSL) for performance metrics (a, b) NSE error log10(1 – NSE) and (c, d) mean bias (bias). Interquartile range (box), 1.5 x interquartile range (whiskers,) median (divider), mean (cross) and outliers (dots). Perfect simulation for log10(1 – NSE) is -∞, for bias is zero percent. Reproduced from: Tefs et al., 2021 (Figure 8).

Using the HHYPE$_{REG}$ and (Appendix B, Tables 2.3-2 and 2.3-3) HHYPE$_{NAT}$ (Appendix B, Table 2.3-1) models, differences in discharge trends are identified for the two largest hydroelectric systems in the HBDB (NCRB, LGRC). The effects of regulation and climate change are shown in normalized discharge and discharge interquartile dispersion between 19-member ensemble (Tefs et al., in revision (b)). These results highlight the differences between the NCRB and LGRC when evaluating ensemble agreement (shown here as normalized dispersion, or the ensemble interquartile range divided by the ensemble mean). Where the LGRC ensemble disagreement (Figure 3.2.25d) is greatest consistently from April to June (during the period when floods are delivered and then retained or passed depending on their severity), the NCRB has greater inter-annual variability of ensemble agreement (Figure 3.2.25c). This suggests that both the flow and the modelled uncertainty are more strongly driven by climatic variability and modelled climatic disagreement in the NCRB.

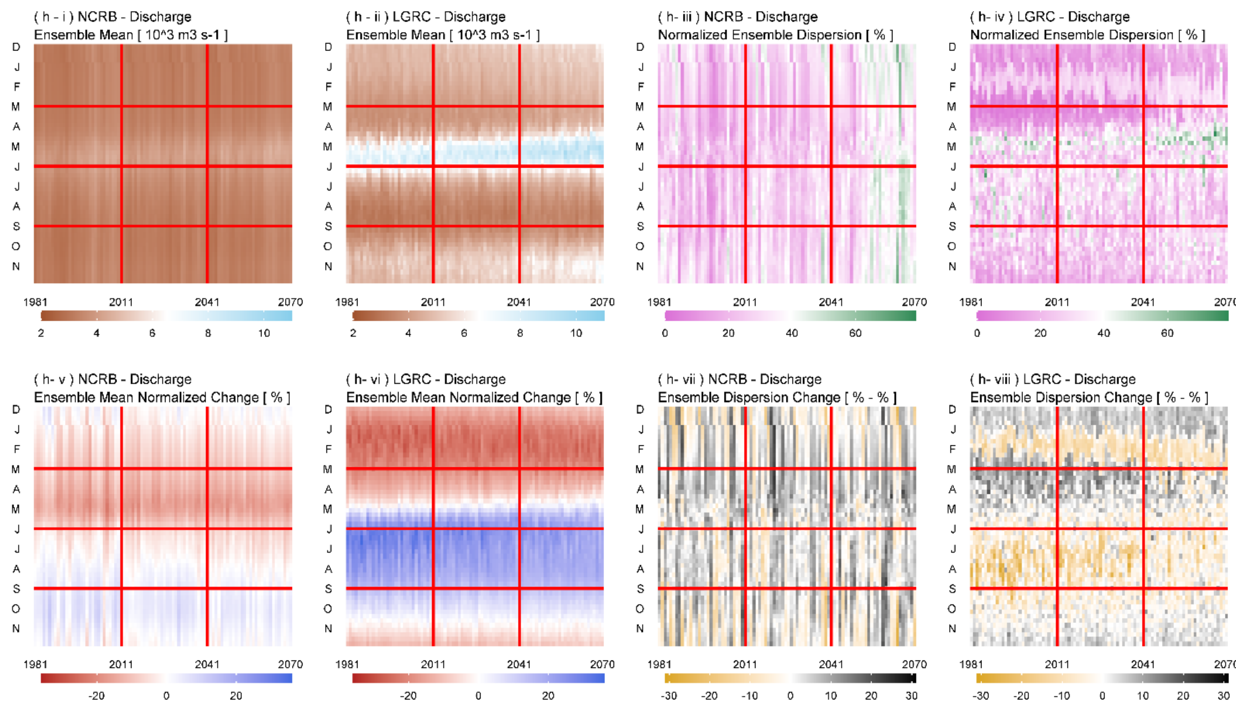

FIGURE 3.2.25 Weekly (y-axis) sum or mean for simulated years (x-axis). Ensemble mean (i, ii; Equation 3b), ensemble dispersion (iii, iv; Equation 3c), model configuration percent change to ensemble mean (v, vi; Equation 3d), and model configuration change to dispersion (vii, viii; Equation 3e). Dispersion greater than 150% is excluded to improve readability. Plots v, vi, vii, and viii are excluded where records exist presenting a change greater than |0.5%|. Red lines correspond to (vertical) 30-year periods and (horizontal) seasons used in Figure 8. Overlaid text denotes mean for period and season. Discharge mean colour-bar labels hidden at the request of collaborators due to industrial privacy concerns. Reproduced from: Tefs et al., in revision (Figure 7h) (Confidential pending publication).

The regulated and naturalized outflow ensembles (Appendix B, Table 2.3-4) have been distributed to Team 3 for use in nutrient flux estimation and carbon flux estimation, and to Team 6 for use in oceanographic modelling (Jafarikhasragh et al., 2019).

Uncertainty Assessment of HBDB Discharge (Task 2.4)

The HBDB uncertainty framework was applied to discharge data generated by HHYPE (regulated and naturalized results). Evaluation of PUB uncertainty transfer was assessed in the LNRB by treating each basin as ungauged and generating an uncertainty estimate using uncertainty transfer methods (Pokorny et al., in preparation). Results suggested that flow signature similarity was important to results quality; basins with notably different flow signatures more often had underestimates of uncertainty than those with similar flow signatures. This result suggests that the uncertainty transferred to HBDB discharge data were conservative.

Uncertainty transfer results show that baseflow-dominated months generated the best transfer results, followed by summer months, which are subject to convective storms, and the worst months were spring freshet months (Figure 3.2.26). The variability in spring event timing meant that uncertainty was often overestimated on the spring melt rising limb and underestimated for peak flows (Figure 3.2.27). Flow signature matching from donors was the sensitive part of the methodology to overall transferred uncertainty. More donors generally improved results, but only if no donors were strong flow signature matches (Figure 3.2.28). To balance the improvements of more donors with lowering weighting to ideal donors, four donor basins were used for all uncertainty transfers.

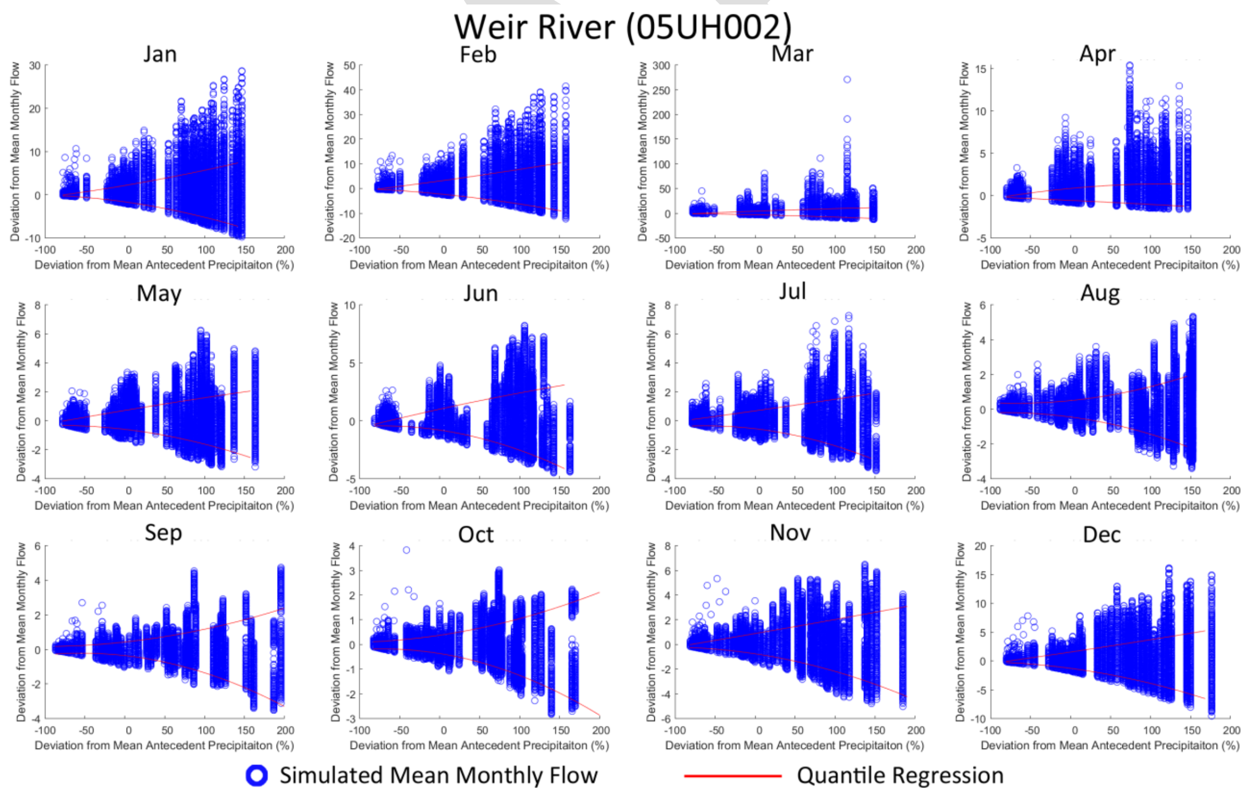

FIGURE 3.2.26 Monthly normalized quantile regressions for the Weir River. Each simulated month is one of the 30 years of that month (e.g. 30 Januarys in 1981-2010) for one parameter set for one of the three model structures. Quantile regression lines are generated for the 10th and 90th quantiles. Reproduced from Pokorny et al. (in preparation) (Confidential pending publication).

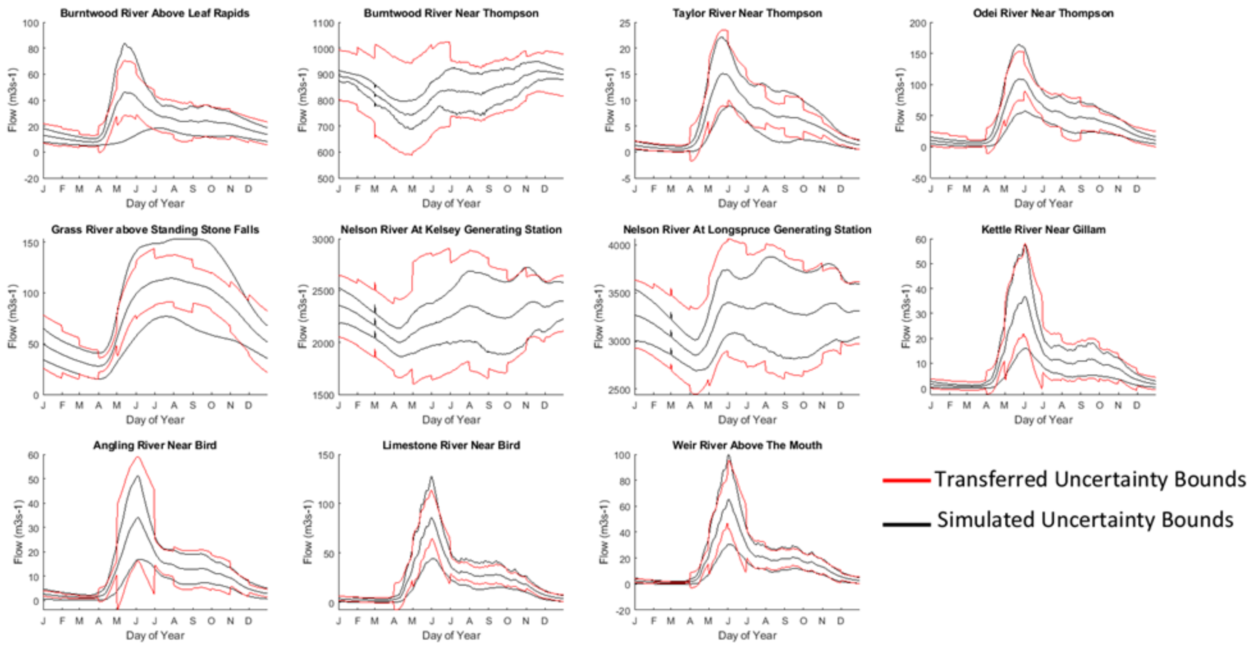

FIGURE 3.2.27 Annual average hydrographs (1981-2010) for each of the 11 gauged locations. The center simulated (black) hydrograph represents the target for uncertainty transfer. Uncertainty was transferred using four donor basins for the 10th and 90th quantiles. Reproduced from Pokorny et al. (in preparation) (Confidential pending publication).

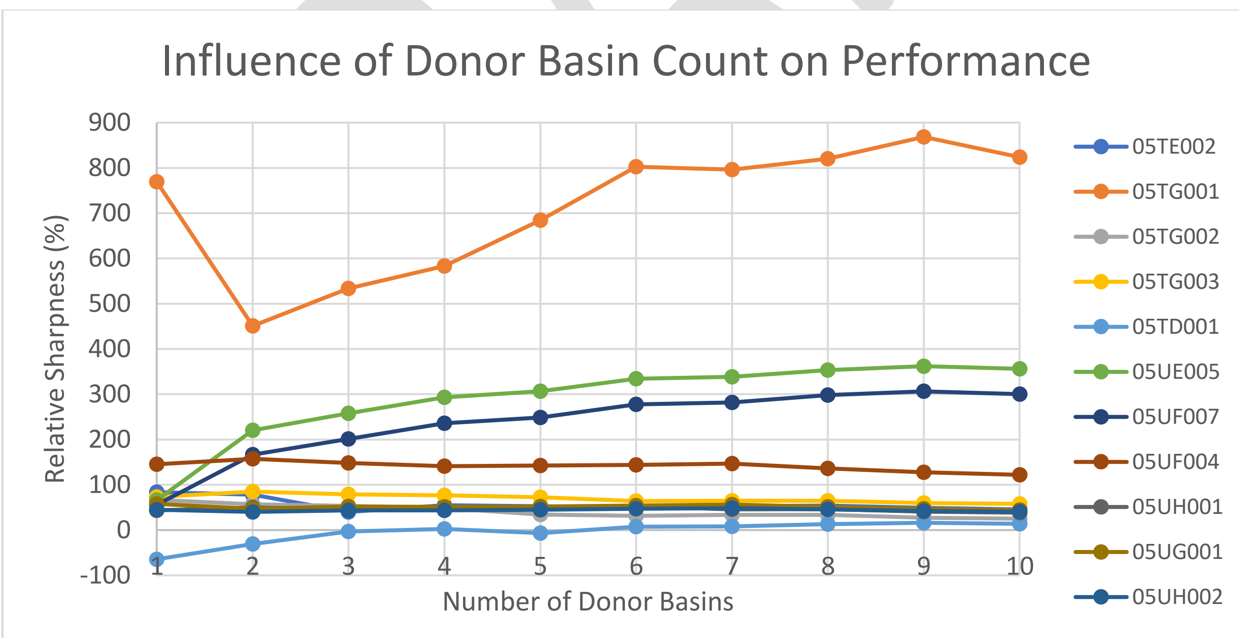

FIGURE 3.2.28 Relative sharpness (RS) calculated for the full 1981-2010 period for each of the 11 gauges with the number of donor basins varied from 1 to 10 donor basins. Reproduced from Pokorny et al. (in preparation) (Confidential pending publication).

Using the LNRB uncertainty results as well as the downscaling uncertainty and the output uncertainty, we have been able to generate an ensemble of uncertainty runs (Appendix B, Table 2.4-1; 1216 possible hydrologic outcomes) specific to the hydrologic characteristics of each river, while keeping the relationship across the bay climatically consistent (Tefs et al., in preparation). This method makes use of analytic concepts, simplified to numeric methods for efficient computing to generate representative output. Assessing the variability in output (discharge) due to ensemble variability, inter-annual climatic variability, and modelling uncertainty, the results indicate that seasonally, modelling uncertainty, and ensemble variability dominate uncertainty (Figure 3.2.29). As periods progress (1981 to 2010, 2011 to 2040, 2041 to 2070), the ensemble variability in the NCRB becomes more dominant in three of four seasons (for both $HHYPE_{REG}$ and $HHYPE_{NAT}$). In the LGRC, modelling uncertainty is greater than ensemble variability, in keeping with results from earlier studies (MacDonald et al., 2018; Stadnyk et al., 2019). In both basins, inter-annual variability is the smallest contributor to uncertainty, although the ensemble variability of the naturalized LGRC is also very small in winter. In the LGRC, the presence of regulation shifts the range of values to the degree that it exceeds the modelling uncertainty in three of four seasons (spring, autumn, and winter). This is not the case in any season in the NCRB.

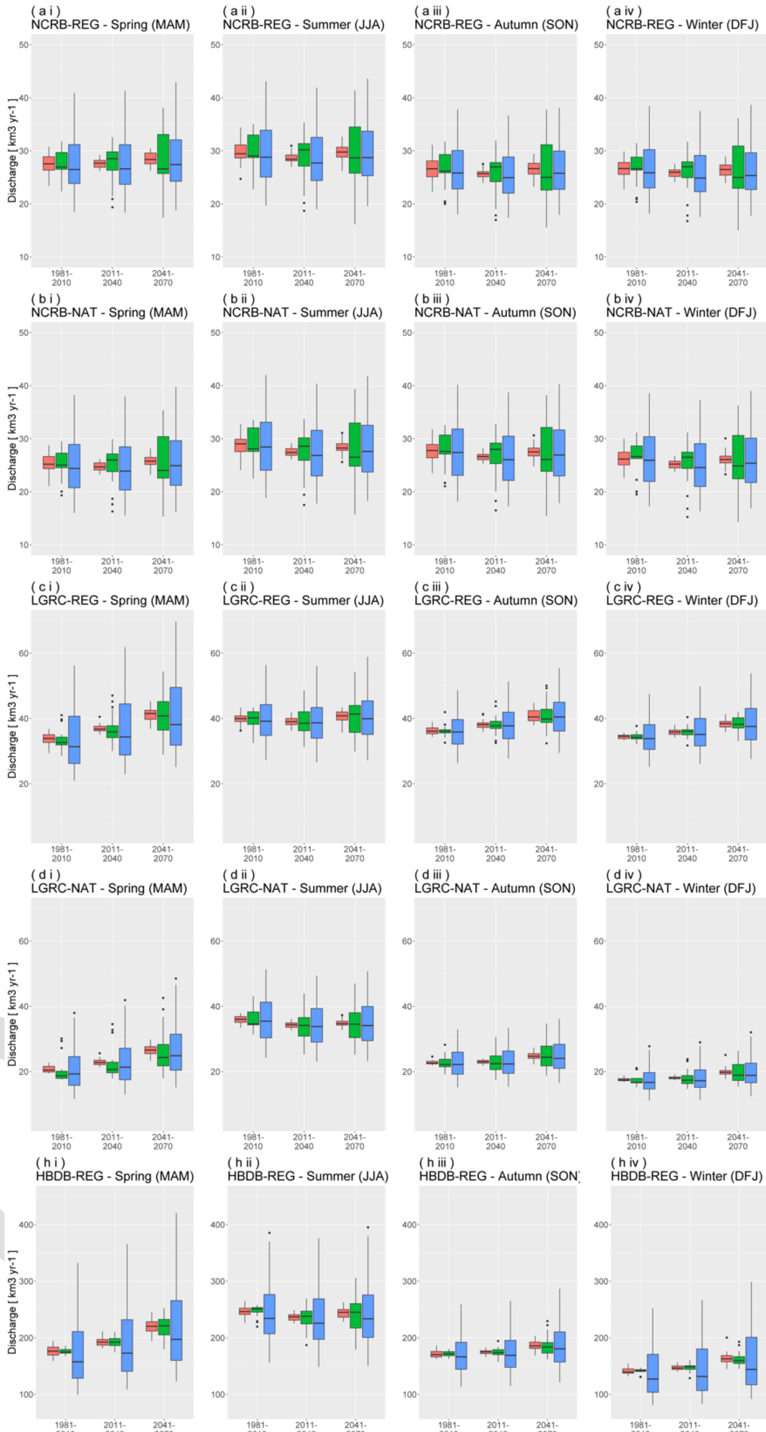

FIGURE 3.2.29 Seasonal, climate-normal period distributions of discharge (all shown in km3 bulk discharge by season) for (red) inter-annual, (green) ensemble members, and (blue) modelling uncertainty storylines. Inter-annual: n = 30, yearly mean of ensemble members and uncertainty storylines. Ensemble: n = 19, member mean of period years and uncertainty storylines. Uncertainty: n = 64, storyline mean of period years and ensemble members. Plotted boxes denote the limits of the interquartile range (IQR), separated by median value, whiskers extending to 1.5 times the IQR, any outliers shown beyond the whiskers as dots. Reproduced from Tefs et al., in preparation (Figure 5). (Confidential pending publication).

3.2.4 Conclusions

The BaySys proposal required Team 2 to address two integrated objectives that were designed to understand the relative impacts of regulation and climate change on freshwater quality and quantity being delivered to the HBC. We conclude this chapter by summarizing the results from our BaySys investigations as they pertain to each stated objective.

> **Hypothesis 2.1:** Freshwater export into Hudson Bay is expected to increase under climate change.
>
> **Hypothesis 2.2:** Regulation is expected to influence the variability and timing of annual peak flows.

Continental-scale HBDB Hydrologic Modelling

By developing and leveraging historical datasets, we have been able to calibrate our models to various elements of the hydrologic cycle (*in-situ* snow course data and FluxNet evapotranspiration datasets). This gives us greater confidence in the robustness of our projections, which also use a significantly descriptive climatic input ensemble. All of this combined provides reliable runoff and terrestrial climate datasets to be used by other BaySys Teams to describe baseline conditions for the HBDB. In studying observed datasets, we gain insight into the historical context for terrestrial freshwater conditions associated with fieldwork seasons.

> ***Hypothesis H2.1 should not be rejected:***
> *Ensemble freshwater runoff generation (not regulated or naturalized) is expected to increase, with Mann-Kendall significance shown for all seasons in the future (2020 to 2070) and winter in the past (1981 to 2005).*
> ***Hypothesis H2.2 should not be rejected:***
> *Historic observations show that regulation affects sub-weekly and intra-annual variability as well as inter-annual variability beyond the extent of historic climate change.*

By developing a comprehensive database of observed, historic climatic and discharge conditions for the HBDB rivers, we can initially assess the effects of both climate change and hydroelectric regulation. Doing so indicates that regulation plays a significant role in changing the annual historic flow regime of regulated rivers in a way that is not seen in those rivers that are not regulated. This is quantified by examining decadal average daily values and the coefficient of variation between the years in those decades as well as spectral decomposition of hydrograph signals. Further evidence is shown for climate change driving increasing trends to all elements of the hydrologic cycle under (global mean) warming of 1.5 and 2.0°C of HBDB regional changes. The coupling of regulation effects and an intensifying hydrologic cycle highlight the need to model the differences between the net and individual effects and to understand the uncertainties inherent in this modelling.

Uncertainty Assessment of LNRB Discharge

By assessing and quantifying model sensitivity and four aspects of modelling uncertainty, we have created the base for a bay-wide framework to assess overall uncertainty in discharge. By focusing this study on the LNRB, we hope to provide the most detailed possible uncertainty bounds for one of the major estuaries studied by other BaySys Teams.

> ***Hypothesis 2.1 should not be rejected:***
> *All sources of uncertainty are important to hydrologic modelling studies in data-sparse regions.*
> ***Hypothesis 2.2 should not be rejected:***
> *Uncertainty is not constant in time and, therefore, requires the inclusion of low likelihood uncertainty tails to be representative of the larger BaySys region.*

Generating a comprehensive uncertainty analysis for the entire HBDB domain was not computationally feasible, therefore, a comprehensive uncertainty estimate for the LNRB was used to study sensitivity, calibration, and uncertainty in a remote, industrially-relevant region (LNRB) and further, to inform uncertainty estimates for the HBDB region through uncertainty transfer. Uncertainties associated with climate data input, model structure, and model parameters were estimated and compared to a simple estimate of observed streamflow uncertainty, which suggested the ensemble was better performing than any of the individual models in the ensemble. The wide range of input uncertainty was further valuable to explore structural and parameter uncertainties under different climate conditions; uncertainty generally converged under very dry conditions while uncertainty bounds became wider under very wet conditions. The results from different climate inputs were valuable to explore the expected effects of future projected climate data and highlight vulnerabilities in single-model studies of data-sparse regions.

Regulated NCRB and LGRC Modelling

The paired regulated and naturalized models (and ensuing datasets) allow Team 2 to contribute quantifiable hydrologic changes caused by (a) climate change, (b) hydroelectric regulation, and (c) simultaneous climate change and hydroelectric regulation. This contributes directly to the BaySys objectives by providing a base for comparing the effects of the drivers of change to the HBC. These datasets have been used by Team 6 as the boundary runoff for comparative NEMO runs and will hopefully be used by all BaySys Teams in the quantification of the effects of climate change and regulation in the cycling of carbon and impacts of contaminants.

> ***Hypothesis H2.1 should not be rejected:***
> *Total annual freshwater runoff generation is expected to increase in the two largest regulated basins, with greater agreement between ensemble members in the LGRC than the NCRB.*
> ***Hypothesis H2.2 should not be rejected:***
> *Regulated and naturalized model configurations show expected differences between (a) total monthly discharge and (b) ensemble dispersion in both the LGRC and NCRB, with inter-annual variability more notable in the NCRB.*

By simulating regulation ($HHYPE_{REG}$) and the absence of hydroelectric regulation ($HHYPE_{NAT}$), we hope to improve the understanding of the downstream effects of hydroelectric regulation (i.e., on the freshwater-marine interface), but also to improve the understanding of the interacting effects of changing hydrology and regulation (i.e., effects on net evaporation upstream of regulated reservoirs). By projecting regulated and non-regulated results, we have shown that as climate change progresses, it may create interannual variability which surpasses the regulated systems' capacity to regulate flow, depending on the basins' upstream storage capabilities. We also show that re-apportionment of discharge intra-annually is driven more extensively by hydroelectric regulation (flows stored for periods of greatest demand) than by climate change (progression from nival to mixed or pluvial regimes). Similarly, our work has indicated the presence of hydropeaking in observed discharge records and shown that regulation within these basins has a discernable impact on the timing and magnitude of peak flows that is progressive as development has occurred.

Uncertainty Assessment of HBDB Discharge

Together, these results contribute to the BaySys objectives by adding uncertainty bounds to the ensemble projections generated. This allows all BaySys Teams to bracket any projections or budgets with plausible uncertainty limits. A selection of these uncertainty time series will also be used for NEMO sensitivity studies, which will help quantify the oceanographic model's sensitivity to certain processes and will help inform the understanding of the changing conditions in the HBC.

> ***Hypothesis H2.1 should not be rejected***
> *Climate change is expected to increase the total discharge to the HBDB, though seasonally the degree of change is unclear due to modelling uncertainty.*
> ***Hypothesis H2.2 should not be rejected***
> *The role of regulation in changing the timing of peak flow exceeds modelled uncertainty for at least half of the flow supplied to the HBDB.*

Antecedent precipitation, normalized to a historical climatic average, was used in conjunction with flow signatures to predict modelling uncertainty from the LNRB to the larger HBDB. Transferred uncertainty bounds were generally similar to the model-generated uncertainty bounds in the LNRB; transferred uncertainty bounds are most conservative where flow signatures of HBDB rivers were notably different from available the LNRB donor basins. Uncertainty time series generated through this work will help inform sensitivity limits of freshwater (as river discharge) to the oceanographic models, allowing a more robust understanding of the realism of modelled processes in marine dynamics, sea ice formation, and biogeochemical processes in the larger HBC, while also helping to describe those hydrologic processes which are best represented. Uncertainty transfer results suggest that transferred modelling uncertainty is more likely to be an underestimate, based on LNRB results. Transferred uncertainty is, therefore, likely conservative for most locations. The method of sampling wide precipitation uncertainty bounds to assess modelling-generated uncertainty produced reasonable results under climate change conditions. Results showed uncertainty estimates were generally robust to climate change-imposed uncertainty.

3.2.5 Gaps and Recommendations

An incredible amount of work was conducted as part of BaySys Team 2, such that it will require significant time beyond the funded BaySys project to utilize its full capacity and to understand all ramifications of the counter opposing forces of water regulation and climate change. We have addressed the deliverables of our objectives and uncovered new processes which have bearing on the overarching objectives of BaySys. We conclude by summarizing these gaps and making recommendations for further work from the perspective of Team 1:

a) Any data produced in Task 2.1 uses a version of the HHYPE model which incorporates the HYPE model's built-in regulation routines, which are shown to be less accurate at adapting reservoir discharge to long-term wet or dry periods. Task 2.1 discharge results for upstream, regulated stations should be treated with caution if using a monthly temporal resolution or finer due to the routines used to govern regulation. Details regarding HYPE routines governing routing and regulated reservoir discharge can be found on the SMHI HYPE wiki ("Rivers and Lakes", 2019).

   Additionally, Task 2.1 results were generated using the version 1 input data (which was bias corrected to NRCan). Because this bias correction product (and the subsequent model parameter calibrations) differs from that used for NEMO (ERA-Interim), these results are not ideally integrated. Hydrologic results can be treated as hydrologically descriptive, but their integration (as boundary runoff) with oceanographic modelling should be treated as less trustworthy than those hydrologic data generated using v2 input data (which are calibrated to the same bias correction dataset as the oceanographic model). Details of the model developed, and the input data used, can be found in MacDonald et al. (2018), Stadnyk et al. (2019), Stadnyk et al. (2020), and Braun et al. (2021).

b) Only bilinear interpolation was used to re-grid the gridded climate datasets; the effects of other spatial interpolation methods were not explored. Ensemble minimum and ensemble maximum precipitation datasets were beyond the uncertain range of observed data; minimum and maximum datasets were used to sample a range of relative partitions of structural and parameter uncertainty but reduced the accuracy of the hydrologic models by deviating from realistic climatic conditions. Additionally, all output from the HYPE model was generated from the early version presented in Task 2.1 (discussed above). Parameter and input sampling was limited by computational budget, additional sampling would have better explored the response surface of the model ensemble.

   Further sampling of meteorological input data would have filled in regions of zero sampling density, which would have better informed how far beyond the range of observed uncertainty the ensemble minimum and ensemble maximum products extended. Model parameter sets were selected without consideration of output uncertainty; output uncertainty was considered in post-processing only. Additional consideration of output uncertainty should be integrated into the calibration of models, as well as the addition of more model structures. Finally, it would be beneficial to develop a simple framework for the estimation of hydrometric flow data uncertainty that would be widely applicable to the larger HBDB without requiring extensive historical rating curve access.

The outcome of the VIC uncertainty assessment is centered around the VARS sensitivity and OLHS uncertainty analysis and is limited to the tools and methods. However, it can be equally useful for advanced modelling practices, by promoting a multi-criteria sensitivity analysis approach and under various conditions for an improved, comprehensive understanding of the model structure, reducing model prediction uncertainty, and conducting a more efficient calibration.

Future work investigating the effect of factors such as initial or boundary conditions and/or other model variables such as soil moisture or evapotranspiration in model sensitivity assessment could add to already in-depth studies of the LNRB.

c) Regulated results for the NCRB (1981 to 2070, daily) were computed using regulation rules determined from historical operations (2001 to 2010, daily) and validated on the reservoirs' operational records within the BaySys historical period (1981 to 2010, daily). These operating rules are a series of inflow-storage-outflow algorithms which are generalized and optimized but not tailored to real-world operations. These operations rules, while striving to maintain intra-annual flow levels, do not adapt to climate change or likely changes to operational policy.

These reservoir outflow records should not in any way be construed as a realistic projection of daily hydropower production. They can be used to project a monthly or seasonal estimate of outflow futures, but only in a future where reservoir safety limits remain unchanged. Details regarding the development of the embedded HHYPE regulation routines and the simulation skill thereof can be found in Tefs et al. (in revision (a)).

Regulated results for the LGRC (1981 to 2070, daily for Rivière Rupert, and weekly for La Grande Rivière) were computed using current regulation rules practiced operationally for Hydro-Québec long-term projections. These rules govern minimum required flow, production optimizing, and water level maintenance. These reservoir outflow records should not be construed as a realistic projection of daily or weekly hydropower production. They can be used to project a monthly or seasonal estimate of outflow futures, but only in a future where reservoir regulatory operations are unchanged.

Naturalized results were generated by approximating natural discharge from reservoirs using stage-discharge curves from pre-development records and pre-development flooded areas. These areas and curves are approximate and daily discharge should not be considered to be realistic predictions but as a monthly or seasonal approximation of climatic representation of natural discharge. Details regarding the development of the HHYPE naturalized results and their comparison to regulated results can be found in Tefs et al. (in revision (b)).

Though regulated and naturalized results are all forced by the climatic ensemble created for v2 (bias-corrected to HydroGFD), the method used to assign the gridded climatic input data to the HYPE sub-basins varies by drainage region and model used (regulated or naturalized). Those watersheds which drain James Bay use v2 input data for naturalized results and v2.1 input data for regulated results. Those watersheds which drain Hudson Bay, the Foxe Basin, Hudson Strait, and Ungava Bay use v2 input data for both regulated and naturalized results. As a result of this input data mixing, it is not possible to analyse the differences between regulated and naturalized results for any given James Bay river or estuary. Differences between regulated and naturalized output in James Bay should only be described when considering James Bay in its entirety (sum of outflows). Those rivers and estuaries outside James Bay can be considered individually when comparing the effects of climate change and hydroelectric regulation, though simulation skill at temporal resolution less than monthly or seasonally is unchanged. The rationale for this input data mixing is detailed in “re: Updated James Bay v2 HYPE Input”, circulated to all BaySys Team leads May 14, 2019.

In view of partially resolving some of these gaps and uncertainties, we recommend certain future work. First is the adaptation of the HYPEREG code to make it usable in Worldwide HYPE (WHYPE). In its current iteration, the reservoir regulation code is more preferable for industry partners but is unviable in larger model domains (requires an individual text file for each reservoir integrated). It would similarly be useful to simulate LGRC regulation using the embedded regulation rules. This would reduce reliance on Hydro-Québec in-kind hours for future work studying uncertainty or self-adaptive regulation. Studying regulation rules which do not remain static (or rules which are self-adaptive) would also be of interest to study changing climate and runoff regimes. Such a study would involve regulation rules designed to re-calibrate regulation parameters every 10-30 years, based on new hydrologic regimes.

d) The development of the hydrologic uncertainty time series (64 x 19 = 1216 possible time series, 1981 to 2070, daily) assumes that each uses a single “seed” for the unperturbed bay-wide discharge. This was done to ensure that each river’s time series is climatically coherent and that each day’s spatial variation (between the rivers) is also coherent. Through the three steps of uncertainty considered (accounting for four types of uncertainty), discharge is perturbed to four points along a synthetic distribution, creating a total of 64 (4 points 3 steps = 64 time series) possible time series per seed.

Results passed to Team 6 for NEMO oceanographic modelling (2 regulated and 2 naturalized) represent a subset of one group of 64 (seeded with MRI-CGCM3-RCP8.5). These two values (per model configuration) were selected to study NEMO sensitivity to uncertainty in freshwater runoff and do not represent a full study of the possible uncertainty inherent in the basin or period hydrology. MRI-CGCM3-RCP8.5 was selected for Team 6 sensitivity study due to it being the “greatest change” scenario. Based on historic discharge (total of the HBDB) and changes (in both the near and far future) to absolute volume difference and monthly standard deviation, they were used to identify the run causing the most change to the historic hydrologic regime. All members of the climatic ensemble being considered equally possible, there is no reason to consider the unperturbed discharge simulated by MRI-CGCM3-RCP8.5 as more likely to occur than any others but selected in this case due to limited computing resources as the most interesting (most extreme) scenario to study oceanographic sensitivity.

It is important to note these values do not represent the entirety of the possible ensemble of values or even the entirety of the possible set of values available within BaySys. Because four discrete points are selected from each distribution of possible values, these should be taken as elements of distribution, not a continuous or analytical solution to total hydrologic uncertainty. These values should be taken as a representative distribution of possible uncertainty, not a descriptive range of discharges. It is equally important to note those aspects of total uncertainty which this study either does and does not include.

Those aspects included are: downscaling uncertainty (assigning gridded GCM-RCP data to HYPE sub-basins), parameter and model structural uncertainty (uncertainty inherent to HYPE model structure, and use of a single parameter set), and calibration observed uncertainty (the use of a reconstructed discrete time series for calibration).

Not included in the uncertainty study are the effects of regulation on hydrologic uncertainty. The discharge records which are serially perturbed are those terminating at Hudson Bay estuaries. Regulated discharge values are perturbed by the uncertainty methodology; perturbed upstream values are not regulated. Future studies will examine the effects of uncertainty in modelled regulation on total hydrologic uncertainty. However, the current set of discharge time series created may surpass (or fail to meet) safe levels prescribed by regulation rules due to the uncertainty perturbations of the time series. These regulated uncertainty discharge records do not represent a descriptive range of realistic discharge but reflect the possible discharge in light of those uncertainty aspects listed above. Details regarding the development of the uncertainty methodology and the limitations of the results can be found in Pokorny et al. (submitted) and Tefs et al. (in preparation).

To close the literature gaps in the uncertainty study, we recommend a future analysis including two other sources of uncertainty: regulation and input. To assess regulation uncertainty, we must reverse the order of operations of uncertainty and regulation to that used in Task 2.4. Work should be done to provide uncertainty Net Basin Supply (NBS) to regulation points rather than evaluating uncertainty at the outlet, where regulation has already taken place. This will require much more computational time for regulated modelling but will give a better understanding of the effects of regulation on the hydrologic uncertainty cascade. Similarly, computationally intensive, it would be useful to undertake multiple hydrologic simulations using multiple GCM initial conditions to first assess GCM uncertainty.

3.2.6 References Cited

The following is a list of publications produced and cited by Teams within the BaySys project.

Barber, D.G. (2014). BaySys – Contributions of climate change and hydroelectric regulation to the variability and change of freshwater-marine coupling in the Hudson Bay system. Retrieved from: http://umanitoba.ca/faculties/environment/department/ceos/mdeia/BaySys_PROJECT _DESCRIPTION.pdf

Braun, M., Thiombiano, A., Vieira, M., Stadnyk, T.A. (2021). Representing climate evolution in ensembles of GCM simulations for the Hudson Bay System. *Elementa: Science of the Anthropocene,* 9(1), 00011. https://doi.org/10.1525/elementa.2021.00011

Déry, S.J., Stadnyk, T.A., MacDonald, M.K., Gauli-Sharma, B. (2016). Recent trends and variability in river discharge across northern Canada. *Hydrology and Earth System Sciences*, 20(12), 4801-4818.

Déry, S.J., Stadnyk, T.A., MacDonald, M.K., Koenig, K.A. (2018). Flow alteration impacts on Hudson Bay river discharge. *Hydrological Processes*, 32(24), 3576-3587.

Déry, S.J., Marco A. Hernández-Henríquez, Tricia A. Stadnyk, Tara J. Troy. (submitted). Vanishing weekly cycles in American and Canadian hydropeaking rivers. Preprint, in revision, *Nature Climate Change* NCOMMS-21-12638. https://www.researchsquare.com/article/rs-441563/v1

Jafarikhasragh, S., Lukovich, J. V., Hu, X., Myers, P. G., Sydor, K., & Barber, D. G. (2019). Modelling Sea Surface Temperature (SST) in the Hudson Bay Complex Using Bulk Heat Flux Parameterization: Sensitivity to Atmospheric Forcing, and Model Resolution. *Atmosphere-Ocean*, 57(2), 120-133.

Lilhare, R., Déry, S J., Pokorny, S., Stadnyk, T.A., & Koenig, K.A. (2019). Intercomparison of Multiple Hydroclimatic Datasets across the Lower Nelson River Basin, Manitoba, Canada. *Atmosphere-Ocean*, 57(4), 262-278.

Lilhare, R., Pokorny, S., Déry, S.J., Stadnyk, T.A., Koenig, K.A., (2020). Sensitivity analysis and uncertainty assessment in water budgets simulated by the variable infiltration capacity model for Canadian subarctic watersheds. *Hydrological Process*. 34, 2057–2075. http://doi.org/10.1002/hyp.13711

Lukovich, J.V., Tefs, A., Jafarikhasragh, S., Pennelly, C., Kirillov, S., Myers, P.G., Stadnyk, T.A., Sydor, K., Wong, K., Stroeve, J., Barber, D.G. (2021a). A baseline evaluation of atmospheric and river discharge conditions in the Hudson Bay Complex during 2016-2018. *Elementa: Science of the Anthropocene*, *9(1), 00126.* https://doi.org/10.1525/elementa.2020.00126

Lukovich, J.V., Jafarikhasragh, S., Tefs, A., Myers, P.G., Sydor, K., Wong, K., Stroeve, J.C., Stadnyk, T.A., Babb, D., Barber, D.G.. (2021b). A baseline evaluation of oceanographic and sea ice conditions in the Hudson Bay Complex during 2016-2018. *Elementa: Science of the Anthropocene*, 9(1), 00128. https://doi.org/10.1525/elementa.2020.00128

MacDonald, M.K., Stadnyk, T.A., Déry, S.J., Braun, M., Gustafsson, D., Isberg, K., Arheimer, B. (2018). Impacts of 1.5 and 2.0 degrees C warming on pan-Arctic river discharge into the Hudson Bay complex through 2070. *Geophysical Research Letters*, 45(15), 7561-7570.

Pokorny, S., Stadnyk, T.A., Lilhare, R., Ali, G., Déry, S. J., Koenig, K.A. (2020a). Towards assessing input data uncertainty in hydrologic models from ensemble-based gridded climate data. *Water*, 932925.

Pokorny, S., Stadnyk, T.A., Ali, G., Déry, S.J., Lilhare, R., Koenig, K. (2020b). Cumulative effects of uncertainty on simulated streamflow in a hydrologic modelling environment. *Elementa: Science of the Anthropocene*, 9(1), 431. https://doi.org/10.1525/elementa.431

Pokorny, S., Tefs, A., Stadnyk, T.A., Ali, G., Koenig, K.A. (submitted). Projecting Hydrologic Modelling Uncertainty across Varying Basin Scales and Temporal Periods. To be submitted to Water Resources Research. Submitted to *Water Resources Research*, 2020WR029082.

Ridenour, N.A., Hu, X., Jafarikhasragh, S., Landy, J.C., Lukovich, J.V., Stadnyk, T.A., Sydor, K., Myers, P.G., Barber, D.G. (2019). Sensitivity of freshwater dynamics to ocean model resolution and river discharge forcing in the Hudson Bay Complex. *Journal of Marine Systems*, 196, 48-64.

Stadnyk, T.A., Tefs, A., Broesky, M., Déry, S.J., Myers, P.G., Ridenour, N.A., Vonderbank, L., Gustafsson, D. (2021). Changing freshwater contributions to the Arctic: a 90-year trend analysis (1981-2070). *Elementa: Science of the Anthropocene,* 9(1), 00098. https://doi.org/10.1525/elementa.2020.00098

Stadnyk, T.A., MacDonald, M.K., Tefs, A., Awoye, O.H.R., Déry, S.J., Gustafsson, D., Isberg, K., and Arheimer, B. (2020). Hydrological modelling of freshwater discharge into Hudson Bay using HYPE. *Elementa: Science of the Anthropocene*, 8, 43. https://doi.org/10.1525/elementa.439

Stadnyk, T.A., Déry, S.J., MacDonald, M.K., Koenig, K.A. (2019). Freshwater System. In Barber, D., Kuzyk, Z., Candlish, L. *An Integrated Regional Impact Assessment of Hudson Bay: Implications of a Changing Environment*. Québec City, QC, Canada.

Tefs, A.A.G., Slota, P., Koenig, K., Stadnyk**,** T.A., MacDonald, M.K. Hamilton, M., Crawford, J. (2021). Simulating river regulation and reservoir performance in a continental-scale hydrologic model. Accepted to *Environmental Modelling & Software.* ENVSOFT_2019_485.

Tefs, A.A.G., MacDonald, M.K., Stadnyk, T.A., Koenig, K.A., Déry, S.J., Slota, P., Guay, C., Hamilton, M., Thiemonge, N., Vieira, M., Pokorny, S. (in revision). Modelling the relative effects of climate change and hydroelectric development on the changing freshwater exports to Hudson Bay. Submitted to Canadian Water Resources Journal.

Tefs, A.A.G.; Stadnyk, T.A.; Koenig, K.A.; Déry, S.J.; Ali, G.; Guay, C.; Pokorny, S. (in prep). Uncertainty in projections of freshwater supply to the Hudson Bay Complex: How quantifying uncertainty leads to greater confidence. Submitted to *Elementa: Science of the Anthropocene*.

Other Works Cited

Ajami, N.K., Duan, Q., Sorooshian, S. (2007). An integrated hydrologic Bayesian multimodel combination framework: Confronting input, parameter, and model structure uncertainty in hydrologic prediction. *Water Resources Research,* 43(1).

Anctil, F., Couture, R. (1994). Cumulative impacts of hydroelectric development on fresh-water levels of Hudson Bay. *Canadian Journal of Civil Engineering,* 21(2), 297-306.

Andersson, J., Pechlivanidis, I., Gustafsson, D., Donnelly, C., Arheimer, B. (2015). Key factors for improving large-scale hydrological model performance. *European Water*, 49, 77-88.

Andréassian, V., Coron, L., Lerat, J., Le Moine, N. (2016). Climate elasticity of streamflow revisited – an elastic index base on long-term hydrometeorological records. *Hydrology and Earth Systems Sciences*, 20, 4503-4524.

Arheimer, B., Donnelly, C., Lindström, G. (2017). Regulation of snow-fed rivers affects flow regimes more than climate change. *Nature Communications*, 8(62).

Asong, Z.E., Razavi, S., Whaeter, H.S., Wong, J.S. (2017). Evaluation of integrated multi-satellite retrievals for GPM (IMERG) over southern Canada against ground precipitation observations: A preliminary assessment. *Journal of Hydrometeorology*, 18(4), 1033-1050.

Bajracharya, A., Awoye, H., Stadnyk, T., Asadzadeh, M. (2020). Time Variant Sensitivity Analysis of Hydrological Model Parameters in a Cold Region using Flow Signatures. *Water*, 12(4), 961.

Berg, P., Donnelly, C., Gustafsson, D. (2018). Near-real-time adjusted reanalysis forcing data for hydrology. *Hydrology and Earth System Sciences*, 22(2), 989-1000.

Beven, K, Binley, A. (1992). The future of distributed models - Model calibration and uncertainty prediction. *Hydrological Processes*, 6(3), 279-298.

Beven, K. (2007). Towards integrated environmental models of everywhere: Uncertainty, data, and modelling as a learning process. *Hydrology and Earth System Sciences*, 11(1), 460-467.

Bring, A., Shiklomanov, A., Lammers, R.B. (2017). Pan-Arctic river discharge: Prioritizing monitoring of future climate change hot spots. *Earth's Future*, 5, 72-92.

Bourgin, F., Andreassian, V., Perrin, C., Oudin, L. (2015). Transferring global uncertainty estimates from gauged to ungauged catchments. *Hydrology and Earth System Sciences*, 19, 2535-2546.

Casajus, N., Perie, C., Logan, T., Lambert, M.C., de Blois, S., Bertaux, D. (2016). An objective approach to select climate scenarios when projecting species distribution under climate change. *PLoS ONE*, 11(3), E0152495.

Charley, W., Pabst, A., Peters, J. (1995). The Hydrologic Modelling System (HEC-HMS): Design and development issues. *Computing in Civil Engineering*, 1-2, 131-138.

Chen, J., Brissette, F.P., Poulin, A., Leconte, R. (2011). Overall uncertainty of the hydrological impacts of climate change for a Canadian watershed. *Water Resources Research*, 47, W12509.

Chen, J., Brissette, F.P., Chaumont, D., Braun, M. (2013). Finding appropriate bias correction methods in downscaling precipitation for hydrologic impact studies over North America. *Water Resources Research*, 49(7), 4187-4205.

Clark, M.P., Wilby, R.L., Gutmann, E.D., Vano, J.A., Gangopadhyay, S., Wood, A.W., Fowler, H.J., Prudhomme, C., Arnol, J.R., Brekke, L.D. (2016). Characterizing uncertainty of the hydrologic impacts of climate change. *Current Climate Change Reports*, 2, 55-64.

Coccia, G., Todini, E. (2011). Recent developments in predictive uncertainty assessment based on the model conditional processor approach. *Hydrology and Earth System Sciences*, 15, 3253-3274.

Courbariaux, M., Barbillon, P., Parent, E. (2017). Water flow probabilistic predictions based on a rainfall-runoff simulator: a two-regime model with variable selection. *Journal of Agricultural, Biological, and Environmental Statistics,* 22(2), 194-219.

Dai, A., Trenberth, K.E. (2002). Estimates of freshwater discharge from continents: Latitudinal and seasonal variations. *Journal of Hydrometeorology,* 3(6), 660-687.

DeBeer, C.M., Wheater, H.S., Carey, S.K., Chun, K.P. (2016). Recent climatic, cryospheric, and hydrological changes over the interior of western Canada: A review and synthesis. *Hydrology and Earth Systems Sciences,* 20, 1573-1598.

Déry, S.J., Stieglitz, M., McKenna, E.C., Wood, E.F. (2005). Characteristics and trends of river discharge into Hudson, James, and Ungava Bays, 1964-2000. *Journal of Climate*, 18, 2540-2557.

Déry, S.J., Mlynowski, T.J., Hernandez-Henriquez, M.A., Straneo, F. (2011). Interannual variability and interdecadal trends in Hudson Bay streamflow. *Journal of Marine Systems*, 88(3) 341-351.

Donnelly, C., Andersson, J.C.M., Arheimer, B. (2016). Using flow signatures and catchment similarities to evaluate the E-HYPE multi-basin model across Europe. *Hydrological Sciences Journal*, 61(2), 255-273.

Dynesius, M., Nilsson, C. (1994). Fragmentation and flow regulation of river systems in the northern third of the world. *Science, New Series,* 266(5186), 753-762.

Eastwood, R.A., Macdonald, R.W., Ehn, J.K., Heath, J., Arrangutainaq, L., Myers, P.G., Barber, D.G., Kuzyk, Z.A. (2020). Role of river runoff and sea ice brine rejection in controlling stratification throughout winter in southeast Hudson Bay. *Estuaries and Coasts,* 43(4) 756-786.

Gan, Y.J., Daun, Q.Y., Gong, W., Tong, C., Sun, Y.W., Chu, W., Ye, A.Z., Miao, C.Y., Di, Z.H. (2014). A comprehensive evaluation of various sensitivity analysis methods: A case study with a hydrological model. *Environmental Modelling & Software,* 51, 269-285.

Gelfan, A., Gustafsson, D., Motovillov, Y., Arheimer, B., Kalugin, A., Krylenko, I., Lavrenov, A. (2017). Climate change impacts om the water regimes of two great Arctic rivers: Modelling and uncertainty issues. *Climatic Change,* 141, 499-515.

Granskog, M.A., Kuzyk, Z.A., Azetsu-Scott, K., Macdonald, R.W. (2011). Distributions of runoff, sea ice melt and brine using δ18O and salinity data: A new view on freshwater cycling in Hudson Bay. *Journal of Marine Systems,* 88(3), 362-374.

Her, Y., Yoo, S.-H., Seong, C., Jeong, J., Cho, J., Hwang, S. (2016). Comparison of uncertainty in multi-parameter and multi-model ensemble hydrologic analysis of climate change. *Hydrology and Earth System Sciences Discussions,* 10.5194/hess-2016-160.

Hong, Y., Hsu, K.-L., Moradkhani, H., Sorooshian, S. (2006). Uncertainty quantification of satellite precipitation estimation and Monte Carlo assessment of the error propagation into hydrologic response. *Water Resources Research,* 42, W08421.

Ingram, R.G., Wang, J., Lin, C., Legendre, L., Fortier, L. (1996). Impact of freshwater on a subarctic coastal ecosystem under seasonal ice (southeastern Hudson Bay, Canada). I. Interannual variability and predicted global warming influence on river plume dynamics and sea ice. *Journal of Marine Systems,* 7(2-4), 221-231.

Koutsoyiannis, D. (2016) Generic and parsimonious stochastic modelling for hydrology and beyond. *Hydrological Sciences Journal*, 61(2), 225-244.

Kouwen, N. (1988). WATFLOOD: a micro-computer based flood forecasting system based on real-time weather radar. *Canadian Water Resources Journal*, 13(1), 62-77.

Krzysztofowicz, R., Kelly, K.S. (2000). Hydrologic uncertainty processor for probabilistic river stage forecasting. *Water Resources Research,* 36(11), 3265-3277.

Lespinas, F., Fortin, V., Roy, G., Rasmussen, P., Stadnyk, T.A. (2015). Performance evaluation of the Canadian precipitation analysis (CaPA). *Journal of Hydrometeorology*, 16(5), 2045-2064.

de Levanne, A., Cudennec, C. (2019). Assessment of freshwater discharge into a coastal bay through multi-basin ensemble hydrological modelling. *Science of the Total Environment*, 669, 812-820.

Liang, X., Lettenmaier, D.P., Wood, E.F., Burges, S.J. (1994). A simple hydrologically based model of land-surface water and energy fluxes for general-circulation models. *Journal of Geophysical Research-Atmospheres*, 99(D7), 14415-14428.

Lindström, G., Pers, C., Rosberg, R., Strömqvist, J., Arheimer, B. (2010). Development and test of the HYPE (Hydrological Predictions for the Environment) model – A water quality model for different spatial scales. *Hydrological Research*, 41(3-4), 295-319.

Lu, G.Y., Wong, D.W. (2008). An adaptive inverse-distance weighting spatial interpolation technique. *Computational Geoscience*, 34(9), 1044–1055.

Madec, G. (2008). the Nemo team (2008) NEMO ocean engine. Note du Pôle de modélisation, Institut Pierre-Simon Laplace (IPSL), France, (27).

Montanari, A., Koutsoyiannis, D. (2012). A blueprint for process-based modelling of uncertain hydrological systems. *Water Resources Research*, 48, W09555.

Pechlivanidis, I., Arheimer, B. (2015). Large-scale hydrological modelling by using modified PUB recommendations: the India-HYPE case. *Hydrology and Earth System Sciences* 19(11), 4559-4579.
Razavi, S., Gupta, H.V. (2016). A new framework for comprehensive, robust, and efficient global sensitivity analysis: Theory. *Water Resources Research,* 52(1), 423-439.

River and Lakes [HYPE Model Documentation]. (2019) Retrieved from: http://www.smhi.net/hype/wiki/doku.php?id=start:hype_model_description:hype_routing.

Taylor, K.E., Stouffer, R.J., Meehl, G.A. (2012). An overview of CMIP5 and the experiment design. *Bulletin of the American Meteorological Society*, 93(4), 485-498.

Tebaldi, C., Knutti, R. (2007). The use of multi-model ensemble in probabilistic climate projections. *Philosophical Transactions of the Royal Society – Mathematical, Physical, and Engineering Sciences*, 365(1857), 2053-2075.

van Meijgaard, E., L. H. van Ulft, W. J. van de Berg, F. C. Bosveld, B. J. J., M. van den Hurk, G. Lenderink, and A. P. Siebesma (2008), The KNMI regional atmospheric climate model, version 2.1, KNMI Technical Report 302, R. Neth. Meteorol. Inst., De Bilt, Netherlands

Vehtari, A., Gelman, A., Gabry, J. (2017). Practical Bayesian model evaluation using leave-one-out cross-validation and WAIC. *Statistics and Computing,* 27(5), 1413-1432.

Verkade, J.S., Brown, J.D., Davids, F., Reggiani, P., Weerts, A.H. (2017). Estimating predictive hydrological uncertainty by dressing deterministic and ensemble forecasts, a comparison, with application to Meuse and Rhine. *Journal of Hydrology,* 555, 257-277.

Vrugt, J.A, ter Braak, C.J.F., Diks, C.G.H., Robinson, B.A., Hyman, J.M., Hidgon, D. (2009). Accelerating Markov Chain Monte Carlo simulation by differential evolution with self-adaptive randomized subspace sampling. *International Journal of Nonlinear Sciences and Numerical Simulation*, 10(3), 273-290.

Wada, Y., Bierkens, M.F.P., de Roo, A., Diermeyer, P.A., Famiglietti, J.S., Hanasaki, N., Konar, M., Liu, J., Schmied, H.M., Oki, T., Pokhrel, Y., Sivapalan, M., Troy, T.J., van Dijk, A.I.J.M., van Emmerik, T., van Huijgevoort, M.H.J., van Lanen, H.A.J., Vorosmarty, C.J., Wanders, N., Wheater, H. (2017). Human-water interface in hydrological modelling: current status and future directions. *Hydrology and Earth System Sciences*, 21, 4169-4193.

Weerts, A.H., Winsemius, H.C., Verkade, J.S. (2011). Estimation of predictive hydrological uncertainty using quantile regression: examples from the National Flood Forecasting System (England and Wales). *Hydrology and Earth System Sciences*, 15, 255-265.

Westerberg, I.K., Wagener, T., Coxon, G., McMillan, H.K., Castellarin, A., Montanari, A., Freer, J. (2016). Uncertainty in hydrological signatures for gauged and ungauged catchments. *Water Resources Research*, 52, 1847-1865.

3.2.7 Appendix A: Additional Figures and Tables

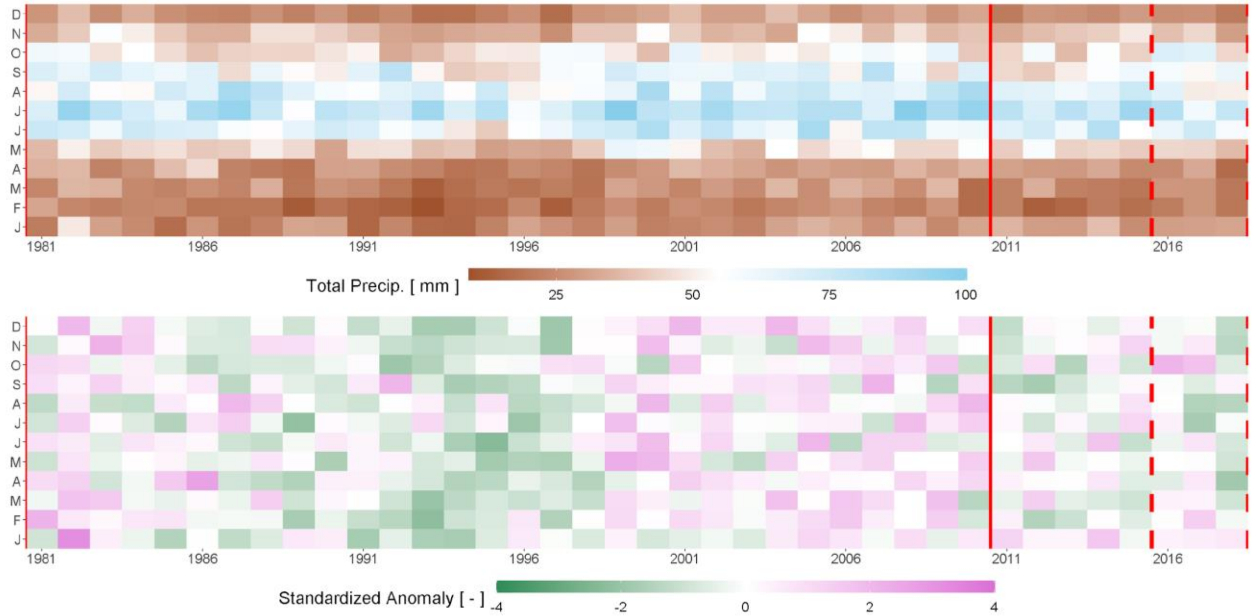

Figure A1: *HBDB monthly HydroGFD total precipitation (top) value and (bottom) standardized anomaly. Anomalies computed relative to mean and standard deviation are computed 1981-2018 for each month. Solid red lines indicate reference period, dashed red lines indicate observation period limits. Reproduced from: Lukovich et al., in preparation (Figures TBD) (Confidential pending publication).*

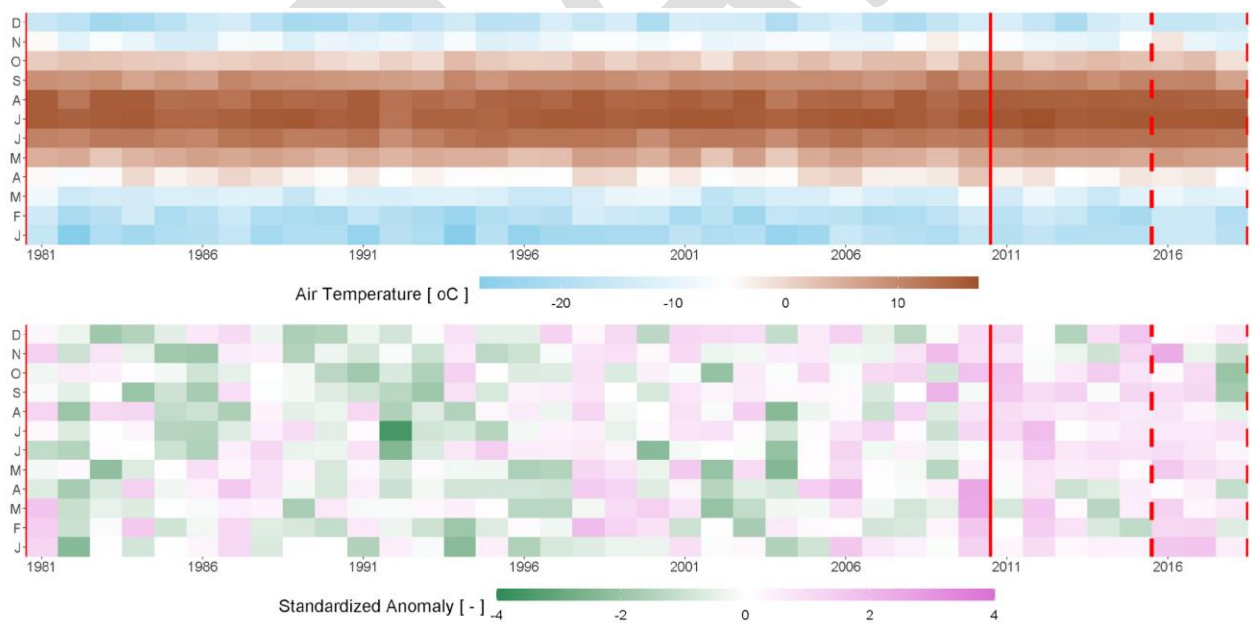

Figure A2: *HBDB monthly HydroGFD air temperature (top) value and (bottom) standardized anomaly. Anomalies computed relative to mean and standard deviation are computed 1981-2018 for each month. Solid red lines indicate reference period, dashed red lines indicate observation period limits. Reproduced from: Lukovich et al., in preparation (Figures TBD) (Confidential pending publication).*

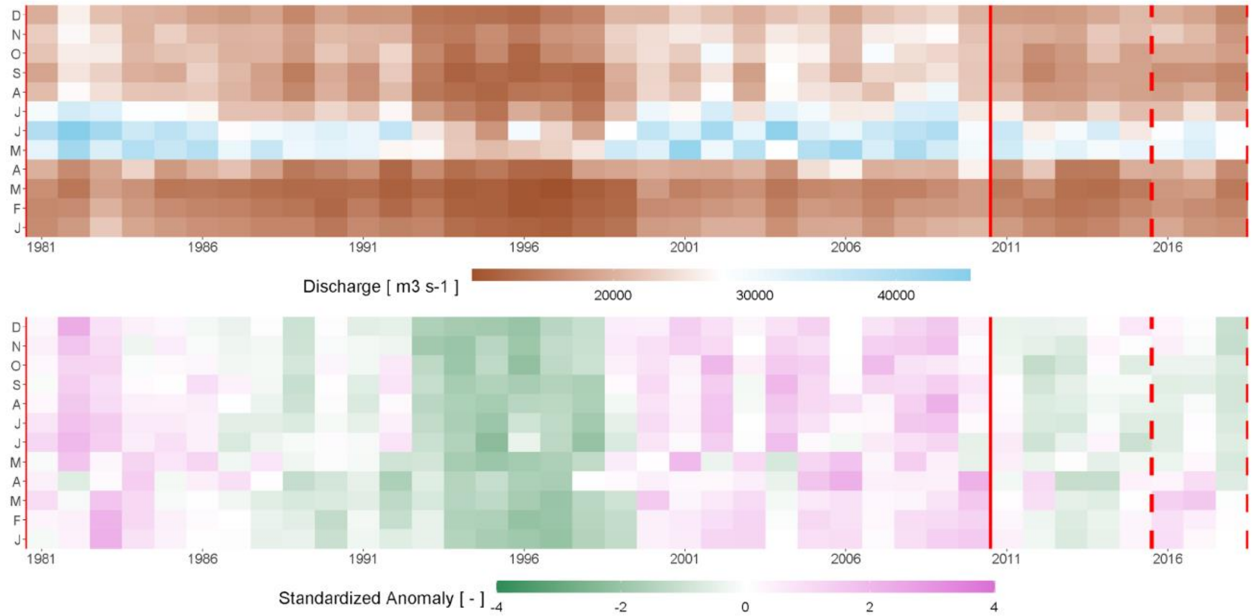

Figure A3: *HBDB monthly (regulated in $HHYPE_{REG}$) HydroGFD discharge (top) value and (bottom) standardized anomaly. Anomalies computed relative to mean and standard deviation are computed 1981-2018 for each month. Solid red lines indicate reference period, dashed red lines indicate observation period limits. Reproduced from: Lukovich et al., in preparation (Figures TBD) (Confidential pending publication).*

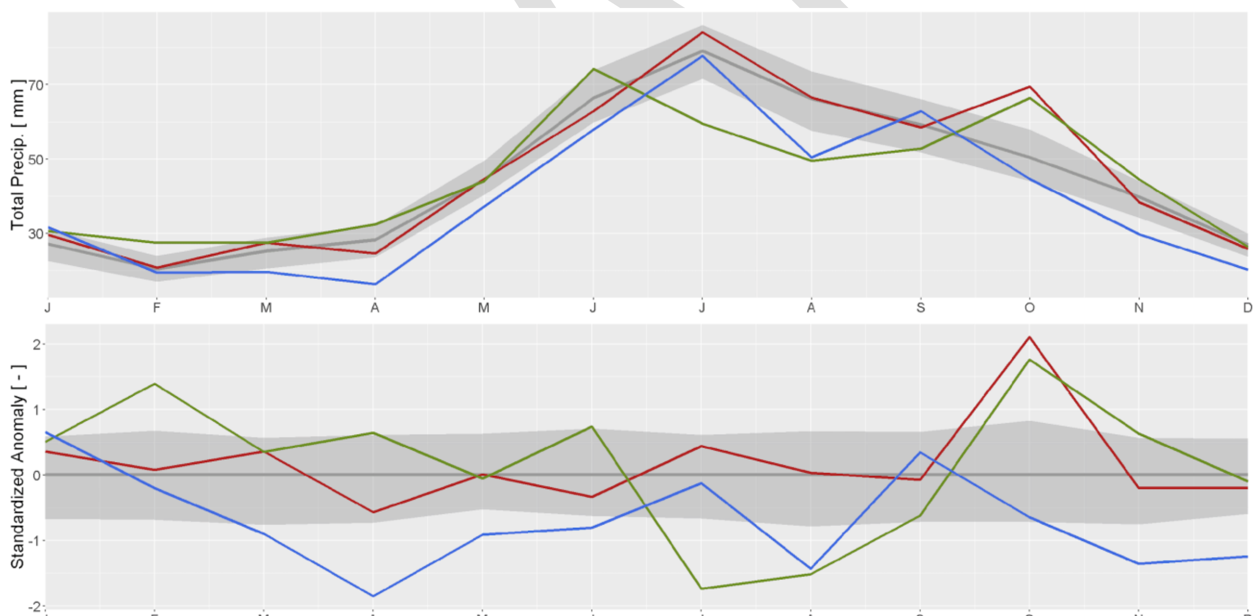

Figure A4: *HBDB monthly HydroGFD total precipitation (top) value and (bottom) standardized anomaly. Anomalies computed relative to mean and standard deviation are computed 1981-2018 for each month. Timeseries shown for (gray region) reference period IQR, (gray line) reference period mean, (red) 2016, (green) 2017, and (blue) 2018. Reproduced from: Lukovich et al., in preparation (Figures TBD) (Confidential pending publication).*

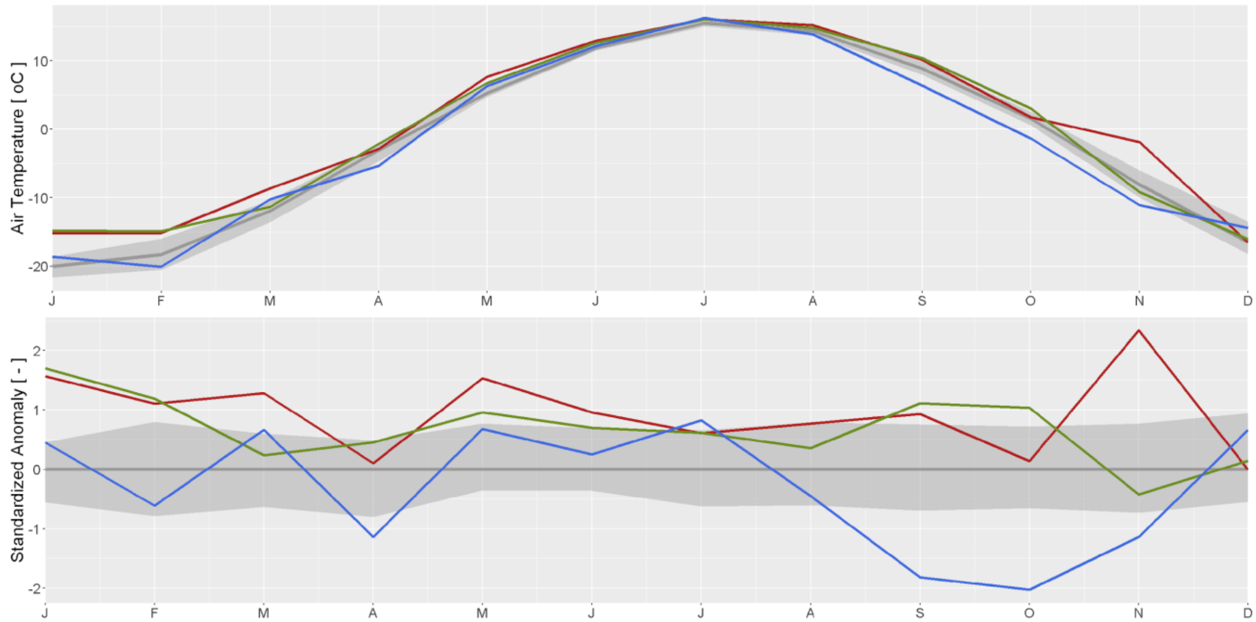

Figure A5: *HBDB monthly HydroGFD air temperature (top) value and (bottom) standardized anomaly. Anomalies computed relative to mean and standard deviation are computed 1981-2018 for each month. Timeseries shown for (gray region) reference period IQR, (gray line) reference period mean, (red) 2016, (green) 2017, and (blue) 2018. Reproduced from: Lukovich et al., in preparation (Figures TBD) (Confidential pending publication).*

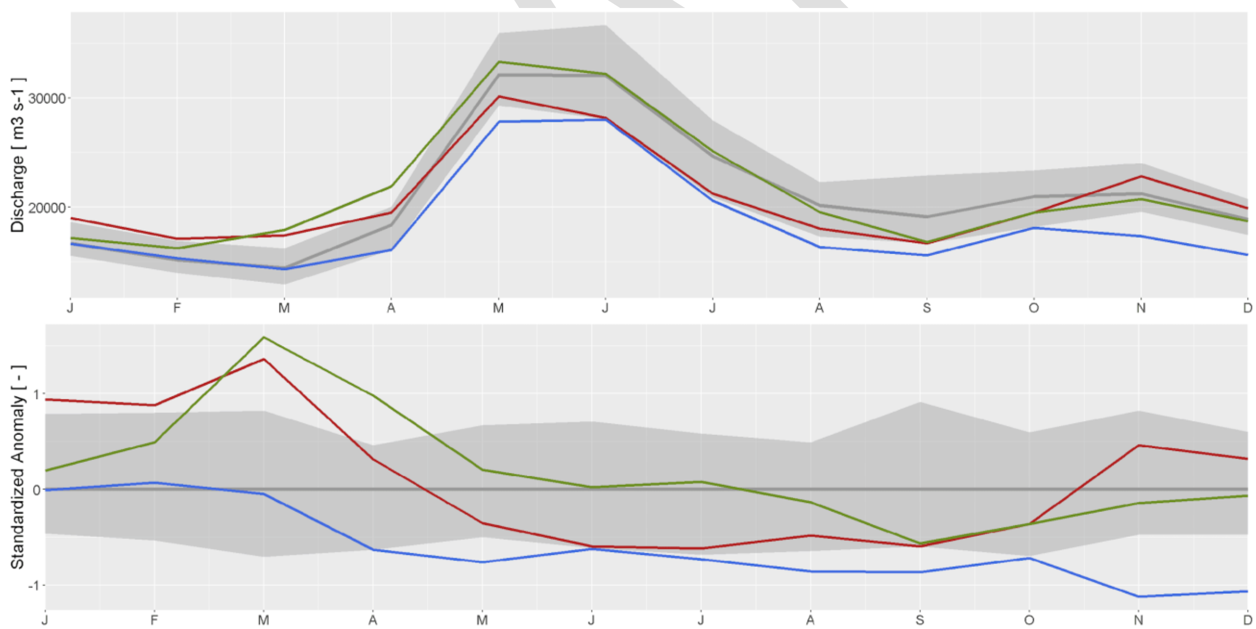

Figure A6: *HBDB monthly (regulated in HHYPE$_{REG}$) HydroGFD discharge (top) value and (bottom) standardized anomaly. Anomalies computed relative to mean and standard deviation are computed 1981-2018 for each month. Timeseries shown for (gray region) reference period IQR, (gray line) reference period mean, (red) 2016, (green) 2017, and (blue) 2018. Reproduced from: Lukovich et al., in preparation (Figures TBD) (Confidential pending publication).*

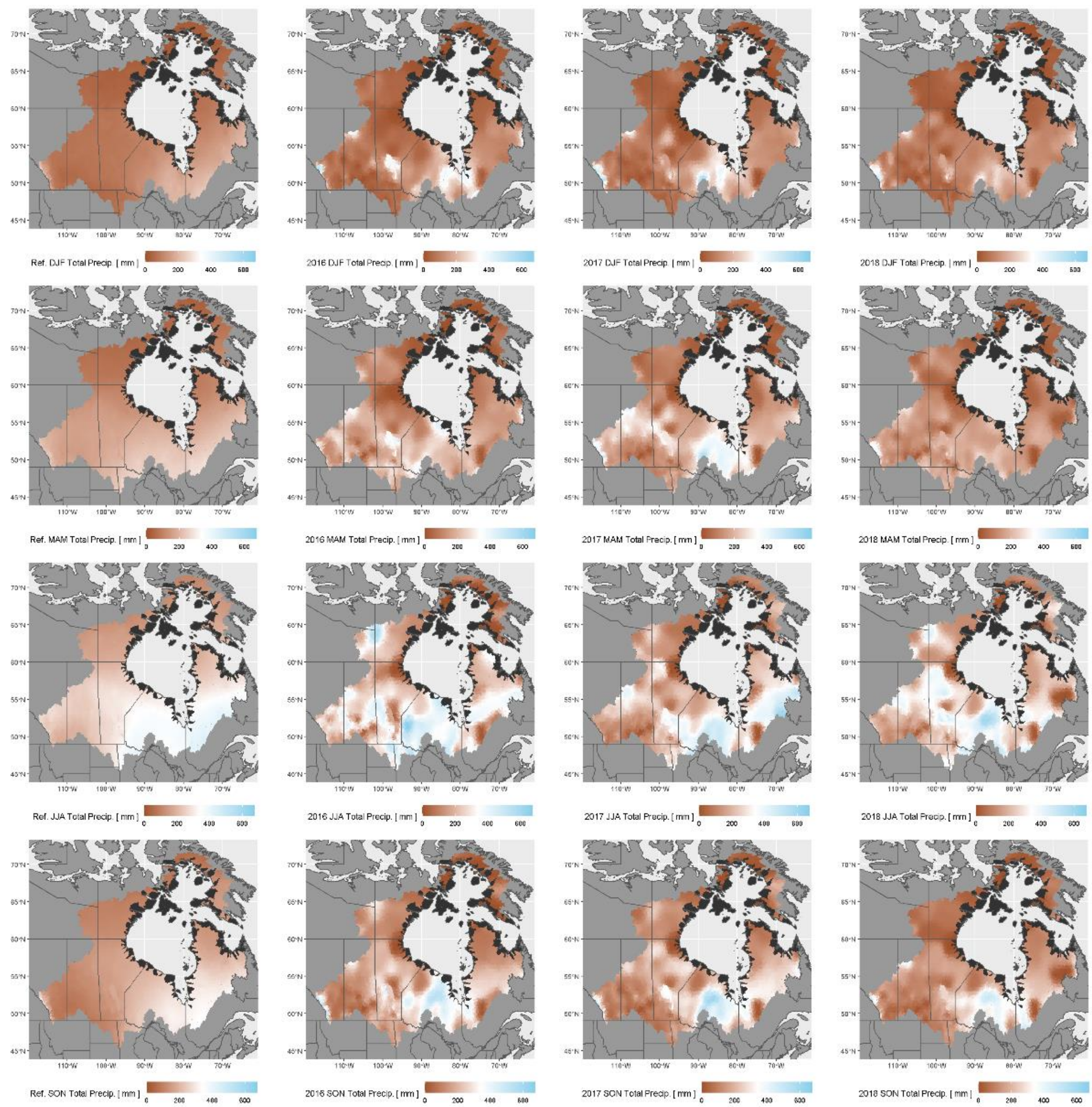

Figure A7: *HBDB seasonal (winter: DJF, spring: MAM, summer: JJA, and autumn: SON) HydroGFD total precipitation for (left) reference period mean, (second left) 2016, (second right) 2017, and (right) 2018. Reproduced from: Lukovich et al., in preparation (Figures TBD) (Confidential pending publication).*

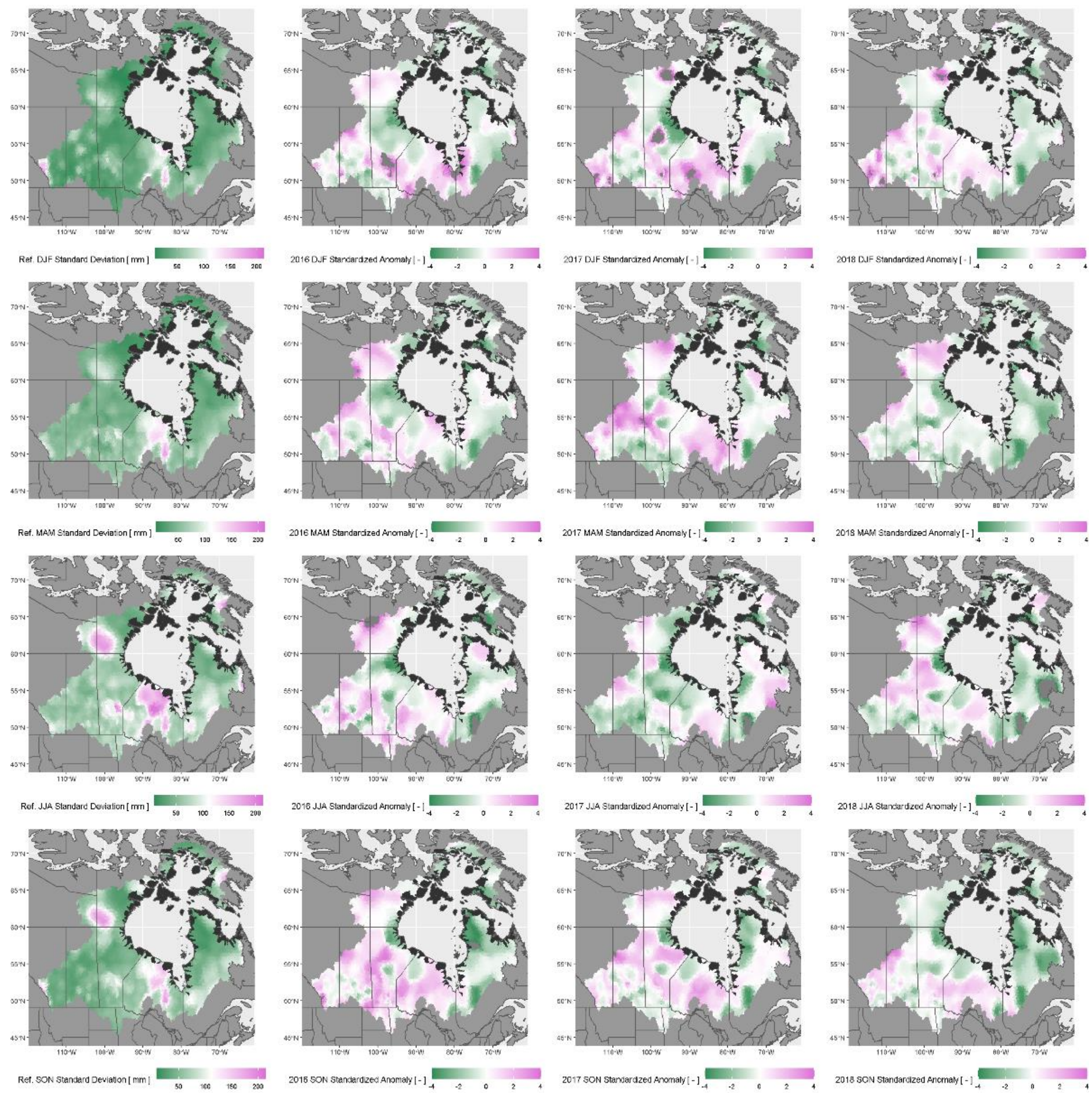

Figure A8: *HBDB seasonal (winter: DJF, spring: MAM, summer: JJA, and autumn: SON) HydroGFD total precipitation for (left) reference period standard deviation and standardized anomaly for (second left) 2016, (second right) 2017, and (right) 2018. Reproduced from: Lukovich et al., in preparation (Figures TBD) (Confidential pending publication).*

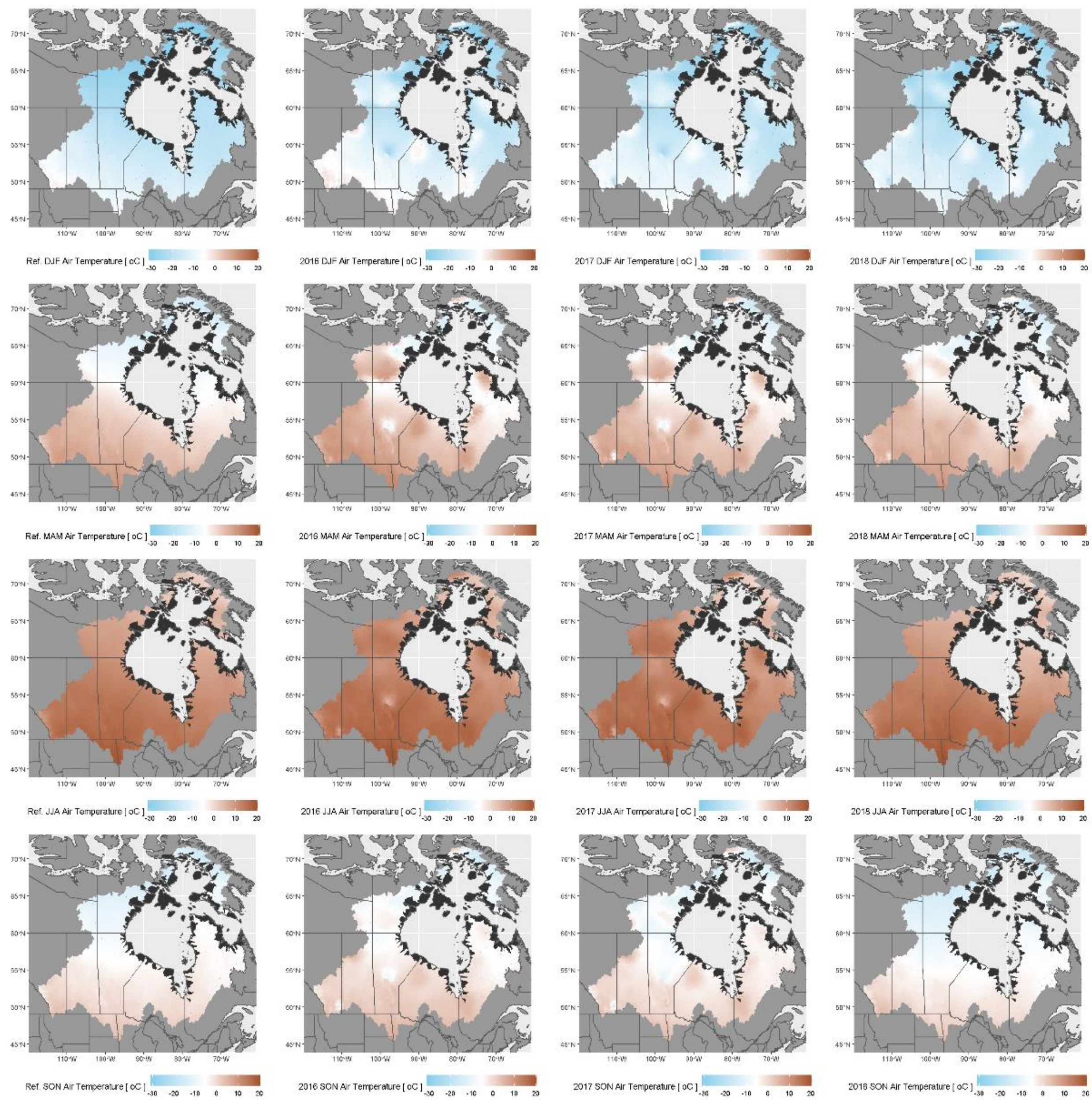

Figure A9: *HBDB seasonal (winter: DJF, spring: MAM, summer: JJA, and autumn: SON) HydroGFD air temperature for (left) reference period mean, (second left) 2016, (second right) 2017, and (right) 2018. Reproduced from: Lukovich et al., in preparation (Figures TBD) (Confidential pending publication).*

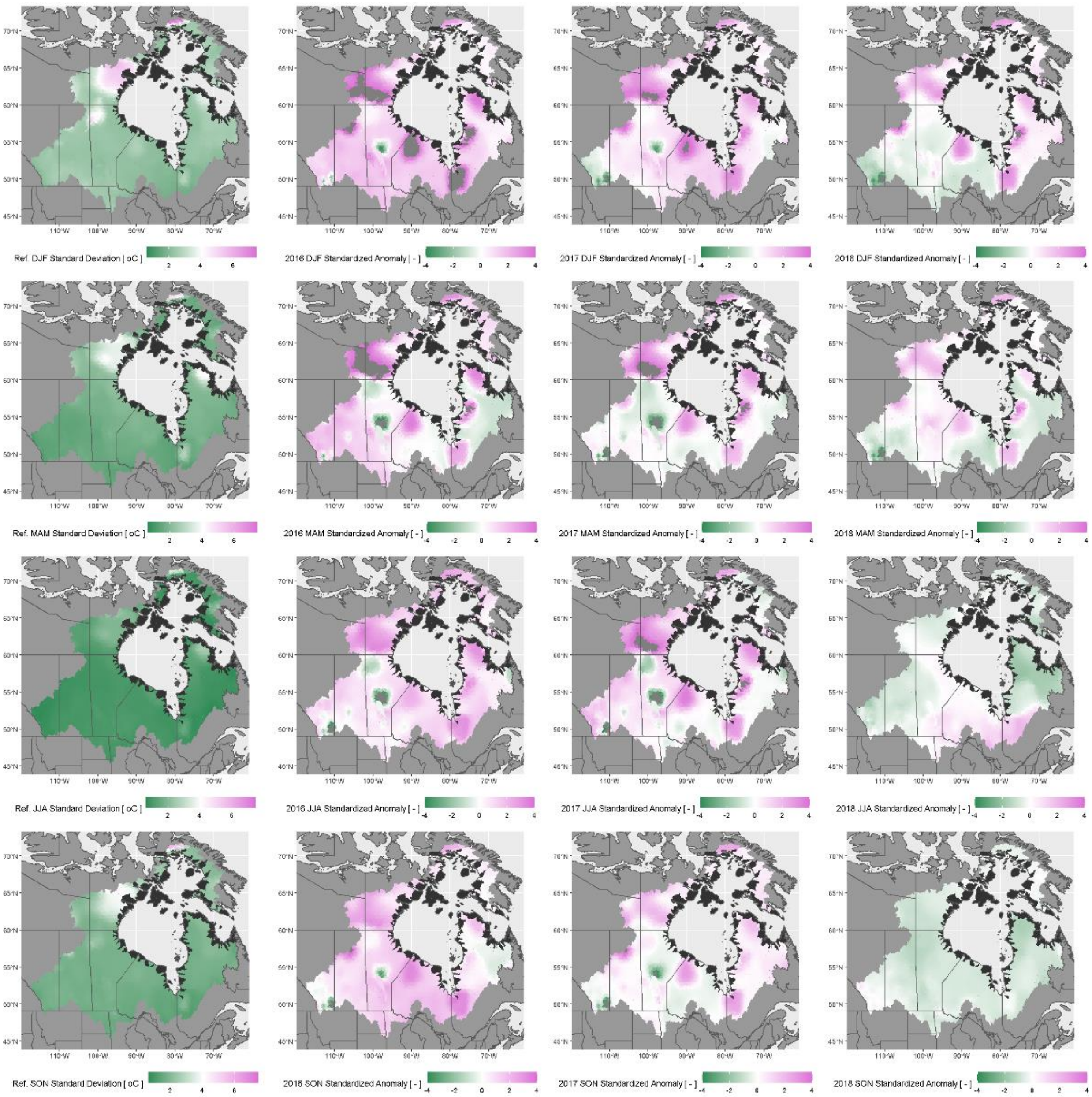

Figure A10: *HBDB seasonal (winter: DJF, spring: MAM, summer: JJA, and autumn: SON) HydroGFD air temperature for (left) reference period standard deviation and standardized anomaly for (second left) 2016, (second right) 2017, and (right) 2018. Reproduced from: Lukovich et al., in preparation (Figures TBD) (Confidential pending publication).*

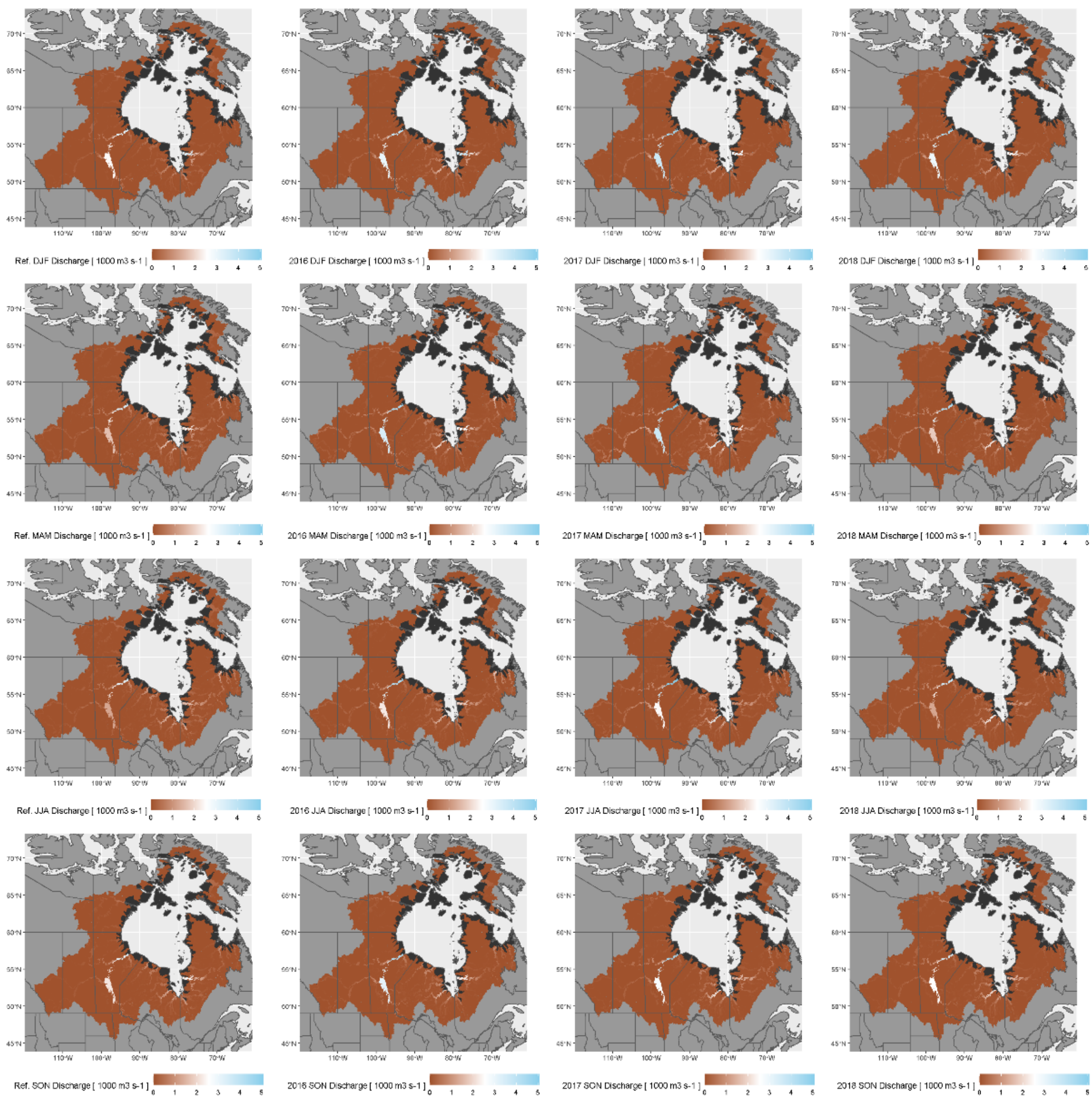

Figure A11: *HBDB seasonal (winter: DJF, spring: MAM, summer: JJA, and autumn: SON) HydroGFD discharge (regulated in $HHYPE_{REG}$) for (left) reference period mean, (second left) 2016, (second right) 2017, and (right) 2018. Reproduced from: Lukovich et al., in preparation (Figures TBD) (Confidential pending publication).*

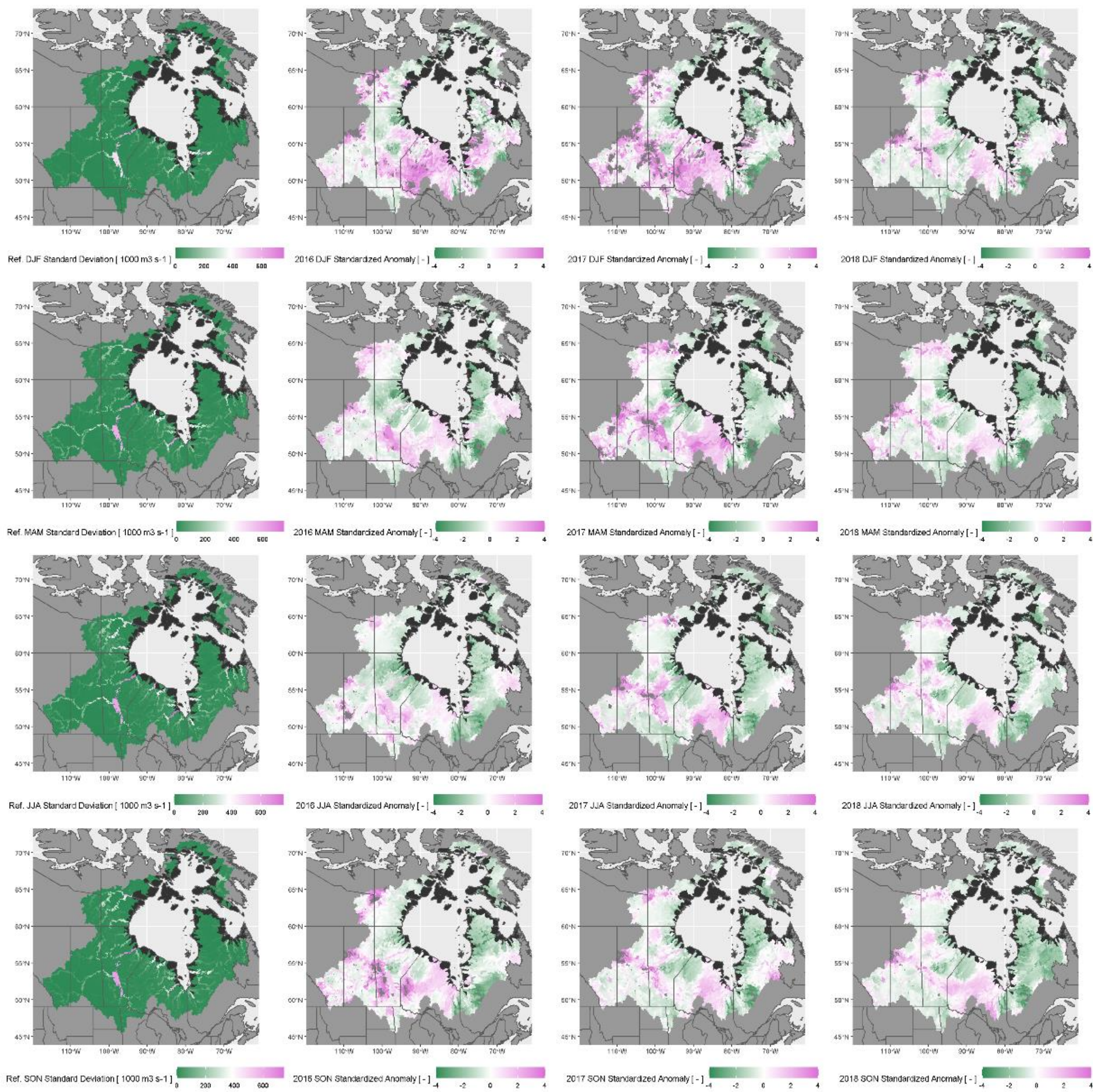

Figure A12: *HBDB seasonal (winter: DJF, spring: MAM, summer: JJA, and autumn: SON) HydroGFD discharge (regulated in* $HHYPE_{REG}$*) for (left) reference period standard deviation and standardized anomaly for (second left) 2016, (second right) 2017, and (right) 2018. Reproduced from: Lukovich et al., in preparation (Figures TBD) (Confidential pending publication).*

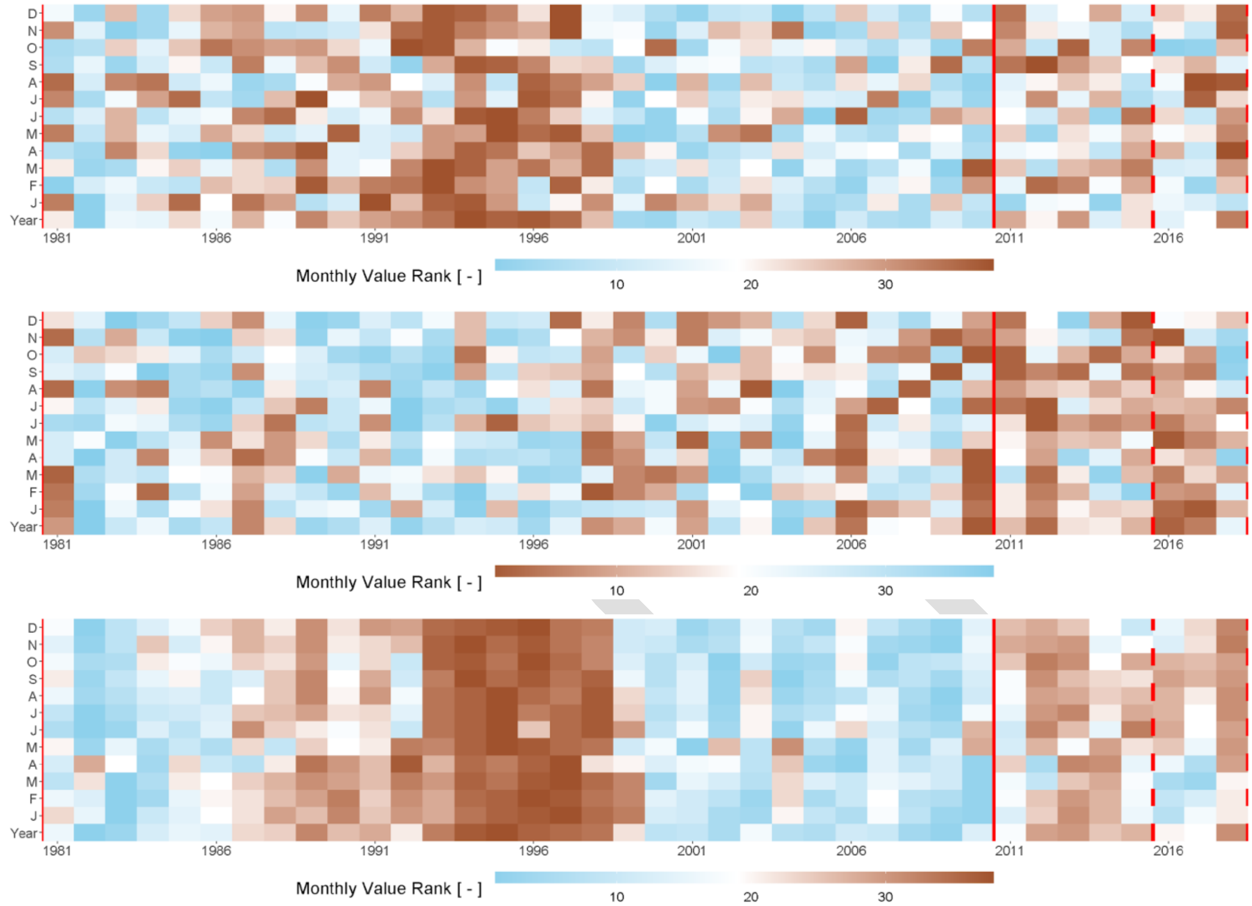

Figure A13: *Descending ranks of HBDB monthly for HydroGFD (top) total precipitation, (middle) air temperature, and (bottom) discharge (regulated in HHYPE$_{REG}$) value. Solid red lines indicate reference period, dashed red lines indicate observation period limits. Reproduced from: Lukovich et al., in preparation (Figures TBD) (Confidential pending publication).*

3.2.8 Appendix B: List of Data Products Used (Input) and Available (Output)

Task 2.1 Continental Scale Modelling

Any questions regarding the preparation and publication of the observed discharge records should contact Stephen Déry (stephen.dery@unbc.ca), those regarding model development results can be addressed by Andrew Tefs (andrew.tefs@ucalgary.ca), those regarding bias-correction of CMIP-5 climatic data to Marco Braun (braun.marco@ouranos.ca).

Table 2.1-1: Climate data used as input for hydrologic modelling

Code	Type	Aspect	Base Data	Modifications / Use
a	Calibration Input	Climate forcing	Hydrologic Global forcing Data (HydroGFD; Berg et al., 2018)	v2: Assigned to subbasins using grid-to-subbasin weighting
b			Global Forcing Data Watch ERA Interim (Berg et al., 2018)	v1: Assigned to subbasins using grid-to-subbasin weighting
c	Projection Input		Ensemble of 19 climatic datasets selected (Stadnyk et al., 2019) from CMIP-5 (Taylor et al., 2012), bias corrected (bias-correction base data listed in “Modifications”; Chen et al., 2013)	v1: Bias-corrected to NRCan, assigned to subbasins using grid-to-subbasin weighting
d				v2: Bias-corrected to HydroGFD, assigned to subbasins using inverse distance weighting (IDW)
e				v2.1: Bias-corrected to HydroGFD, assigned to subbasins using nearest neighbour

Table 2.1-2: Data used in HBDB HYPE model setup (HHYPE v1)

Code	Type	Aspect	Base Data	Modifications / Use
a	Calibration Input	Climate Input	v1: see Table 2.1-1b	None
b	Model Data	Topography	USGS Hydro 1k (https://lta.cr.usgs.gov/HYDRO1K)	Used to delineate subbasin polygons and subbasin slope

c		Lakes and reservoirs	Global Lake and Wetland Database (GLWD; Lehner and Döll, 2004), Global Lake Database v2 (Kourzeneva, 2010), Global Reservoir and Dam database (GRanD v1.1; Lehner et al., 2011)	Used to determine lake subbasin polygons and properties of lake and dam parameters
d		Soil type	Harmonised World Soil Database (Nachtergaele et al., 2012)	Assigned to subbasins by weighting native grids to polygons
e		Land cover	ESA CCI LC 2010 v1.4 (ESA Climate Change Initiative – Land Cover Project 2014)	
f	Calibration Dataset	Observed river discharge	ECCC Water Survey of Canada; USGS National Water Information System	Re-construction (Déry et al., 2011) of major river outlets
g	Model Process	Various	Frozen soil representation improved, dynamic non-contributing areas added, and lakes physiographically parameterized	Model processes improved per Stadnyk et al. 2020)
h	Model Data	Parameters	ArcticHYPE base parameters (Andersson et al., 2015)	Calibrated for BaySys period and rivers of interest per Stadnyk et al. (2020)
i	Model	Calibrated hydrologic model	Note that: b, c, d, e, g, and h together (known as HHYPE v1)	None

Table 2.1-3: Data used in HHYPE v1 historic and projected hydrologic cycle modelling

Code	Type	Aspect	Base Data	Modifications / Use
a	Projection Input	Climate Input	v1: see Table 2.1-1c	None
b	Model	Calibrated Hydrologic Model	HHYPE v1: see Table 2.1-2i	None
c	Output Dataset	Hydrologic Cycle Output	Precipitation, temperature, evapotranspiration, and discharge; simulated 1981 to 2070	Daily computation aggregated to annual for output

Task 2.2 Localized Sensitivity Analysis

Any questions regarding climatic input sensitivity or LNRB modelling uncertainty data should contact Scott Pokorny (umpokors@myumanitoba.ca) or Rajtantra Lilhare (lilhare@unbc.ca).

Table 2.2-1 Data used in sensitivity study

Code	Type	Aspect	Base Data	Modifications / Use
a	Climate Data	Climate Input	NARR (Mesinger et al. 2006); WFDEI (Weedon et al. 2014); NRCAN (Hutchinson et al. 2009); ERA-Interim (Dee et al. 2011); HydroGFD (Berg et al., 2018)	Bilinearly interpolated to match NRCAN's spatial grid over the Nelson Churchill Watershed
b	Validation Data	Climate Data	AHCCD (Mekis and Vincent 2011)	None
c	Calibration Data	Climate Input	Ensemble min., mean and max. (Pokorny et al. submitted (a))	None

Table 2.2-2 Models used for uncertainty analysis

Hydrologic Model	Hydrologic Processes	Selected methods	Comments
VIC (Liang et al, 1994)	Infiltration	Variable infiltration capacity curve	Large-scale, semi-distributed hydrologic model with 10 km grid spacing over the LNRB 1925 total VARS samples and 600 total OLH samples for the LNRB
	Evapotranspiration	Penman-Monteith equation	
	Snowmelt	Temperature and Radiation Index	
	Routing	Linearized Saint-Venant equation	
HYPE (Lindstrom et al., 2010) (Stadnyk et al., 2020	Infiltration	HYPE default infiltration	Semi-lumped sub-basin model with basin sizes generally around 400 km2 with 6900 total OLHS samples used
	Evapotranspiration	Priestly-Taylor	
	Snowmelt	Temperature + Radiation Index	
	Routing	Lag, Recession, and Attenuation	
WATFLOOD (Holmes, 2016)	Infiltration	Phillips Formula	Gridded model with 10 km grid spacing 15300 total OLHS samples used
	Evapotranspiration	Hargreaves	
	Snowmelt	Temperature Index	
	Routing	Storage routing	
HEC-HMS (Sagan, 2017)	Infiltration	Soil Moisture Accounting	

	Evapotranspiration	Priestly-Taylor	Semi-lumped sub-basin model with basin sizes ranging from 360 – 12,000 km2 18900 total OLHS samples used
	Snowmelt	Temperature Index	
	Routing	Muskingum	

Table 2.2-3 Data used in uncertainty study

Code	Type	Aspect	Base Data	Modifications / Use
a	Model	Calibrated Model	HEC-HMS (Sagan 2017); WATFLOOD (Holmes 2016); HYPE (see Table 2.1-2i)	HEC-HMS parameters and methods were updated for climate change studies
b	Calibration Data	Climate input	Ensemble minimum, mean and maximum (see Table 2.2-1)	None
		Hydrometric data	Water survey of Canada data (See table 2.2-4)	None
c	Model Data	Parameters	HEC-HMS (Sagan 2017); WATFLOOD (Holmes 2016); HYPE (see Table 2.1-2i)	Parameters generated with OLHS

Table 2.2-4 Hydrometric gauge data used for calibration and uncertainty analysis

Station Name	ID	Lon. (°W)	Lat. (°N)	Gauged Drainage Area (km^2)	Mean Annual Flow (m^3s^{-1})	Reg.
Footprint River above Footprint Lake	05TF002	98.88	55.93	643	3	No
Taylor River near Thompson	05TG002	98.19	55.48	886	5	No
Kettle River near Gillam	05UF004	94.69	56.34	1090	13	No
Angling River near Bird	05UH001	93.64	56.68	1560	11	No
Weir River above the Mouth	05UH002	93.45	57.02	2190	16	No
Limestone River near Bird	05UG001	94.21	56.51	3270	22	No
Burntwood River above Leaf Rapids	05TE002	99.22	55.49	5810	23	No
Odie River near Thompson	05TG003	97.35	55.99	6110	34	No
Grass River above Standing Stone Falls	05TD001	97.01	55.74	15400	65	No

Burntwood River near Thompson	05TG001	97.9	55.74	18500	867	Yes
Nelson River at Kelsey GS	05UE005	96.59	55.94	1050000	2350	Yes
Nelson River at Kettle Generating Station	05UF006	94.37	56.4	1100000	3550	Yes
Nelson River at Long Spruce Generating Station	05UF007	94.37	56.4	1100000	3550	Yes
Rat River below Notigi Control Structure	05TF003	99.29	55.86	6140	790	Yes
Nelson River (West Channel) at Jenpeg	05UB009	98.05	54.5	974500	1880	Yes
Nelson River (East Channel) below Sea River Falls	05UB008	97.59	54.24	976000	361	Yes

Task 2.3 Regulated System Modelling

Any questions regarding regulated and naturalized modelling and results can be addressed to Andrew Tefs (andrew.tefs@calgary.ca).

Table 2.3-1: *Data used in naturalized HHYPE model setup (HHYPE$_{NAT}$)*

Code	Type	Aspect	Base Data	Modifications / Use
a	Projection Input	Climate Input	v2: see Table 2.1-1d	None
b	Model Data	Land-cover Changes	Pre-development (period varies by reservoir) reservoir extents (shapefiles or gross area). Sources in Tefs et al., in revision (b)	Used to determine pre-development land-use for flooded reservoirs
c	Model Data	Lake Outflow Changes	Pre-development (period varies by reservoir) stage and discharge data. Sources in Tefs et al., in revision (b)	Used to determine pre-development stage-discharge relationships
d	Model	Calibrated Hydrologic Model	HHYPE v1: see Table 2.1-2i	see Table 2.3-1b and Table 2.3-1c
e	Output Dataset	Hydrologic Cycle Output	10 water cycle variables, 6668 subbasins, at monthly resolution, simulated 1981 to 2070	Daily computation aggregated to monthly for output
f	Output Dataset	Outlet Discharge Output	Discharge data at 398 outlets to Hudson Bay, at daily resolution, simulated 1981 to 2070	None

Table 2.3-2: *Data used in regulated HHYPE model setup (HHYPE$_{REG}$) outside James Bay*

Code	Type	Aspect	Base Data	Modifications / Use

a	Projection Input	Climate Input	v2: see Table 2.1-1d	None
b	Model Process	Reservoir Regulation	Regulation added at 13 reservoirs throughout the NCRB	For regulation of reservoirs
c	Model	Calibrated Hydrologic Model	HHYPE v1: see Table 2.1-2i	Uses HHYPE v1 with regulation added: see Table 2.3.-2b
d	Output Dataset	Hydrologic Cycle Output	10 water cycle variables, 5545 subbasins, at monthly resolution, simulated 1981 to 2070	Daily computation aggregated to monthly for output
e	Output Dataset	Outlet Discharge Output	Discharge data at 356 outlets to Hudson Bay, at daily resolution, simulated 1981 to 2070	None

Table 2.3-3: *Data used in regulated HHYPE model setup (*$HHYPE_{REG}$*) for James Bay*

Code	Type	Aspect	Base Data	Modifications / Use
a	Projection Input	Climate Input	v2.1: see Table 2.1-1e	None
b	Model	Calibrated Hydrologic Model	HHYPE v1: see Table 2.1-2i	None
c	Post-Processing	LGRC Regulation	Hydro-Québec regulation rules, using net basin supply inflows at 12 regulation points from HYPE	None
d	Output Dataset	Hydrologic Cycle Output	10 water cycle variables, 1123 subbasins, at monthly resolution, simulated 1981 to 2070	Daily computation aggregated to monthly for output
e	Output Dataset	Outlet Discharge Output	Discharge data at 42 outlets to Hudson Bay, at daily resolution, simulated 1981 to 2070	Regulation applied to La Grande Rivière and Rivière Rupert: see Table 2.3-3c

Table 2.3-4 *Hydrologic data distributed to Team 6 for NEMO simulations*

Code	Type	Aspect	Base Data	Modifications / Use
a	Output Dataset	Outlet Discharge Output	Naturalized discharge to Hudson Bay (Table 2.3-1f)	Subset of climate ensemble outputs used: MIROC5 (RCPs 4.5, 8.5), MRI-
b			Regulated discharge outside James Bay (Table 2.3-2e)	

c			Regulated discharge to James Bay (Table 2.3-3e)	CGCM3 (RCPs 4.5, 8.5), and GFDL-CM3 (RCP 4.5)

Table 2.3-5 *Other hydrologic datasets available for distribution*

Code	Type	Aspect	Base Data	Modifications / Use
a	Output Dataset	Outlet Discharge Output	Naturalized discharge to Hudson Bay (Table 2.3-1f)	None
b	Output Dataset	Outlet Discharge Output	Regulated discharge outside James Bay (Table 2.3-2e)	None
c	Output Dataset	Outlet Discharge Output	Regulated discharge to James Bay (Table 2.3-3e)	None
d	Output Dataset	Hydrologic Cycle Output	Naturalized variables within HBDB (Table 2.3-1e)	None
e	Output Dataset	Hydrologic Cycle Output	Regulated discharge within James Bay drainage (Table 2.3-2d)	None
f	Output Dataset	Hydrologic Cycle Output	Regulated discharge outside James Bay drainage (Table 2.3-3d)	None

Table 2.3-6: *Naturalized re-analysis hydrologic simulations*

Code	Type	Aspect	Base Data	Modifications / Use
a	Calibration Input	Climate Input	HydroGFD: see Table 2.1-1a	None
b	Model	Calibrated Hydrologic Model	$HHYPE_{NAT}$: see Table 2.3-1d	None
c	Output Dataset	Outlet Discharge Output	Discharge data at 398 outlets to Hudson Bay, at daily resolution, simulated 1981 to 2070	None
d	Output Dataset	Hydrologic Cycle Output	10 water cycle variables, 6668 subbasins, at monthly resolution, simulated 1981 to 2070	Daily computation aggregated to monthly for output

Table 2.3-7: *Regulated re-analysis hydrologic simulations*

Code	Type	Aspect	Base Data	Modifications / Use
a	Calibration Input	Climate Input	HydroGFD: see Table 2.1-1a	None

b	Model	Calibrated Hydrologic Model	HHYPE$_{REG}$: see Table 2.3-2c	
c	Output Dataset	Outlet Discharge Output	Discharge data at 398 outlets to Hudson Bay, at daily resolution, simulated 1981 to 2070	
d	Output Dataset	Hydrologic Cycle Output	10 water cycle variables, 6668 subbasins, at monthly resolution, simulated 1981 to 2070	Daily computation aggregated to monthly for output

Task 2.4 Bay-wide Discharge Uncertainty Study

Any questions regarding HBDB uncertainty, transfer of uncertainty data from the LNRB, or available uncertainty timeseries should contact Scott Pokorny (umpokors@myumanitoba.ca) or Andrew Tefs (andrew.tefs@ucalgary.ca).

Table 2.4-1: *Data used in formulation of uncertainty timeseries*

Code	Type	Aspect	Base Data	Modifications / Use
a	Calibration Input	Climate Input	HydroGFD: see Table 2.1-1a	Used to determine historic relationship (temporal) between input and output
b	Output Dataset	Outlet Discharge Output	HydroGFD naturalized discharge: see Table 2.3-6c	
c	Projection Input	Climate Input	Varies by outlet location (inside or outside of James Bay) see Table 2.1-1d or Table 2.1-1e	Used with HydroGFD input (Table 2.4-1a) to assess downscaling uncertainty
d	Output Dataset	Outlet Discharge Output	Varies by outlet (inside or outside of James Bay) see Tables 2.3-4a, 2.3-4b, or 2.3-4c	Used to assess output ensemble uncertainty
e	Calibration Dataset	Observed River Discharge	Observed dataset: see Table 2.1-2f	
f	Output Dataset	Outlet Discharge Output	Single timeseries of discharge used as "seed" for perturbed uncertainty timeseries to be generated, simulated daily 1981 to 2070	Varies by end-use: see Table 2.4-2a, 2.4-3a
g	Output Dataset	Outlet Uncertainty Timeseries	Timeseries of discharge generated by the models summarized in Table 2.2-2	Computed and saved at daily, aggregated to seasonal for publication

h	Output Dataset	Outlet Uncertainty Timeseries	Table 2.4-1a to 2.4-1f used to compute 64 timeseries describing hydrologic uncertainty, this can be considered the ‘uncertainty model’	None

Table 2.4-2: *Uncertainty timeseries passed to Team 6 for oceanographic sensitivity study*

Code	Type	Aspect	Base Data	Modifications / Use
a	Output Dataset	Outlet Discharge Output	MRI-CGCM3-RCP8.5 used (most-change to historic discharge) as seed timeseries see: Table 2.4-1f	None
b	Output Dataset	Outlet Uncertainty Timeseries	1 x 64 timeseries see: Table 2.4-1h	25-25-25 and 75-75-75 timeseries selected (for both regulated and re-naturalized results)

3.3 Marine Ecosystems (Team 3)

Team Member	Affiliation	Tasks Contributed to				Role
Jean-Éric Tremblay	*a*	*3.1*	*3.2*	*3.3*	*3.4*	*Science Lead*
Gary Swanson	*b*	*3.1*	*3.2*	*3.3*	*3.4*	*Hydro Lead*
Marilynn Kullman	*b*	*3.1*	*3.2*	*3.3*	*3.4*	*Hydro Lead*
Frédéric Maps	*a*	*3.1*	*3.2*	*3.3*	*3.4*	*Contributor*
Louis Fortier	*a*	*3.1*	*3.2*	*3.3*	*3.4*	*Contributor*
Connie Lovejoy	*a*	*3.1*	*3.2*	*3.3*	*3.4*	*Contributor*
Simon Bélanger	*c*	*3.1*	*3.2*	*3.3*	*3.4*	*Contributor*
Philippe Archambault	*a*	*3.1*	*3.2*	*3.3*	*3.4*	*Contributor*
C.J. Mundy	*d*	*3.1*	*3.2*	*3.3*	*3.4*	*Contributor*
Gabriele Deslongchamps	*a*	*3.1*	*3.2*	*3.3*	*3.4*	*Contributor*
Jonathan Gagnon	*a*	*3.1*	*3.2*	*3.3*	*3.4*	*Contributor*
Sylvain Blondeau	*a*	*3.1*	*3.2*	*3.3*	*3.4*	*Technician*
Inge Deschepper	*a*	*3.1*	*3.2*	*3.3*	*3.4*	*Contributor*
Marie PierreJean	*a*	*3.1*	*3.2*	*3.3*	*3.4*	*Contributor*
Sarah Schembri	*a*	*3.1*	*3.2*	*3.3*	*3.4*	*Contributor*
Loïc Jacquemot	*a*	*3.1*	*3.2*	*3.3*	*3.4*	*Contributor*
Lucas Barbedo de Freitas	*c*	*3.1*	*3.2*	*3.3*	*3.4*	*Contributor*
Janghan Lee	*a*	*3.1*	*3.2*	*3.3*	*3.4*	*Contributor*
Lisa Matthes	*d*	*3.1*	*3.2*	*3.3*	*3.4*	*Contributor*
Laura Dalman	*d*	*3.1*	*3.2*	*3.3*	*3.4*	*Contributor*

a) Department of Biology, Université Laval, Quebec City, Quebec, Canada.
b) Manitoba Hydro, Winnipeg, Manitoba, Canada.
c) Université Québec à Rimouski, Rimouski, Québec, Canada.
d) Centre for Earth Observation Science, University of Manitoba, Winnipeg, Manitoba, Canada.

3.3.1 Introduction and Objectives

In Hudson Bay, river runoff, sea ice dynamics, and ocean physics (Ingram et al., 1996) influence the growth conditions of marine organisms (Figure 3.3.1). The relative importance of the different factors and their interactions vary in space (locally, regionally) and time (seasonally, inter-annually) (Legendre et al., 1996; Kuzyk et al., 2010). A modelling study proposed that under climate warming, increased river flow reduced ice formation, and decreased winter convection is expected to reinforce vertical stratification, decrease upward nutrient supply, and lower overall biological productivity at the bay-wide scale (Joly et al., 2011). Horizontal nutrient deliveries by rivers will probably make a greater contribution to coastal productivity in such a setting unless storms became sufficiently frequent or powerful to erode the vertical stratification. These changes are also likely to shift the seasonal peak of primary production (PP) forward, thereby affecting the coupling between primary producers and consumers as well as the vertical export of organic matter to the benthos. In the near-shore zone, the timing of biological production will be impacted by the quantity and quality of runoff.

The objective of Team 3 is to assess how different drivers collectively affect biological productivity and the diversity and interaction of water column organisms (microbes, algae, and consumers) and the benthos, with an aim to identify the fate of nutrients entering Hudson Bay through marine gateways and regulated versus unregulated rivers.

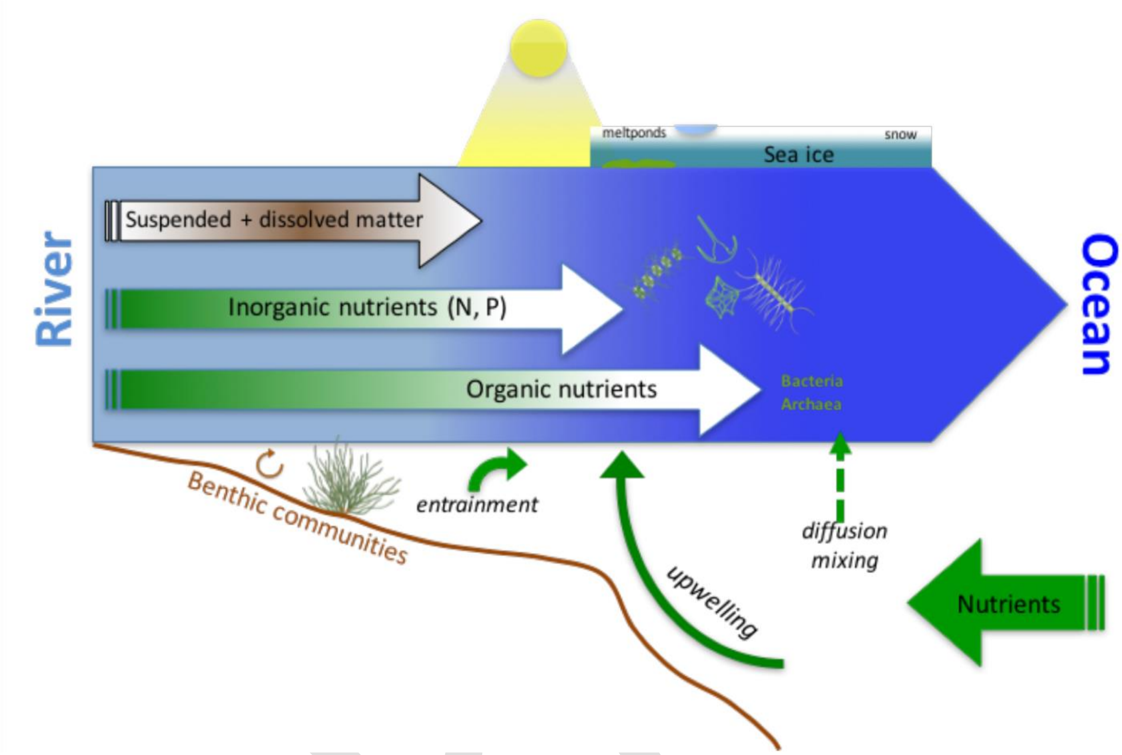

FIGURE 3.3.1 Schematic view of freshwater-marine coupling with respect to light availability and the main sources of new (green) and recycled nutrients (white) for primary producers and the lower pelagic and benthic food webs.

3.3.2 Analysis and Methods

Fieldwork

Throughout the BaySys program, Team 3 participated in four expeditions (Figure 3.3.2). During the two ship-based expeditions (autumn 2016 and summer 2018), a suite of core physical, biological and chemical parameters were recorded. Spatial coverage of the bay was more comprehensive during the main expedition of summer 2018 and several additional types of chemical and biological samples were obtained. The two other expeditions (winter and spring 2017) were shore-based and mostly limited to nearshore sampling of the water column and sea ice in the estuaries of the Churchill (February and late April) and Nelson (March-April) rivers. For the Churchill expedition, a few offshore sites were accessed by helicopter to provide marine nutrient samples. During the 2018 expedition, the nearshore work examining the freshwater-marine gradient focused on the Nelson River. Surface and bottom samples were collected across the estuarine transition zone, with sampling stations set up to adequately cover the salinity gradient, which meant that the stations were not evenly spaced. This sampling strategy maximized the probability of sampling different mixtures of fresh and marine waters. Additional, but more limited sampling along salinity gradients was carried out in the Churchill estuary in 2018 and near the Great Whale River that was opportunistically sampled in 2017. The details of stations locations, sample collection, treatment, and processing can be found in the Phase 1 report.

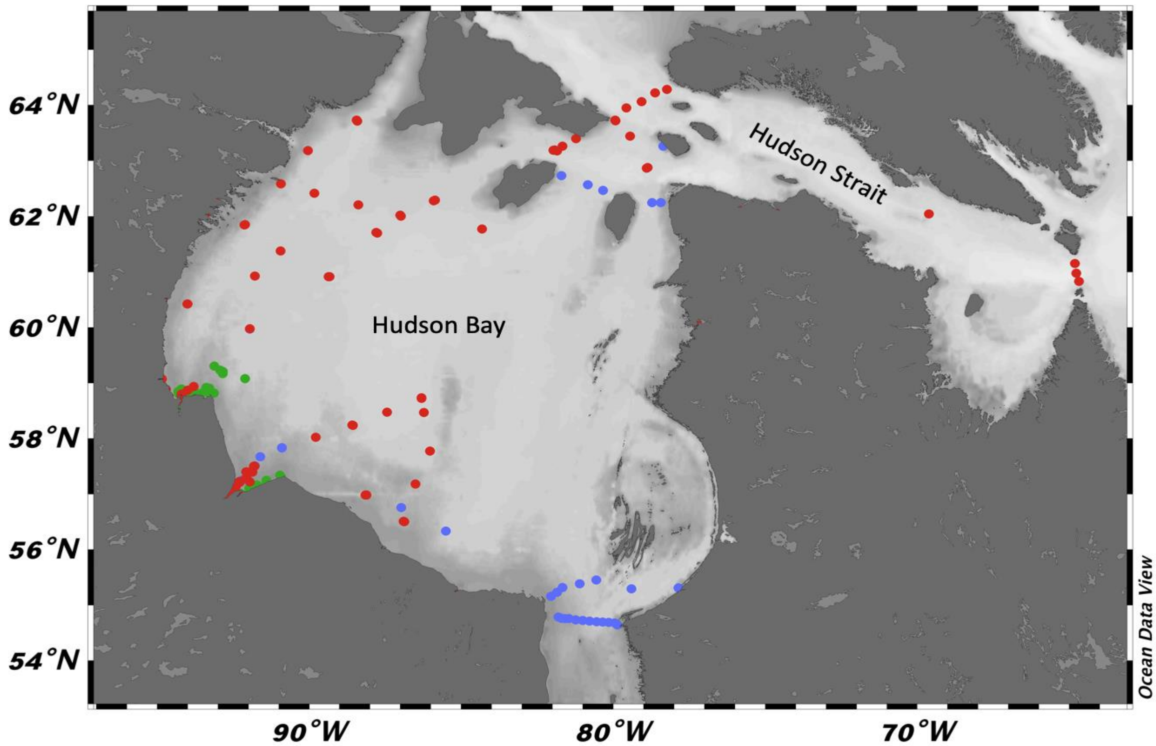

FIGURE 3.3.2 Map of sampling locations during the BaySys field campaigns. The colors indicate the sampling expeditions (Fall 2016 = blue, Winter 2017 = green, and Summer 2018 = red).

Remote Sensing

The concentration of chlorophyll *a* (Chl*a*), a proxy for algal biomass, was assessed from satellite measurements of sea-leaving radiance (Rrs) under ice-free conditions, using semi-analytical algorithms such as GSM (Maritorena et al., 2002) and quasi-analytical algorithms such as QAA (Lee et al., 2002, 2005). Different ocean color data products (SeaWiFS, MODIS, MERIS, VIIRS, OLCI) were merged to obtain the longest time series possible given the limited lifespan of different satellites. The extra step of estimating rates of primary production (PP), which provides the amount of carbon fixed per unit time by the algae, was based on the model of Bélanger et al. (2013). The model uses Chl*a* and additional satellite observations of the diffuse attenuation of downwelling irradiance (kd), solar irradiance (Ed), and the parameters of photosynthesis-irradiance curves (from the literature and the BaySys experiments described below). The approach was refined to reduce the uncertainty of parameters and constants; tuning the algorithm to the specific conditions prevailing in Hudson Bay (e.g., Huot et al., 2013; Ardyna et al., 2013). The final product consists of PP estimates at an 8-day resolution from 1998 onward.

Strategies were employed to fill observation gaps caused by sea ice, cloud cover, or signal contamination by CDOM and re-suspension in nearshore areas (Babin et al., in prep; IOCCG report, in prep). Given the aggregate uncertainties inherent to the PP estimation method, a large portion of the analyses presented here is based on Chl*a* and its relationship to cryospheric and atmospheric processes in the bay. Spatial patterns, as well as the temporal trends and variability in the timing, intensity, and duration of the phytoplankton spring-summer bloom (Zhai et al., 2012), was related to the riverine, oceanic, and atmospheric drivers provided by Teams 1 and 2.

Nutrients

During winter expeditions, nutrient samples were obtained from melted ice cores and surface waters through leads or holes drilled in the ice. The nutrient data obtained by helicopter at the offshore station located off Churchill are the first of their kind and enabled us to examine the pre-conditioning of the spring bloom in the upper part of the water column. During the ship-based expeditions of fall 2016 and summer 2018, the nutrient samples were collected over larger areas and a greater vertical extent, including the surface and the sub-surface chlorophyll maximum (SCM) as well as up to 15 standard depths depending on bottom depth. Analyses of in-river nutrient data were based on historical data and new samples obtained during the BaySys expeditions of fall 2016 (Winisk and Severn rivers), winter 2017 (Nelson, Churchill, and Hayes rivers), and the main expedition of summer 2018 (Nelson and several other rivers across the bay).

To assess the importance of river nutrients for PP, historical and recent data on nutrient concentration and water discharge for the Nelson and Churchill rivers (upstream and downstream of the Churchill River diversion) and the Hayes River were provided by Manitoba Hydro's CAMP and Conawapa programs (2004 to 2013). Data from other rivers collected using helicopter support during the bay-wide expedition of the *CCGS Amundsen* was used to compare nutrient concentration across watersheds and between regulated and unregulated rivers. River nutrient transports were estimated by combining concentration data, discharge-concentration relationships (where possible), and volume discharge data provided by Team 2. The transport estimates were used to assess the relative contribution of rivers to overall productivity in Hudson Bay, based on the assumption that all river nutrients are eventually converted to phytoplankton biomass at the surface.

A nutrient budget was calculated by combining these riverine fluxes with nutrient transports across the northern oceanic gateways leading in and out of the bay. This budget provides validation for the biogeochemical model, which will then be used to project productivity into the future based on the sea ice and runoff scenarios provided by Teams 1 and 2. In the initial proposal, we were planning to assess marine productivity by following sequential changes in nutrient inventories between fall 2016, winter 2017, and spring-summer 2018 (i.e., the fall and winter pre-condition the following productive season through the vertical re-injection of nutrients at the surface). However, postponing the 2017 expedition to 2018 interrupted the sequence. This shortcoming was circumvented by using the nutrient-salinity relationships observed during winter 2017 and assuming that those relationships, which are conservative during winter, can be used to infer the pre-bloom nutrient levels of winter 2018 from the salinity measurements made during the spring-summer expedition.

Point Estimates of Primary Production and Nitrogen Cycling

Point estimates of total, net, and regenerated PP in sea ice and the water column were obtained *in vitro* during incubations with ^{13}C and ^{14}C tracers. For the ^{14}C method, radio-labeled carbon was used in photosynthesis-irradiance (PE) incubations to provide estimates of light-dependent photosynthetic parameters (i.e., photo-acclimation parameters) and the rate of carbon fixation (primary production) by ice algae and phytoplankton (Lewis & Smith, 1983). Nitrogen assimilation was assessed using trace additions of ^{15}N-labelled substrates (NH_4^+, NO_3^- or urea) following the methods described in Tremblay et al. (2006). Rates of other key nitrogen cycling steps, including ammonification and nitrogen fixation, were also assessed in vitro using ^{15}N-labeling techniques (Christman et al., 2011; Mohr et al., 2010; Rysgaard et al., 2004). Complementary data on the biomass of algal pigments (Chl*a* and others) and the concentration of particulate organic carbon and nitrogen were also obtained. The dominant algal groups were microscopically identified and enumerated from the bottom sections of melted ice cores and samples from the surface and subsurface chlorophyll maximum in the water column. To evaluate the environmental factors controlling PP and N cycling rates, the data were compared with a suite of environmental variables measured by Team 3 as well as Teams 1 and 2. Those included sea ice characteristics, ocean properties, and comprehensive measurements of light propagation in sea ice and the upper water column. The plausible impacts of long-term changes in the timing of different lower food-web processes under different physical forcing scenarios (provided by Teams 1 and 2) are being assessed with a numerical biogeochemical model.

Microbial Diversity and Gene Surveys

The biodiversity and distribution of pelagic microbes were assessed with molecular and bioinformatics techniques following the approach of Comeau et al. (2011). The bulk of these RNA and DNA analyses is based on water samples obtained at four different depths in and east of Hudson Bay’s northwestern polynya (Figure 3.3.3A) and during the freshwater-marine gradient work near the Nelson, Churchill, and Great Whale rivers (Figure 3.3.3B).

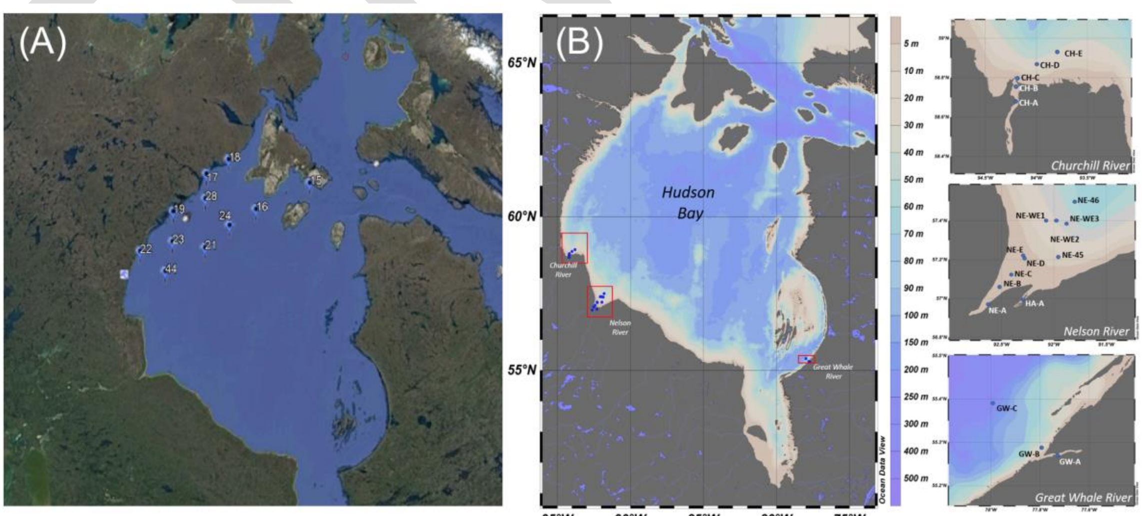

FIGURE 3.3.3 Station sampled in 2018 in (A) Hudson Bay’s northwestern polynya and (B) during the freshwater-marine gradient work near the Nelson, Churchill, and Great Whale rivers for microbial and gene surveys.

Benthic Ecology

The composition and distribution of the epibenthic megafaunal communities were established with samples taken during the main expedition in 2018. The epifauna (organisms living on the surface of the sediment) collected during Agassiz trawl deployments were counted and identified to the lowest taxonomic level possible. Species names were verified using the World Register of Marine Species (http://www.marinespecies.org/index.php) and the Integrated Taxonomic Information System (www.ITIS.gov). To relate the abundance and biodiversity of these organisms to the physical environment, a suite of environmental variables was collected. Surface particulate organic carbon content (POC; mg m^{-3}) and mean annual surface PP (mg C m^{-2} y^{-1}) were extracted from interpolated environmental data layers generated at the global scale as well as in the Eastern Canadian Arctic and Sub-Arctic regions (Basher et al., 2018; Beazley et al., 2019). The substratum type was classified into three separate classes based on Henderson (1989) and Pelletier (1986).

To define distinct communities from the co-distributions of individual species, Bray–Curtis dissimilarity measures were used to build a community dissimilarity matrix. This matrix was subjected to a hierarchical cluster (Ward, 1963) and clusters corresponding to the dissimilarity between communities of less than 20% were selected. Statistical relationships between epibenthic community composition and different environmental variables were evaluated using canonical correspondence analysis (CCA) (ter Braak & Verdonschot, 1995).

Pelagic Zooplankton and Ichthyoplankton

The abundance and diversity of zooplankton and fish were assessed using a combination of direct sampling, imaging, and acoustics during the *CCGS Amundsen* expedition. Zooplankton were collected by vertical net tows. The ichthyoplankton assemblage was also sampled directly with a Double Square Net sampler (DSN). When it was not possible to deploy the DSN under high ice conditions and in shallow estuaries unreachable by ship, the hand-operated ring net was deployed from the zodiac. Benthic fish were sampled using a beam trawl that skims the sea floor and collects fish in its path. The ichthyoplankton and adult fish captured during the different net tows were identified, measured, and preserved onboard. For fish that require closer examination for identification and zooplankton, identification was done at the Laval laboratory. Fish larvae in the Osmeridae family were identified via genetic analysis. These standard sampling methods for fish and zooplankton assure comparability with older data sets from Hudson Bay that were compiled to extend the analysis.

Biogeochemical Modelling

The biogeochemical model used runs with the available historical and future forcings from Team 6. Firstly, the model was run for 2016 to 2018 and compared to the observations obtained from 2017 to 2018 assessing the model's ability to simulate the present environment. Secondly, the model was run to investigate the past physical environmental impacts on the biogeochemical cycle (1981-2010). Both regulated and unregulated river forcings from Team 2 were used to assess the impact of regulation on the cycles. Thirdly, the future forcing was used to assess the impact of climate change (RCP 8.5 scenario) on the biogeochemical cycle in the future (2010-2070). Future regulated and unregulated runoff was used to assess the respective impacts of climate change and regulation.

3.3.3 Results and Discussion

Team 3 results follow four tasks that were established at the onset of the BaySys project. The analytical results are then discussed within the greater context of the Team's objectives, and overarching project. The initial tasks were:

Task 3.1 Assess the timing of primary production - to characterize the spatial distribution and seasonal evolution of phytoplankton biomass and PP in open waters.

Task 3.2 Estimate the magnitude of primary production – to calculate a nutrient budget by combining riverine fluxes with nutrient transports across the northern oceanic gateways leading in and out of the bay.

Task 3.3 Evaluate nutrient processing along freshwater-marine gradients - to assess the chemical form under which nutrients spread and how far they reach into the bay depends on several processes, including biomass synthesis and bacterial transformations along flow.

Task 3.4 Biogeochemical modelling - coupled 3D ecosystem model to predict plausible changes in the timing and magnitude of primary and secondary production associated with the sea ice and within the water column of Hudson Bay, in response to climate change and freshwater inputs.

Assess the timing of primary production (Task 3.1)

Retrospective analyses of remote-sensing data for the period 1998-2018 demonstrated that phytoplankton abundance in the marginal ice zone (MIZ) has a strong spatial-temporal and inter-annual variability in Hudson Bay (Figure 3.3.4). As observed in other sectors of the Arctic and Sub-Arctic, the timing of the spring-summer phytoplankton bloom is controlled by the dynamics of sea ice and its associated snow cover through their impact on the availability of light in the upper ocean layer throughout the marginal ice zone (MIZ) of Hudson Bay. Sea ice break-up in the bay typically occurs between mid-June and mid-July (60% of the time) and Chl*a* concentrations at this time are close to 0.5 mg m^{-3} and therefore already elevated with respect to winter background levels, yet lower than the maximum values that occur during the ice-free season. The results also underscore that the development of phytoplankton blooms in the Northwestern polynya, a key ecological site for marine life in the bay. We show that the bloom is very sensitive to the Arctic Oscillation (AO) (Figure 3.3.5). During positive AO phases, strong westerly winds are associated with a relatively early ice retreat and a wide expansion of the polynya.

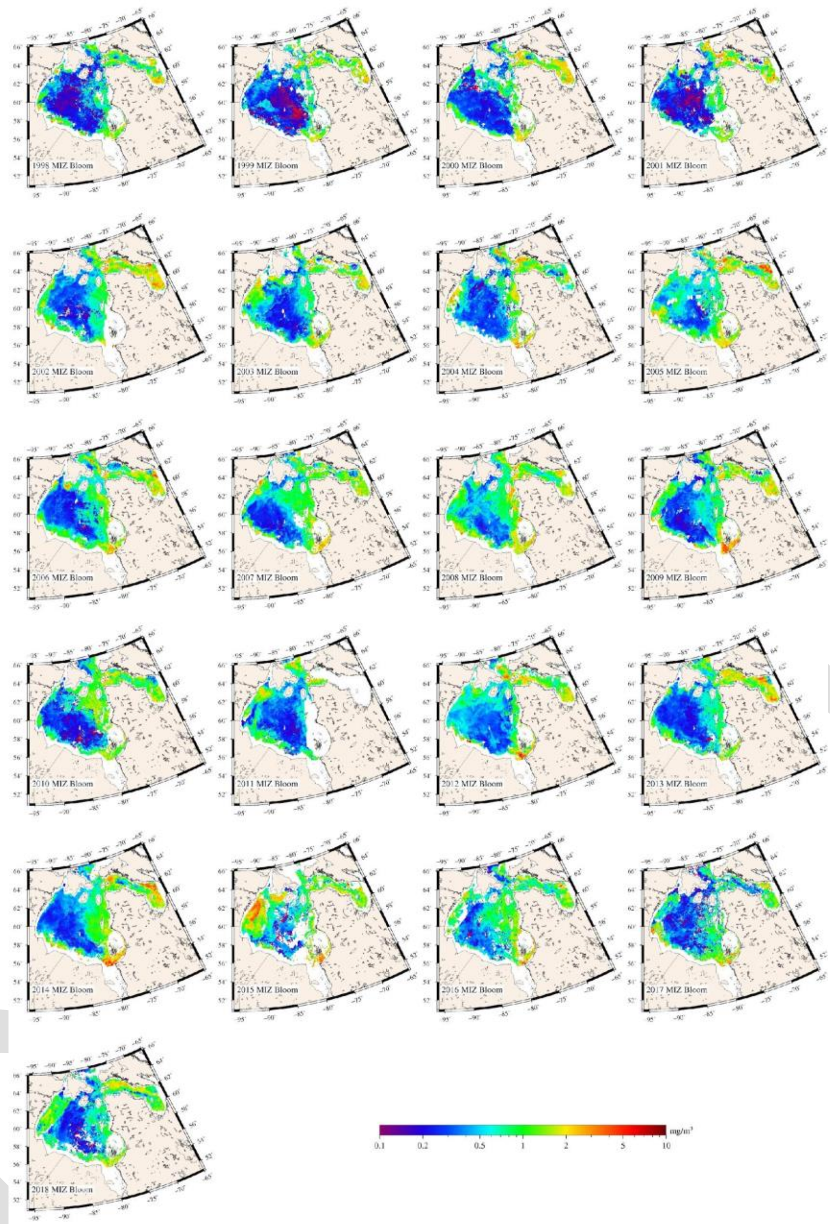

FIGURE 3.3.4 Marginal ice blooms detected by the maximum [Chl*a*] during the follow 24 days after the sea ice retreat (first day of continuous SIC < 10%) (Perrette et al., 2011) between 1998 and 2018.

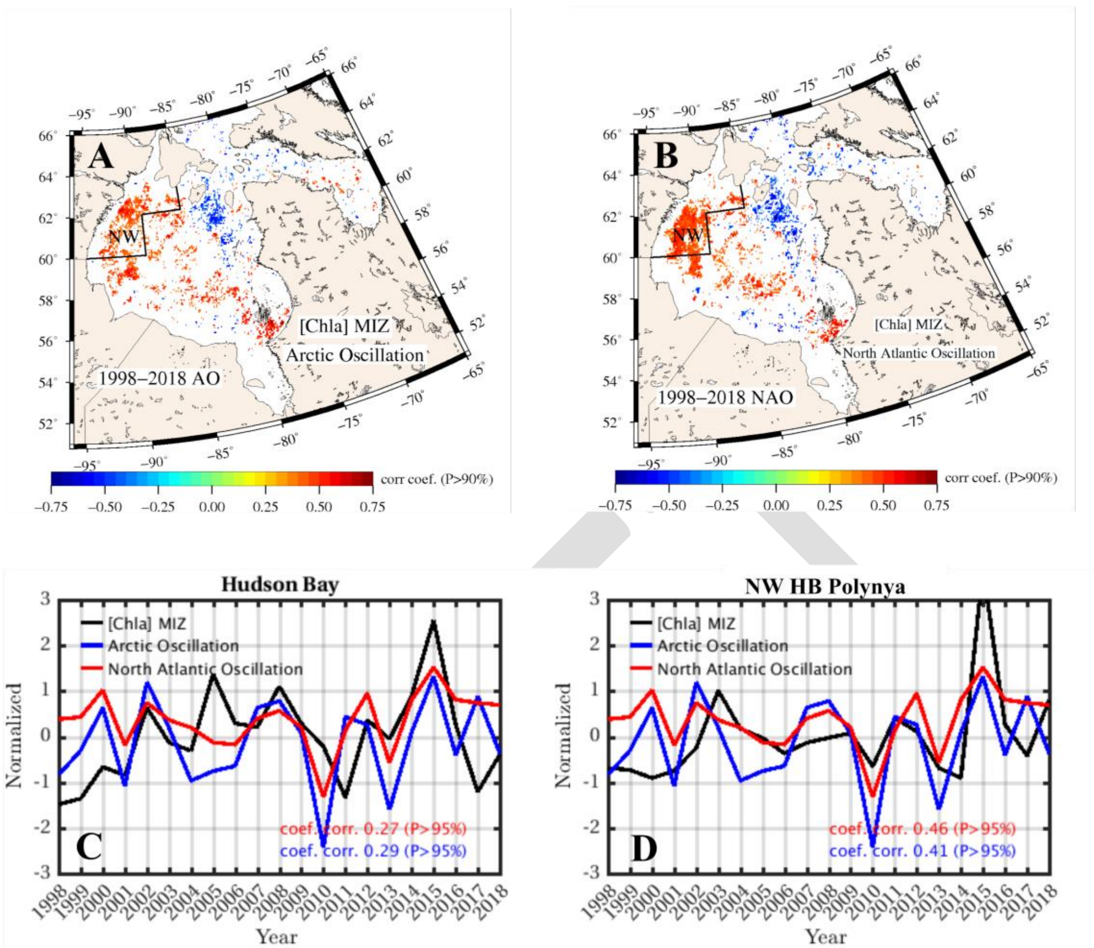

FIGURE 3.3.5 Arctic Oscillation (AO) and North Atlantic Oscillation (NAO) teleconnections with marginal ice blooms. Map of correlations coefficient ($p < 0.05$) between [Chl*a*] maxima annual in (A) the marginal ice zone and AO and (B) the marginal ice zone and NAO between 1998 and 2018 generated using the [Chl*a*] GSM algorithm from Globcolour and climatic indexes obtained from CPC/NOAA. Pearson's correlation with t-test smaller than 90% confidence interval was removed. Time series of climatic indexes AO, NAO, and normalized mean values of [Chl*a*] maxima annual in the marginal ice zone for (C) whole HBS and (D) in the NW HB polynya, a 95% confidence interval was applied.

Concerning ice algae, biomass accumulation was >2 mg Chl*a* m^{-2} at marine sites when ice was first sampled in February 2017. In both Nelson and Churchill estuaries, ice algal biomass significantly increased away from the riverine influence, reaching their maxima at marine sites (Figure 3.3.6). Ice algal biomass peaked at 9.6 mg Chl*a* m^{-2} in early April near the Nelson River Estuary, decreasing to <2 mg Chl*a* m^{-2} at marine sites near Churchill in late April. Due to a lack of time series data, it is difficult to say with certainty, but warm air intrusions coupled with significant snowstorm events in March through early April likely had a strong impact on ice algal biomass (Figure 3.3.7). The decrease in ice algal biomass by late April appeared to be associated with events that promoted ice ablation or light limitation of algal production at the ice bottom.

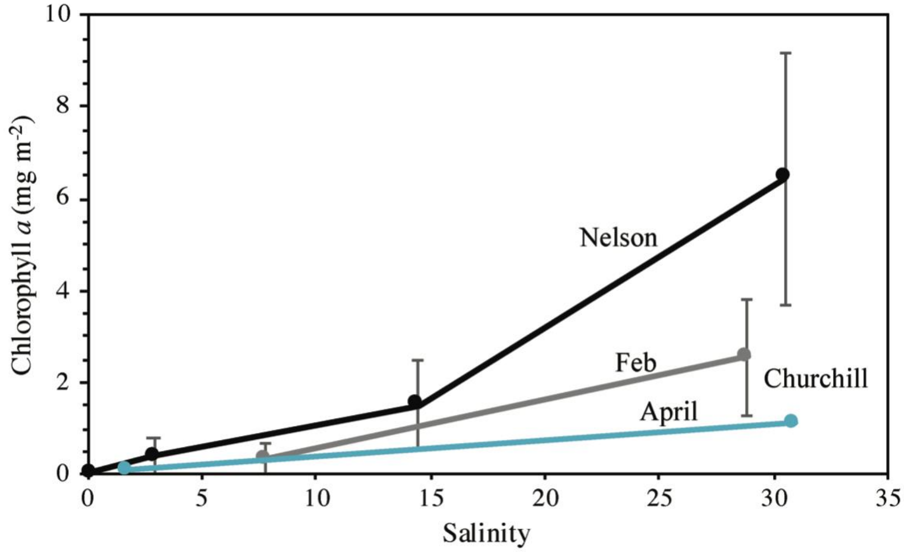

FIGURE 3.3.6 Averaged (± standard deviation error bars) bottom-ice [Chl*a*] along transects from the estuary to the marine system. Nelson River, Churchill River February, and April sites are depicted in black, grey, and blue, respectively.

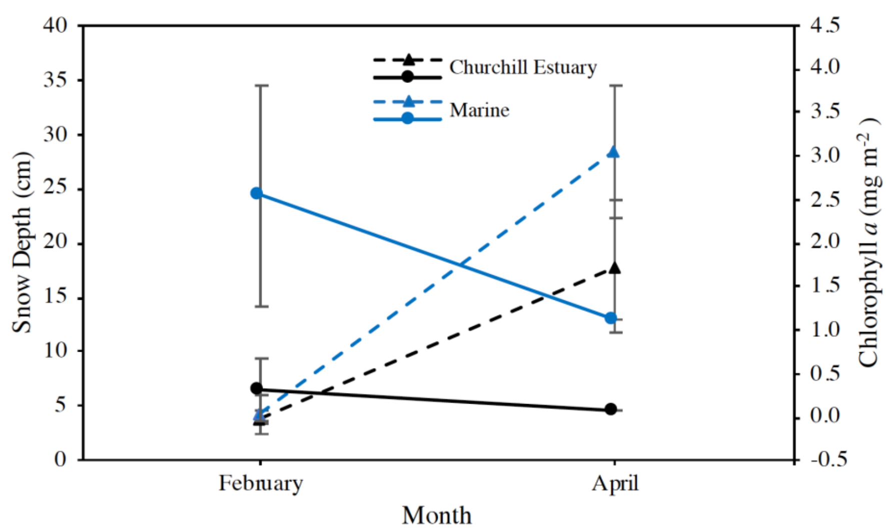

FIGURE 3.3.7 Averaged (± standard deviation error bars) snow depth (dashed lines) and chlorophyll *a* concentration (solid line) for Churchill estuary (black) and marine sites (blue).

Until now, no study had directly observed PP for either ice algae or phytoplankton in central Hudson Bay during the spring to summer sea ice melt transition. Results show a strong pulse of algal production in early summer while the ice cover rapidly ablated. However, the timing of primary production varied between the different regions and between the different algal groups. Ice algal communities at the bottom of mobile ice floes were found throughout the bay, sometimes in relatively high concentrations. PP estimates of ice-algal communities, sampled within the bottommost centimeters of the sea ice layer, varied between 2.72 mg C m^{-2} d^{-1} in the entrance to Hudson Bay (Narrows) and 1.76 mg C m^{-2} d^{-1} in the ice-covered central Hudson Bay (Figure 3.3.17). The observed ice-algal communities had a much lower biomass and PP compared to previous observations in landfast sea ice of Hudson Bay (Gosselin et al., 1986, Welch et al., 1991, Michel et al., 1993) and were likely already in a postbloom state with partial biomass loss through ice bottom melt. The contribution of melt pond communities to regional production was also negligible. Interestingly, unexpectedly high biomass of the ice-suspended algal community dominated by *Melosira arctica*, was observed on the underside of first-year ice floes mainly in the Narrows) and the central northern section of Hudson Bay (Figure 3.3.8). Samples of *M. arctica* were collected at two stations and showed a PP of 378 ± 119 mg C m^{-2} d^{-1}. These are the first observations of this species in the pack-ice of the Canadian sub-Arctic indicating a potentially large contribution to under-ice primary production in late spring.

FIGURE 3.3.8 *Melosira arctica*, a sub-ice algal community on first-year ice in northern Hudson Bay (photo by Laura Dalman on June 5, 2018).

Phytoplankton pelagic primary production ranged from 0.02 to 1.32 g C m^{-2} d^{-1} in the distinct light environments sampled during the spring-to-summer transition in the Hudson Bay System. Stations 9, 16, and 18 grouped as high light attenuation marginal ice zones were the most productive with 0.86±0.65 g C m^{-2} d^{-1}, with the highest production being 278 at station 16 in northern Hudson Bay. Marginal ice zone stations grouped as moderate attenuation sampled at stations 22B, 36, and 48 had a production of 0.44±0.18g C m^{-2} d^{-1}, low attenuation stations 15, 15, and 44 had a production of 0.22±0.11 g C m^{-2} d^{-1}. South Hudson Bay coastal water stations 32, 34, and 46 had a production of 0.26±.15 g C m^{-2} d^{-1}, However, at station 45, a new natural small lead surrounded by landfast sea ice in southern Hudson Bay, the production was 0.09 g C m^{-2} d^{-1}. The less productive light environment was 283 the Nelson River shallow and extremely turbid waters sampled in the stations BN1 and BN5, where production was 0.03±0.02 g C m^{-2} d^{-1}. However, production rose almost six-fold (0.11 g C m^{-2} d^{-1}) when sediment plume just began to dissipate at station BN6.

A phytoplankton bloom with a pronounced SCM was observed in the northwestern polynya, which opened up in May, highlighting the importance of ocean-atmosphere coupling for biological productivity in this region (Figure 3.3.9). The presence of an SCM in the water column overlapped with an observed nutrient depletion at the surface, suggesting that a surface bloom had occurred prior to the ship-based observation. Measured under-ice phytoplankton production was consistently low throughout the bay, although nutrient concentrations were higher in the ice-covered surface water compared to the adjacent open water surface waters. Additionally, under-ice transmitted light levels increased over the duration of the expedition due to the formation of melt ponds on the surface of the sea ice, and the surface layer became more stabilized due to increasing air temperatures and sea ice melt. These conditions promote the development of substantial under-ice blooms (Matthes et al., 2021) and Chl*a* concentrations were highest directly beneath the ice, where phytoplankton communities were acclimated to exploit low quantities of light.

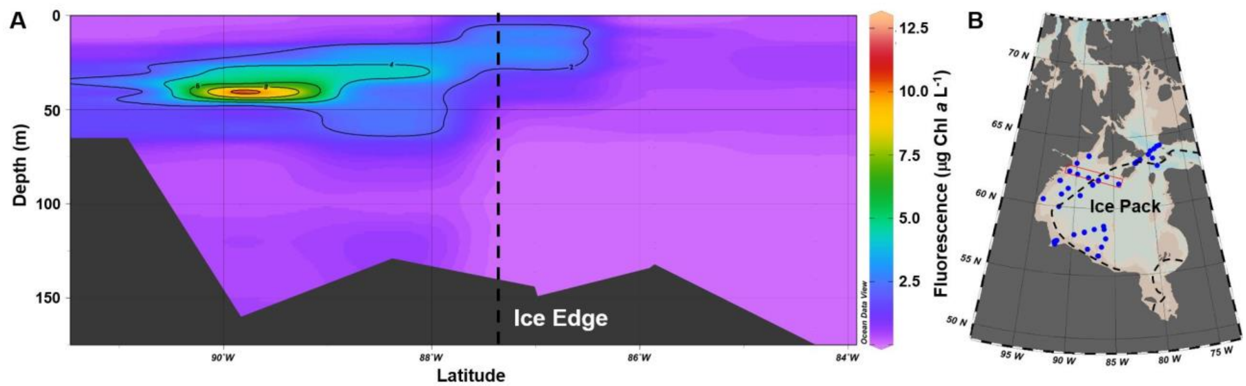

FIGURE 3.3.9 (A) Transect of Chl*a* fluorescence from the open water into the ice pack in (B) the northwestern region of Hudson Bay. The extent and location of the edge of the ice pack are highlighted by the dashed line. The stations along the plotted transect are marked with a red box.

The different surface freshwater signals, from temperature-salinity (TS) properties, were used to track the progress of microbial community structure relative to the transition from ice-free coastal waters to ice-covered stations (Jacquemot et al., in prep). Sea ice melt and river discharge both contribute to the stratification of the water column and thereby influence the assembly of microbial communities (Monier et al., 2013). Amplicon reads of marker genes from both DNA and RNA along these freshwater gradients revealed that eukaryotic and prokaryotic communities across the northwestern polynya and adjacent eastern stations were associated with ice conditions at the time of sampling. The relative abundance of reads associated with specific diatoms in the deeper waters of the bay was consistent with sinking phytoplankton, and the main spring bloom occurring prior to the time we were able to sample the polynya.

The seasonal timing of algal blooms is generally regarded as crucial for the development of the food web, which is based on algal biomass becoming the food that is transferred to fish via zooplankton. Another key variable intervening in fish development is temperature since it modulates the growth rate of larval fish and therefore the coupling between their seasonal feeding window and the availability of food. Arctic cod hatching strategies include using fresh water as a thermal refuge and eggs tend to hatch earlier when they are in estuaries (Bouchard and Fortier, 2011). Regulation of freshwater run-off might influence the timing of Arctic cod hatching; generally, Arctic cod that hatch earlier are more likely to be recruited into the adult population (Figure 3.3.10). Regulation of fresh water means that more fresh water is available in winter, therefore creating more under-ice river plumes which are potential thermal refugia for the eggs of Arctic cod. We hypothesise that more thermal refugia would drive earlier hatching of Arctic cod and subsequently, more recruitment of adult Arctic cod. Although a mechanistic connection between temperature and hatch date is only inferred, our results show that a slight increase in temperature (about 0.5˚ C) at the hatch location was accompanied by an earlier hatch date (Fig. 3.3.10) and increased pre-winter size. Larvae that achieve a larger size by the end of summer are more likely to survive the winter months. The manuscript for this study has been submitted to the Elementa BaySys special issue and is under review. Arctic cod also face competition from Capelin which has always been present in large numbers in the Nelson and Churchill estuaries but might be expanding their habitat. Initial results were published in the “Fish and Fisheries” chapter of the integrated regional impact study for Hudson Bay (Schembri et al., 2019). The manuscript about the distribution and role of Arctic cod, Capelin, and the other fish species in the Hudson Bay is being written. Zooplankton in Hudson Bay shows greater seasonality through the spring and summer seasons, compared to the higher Arctic. Large, lipid-rich copepods such as *Calanus glacialis* are more abundant during the ice break-up period while smaller copepods such as *Pseudocalanus* sp. dominate during the ice-free period. This could be an effect of the brief intense phytoplankton bloom and rapid switch to oligotrophic conditions seen in the bay. The manuscript about seasonality of zooplankton is also being written to submit to the BaySys Special Feature in *Elementa*.

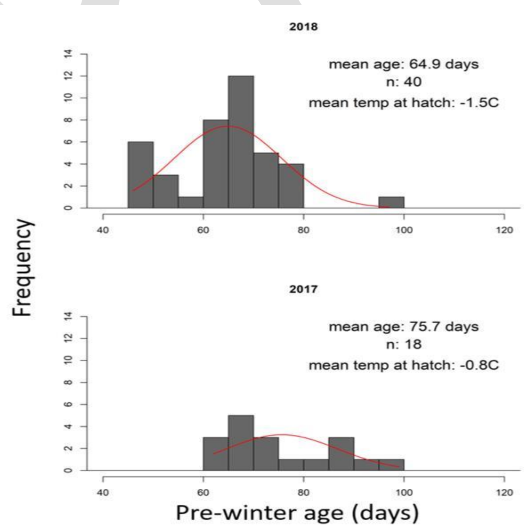

FIGURE 3.3.10 Frequency distribution of the estimated age (in days) of Arctic cod in Hudson Bay on 2nd October in 2018 (top) and 2017 (bottom). The trajectory of each larvae from the location of sampling to the hatch location was modelled using a langrangian tool for simulating ichthyoplankton dynamics. The mean temperature at the estimated hatch locations is shown on the upper right. In 2017 the hatch location was on average warmer and by the end of summer, the mean age of the larvae was 10 days more than in 2018. Ten days of additional growth implies that in 2017 the larvae achieved a larger size and were more likely to survive the winter months. Warmer hatch locations correspond to nearshore locations were under-ice freshwater accumulates during winter.

The timing of biological production in the offshore water column of Hudson Bay was positively affected by enhanced light transmission through sea ice melt and break up. During the June expedition 2018, phytoplankton production was much higher in the open water of the northwestern Hudson Bay polynya by contrast to consistently low under-ice primary production elsewhere. This distribution highlights the importance of an early ice-break-up in triggering biological productivity in the bay. In addition to the elevated phytoplankton biomass in the polynya, depleted nutrient concentrations near the surface indicate that production had begun up to several weeks before sampling took place, and the peak of the bloom had passed. This notion is consistent with the composition of the microbial community, which showed a succession from typical bloom assemblages to post-bloom ones, as well as the occurrence of planktonic diatoms in bottom waters. The latter indicates that a part of the phytoplankton biomass produced during the bloom had already sunk out of the surface layer and affected deep microbial communities and the benthic food web. This early and enhanced production kick starts the feeding period for higher trophic levels of the food web and contributes to the area's status as a relative hotspot of marine wildlife.

Estimate the magnitude of Primary Production (Task 3.2)

In Arctic and sub-Arctic waters, the magnitude attained by phytoplankton blooms under ice-free conditions is generally proportional to the supply of nutrients and more specifically nitrogen, which is considered as the limiting element for marine algal biomass. In the Hudson Bay system, this nutrient supply can occur through vertical mixing during winter that brings nutrients from the deep reservoir to the surface, horizontal deliveries by rivers and ocean gateways throughout the year, and other relatively minor inputs such as precipitation and bacterial nitrogen fixation. In this context, the magnitude of primary production can be assessed directly in the field through measurements of algal biomass and carbon fixation rates, which works for both ice algae and phytoplankton. The latter provides instantaneous data that are particularly useful for understanding environmental drivers at a particular time. Another approach consists of assessing nutrient deliveries by rivers and the winter re-supply of nutrients in offshore areas, which provides the potential productivity of the system. Since river deliveries are shallow and encompass the sunlit layer, we assume that these nutrients will be used entirely in the coastal domain during the productive period. In offshore areas, where vertical re-supply dominates, the time-integrative cumulated production of the system can be assessed from the difference between the pre-bloom, winter nutrient inventory in the euphotic zone, and the residual nutrient stock observed at the moment of sampling during summer.

Since ship-based sampling is temporally and spatially limited, remote-sensing provides a way to observe primary production at the bay-wide scale and to follow how this productivity changes or fluctuates within a given productive season or among years. For the time being, Chl*a* biomass is the only remote-sensing product available, but a revised PP estimation algorithm is currently being tested and tuned to the Hudson Bay system using a combination of remote sensing data and *in situ* data on radiometry, Chl*a*, and photosynthetic parameters obtained during the sampling campaigns in Hudson Bay (Figure 3.3.11). Available results show that the model's performance is superior to that of generalized polar parametrizations (not shown).

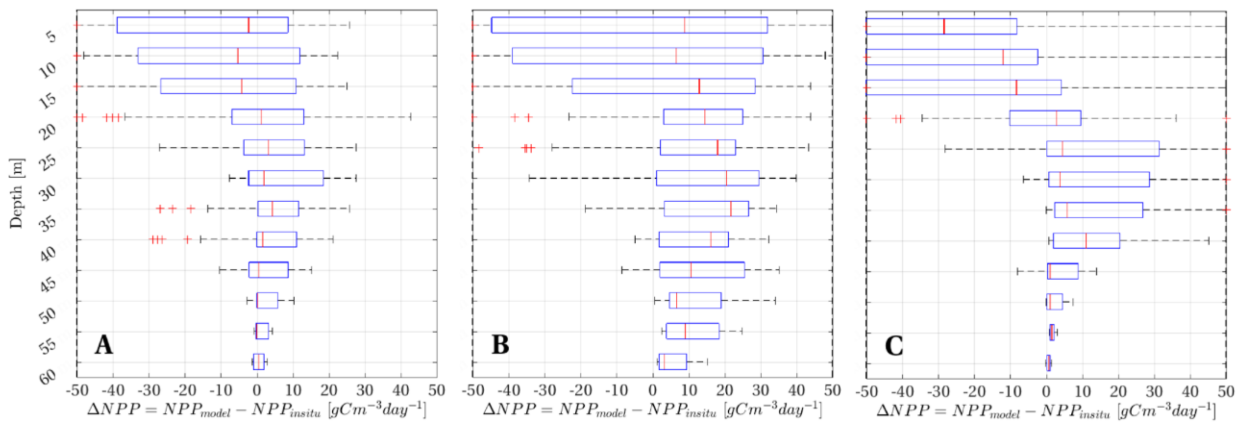

FIGURE 3.3.11 Boxplots of the difference between Net Phytoplankton Production NPP reference and using distinct strategies to resolve [Chl*a*] profiles (ΔNPP = NPP_{model}-$NPP_{reference}$) (A) vertical homogeneous [Chl*a*] profiles [Belanger et al., 2013]; (B) climatological [Chl*a*] selected by trophic descriptors (Ardyna et al., 2013); (C) profiles of [Chl*a*] measured by in vivo fluorimetry corrected for fluorescence quenching using backscattering coefficient ($b_{bp}(700)$ (Swart et al., 2015)).

The remote sensing Chl*a* data show that the early sea ice retreat occurring during positive AO phases not only triggers the early development of phytoplankton but is associated with higher algal biomass at the peak of the bloom (Figure 3.3.12). Correlation between the AO index and phytoplankton biomass is much weaker elsewhere in the bay, where maximum Chl*a* concentrations are generally lower than in the polynya. During some years, no MIZ blooms were detected from space, and the absence was more striking in the central part of Hudson Bay where the vertical stratification of the water column is particularly strong. This occasional absence of blooms could indicate that the bloom occurred under the ice during these years.

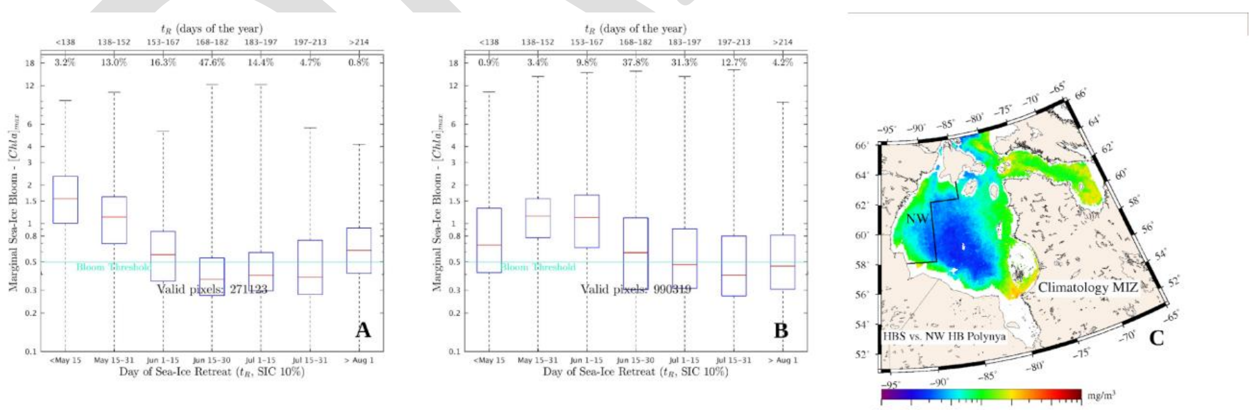

FIGURE 3.3.12 (A) Boxplots of [Chl*a*] in the marginal sea ice zone in relation to the date of sea ice retreat (tR) in NW HB polynya and (B) all HBS. [Chl*a*] above the threshold of 0.5 mg m−3 (green line) defines the marginal ice bloom occurrence (Perrette et al., 2011). (C) Climatology of [Chl*a*] in the marginal ice zone between 1998 and 2018.

Our compilation of nutrients for rivers showed that nitrate concentrations (the main form of bioavailable nitrogen) ranged 30-fold among rivers and were highest in the Southwest sector and the Nelson River in particular (Figure 3.3.13). Given the wide spread of concentrations across unregulated rivers, the small sample size for impacted rivers, and the diversity of natural factors that may impact the nutrient load of impacted and unimpacted rivers alike, the data were inconclusive with respect to a possible impact of regulation on nutrient load. The rivers for which data were available at more than one time during the year exhibited seasonal differences, with concentrations being generally higher in the winter/spring period than during summer/fall. Molar ratios for the different nutrients also varied substantially between watersheds and seasons (Figure 3.3.14). Apart from northern rivers, all rivers exhibited inorganic N:P ratios below 16:1 (the ratio required by phytoplankton, on average), indicating that coastal phytoplankton using river nutrients will run out of nitrate first and that phosphate will accumulate in the bay unless other sources of nitrogen (DON) are used by phytoplankton. This relative nitrate deficiency tended to be more severe during summer/fall than in winter/spring and was particularly acute in the South. The Si:N ratios were systematically above 1:1, which implies that all river waters were favourable for the production of diatoms (this group has an absolute requirement for silicon), a taxa considered to critically sustain the marine food web.

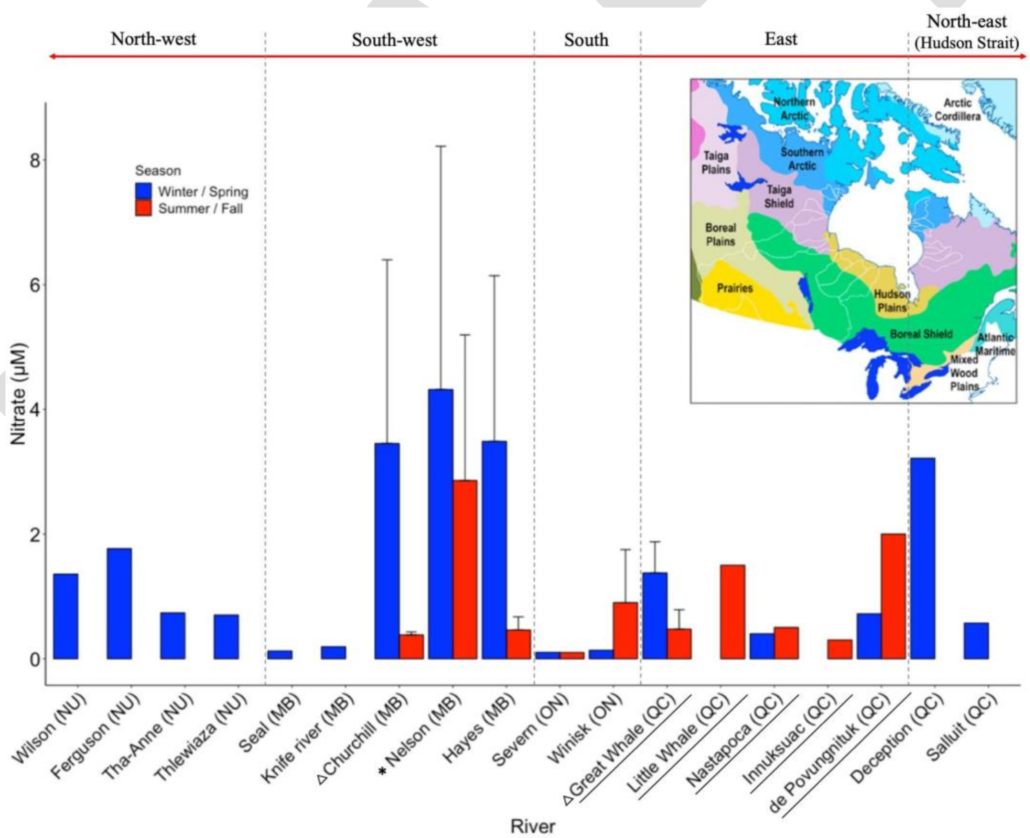

FIGURE 3.3.13 Concentrations of nitrate in different rivers during the summer-fall (July – October) and/or winter-spring (November –June) periods using historical data and BaySys measurements (for more detail, see Lee et al. in prep.). Regulated and partially diverted rivers are denoted with an asterisk (*) and a triangular symbol (△), respectively, and those for which literature data were used are underlined (Hudon et al., 1996; Kuzyk et al., 2010). The inset shows the diversity of vegetation zones spanning the Hudson Bay drainage area (adapted from Godin et al., 2016).

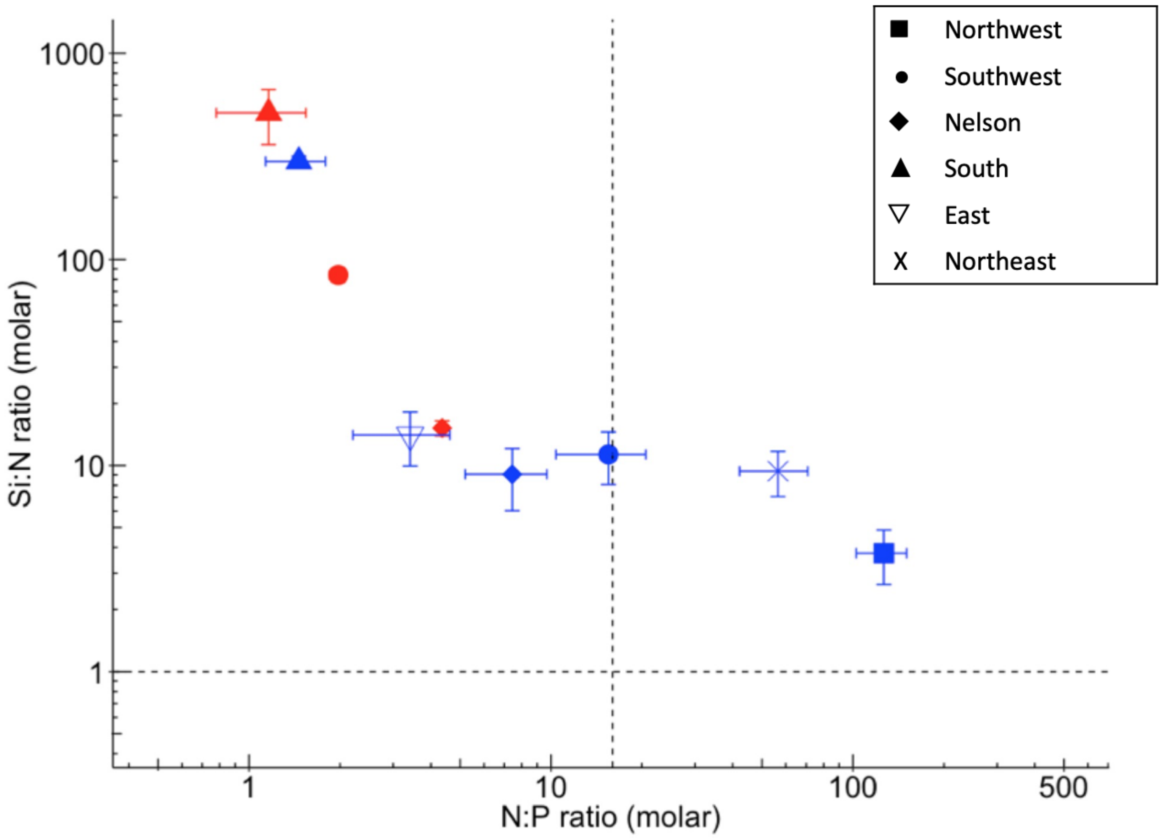

FIGURE 3.3.14 Average nutrient ratios in sub-Arctic rivers. Colors indicate the period (winter/spring = blue, summer/fall = red) and symbols denote regions or rivers (northwest = ■, southwest = ●, Nelson = ◆, south = ▲, east = ▽, northeast = X). Dashed lines indicate the Redfield value for N:P (16) and an average Si:N ratio of 1 for diatoms.

By combining a suite of discharge estimates (from different model runs implemented by Team 2) and the nitrogen concentrations we measured in several rivers (extrapolations were performed for rivers with no data), we estimated an annual nitrate input of 2 x 10^{10} g N for the whole bay. For specific rivers, the estimated nutrient transports were not sensitive to the model used (Figure 3.3.15). For regulated rivers or those impacted by flow diversion, the proportion of the annual flux that was delivered during winter was high (Figure 3.3.16) and larger than in other rivers. A comparison between the total annual nitrate input given above with the estimated winter re-supply of nitrate from marine sources at the bay-wide scale shows that the latter is at least an order of magnitude larger (124 x 10^{10} g N, assuming a total area of 5.48 x 10^5 km^2 for marine waters).

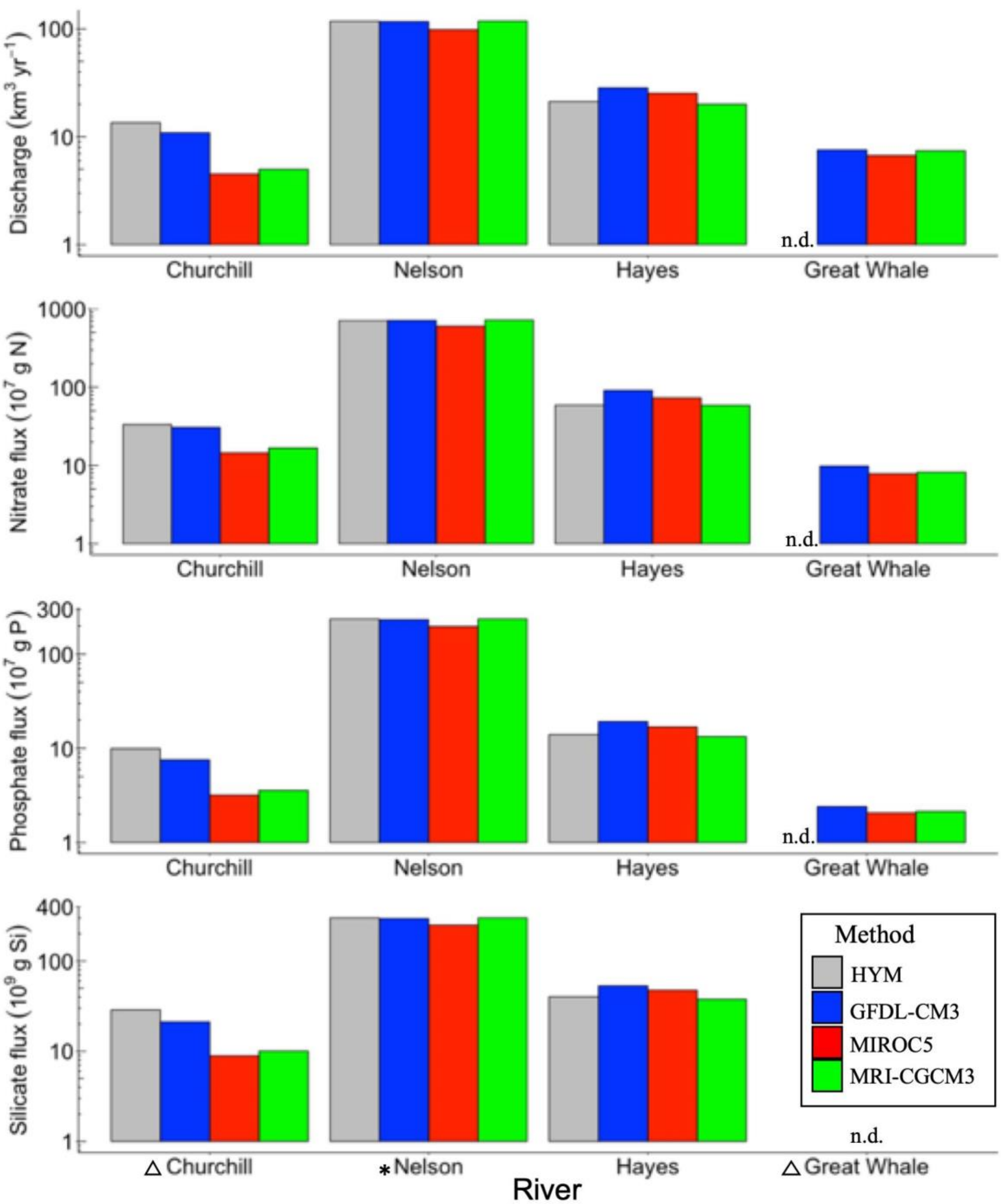

FIGURE 3.3.15 Annual discharge and nutrient transports for 4 major rivers, calculated by combining measured nutrient concentrations with discharge estimates from hydrometric data (HYM) and the three model outputs.

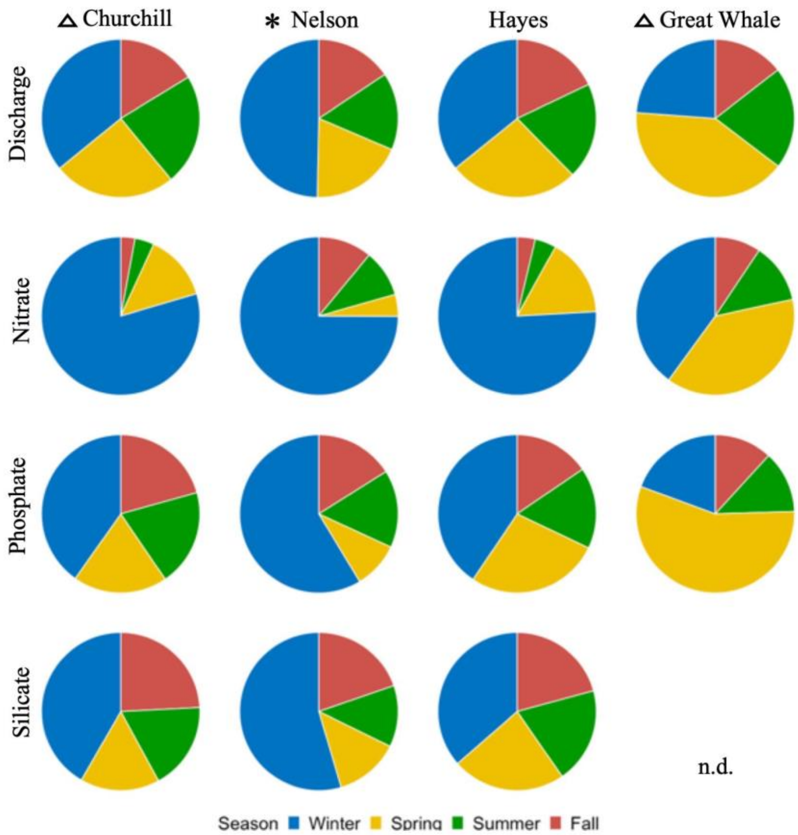

FIGURE 3.3.16 Percentage of nutrient inputs between seasons for 4 major rivers, based on averages from the 3 model outputs. The four seasons are taken here as winter (November to April), spring (May to June), summer (July to August), and fall (September to October).

The calculated average rate of PP by phytoplankton in the water column during the main expedition was 437 mg C m^{-2} d^{-1}, which is higher than the published average summer PP of 320 mg C m^{-2} d^{-1} in central Hudson Bay (Ferland et al., 2011). Spatial patterns of phytoplankton production also show comparable trends with the highest phytoplankton biomass and PP in the northwestern polynya (Figure 3.3.17), which were associated with relatively high concentrations of nutrients at depth in the polynya region. Beneath the mobile sea ice cover in central Hudson Bay, phytoplankton communities were less productive compared to those found in the open waters, although the mobile sea ice cover was melting and allowed a greater amount of incoming light to be transmitted to the underlying water column for algal photosynthesis. By combining these new PP estimates with those published in other studies for different periods, Matthes et al. (2021) revised the estimate of annual primary production upward from 21.5 – 39 g C m^{-2} yr^{-1} to 72 g C m^{-2} yr^{-1}. The increase was largely attributed to the inclusion of novel measurements of PP by ice algae (including *Melosira*) as well as phytoplankton under the ice and in the northwestern polynya.

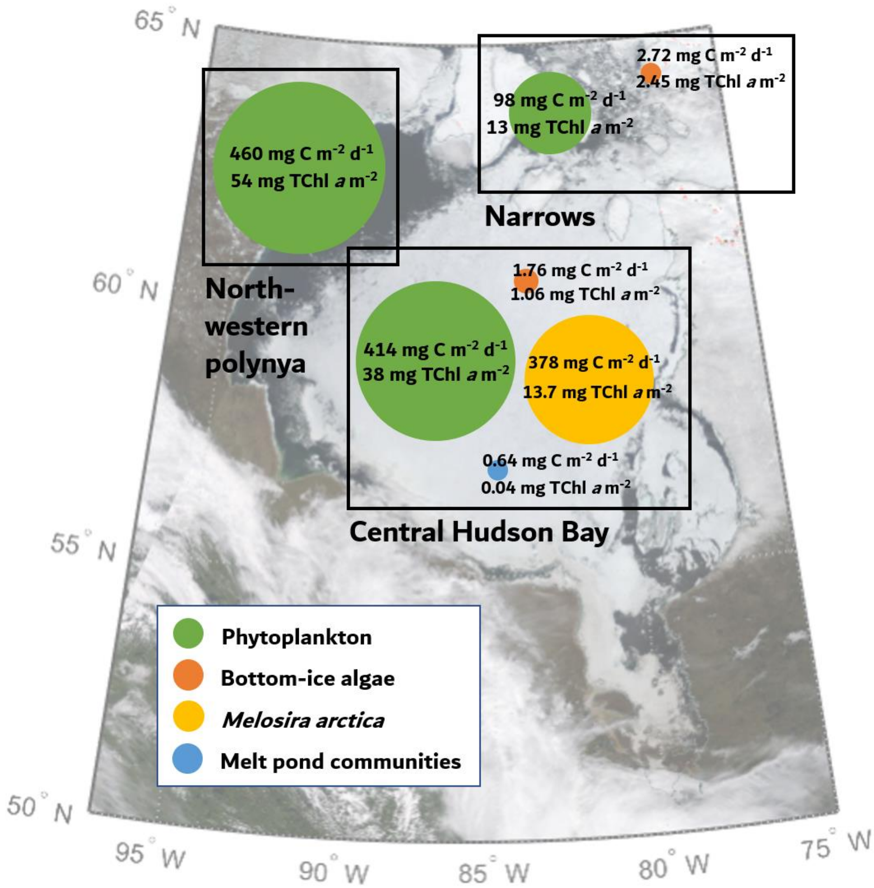

FIGURE 3.3.17 Summary of contribution of different microalgal communities to late spring primary production in the Narrows, northwestern polynya and central Hudson Bay. Biomass expressed as total chlorophyll *a* (mg TChl *a* m^{-2}) and primary production (mg C m^{-2} d^{-1}) is provided for each community in the corresponding circle for each region. Satellite image (MODIS) of sea ice conditions in Hudson Bay on 13 June 2018. Modified after Matthes (2021).

In the Nelson River Estuary, the PP rates and biomass of phytoplankton and ice algae were investigated along a salinity gradient. In early spring, ice algal biomass in the landfast ice adjacent to the Nelson River Estuary increased with increasing surface salinity and distance from the estuary. PP rates showed the same trend during the spring-summer transition. Final calculations and analyses are still underway. Results for the spatial distribution of ice algal and phytoplankton biomass and production along a salinity gradient in the Nelson estuary are also being interpreted (Dalman et al., *in prep.*).

Salinity was the major environmental parameter structuring microbial communities along the three transects (Nelson, Churchill, and Great Whale rivers; Figure 3.3.18A, Jacquemot et al., 2021), which suggests that the Arctic communities in summer are driven by similar salinity constraints as reported in temperate estuaries for protist communities (Muylaert et al., 2000; Bazin et al., 2014; Lee et al., 2017, Filker et al., 2019). At the marine ecosystem scale, coastal microbial assemblages clustered by region are mostly driven by nutrient availability (Figure

3.3.18B). In particular, Nelson River was associated with the development of a diatom community of *Rhizosolenia* spp. within the brackish waters of the estuary. River runoff is a source of heterogeneity and drives biodiversity differences in coastal communities. Distinct communities of heterotrophic protists were identified in the three estuarine transition zones, the most marked at the turbidity front of the Nelson River, suggesting that the convergence of fresh and marine waters creates a distinct habitat for a specialized community (Jacquemot et al., 2021). The timing, position, and composition of the phytoplankton blooms in estuaries seemed to be directly linked to the volume of freshwater discharge.

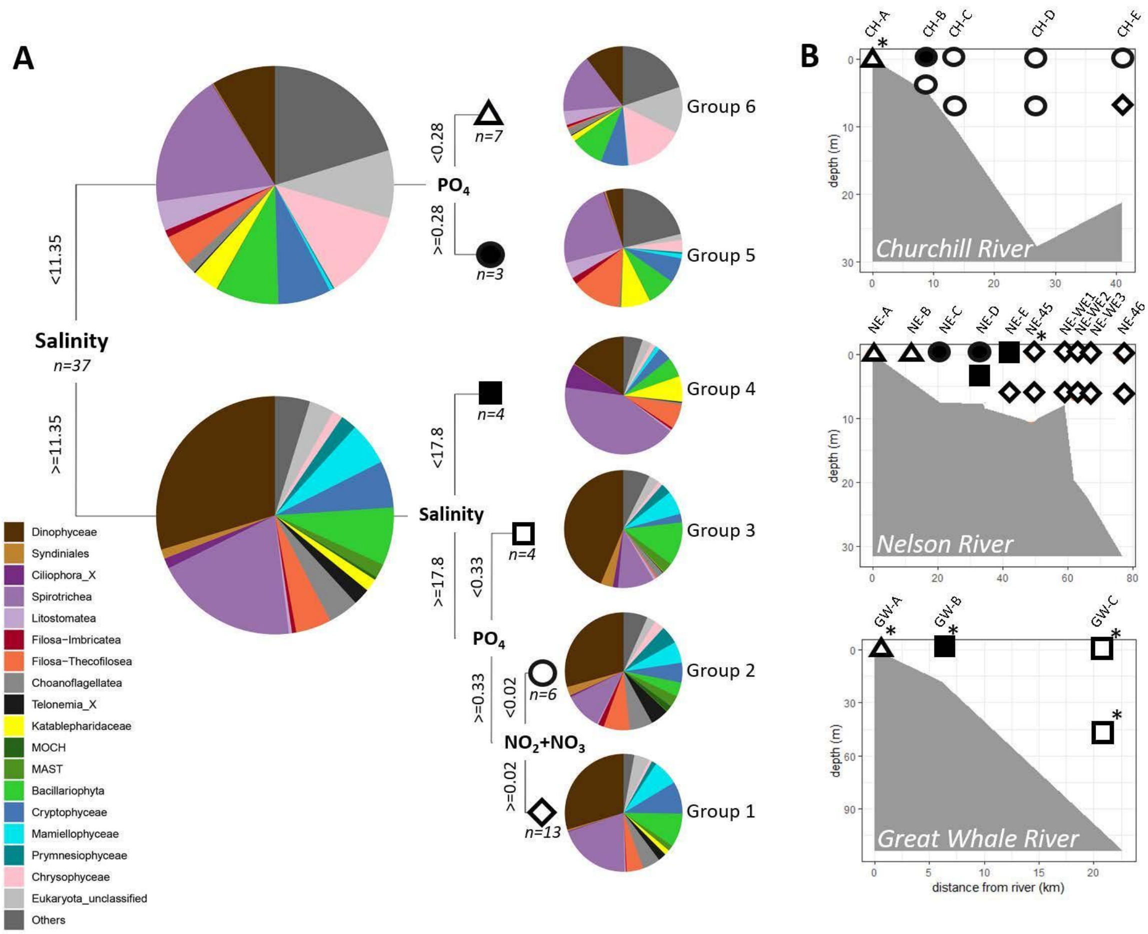

FIGURE 3.3.18 (A) Distance-based multivariate regression tree (db-MRT) analysis based on Bray-Curtis distance between 37 samples. Singletons were removed from the species table. Distances are based on the composition of 6010 OTUs variables. Environmental variables considered are salinity, phosphate, silicate, nitrite + nitrate, temperature, depth, and total phytoplankton concentration. Pie-chart represents the proportion of each clade within the subgroups. (B) Location of each subgroup along estuarine transects. Asterisks (*) indicate additional replicates. Note that the station at the Hayes River (HA-A) cannot be displayed on the plot but belong to subgroup 6.

Our work resulted in an increase in observed epibenthic taxa richness (n= 380) relative to prior studies. According to the non-parametric Chao2's index (Chao, 1987), which was used to predict the number of different epibenthic taxa that can be expected in the Hudson Bay Complex (HBC) (calculated using the "vegan" package; Oksanen et al., 2017), the number of taxa we observed represents 71% of the taxa expected (539± 34 taxa), indicating that about one-third of the expected species pool remains unrecorded (Pierrejean et al., 2020). Bottom salinity and particulate organic carbon content (POC) were the main environmental factors explaining epibenthic biomass, density, and taxonomic richness within the geographical areas of HBC. The lowest density, biomass, and taxonomic richness, observed along the coast, were associated with a high POC content and a low salinity mostly influenced by river runoff. The middle of the bay presented low values of benthic characteristics (density, biomass, and taxonomic richness) and was related to the more extended ice cover period, whereas polynyas were associated with large, abundant, and diverse epibenthic organisms. At the scale of the bay, three communities were defined based on their biomass-taxonomic composition and were primarily associated with the substrate type, then salinity, and annual primary production (Figure 3.3.19). The first community, associated with coarse substrate, was distributed along the coastlines and near the river mouths. This community was characterized by the lowest density and taxonomic richness and the highest biomass of filter and suspension feeders. The second community, mostly composed of deposit feeders and small abundant epibenthic organisms, was associated with soft substrate and distributed in the deepest waters. The third community, associated with a mixed substrate, was mostly located in polynya areas and was characterized by large and diverse epibenthic organisms. This community was not dominated by any specific taxa, showing a very diverse composition relative to other communities.

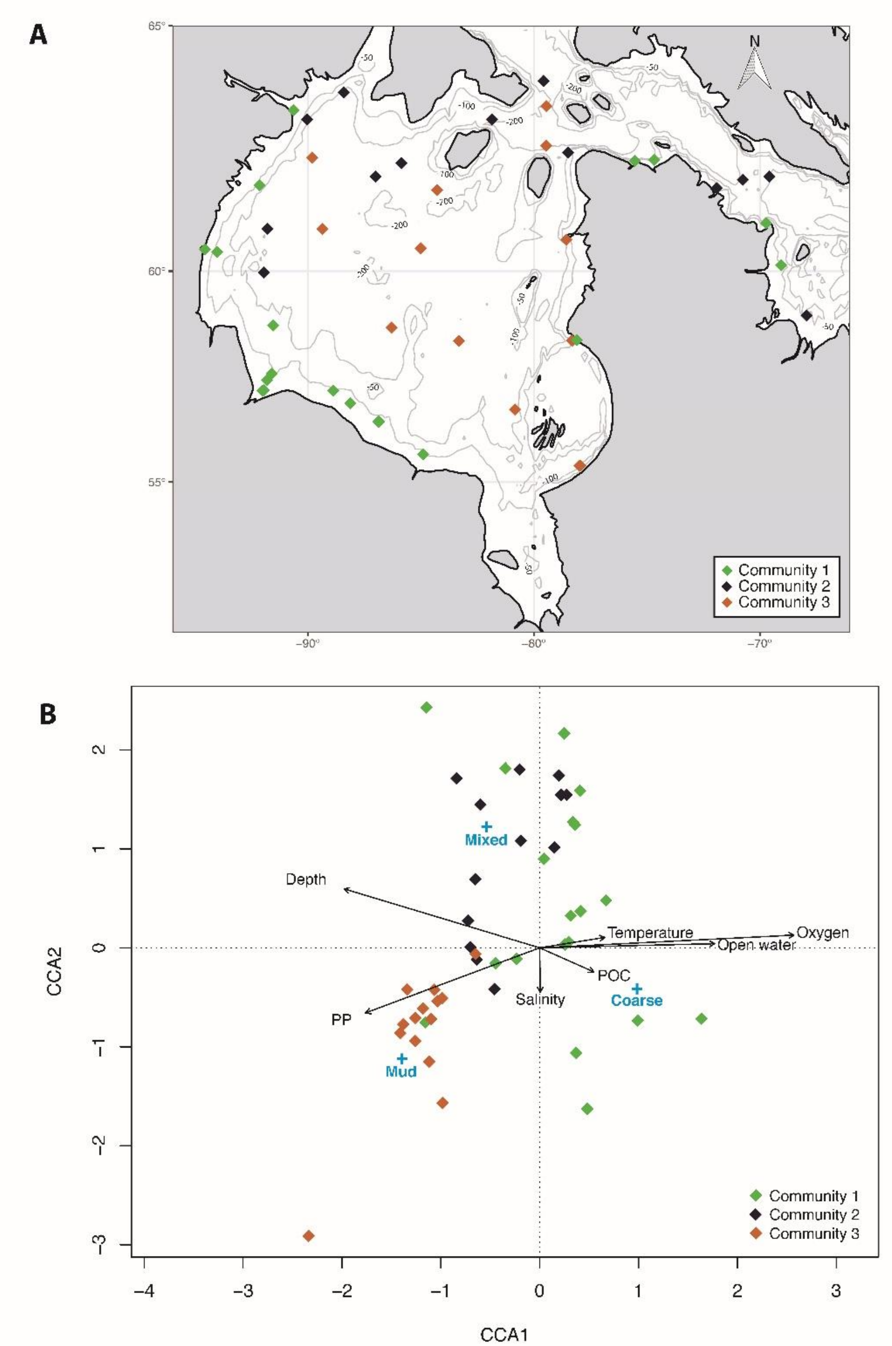

FIGURE 3.3.19 Epibenthic communities in the HBC. (A) Spatial distribution of the three distinct communities corresponding to coarse (green), soft (dark purple), and mixed (brown) bottom substrates (B) Canonical correspondence analysis (CCA) with ordination biplots of the epibenthic composition based on biomass data. In the ordination biplot, the quantitative environmental variables are illustrated by arrows, and the qualitative variable (type of substrate) is illustrated by the centroids (light blue crosses).

While the surface was nutrient-depleted in the polynya, subsurface waters were richer in nutrients than in adjacent ice-covered regions consistent with deeper convection in winter having a positive impact on upward nutrient supply and biological productivity. The temperature and salinity characteristics of the ice-free water column in the polynya (Team 1) showed that deep waters there were colder and saltier than elsewhere in the bay, suggesting deep winter mixing and enhanced nutrient supply to the surface. The remote-sensing approach provided crucial insights into the processes that affect productivity in northwestern Hudson Bay and the marginal ice zone (MIZ) in particular. Correlations between climate indices, i.e., the North Atlantic Oscillation and Arctic Oscillation (NAO/AO), and stocks of Chl*a* in surface waters implied that the bloom responds to large-scale atmospheric circulation patterns in the Northern Hemisphere. During positive NAO/AO phases, the strong polar vortex during winter strengthens westerly winds. This condition favors the formation of the polynya, where ice production and export, brine rejection, and nutrient replenishment are more efficient. As a result, the winter climate pre-conditions the upper layer of Hudson Bay for the subsequent development of MIZ blooms. Overall, this analysis suggests that primary productivity in the Hudson Bay system and the northwest polynya, in particular, was likely to decrease in the context of a decline in NAO/AO strength with Arctic warming.

East of the polynya, the absence of high phytoplankton biomass under mobile sea ice during the June expedition was intriguing since measured under-ice light levels at the time were sufficient to support phytoplankton growth. In the North, an under-ice bloom was potentially within its initial stages since above-background algal fluorescence was detected and nutrient concentrations remained elevated albeit slightly lower than estimated pre-bloom concentrations. The concomitant and novel observation of *Melosira arctica*, a filamentous diatom that attaches to the ice and extends into the upper water column, suggested an important role of this species in the early stages of the productive season there. In the South, under-ice algal fluorescence was higher than in the North while nutrient concentrations were reduced, suggesting that phytoplankton development was more advanced. These observations show that pelagic phytoplankton productivity can be initiated under the ice in Hudson Bay but that open-water conditions, such as those that prevailed in the polynya, are required to reach full bloom conditions.

Habitat suitability and surface salinities followed similar trends to those observed previously in southeastern Hudson Bay (Legendre et al., 1991; Gosselin et al., 1986; Monti et al., 1996). The positive correlation between ice algal Chl*a* concentrations and the salinity of both sea ice and surface water supports the notion that growth conditions were more favorable away from the estuaries. While the negative influence of low salinity appeared to be highly localized in the estuary, it is plausible that enhanced winter discharge in regulated rivers exacerbates the effect (Prinsenberg & Ingram, 1991).

During summer, where biological activity peaks due to warming and an abundance of sunlight for photosynthesis, most if not all inorganic nitrogen transported by rivers into the bay is converted into new phytoplankton biomass before it can disperse offshore, precluding any long-ranging influence for the bay as a whole. Algal growth within the rivers also partially depletes the riverine nutrient load and the potential for nutrient fertilisation of estuaries. In addition, dams modify the ratios of N, P, and Si riverine fluxes (Maavara et al., 2020) suggesting the management of upstream dams could also have consequences for nutrient river inputs.

The variability of nutrient concentrations and ratios among rivers located in different sectors of the bay is striking and can be attributed to the diversity of watersheds and littoral conditions and their environmental settings (land cover and local climate) and biological activity (vegetation growth and uptake of nutrients by microbes). With our current understanding, aside from the seasonal partitioning of nutrient deliveries to the bay, these differences mask any net influence of flow regulation on nutrient concentrations and ratios. In the absence of pre and post-regulation assessments for specific rivers, a proper ground-truthing evaluation of this influence would require the comparison of rivers that differ with respect to the presence/absence of regulation but otherwise are in the same watershed and share near-identical flow rates. Unfortunately, such a comparison remains unrealistic.

Evaluate nutrient processing along freshwater-marine gradients (Task 3.3)

The chemical form of nutrients that enter the bay and how far they move offshore depends on several processes, including biomass synthesis and bacterial transformations along the flow. Local changes in the composition of nutrients as well as in the stable isotopic signature of inorganic nitrogen pools along several freshwater-marine gradients were assessed. These measurements were related to discharge and chemical tracers of freshwater (Teams 2 and 1; see (Granskog et al., 2011)) and contrasted between regulated and unregulated rivers and watersheds.

In situ nutrient concentrations highlighted several trends, during winter 2017, the nitrate and silicate concentrations were higher in the freshwater than in marine waters. The concentrations decreased towards the ocean within the estuarine transition zone. In spring and fall, nitrate was depleted, whereas other nutrients (phosphate and silicate) were not. From these results, we examined the changes in nutrient concentrations and molar ratios to assess the detailed nitrogen fluxes in the stable isotopic signature of dissolved and particulate nitrogen pools. For selected rivers (Nelson, Hayes, and Churchill rivers) and their estuaries (freshwater-marine zone), incubations were performed in ship-board microcosms to investigate the degree of nutrient limitation as well as major cycling pathways of nitrogen. The experiments assessed nitrate assimilation into biomass, nitrogen fixation, ammonification, and nitrification, and will be used to close some of the outstanding nitrogen source-sink questions emerging from our observational data. Worldwide, preferential removal of P over N in reservoirs increases the N:P ratios of waters delivered to the ocean, raising the potential for P limitation of coastal productivity (Maavara et al., 2020). The Nelson River with higher P versus N seemed to contradict this trend. Maavara et al. (2020) also report that greater removal of silicon over nitrogen in reservoirs decreases Si:N ratios at river mouths, with a possible negative impact on the production of diatoms in estuaries. We found no indication here that the Nelson and La Grande River exhibit such this behavior, this discrepancy could be linked to the relatively low agricultural activity (little phosphate fertilizer addition) and associated extractive activity (Si is removed from the watershed in the process of plant harvests, and forestry) in the source watersheds.

Molecular techniques were employed to evaluate the degree to which freshwater microbes entering the marine ecosystem die off or survive with respect to gradients in salinity and nutrient availability. Bacterial and protist communities along 3 river gradients showed a strong decrease in freshwater communities from river to marine waters (Morency et al., in review). However, heterotrophic and mixotrophic dominated protist communities were found in the transition zone (Jacquemot et al., 2021). In temperate estuaries, convergence of river runoff and tidal forcing traps suspended sediment and planktonic organisms in a maximum turbidity zone (MTZ) (Frenette et al., 1995; Hetland & Hsu, 2013), creating conditions of low light, organic matter accumulation, and high microbial activity (Herfort et al., 2011). A MTZ was evident in the Nelson Estuary, in keeping with heterotrophy and mixotrophy being favored. Comparing these results with residence time and river discharge tendencies in the Nelson and Churchill estuaries will facilitate understanding the development of the specialized estuarine communities.

Overall nitrogen is in short supply relative to phosphate and silicate in the late spring surface of Hudson Bay waters. This implies that nitrogen, which is mainly in the form of nitrate is depleted first when phytoplankton accumulates biomass and can be considered as limiting for biological productivity. Nitrogen availability, therefore, sets an upper cap on the carrying capacity of Hudson Bay in terms of primary production and upper trophic levels. For this reason, our overall budget of nutrients for the bay focuses on nitrogen. A comparison of the annual deliveries of nitrate by rivers, which can be assumed to be fully converted into algal biomass during the productive season, with an estimate of the bay-wide replenishment of nitrate in the euphotic zone (resulting from vertical mixing processes and horizontal inputs through ocean gateways) shows that river nutrients make a measurable but minor contribution to biological productivity in the Hudson Bay system. The net or new annual primary production that can be supported by the estimated vertical replenishment of nitrate during winter amounts to 13 g C m^{-2} on average (calculated by converting nitrate supply into carbon equivalent and dividing by the marine area of Hudson Bay), which is much lower than the estimate of total primary production (PP, 72 g C m^{-2}) provided by Matthes et al. (2021). The difference indicates that roughly 80% of total PP is fueled internally by the recycling of nutrients (as ammonium or dissolved organic N) by microbes and grazers, a common situation in relatively unproductive ecosystems (Eppley & Peterson, 1970). This low ratio of new to total PP (0.2) implies that only a low and corresponding proportion of total PP can be transferred toward exploitable resources (e.g., fish) in the Hudson Bay.

The variable combinations of river runoff, nutrient concentrations, stoichiometric nutrient ratios, and tidal forcing across the estuaries surveyed impacted the productivity and structure of microbial communities and the position of different assemblages in the estuarine transition zone during early spring/summer. Estuarine circulation was a major driver of the dynamics and composition of microbial communities, leading to the formation of distinct ecological niches for microbial eukaryotes. Overall, local phytoplankton production in the Nelson estuary at this time was controlled by a spatial transition from light limitation in turbid river waters to nutrient limitation in marine waters. The combination of high Chl*a* concentrations and low primary production at the mouth of the Nelson River was interpreted as indicative of the export of freshwater algae that accumulated upstream in the river but became metabolically impaired by the osmotic stress in the more saline waters in the transition zone. At this point, the phytoplankton community was infiltrated by the marine diatom *Rhizosolenia* spp. across the strong front occurs where freshwater input meets marine waters. In parallel, the trapping of heterotrophic protists such as *Katablepharis*, *Cercozoa*, and ciliates at the turbidity front of the estuary sustains carbon remineralization and nutrient regeneration through phagotrophy and grazing. These processes could directly influence higher trophic levels at the scale of the estuarine and coastal systems. By affecting river discharge, regulation has the potential to influence estuarine circulation and modify the width, position, and stability of the salt transition zone, which, in turn, affects local plankton communities.

The biomass, density, and taxonomic richness of epibenthic communities were comparable to those of other Arctic regions (Grebmeier et al., 2006; Piepenburg et al., 2011; Roy et al., 2015). Coastal waters subject to the influence of rivers harbored the lowest epibenthic density, biomass, and taxonomic richness. The higher, but modest values of these epibenthic characteristics in central Hudson Bay were consistent with those of other studies (Ferland et al., 2011; Kenchington et al., 2011; Sibert et al., 2011). The most abundant and diverse communities were found in the northwestern region and are consistent with the BaySys results showing enhanced levels of primary production there as well as prior studies conducted in other polynyas (Ambrose & Renaud, 1995; Link et al., 2011).

Arctic cod, carry out complete life cycles in Hudson Bay and a comparison with other studies shows that the larvae of this key fish species hatch relatively early in the HBC (Bouchard & Fortier 2011). The results of modelling and chemical analysis of otoliths showed that the earliest hatching Arctic cod generally do so in coastal areas influenced by freshwater. This precocious hatching, where freshwater is present, is presumed to be linked to warmer surface waters. This has implications for freshwater regulation, more freshwater in winter possibly sets up conditions for the creation of suitable habitat for early hatching, once near-surface water is warmed by longer days in spring. However, the advantage for the larvae benefitting from a longer growing season could be counteracted by a mismatch between predator and prey, and competition from other species such as the sand lance (Fortier et al., 1995). The net trade-off for fish larvae as ice conditions continue to change is unknown. A major data gap is the seasonality of zooplankton assemblages related to the yearly formation and melting of sea ice and whether low summer zooplankton species, biomass, and general distribution in Hudson Bay are similar during early spring.

Capelin are considered sub-arctic species and have been increasing as a primary food source relative to Arctic cod for marine birds in Hudson Bay since the mid-1990s, with the switch corresponding to the step-change in sea ice cover that occurred about the same time (Gaston et al., 2012). It is difficult to determine whether shifts in species distribution have been exacerbated or tempered by regulation of rivers and more targeted monitoring of fish survival and recruitment throughout Hudson Bay is needed. Other mobile species could also potentially invade Hudson Bay, mirroring the Atlantification of other Arctic Seas by intruding Atlantic waters, resulting in species typically confined to the Atlantic expanding northwards.

Biogeochemical modelling (Task 3.4)

All observational data acquired during this project contributed to the refinement of a biogeochemical model of the bay, schematically represented in Figures 3.3.20, 3.3.21, and 3.3.22. This model was originally developed and validated mainly based on late-summer data (Sibert et al., 2011). This model currently includes the dynamics of both the sympagic (organisms associated with the sea ice) and the pelagic (plankton within the water column) systems and their interaction. Primary producers (micro-algae) are split into a large and a small fraction (respectively called diatoms and flagellates in the model), as are zooplankton consumers (mesozooplankton and microzooplankton). The currency of this mass-balanced model is nitrogen that primary producers can use in two forms from distinct nitrate and ammonium pools. Dynamic links of all these components to particulate and dissolved organic nitrogen pools complete the ecosystem model.

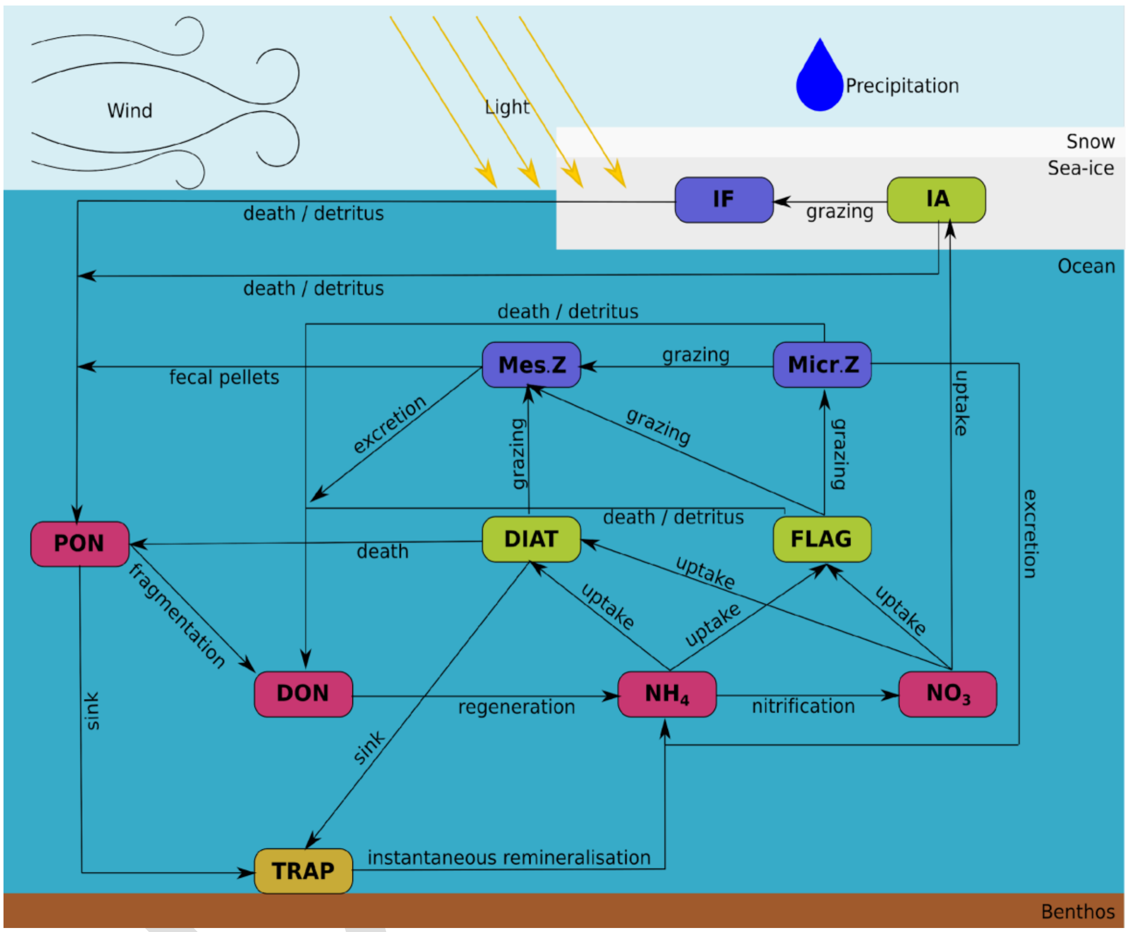

FIGURE 3.3.20 The conceptual model of the BioGeoChemical Ice Incorporated Model (BiGCIIM) was originally based on the Sibert et al. 2010 & 2011 model. Primary producers are in green, diatoms (DIAT), flagellates (FLAG), and ice algae (IA). Primary consumers in blue, microzooplankton (Micr.Z), Mesozooplankton (Mes.Z), and ice fauna (IF). The nutrient components are in pink, particulate organic nitrogen (PON), Dissolved organic nitrogen (DON), ammonium (NH4), and nitrate (NO3). The burial compartment is in yellow (TRAP). The fluxes and flow of matter between compartments are represented with black arrows.

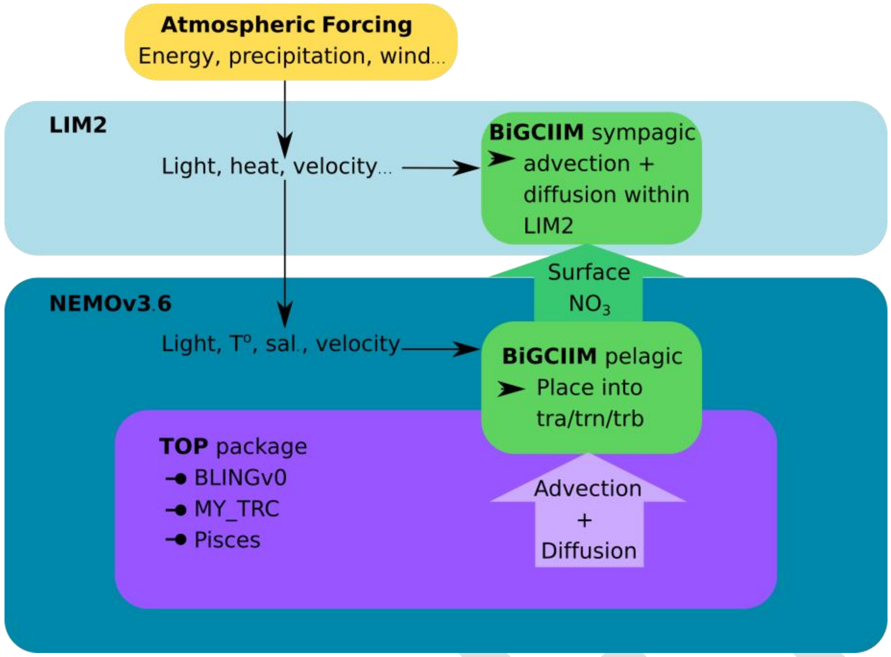

FIGURE 3.3.21 The coupling of BiGCIIM into NEMOv3.6 and LIM2.

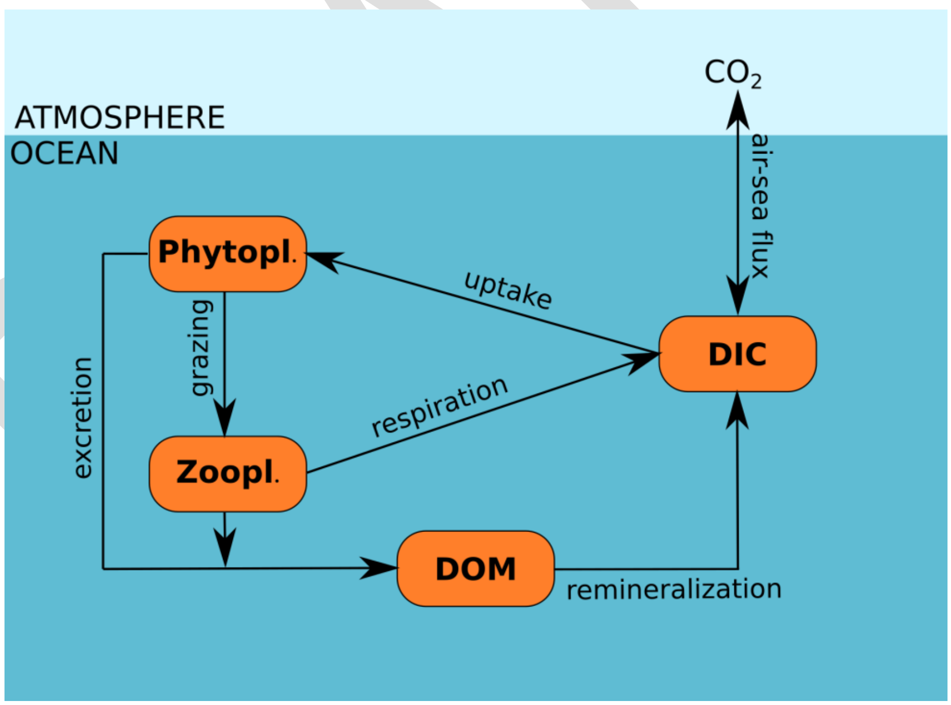

FIGURE 3.3.22 Carbon conceptual module incorporated into the BiGCIIM model. Compartments represented as orange boxes: phytoplankton (Phytopl.), zooplankton (Zoopl.), dissolved organic matter (DOM), and dissolved inorganic carbon (DIC). Fluxes and matter transfer between compartments are represented as black arrows.

The original Sibert et al. (2011) model required many updates and upgrades of the code to ensure a more accurate representation of what happens in the biogeochemical cycle. The model was converted from Fortran 77 to Fortran 90 to ensure compatibility with the physical circulation model it had to be coupled to (Team 6).

The next major improvements were to the rates between biological compartments. Firstly, nitrification, which was missing from the original model code, was implemented as a function of depth and light (Denman, 2003). The nitrification rate also has an ammonium limitation so that an absence of nitrification is assumed if concentrations of ammonium are less than 0.05 mmol N m^{-3} (Lavoie, pers. comm.).

Remineralisation rates were also improved to follow the salinity relationship shown in Al Azhar et al. (2017). This allows for larger sinking rates in areas with lower salinity due to the contribution of POM from river inputs and therefore lower remineralisation rates. In areas of higher salinity remineralization rates will be higher and sedimentation lower.

Within the original model, there is a trap compartment where POM sediments are exported to the bottom of the ocean and then are stored over long-time frames, called ‘permanently’. An instantaneous remineralisation rate of the organic matter reaching the bottom was implemented to ensure that there was no complete loss of nutrients and to allow for deeper ocean nutrient availability and recirculation towards upper layers via vertical turbulent mixing (Lavoie, pers. comm.). The transfer of nutrients into the ice was improved to be based on molecular diffusion gradients (Mortenson et al., 2017; Rebreanu et al., 2008) and under-ice surface roughness (Lavoie, 2015). One of the main mechanisms impacting nutrient transfer to the ice is that turbulence under ice allows for the replenishment of nutrients into the stratified surface layer, allowing nutrient-rich water to diffuse into nutrient deplete sea ice (Dalman et al., 2019).

Growth dependency by phytoplankton on light was improved to follow the methods used in Long et al. (2015). In the majority of biogeochemical models, the subgrid content of photosynthetically available radiation (PAR, 400 – 700 nm), i.e., the amount available within one cell of the model, is computed as the percentage of light that penetrates through open water and ice and then used to compute growth rate. Based on simple mathematical principles, Long et al. (2015) showed that it is the growth rates that have to be calculated for each subgrid level of light to be averaged thereafter. Their corrected approach results in a more representative growth rate for phytoplankton that is often lower than what the incorrect, yet widespread approach produces.

A carbon model was added to the model as well. This allows us to understand the change in alkalinity and dissolved inorganic carbon (DIC) (Lavoie, pers. comm.). The carbon module is added to the biogeochemical model to be dependent on the nitrogen components but may be deactivated as well.

The Biogeochemical model was also coupled to the physical ocean and ice model used by Team 6: NEMO 3.6 (Nucleus for European Modelling of the Ocean version 3.6; (Madec & the NEMO Team, 2008)) and LIM2 (Louvian-la-neuve Ice Model version 2; (Fichefet & Morales Maqueda, 1997; Bouillon et al., 2009)). The physical model is run over the Arctic Northern Hemisphere Atlantic ¼ degree domain (http://knossos.eas.ualberta.ca). Within NEMO 3.6 there is a TOP module, which is a mechanism that allows to input different tracers that will be transported by advection and diffusion calculated within the physical ocean model. Within LIM2, compartments must be placed directly into the model to be advected and diffused at the same time as the LIM2 model is calculated (Madec et al., 2008). Coupling the biogeochemical model online provides physical forcing that is at a higher time resolution for temperature, salinity, light, and velocity information than an offline simulation. This also allows us to run the model for the same period as the physical model, but also to capture the impacts of higher frequency of the climatological, hydrological, and glacial forcing, which sea ice dynamics is highly sensitive.

3.3.4 Conclusions

The BaySys proposal required Team 3 to address three highly integrated objectives through a combination of observational and modelling (Team 2 and 6) studies. We conclude this chapter by summarizing the results from our BaySys investigations as they pertain to each stated objective.

> **Hypothesis 3.1**: Through their impacts on light transmission and mixed-layer thickness, sea ice/snow dynamics, winter convection, and/or river runoff determine the timing of biological production.

> **Hypothesis 3.2**: River runoff and physical oceanic processes are both important drivers of nutrient loading, which controls productivity of the lower food web.

> **Hypothesis 3.3**: Processing of the inorganic and organic nutrients transported by rivers modulates their impact on Hudson Bay.

Overall, the results support our working hypotheses with respect to H3.1) the importance of sea ice/snow dynamics, river discharge, and winter convection in affecting the timing and magnitude of biological production in the Hudson Bay system, and H3.2) the role of estuarine transition zones in modulating the impact of river nutrients on the bay as a whole. The following discussion integrates the different observations and highlights how the variability in physical settings across different sectors of the bay affects the spatial and temporal patterns of biological productivity as well as the biodiversity and distribution of pelagic and benthic organisms. For the bay as a whole, our results support those of previous studies in showing that primary production, on average, is low with respect to other areas of the Arctic and sub-Arctic (Tremblay et al., 2019). While the new estimate of annual PP (67 g C m^{-2} yr^{-1}) produced by Matthes et al. (2021) is 1.7 to 2.8 times higher than previous ones, it remains relatively low when compared to highly productive Arctic regions (e.g., annual PP of 254 g C m^{-2} yr^{-1} in northern Baffin Bay and 462 g C m^{-2} yr^{-1} in the Bering Sea (Klein et al., 2002)).

Our hypothesis stating that the processing of the inorganic and organic nutrients transported by rivers modulate their impact on Hudson Bay H3.3) was also supported by the results, albeit with a clear seasonal distinction in the role that organisms play in this modulation. Data from the winter, when bacteria and phytoplankton activity is relatively low, showed that nutrients disperse unabated away from the Nelson and Churchill estuaries and simply mix conservatively with marine waters offshore. In this case, the nutrients delivered by rivers have a delayed impact since the resulting enrichment of marine waters paves the way for a larger spring bloom in the receiving areas, which may extend further offshore than otherwise if microbes consumed the nutrients within the estuaries. The enhancement of winter river discharge and nutrient transport by flow regulation, which occurs in the Nelson River, may therefore promote such delayed effects in western Hudson Bay.

While low by comparison with the summer pelagic production, ice algal activity in estuaries is present during winter/early spring. Although nutrients were relatively high at this time in southwestern Hudson Bay estuaries, ice algae were negatively influenced by low salinities from riverine input.

Our results concur with those of previous studies in showing that primary production, on average, is low with respect to other Arctic and sub-Arctic regions (Tremblay et al., 2019). This situation occurs despite relatively low ice thickness and the shorter duration of the ice-cover during the year in the bay, which favors light penetration and should promote PP. However, this advantage in light penetration is counteracted by the contribution of freshwater from rivers to stratification in the upper water column, which would be enhanced by concurrently occurring sea ice melt in the central Bay. This stratification curtails the upward re-supply of nutrients during winter, which ultimately limits the ability of ice algae and phytoplankton to accumulate biomass. The nutrient supply is greater in the northwestern polynya, where the wind patterns linked to the North Atlantic Oscillation reduce the ice cover, but also enhance vertical mixing in some years. The resulting early-onset and intensification of primary production in this sector of Hudson Bay quickly start the intense biological activity contributing to a food web supporting the area as a hotspot of marine wildlife. The supply of river nutrients in estuaries potentially provides nutrients to nearshore areas but would be variable due to the wide-ranging concentrations of nutrients across rivers. The nutrient loads of the different rivers were primarily attributed to differences in their natural setting, with no visible effect of regulation. However, regulation increased the relative contribution of nutrients in freshwater in winter. Because winter nutrient transport occurs during a period of relatively low productivity, the nutrients could move further offshore and contribute to a more intense spring bloom than otherwise expected.

Estuarine transition zones were characterized by a diversity of productivity levels and microbial communities that occupied the distinct niches created by varied combinations of runoff, nutrient concentrations/ratios, and tidal forcing during early spring/summer. For the Nelson Estuary, in particular, local phytoplankton production was controlled by the spatial transition from light limitation in turbid river waters to nutrient limitation in marine waters. Low salinities near the mouth of estuaries also had an adverse impact on the ice algae during winter/spring. By affecting river discharge, its partitioning between seasons, and the stability of the salt transition zone, regulation along with future changes in precipitation could therefore influence the structure and productivity of local plankton communities.

Except for the northwestern polynya, where all components of the lower food web were enhanced, spatial patterns of epibenthic communities differed from what would be expected from the distribution of primary production. Despite the relatively low levels of algal productivity offshore, the diversity and biomass of epibenthos were generally similar to those observed in other Arctic regions. The coastal waters subjected to the influence of rivers harbored the lowest epibenthic density, biomass, and richness, presumably due to a negative impact of sediment loading. Enhanced winter discharge for regulated rivers has the potential to exacerbate this negative impact by covering the organisms with sediment before they can gain access to fresh food in the spring/summer.

In the HBC, Arctic cod hatch relatively early in comparison with other seasonally ice-covered regions. The earliest hatchers in the bay can be traced back to coastal waters that are exposed to relatively warm water in winter, which supports the so-called 'freshwater refuge' hypothesis whereby warmer temperatures allow for a higher growth rate and longer feeding season for the fish that hatch there. This enhancement may be particularly crucial for the survival of Arctic cod in Hudson Bay given the relatively low levels of PP and zooplankton biomass we observed. In this context, the relatively high winter discharge observed in regulated rivers may prove beneficial for the success of Arctic cod, provided that the fish do not hatch so early as to lack food.

Finally, the work of Team 3 has provided insights into the ecological functioning of Hudson Bay, showing that the biological carrying capacity of marine waters is relatively low. In such a setting, the input of river nutrients into the coastal zone and the enhanced vertical replenishment of nutrients in the northwestern polynya are particularly crucial in supplying grazers and upper trophic levels with food in those key areas. For the polynya, inter-annual variations in productivity levels are controlled primarily by long-range climatic forcing. While no effect of regulation on in-river nutrient concentrations was detected, regulation potentially impacts the food web through the seasonal shift in river discharge, which affects the timing and offshore transport of nutrients. In addition, the input of sediment and organic matter that affects water transparency and the benthic habitat is affected by the seasonal shift in river discharge. By favoring early hatching, the enhanced delivery of relatively warm waters during winter months in regulated rivers possibly has a positive effect on the growth and survival of Arctic cod larvae.

3.3.5 Gaps and Recommendations

An incredible amount of data were collected as part of BaySys Team 3, such that it will require significant time beyond the funded BaySys project to exploit fully. Additional analysis of the data will also contribute to understanding the more long-term ramifications of counter-opposing forces of water regulation and climate change. We have addressed the deliverables of our objectives and uncovered new processes, which have bearing on the overarching objectives of BaySys. We conclude by summarizing the major gaps and making recommendations for further work from the perspective of Team 3:

a) Satellites cannot see under the ice, so the contribution of under-ice primary production to the total annual primary production remains to be established in the bay. The data suggest that in some years, the main phytoplankton bloom likely occurs under the ice because biomass peaks are not observed later under ice-free conditions.
b) In estuaries, the difficulty of isolating Chl*a* from other constituents in the water precludes a spatial and temporal analysis of possible relationships between discharge data and satellite-based estimates of primary production.
c) The eastern side of the bay was poorly covered by the sampling expeditions, which focused on the western side in part by design and in part due to logistical constraints at

sea. Estimates of Bay-wide PP must therefore be considered as provisional. The same limitation applies to our estimates of pre-bloom nutrient levels, which were established more than a year prior to the main spring/summer expedition.

d) The nature of the dataset prevents a conclusive analysis of the impact of flow regulation on the in-river concentration of different nutrients. This results from the low sample size of regulated rivers and the large variability in concentrations observed for unregulated rivers, both within and between distinct watersheds.

e) Given the combination of high natural variability and low sample size for regulated rivers, a spatial analysis comparing these rivers with unregulated ones in terms of nutrients, productivity, zooplankton, fish and benthos cannot be substituted for the now unattainable comparison of pre- versus post-regulation eras for a specific estuary.

f) The rapid response of microbes to small-scale environmental variability across complex estuarine zones complicates comparisons between rivers in terms of their upstream characteristics and overall influence on estuaries as a whole. This would require sustained monitoring of both regulated and unregulated rivers through time instead of the snapshot approach used here.

g) While our data suggest that the filamentous algae *Melosira arctica* could contribute significantly to the primary production of Hudson Bay under the ice during late spring, technical limitations preclude a quantitative sampling of these algae. In addition, more observations are needed since this was a one-off chance observation.

3.3.6 References Cited

The following is a list of publications produced and cited by Teams within the BaySys project.

Dalman, L. A., Matthes, L. C., Barber, D. B., Kuzyk, Z., Tremblay, J.-É., Lee, J., Lovejoy, C., Jacquemot, L., & Mundy, C. J. (in prep). Response of microalgal communities to a seasonal freshwater gradient in southwestern Hudson Bay, Canada. *Elementa: Science of the Anthropocene 2021*.

Jacquemot, L., Kalenitchenko, D., Matthes, L., Mundy, C. J., Tremblay, J.-É., and Lovejoy, C. (2021). Protist communities along Hudson Bay (Canada) freshwater-marine transition zones. *Elementa Science of the Anthropocene*, 9(1), 00111. 10.1525/elementa.2021.00111

Jacquemot, L., Vigneron, A., Tremblay, J.-É., Lovejoy, C. (in prep). Sea Ice melt and extent drives major transitions in the microbial food web throughout the water column of Hudson Bay, Arctic Canada.

Lee, J., Tefs, A., Standnyk, T., and Tremblay, J-É. (in review). Nutrient inputs from subarctic rivers into Hudson Bay. *Elementa: Science of the Anthropocene 2021.*

Lee, J., & Tremblay, J-É. (in prep). A contemporary nutrient budget for Hudson Bay.

Matthes, L.C., Ehn, J.K., Dalman, L. A., Babb, D.G., Peeken, I., Harasyn, M., Kiriliov, S., Lee, J., Bélanger, S., Tremblay, J.-É., Barber, D.G. and Mundy, C.J. (2021). Environmental drivers of spring primary production in Hudson Bay. *Elementa: Science of the Anthropocene*, 9(1), 00160. https://doi.org/10.1525/elementa.2020.00160

Matthes, L.C. (2021). Light propagation in ice-covered environments: seasonal progression and biological implications. *PhD thesis*. University of Manitoba. http://hdl.handle.net/1993/35352

Morency, C. Jacquemot, L., Potvin, M. Lovejoy C. (in review). A microbial perspective on the local influence of Arctic Rivers and estuaries on Hudson Bay (Canada) *Elementa: Science of the Anthropocene*

Pierrejean, M., Babb, D.G., Maps F., Nozais C. & P. Archambault (2020). Spatial distribution of epifaunal communities in the Hudson Bay system. *Elementa Science of the Anthropocene*, 8(1). doi.org/10.1525/elementa.00044

Schembri, S., Fortier, L., Maps, F. (in prep). Arctic cod hatching and thermal refugia in Hudson Bay. *Elementa: Science of the Anthropocene.*

Schembri, S., LeBlanc, M., Bernatchez, S., Arnold, S., Kamula, M., Litvinov, A., Kennedy, J., Bernatchez, L., & Fortier, L. (2019). Hudson Bay Fish and Fisheries. In: Kuzyk, Z., Candlish, L. (Ed.), *From Science to Policy in the Greater Hudson Bay Marine Region: An Integrated Regional Impact Study (IRIS) of Climate Change and Modernization* (254-273). ArcticNet, Quebec, Canada.

Tremblay, J-É., Lee, J., Gosselin, M., & Bélanger, S. (2019). Nutrient Dynamics and Marine Biological Productivity in the Greater Hudson Bay Marine Region. In: Kuzyk, Z., Candlish, L. (Ed.), *From Science to Policy in the Greater Hudson Bay Marine Region: An Integrated Regional Impact Study (IRIS) of Climate Change and Modernization* (225-243). ArcticNet, Quebec, Canada.

Other Works Cited

Al Azhar, M., Lachkar, Z., Lévy, M., and Smith, S. (2017). Oxygen minimum zone contrasts between the Arabian Sea and the Bay of Bengal implied by differences in remineralization depth. *Geophysical Research Letters*, 44(11), 106-11. 10.1002/2017GL075157.

Ambrose, W.G., and Renaud, P.E. (1995). Benthic response to water column productivity patterns: Evidence for benthic-pelagic coupling in the Northeast Water Polynya. *Journal of Geophysical Research*, 100, 4411–4421. doi.org/10.1029/94JC01982.

Ardyna, M., Babin, M., Gosselin, M., Devred, E., Bélanger, S., Matsuoka, A., and Tremblay, J.-É. (2013). Parameterization of vertical chlorophyll a in the Arctic Ocean: impact of the subsurface chlorophyll maximum on regional, seasonal, and annual primary production estimates Dynamics. *Biogeosciences*, 10, 4383-4404. 10.5194/bg-10-4383-2013.

Babin, M., Bélanger, S., Ellingsen, I., Forest, A., Fouest, V. L., Lacoura, T., Ardynaa, M., and Slagstad, D. (2015). Estimation of primary production in the Arctic Ocean using ocean colour remote sensing and cou- pled physical-biological models: Strengths, limita- tions and how they compare. *Progress in Oceanography*, 139. 10.1016/j.pocean.2015.08. 008.

Bazin, P., Jouenne, F., Friedl, T., Deton-Cabanillas, A. F., Le Roy, B., and Véron, B. (2014). Phytoplankton diversity and community composition along the estuarine gradient of a temperate macrotidal ecosystem: combined morphological and molecular approaches. *PloS one*, 9(4).

Basher, Z., Bowden, D. A., and Costello, M. J. (2018). Global Marine Environment Datasets (GMED). *World Wide Web Electron. Publ. Version 2.0.* URL http://gmed.auckland.ac.nz (accessed 2.3.20).

Beazley, L., Guijarro-Sabaniel, J., Lirette, C., Wang, Z., and Kenchington, E. (2019). Characteristics of Environmental Data Layers for Use in Species Distribution Modelling in the Eastern Canadian Arctic and Sub-Arctic Regions. *Mendeley, Data, V2*.

Bélanger, S., Babin, M., and Tremblay, J.-É. (2013). Increasing cloudiness in Arctic damps the increase in phytoplankton primary production due to sea ice receding. *Biogeosciences*, 10(6), 4087-4101. 10.5194/bg-10-4087-2013.

Bouchard C and Fortier F. (2011). Circum-arctic comparison of the hatching season of polar cod Borogdus saida: A test of the freshwater winter refuge hypothiseis. *Progress in Oceanography*, 90(1-4)105-116. 10.1016/j.pocean.2011.02.008

Bouillon, S., Morales Maqueda, M.A., Legat, V., and Fichefet, T. (2009). An elastic-viscous-plastic sea ice model formulated on Arakawa B and C grids. *Ocean Modelling*, 27, 174-184. 10.1016/j.ocemod.2009.01.004.

Chao, A. (1987). Estimating the population size for capture-recapture data with unequal catchability. *Biometrics*, 43, 783–791.

Christman, G.D., Cottrell, M.T., Popp, B.N., Gier, E., and Kirchman, D.L. (2011). Abundance, diversity, and activity of ammonia-oxidizing prokaryotes in the coastal Arctic Ocean in summer and winter. *Applied and Environmental Microbiology*, 77(6), 2026-2034.

Comeau, A.M., Li, W.K., Tremblay, J.-É., Carmack, E.C., and Lovejoy, C. (2011). Arctic Ocean microbial community structure before and after the 2007 record sea ice minimum. *PloS one*, 6(11), e27492.

Dalman, L.A., Else, B.G.T., Barber, D., Carmack, E., Williams, W.J., Campbell, K., Duke, P.J., Kirillov, S., and Mundy, C.J. (2019). Enhanced bottom-ice algal biomass across a tidal strait in the Kitikmeot Sea of the Canadian Arctic. *Elementa: Science of the Anthropocene*, 7, 22. doi.org/10.1525/elementa.361.

Denman, K.L. (2003). Modelling planktonic ecosystems: parameterizing complexity. *Progress in Oceanography*, 57(3-4), 429-452.

Eppley, R., and Peterson, B. (1979). Particulate organic matter flux and planktonic new production in the deep ocean. *Nature*, 282, 677-680. doi.org/10.1038/282677a0.

Ferland, J., Gosselin, M., and Starr, M. (2011). Environmental control of summer primary production in the Hudson Bay system: The role of stratification. *Journal of Marine Systems*, 88, 385-400.

Fichefet, T., and Morales Maqueda, M.A. (1997). Sensitivity of a global sea ice model to the treatment of ice thermodynamics and dynamics. *Journal of Geophysical Research*, 102(12), 609-12. 10.1029/97JC00480.

Filker, S., Kühner, S., Heckwolf, M., Dierking, J., and Stoeck, T. (2019). A fundamental difference between macrobiota and microbial eukaryotes: protistan plankton has a species maximum in the freshwater-marine transition zone of the Baltic Sea. *Environmental microbiology*, 21(2), 603-617.

Fortier, L., Ponton, D., and Gilbert (1995). The Match mismatch hypothesis and the feeding success of fish larve in ice-covered southeaster Hudson-Bay. *Marine Ecology Progress Series*, 120, 11-21. 10.3354/meps120011.

Frenette, J.J., Vincent, W.F., Dodson, J.J., and Lovejoy, C. (1995). Size-dependent variations in phytoplankton and protozoan community structure across the St. Lawrence River transition region. *Marine ecology progress series*, 120(1), 99-110.

Gaston, A.J, Smith, P.A., Provencher, J.F. (2012). Discontinuous change in ice cover in Hudson Bay in the 1990s and some consequences for marine birds and their prey. *ICES Journal of Marine Science*, 69(7), 1218–1225.

Gosselin, M., Legendre, L., Therriault, J.-C., Demers, S., and Rochet, M. (1986). Physical control of the horizontal patchiness of sea ice microalgae. *Marine Ecology Progress Series*, 29, 289-296.

Granskog, M.A., Kuzyk, Z.Z., Azetsu-scott, K. and Macdonald, R.W. (2011). Distributions of runoff, sea ice melt and brine using δ 18O and salinity data - A new view on freshwater cycling in Hudson Bay. *Journal of Marine Systems*, 88(3), 362–374. 10.1016/j.jmarsys.2011.03.011.

Grebmeier, J.M., Cooper, L.W., Feder, H.M., and Sirenko, B.I. (2006). Ecosystem dynamics of the Pacific-influenced Northern Bering and Chukchi Seas in the Amerasian Arctic. *Progress in Oceanography*, 71, 331-361. doi.org/10.1016/j.pocean.2006.10.001.

Henderson, P. (1989). Provenance and depositional facies of surficial sediments in Hudson Bay, a glaciated epeiric sea. PhD thesis, Department of Geology, University of Ottawa, Ontario.

Herfort, L., Peterson, T. D., McCue, L. A., and Zuber, P. (2011). Protist 18S rRNA gene sequence analysis reveals multiple sources of organic matter contributing to turbidity maxima of the Columbia River estuary. *Marine Ecology Progress Series*, 438, 19-31.

Hetland, R. D., and Hsu, T. J. (2013). Freshwater and sediment dispersal in large river plumes. *Biogeochemical Dynamics at Large River-Coastal Interfaces: Linkages with Global Climate Change*, 55-85.

Huot, Y., Babin, M., and Bruyant, F. (2013). Photosynthetic parameters in the Beaufort Sea in relation to the phytoplankton community structure. *Biogeosciences*, 10(5), 3445-3454. 10.5194/bg-10-3445-2013.

Ingram, R. G., Wang, J., Lin, C., Legendre, L., & Fortier, L. (1996). Impact of freshwater on a subarctic coastal ecosystem under seasonal sea ice (southeastern Hudson Bay, Canada), I. Interannual variability and predicted global warming influence on river plume dynamics and sea ice. *Journal or Marine System*, 7(2-4), 221-231. 10.1016/0924-7963(95)00006-2.

Joly S., Senneville S., Caya D., and Saucier, F.J. (2011). Sensitivity of Hudson Bay sea ice and ocean climate to atmospheric temperature forcing. *Climate Dynamics*, 36, 1835-1849.

Kenchington, E. L., Link, H., Roy, V., Archambault, P., Siferd, T., Treble, M., & Wareham, V. (2011). Identification of Mega- and Macrobenthic Ecologically and Biologically Significant Areas (EBSAs) in the Hudson Bay Complex, the Western and Eastern Canadian Arctic. *DFO Canadian Scientific Advisory Secretariat Research Document*, 52 p.

Klein, B., LeBlanc, B., Mei, Z.-P., Beret, R., Michaud, J., Mundy, C.-J., H von Quillfeldt, C., Garneau, M.-É., Roy, S., Gratton, Y., Cochran, J. K., Bélanger, S., Larouche, P., Pakulski, J. D., Rivkin, R. B., & Legendre, L. (2002). Phytoplankton biomass, production and potential export in the North Water. *Deep Sea Research Part II: Topical Studies in Oceanography*, 49(22), 4983-5002. doi.org/10.1016/S0967-0645(02)00174-1.

Kuzyk, Z. Z., Macdonald, R. W., Tremblay, J-É., & Stern, G. A. (2010). Elemental and stable isotopic constraints on river influence and patterns of nitrogen cycling and biological productivity in Hudson Bay. *Continental Shelf Research*, 30(2), 163-176. 10.1016/j.csr.2009.10.014.

Lavoie, D., Denamn, K., & Michel, C. (2005). Modelling ice algae growth and decline in a seasonally ice-covered region of the Arctic (Resolute Passage, Canadian Archipelago). *Journal of Geophysical Research*, 110, C11009. 10.1029/2005JC002922.

Lee, Z.P., Du, K.P, & Arnone, R. (2005). A model for the diffuse attenuation coefficient of downwelling irradiance. *Journal of Geophysical Research*, 110(C2), C02016. 10.1029/2004JC002275.

Lee, Z.P., Carder, K.L., & Arnone, R.A. (2002). Deriving inherent optical properties from water color: a multiband quasi-analytical algorithm for optically deep waters. *Applied Optics*, 41(27), 5755-5772.

Lee, J.E., Chung, I.K., & Lee, S.R. (2017). Dynamic genetic features of eukaryotic plankton diversity in the Nakdong River estuary of Korea. *Chinese Journal of Oceanology and Limnology*, 35(4), 844-857.

Legendre, L., and Gosselin, M. (1991). *Insitu* spectroradiometric estimation of microalgal biomass in 1st-year sea ice. *Polar Biology*, 11(2), 113-115.

Legendre, L., Robineau, B., Gosselin, M., Michel, C., Ingram, R. G., Fortier, L., Therriault, J. C., Demers, S., and Monti, D. (1996). Impact of freshwater on a subarctic coastal ecosystem under seasonal sea ice (southeastern Hudson Bay, Canada). *Journal of Marine Systems*, 7, 233-250. 10.1016/0924-7963(95)00006-2.

Lewis, M.R., & Smith, J. C. (1983). A small volume, short-incubation-time method for measurement of photosynthesis as a function of incident irradiance. *Marine Ecology Progress Series*, 13(1), 99-102.

Link, H., Archambault, P., Tamelander, T., Renaud, P.E., and Piepenburg, D. (2011). Spring-to-summer changes and regional variability of benthic processes in the western Canadian Arctic. *Polar Biology*, 34, 2025-2038. doi.org/10.1007/s00300-011-1046-6.

Long, M. C., Lindsay, K., and Holland, M.M. (2015). Modelling photosynthesis in sea ice-covered waters. *Journal of Advances in Modelling Earth Systems*, 7, 1189-1206. 10.1002/ 2015MS000436.

Madec, G., and the NEMO team. (2008). NEMO ocean engin. *Note du Pôle de modélisation*, Institut Pierre-Simon Laplace (IPSL), France, 27, 1288-1619.

Maavara, T., Akbarzadeh, Z., and Van Cappellen, P. (2020). Global Dam-Driven Changes to Riverine N:P:Si Ratios Delivered to the Coastal Ocean. *Geophysical Research Letters*, 47(15). 10.1029/2020GL088288.

Maritorena, S., Siegel, D.A., and Peterson, A.R. (2002). Optimization of semi-analytical ocean color model for global-scale applications. *Applied Optics*, 41(15), 2705-2714.

Michel, C, Legendre, L, Therriault, J-C, Demers, S, Vandevelde, T. (1993). Springtime coupling between ice algal and phytoplankton assemblages in southeastern Hudson Bay, Canadian Arctic. *Polar Biology*, 13(7), 441–449.

Mohr, W., Grosskopf, T., Wallace, D.W., and LaRoche, J. (2010). Methodological underestimation of oceanic nitrogen fixation rates. *PloS one*, 5(9), e12583.

Monier, A., Terrado, R., Thaler, M., Comeau, A., Medrinal, E., and Lovejoy, C. (2013). Upper Arctic Ocean water masses harbor distinct communities of heterotrophic flagellates. *Biogeosciences*, 10(6), 4273-4286.

Monti, D., Legendre, L., Therriault, J. C., and Demers, S. (1996). Horizontal distribution of sea ice microalgae: Environmental control and spatial processes (southeastern Hudson Bay, Canada). *Marine Ecology Progress Series*, 133, 229-240. doi :10.3354/meps133229.

Mortenson, E., Hayashida, H., Steiner, N., Monahan, A., Blais, M., Gale, M.A., and Mundy, C.J. (2017). A model-based analysis of physical and biological controls on ice algal and pelagic primary production in Resolute Passage. *Elementa: Science of the Anthropocene*, 5(39). 10.1525/elementa.229.

Muylaert, K., Sabbe, K., and Vyverman, W. (2000). Spatial and temporal dynamics of phytoplankton communities in a freshwater tidal estuary (Schelde, Belgium). *Estuarine, Coastal and Shelf Science*, 50(5), 673-687.

IOCCG. (2015). Ocean colour remote sensing in polar seas. In: Babin, M., Arrigo, K., Bélanger, S., Forget, M.-H., editors. Dartmouth, NS, Canada, *Reports of the International Ocean Colour Coordinating Group, Dartmouth, Canada*. 10.25607/OBP-107.

Ovaskainen, O., Tikhonov, G., Norberg, A., Guillaume Blanchet, F., Duan, L., Dunson, D., Roslin, T., & N. Abrego (2017). How to make more out of community data? A conceptual framework and its implementation as models and software. Ecological Letters 20, 561–576. doi.org/10.1111/ele.12757

Pelletier, B.R. (1986). Seafloor Morphology and Sediments. *Elsevier Oceanography Series*, 143-162. doi.org/10.1016/S0422-9894(08)70901-2.

Piepenburg, D., Archambault, P., Ambrose Jr., W.G., Blanchard, A.L., Bluhm, B.A., Carroll, M.L., Conlan, K.E., Cusson, M., Feder, H.M., Grebmeier, J.M., Jewett, S.C., Lévesque, M., Petryashev, V.V., Sejr, M.K., Sirenko, B.I., and Wlodarska-Kowalczuk, M. (2011). Towards a pan-Arctic inventory of the species diversity of the macro- and megabenthic fauna of the Arctic shelf seas. *Marine Biodiversity Special Issue*, 41(1), 51-70.

Prinsenberg, S.J., and Ingram, R.G., (1991). Under-ice physical oceanographic processes. *Journal of Marine Systems*, 2(1), 143-152. doi.org/10.1016/0924-7963(91)90020-U.

Rebreanu, L., Vanderborght, J.-P., and Chou, L. (2008). The diffusion coefficient of dissolved silica revisited. *Marine Chemistry*, 112(3-4), 230-233. 10.1016/j.marchem.2008.08.004.

Roy, V., Iken, K., and Archambault, P. (2015). Regional Variability of Megabenthic Community Structure across the Canadian Regional Variability of Megabenthic Community Structure across the Canadian Arctic. *Arctic*, 68, 180-192. doi.org/10.14430/arctic4486.

Rysgaard, S., Glud, R.N., Risgaard-Petersen, N., and Dalsgaard, T. (2004). Denitrification and anammox activity in Arctic marine sediments. *Limnology and Oceanography*, 49(5), 1493-1502.

Sibert, V., Zakardjian, B., Gosselin, M., Starr, M., Senneville, S., LeClainche, Y., (2011). 3D bio-physical model of the sympagic and planktonic productions in the Hudson Bay system *Journal of Marine Systems*, 88, 401–422. https://doi.org/10.1016/j.jmarsys.2011.03.014

ter Braak, C., and Verdonschot, P. (1995). Canonical correspondence analysis and relate multivariate methods in aquatic ecology. *Aquatic Sciences*, 57, 255-289. 10.1007/ BF00877430.

Tremblay, J.-É., Hattori, H., Michel, C., Ringuette, M., Mei, Z. P., Lovejoy, C., Fortier, L., Hobson, K. H., Amiel, D., and Cochran, K. (2006). Trophic structure and pathways of biogenic carbon flow in the eastern North Water Polynya. *Progress in Oceanography*, 71, 402–425.

Vannier, T., Leconte, J., Seeleuthner, Y., Mondy, S., Pelletier, E., Aury, J. M., and Wincker, P. (2016). Survey of the green picoalga Bathycoccus genomes in the global ocean. *Scientific reports*, 6, 37900.

Ward, J. H. (1963). Hierarchical grouping to optimize an objective function. *Journal of the American Statistical Association*. 58, 236-244.

Welch, H, Bergmann, M, Siferd, T, Amarualik, P. (1991). Seasonal development of ice algae near Chesterfield Inlet, NWT, Canada. *Canadian Journal of Fisheries and Aquatic Sciences*, 48(12), 2395–2402. http://dx.doi.org/10.1139/f91-280.

Zhai, L., Gudmundsson, K., Miller, P., Peng, W., Guðfinnsson, H., Debes, H., Hátún, H., White III, G.N., Hernández Walls, R., Sathyendranath, S., Platt, T. (2012). Phytoplankton phenology and production around Iceland and Faroes. *Continental Shelf Research*, 37, 15-25. 10.1016/j.csr.2012.01.013.

3.4 Carbon System (Team 4)

Team Member	Affiliation	Tasks contributed to					Role
Tim Papakyriakou	a	**4.1**	**4.2**	**4.3**	**4.4**	**4.5**	Science Lead
Bob Gill	b	**4.1**	**4.2**	**4.3**	**4.4**	**4.5**	Hydro Lead
Mohamed Ahmed	c	4.1	4.2	**4.3**	**4.4**	4.5	Contributor
Brian Butterworth	d	4.1	4.2	**4.3**	4.4	4.5	Contributor
Dave Capelle	a	**4.1**	**4.2**	**4.3**	4.4	**4.5**	Contributor
Inge Deschepper	e	4.1	4.2	4.3	4.4	**4.5**	Contributor
Brent Else	c	4.1	4.2	**4.3**	**4.4**	4.5	Contributor
Sohidul Islam	f	**4.1**	4.2	**4.3**	4.4	4.5	Contributor
Céline Guéguen	g	**4.1**	4.2	**4.3**	4.4	4.5	Contributor
Zou Zou Kuzyk	a	**4.1**	**4.2**	**4.3**	4.4	4.5	Contributor
Samantha Huyghe	a	4.1	4.2	**4.3**	4.4	4.5	Contributor
Zakhar Kazmiruk	a	**4.1**	**4.2**	**4.3**	4.4	4.5	Contributor
Fredrick Maps	e	4.1	4.2	4.3	4.4	**4.5**	Contributor
Rob Macdonald	h	4.1	4.2	4.3	4.4	**4.5**	Collaborator
Lisa Miller	h	4.1	4.2	**4.3**	4.4	4.5	Contributor
Richard Sims	c	4.1	4.2	**4.3**	4.4	4.5	Contributor
Søren Rysgaard	a	**4.1**	**4.2**	4.3	4.4	4.5	Contributor

a) *Centre for Earth Observation Science, University of Manitoba, Winnipeg, Manitoba, Canada.*
b) *Manitoba Hydro, Winnipeg, Manitoba, Canada.*
c) *University of Calgary, Calgary, Alberta, Canada.*
d) *University of Wisconsin*
e) *Department of Biology, Université Laval, Quebec City, Quebec, Canada.*
f) *Trent University*
g) *University of Sherbrooke*
h) *Fisheries and Ocean Canada*

3.4.1 Introduction and Objectives

The ongoing increase in atmospheric CO_2 concentration continues to be the largest single driver of contemporary climate change (IPCC 2013). The world's oceans represent a significant sink of atmospheric CO_2, having absorbed between 20%-30% of the total anthropogenic CO_2 emissions since 1750 (Ciais et al., 2013; Friedlingstein et al., 2019), which has slowed the accumulation of atmospheric CO_2 in the atmosphere. The Arctic Ocean in particular plays a strong role in oceanic CO_2 uptake, despite representing only 3% of the global ocean surface (Bates & Mathis, 2009; MacGilchrist et al., 2014; Yasunaka et al., 2018). Water will take in atmospheric CO_2 when the concentration of dissolved CO_2 at the water surface is less than in overlying air. On contact with water, the CO_2 from the atmosphere reacts forming carbonic acid [H_2CO_3], which then dissociates largely into bicarbonate ion [HCO_3^-], and to a lesser extent carbonate ion [CO_3^{2-}], while releasing one or more protons [H^+], the latter leading to a reduction in water pH. Collectively, dissolved CO_2 [CO_{2w}], [HCO_3^-] and [CO_3^{2-}] constitutes water's dissolved inorganic carbon (DIC) load. Dissolved CO_2 in seawater is often expressed in terms of the CO_2 partial pressure in seawater (pCO_2) in units of μatm. Additionally, the formation/dissolution of $CaCO_3$ results in the release or withdrawal of CO_2 either adding to or reducing seawater's stock of dissolved CO_2. These reactions are dictated by the thermodynamic equilibria of inorganic carbon (Zeebe & Wolfe, 2001), which is also a function of seawater temperature, salinity,, and pressure. For example, the pCO_2 in water will double for every 16°C increase in temperature (Takahashi et al., 1993).

While an accumulation of CO_2 in seawater will cause a decrease in pH (i.e., the seawater becoming more acidic), the water's total alkalinity (TA) buffers against a pH change with absorbed CO_2. A drop in pH also leads to a decline in the carbonate ion concentration (Doney et al., 2009) that has implications on how easily marine calcifiers can form calcium carbonate ($CaCO_3$) minerals. The saturation state (Ω) of a solution with respect to carbonate minerals is proportional to the product of concentrations of Ca^{2+} and CO_3^{2-} in the solution. Both aragonite and calcite are important biogenic $CaCO_3$ minerals and are denoted by subscripts Ar and Ca, respectively (e.g., Ω_{Ar} and Ω_{Ca}). In general, if the saturation state of the solution Ω is greater than 1, the mineral is stable, but if Ω is less than 1, the mineral is vulnerable to dissolution. Collectively, the reduction in pH and drop in Ω for aragonite and calcite are symptoms of ocean acidification (OA). The progression of OA may have serious negative implications for the marine ecosystem (AMAP, 2013), but specifics remain a subject of active research (e.g., Niemi et al., 2021).

In coastal seas, the cycling of carbon is complicated by shallow water processes and inputs of heat, river water, and associated carbon, nutrients and other dissolved and suspended load from the ecosystems within the draining watersheds (Duarte et al., 2013). The situation is further complicated in high latitude seas where seasonal cycles in sea ice add and remove freshwater during respectively the late spring/summer melt and the winter freeze up. Many of the processes that define the carbon cycle in coastal zones are illustrated graphically in Figure 3.4.1. From an abiotic standpoint, the addition of river water to the coastal ocean is important because it is characteristically *lower* in alkalinity and carbonate ions than seawater, which reduces the water's ability to buffer against a pH change with increasing CO_2, also contributing to a concomitant drop in Ω (Azetsu-Scott et al., 2010), and raises seawater pCO_2 that has bearing on air-sea CO_2 exchange. From a biotic standpoint, the addition of river water is important because it supplies organic matter including dissolved and particulate organic carbon (DOC and POC, respectively).

In Figure 3.4.1, 'terr' and 'mar' refer to terrestrial and marine forms of OC, respectively. The inflow of organic carbon (OC_{terr}) from rivers and also internal sources like shoreline erosion and intertidal/subtidal sediment (+POC) resuspension, moderates pCO_2 through the biological processes of respiration (acts to increase pCO_2) and photosynthesis (acts to decrease pCO_2). These processes occur both in the water column (heterotrophic bacteria and microalgae or phytoplankton) and on the seafloor of the coastal shelf (e.g., benthic algae and eelgrass) with impacts on the carbon system (e.g., Duarte et al., 2013; Hendriks et al., 2010). In the following, we refer to organic material and organic carbon. Dissolved organic material (DOM) is defined as part of the organic matter pool that passes through 0.22-0.7 μm filters. DOM contains nitrogen, phosphorus, oxygen, carbon among other elements, while DOC is the concentration of dissolved carbon in DOM. Nutrients bound in the OM are liberated when the material is degraded (also termed mineralized or remineralized) and available to support biological production in the presence of the other requirements for photosynthesis, most notably available photosynthetically active radiation. When exposed to sunlight, chromophoric dissolved organic material (CDOM) can also be broken down photochemically to DIC or altered so that the OM is more readily degraded to CO_2. Sediments bury POC (and DOC that has become sorbed to particles, converting it to POC) and preserve some of it over long time scales.

Similar to river water in its low salinity, but even more mineral-free, sea ice melt floods surface seawater with water that is typically colder than ambient conditions, and also low in TA and DIC, locally depressing both pCO_2 and Ω. Stratification resulting from inputs of freshwater (sea ice melt and inflow of meteoric water from precipitation and rivers) impedes vertical water mixing and air-sea exchange, causing CO_2 produced by respiration in deep waters to build up in those water masses and causing a drop in both pH and Ω (sometimes dangerously so). Ice formation, on the other hand, expels brine, which is both saltier and colder than seawater, thus denser, which promotes vertical mixing; furthermore, sea ice brine is well stocked in salts, alkalinity, and DIC. Sea ice cover acts to impede the direct air-sea transfer of momentum, heat, and CO_2 exchange. A final component of the carbon cycle in Figure 3.4.1 is the release of methane (CH_4) from sediments. In low oxygen, organic-rich environments, like some sediments, methane can be produced by microbial degradation of organic material. Methane can be oxidized to CO_2, and while a portion of the CH_4 released to the water column from the sediments can contribute to the water column stock of DIC, methane can also be released to the atmosphere when the ebullition rate from the sediments exceeds the oxidation rate within the water column. All considered, freshwater-dominated, high latitude shelf seas are relatively prone to OA and CO_2 outgassing (AMAP 2017).

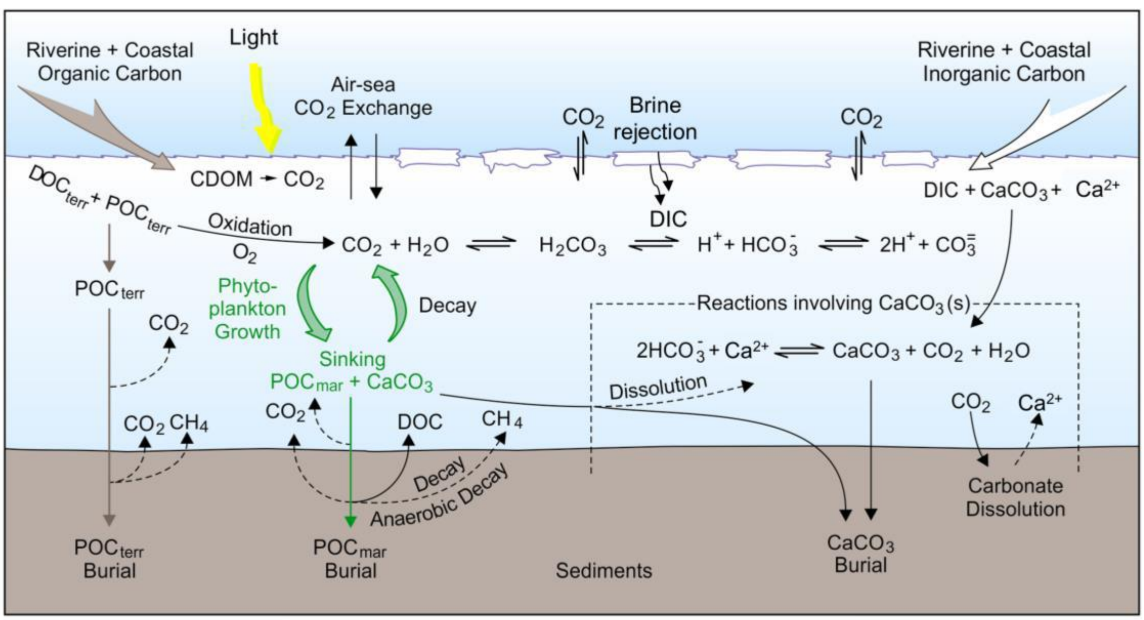

FIGURE 3.4.1 Schematic showing major processes related to the Carbon Cycle in high-latitude shelf seas (Capelle et al., 2020a). Subscripts ‘terr’ and ‘mar’ refer to terrestrial and marine forms of OC, respectively.

Hudson Bay is the largest continental shelf sea in the world and receives an annual freshwater loading of about 760 km^3 from more than 42 rivers (Déry et al., 2011). Local drainage is over carbon-rich soils largely underlain by continuous or discontinuous permafrost, particularly in the

Hudson Plains lying to the southwest and south of Hudson Bay. An additional freshwater flux, estimated seasonally at 1200 km^3 or more (Prinsenberg, 1988; Granskog et al., 2011), is withdrawn from or added to the water column due to the formation or decay of sea ice in the bay.

Like other Arctic Seas, Hudson Bay is transforming under the influence of anthropogenic climate change (AMAP, 2017). Sea ice cover in the bay has declined with a lengthening ice-free season (Hochheim et al., 2011; Hochheim & Barber, 2014; Landy et al., 2017) creating an opportunity for earlier commencement of spring phytoplankton blooms. Additionally, freshwater inputs to Hudson Bay continue to increase from various sources, including increasingly fresh surface waters imported from the Arctic Ocean (Carmack et al., 2016) and increased river discharge (Déry et al., 2016) in response to an Arctic wide- intensification of the hydrological cycle. Most of the river water and associated terrestrial carbon enters along the bay's southern coast, and many of the largest rivers are regulated for hydroelectric production (Déry et al., 2011). These regulated rivers include the Nelson, Churchill, Moose, Eastmain, and La Grande Rivière. The impact of regulation in Manitoba is a suppression of strong seasonality (i.e., flattening) in the annual hydrograph, with the implication of a reduction/increase in spring/winter discharge (Déry et al., 2018). At La Grande Rivière (Quebec), there is a reversed seasonality with highest flows in winter (about 10-times the natural winter flows). While studies have examined the potential impacts of regulation on river discharge (e.g., Déry et al., 2005, 2011, 2016, 2018) and Hudson Bay's freshwater budget (e.g., Anctil & Couture, 1994; Prinsenberg, 1980, 1983), none have explicitly examined the impact on the cycling of carbon in Hudson Bay, including effects on the bay's CO_2 sink capacity, or ocean acidification.

Insight into the bay's inorganic carbon system primarily results from ship cruises that have occurred in the late summer and early fall (e.g., Else et al., 2008a, 2008b; Azetsu-Scott et al., 2014; Burt et al., 2016). The results suggest that patterns in DIC and TA generally follow the distribution of freshwater (sea ice melt and meteoric water). The delivery of DIC and TA by rivers was found to be strongly influenced by the geology of the watersheds (Azetsu-Scott et al., 2014; Burt et al., 2016; Tank et al., 2012, Rosa et al., 2012). River water from the limestone-rich basins in southwestern Hudson Bay have relatively high DIC and TA compared to the eastern rivers (Tank et al., 2012), leading to aragonite super-saturation ($\Omega_{Ar} > 1$) in southwestern Hudson Bay coastal waters despite the abundance of freshwater in this region (Azetsu-Scott et al., 2014; Burt et al., 2016). While low saturation states for aragonite (i.e., Ω_{AR}) have been observed, particularly in the southeast of the bay, observations in surface waters have mostly been above 1 (Burt et al., 2016), except in proximity to the entrance of James Bay, were aragonite undersaturation was observed in surface waters (Azetsu-Scott et al., 2014). In southeastern Hudson Bay the saturation horizon (i.e., the water depth at which Ω_{AR} =1) was observed to the shoal to within 20 m of the surface, meaning deeper waters were undersaturated with respect to aragonite, and hence possibly corrosive to $CaCO_3$ minerals.

Else et al., (2008a, 2008b) noted that pCO_{2w} was in excess of atmospheric values in coastal waters dominated by river inflow, and attributed the observation to negative net community production (NCP), that is respiration of organic carbon in excess of local photosynthesis. Those results suggest that Hudson Bay was a net source of CO_2 to the atmosphere during the ice-free season. Regionally, Hudson Bay waters ranged from strong CO_2 evasion in the nearshore (particularly southeastern Hudson Bay and James Bay) to CO_2 sinks in the offshore and northern

Hudson Bay, including Foxe Basin (Else et al., 2008a, 2008b). Other studies show a relatively high degree of heterogeneity in primary production, but overall relatively low productivity (Ferland et al., 2011; Sibert et al., 2011; Kuzyk et al., 2010).

Estimates suggest that rivers supply Hudson Bay with approximately 5.5 Tg C yr^{-1} of DOC (Mundy et al., 2010) and 0.46 ± 0.33 Tg C yr^{-1} of POC (Kuzyk et al., 2009). POC_{terr} composition varies widely and includes both soil organic matter and relatively fresh vascular plant debris (Kuzyk et al., 2009). Godin et al. (2017) observed that both the riverine fluxes and the age and composition of DOC_{terr} vary widely within the Hudson Bay system. Gueguen et al. (2011, 2016) also noted variation in the composition and reactivity of DOC_{terr} in Hudson Bay. However, the fate of the POC_{terr} and DOC_{terr} in the bay, that is, what proportion is buried, transported out the system, or mineralized to CO_2 and evaded to the atmosphere, remains mostly unknown. Thus, while limited research to date suggests that river inflow, or in general freshwater, exerts a strong influence on the carbon system of Hudson Bay, we are not sure about the role of rivers in moderating the overall CO_2 source or sink status of Hudson Bay. Because POC_{terr} and DOC_{terr} sources (supply and composition) will be affected uniquely by climate change, there is increased urgency to understanding the specific fate of the various components. Long-term we are unsure of the relative role of changes in river discharge, including that associated with flow regulation, versus the influence of climate change in influencing the bay's overall role as an atmospheric source or sink.

To better understand the role of rivers on the bay's carbon system we have developed two main objectives:

> **First**, to characterize the seasonal impacts on Hudson Bay's carbon system, including the bay's overall CO_2 source or sink status, associated with variations in river discharge, primary production, and cycles of sea ice melt and formation; and
>
> **Second**, to assess long-term changes in Hudson Bay's carbon system, including the bay's overall CO_2 source or sink status, separating the relative influence of river flow regulation and climate change.

The report is divided into 6 sections. Having established the background, context, and objectives of the study, we next present the laboratory and modelling methods. Results are then presented sequentially in support of our first and second objectives, followed by an expert assessment of findings.

3.4.2 Analysis and Methods

Fieldwork

Details regarding field programs and methods are provided in the Phase 1 report and only briefly described below. Computational methods, and approaches to data analyses and interpretations are described in detail.

Underway Continuous pCO₂

During the 2018 cruise, we operated an automated underway pCO_2 system (General Oceanics model GO 8050; Pierrot et al., 2009) by directing water flow from a high-volume inlet located at about 7-m depth in the ship's hull through a shower-type equilibrator at a nominal flow rate of 2.5 L min^{-1}. The precision of the underway pCO_2 system is 0.1 µatm, with an overall accuracy estimated at 2 µatm (Pierrot et al., 2009). The system was calibrated every 8 hours using three certified standard gases (ultrahigh purity N_2 as a zero gas and two CO_2/air mixtures between 300 and 600 ppm) traceable to World Meteorological Organization standards. The underway pCO_2 system also contains a flow-through conductivity-temperature-depth (CTD; Idronaut model Ocean Seven 315), which provides continuous measurements of surface water temperature, salinity, and dissolved oxygen. However, we opted to use temperature and salinity measurements (for calculations and mapping) from a separate thermosalinograph (TSG) instrument, which draws water from the same intake line but is installed closer to the ship inlet than the underway pCO_2 system. We measured the chlorophyll a (Chl-a) concentration using a WestStar fluorometer included with the thermosalinograph system. Furthermore, we used a Fluorescing dissolved organic matter (FDOM) sensor (WETLabs ECOFLD) to measure the variability of FDOM.
The underway measurements of CO_2 mixing ratio were converted to pCO_2 at 2-minute intervals following Dickson et al. (2007):

$$pCO_2 = xCO_2 \times (P - pH_2O) \qquad (1)$$

where pCO_2 and pH_2O are the partial pressures of CO_2 and water (i.e., saturated vapour pressure, after Weiss & Price, 1980) inside of the systems equilibration chamber, xCO_2 is the dry-air mixing ratio, and P is atmospheric pressure. Calculated pCO_2 was adjusted for the temperature difference between the system's equilibrator and the TSG (taken as representative of the in-situ seawater temperature) following Takahashi et al. (1993). Propagating the maximum uncertainty in the *in-situ* seawater temperature measurements through the pCO_2 temperature correction, we estimate that the total uncertainty in the final pCO_2 measurements is < 2%. We processed the underway data to remove any measurements collected when the system was being cleaned or calibrated, or when water flows were restricted (i.e., water flow < 1.5 L m^{-1}) due to icebreaking operations. Additional details on the system can be found in Ahmed et al. (2020).

Analyses on Discrete Water Samples: Seawater Carbonate System and ^{18}O-H_2O

Both DIC (coulometric) and TA (potentiometric titrations with non-linear least squares end-point determination) were analyzed on bottle water sampled using the ship's CTD/Rosette system at predetermined stations (see Figure 3.4.2) and depths during the 2018 summertime cruise using standard methods (Dickson et al., 2007) at the Institute of Ocean Sciences (IOS, DFO, Sydney, BC). Accuracy was assured by calibration against certified reference materials (provided by Andrew Dickson, Scripps Institute of Oceanography), and we estimate the precision of the analyses at 1 µmol/kg for TIC and 3 µmol/kg for TA. Our near-surface samples that were collected independent of the ship's rosette and the DIC and TA for these samples were measured at the University of Calgary using an automated infrared inorganic carbon analyzer (AIRICA, Marianda Company, Kiel, Germany) and a semiautomated open-cell potentiometric titration system (AS-ALK2, Apollo SciTech, Newark, Delaware, USA) based on the modified Gran titration method, respectively. The precision of these measurements for DIC and TA were ±2 and ±3 μmol kg^{-1}, respectively.

Discrete salinity samples were collected at all stations and depths and were analyzed onboard the *Amundsen* using a Guildline Autosal Salinometer 8400B, with a precision better than ± 0.002 practical salinity units (PSU). The salinometer was calibrated with IAPSO Standard Sea Water provided by Ocean Scientific International Ltd (OSIL) before running the samples, and results are presented on the Practical Salinity Scale (PSU). Seawater pH and saturation state for aragonite (Ω_{ar}) were calculated for the discrete water samples using the software CO_2SYS (Pierrot & Wallace, 2006), with measured DIC, TA, seawater temperature, and salinity, the latter two from a SeaBird 911+CTD attached to the ship's rosette. Additional details are available from Burgers et al. (2020).

Samples for the determination of $\delta^{18}O$ were analyzed at the GEOTOP stable isotope laboratory at the Université du Québec à Montréal. Measurements were made using the CO_2 equilibration method, where 200 μL of sample water was equilibrated with CO_2 for 7 hours at 40 °C. The CO_2 was then analyzed on a Micromass Isoprime™ universal triple collector mass spectrometer in dual inlet mode with an AquaPrep™ system (Isoprime Ltd., Cheadle, UK). Results are expressed in the δ notation in ‰ versus Vienna Standard Mean Ocean Water. For each analytical sequence, two internal reference water samples were used to normalize the sample data ($\delta^{18}O$ = –6.71 ‰ and –20.31 ‰). Uncertainties in replicate measurements were ± 0.05 ‰ (1σ).

DOC concentration in water samples was measured at the Université du Québec à Rimouski using a Shimadzu TOC-Vcpn carbon analyzer equipped with a TNM-1 module (Total Nitrogen Measurement unit) simultaneously measuring the dissolved nitrogen concentration (DN, inorganic plus organic). Potassium hydrogen phthalate and potassium nitrate were used to standardize DOC and DN measurements, respectively. In addition, samples were systematically checked against Nanopure water (Barnstead Nanopure Infinity) and Bedford Basin secondary reference seawater (115-121 µmol C L^{-1} and 11-13 µmol N L^{-1}) every seventh sample analysis. The secondary standard was referenced to deep seawater reference from Florida Strait (43-45 µmol C L^{-1} and 32-33 µmol N L^{-1}) produced by the Hansell's consensus reference materials (CRM) program. The coefficient of variation on three replicate injections were typically <2% for DOC and <5% for DN.

Freshwater and seawater fractions

The fractions of sea ice meltwater (F_{SIM}), meteoric water (F_{MW}), and seawater (F_{SW}) were estimated for discrete water samples using $\delta^{18}O$ and salinity in a three-endmember mixing model (e.g., Östlund & Hut, 1984). Details can be found in Ahmed et al. (2020).

The impact of mixing of waters of different carbonate chemistry (e.g., freshwater and seawater) on the regional CO_2 source/sink is not easily quantified (e.g., Meire et al., 2015). While salinity, TA, and DIC are conservative water properties, the pCO_2 of the water does not change linearly when water masses are mixed (Zeebe & Wolfe Gladrow, 2001). The salinity (S), TA, and DIC in the coastal corridor resulting from the mixing of sea and river waters can be calculated following:

$$S_{mix}, DIC_{mix}, TA_{mix} = M_1 \times (S_1, TA_1, DIC_1,) + M_2 \times (S_2, TA_2, DIC_2), \quad (2)$$

where M_1 and M_2 are the mass proportions (0 to 1) of water masses 1 and 2, of respective endmember concentrations of S, TA and DIC. The pCO_2 of the mixed water can then be calculated using S_{mix}, $TA_{mix,}$ and DIC_{mix} for a given temperature using carbonate equilibria expressions.

Bulk Flux Estimates

The air-sea CO_2 flux (FCO_2) was calculated using the bulk formulation:

$$FCO_2 = \alpha k \cdot \Delta pCO_2 \left(1 - {C_i}/{100}\right), \quad (3)$$

where $\Delta pCO_2 = (pCO_{2sw} - pCO_{2atm})$ is the difference in partial pressure of CO_2 in the near-surface seawater (pCO2sw) and the near-surface atmosphere ($pCO2_{atm}$); α is the CO_2 solubility in seawater calculated using measured seawater temperature and salinity according to Weiss (1974); k is the gas transfer velocity as a function of 10 m horizontal windspeed (Wanninkhof, 2014). The flux was scaled with the concentration of open water, where C_i is the percentage of sea ice cover. To account for vertical pCO_2 gradients resulting from freshwater stratification, we applied a correction for the pCO_2 measurements in areas we occupied 1-5 weeks after ice breakup using a linear relationship proposed by Ahmed et al. (2020) to align the underway pCO_2 measurements with surface conditions (stratification-corrected measurements = 0.80 × uncorrected obs. + 65.7). pCO_{2atm} was calculated from CO_2 mixing ratio measurements made directly on air drawn into a gas analyzer (LI-COR, model 7000) from 17 m above the water surface. The LI-7000 was calibrated twice a day with two certified gas standards traceable to NOAA standards, and the mixing ratio measurements were converted into pCO_{2atm} following Dickson et al. (2007). Wind speed and air temperature were measured using a conventional propeller anemometer (RM Young Co. model 15106MA) and HMP45C212 temperature sensor, respectively. These sensors were mounted on the meteorological tower at a height of approximately 16-m above sea level. Wind speed was corrected to a height of 10 m assuming a log-linear wind profile and a neutral surface layer (Stull, 1988). Additional details on the flux calculation appear in Ahmed et al. (2021), and the field measurements of surface meteorology and gas concentrations are detailed in the Phase 1 report.

Carbon Degradation Experiments

Water samples were collected during the 2016/2017 ice camp and 2017 fall cruises for incubation experiments to determine rates of microbial and photochemical OC remineralization in Hudson Bay coastal waters. Sampling details appear in the Phase 1 report and Kazmiruk et al. (2021). In separate experiments, river, estuarine and coastal waters were either irradiated in a solar simulator for 48h (representing ~7 days of ambient sunlight) to measure photochemical degradation or incubated for 7-days to measure microbial degradation. DOM degradation was determined by the difference in before and after concentrations in organic matter (measured by absorbance and fluorescence spectroscopy) and in CO_2 and O_2 (measured by mass spectrometry). Details appear in Islam (2021).

Remote Sensing Methods

Daily satellite Level 3 (L3) sea surface temperature (SST) (4 km^2 resolution) was acquired from the MODIS Aqua platforms (NASA, 2019) between May and October 2018 for Hudson Bay. Areal estimates of ice-free surface seawater pCO_2 were inverted from the SST data using an algorithm detailed by Ahmed et al. (2021) using the 2018 springtime cruise data. An integrated sea-air flux of CO_2 for the HBC was estimated based on the bulk flux algorithm shown (Eq. 3). Wind speed for the gas transfer velocity was derived from the cross-calibrated multi-platform wind vector analysis (CCMP) at 6-hr resolution, and daily sea ice concentrations were derived from the Advanced Microwave Scanning Radiometer 2 (AMSR2; Spreen et al., 2008).

Numerical Modelling Methods

<u>Box Model:</u> A method to estimate the impacts of river inflow on the Hudson Bay Carbon System involved the use of a box model described by Capelle et al. (2020). The model provided an assessment of baseline biogeochemical controls on the bay's carbon system, including marine primary production, sea-air CO_2 flux, and indices of OA associated with the river delivery of OC_{Terr} (Capelle et al., 2020).

Briefly, the bay was divided into 'surface (0 – 50m)' and 'deep (50m – bottom)' layers for the coastal domain, where river runoff is relatively abundant, and the offshore domain, where runoff is less abundant. The average water properties (e.g., temperature, salinity, DIC, TA, nutrients, etc.) of each compartment and rates/magnitudes of relevant biogeochemical processes (e.g., primary production, carbon delivery, and transformation between organic and inorganic forms, water mass mixing) were estimated for each compartment based on available data prior to the BaySys project. Each compartment in the model was considered for both the open water season (May-Nov) and the ice-covered season (Dec-Apr). Empirical relationships between the chemical water properties (e.g., temperature, salinity, DIC, TA, nutrients) were then used to derive changes in pCO_2 (proxy for CO_2 flux) and aragonite-saturation (Ω_{Ar}; proxy for ocean acidification) for each compartment during each season using the software CO_2SYS (Pierrot & Wallace, 2006). This approach enabled us to isolate specific biogeochemical processes and determine their specific impact on pCO_2 and Ω_{Ar}.

<u>Biogeochemical Model: BLING</u>: The implementation of BLING was orchestrated by BaySys Team 6. BLING is a marine biogeochemical model: Biogeochemistry with Light Iron and Nutrient limitation and Gases (BLING) Version 0 + DIC (Galbraith et al., 2010, 2015). It ran within the BaySys Nucleus for European Modelling of the Ocean (NEMO) modelling framework for 3 climate scenarios (MRI, MIROC, GFDL – refer to section 3.6; Chapter 10 of the Phase 1 Report) over the historical period of 1980-2005 for both regulated and naturalized river runoff. For the future periods, various practical considerations limited the future experiments with BLING to just the RCP8.5 (IPCC, 2013) scenarios of MRI and MIROC. In each case, 2006-2070 was run for each forcing scenario for both naturalized and regulated runoff (refer to section 3.2). For this report, only the <u>ensemble average</u> considering the MRI and MIROC scenarios were analyzed.

BLING version 0 + DIC is a reduced complexity phosphorus-based biogeochemical model that includes iron, nutrients, and light limitation. The four prognostic tracers are inorganic phosphate, dissolved organic phosphate, oxygen, and iron. The model solves for Chl-a, phytoplankton production, and particle export considering light, macronutrient, and iron limitations, as well as a temperature dependency. The carbon module solves for dissolved inorganic carbon (DIC), total alkalinity (TA) concentration, dissolved oxygen concentration (DO), and chlorophyll-a concentration (Chl-a). Despite having a small number of prognostic tracers, BLING has been shown to reproduce basic bloom dynamics and magnitude within the HBC (Castro de la Guardia et al., 2019). BLING only considers the pelagic (plankton within the water column) system and not the sympagic system associated with a sea ice cover.

Biological fields in the model were initialized from the World Ocean Atlas 2012 version 2 (WOA13; Garcia et al., 2014). Dissolved iron and organic phosphate came from the Geophysical Fluid Dynamics Laboratory (GFDL) Earth System Model version 2 (ESM2M) (Galbraith et al., 2015). The GFDL ESM2M simulation is a global configuration at 1-degree nominal resolution and geopotential vertical coordinates. The simulation had a 100-year spin-up period using year 1860 forcing and an atmospheric carbon dioxide partial pressure (pCO_2) of 286 ppm. The initial conditions for the biological fields were built using the average of the last 20 years of the spin-up period.

The initial conditions of total alkalinity and dissolved inorganic carbon were derived from the mapped observational data product of the Global Ocean Data Analysis Project version 2 (GLODAP2; Key et al., 2015; Lauvset et al., 2016; and Oslen et al., 2016). These fields were remapped onto the ANHA4 grid with units of mol m^{-3}. The initial DIC concentration was normalized to the simulation start year (DICic = DICGLODAPv2 - DICdiff), where DICdiff is the anthropogenic carbon using DeVries (2014) estimates.

The default sign convention for the calculated surface DIC flux (as CO_2, termed SFDIC in output) in BLING Version 0 + DIC is positive when directed from the atmosphere into the ocean, and units are mmol $m^{-2}s^{-1}$. We transformed the flux so that a **negative** value denotes a flux of DIC into the seawater to be consistent with field process studies discussed in Section 3.4.4.6, and the units have also been changed to mmol m^{-2} day^{-1} for this report.

We evaluated projected climate change and regulation impacts on the carbon biogeochemistry in the Hudson Bay Complec (HBC) by season for both above and below the mixed layer depth (MLD) using historical (H; 1981 - 2010) and projected (P1 = 2021-2050 and P2=2041-2070) natural (N) and regulated (R) experiments. The MLD was defined as the depth where the seawater density anomaly, (σ_T):

$$\sigma_T = \rho\text{-}1000 \text{ kg m}^{-3}, \qquad [4]$$

(where ρ is the seawater density) differed from that at the surface by 0.01 kgm^{-3}. Monthly averages for the biogeochemical variables were grouped by season: Winter = January, February, and March; Spring = April, May, and June; Summer = July, August, and September; Fall = October, November, and December. Biogeochemical variables considered in the assessment include surface seawater pCO_2, the surface CO_2 exchange with the atmosphere (SFDIC), total alkalinity (TA), dissolved inorganic carbon (DIC), and pH. TA, DIC, and pH were calculated throughout the water column, while pCO_2 and the surface flux are variables specific to the sea surface. Dissolved oxygen (DO) was examined to support our interpretation of pCO_2 trends.

Aragonite saturation (Ω_{Ar}) was calculated using carbonate equilibria expressions with pH, TA, water temperature, and salinity within the CO_2SYS processing environment (Pierrot & Wallace, 2006) as input. Seawater temperature and salinity were also considered in the analysis because of their strong influence on the marine carbonate system.

Parts of our analysis followed Lukovich et al. (2021). In that work the impacts of climate change and regulation are evaluated using:

$$CC_{1,2} = N_{1,2} - HN; \quad [5]$$
$$CCR_{1,2} = R_{1,2} - HR; \quad [6]$$
$$Rh = HR - HN; \quad [7]$$
$$RC_{1,2} = CCR_{1,2} - CC_{1,2}, \quad [8]$$

where subscripts 1 and 2 represent projections associated with the two historical periods defined above (P1 or P2), N represents the naturalized scenario, R represents the regulated scenario, and H indicates historical averages. Thus, the impact of climate change ($CC_{1,2}$) is simply the difference in average values between the future projections and the historical average for the naturalized scenario (HN). Similarly, the combined regulation and climate change ($CCR_{1,2}$) impact is the difference between the projections and the historic period under the regulated scenario. The impact of historical regulation (Rh) is simply the difference between the regulated and naturalized scenarios for the 30 years contained in the historic runs, and cumulative regulated impacts are taken as the difference between the combined climate change and regulation impact (CCR) and climate change impact (CC) over P1 or P2. The percent relative climate change and regulation impacts are computed as:

$$\%CC_{1,2} = \left(CC_{1,2}/\left(\left|CC_{1,2}\right| + \left|RC_{1,2}\right|\right)\right) \cdot 100 \text{ and} \quad [9]$$
$$\%Reg_{1,2} = \left(RC_{1,2}/\left(\left|CC_{1,2}\right| + \left|RC_{1,2}\right|\right)\right) \cdot 100, \quad [10]$$

respectively, where again subscripts 1 and 2 correspond to the future periods P1 and P2 defined above. Each is also multiplied by the sign of the change in CCR to indicate whether the relative contribution from each reinforces or counteracts the projected combined climate change and regulation impacts.

It was anticipated that a second biogeochemical model, the BioGeoChemical Ice Incorporated Model (BiGCIIM), would be used to forecast changes in carbon cycling within Hudson Bay as part of the BaySys NEMOv3.6 and LIM2 modelling initiative. The model is based on Sibert et al. (2010; 2011) and has enhanced complexity relative to BLING. Due to the time constraints linked to BaySys deadlines, and the extent of work required to get BiGCIIM working, analyses based on BiGCIIM will not be available for this report. In the future, BLINGv0-DIC output will be compared to BiGCIIM, and additionally, BiGCIIM will be used to examine the roles of climate change and flow regulation on carbon cycling within the bay.

3.4.3 Results and Discussion

Team 4 results follow five tasks that were established at the onset of the BaySys project. The analytical results are then discussed within the greater context of the Team's objectives, and the overarching project. The initial tasks were:

Task 4.1 Fall Cruise (Mooring Deployment) - to investigate the effects of freshwater/marine mixing on carbon system parameters. Although the sampling duration will be limited, this survey will be an important part of establishing the seasonal carbon cycle in the Nelson estuary (hypothesis H4.1).

Task 4.2 Winter Camp - to allow an understanding of the impact of sea ice formation and melt on surface carbon chemistry in estuarine systems characterized by high (Nelson River) and low (Churchill River) winter season discharge.

Task 4.3 Bay-Wide Survey - to broadly sample variables regionally across shelf, basin, and estuarine environments of the bay (Figure 3.4.3). We will make use of our underway systems, ship's rosette, and sediment coring equipment for surface, water column, and benthos sampling along the ship track.

Task 4.4 Remote Sensing – to ensure that regional trends may be assessed relative to observed variation in atmospheric, hydrologic, and oceanic drivers to provide an independent satellite-based assessment of pCO_2, surface flux, including the contributions of thermodynamics and biology across the bay to assess the regional and Bay-wide influence of processes on pCO_2 and associated flux.

Task 4.5 Biogeochemical Modelling - to distinguish effects of climate variability from hydroelectric regime forcing on the bay's carbon system parameters, and net CO_2 exchange budgets.

3.4.3.1 Carbonate System Components in Surface Waters of Hudson Bay

The discrete sampling stations during the 2018 summertime cruise of the Amundsen are shown in Figure 3.4.2. In total 796 water samples for DIC and TA were collected between May 31 and July 12 providing comprehensive spatial coverage of the carbon system in the north, west, and south of the bay. Thick ice limited sampling in the central and eastern portions of the bay (Figure 3.4.3).

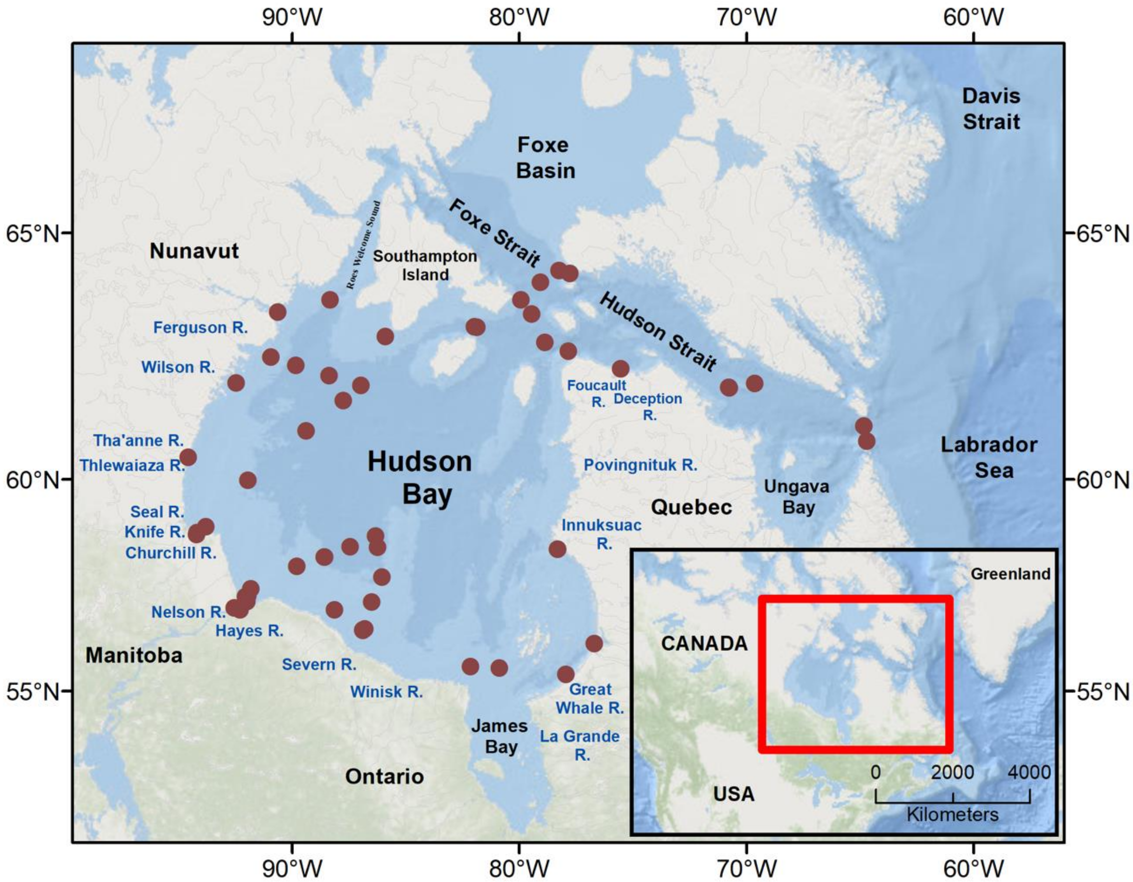

FIGURE 3.4.2 Surface sampling locations in Hudson Bay and Hudson Strait during the 2018 BaySys cruise (adapted from Ahmed et al., 2020). Also shown on the map are select rivers entering Hudson and James Bay.

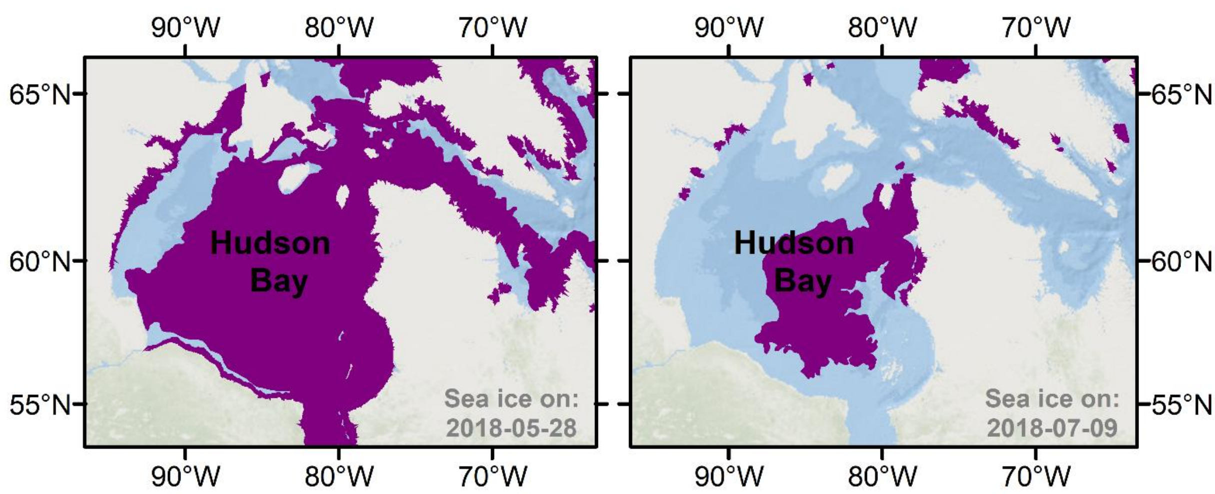

FIGURE 3.4.3 Sea ice concentration (>9/10th) at the beginning (left panel) and the end (right panel) of BaySys cruise in 2018 is shown in purple, based on using weekly ice charts provided by the Canadian Ice Service (Ahmed et al., 2020).

A synoptic perspective on the distribution of the major components of the bay's inorganic carbon system in the upper 20 cm of surface waters, in addition to surface salinity and temperature, is shown in Figure 3.4.4. As reported by others (i.e., Azetzu-Scott et al., 2014; Burt et al., 2016), the surface distribution of inorganic carbon largely followed the distribution of salinity and correspondingly the distribution of freshwater, both in the form of sea ice melt and river inflow. During the 2018 BaySys cruise, seawater salinity, which reflects total freshwater additions, was highest in the north and northwest of the bay and decreased along the coastal corridor into the southwest, south, and eastern areas of the bay.

Using salinity together with oxygen isotope data allows a three-component estimation of the composition of each water sample (see, for example, Ostlund & Hut, 1984). Following previous workers (Granskog et al., 2009, 2011; Eastwood et al., 2020; Ahmed et al., 2020), samples were decomposed into meteoric water (mostly river water in Hudson Bay), sea ice melt, and seawater. The fraction of sea ice melt was highest within the zone connecting the southwest to the southeast of the bay (see also Section 3.1.1). Meteoric water contributed most significantly to surface water in the south and southeast of the bay. The warmest water was observed along the southwestern coast between Cape Churchill and the Nelson River outlet, and then along a coastal corridor extending from the Nelson River to the east coast of the bay, mimicking the distribution of meteoric water. Total alkalinity (TA) had its highest surface concentration in the west and north of the bay, and lowest concentrations in the south and southeast, where dilution by river water and sea ice melt was greatest. While TA in the southwest of the bay was lower relative to the northwest, it was much higher than observed in the south and southeast. Both pH and Ω_{Ar} followed a similar trend to TA - that is, water with high pH and $\Omega_{ar} > 1$ was observed in the north and west of the bay, while $\Omega_{ar} \leq 1$ was observed in water with a high fractional composition of sea ice melt and meteoric water. Regionally high TA, pH, and Ω_{ar} were observed in the bay's southwest.

The observation of high seawater pH and Ω_{ar} (> 1) in surface waters at the confluence with James Bay, south of the Belcher Islands, is curious given high fractional compositions of both sea ice melt and meteoric water in those regions, and the presence of seawater with low pH and Ω_{ar} directly north of this region. Rosette sampling for water was sparse in that area, and the regional interpolation of the surface field is disproportionately influenced by only a few surface samples. TA was at a bay-wide minimum in that area which would otherwise tend to be associated with low pH and low Ω_{ar}. Seawater was intensely undersaturated in pCO_2 (<150 μatm) relative to atmospheric levels (~ 408 ± 2.8 μatm; Ahmed et al., 2021) in that area, which should support higher, rather than lower pH. This underscores the non-linear relationships between CO_2 system and oceanographic variables.

The water properties in Hudson Strait showed a large degree of variability, particularly in sea surface temperature, pCO_2, TA, pH, and $\Omega_{Ar.}$ Hudson Strait is the main corridor for water influx and outflow, hence the southern and northern portions of Hudson Strait reflect the properties of water leaving Hudson Bay, while the northern portion reflects water entering Hudson Bay from Baffin Bay. Inflow to the bay along the northern portion of the Strait was characteristically higher in salinity, TA, and pCO_2.

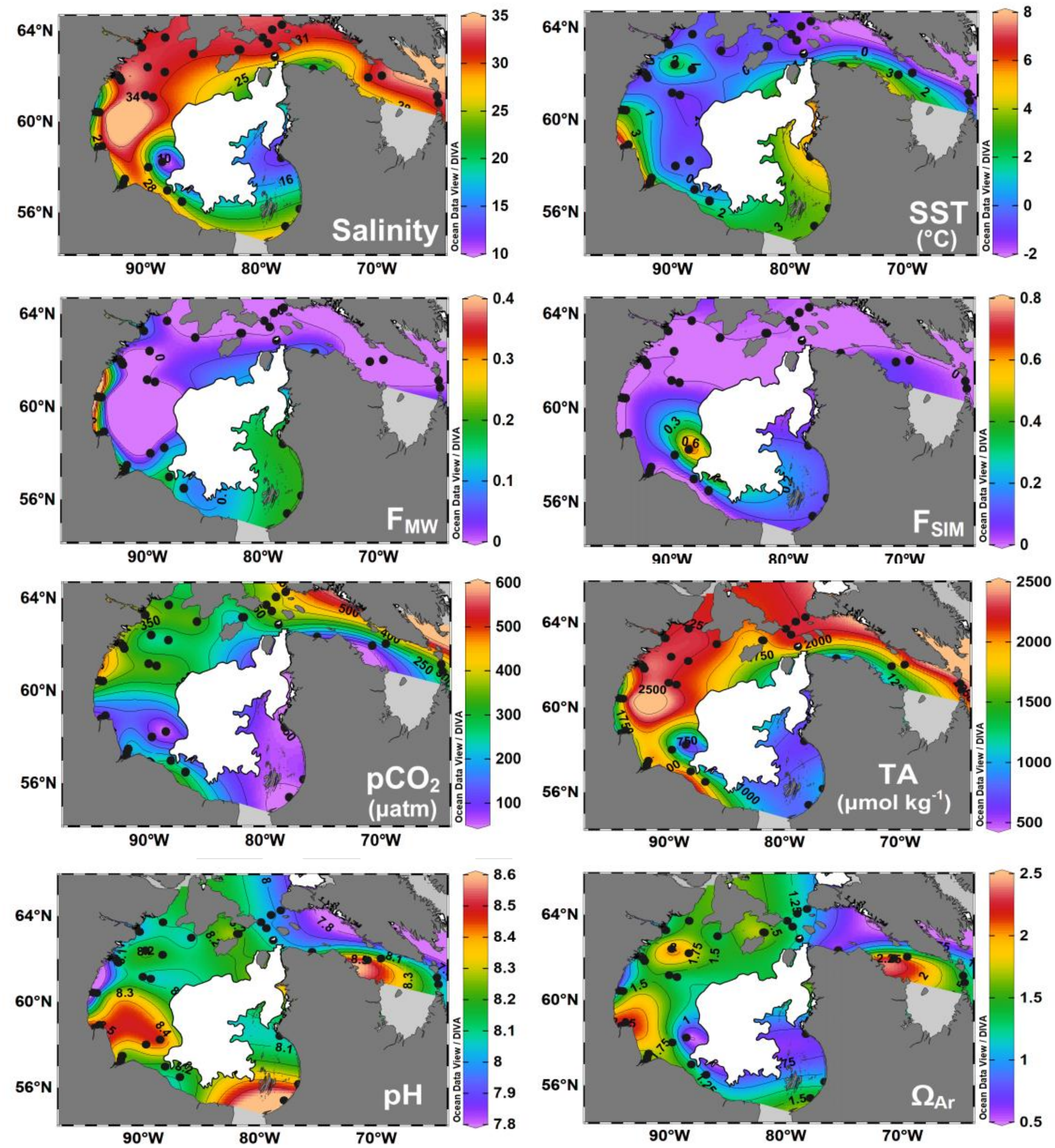

FIGURE 3.4.4 Surface distributions of (a) salinity (on the practical salinity scale, PSU), (b) sea surface temperature (SST), (c) meteoric water fraction (F_{MW}), (d) sea ice melt fraction (F_{SIM}), (e) seawater $p$$CO_2$ (calculated), (f) total alkalinity (TA), (g) pH and (h) aragonite saturation state (Ω_{Ar}). Data shown resulted from the 2018 BaySys summer cruise. The white area represents sea ice cover (> 9/10) as of 9 July 2018, based on weekly ice charts provided by the Canadian Ice Service (modified after Ahmed et al. 2020).

Measured pCO_2 (at ~ 7 m depth) along the ship track is shown in Figure 3.4.5 for the summer 2018 cruise, along with sea ice concentration, salinity, and temperature. Ahmed et al. (2020; 2021) summarized the data and reported that pCO_2 averaged 316.8$\pm$ 61 µatm in the surface seawater, and ranged between 125 and 650 µatm. They observed that the mixing of water masses was the main driver for pCO_2 variability across the study area with minor influence of biological production and remineralization of organic matter. The lowest pCO_2 values were observed close to the ice edges in the eastern and northwestern parts of the bay, and in Hudson Strait (125–280 µatm). The highest $p$$CO_2$ values (380–550 µatm) were mainly observed in ice-covered waters along the coast in southeastern Hudson Bay in areas with warm water of low salinity, close to the Churchill and Nelson Estuaries (390–465 μatm) (refer also to Figure 3.4.6). The undersaturated pCO_2 in offshore waters is probably a result of ice melt dilution, and possibly biological productivity promoted by mixing with high-nutrient sub-surface waters, particularly in the polynya located in the northwest of the bay, and in Hudson Strait. Sea ice meltwater is initially undersaturated in pCO_2 (e.g., Geilfus et al., 2015), whereas Arctic river waters tend to be relatively warmer than receiving seawater, and with pCO_2 close to, or in excess of atmospheric values, as a result of degrading terrestrial organic carbon and low pH (e.g. Semiletov et al., 2016). Therefore, the expectation is for regions dominated by sea ice melt and riverine input to experience undersaturated and supersaturated pCO_2 relative to the atmosphere, respectively.

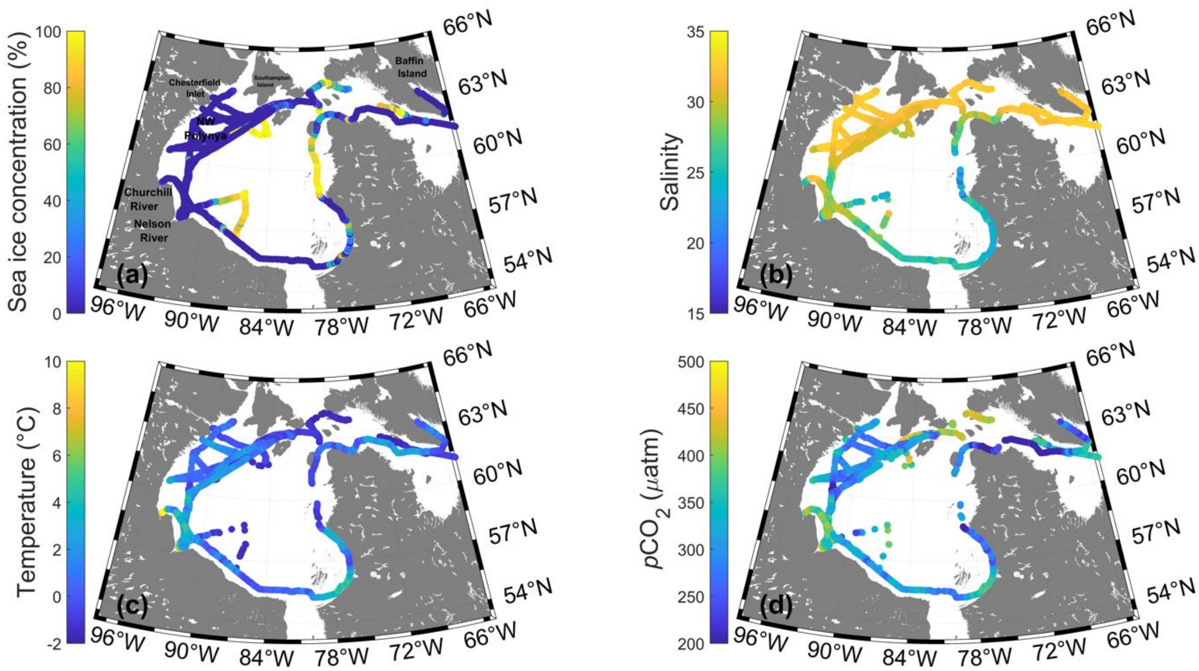

FIGURE 3.4.5 Spatial variability of sea ice concentration using the AMSR2 ice data (a), and underway measurements of (b) sea surface salinity (PSU), (c) sea surface temperature, and (d) surface seawater pCO_2 along the ship track in Hudson Bay from May 25 to July 13, 2018 (Ahmed et al. 2021).

Ahmed et al. (2021) demonstrated that the pCO_2 (at 7 m) in Hudson Bay was highly correlated with respective temperature (Pearson's r=0.65) and salinity (Pearson's r=-0.71). The pCO_2 is plotted as a function of temperature and salinity in Figure 3.4.6. Seawater with high pCO_2 was also observed under sea ice and generally results from the dominance of respiration over photosynthesis, as well as brine rejection from sea ice during the winter season, coupled with sea ice cover limiting air-sea gas exchange (see also Else et al., 2012c; Shadwick et al., 2011; Miller et al., 2011; Rysgaard et al., 2007). Upwelling can also lead to high surface pCO_2 (see also Else et al., 2012c; Mathis et al., 2012), which may explain the occurrence of high pCO_2 in cold saline surface waters (dashed rectangle in Figure 3.4.6) as observed south of Southampton Island (Figure 3.4.5d) (Ahmed et al., 2021).

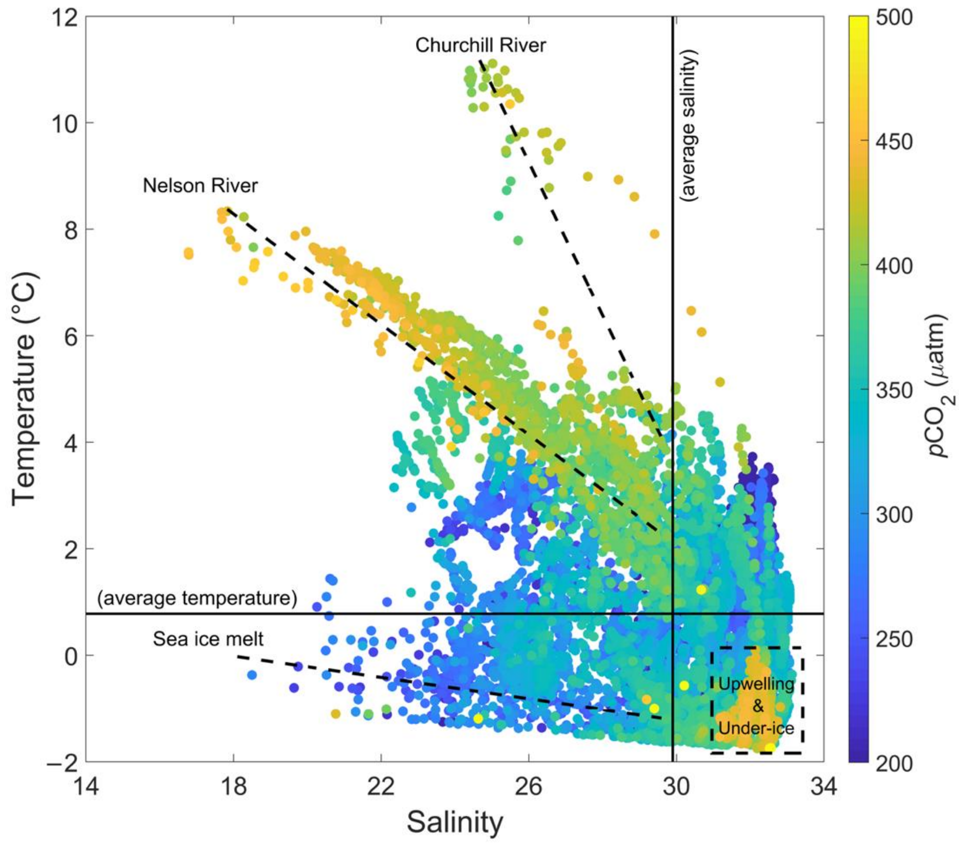

FIGURE 3.4.6 Temperature-salinity (as PSU) diagram visualized with surface water pCO_2 using data from the 2018 BaySys summer cruise (May 25 to July 13, 2018). The solid lines show the weighted area average of salinity and temperature, the dashed lines are mixing lines of freshwater sources, and the dashed rectangle highlights the source of high-pCO_2 marine waters (Ahmed et al., 2021).

3.4.3.2 The coastal corridor of Hudson Bay

The track of the 2018 cruise provides the opportunity to examine carbon biogeochemistry along the bay's coastal corridor. The variation in the water column carbonate system parameters and freshwater fractions along the coastal corridor is shown in Figure 3.4.7. The accumulation of meteoric water extended across the upper 50 m of the water column along the bay's southern coast, with the highest fractional composition across the mouth of James Bay and south of the Belcher Islands (southeastern Hudson Bay). While sea ice melt was also observed in these areas, the meteoric water was by far the prominent freshwater source, reaching fractional compositions of 25% at the mouth of James Bay. The highest fractional composition of sea ice melt was observed near the Nelson River outflow. In the figure, the negative fractional composition of sea ice melt is indicative of the brine signal associated with sea ice growth and negative F_{sim} values may be considered evidence of brine addition exceeding sea ice melt. Negative F_{sim} was observed both upstream and downstream of the Nelson River outlet, particularly in waters deeper than 25 m.

The low concentrations of TA (and DIC) were noticeably depressed in the upper 50 m of the water column at the mouth of James Bay. The seawater was supersaturated in aragonite north of the Nelson River (i.e., Ω_{Ar} >1), but the saturation horizon (depth below which waters become undersaturated in aragonite, i.e., Ω_{Ar} <1) shoals to the surface at the mouth of James Bay, with waters undersaturated in aragonite (i.e., potentially corrosive to aragonite) extending throughout the water column. The seawater pH generally follows the distribution of Ω_{Ar}, with lowest Ω_{Ar} (and pH) observed at depth in southeastern Hudson Bay. The general trend observed in this data set is in line with others (e.g., Burt et al., 2016), and in particular Azetsu-Scott et al., (2014) who 1reported aragonite undersaturation in southeastern Hudson Bay surface waters with high river-run-off fractions (>10%).

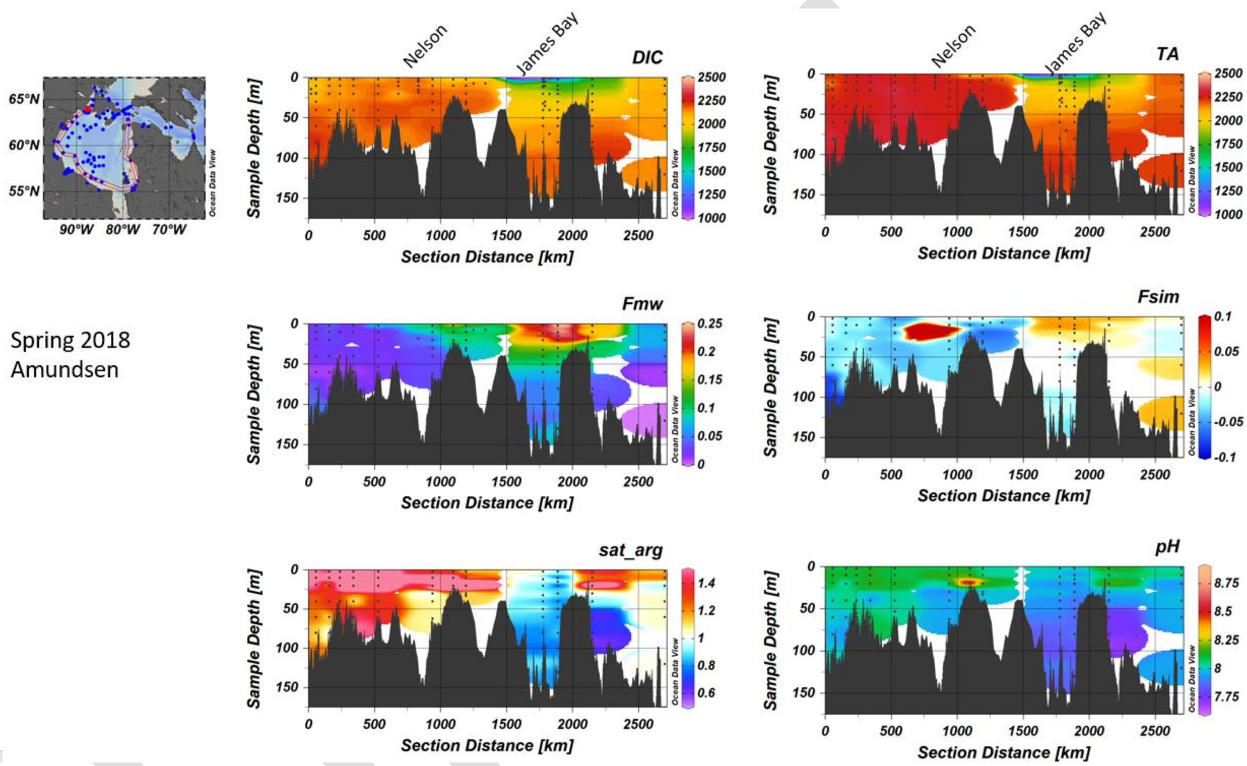

FIGURE 3.4.7 Seawater properties along a coastal transect starting in northwestern Hudson Bay and continuing counter-clockwise around the bay terminating in the northeast. Data in the figure are from the 2018 BaySys summertime cruise. Shown in colours are: a) dissolved inorganic carbon (DIC), b) total alkalinity (TA), c) meteoric water fraction (F_{mw}), d) sea ice melt fraction (F_{sim}), e) aragonite-saturation state (sat_arg = Ω_{Ar}), and f) pH. The red line on the inset map shows the position of the transect. Discrete sample locations are shown by blue dots on the inset map and black dots on the contour panels. The figure is adapted from Capelle et al. (2020b).

3.4.3.3. The Nelson River Estuary

The Nelson River has the largest discharge of the 42 rivers entering Hudson Bay (Déry et al., 2005, 2011) and to date, there is no published information on carbon dynamics in its estuary. The 2018 BaySys cruise provided the opportunity to observe water property mixing, and to measure carbonate system parameters, as the water transits from the river to sea within the estuary.

The spatial distribution of surface seawater pCO_2 in proximity to the Churchill and Nelson Rivers is shown in Figure 3.4.8. The highest pCO_2 values were observed in proximity to the river outlets, but interestingly not necessarily at the furthest points upstream. The pCO_2 appeared slightly undersaturated, or at least near equilibrium with the atmosphere in the samples closest to the river mouths. This observation may result from the diluting effect of the river water on TA and DIC, or sea ice melt associated with ice remnants along the coast. Seaward, the surface pCO_2 values fell off rapidly as the ship progressed toward the remnants of the sea ice pack. The average atmospheric pCO_2 was 408 ± 2.8 µatm during the study, hence seawater supersaturation appears, with some exceptions, limited regionally to the river estuaries or associated plumes (including the Churchill River) within the coastal conduit.

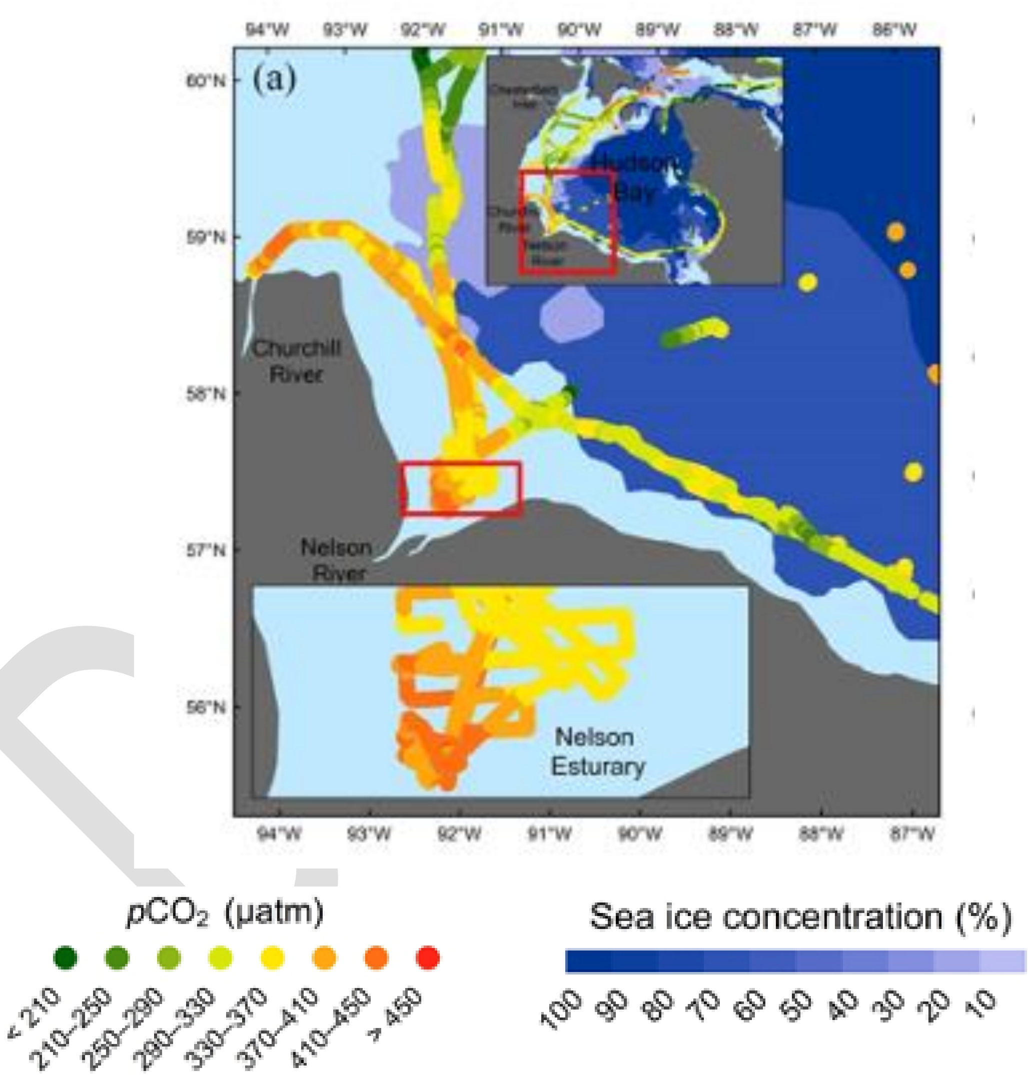

FIGURE 3.4.8 Underway measurements of pCO_2 (at ~ 7m of depth) in Nelson and Churchill River Estuaries**.** Also shown is with sea ice concentration (as of 2 July 2018) (Ahmed et al. 2021).

A closer look at the water properties along a transect seaward from the Nelson River is provided in Figures 3.4.9 to 3.4.12. The data presented results from ship- and boat-based sampling. As expected, water with high meteoric and sea ice melt fractions had lower salinity than surrounding seawater, however, the distribution of the freshwater fractions was patchy in a small geographic space in the river estuary, likely attributed to currents, water mixing, and remnants of melting sea ice (Figures 3.4.9a-c). The distribution of carbon variables (Figure 3.4.10 a-d) shows similar spatial complexity. The impact of sea ice melt led to lower TA, DIC, pCO_2. Conspicuous are values for carbon variables at Station 40, which possessed the highest sea ice melt fraction at the surface, and correspondingly lowest TA, DIC, pCO_2, and the only sampling station in the transect where Ω_{Ar} was less than 1 at the surface.

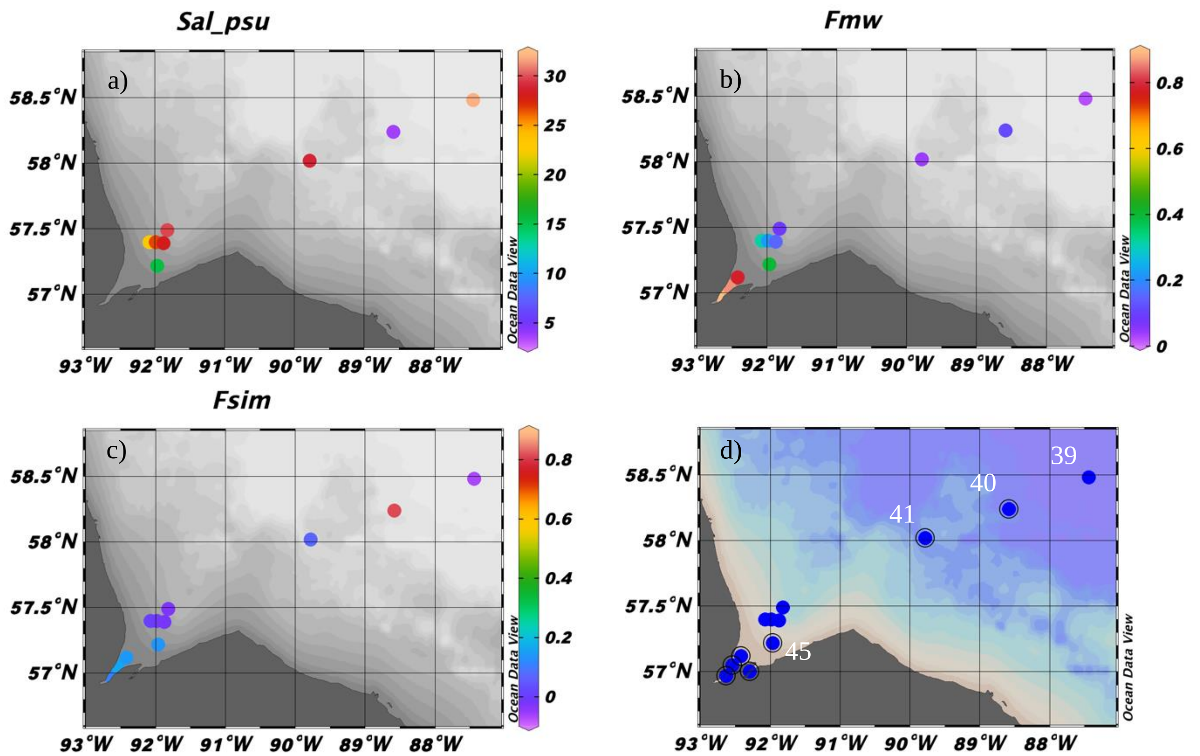

FIGURE 3.4.9 Near-surface seawater a) salinity (on the practical salinity scale), b) freshwater and c) sea ice melt fractions along a transect extending seaward from the Nelson River between June 24-30, 2018. Water was sampled at 0.2 m by barge (circled spheres in d) and at ~ 2 m depth at all other locations. Sampling stations 39, 40, 41, and 45 are identified in (d).

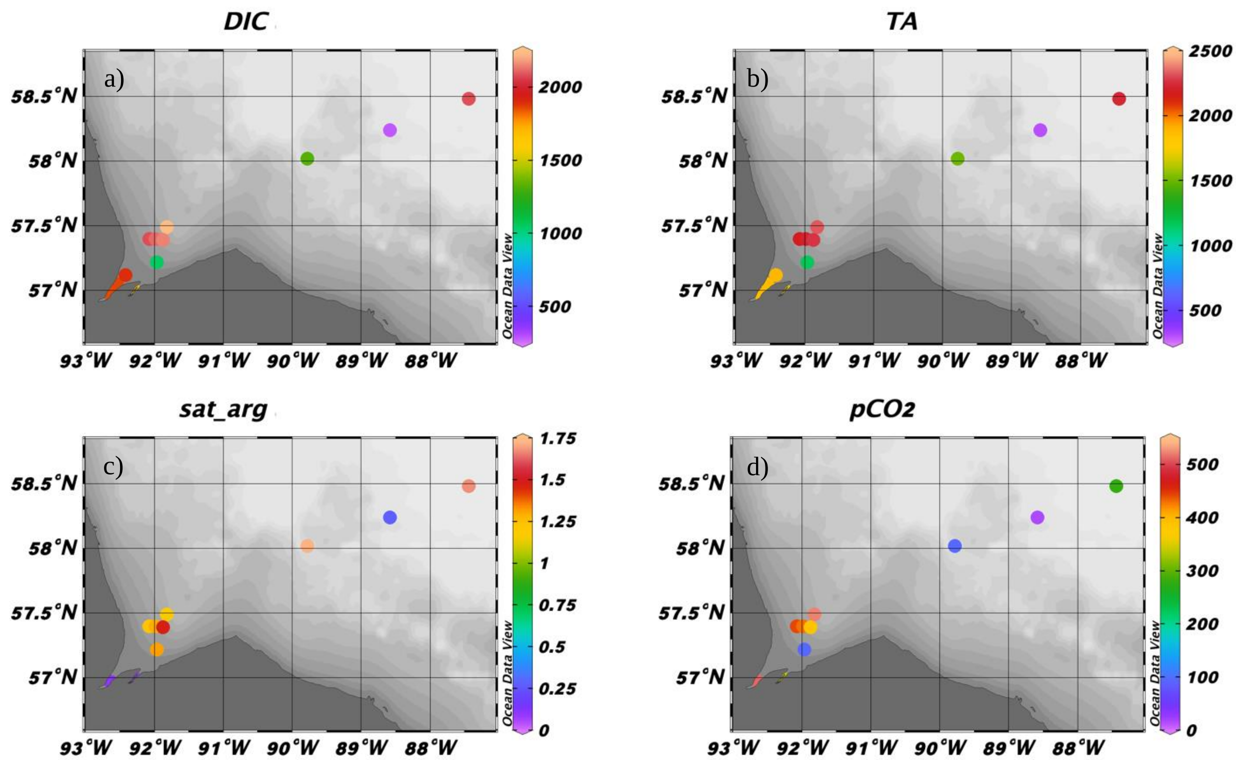

FIGURE 3.4.10 Near-surface seawater: (a) DIC (μmol/kg), (b) TA (μmol/kg), (c) Ω_{Ar} (sat_arg), and (d) pCO_2 (μatm) along the same transect identified in Figure 3.4.9d. pCO_2 was calculated using DIC and TA in CO_2SYS.

Ahmed et al. (2020) examined the salinity and temperature structure along a transect seaward to the sea ice edge from the Nelson River (Figure 3.4.11) and highlights the presence of the river freshwater lens atop saltier seawater that extended to ~ 50 km from the river outlet. The surface river flooding (evidenced by seawater of salinity less than ~ 28, and temperature far in excess of surrounding seawater), and associated stratification diminished rapidly from the freshwater sources (river and sea ice melt). While sea ice melt at the northeastern edge of the transect reduced salinity in the upper water column, its temperature was close to that of the surrounding seawater.

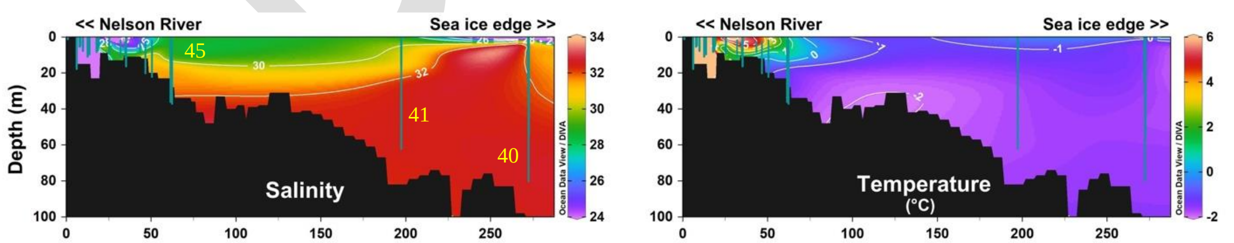

FIGURE 3.4.11 Cross-section of seawater (a) salinity (PSU) and (b) temperature along a subset of the transect identified in Figure 3.4.9d. Stations 45, 41, and 40 are identified in the figure. The vertical bars denote the location and depth of CTD profile. Data were collected between June 24 and 30, 2018 (Ahmed et al., 2020).

Seawater was sampled with depth for analyses at stations 39, 40, 41, and 45 (Figure 3.4.12 and 3.4.13). The river water fraction was high in the upper 20 m at stations 45, 41, and 40. The highest fraction was observed at Station 40 (the closest to the Nelson outlet). SIM was also evident at these stations, particularly at Station 40.

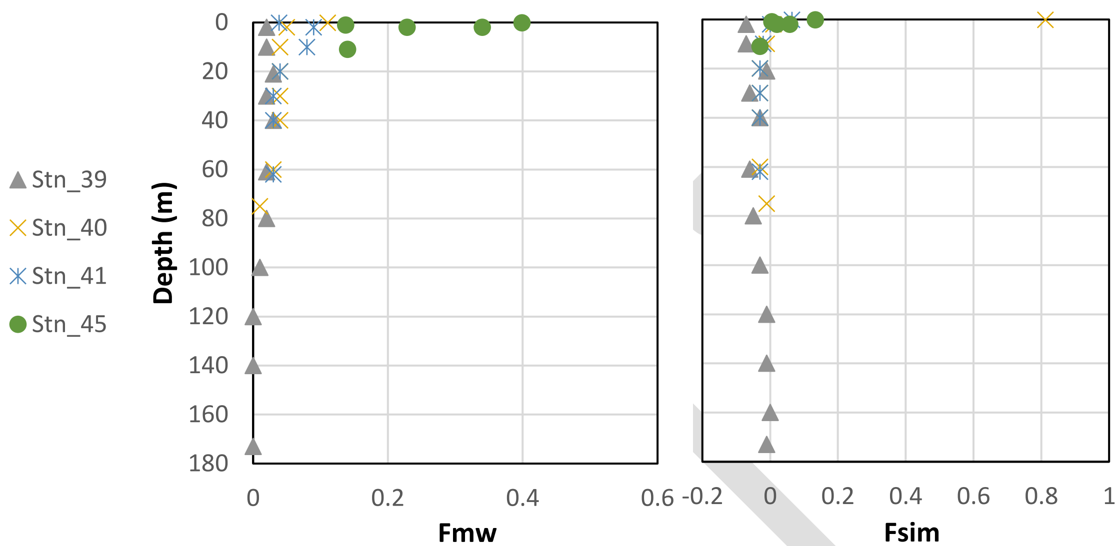

FIGURE 3.4.12 Freshwater fractions (meteoric water – F_{mw} and sea ice melt – F_{sim}) with depth across stations 39, 40, 41, and 45 (refer to Figure 3.4.9d for station locations). Samples were collected between June 24 and 30, 2018.

The corresponding carbon variables (pCO_2, Ω_{Ar}, pH, in addition to TA) for these stations, and from the Nelson and Hayes Rivers appear in Figure 3.4.13. The river water is super-saturated in pCO_2 at the Nelson outlet and near-saturated at the outlet of the Hayes River. Seawater samples from all stations in the upper 25-30 m (with few exceptions) showed undersaturation (and some exceedingly so) in pCO_2, including from station 45, which was only between 20 km to 30 km from the outlet of the Nelson River (Figure 3.4.13a). While Ω_{Ar} computed for these rivers showed pronounced undersaturation in aragonite ($\Omega_{Ar} < 1$), only two seawater samples in the upper 30 m of the water column were undersaturated in aragonite (Figure 3.4.13b). The river water is likely undersaturated in aragonite because of low concentration of calcium ions, typical of most rivers (AMAP, 2013). The TA from these rivers was less than measured in the majority of seawater samples, however, they were still higher than surface samples from Stations 45, 41, and 40 (Figure 3.4.13d). All samples from Station 45, the closest to the river outlet, were saturated in aragonite (i.e., $\Omega_{Ar} > 1$). Seawater in all samples deeper than ~ 70 m had $\Omega_{Ar} \leq$ ~1, and seawater was most acidic in deep waters of Station 39 (Figure 3.4.13c). Interestingly, most seawater samples near to the surface were more acidic than the river water samples (Figure 3.4.13c), highlighting pCO_2 undersaturation in surface waters of the estuary, and strong buffering capacity of rivers draining the Hudson Plains.

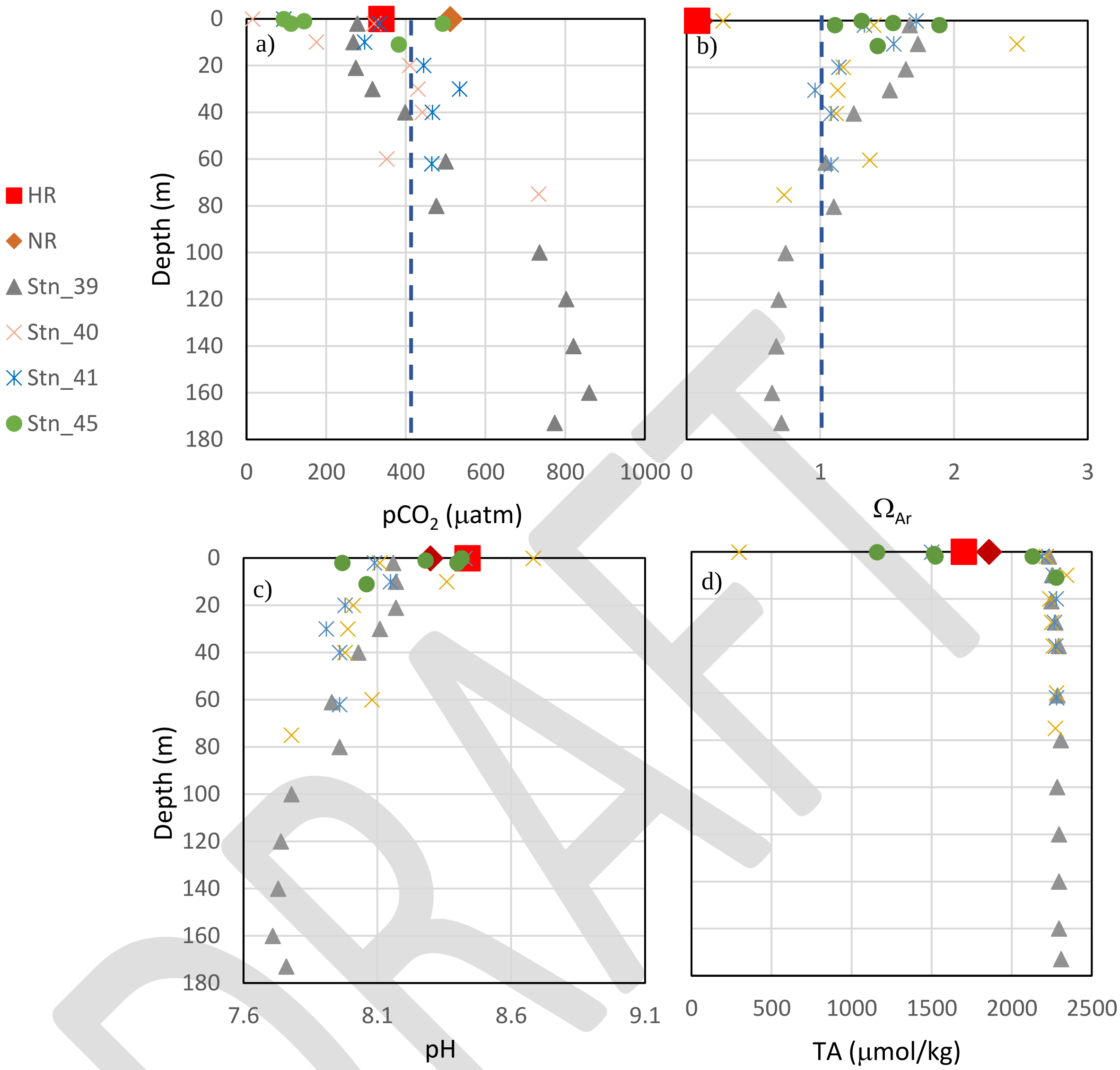

FIGURE 3.4.13 Carbon system variables: (a) pCO_2, (b) W_{Ar}, (c) pH, and (d) TA shown with depth across stations 39, 40, 41 and 45 (refer to Figure 3.4.9d for station locations). pCO_2 was calculated using carbon equilibria expressions (CO_2SYS, Pierrot & Wallace, 2006). The dashed line in (a) shows the average atmospheric pCO_2 from the BaySys cruise (408 matm). The dashed line in (b) shows the saturation state threshold (i.e., W_{Ar} =1). Samples were collected between June 24 and 30, 2018. HR and NR refer to respectively the Hayes River and Nelson River, sampled at the river outlets.

The data presented in Figures 3.4.9 to 3.4.13 represent a snapshot of conditions representative of the mixing environment over a 6-day sampling period and highlights that linear gradients in water properties along freshwater-marine mixing zones should not be expected owing to the complexity of both the mixing environment and carbonate equilibria (for the carbon variables). The carbonate system of estuaries is acknowledged to be highly complex (Abril & Borges, 2004). The distribution of the carbon system parameters should vary with changing river discharge, estuarine mixing augmented by tides and wind, freshwater residence time, the presence of water column stratification associated with the regional distribution of freshwater, and sea ice. Processes associated with ice (river and marine) may substantively change the estuarine mixing environment during the winter season. A deeper understanding of the carbon system of the Nelson Estuary, including its relationship to river outflow will require high-resolution measurements (in time and space) as part of a dedicated field and modelling study.

3.4.4.4 Carbon chemistry of rivers in Hudson Bay

The BaySys 2018 summertime cruise presented the opportunity to sample several rivers (see Figure 3.4.2) draining into Hudson Bay. The concentrations of DIC, TA, pCO_2, and DOC derived from water samples taken at the mouth of these rivers are shown in Figure 3.4.14, and data are summarized in Table 3.4.1. The pCO_2 in river water was calculated using CO_2SYS (Pierrot & Wallace, 2006) using measured DIC and TA. Representative values for concentrations of TA and DIC from sea ice melt and surface waters in Hudson Bay are provided in Table 3.4.1 for comparison. The southwestern rivers (Knife, Churchill, Nelson, Hayes, Severn, and Winisk Rivers) drain watersheds dominated by the carbonate-based bedrock of the Hudson Bay Plains. These rivers export (with the exception of the Knife River) water with concentrations of DIC and TA that were in excess of 1000 μmol kg^{-1} each. By comparison, the concentrations of DIC and TA in rivers in other parts of Hudson Bay that drain Precambrian rock of the Canadian Shield (Povungnituk, Foucault, Deception, Seal, Ferguson, and Thlewiaza Rivers) had concentrations < ~ 300 μmol kg^{-1}, substantially lower than concentrations measured in rivers in the southwest of Hudson Bay. Thus, in the marine system, the runoff from southwest of the bay is better buffered against acidification than areas influenced by runoff from the northwestern or eastern portions of the bay. The Nelson River had high TA:DIC ratios (>1) making this water particularly well buffered against acidification relative to rivers draining Precambrian Shield where the TA:DIC ratio was always less than 0.7. All the rivers sampled were oversaturated in pCO_2 relative to atmospheric concentrations, except the Hayes and Winisk Rivers, which appear in near equilibrium with the atmosphere.

Organic components of the carbon system also were measured in river waters. The concentration of DOC in Hayes, Nelson, and Winisk river water (10-13 mg/L) was ~ 2.5 times that observed in the other rivers (Figure 3.4.14). The mean marine DOC provided in Table 1 (1.1 mg/L) is similar to median values reported in Mundy et al. (2010) for Hudson Bay (1.31 mg/L) and roughly 10 times lower than observed for the southwest rivers.

The regionally high TA in southwest Hudson Bay identified in the text surrounding Figure 3.4.4 is at least partly because rivers entering the bay in southwest Hudson Bay have the highest TA of rivers entering Hudson Bay. The southeast of Hudson Bay had lower salinity and higher fractional composition of freshwater, indicative of the greater extent to which that area is impacted by cumulative river inflow and sea ice melt than the western area of the bay, due to the cyclonic circulation of the bay's outer boundary.

TABLE 3.4.1: Endmember values of salinity (S on the practical salinity scale - PSU), TA, DIC, and DIC_{Sat}[+] for surface waters of Hudson Bay (Marine), sea ice melt (SIM), and select rivers. The SW Rivers include The Hayes, Nelson, Winisk, and Churchill Rivers. The Other Rivers include the Ferguson, Tha'anne, Thlewiaze, Seal, Povungnituk, and Foucault Rivers. Uncertainty (1 standard deviation) is provided in situations when a sample of values where available. Uncertainty estimates in TA, DIC are DOC are provided in Section 3.4.2.

	S	TA (µmol/kg)	DIC (µmol/kg)	DIC_{Sat}[+] (µmol/kg)	DOC (mg/L)
Marine	31.3	2244±103	2130±98	2147	1.1±0.1
SIM[++]	6	415±35	330±30	442	-
SW Rivers	0	1437±369	1433±348	1449	11.8±0.9
Other Rivers	0	239±299	299±240	270	4.0±1.3
Nelson	0	1858	1851	1857	11.3
Winnisk	0	1173	1180	1191	12.9
Focault	0	138	200	170	-
LaGrande[+++]	0	46	116.3	78	-

[+] DIC_{Sat} was calculated using values of TA and seawater pCO_2 at equilibrium with the atmosphere at 0ºC.
[++] SIM from Lansard et al. (2012), Miller et al. (2011) and Rysgaard et al. (2007)
[+++] Data for the LaGrande River from Rosa et al. (2012). All other values are from the BaySys 2018 summer cruise.

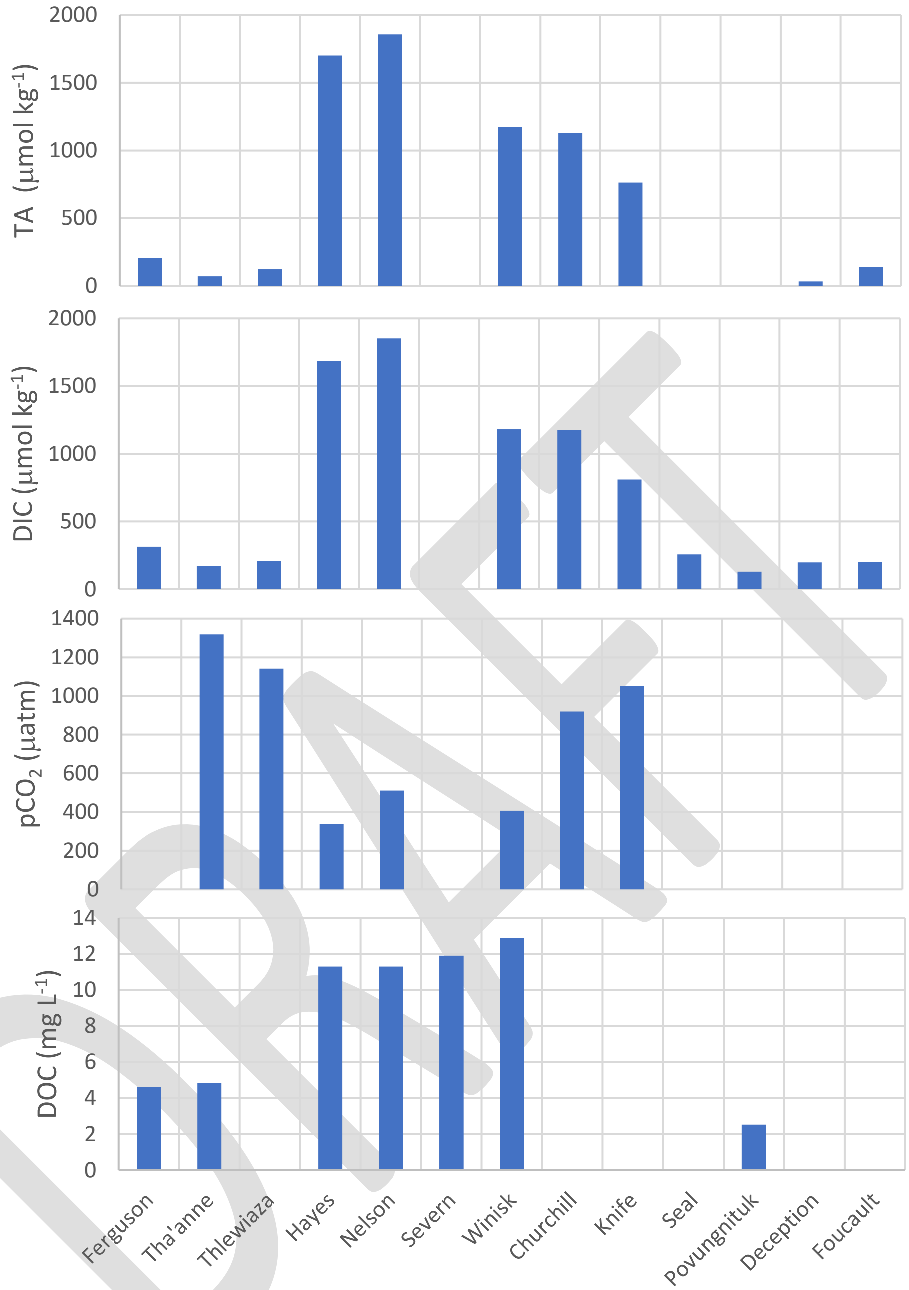

FIGURE 3.4.14. DIC, TA, pCO_2, and DOC at the mouth of rivers sampled during the 2018 BaySys cruise. pCO_2 was calculated using carbonate equilibria expressions within CO_2SYS (Peirrot and Wallace, 2006).

The annual discharge for 35 rivers entering Hudson and James Bay is provided by Déry et al. (2005). Concentration data are available for a subset of these rivers from the 2018 BaySys summer cruise, including the Nelson, Churchill, Hayes, Winisk, Thlewiaza, Tha-anne, and Ferguson Rivers). Concentration data for the Great Whale, La Grande Pontax, Rupert, Broadback, and Harricana Rivers are available from Rosa et al. (2012), that together with discharge allowed the calculation of river loads of DIC, TA, and DOC. We estimated the loads for the remaining rivers listed in Déry et al. (2005) depending on if they drained the Hudson

Plains or Precambrian Shield, using concentration data from categories ‘SW Rivers’ and ‘Other Rivers’ listed in Table 3.4.1. The resulting river loads for the carbon variables DIC, TA, and DOC are shown in Figure 3.4.15. The input of DIC and TA into the upper 20 m of the water column by SIM was also calculated for the coastal conduit using the concentration estimates from Table 3.4.1, estimates of sea ice melt for Hudson Bay (i.e., 1200 km^3 from Prinsenberg, 1988; Granskog et al., 2011), and scaled for the area of the coastal conduit (579,000 km^2), the latter provided by Capelle et al. (2020a).

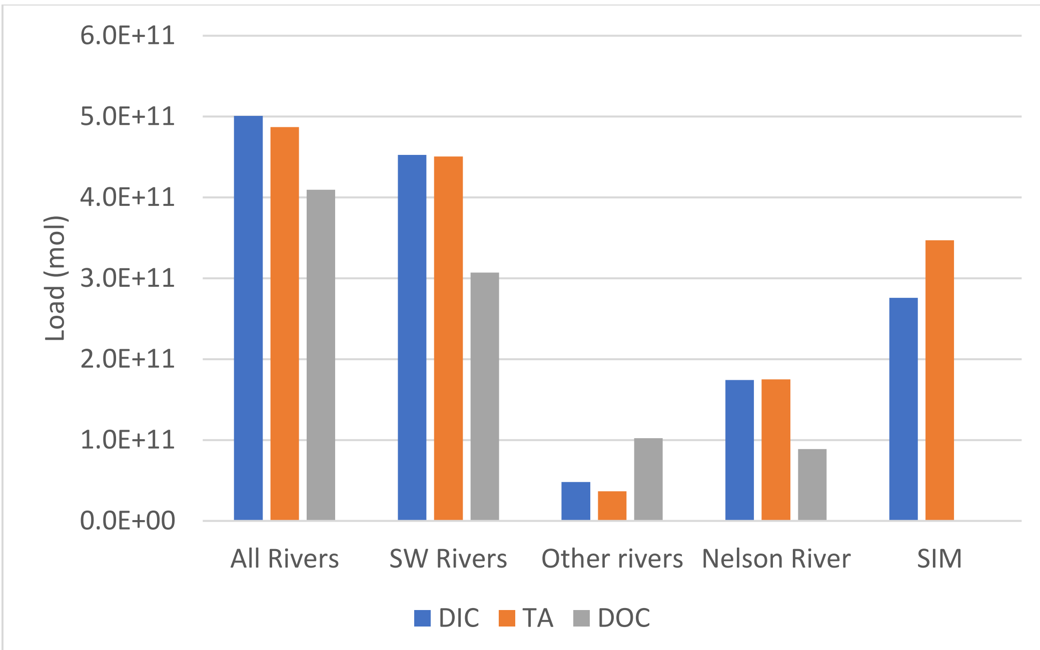

FIGURE 3.4.15 Annual load (moles) of DIC, TA, and DOC for rivers entering Hudson and James Bay. Included is the seasonal injection of DIC and TA associated with sea ice melt (SIM) within the coastal conduit; note that the SIM contribution does not represent a net annual change, as that same material was initially incorporated into the ice from the waters of Hudson Bay. The category ‘All Rivers’ includes 35 rivers with outlets in Hudson Bay and James Bay (see Table 1 in Déry et al., 2005). SW Rivers includes those rivers listed in Déry et al. (2005) that drain the Hudson Plains (ie., the Nelson, Moose, Nottawy, Albany, Rupert, Severn, Churchill, Hayes, Winisk, Attawapiskat, Harricana, Thlewiaza, Tha-anne, Ekwan, and Ferguson Rivers). The ‘Other Rivers’ include those in the ‘All Rivers’ category not classified as ‘SW Rivers’.

Over the annual cycle, rivers deliver approximately $5.0x10^{11}$ moles (6.0 TgC) of DIC, $4.9x10^{11}$ moles of TA, and $4.1x10^{11}$ moles (4.9 TgC) of DOC to Hudson Bay, with over 90% of the DIC and TA delivery, and ~ 75% of the DOC delivery attributed to rivers from southwest Hudson Bay (including James Bay rivers draining the Hudson Plains). Pre-BaySys estimates for DOC load are between 3.6 and 5.5 TgC/yr (Kuzyk et al., 2009; Mundy et al., 2010; Capelle et al., 2020), with another 0.46 Tg/yr received as POC. Our annual DIC load estimate is higher than other major rivers draining Arctic watersheds (Ob’, Lena, Kolyma, and Yukon), but smaller than estimates for the Yenisey and MacKenzie Rivers (Tank et al., 2012). Our data from BaySys indicate that an earlier estimate of the riverine DIC delivery to Hudson Bay (Tank et al., 2012) overestimated the flux by ~38%.

We estimate there were approximately $2.5x10^{13}$ moles DIC, $2.6x10^{13}$ moles TA, and $1.0x10^{12}$ moles of DOC in the surface 20 m of the coastal conduit at the time of the 2018 BaySys cruise (Table 3.4.1). Thus, the rivers entering Hudson Bay contribute each year the equivalent of only ~ 2% of the store of both TA and DIC in surface waters of the coastal conduit, but 39% of the marine store of DOC. The rivers from southwest Hudson Bay are well stocked in the carbon species, and on its own, the Nelson River supplies about 1% of the DIC and TA in the upper 20 m of the coastal conduit, but 8% of the DOC store. For comparison, SIM represents ~1% of the summertime Hudson Bay coastal surface water store of DIC and TA. The proportional contributions listed assume distribution across the surface waters of the coastal conduit, but the cyclonic circulation of the bay concentrates both meteoric water and sea ice melt in the south and east of the bay, which following the discussion surrounding Figures 3.4.4 and 3.4.7, can lead to pronounced impacts on both pCO_2 and aragonite saturation state.

3.4.4.5 Impact of rivers on the carbon system of Hudson Bay

The impact of mixing seawater various freshwaters (different rivers and sea ice melt) on the air-sea difference in pCO_2 and DIC uptake potential (ΔDIC) was explored following the approach outlined by Meire et al. (2015). The rivers were selected to contrast the impact on the marine inorganic carbon system from rivers draining the Hudson Plains (Nelson and Winisk) and Precambrian Shield (Foucault, and LaGrande). In Figure 3.4.16, $\Delta pCO_{2mix\text{-}sat}$ is the difference in pCO_2 for mixed seawater and pCO_2 at saturation (i.e., $\Delta pCO_{2mix\text{-}sat}=pCO_{2mix}-pCO_{2sat}$, where pCO_{2sat}=408 μatm). The term ΔDIC in Figure 3.4.17 is the difference between DIC when pCO_2 in the water is at equilibrium with the atmosphere (i.e., DIC_{sat}), and the DIC corresponding to the freshwater-marine mixture (DIC_{mix}), and it can be interpreted as the capacity to carry DIC (μmol/kg) in excess of mixed values (i.e., $\Delta DIC=DIC_{Sat}-DIC_{Mix}$). It represents the potential of the seawater to absorb more inorganic carbon from the atmosphere or retain inorganic carbon released by respiration. Both variables were obtained by inputting salinity, TA, and DIC for mixed water mass fractions across a salinity range of 0 (i.e., 100% freshwater source) to 31.3 (100% surface waters of Hudson Bay) using Eq (2), endmembers provided in Table 3.4.1, and CO_2SYS (Pierrot & Wallace, 2006) for the calculation of pCO_{2mix}, $DIC_{mix,}$ and DIC_{Sat}, while assuming the river, sea ice melt and marine end-members to be in equilibrium with the atmosphere (i.e., pCO_2 of 408 μatm). Water temperature was held constant at 0^{o}C.

The results shown in Figures 3.4.16 and 3.4.17 support the concept that mixing of two water masses at pCO_2 saturation with the atmosphere need not result in the mixed water being saturated (Meire et al. 2015). A consistent pattern emerges wherein mixed waters have a greater potential to draw down atmospheric CO_2 and hold more DIC than either pure river waters or seawater, however, the impact on mixing depends strongly on the freshwater source and salinity. Both rivers coming off the Precambrian Shield (Focault and La Grande Rivers) lead to large negative ΔpCO_2 on mixing with marine water, with ΔpCO_2 reaching -210 μatm around a salinity of ~9 (Figure 3.4.16), and maximum DIC uptake potential occurring at a salinity of approximately 16 (Figure 3.4.17). On mixing SIM also drives drive large negative ΔpCO_2 (peak ΔpCO_2 ~-145 μatm) and high ΔDIC (peak DDIC~ 25 μmol/kg), but has less of an impact relative to the rivers draining the Precambrian Shield. Mixing the southwestern rivers (Nelson and Winisk Rivers) with seawater drives modest pCO_2 undersaturation with minimum ΔpCO_2

approaching -35 μatm and -80 μatm when salinity is approximately 12, respectively for the Nelson and Winisk Rivers. Meteoric water fractions are between 0.5 and 0.7 for salinity between 9 and 15 based on the application of Eq (2) and salinity endmembers from Table 3.4.1. Peak ΔDIC for the southwest rivers is ~ 8 μmol/kg and 16 μmol/kg for the Nelson and Winisk Rivers. Thus, at its peak, the level of pCO_2 undersaturation induced by mixing can be over 5 times higher for the rivers draining the Precambrian Shield than expected for rivers draining the Hudson Plains. As noted above, the rivers from southwestern Hudson Bay (i.e., the Winisk and Nelson Rivers) have high concentrations of TA, and TA:DIC ratios close to 1, and consequently they have less impact on ΔpCO_2 and ΔDIC on mixing with seawater than the rivers draining the Precambrian Shield or SIM.

Results for the Great Whale River, the 13th largest river entering Hudson Bay (not shown), were virtually identical to the results provided for the La Grande River using concentration data from Rosa et al. (2012). This strongly suggests that rivers draining into Hudson Bay from the Precambrian Shield dilute alkalinity and DIC to a greater extent than even sea ice melt, leading to the potential for highly negative ΔpCO_2 and excess DIC uptake and retention in the marine environment.

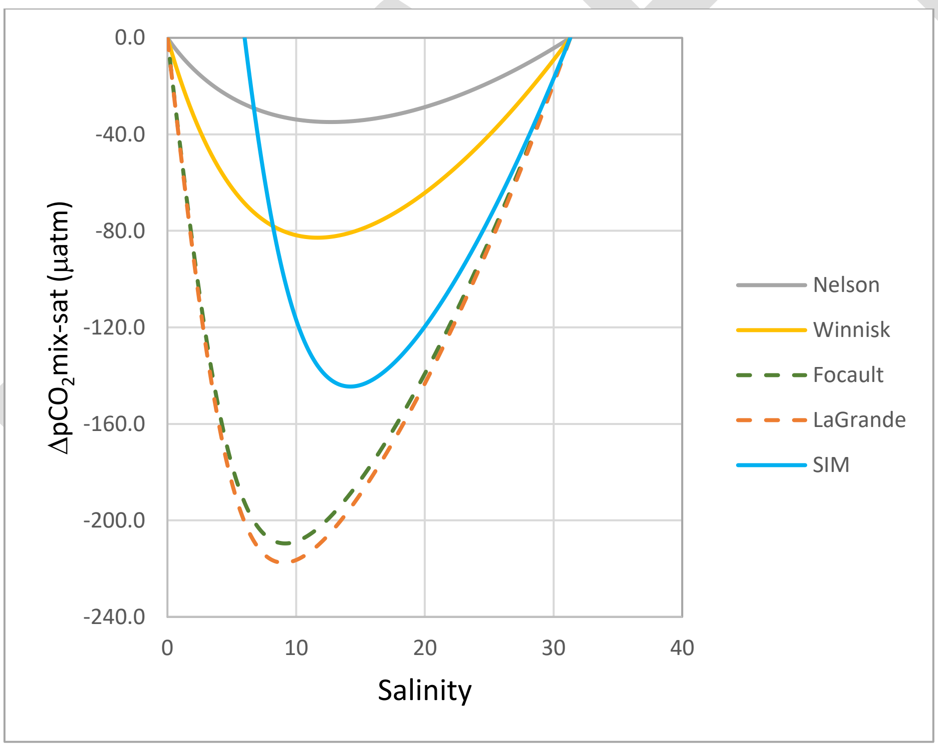

FIGURE 3.4.16 Resulting ΔpCO_2 shown along a salinity mixing gradient for select rivers and sea ice melt (SIM) at 0°C and assuming endmembers to be at equilibrium at atmospheric concentration of 408 μatm. Dashed lines represent rivers draining the Precambrian Shield.

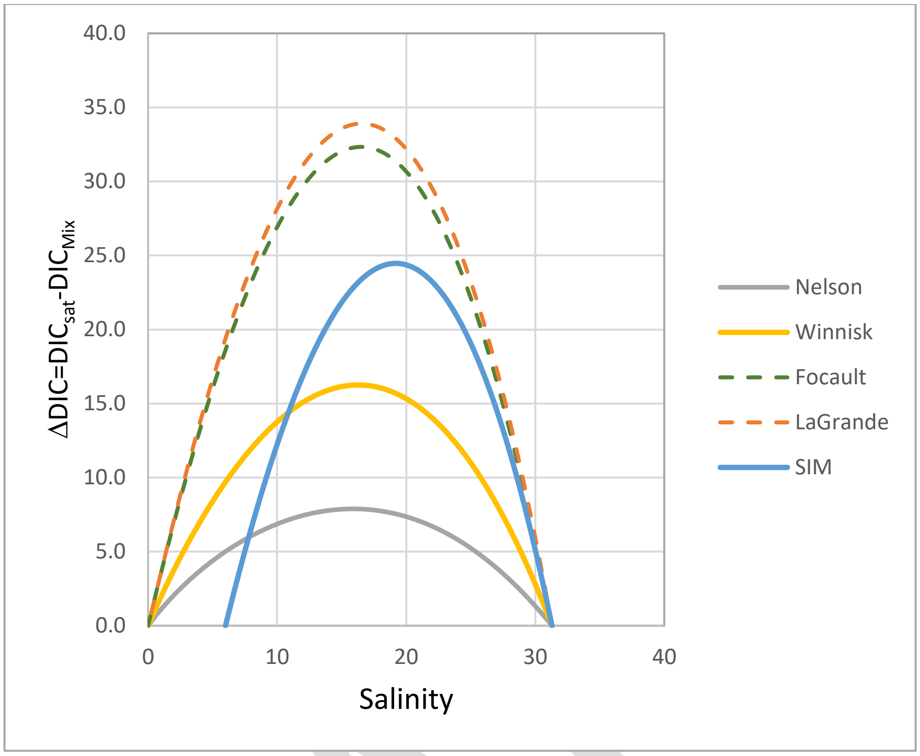

FIGURE 3.4.17 Same as for Figure 3.4.16, except showing ΔDIC shown along the salinity mixing gradient.

The discussion thus far has focussed on the impact of riverine inorganic carbon on the marine system. Organic carbon data for Hudson Bay, and thus information on the role of organic carbon on the bay's carbon cycle remains relatively scarce. Recall from the discussion surrounding Figure 3.4.1 that the mineralization of OC contributes to the seawater stock of inorganic carbon, including pCO_2. A previously constructed organic carbon budget based mostly on river and sediment core data indicates that about 65% of the terrestrial particulate organic carbon (POC_{terr}) that enters the system is remineralized in the water column, and as much as another 15% is remineralized in surface sediments (Kuzyk et al., 2009). According to the same work, an estimated 93% of the marine particulate organic carbon exported below the euphotic zone is remineralized in deep waters, and an additional 3% is remineralized in surface sediments. However, little information existed before BaySys about the extent of remineralization of DOC, and in particular terrigenous DOC. The BaySys project provided new information on when, where, and to what extent terrigenous DOC is remineralized, as well as new sedimentary organic carbon data that confirms previous findings of the low extent of carbon sequestration in Hudson Bay sediments.

Using 42-day bottle incubations, Kazmiruk et al. (2021) examined the biodegradability of DOC during the late winter (pre-freshet) in riverine and coastal waters of Hudson Bay. The proportion of DOC that was biodegradable (%BDOC) was observed to vary for different rivers and coastal waters (Figure 3.4.18). In the figure, the lability of BDOC describes how fast the degradation of DOC occurs: BDOC degraded within 3 days was defined as labile (L-BDOC) and the BDOC degraded from day 3 to day 45 was defined as semi-labile (SL-BDOC). Considering the prevailing view that terrigenous organic matter delivered by Arctic rivers is largely refractory because of extensive degradation on land, the riverine DOC was found to be surprisingly biodegradable, especially in the southwestern rivers (Nelson and Hayes). The incubations showed that 24-60% of the DOC in the rivers and on average 21% of the DOC in the immediate coastal waters was biodegradable. Approximately one-half of the BDOC in southwestern Hudson Bay (SWHB) coastal waters and about three-quarters of the BDOC in southeastern Hudson Bay (SEHB) coastal waters was defined as L-BDOC. The BDOC in the Nelson River was dominated by labile BDOC, whereas the Hayes River water and the SWHB coastal water had even contributions of labile and semi-labile BDOC. Interestingly, the Great Whale River BDOC was mostly semi-labile, but the BDOC in the SEHB coastal waters was dominated by the labile fraction, implying that much of the DOC in the coastal waters was not derived from the Great Whale River. Differences in biodegradability seem to be dependent on the properties of the water (seawater and rivers), including characteristics of watersheds and physical and biochemical processes in aquatic environments. A sampling of a greater number of rivers is required to better understand the reasons for the differences, and the possible role of regulation.

The Nelson River had high DOC concentrations relative to other rivers, both pre-freshet (Figure 3.4.19; Kazmiruk et al., 2021) and post-freshet (Figure 3.4.14), and the DOC associated with the river appears highly degradable. The 60% BDOC of the Nelson River is exceptional (Figure 3.4.18) and Kazmiruk et al. (2021) speculate that a steady DOC supply from the river’s lower reaches, associated with reservoirs in peatland systems with extensive permafrost, contributes to the observed high biodegradability of Nelson River DOC. Permafrost DOC can be rapidly biodegraded once in the river network (Drake et al., 2015; Mann et al., 2015; Spencer et al., 2015; Ward & Cory, 2015; Muller et al., 2018). The production, store, and transport of aquatic DOC that arises through biological production in the shallow reservoirs on the lower Nelson may also contribute to the biodegradability of water within the Nelson Estuary. However, while the POC in the lower reaches of the Nelson River appears sourced primarily from the local material (i.e., soils introduced by riverbank erosion and suspended sediments and resuspension of riverbed sediment; Stainton, 2018), we don’t know with any confidence the source of the DOC delivered to the bay in the river water. It may be expected that DOC sources and composition vary seasonally, but such variability remains unassessed, as our samples are only from late winter.

Bench top experiments conducted during BaySys showed that oxidative photodegradation processes are important in degrading dissolved organic material (DOM) in river water and Hudson Bay surface waters (Islam, 2021). Soil leachates, algal leachates, and samples of river water and bay surface waters were all photoreactive. Among the river and marine samples, only 4% (± 5 %) of the DOM was found to be resistant to photodegradation, which is much lower than the proportion of resistant DOM found at lower latitudes (Islam, 2021). Despite comparable CDOM loss, significant differences in decay rates and molecular composition were found between the river and coastal DOM, and photodegradation appeared to be strongly governed by the initial CDOM concentration in the waters. Microbial degradation was also studied in rivers, estuaries, and bay waters. Photochemical processes had a greater influence on the CDOM absorbance and fluorescence than microbial degradation in all samples, but when considering the molecular composition of DOM (based on FT-ICR-MS analysis), microbial processes had a greater impact on DOM originating from riverine and estuary sources, and photochemical processes dominated only for bay waters.

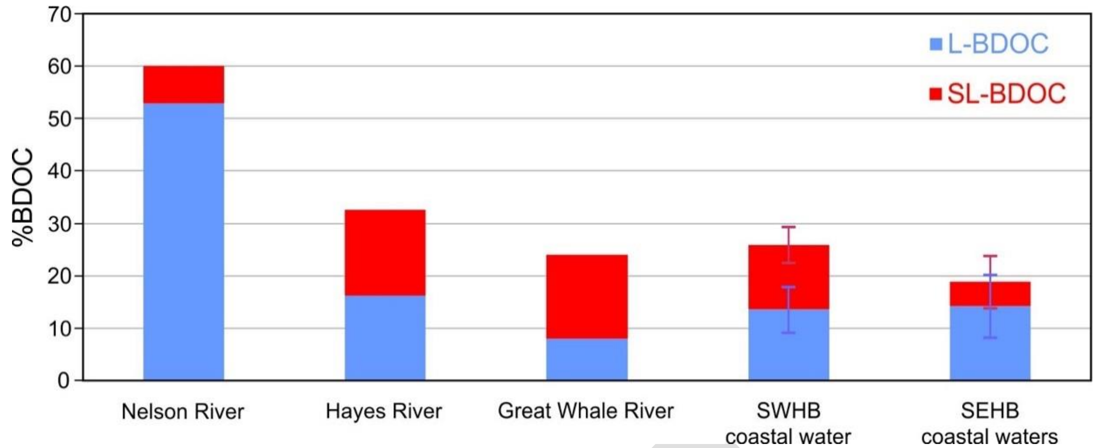

FIGURE 3.4.18 Biodegradable fraction of total DOC (%BDOC) and relative proportions of labile (L-BDOC) and semi-labile (SL-BDOC) BDOC for river samples (N=1), in addition to coastal waters from the southwest (SWHB; N=9) and southeast (SEHB; N=15) Hudson Bay. Error bars in the coastal samples representing one standard error in measurement surrounding mean values. Source: Kazmiruk et al. (2021).

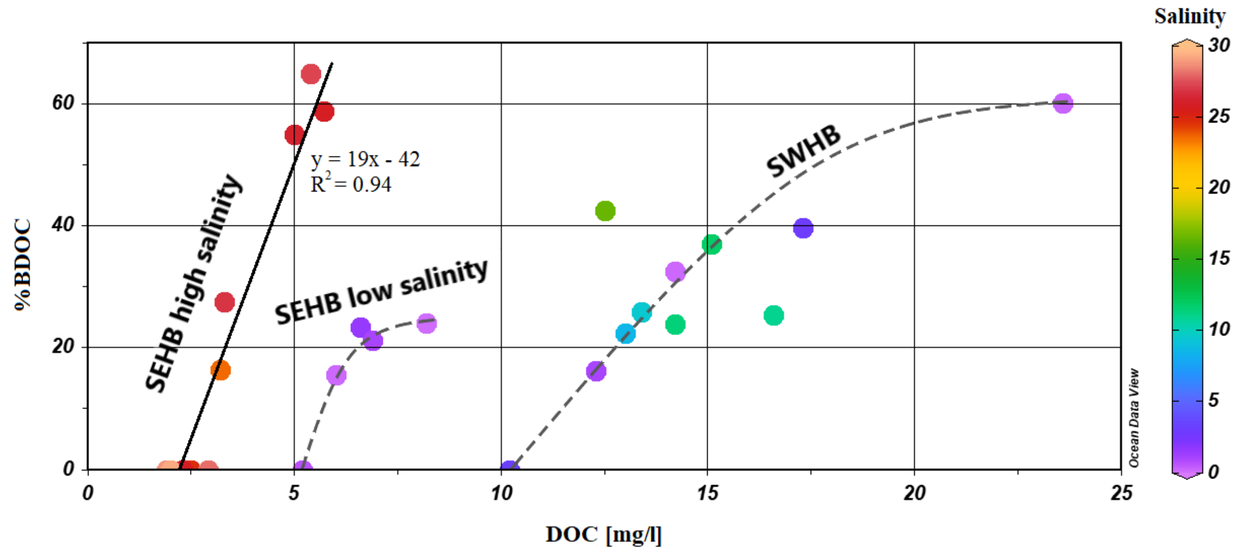

FIGURE 3.4.19 Relationship between %BDOC and initial DOC concentration with salinity displayed using colour shading (scale at right). The black solid line represents a significant linear trend for the SEHB high salinity samples, while the grey dashed lines represent estimated exponential trends for the SEHB low salinity and SWHB samples. Source: Kazmiruk et al. (2021).

Based on pre-BaySys and new sedimentary carbon data, Capelle et al. (2020) constructed a box model of coupled organic-inorganic carbon cycling in Hudson Bay to examine the influence of organic carbon of terrestrial origin on both pCO_2 and Ω_{Ar}. They observed that over the annual cycle the mineralization of DOC_{Terr} was the main driver of pCO_2 accumulation and Ω_{ar} undersaturation in coastal surface waters (Figure 3.4.20). By comparison, the mineralization of POC_{Terr} had a relatively small impact, because the river POC_{Terr} load was much smaller than DOC_{Terr}. Below the surface layer and in the bay's interior the remineralization of DOC of marine origin increases the amount of pCO_2 that contributes to the undersaturation of Ω_{Ar}. It is evident from Figure 3.4.20 that little organic carbon of terrestrial origin is available for mineralization beneath the mixed layer, consistent with the observations of Kazmiruk et al. (2021) that OC_{terr} is rapidly and effectively degraded in the surface layer.

An important finding of Capelle et al. (2020) was that new and regenerated production (see the text surrounding Figure 3.4.1 in Section 3.4.1) is effective at offsetting the accumulation of CO_2 and aragonite under-saturation in nearshore surface waters, and the mineralization of terrestrial organic material is more effective at fueling production than the mineralization of marine organic material given a greater proportion of nitrogen relative to carbon (i.e., a smaller C:N ratio) in the terrestrial organic material. The implications are that an increase in the delivery of terrestrial organic carbon may not appreciably increase susceptibility to CO_2 accumulation (and outgassing) and aragonite under-saturations when light is seasonally sufficient to drive biological production. In deeper waters, the model revealed that the dissolution of particulate inorganic carbon (as $CaCO_3$) offsets the impact of respiration, partially mitigating aragonite under-saturation, with this effect being more pronounced in offshore deep waters. Such detrital carbonate is supplied primarily by Hudson Plains rivers entering southwestern Hudson Bay, like the Nelson.

Capelle et al. (2020) concluded that both the pCO_2 and Ω_{Ar} in the surface layer in the coastal corridor are significantly influenced by the river inflow of terrestrial carbon and that the process is complicated by the amount, quality, and timing of the organic material inflow. Inorganic carbon provided by rivers and sea ice melt in the form of DIC and TA was not explicitly considered in their work but, as revealed by BaySys analyses presented in Figures 3.4.16 and 3.4.17, could be important counter-agents to the build-up of CO_2 in response to the degradation of DOC. The observations of high pCO_2 in areas of Hudson Bay's coastal conduit (Ahmed et al., 2021; Else et al., 2008a, 2008b) suggest that the impact of remineralization of terrigenous DOC on pCO_2 appears to outweigh the impact of dilution (on TA and DIC) away from the river estuary. The net impact of river carbon on pCO_2, and by extension on air-sea CO_2 exchange, however, will depend on the amount and speciation of inorganic carbon (i.e., concentrations of TA and DIC), and the amount and quality of OC, and where the bulk of the OC is degraded. Numerical modelling is well suited to address multivariate complex process interactions such as those associated with the bay's carbon cycle. We review the bay's CO_2 source/sink status in the following section, and the results of a numerical model are discussed in Section 3.4.4.7.

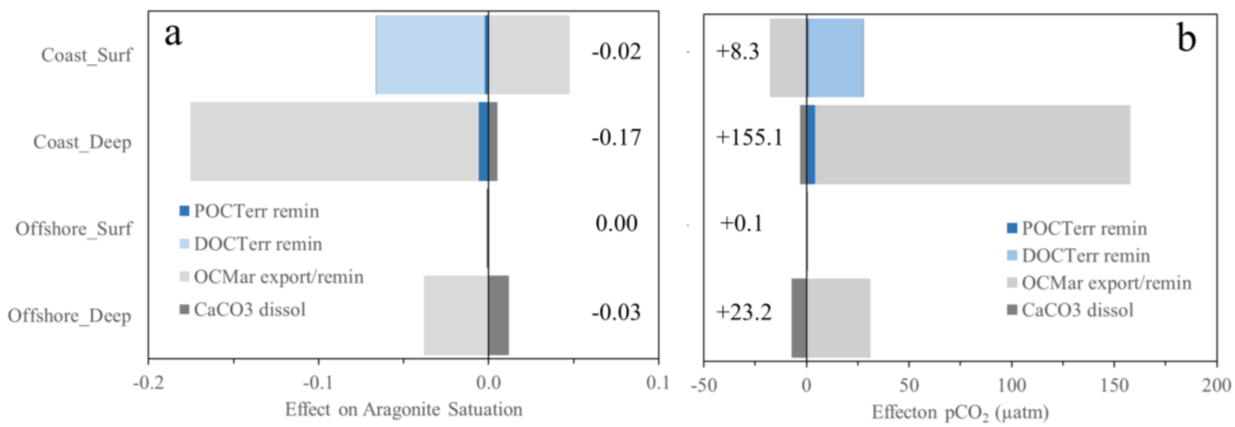

FIGURE 3.4.20 Independent effects on Ω_{Ar} (panel a) and pCO_2 (panel b) of carbon cycle processes occurring within each model compartment on an annual basis (Capelle et al., 2020). Processes include remineralization of POC_{terr} and DOC_{terr}; production and/or remineralization of OC_{mar}; and PIC dissolution. Bar lengths represent the effect of each process on Ω_{Ar} and pCO_2. Processes that reduce Ω_{Ar} or pCO_2 are stacked on the left side of the y-axis, and processes that increase them are on the right. The net impact of C-transformations is indicated by the text label next to each bar.

3.4.4.6 Contemporary CO_2 Source/Sink Status of Hudson Bay

Ahmed et al. (2021), and before them Else et al. (2008a, 2008b), suggested the mineralization of organic carbon as an important process for promoting high surface pCO_2 in river estuaries and coastal zones of Hudson Bay. It has been difficult to assess the relative importance of organic carbon remineralization versus other processes, including primary production, at the bay-wide scale, in part because of the late timing (August – October) of previous cruises, which is well after the peak productive season in Hudson Bay. During the BaySys cruise an area-weighted average of pCO_2 measurements across Hudson Bay was 317 ± 61 µatm, which was lower than the average of atmospheric pCO_2 (408 ± 2.8 µatm), indicating that overall, Hudson Bay was undersaturated in pCO_2 relative to the atmosphere. It may be inferred that the bay was acting as a carbon sink (Ahmed et al., 2021). The distribution of the sea-to-air CO_2 flux (Figure 3.4.21) shows pronounced spatial variation associated with both variation in pCO_2 (Figure 3.4.5), and wind speed. Over the 5-week cruise CO_2 uptake (Equation 3) averaged ~ -5.1 ± 9.3 mmol $m^{-2}day^{-1}$ (negative signifying uptake into the ocean; Ahmed et al., 2021). The uncertainty in the flux estimation was assessed at ~38%.

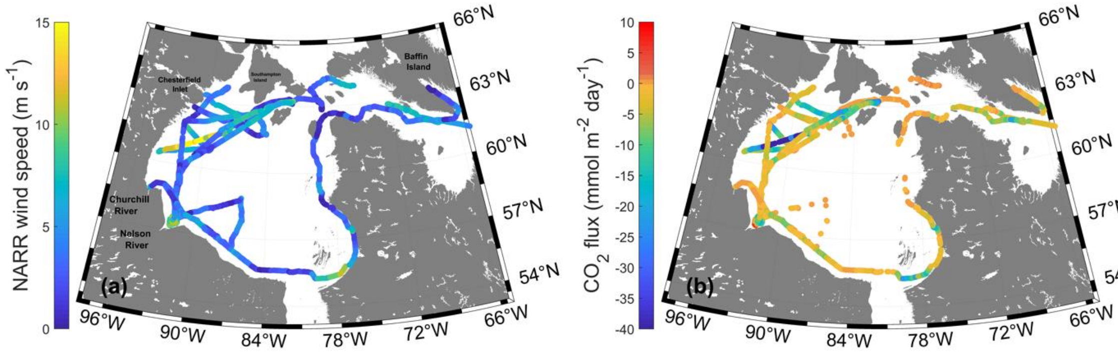

FIGURE 3.4.18 Spatial variability of sea-air CO_2 fluxes in Hudson Bay. Spatial variability of (a) wind speed, and (b) sea-air CO_2 fluxes based on wind data along the ship track from May 25 to July 13, 2021 (Ahmed et al., 2020).

Ahmed et al. (2021) extended the 5-week carbon exchange budget from May into July, assuming an average ice-free sink of -5 mmol CO_2 m^{-2} day^{-1} and scaling the flux using sea ice data from the Canadian Ice Service (https://iceweb1.cis.ec.gc.ca/Archive/page1.xhtml?lang=en) between May and July 2018, and assuming an area of 807,000 km^{-2}. The resulting open water areal-averaged CO_2 flux totals were -0.3, -1.1, and -1.9 Tg C in respectively May, June, and July, for a total of -3.3 ($\pm$ 1.2) TgC for the spring to early summer**.** Ahmed et al. (2021), following Else et al. (2008b), then exploited the dependency of pCO_2 on temperature to calculate open-water fluxes for August, September, and October using satellite-derived average seawater temperature from Level-3 MODIS Aqua, and monthly average wind speed from modelled North American Regional Reanalysis (NARR) product (https://www.ncdc.noaa.gov/data-access/model-data/model-datasets/north-american-regional-reanalysis-narr). The estimated CO_2 exchange budget during the 2018 months of August, September, and October were −0.6 Tg C, −1.2 Tg C, and −2.2 Tg C. The resulting total open-water CO_2 flux for 2018 (May to October) was -7.2 Tg C, which is ~5% of the annual net CO_2 flux recently estimated for the entire Arctic (Manizza et al., 2019). The annual uptake for Hudson Bay will be smaller than the open water total because of extensive remineralization of terrigenous DOC in the winter season, and a lack of primary production during those winter months (Capelle et al., 2020). Nonetheless Hudson Bay appears a low to moderate CO_2 sink relative to other Arctic shelf regions (Table 3.4.2).

TABLE 3.4.2 Comparison of sea-air CO_2 fluxes in this study with fluxes in other Arctic Shelves. Areas, depths, river inflow, and sea-air CO_2 flux are provided for several Arctic continental shelves[a] (Ahmed et al., 2021).

Shelf sea	Area (10^3 km^2)	Mean depth (m)	River inflow (Km^3 yr^{-1})	Sea-air CO_2 flux (mmol m^{-2} day^{-1})	Season	Reference
Barents Sea	1512	200	463	−11.1	Annual	Lauvset et al. (2013)
Kara Sea	926	131	1133	−18.3 to −32.8	Summer-Fall	Pipko et al. (2017)
Laptev Sea	498	48	767	−0.8 to −15.7	Summer-Fall	Pipko et al. (2017)
E. Siberian Sea	987	58	213	0.8 to 11.5	Summer	Pipko et al. (2011)
Chukchi Sea	620	80	78	−14.8	Annual	Bates (2006)
Beaufort Sea	178	124	330	−10.0	Summer	Murata and Takizawa (2003)
Canadian Archipelago	1490	290	270	−3.0	Annual	Ahmed and Else (2019)
Hudson Bay	841	150	900	−0.73 1.98	Fall Summer-Fall	Else et al. (2008a) Else et al. (2008b)
Hudson Bay & Hudson Strait	1041	150	900	−4.8 −4.3	Spring-early Summer Open water	Ahmed et al (2021)

[a]Negative annual CO_2 fluxes indicate oceanic sink.

A possible fate of carbon associated with the atmospheric CO_2 uptake totals listed in Table 3.4.2 is photosynthetic conversion to organic matter and eventual burial in the sediments. The BaySys data on Hudson Bay's sedimentary carbon sink include newly collected and analyzed sediment cores, which provide coverage for the first time in the northwest and southwest Hudson Bay. Particle size analysis revealed a wide range of particle sizes with coarse-grained sediments more common in western Hudson Bay than offshore or in eastern areas. All of the cores in northwest Hudson Bay and near Southampton Island were sand- rather than silt-dominated (Figure 3.4.22). The percentage of organic carbon (%OC) in the surface slices of the cores ranged from 0.071% to 1.111%, which is below average compared to previously collected cores from Hudson Bay (Huyghe in preparation). Inventories of excess ^{210}Pb and ^{137}Cs also were low in the sediments from the western part of the bay (Figure 3.4.23). The calculated sedimentation rates ranged from 0.05 to 0.14 cm/yr (Huyghe in preparation). All in all, the conclusion from the sediment core analyses is that western Hudson Bay has scarce modern sediment deposition. Most of the seabed consists of a coarse lag deposit, as expected for an energetic region in which bottom currents remove deposited fines. Sand-sized material may be added by ice rafting and/or energetic processes like turbidity currents, but low amounts of radioisotope tracers are incorporated through these processes. Based on the lack of ^{137}Cs, which sorbs strongly to clays in terrestrial environments, it may be inferred that minimal sediment accumulating on the seafloor in northwest Hudson Bay is sourced from watersheds.

A review of a seismic data set including observations from the 1970s and recent imagery from 2003-2018, supports the conclusion of scarce modern sediment deposition in western Hudson Bay and offshore (Huyghe in preparation). Surficial sediment deposits, which include areas of active sedimentation, as well as previous postglacial deposits that are acoustically indistinguishable, are scarcely seen in seismic profiles for offshore and western Hudson Bay (Figure 3.4.24). Sediment deposits typically occur below 50 m water depth, with the majority of the deposits between 50 and 85 m. Most of the detected deposits occur in eastern Hudson Bay and deposits are abundant in a north-south trending band off the east coast. Some sediment deposits were found in seismic profiles in northwest Hudson Bay but mostly as isolated spots or small clusters. One cluster of deposits occurred south of Roes Welcome Sound and two others at locations further south along the northwest coast. Smaller localized deposits occurred in the south and central Hudson Bay. Deposits near the western and eastern coasts are located near the bottom of slopes and near mapped geological contacts. There is also regional variation in the appearance of the sediment deposits. Northwestern Hudson Bay is characterized by a rough, uneven seabed with sediment deposits in localized depressions within larger troughs. Southern Hudson Bay is characterized by a fairly smooth bottom with sediment deposits in shallow localized depressions. In both these areas, the deposits resemble a thin drape. Eastern Hudson Bay is characterized by large, deep sediment deposits (Figure 3.4.24). This new data supports the prevailing view that the area of active sedimentation (and thus organic carbon accumulation) is small in Hudson Bay, perhaps only 15% of the total seafloor area, as previously estimated (Kuzyk et al., 2009).

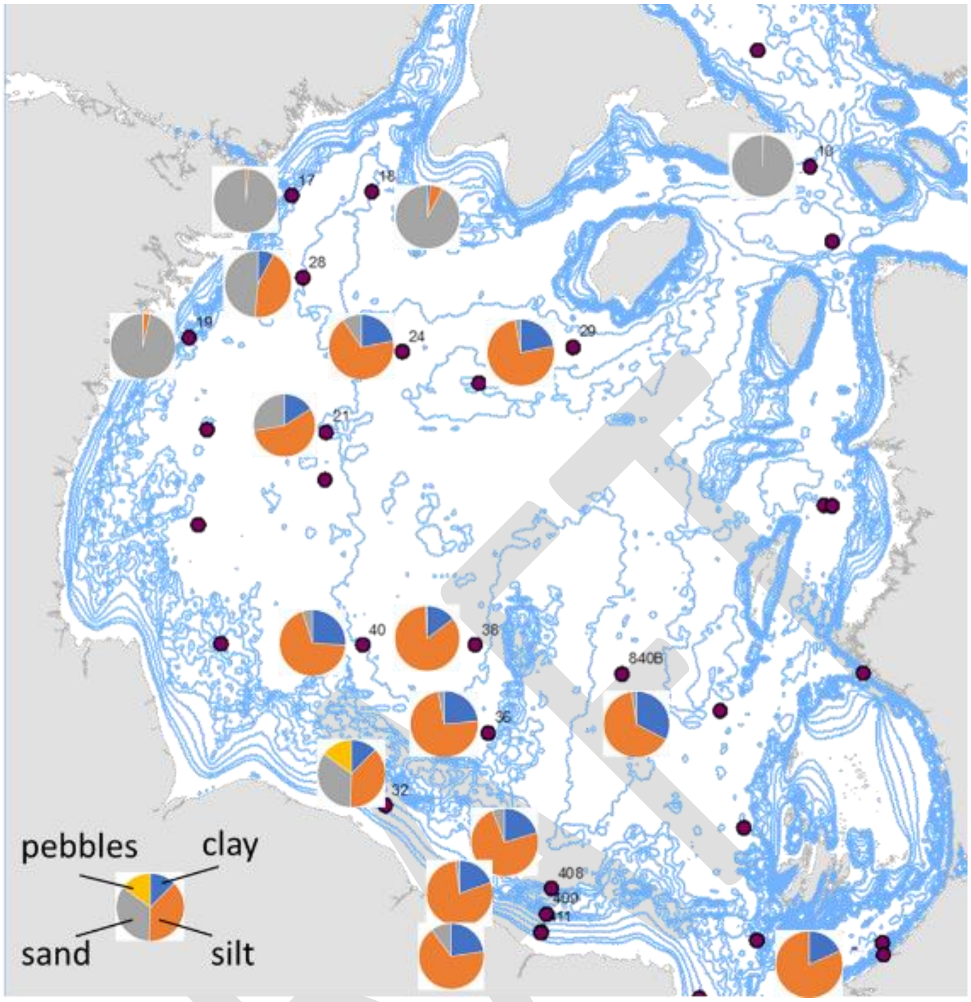

FIGURE 3.4.22 Fractions of pebble, sand, silt, and clay-sized materials in surface sediments (Huyghe, in preparation).

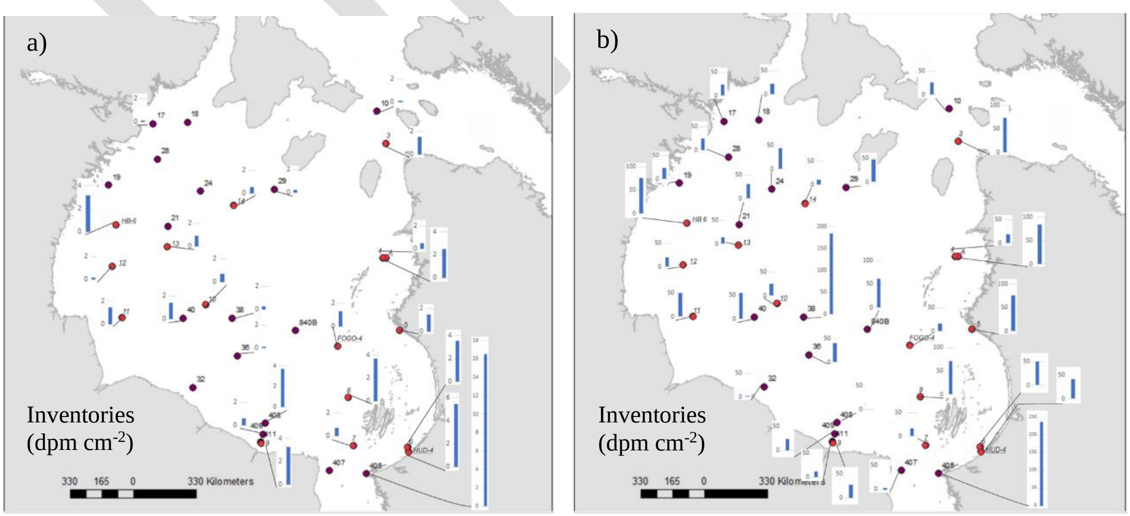

FIGURE 3.4.23 ^{137}Cs (a) and ^{210}Pb (b) inventories in the cores (Huyghe, in preparation).

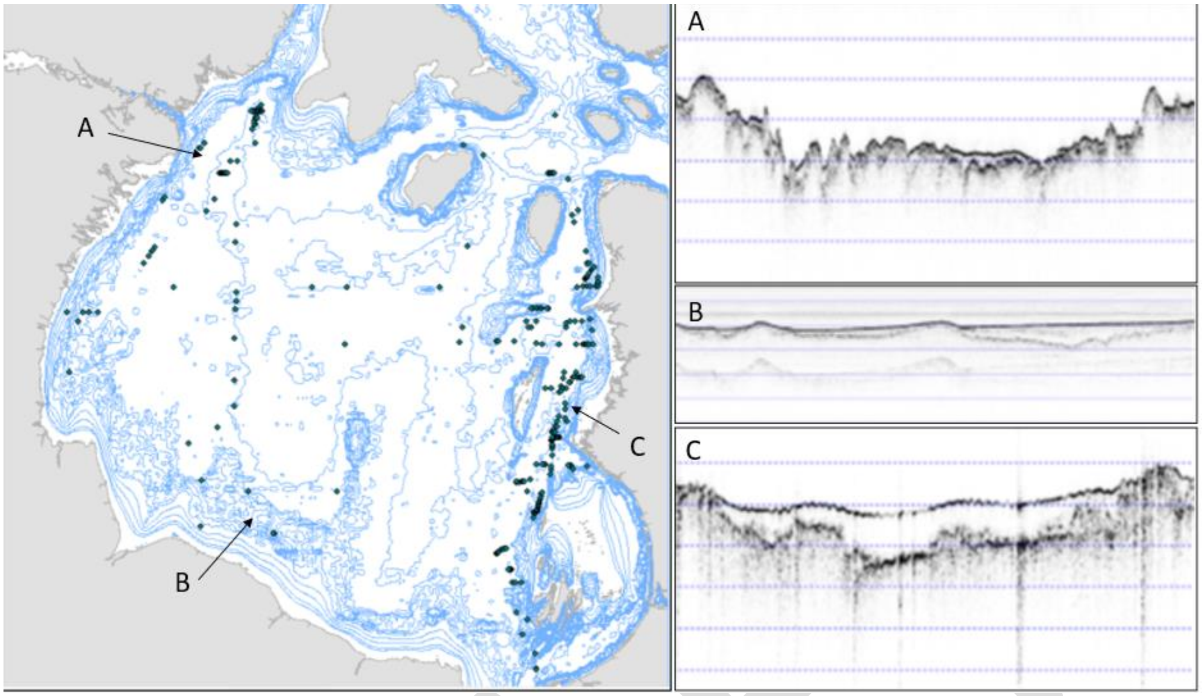

FIGURE 3.4.24 Locations of surficial sediment deposits is Hudson Bay as identified from seismic profiles and examples of typical profiles for deposits in northwest Hudson Bay (A), southwest Hudson Bay (B), and eastern Hudson Bay (C). Isobaths (in blue) are provided in the left-hand side map (Huyghe, in preparation).

3.4.4.7 Contemporary and Future Carbon Cycling in Hudson Bay – Biogeochemical Modelling

The implementation of BLING Version 0 + DIC (Galbraith et al., 2010, 2015) is outlined in Section 3.4.2. Variations in temperature and salinity, and their impacts, are included in our analysis given their strong relationship with the carbon system. The synthesis of model results in support of project objectives follows.

<u>Temperature and Salinity:</u> The average seawater temperature and salinity above the mixed layer depth (MLD) in Hudson Bay for the historic (H; 1981 - 2010) and projected periods P1 and P2 (P1 = 2021-2050 and P2=2041-2070) is shown by month in Figures 3.4.25 and 3.4.26, respectively, while the 2020 to 2070 time series of temperature and salinity are shown by season appears in Figures 3.4.27 and 3.4.28. The seasonal and annual averages from the simulations are provided in Table 3.4.3.

The largest change in monthly average water temperature is forecast to occur in the summer months for both naturalized and regulated flow scenarios (Table 3.4.3), while little change in seawater temperature is expected during the winter and early spring (January to May), over H, P1, and P2 (Figure 3.4.25). There appears a large difference in the average seawater temperature between January and December, particularly in the future projections; an observation that perhaps can be attributed to the difference in simulated sea ice cover between months. The future warming rate is projected to be less severe in winter than during the other seasons (Figure 3.4.27). Summer surface seawater temperature is forecasted to be 2.24°C and 2.28°C warmer for naturalized and regulated scenarios, respectively, in mid-century relative to the historical period (Table 3.4.3). Regulation has a small impact on seawater temperature, and over both P1 and P2, the regulation increases surface seawater temperature by less than 0.04°C (Figures 3.4.25 and 3.4.27 and Table 3.4.4).

The seasonal cycle in average seawater salinity is consistent between the simulation scenarios (H to P2), with the highest values between February and April and the lowest in July and August (Figure 3.4.26). Salinity however drops across all months in the future scenarios. Regulation also decreases salinity, with a larger impact in the future than in the historical scenarios (as is also shown in Figure 3.4.28). The greatest decreases in salinity with time are projected for the spring and winter months under the regulated scenarios (Figure 3.4.28, Table 3.4.3). Average springtime salinity is expected to drop by 0.55 g/kg and 0.78 g/kg between H and P2 for naturalized and regulated flow scenarios. Regulation will, according to projections, lead to lower salinity relative to naturalized scenarios in all seasons. Historically, regulation has lowered the salinity of Hudson Bay by 0.15 g/kg, with small variations between seasons (Table 3.4.4). In future scenarios, regulation decreases the surface salinity of the bay by no more than 0.23 g/kg.

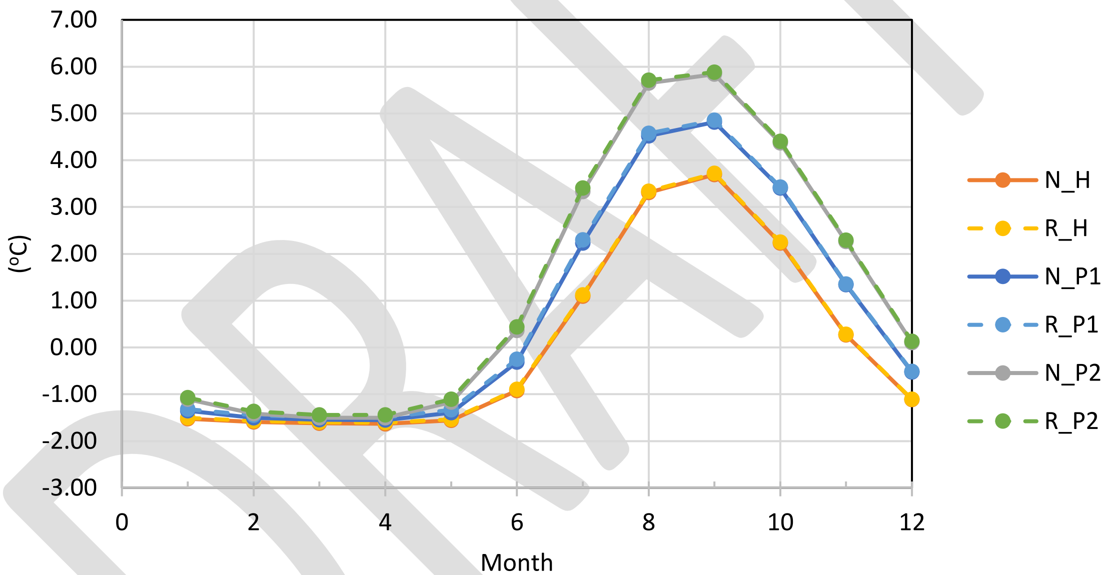

FIGURE 3.4.25 Average seawater temperature above the MLD by month over the historical (H), and projected periods (P1: 2021-2050 and P2: 2041-2070) for naturalized (N) and regulated scenarios for above the MLD.

TABLE 3.4.3 Ensemble-average temperature and salinity by season for naturalized (N) and regulated (R) scenarios for historical (H=1981 to 2019) and projected runs (P1=2021 to 2050 and P2=2041 to 2070). In table W, SP, SU, F, and AN refer to winter (JFM), spring (AMJ), summer (JAS), fall (OND), and annual.

	W	SP	SU	F	AN	W	SP	SU	F	AN
	N	N	N	N	N	R	R	R	R	R
AVERAGE TEMPERATURE (^{O}C)										
H	-1.58	-1.37	2.70	0.46	0.05	-1.56	-1.35	2.72	0.47	0.07
P1	-1.47	-1.09	3.85	1.41	0.68	-1.42	-1.03	3.91	1.42	0.72
P2	-1.34	-0.77	4.94	2.24	1.27	-1.29	-0.70	5.00	2.27	1.32
	CC_1	**CC_1**	**CC_1**	**CC_1**	**CC_1**	**CCR_1**	**CCR_1**	**CCR_1**	**CCR_1**	**CCR_1**
P1-H	0.11	0.28	1.15	0.95	0.62	0.14	0.32	1.18	0.95	0.65
	CC_2	**CC_2**	**CC_2**	**CC_2**	**CC_2**	**CCR_2**	**CCR_2**	**CCR_2**	**CCR_2**	**CCR_2**
P2-H	0.24	0.60	2.24	1.78	1.22	0.27	0.64	2.28	1.80	1.25
AVERAGE SALINITY (g/kg)										
H	32.40	32.12	31.30	31.76	31.90	32.27	31.97	31.14	31.62	31.75
P1	31.93	31.64	31.00	31.33	31.47	31.60	31.26	30.62	30.98	31.12
P2	31.87	31.57	31.05	31.30	31.45	31.52	31.18	30.67	30.95	31.08
	CC_1	**CC_1**	**CC_1**	**CC_1**	**CC_1**	**CCR_1**	**CCR_1**	**CCR_1**	**CCR_1**	**CCR_1**
P1-H	-0.47	-0.49	-0.30	-0.44	-0.42	-0.67	-0.70	-0.52	-0.64	-0.63
	CC_2	**CC_2**	**CC_2**	**CC_2**	**CC_2**	**CCR_2**	**CCR_2**	**CCR_2**	**CCR_2**	**CCR_2**
P2-H	-0.53	-0.55	-0.25	-0.46	-0.45	-0.74	-0.78	-0.48	-0.67	-0.67

TABLE 3.4.4 Impacts on temperature and salinity of historical regulation ($Rh = HR - HN$) and cumulative regulation impacts ($RC_{1,2} = CCR_{1,2} - CC_{1,2}$) across seasons (W, SP, SU, F) and over the annual cycle (AN) over projection periods P1=2021 to 2050 and P2=2041 to 2070.

	W	SP	SU	F	AN
TEMPERATURE DIVERGENCE (^{O}C)					
Rh	0.02	0.02	0.03	0.01	0.02
RC_1	0.03	0.04	0.03	0.00	0.02
RC_2	0.03	0.04	0.04	0.02	0.03
SALINITY DIVERGENCE (g/kg)					
Rh	-0.14	-0.16	-0.16	-0.14	-0.15
RC_1	-0.20	-0.22	-0.22	-0.20	-0.21
RC_2	-0.21	-0.23	-0.23	-0.21	-0.22

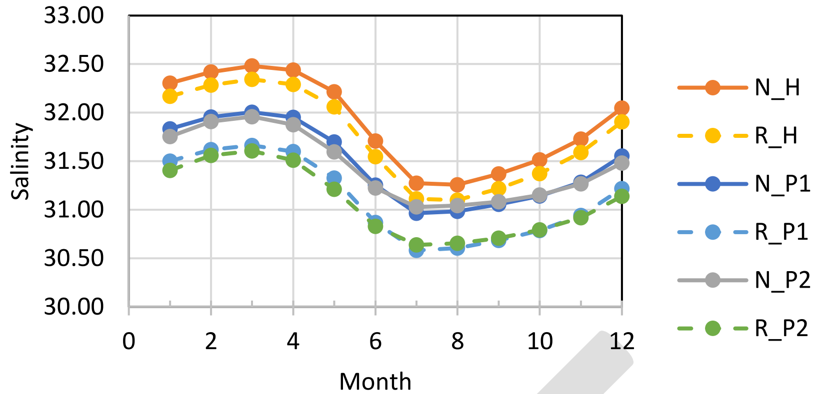

FIGURE 3.4.26 Average seawater salinity (g/kg) by month over the historical (H), and projected periods (P1 and P2) for naturalized (N) and regulated scenarios above the MLD.

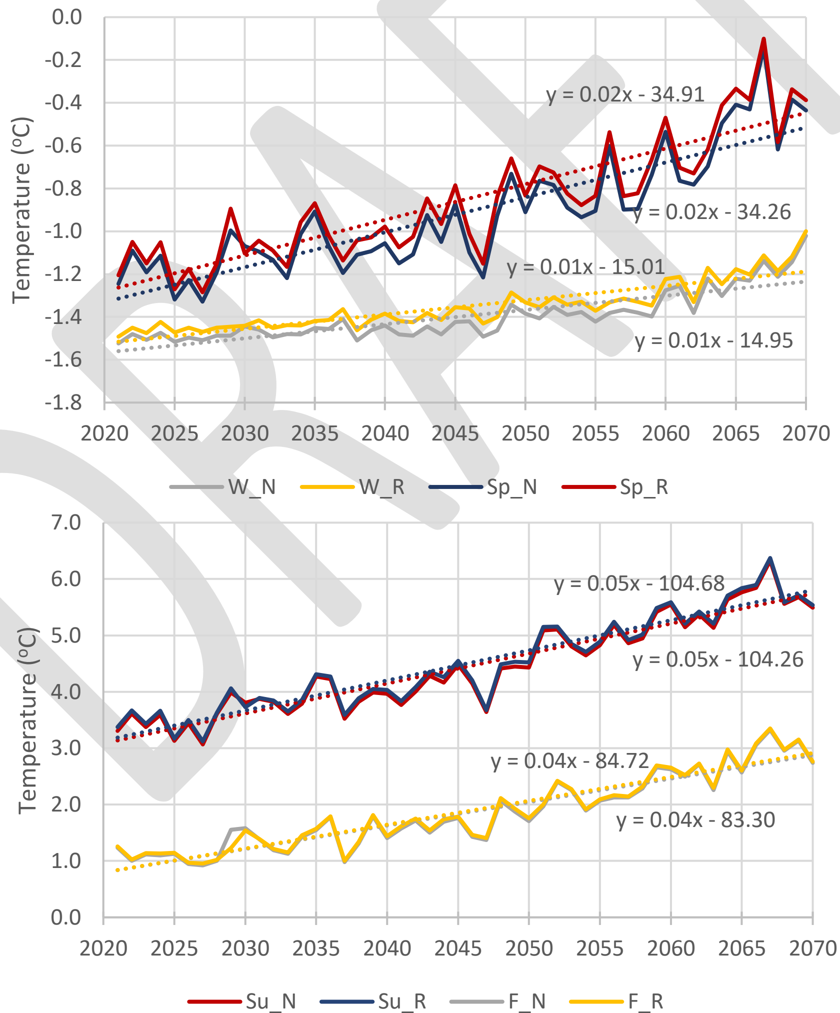

FIGURE 3.4.27 Ensemble-averaged seawater temperature above the MLD for each season. N and R refer to naturalized and regulated. W, Sp, Su, and F refer to the winter, spring, summer, and fall. Dotted lines indicate the trends in the naturalized runs from 2021 to 2070. All slopes are significant (p-value < 0.01).

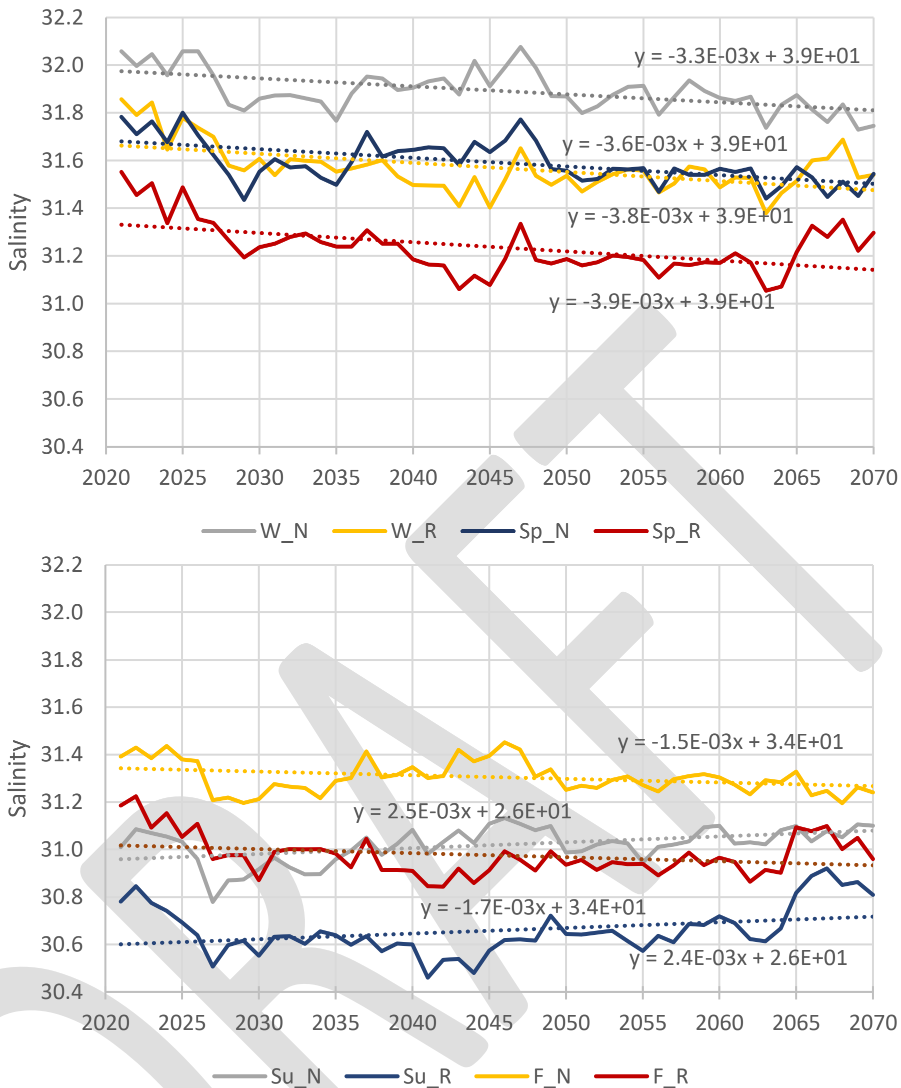

FIGURE 3.4.28 Ensemble-averaged seawater salinity (g/kg) above the MLD for each season. N and R refer to naturalized and regulated. W, Sp, Su, and F refer to the winter, spring, summer, and fall. Trend lines (2010 to 20170) are provided for each of the seasons as dotted lines. All slopes are significant (p-value < 0.01) for winter and spring (N and R), but not for summer and fall (N and R).

Surface Flux of DIC and the Inorganic Carbon System: The BLING simulations for the bay's carbon system are forced by climate, including prescribed annual increases in atmospheric CO_2 concentration, and river flow regulation. The atmospheric pCO_2 is prescribed to increase from 340 µatm to 526 µatm between 1981 and 2070 following the RCP8.5 forcing. The average atmospheric pCO_2 is 363 µatm, 453 µatm, and 500 µatm during periods H (1981-2010), P1 (2021-2050), and P2 (2041-2070), respectively. The atmospheric pCO_2 is held constant within each year. In the following, we present and discuss the simulated carbon system parameters and attribute the role of regulation and climate change on projected variables.

The monthly average surface water pCO_2, total alkalinity (TA), dissolved inorganic carbon (DIC), dissolved oxygen (DO), and flux of DIC (SFDIC) for H, P1, and P2 are provided in Figures 3.4.29, 3.4.30, 3.4.31, 3.4.32, and 3.4.33, respectively for seawater above the MLD, and averages by season appear in Table 3.4.5. The difference in surface seawater pCO_2 and atmospheric values defines the direction of the air-sea DIC (as CO_2) flux. Over the historic period the average monthly pCO_2 cycles from winter maximum between February and March to mid-summer minimum in June and July, then rising over the fall season (Figure 3.4.29). The increase in average monthly (Figure 3.4.29) and seasonally projected pCO_2 (Table 3.4.5) from H to P2 corresponds to increasing atmospheric CO_2 concentration associated with the RCP8.5 climate forcing. Nonetheless, on average Hudson Bay remains undersaturated relative to prescribed atmospheric CO_2 concentrations through mid-century. However, conspicuous is the large increase in pCO_2 forecasted to occur between August to December in P1 and P2, relative to the historic period, implying that the maximum in surface pCO_2 will shift from winter to fall, and thus should generate a high rate of autumn CO_2 outgassing. These projected extreme changes in autumn conditions appear to be related to the autumn temperature increases shown in Figures 3.4.25 and 3.4.27. The 1.78^{o}C temperature increase in the fall between H and P2 (Table 3.4.1) accounts for roughly 75% of the predicted H to P2 rise in pCO_2 (i.e., ~375 μatm to ~535 μatm; Table 3.4.5) based solely on thermodynamics. Both Else et al. (2008b) and Ahmed et al. (2021) report that variability in temperature was a good predictor of the observed variation in surface seawater pCO_2. The remaining increase in pCO_2 is likely the result of reduced NCP, given low projections for annual DO minima during the fall season (Figure 3.4.32; Table 3.4.5). The discontinuity between the December and January points for pCO_2 in future scenarios (i.e., Figure 3.4.29) is also likely a consequence of seawater temperature yet to be assessed.

TABLE 3.4.5 Average (with standard deviations in parentheses) simulated air-sea carbon exchange (SFDIC), pCO2, pH, TA, DIC, and DO in seawater above the MLD. Ω_{Ar} is included in the Table and was calculated using CO_2Sys (Pierrot and Wallace, 2006) with average pH, TA, salinity, and temperature from BLING. W, SP, SU, F, and AN refer to winter, spring, summer, fall, and annual, respectively. N and R refer to naturalized and regulated scenarios. H, P1, and P2 are historical (1981-2010), (2021-2050), and (2041-270) periods.

	W	SP	SU	F	AN	W	SP	SU	F	AN
	N	N	N	N	N	R	R	R	R	R
SFDIC (mmol C m^{-2}d^{-1})										
H	0.29 (0.36)	-1.03 (0.47)	-3.14 (1.96)	-0.39 (3.16)	-1.07 (1.33)	0.37 (0.38)	-0.85 (0.48)	-2.88 (1.95)	-0.06 (3.22)	-0.85 (1.96)
P1	0.53 (0.22)	-1.48 (0.38)	-2.48 (0.38)	2.01 (0.89)	-0.36 (0.29)	0.72 (0.29)	-1.13 (0.25)	-2.69 (0.42)	3.17 (1.04)	0.02 (0.25)
P2	0.80 (0.36)	-2.37 (0.60)	-2.18 (0.54)	2.28 (0.87)	-0.37 (0.21)	1.19 (0.50)	-2.08 (0.65)	-2.88 (0.35)	3.86 (1.20)	0.02 (0.35)
pCO2 (μatm)										
H	410.30 (66.57)	348.35 (53.59)	319.17 (35.78)	375.44 (46.48)	363.32 (50.16)	415.63 (68.11)	352.69 (54.28)	322.02 (35.70)	378.42 (47.14)	367.19 (50.85)
P1	449.99 (15.81)	375.50 (9.50)	390.46 (17.72)	487.80 (26.92)	425.94 (15.67)	466.01 (17.93)	387.08 (11.17)	411.08 (20.68)	498.46 (28.09)	440.66 (17.21)
P2	465.90 (10.30)	378.69 (9.74)	427.99 (18.36)	535.08 (19.64)	451.92 (10.85)	484.39 (12.30)	390.01 (13.40)	449.41 (16.69)	548.29 (20.69)	468.03 (11.19)
pH										
H	8.027 (0.068)	8.084 (0.062)	8.125 (0.044)	8.059 (0.047)	8.074 (0.054)	8.024 (0.069)	8.081 (0.062)	8.123 (0.043)	8.057 (0.047)	8.071 (0.055)

P1	8.021 (0.011)	8.088 (0.008)	8.080 (0.014)	7.987 (0.020)	8.044 (0.011)	8.007 (0.013)	8.076 (0.010)	8.059 (0.018)	7.976 (0.022)	8.029 (0.014)
P2	8.014 (0.007)	8.093 (0.010)	8.053 (0.013)	7.955 (0.012)	8.029 (0.006)	7.995 (0.009)	8.077 (0.014)	8.028 (0.013)	7.940 (0.014)	8.010 (0.008)
TA (mol m^{-3})										
H	2.40 (0.06)	2.36 (0.06)	2.30 (0.06)	2.36 (0.06)	2.36 (0.06)	2.4 (0.06)	2.36 (0.06)	2.31 (0.06)	2.36 (0.06)	2.36 (0.06)
P1	2.59 (0.01)	2.55 (0.01)	2.51 (0.02)	2.55 (0.01)	2.55 (0.01)	2.57 (0.01)	2.53 (0.01)	2.49 (0.01)	2.53 (0.01)	2.53 (0.01)
P2	2.61 (0.01)	2.57 (0.01)	2.55 (0.02)	2.57 (0.01)	2.57 (0.01)	2.56 (0.01)	2.53 (0.01)	2.51 (0.01)	2.53 (0.01)	2.53 (0.01)
DIC (mol m^{-3})										
H	2.3 (0.07)	2.23 (0.07)	2.14 (0.07)	2.23 (0.07)	2.23 (0.07)	2.30 (0.07)	2.24 (0.07)	2.15 (0.07)	2.24 (0.07)	2.23 (0.07)
P1	2.48 (0.01)	2.42 (0.01)	2.33 (0.02)	2.41 (0.01)	2.41 (0.01)	2.49 (0.01)	2.43 (0.01)	2.34 (0.01)	2.42 (0.01)	2.42 (0.01)
P2	2.50 (0.01)	2.44 (0.01)	2.36 (0.02)	2.43 (0.01)	2.43 (0.01)	2.50 (0.01)	2.43 (0.01)	2.360 (0.01)	2.43 (0.01)	2.43 (0.01)
DO (mol m^{-3})										
H	0.35 (0.00)	0.37 (0.00)	0.36 (0.00)	0.35 (0.00)	0.36 (0.00)	0.35 (0.00)	0.37 (0.00)	0.36 (0.00)	0.35 (0.00)	0.36 (0.00)
P1	0.35 (0.00)	0.38 (0.00)	0.35 (0.00	0.34 (0.003)	0.35 (0.00)	0.35 (0.00)	0.38 (0.00)	0.35 (0.004	0.34 (0.00)	0.35 (0.001)
P2	0.35 (0.00)	0.38 (0.00)	0.34 (0.01)	0.33 (0.00)	0.35 (0.00)	0.35 (0.00)	0.38 (0.00)	0.34 (0.01)	0.33 (0.00)	0.35 (0.00)
Ω_{Ar}										
H	1.2	1.4	1.7	1.4	1.4	1.2	1.4	1.7	1.4	1.4
P1	1.3	1.50	1.7	1.3	1.5	1.3	1.4	1.6	1.3	1.4
P2	1.3	1.6	1.7	1.3	1.5	1.2	1.5	1.6	1.2	1.4

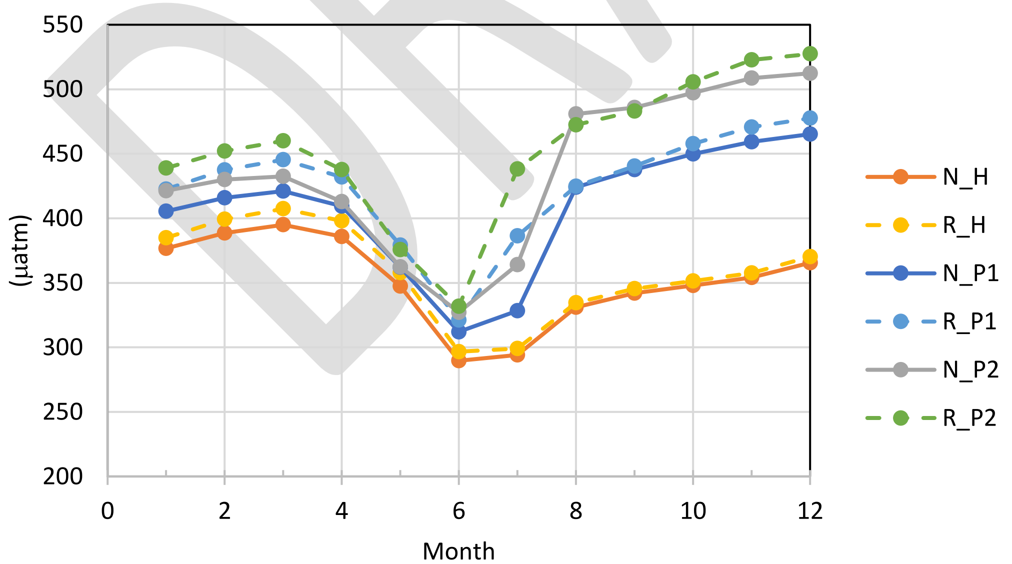

FIGURE 3.4.29 The monthly average seawater pCO_2 at the sea surface over the historical (H), and projected periods (P1 and P2) for naturalized (N) and regulated scenarios.

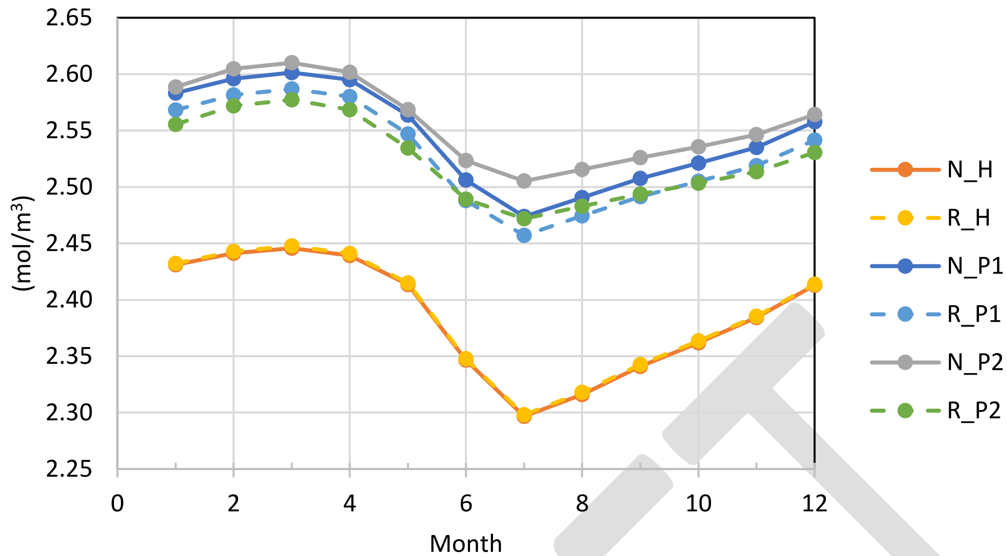

FIGURE 3.4.30 Monthly average total alkalinity (TA) above the MLD over the historical (H), and projected periods (P1 and P2) for naturalized (N) and regulated scenarios.

Total alkalinity (TA) dictates the buffering capacity of seawater against a change in pH with CO_2 uptake and changing DIC concentrations. Collectively with DIC, it also moderates pCO_2. Over the historic period, the seasonal variations in surface TA and DIC (Figures 3.4.30 and 3.4.31) mimic seawater salinity (Figure 3.4.26) above the MLD, that is highest monthly average alkalinity and DIC are observed in the winter and early spring (February to April), with the annual minimum in July. Surface seawater alkalinity and DIC are projected to increase in the future, with regulation reducing that increase somewhat.

Average annual alkalinity (Table 3.4.6) beneath the MLD is expected to range between 2.39 mol/m^3 (for H) to 2.59 mol/m^3 (for P2), marginally higher than expected above the MLD (TA= 2.36 mol/m^3 and 2.57 mol/m^3 for H and P2 respectively). Highest/lowest alkalinity is projected to occur in the winter/summer for P1 and P2, also consistent with observations from above the MLD.

Dissolved oxygen (DO in Figure 3.4.30) shows annual maxima and minima in the summer and fall respectively. The timing of maxima and minima is out of phase with pCO_2 (Figure 3.4.29), that is the timing of maximum pCO_2 corresponds with minimum DO, and vice versa, suggesting an element of biological control on both dissolved gases.

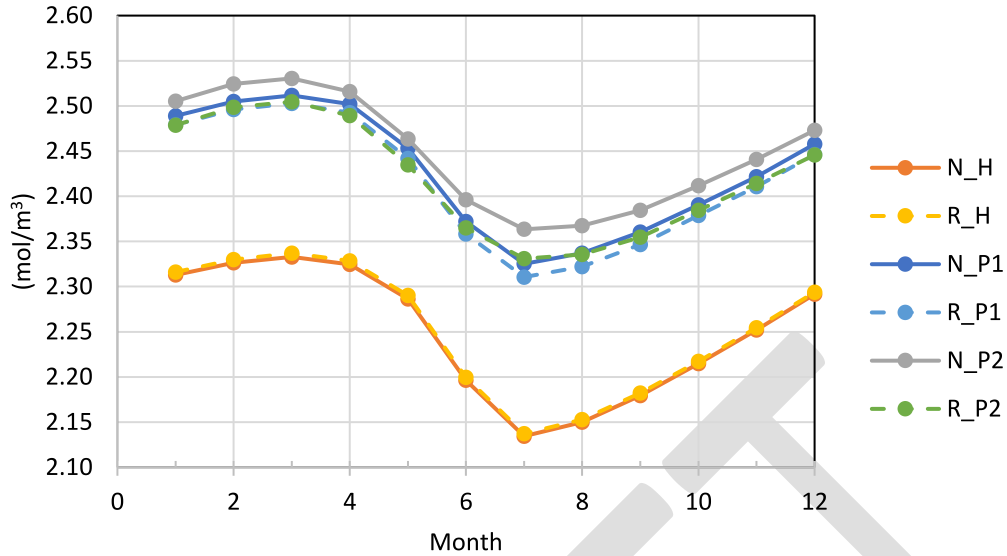

FIGURE 3.4.31 Monthly average dissolved inorganic carbon (DIC) above the MLD over the historical (H), and projected periods (P1 and P2) for naturalized (N) and regulated scenarios.

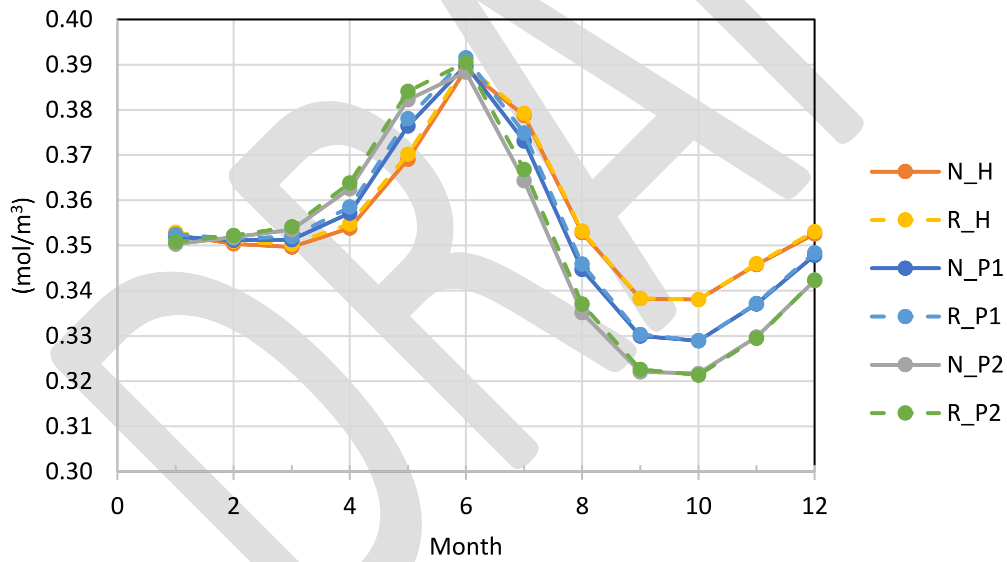

FIGURE 3.4.32 Monthly average dissolved oxygen (DO) above the MLD over the historical (H), and projected periods (P1 and P2) for naturalized (N) and regulated scenarios.

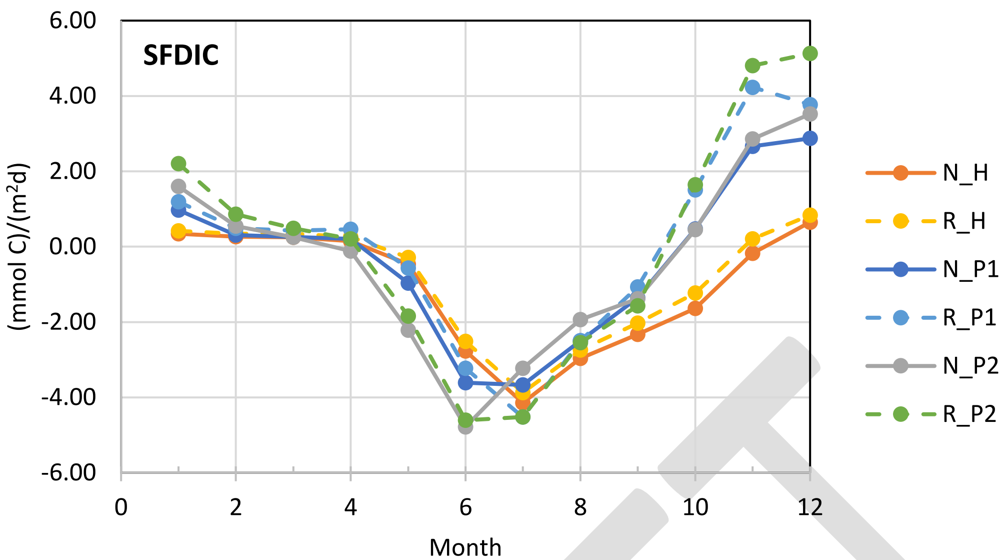

FIGURE 3.4.33 Average surface flux of DIC (as CO_2) by month over the historical (H), and projected periods (P1 and P2) for naturalized (N) and regulated scenarios.

The annual cycle of the surface DIC flux (as CO_2) during the historic period is characterized by low-level outgassing (< 1 mmol C $m^{-2}d^{-1}$) during the cold dark months: December, January, February, and March, with uptake observed between May and November for naturalized and regulated scenarios (Figure 3.4.33). Peak uptake (around -4 mmol C $m^{-2}d^{-1}$) is expected in July. Average uptake is projected to increase in June over the next few decades, while still peaking in July. Peak uptake shifts into June in P2, with a marginally greater uptake rate. In future scenarios, the expectation is for spring-time uptake to increase from 1.03 to 2.37 mmol C $m^{-2}d^{-1}$ between historical and P2 periods, while summertime uptake is expected to decrease (Table 3.4.5), suggesting the system will continue to be oligotrophic in the future (refer to section 3.3). The average rate of winter CO_2 emission from the ocean is projected to increase slightly, and during the autumn, the flux is expected to shift from a small uptake to a significant release (Table 3.4.5). Figure 3.4.34a quantifies these trends and indicates the extent to which they are exacerbated, or not, by river regulation. That is, the slopes of the trend lines are slightly higher for the regulated scenarios in fall and winter, but slightly lower in spring and summer. Note also that the slopes of the summer trendlines are very small, and indeed cannot be considered significant for the regulated scenario. Trend lines in the figures are calculated between 2021 to 2070. The net result, over the annual cycle, is that the seasonal increases and decreases in air-sea carbon flux will balance, and little net change in the total annual flux is projected (Figure 3.4.34b). Thus, on average, and over the annual cycle, the source/sink strength of Hudson Bay is projected to be near zero, with values ranging from ~-0.3 mmol $m^{-2}day^{-1}$ over P1 and P2 for naturalized scenarios and ~0.02 mmol $m^{-2}day^{-1}$ over the future scenarios for regulated scenarios (Table 3.4.5). It would be difficult to rationalize if the model predicted stronger uptake over the annual cycle given the small carbon store in Hudson Bay sediments (Kuzyk et al., 2009).

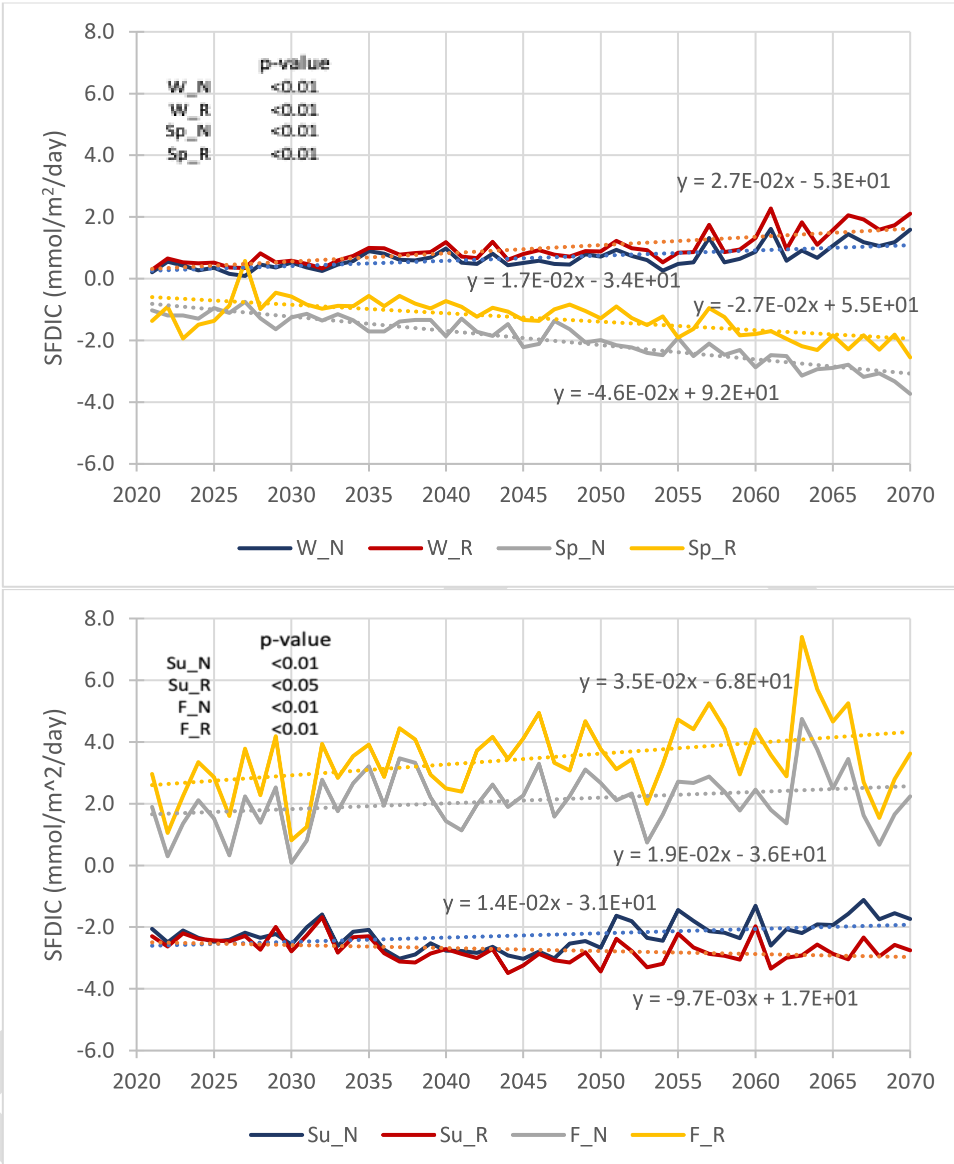

FIGURE 3.4.34a Surface flux of DIC for each of the seasons: winter (W), spring (Sp) (top panel), and summer (Su), and Fall (F) (bottom panel) for naturalized (N) and regulated (R) scenarios. Trend lines (y=b+mx) are dashed and p-values are provided for slopes (H_1: m≠0).

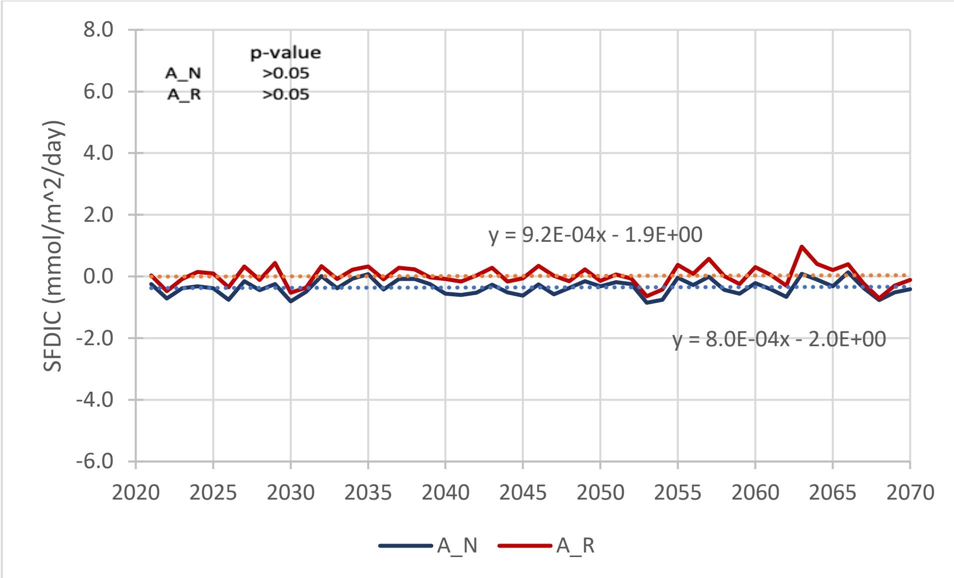

FIGURE 3.4.34b Surface flux of DIC for annually averaged flux (A) for naturalized (N) and regulated (R) scenarios. Trend lines (y=b+mx) are dashed and p-values are provided for slopes (H_1: m≠0).

Ocean Acidification: The annual cycle in pH above the MLD mirrors the trend described for pCO_2, that is, highest pH (i.e., least acidic) in the summer months (corresponding to the periods with the lowest pCO_2) and lowest pH (i.e., most acidic) in the winter and fall seasons (corresponding to periods of highest pCO_2) for the historic period (Figure 3.4.35). The projection for the future is that the pH minimum will shift from winter to autumn, and that regulation will increasingly enhance those minima.

The year-to-year variation in seawater pH above the MLD is provided in Figures 3.4.36a and b, for each season with long-term means tabulated in Table 3.4.5. We comment above that the lowest pH is projected to occur in the fall season (Figure 35). The pH time series shows that pH will drop at the highest rate in the fall and summer (in that order). Annually, the pH in Hudson Bay is projected to drop at a low, but the statistically significant rate (0.0008 and 0.0009 per year for naturalized and regulated scenarios, with ± 0.0001 95% confidence), between 2010 and 2070 (Figure 3.4.36b). The reduction in pH during fall seasons over the simulation record is projected to be approximately twice this rate. Interestingly, the pH above the MLD is projected to change very little during the spring season (Figure 3.4.36a top panel), and the projection for naturalized flow regime shows that the pH is expected to increase in the spring, ranging from an average of 8.08 during H to 8.09 during P2. The tendency is for pH to decrease in all other seasons.

Aragonite saturation (Ω_{Ar}) was calculated with CO_2SYS (Pierrot and Wallace, 2006) using the average simulated TA, pH, salinity, and temperature of seawater for each season and flow regime, and values are shown in Table 3.4.5 and 3.4.6 for above and below the MLD, respectively. The calculations indicate that the bay-wide surface Ω_{Ar} will remain well above 1 during each season above the MLD with the seasonally lowest expected values in the fall. Recall that aragonite minerals are stable when Ω_{Ar} >1, and may be subject to dissolution when Ω_{Ar} <1. Marginally lower Ω_{Ar} is expected in P1 and P2 in the fall relative to historic values, while on the other hand Ω_{Ar} is expected to increase slightly in the spring and summer for naturalized flow.

The effect of regulation is to slightly lower Ω_{Ar}, however, values remain well above 1. With some regional exceptions, Ω_{Ar} was observed to be greater than 1 in surface waters during the BaySys summertime cruise. Additional work is required to examine projected spatial trends for both pH and Ω_{Ar} regional OA risk in surface waters of Hudson Bay using BLING v0+DIC.

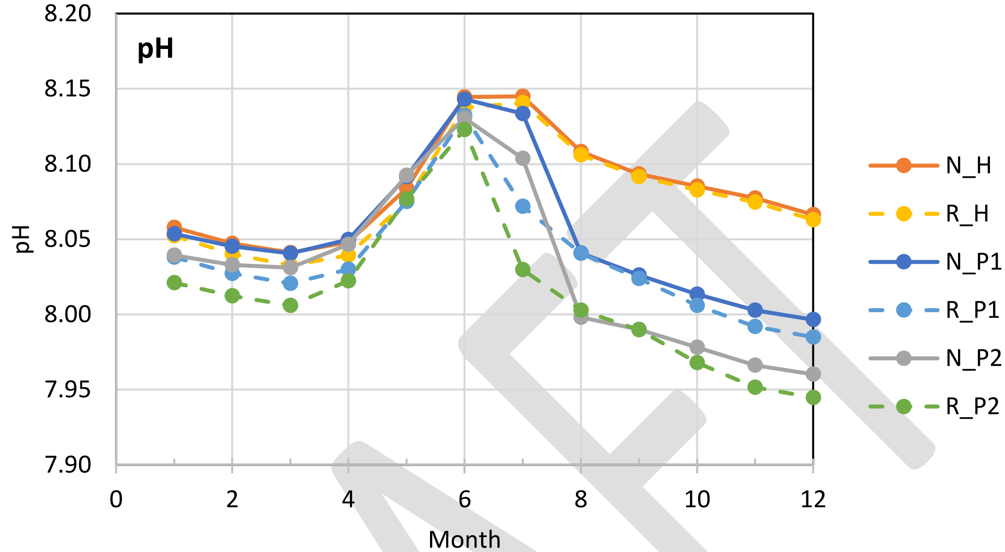

FIGURE 3.4.35 Monthly average pH above the MLD over the historical (H), and projected periods (P1 and P2) for naturalized (N) and regulated scenarios.

Because of strong water column stability and limited mixing, inorganic carbon concentrations tend to increase, and thus pH declines beneath the MLD (Figures 3.4.37a and b). Below the mixed layer, the long-term annual average pH for Hudson Bay (Table 3.4.6) is predicted to decrease from 7.84 during the historical period to 7.74 in mid-century for naturalized discharge, substantially lower values, and undergoing a greater change than in the surface waters (Table 3.4.5). The expectation is for pH in deep waters to decrease in all seasons under both regulated and unregulated scenarios, with faster decreases under the regulated scenarios (Figure 3.4.37a and b). The lowest deep-water pH is projected for the fall season, in line with projections for above the MLD. The average pH in the fall below the MLD is expected to range from7.68 and 7.62 for P1 and P2, which are lower relative to projections for above the MLD (average pH=7.99 and 7.96 for P1 and P2). Contrasting the time series shown in Figures 3.4.36 and 3.4.37, the rate at which pH is expected to drop is marginally faster beneath the MLD relative to above the MLD in all seasons.

Aragonite saturation state is also provided in Table 3.4.6. In all seasons Ω_{Ar} will be less than 1 in bay-wide deep waters for historic and future projections and both flow regimes. The lowest values are expected to occur in the fall, corresponding to the highest pCO_2. We observed $\Omega_{Ar} < 1$ to be widespread during the 2018 BaySys summer cruise in the deep waters and Azetsu-Scott et al. (2014) reported that over 67% of the bottom water in Hudson Bay was undersaturated with respect to aragonite in 2005. Our calculations indicate that the deep waters in Hudson Bay will just become more corrosive to aragonite in the future.

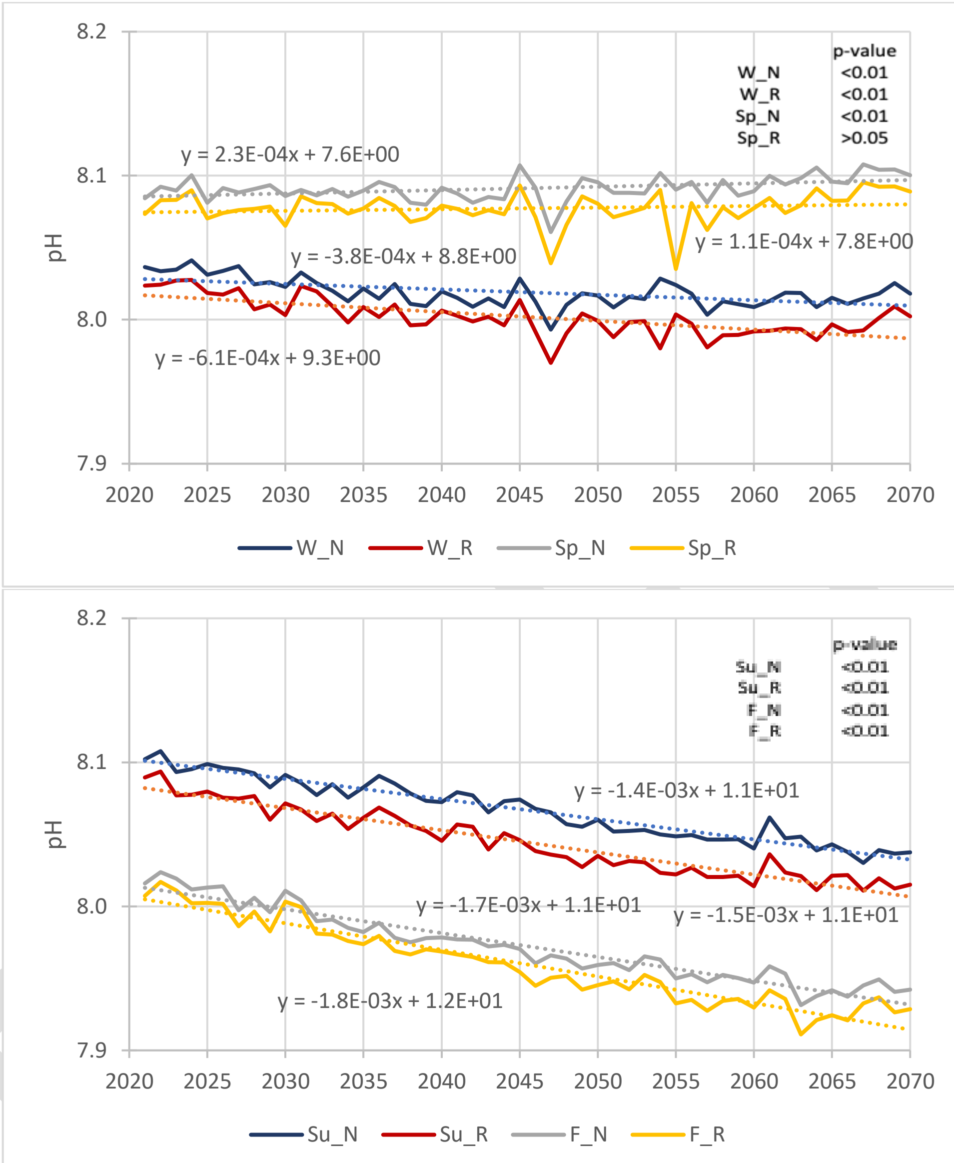

FIGURE 3.4.36a pH for each of the seasons above the MLD: winter (W), spring (Sp) (top panel), and summer (Su) and fall (F) (bottom panel) for naturalized (N) and regulated (R) scenarios. Trend lines (y=b+mx) are dashed and p-values are provided for slopes (H_1: m≠0).

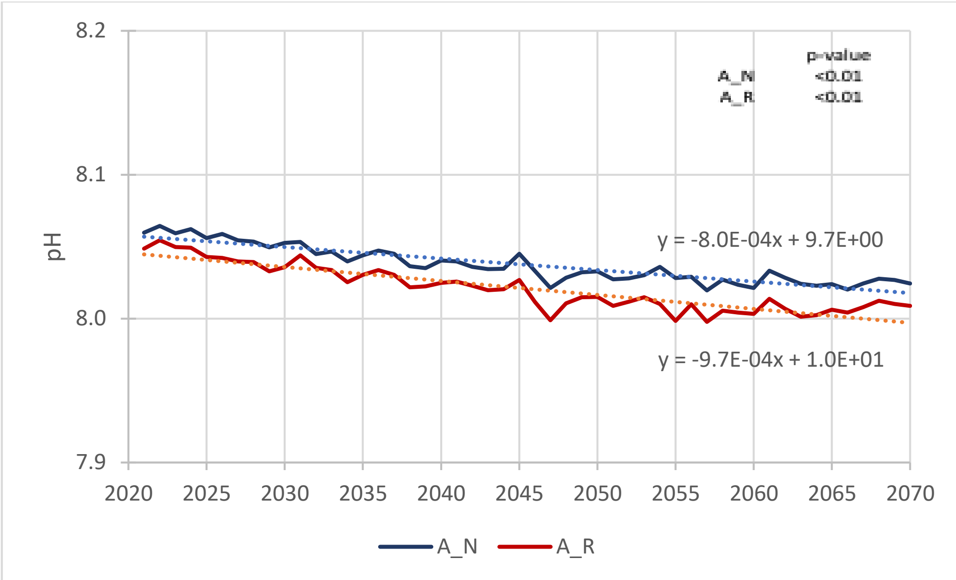

FIGURE 3.4.36b pH for annually-averaged pH (A) above the MLD for naturalized (N) and regulated (R) scenarios. Trend lines (y=b+mx) are dashed and p-values are provided for slopes (H_1: m≠0).

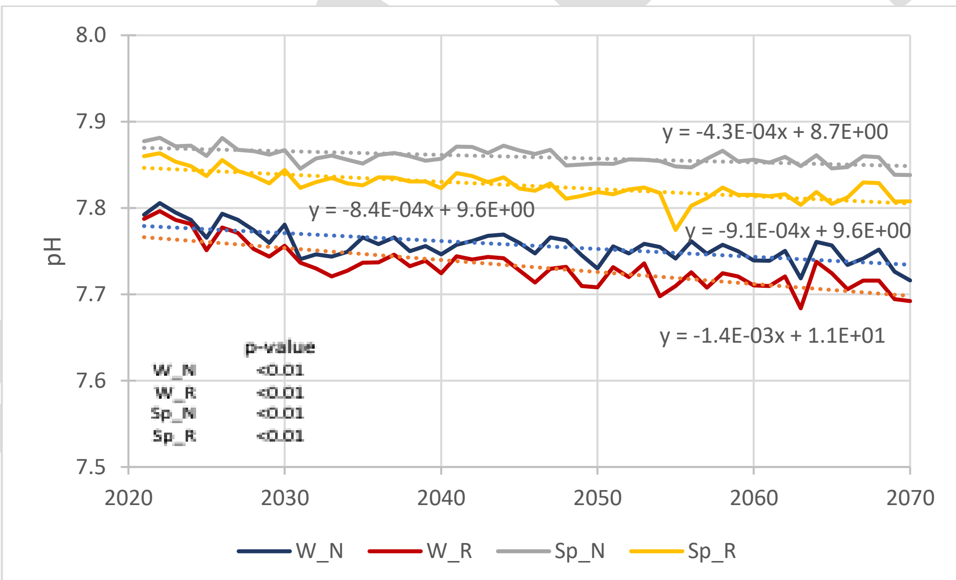

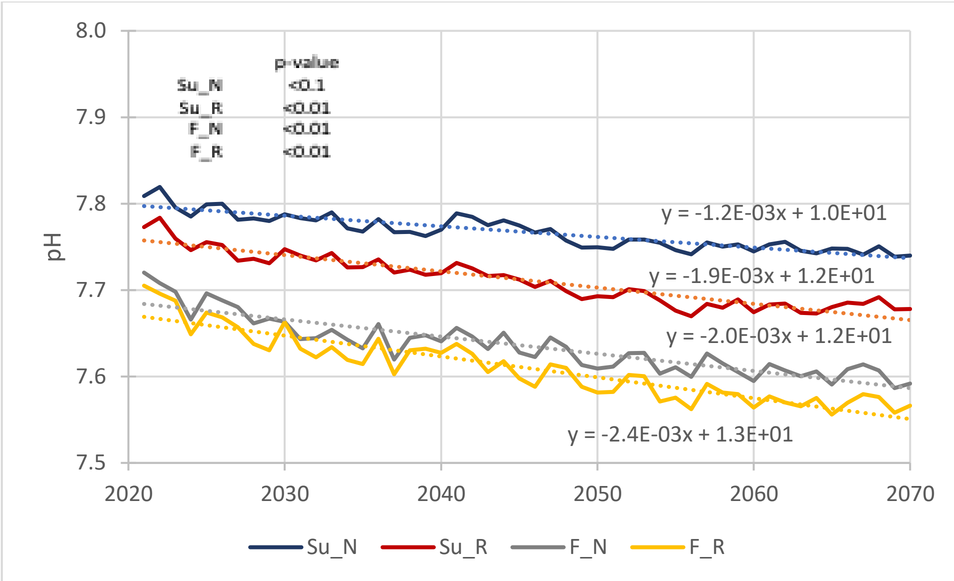

FIGURE 3.4.37a pH for each of the seasons below the MLD: winter (W), spring (Sp) (top panel), and summer (Su), and fall (F) (bottom panel) for naturalized (N) and regulated (R) scenarios. Trend lines (y=b+mx) are dashed. P-values are provided for slopes (H_1: m≠0).

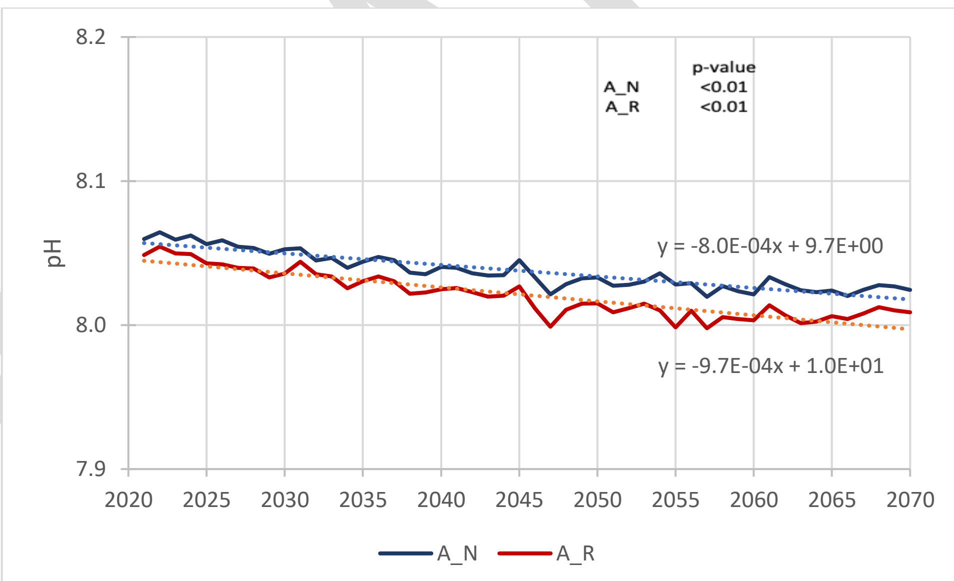

FIGURE 3.4.37b pH for annually-averaged pH (A) above the MLD for naturalized (N) and regulated (R) scenarios. Trend lines (y=b+mx) are dashed and p-values are provided for slopes (H_1: m≠0).

TABLE 3.4.6 Averages for pH, TA, DIC and DO in seawater beneath the MLD. pCO_2 and Ω_{Ar} are also provided using calculations based on CO_2Sys (Pierrot and Wallace, 2005) with the averages of TA, pH, temperature, and salinity, provided by BLING. In the table W, SP, SU, F, and AN refer to winter, spring, summer, fall, and annual. N and R refer to naturalized and regulated scenarios. H, P1, and P2 are historical (1981-2010), (2021-2050), and (2041-270). P1H and P2H refer respectively to differences between P1 and H and P2 and H.

	W	SP	SU	F	AN	W	SP	SU	F	ANN
	N	N	N	N	N	R	R	R	R	R
pH										
H	7.823 (0.109)	7.900 (0.091)	7.869 (0.091)	7.776 (0.091)	7.842 (0.095)	7.821 (0.111)	7.893 (0.093)	7.860 (0.093)	7.773 (0.092)	7.837 (0.095)
P1	7.764 (0.018)	7.863 (0.009)	7.778 (0.017)	7.652 (0.028)	7.764 (0.017)	7.744 (0.023)	7.834 (0.013)	7.729 (0.023)	7.631 (0.032)	7.734 (0.022)
P2	7.749 (0.014)	7.856 (0.009)	7.756 (0.014)	7.616 (0.018)	7.744 (0.012)	7.719 (0.016)	7.817 (0.013)	7.692 (0.016)	7.586 (0.021)	7.704 (0.015)
TA (mol m^{-3})										
H	2.42 (0.06)	2.41 (0.06)	2.36 (0.06)	2.39 (0.06)	2.40 (0.06)	2.41 (0.06)	2.41 (0.06)	2.37 (0.06)	2.39 (0.06)	2.39 (0.06)
P1	2.59 (0.01)	2.58 (0.01)	2.55 (0.01)	2.56 (0.01)	2.57 (0.01)	2.56 (0.01)	2.56 (0.01)	2.52 (0.01)	2.54 (0.01)	2.55 (0.01)
P2	2.60 (0.01)	2.60 (0.01)	2.57 (0.01)	2.58 (0.01)	2.59 (0.01)	2.55 (0.01)	2.55 (0.01)	2.52 (0.01)	2.53 (0.01)	2.54 (0.01)
DIC (mol m^{-3})										
H	2.38 (0.08)	2.33 (0.08)	2.28 (0.08)	2.34 (0.08)	2.33 (0.08)	2.36 (0.09)	2.33 (0.08)	2.28 (0.08)	2.34 (0.08)	2.33 (0.08)
P1	2.57 (0.01)	2.51 (0.01)	2.46 (0.01)	2.52 (0.01)	2.52 (0.01)	2.55 (0.01)	2.51 (0.01)	2.47 (0.01)	2.53 (0.01)	2.52 (0.01)
P2	2.59 (0.01)	2.53 (0.01)	2.48 (0.01)	2.54 (0.01)	2.53 (0.01)	2.56 (0.009)	2.52 (0.018)	2.48 (0.01)	2.53 (0.01)	2.52 (0.01)
DO (mol m^{-3})										
H	0.35 (0.00)	0.37 (0.00)	0.36 (0.00)	0.35 (0.00)	0.36 (0.00)	0.30 (0.01)	0.32 (0.01)	0.31 (0.01)	0.28 (0.01)	0.30 (0.01)
P1	0.35 (0.00)	0.37 (0.00)	0.35 (0.00)	0.34 (0.00)	0.35 (0.00)	0.29 (0.00)	0.31 (0.00)	0.29 (0.00)	0.27 (0.00)	0.29 (0.00)
P2	0.35 (0.00)	0.38 (0.00)	0.34 (0.00)	0.33 (0.00)	0.35 (0.00)	0.29 (0.00)	0.32 (0.00)	0.29 (0.00	0.26 (0.00)	0.29 (0.00)
pCO_2 (µatm)										
H	685.1	565.0	598.9	760.3	648.3	687.9	574.6	612.6	765.2	656.0
P1	848.2	664.4	806.2	1098.5	841.6	880.9	706.1	898.9	1143.2	896.0
P2	883.3	679.6	857.7	1204.7	888.9	932.3	734.0	983.1	1270.3	961.2
Ω_{Ar}										
H	0.81	0.96	0.88	0.73	0.84	0.81	0.94	0.86	0.72	0.83
P1	0.77	0.95	0.78	0.59	0.76	0.73	0.88	0.69	0.56	0.71
P2	0.75	0.94	0.75	0.55	0.73	0.68	0.85	0.64	0.51	0.66

<u>Evaluation of BLING Performance:</u> There are very few accounts of seasonal changes in carbon system parameters over the annual cycle in Arctic seas with which to compare the simulated values reported here. However, in coupling the results from the few year-long expeditions that have included CO_2 system sampling (Miller et al., 2011; Lansard et al., 2012; Else et al., 2012, 2013) with seasonal studies (e.g., Yager et al., 1995; Anderson et al., 2004; Fransson et al., 2017) a generalized, conceptual model of the annual CO_2 cycle in Arctic waters has emerged. Summer

draw-down in pCO_2 is driven by primary production and pCO_2 undersaturation (relative to atmospheric concentration) in surface waters, persisting into the fall because of late-season algal blooms and cooling seawater. Autumn drawdown can be as high or higher than in summer because of increasing storms and associated high wind speeds. As seawater freezes, CO_2 is released; initially, some of that CO_2 escapes to the atmosphere, but once the ice cover is established, further ice growth occurs only from the bottom of the ice, and CO_2 is released exclusively to the underlying water. Through the winter, surface water (i.e., under-ice) pCO_2 increases, not only because of sea ice growth but also due to negative net community production (i.e., respiration in excess of photosynthesis). At the end of winter and through spring, increasing light promotes primary production both within the ice and in the underlying water. Thanks to that biological production, as well as the innate undersaturation of sea ice melt, the surface waters are undersaturated in CO_2 as the sea ice retreats, promoting absorption from the atmosphere. During summer, strong stratification of the surface waters due to freshwater inputs from both sea ice melt and rivers ultimately limits how much atmospheric CO_2 can be absorbed, and warming can lead to outgassing in some cases.

The carbon dynamics in sea ice are not represented in BLING v0+DIC, and thus in this study sea ice exists as an impermeable slab from the perspective of the carbon system. A thorough assessment of the application of BLING v0+DIC carbon module for Hudson Bay, as part of the BaySys modelling program, is in progress using available field data from past ArcticNet cruises in Hudson Bay, in addition to observations from the BaySys program (Deschepper et al., in prep.). Results however are not yet available at the writing of this report. Nonetheless, in the following, we provide information on the performance of the BLING v0+DIC module.

The simulated surface flux of DIC over the historic period in Hudson Bay followed a typical annual cycle of uptake between May and October, with peak uptake occurring in July, countered by low-level outgassing in the late fall and winter. The simulated peak uptake in July was ~-4$\pm$2 mmol $m^{-2}d^{-1}$ which agrees with the ~ -5 mmol $m^{-2}d^{-1}$ estimate for Hudson Bay in early summer based on data from the 2018 BaySys (Ahmed et al., 2021). The average simulated pCO_2 in summer surface waters (320$\pm$36 μatm for the historic period) also agrees with the observations during the 2018 BaySys cruise (361$\pm$61 μatm; Ahmed et al., 2021). The simulated air-sea carbon flux of 0.4$\pm$3 mmol $m^{-2}d^{-1}$ also agrees with the estimate Else et al. (2008b) (-0.7 mmol $m^{-2}d^{-1}$) derived using remote sensing. Thus, the simulated flux of DIC and associated drivers are within expected ranges based on observation.

The seasonal cycles in the simulated surface flux of carbon (as well as the pCO_2 and pH cycles) correspond primarily to seasonality in net ecosystem production – that is primary production in excess of respiration in the summer (i.e., positive net community production – NCP) leading to a drop in pCO_2 and DIC and increase in each of pH DO, and respiration in excess of primary production in winter (i.e., negative NCP, increases in pCO_2 and DIC, and decreases in pH and DO). Much of the projected increase in pCO_2 during the fall (Figure 3.4.29), may be attributed to temperature (Figure 25 and 27), both directly through its effect on pCO_2, and indirectly through its impact on microbial respiration (Rivkin and Legendre, 2001) and the remineralization of organic carbon to CO_2. The modelled dissolved oxygen (Figure 3.4.32) shows annual maxima and minima in the summer and fall, respectively.

The simulated pH values from the historical run (8.08±0.06 in spring, 8.12±0.04 in summer, and 8.06±0.05 in fall) for Hudson Bay falls within the range of values reported from field studies in Hudson Bay, including BaySys (early summer value of 7.99±0.23) and Azetsu-Scott et al. (2014) (autumn values between 7.77 and 8.22).

While pCO_2 in surface water underpins the surface flux, it is related to the carbon variables DIC, TA, and pH through equilibria relations discussed in Section 3.4.2. The increased TA in P1 and P2 occurs hand in hand with increasing seawater DIC (Figure 3.4.33), which can be attributed to the accumulation of DIC as a result of uptake (as CO_2) from the atmosphere, but also possibly through DIC input into Hudson Bay from the Arctic Ocean and Baffin Bay via Hudson Strait or Fury and Hecla Strait. Both the concentration of the carbonate ion (CO_3^{2-}) and $CaCO_3$ dissolution rate are projected to be higher in P1 and P2 than in H (not shown) contributing to the observation of higher TA and DIC in the future simulations.

The patterns observed in pH above the MLD respond to the processes affecting pCO_2 and described above. Simulated pH across Hudson Bay over the historical period and for naturalized scenarios averaged 8.07± 0.05 above the MLD over the annual cycle, with the lowest average pH occurring in the winter (8.03±0.07) and fall (8.06±0.05). The expectation for relatively higher pH in the summer is likely the results from the seasonally low pCO_2 forecasted in the future scenarios for that season (Table 3.4.5). The higher buffering capacity in winter seawater may be one part of the reason pH is expected to be lower in the fall (i.e., more acidic), relative to the winter season in the future projections. Low TA in the fall likely results from the influx of sea ice melt and accumulation of river inflow (as discussed in Sections 3.4.3.1 and 3.4.3.2).

Beneath the MLD the maximum and minimum pH across the bay ranged from 8.30 to 7.98. By way of comparison, Azetsu-Scott et al. (2014) reported a pH range in the fall between 7.77 and 8.22. The overall average pH measured during the 2019 BaySys experiment was 7.99±0.23. Simulated pH in the fall appears in line with the observed range reported by Azetzu-Scott, however, a more comprehensive comparison is warranted taking into consideration spatial and temporal variability in both observed and simulated pH. Deeper waters being more acidic than surface waters have been widely observed in Arctic seas, including Hudson Bay (e.g., Burt et al., 2016; Azetsu-Scott et al., 2014) and attributed to the mineralization of organic carbon and stratification trapping the CO_2 product of respiration. Both simulated pH and DO are lower beneath the MLD (relative to above the MLD), while calculated pCO_2 is higher (Table 3.4.6), suggesting BLING captures the respiration signal.

On the Role of Climate Change and Regulation on Carbon System Variables: A BLING Synthesis

The impacts of climate change and river regulation on the inorganic carbon system of Hudson Bay are summarized in Tables 3.4.7a and b, but thus far have only been discussed to a limited extent. Regulation acts to flatten the annual hydrograph of river discharge, with water held back in reservoirs during the spring and summer and released in the winter to meet the heightened hydroelectric demands of that season (refer to Section 3.4.1). We make a note above (Figures 3.4.26 and 3.4.28; Tables 3.4.3 and 3.4.4) that regulation strongly impacts salinity across seasons, and thus the major impact of regulation on the surface flux is likely a consequence of freshwater on water column stratification (limiting the availability of nutrients for biological production outside of the winter season, as well as the capacity for air-sea flux). The impact of historical regulation (Rh) on the modern air-sea carbon flux (Table 3.4.7a) is very small across each of the seasons ($|Rh| \leq 0.33$ mmol $m^{-2}d^{-1}$), being the largest in the fall (increasing outgassing by 0.33 mmol $m^{-2}d^{-1}$) and summer (increasing uptake by -0.26 mmol $m^{-2}d^{-1}$; recall a negative flux denotes uptake). While there is a small difference in the average flux across seasons between regulated and naturalized flow regimes during the historic period, these differences are not statistically significant (p-value >0.01) based on a Wilcoxen/Kruskal-Wallis Rank Sums Test.

In general, the impact of regulation in future simulations is to reduce the absorption of atmospheric carbon into Hudson Bay, decreasing spring and summer uptake and increasing fall and winter release (Figure 3.4.31). In future scenarios, the impacts of regulation ($RC_{1,2}$) on the surface flux are largest in the fall and summer seasons. The SFDIC is different between regulated and naturalized flow in the future projections based on a Wilcoxen/Kruskal-Wallis Rank Sums Test (p-value<0.01) for all seasons except spring (p-value<0.05). The largest change in the air-sea flux with time is expected to occur in the fall season, with the flux projected to increase by up to 2.7 mmol C $m^{-2}d^{-1}$ in P2 relative to historic naturalized estimates (i.e., CC_2 in Table 3.4.7b). Roughly a third (32%) of the total predicted increase in autumn carbon outgassing between H and P2 can be attributed to river regulation, with 68% attributed to climate change (%Reg and %CC in Table 3.4.7b).

In other seasons, climate change also accounts for the majority of the changes in air-sea carbon fluxes, although in summer the attribution is almost equal between climate change and river regulation (Table 3.4.7b). The projected changes in summertime uptake are small (Table 3.4.5), thus impacts of both climate change and regulation will be small in this season. Over the annual cycle regulation has a moderate impact (i.e., %Reg of 20% in Table 3.4.7b) on Hudson Bay's overall carbon source/sink status, with the residual attributable to climate change (%CC of 80% in Table 3.4.7b).

TABLE 3.4.7a Impacts of historical ($Rh = HR - HN$) and future regulation ($Rc_{1\&2} = CCpR_{1,2} - CC_{1,2}$) on the air-sea flux of carbon (SFDIC in mmol C $m^{-2}d^{-1}$).

	W	SP	SU	F	AN
SFDIC (mmol C $m^{-2}d^{-1}$)					
Rh	0.08	0.18	-0.26	0.33	0.21
RC_1	0.05	0.06	-0.47	0.55	0.05
RC_2	0.30	0.11	-0.96	1.25	0.18

TABLE 3.4.7b A summary of climate change and regulation regulation-related impacts for SDFIC. In the table W, SP, SU, F, and AN refer to winter, spring, summer, fall, and annual. N and R are naturalized and regulated flow regimes. H, P1, and P2 are historical (1981-2010), (2011-2040), and (2041-2070) periods. P1H and P2H refer respectively to differences between P1 and H and P2 and H. %CC and %Reg represent the proportions of the total projected change that can be attributed to climate change and river regulation, respectively (described by Equations 5-6 and 9-10).

	W	SP	SU	F	AN	W	SP	SU	F	AN
	N	N	N	N	N	R	R	R	R	R
SFDIC (mmol C $m^{-2}d^{-1}$)										
CC_1						**CR_1**				
P1H	0.24	-0.45	0.66	2.40	0.71	0.35	-0.28	0.19	3.23	0.87
CC_2						**CR_2**				
P2H	0.51	-1.35	0.96	2.66	0.70	0.82	-1.24	0.00	3.92	0.88
%CC						**%REG**				
P1H	68.35	72.91	58.48	74.22	81.63	31.65	-27.09	-41.52	25.78	18.37
P2H	62.88	92.44	50.05	67.98	79.70	37.12	-7.56	-49.95	32.02	20.30

The relative impacts of climate change and regulation are tabulated for surface water pCO_2, pH, and TA in Table 3.4.8a. Regulation has had little impact on pCO_2 during the historical period (Figure 3.4.29; Rh in Table 3.4.8a). The simulations show the largest impact in winter and spring (Rh = 5.3 and 4.3, respectively), which is only 1% of the average seawater pCO_2 for the historical period (Table 3.4.5). In future projections regulation is forecasted to increase pCO_2, with the greatest impact realized in the summer (11 μatm and 18 μatm, respectively in P1 and P2), which is consistent with the discussion surrounding Figure 3.4.29. As with the air-sea carbon flux, projected changes in pCO_2 for future scenarios are mostly attributable to climate change, with 12% of the net annual change in surface pCO_2 attributable to river regulation (i.e., %Reg in Table 3.4.8b).

TABLE 8a Impacts of historical ($Rh = HR - HN$) and future regulation ($Rc_{1,2} = CCpR_{1,2} - CC_{1,2}$) pCO_2 (μatm) at the sea surface, and pH, and alkalinity (TA in mol m^{-3}) above the MLD.

	W	SP	SU	F	ANN
pCO2 (μatm)					
Rh	5.33	4.34	-2.85	2.98	3.87
RC_1	8.48	6.23	11.23	6.93	8.22
RC_2	13.16	6.98	18.57	10.23	12.24
pH					
Rh	-0.003	-0.003	-0.002	-0.002	-0.003
RC_1	-0.009	-0.008	-0.013	-0.008	-0.009
RC_2	-0.016	-0.012	-0.022	-0.013	-0.016
TA (mol m^{-3})					
Rh	0.002	0.001	0.001	0.001	0.001
RC_1	-0.014	-0.015	-0.014	-0.014	-0.014
RC_2	-0.043	-0.044	-0.042	-0.043	-0.044

TABLE 8b A summary of climate change and regulation regulation-related impacts for pCO_2, pH, and TA above the MLD. In the table W, SP, SU, F, and AN refer to winter, spring, summer, fall, and annual. N and R are naturalized and regulated flow regimes. H, P1, and P2 are historical (1981-2010), (2011-2040), and (2041-2070) time periods. P1H and P2H refer respectively to differences between P1 and H and P2 and H. %CC and %Reg represent the proportions of the total projected change that can be attributed to climate change and river regulation, respectively (described by Equations 5-6 and 9-10).

	W	SP	SU	F	AN	W	SP	SU	F	AN
	N	N	N	N	N	R	R	R	R	R
pCO2 (μatm)										
CC₁						CR₁				
P1H	39.69	27.15	71.29	112.36	62.62	50.38	34.39	89.06	120.04	73.47
CC₂						CR₂				
P2H	55.60	30.34	108.82	159.64	88.60	68.76	37.32	127.39	169.87	100.84
%CC						%REG				
P1H	78.77	78.94	80.05	93.60	85.24	21.23	21.06	19.95	6.40	14.76
P2H	80.86	81.30	85.42	93.98	87.87	19.14	18.70	14.58	6.02	12.13
pH										
CC₁						CR₁				
P1H	-0.006	0.004	-0.045	-0.072	-0.030	-0.017	-0.005	-0.064	-0.081	-0.042
CC₂						CR₂				
P2H	-0.013	0.009	-0.072	-0.104	-0.045	-0.029	-0.004	-0.094	-0.117	-0.061
%CC						%REG				
P1H	35.73	-32.66	69.67	89.28	71.09	64.27	67.34	30.33	10.72	28.91
P2H	43.43	-41.68	76.57	88.85	73.82	56.57	58.32	23.43	11.15	26.18
TA (mol m^{-3})										
CC₁						CR₁				
P1H	0.190	0.190	0.208	0.189	0.194	0.168	0.166	0.184	0.166	0.171
CC₂						CR₂				
P2H	0.209	0.212	0.244	0.213	0.219	0.166	0.167	0.200	0.170	0.176
%CC						%REG				
P1H	89.50	88.81	89.79	89.16	89.32	-10.50	-11.19	-10.21	-10.84	-10.68
P2H	82.83	82.72	84.85	83.08	83.42	-17.17	-17.28	-15.15	-16.92	-16.58

Surface seawater pH is expected to decrease in all seasons, except for the spring under the unregulated scenario (Table 3.4.5, and $CC_{1,2}$ in Table 3.4.8b), where a very small increase is expected. The largest drop in pH is projected to occur in the fall season, consistent with projections of the highest pCO_2 in this season. Regulation appears to have a negligible impact on simulated pH during H (Tables 3.4.5, 3.4.8a). In future scenarios, regulation is associated with marginally lower surface pH than in the naturalized scenarios in all months, with the largest impacts of regulation evident in the summertime. Climate change is the dominant influence on projected pH only in the summer and fall seasons, and river regulation has a greater impact in the winter and spring (%Reg in Table 3.4.8b). Changes expected in TA are mainly attributed to climate change (e.g., $\%CC_1 > 88\%$ and $\%CC_2 > 82\%$ in Table 3.4.8b).

The effect of regulation on historical pH below the surface (Tables 3.4.6, 3.4.9a) is most strongly realized during the summer (Rh=-0.009), consistent with simulations for the surface waters. The simulations show that river regulation acts to lower deep-water pH throughout the year. In future projections impact of regulation ($RC_{1\&2}$) on pH is also strongest in the summer, particularly over the longer timescale (Table 3.4.9a). Changes in pH beneath the MLD are mainly attributed to climate change, however, less so than reported for pH above MLD. Below the MLD regulation accounts for up to 32% of the change during the summer season (Table 3.4.9b).

TABLE 9a Impacts of historical regulation ($Rh = HR - HN$) and future regulation ($Rc_{1,2} = CCpR_{1,2} - CC_{1,2}$) on pH, and alkalinity (TA in mol m^{-3}) beneath the MLD.

	W	SP	SU	F	AN
pH					
Rh	-0.002	-0.007	-0.009	-0.003	-0.005
RC_1	-0.027	-0.025	-0.024	-0.026	-0.025
RC_2	-0.030	-0.039	-0.064	-0.030	-0.041
TA (mol m^{-3})					
Rh	-0.002	-0.001	0.001	-0.001	-0.001
RC_1	-0.01	-0.01	-0.01	-0.01	-0.01
RC_2	-0.047	-0.046	-0.044	-0.046	-0.046

TABLE 9b A summary of climate change and regulation regulation-related impacts for pH and TA below the MLD. In the table W, SP, SU, F, and AN refer to winter, spring, summer, fall, and annual. N and R are naturalized and regulated. H, P1, and P2 are historical (1981-2010), (2011-2040), and (2041-2070) periods. P1H and P2H refer respectively to differences between P1 and H and P2 and H. %CC and %Reg represent the proportions of the total projected change that can be attributed to climate change and river regulation, respectively.

	W	SP	SU	F	HB	W	SP	SU	F	HB
	N	N	N	N	N	R	R	R	R	R
pH										
	CC	CC	CC	CC	CC	CCpR	CCpR	CCpR	CCpR	CCpR
P1H	-0.06	-0.04	-0.08	-0.10	-0.07	-0.07	-0.06	-0.11	-0.11	-0.09
P2H	-0.07	-0.04	-0.11	-0.16	-0.10	-0.10	-0.08	-0.17	-0.19	-0.13
%CC						**%REG**				
P1H	84.79	75.38	73.64	88.47	81.02	15.21	24.62	26.36	11.53	18.98
P2H	72.69	57.83	67.37	85.36	73.38	27.31	42.17	32.63	14.64	26.62
TA (mol m^{-3})										
	CC	CC	CC	CC	CC	CCpR	CCpR	CCpR	CCpR	CCpR
P1H	0.16	0.16	0.16	0.16	0.16	0.15	0.15	0.15	0.14	0.15
P2H	0.18	0.19	0.20	0.19	0.19	0.14	0.14	0.16	0.14	0.15
%CC						**%REG**				
P1H	91.95	91.77	91.79	91.67	91.80	-8.05	-8.23	-8.21	-8.33	-8.20
P2H	80.47	80.72	81.99	80.56	80.96	-19.53	-19.28	-0.18	-19.44	-19.04

3.4.5 Summary and Conclusions

The BaySys proposal required Team 4 to address two highly integrated objectives through a combination of observational and modelling studies. We conclude this chapter by summarizing the results from our BaySys investigations as they pertain to each objective.

> **First Objective:** to characterize the impact on Hudson Bay's carbon system, including the bay's overall CO_2 source or sink status, associated with seasonal variations in rivers discharge, primary production, and cycles of sea ice melt and formation.

Second Objective: to assess long-term changes in Hudson Bay's carbon system, including the bay's overall CO_2 source or sink status, separating the relative influence of river flow regulation and climate change.

Objective 1: Impacts on Hudson Bay's Contemporary Carbon System

BaySys research demonstrates that several processes influence the bay's CO_2 exchange budget with the atmosphere over a range of temporal and spatial scales. The total open water (May to October) CO_2 sink was estimated to be 7.2 TgC for the entire Hudson Bay Complex (HBC). BLING simulations over the 1981-2010 historical period further supported the conclusion that Hudson Bay is overall a weak CO_2 sink. The simulations confirm that the peak uptake occurs in July with a magnitude comparable to that observed by Ahmed et al. (2021) in the early summer. The simulations also indicate that the bay is a CO_2 source during the five months (November, December, January, February, March, and April) not considered by Ahmed et al. (2021), losing on average ~ 0.4 mmol C $m^{-2}d^{-1}$ (Figure 3.4.33), totalling a 0.9 Tg C loss to the atmosphere assuming an area 1.041×10^6 km^2 (Hudson Bay and Hudson Strait). Adding this carbon loss to the open-water season uptake estimated by Ahmed et al. (2021) suggests that the annual total uptake for Hudson Bay might be closer to 6 TgC, which is within the range of the annual average historical flux simulated by BLING (-4.9 $\pm$ 6.1 TgC), again assuming an area of 1.041×10^6 km^2 and average daily rate of -1.07 $\pm$1.33 mmol $C^{-1}m^{-2}d^{-1}$ (Table 3.4.5). This establishes the bay as a weak to moderate CO_2 sink, and comparable in size to other Arctic peripheral seas (e.g., Laptev and East Siberian Seas) based on data provided by Ahmed et al. (2021).

While the mean of modelled fluxes over the historical period is surprisingly close to our observationally derived estimate, the interannual variability within the simulation is quite high, and with the uncertainty on that average annual flux, it is not different from zero. Comparison between the observations of Ahmed et al. (2021), who found that the bay was a net CO_2 sink in late summer 2018, and those of Else et al. (2008b), who found that the bay was a net CO_2 source to the atmosphere in late summer 2005, further demonstrates that there can be substantial inter-annual variability in the seasonal CO_2 source/sink status of the bay. Higher resolution and longer observation time series would help better constrain the variability in the carbon fluxes of the bay. New data confirmed that river water dilutes TA and DIC, while augmenting the availability of organic carbon in the marine system. Additionally, we established that rivers in the southwest of Hudson Bay have much higher concentrations of DIC and TA than rivers draining Precambrian Shield. Sea ice melt typically has lower concentrations for both DIC and TA relative to the southwest rivers, but not necessarily relative to rivers that drain other parts of the bay's watershed. Diluting river waters draining the Precambrian Shield and sea ice melt can lead to pronounced CO_2 undersaturation relative to the atmosphere. The main impacts of such dilution are highly localized, rapidly dissipating upon mixing with seawater. Thus, our BaySys observations confirmed that the distribution of carbon system variables in the surface waters of Hudson Bay generally followed the distribution of salinity, consistent with previous observations (i.e., Burt et al., 2016; Azetsu-Scott et al., 2014).

Seawater temperature is an important control on pCO_2, and when the temperature is variable (i.e., in summer and fall), it dominates the observed variations in pCO_2, and as the temperature rises, previously undersaturated waters can outgas (e.g., Ahmed et al., 2021; Else et al., 2008a, 2008b). Localized upwelling also contributed to high surface pCO_2 in some areas (particularly south of Southampton Island), while the biological production was an important factor decreasing pCO_2, particularly in the marginal ice zone in spring. Respiration also served to increase pCO_2 in some places but was most important in sub-surface waters. Pockets of CO_2 saturation and oversaturation observed in the low salinity and warm waters of the coastal corridor were attributed to the mineralization of terrestrial organic carbon, as well as warmer water temperatures.

Over the annual cycle and within the coastal corridor, the mineralization of organic carbon was shown to be a major contributor not only to elevated pCO_2 but also low pH and aragonite saturation state (Ω_{Ar}) (Capelle et al., 2020). BaySys results showed that organic material of terrestrial origin was rapidly degraded in rivers, estuaries, and bay surface waters, with contributions from light (photodegradation) as well as microbial activity (Kazmiruk et al., 2021; Islam, 2021). Organic material carried by rivers has a complex composition, differs between watersheds, and possibly between seasons. Depending on the nutrient ratio of the material, the build-up of pCO_2 and associated implications for gas exchange and acidification may be offset to some degree by new primary production made possible through the release of nutrients from remineralized organic material. Thus, the net impact of river inflow on the marine carbon system is determined by a combination of the river's discharge, inorganic carbon chemistry of the river water, load and composition of organic carbon, together with the properties of the receiving seawater. Where the impact of riverine carbon load is realized (i.e., estuary, coast zone, depth) depends on mixing and residence time. The fate of the riverine DOC that is not degradable within the short time-frames established by our incubation experiments is not known but may include export to Hudson Strait or sorption onto particles and sedimentation.

With no evidence of an effective biological pump in the sediment record (Section 3.4.4.6) of the bay, likely, much of the carbon taken into the system (from rivers and gas exchange at the sea surface) is exported to Baffin Bay and the North Atlantic through Hudson Strait. The Hudson Strait outflow is estimated at ~1.45 x 10^6 m^3s^{-1} to Baffin Bay (Ridenour, pers. comm.), and the associated transport of carbon has not been quantified. Hence, reiterating from above, the bay is a low-level carbon sink and we do not know how much of an annual carbon sink is advected from the system.

Potentially corrosive seawater (i.e., $\Omega_{ar} < 1$) was widely observed in deep waters and shoaled to within 25 m of the surface east of James Bay, consistent with observations from other studies (e.g., Burt et al., 2016; Azetsu-Scott et al., 2014). The pervasive and sometimes strong surface layer stability reported by Ahmed et al. (2020) that resulted from freshwater pooling at the surface facilitates the build-up of pCO_2 in deeper waters, contributing to observations of low pH and $\Omega_{ar.}$ BaySys results (Capelle et al., 2020) indicate that much of the OC material degraded in the deep water and the bay's interior is of marine origin.

The impact of high primary production on lowering pCO_2 was discernable during the BaySys cruise in the bay's northwest polynya and Hudson Strait (Ahmed et al., 2021). The primary production signal on pCO_2 in other areas showing evidence of high primary production (e.g., in proximity to the Nelson Estuary) was, we believe (e.g., Ahmed et al., 2021), masked by other processes tending to increase pCO_2 (notably respiration and elevated water temperature). The numerical modelling results, however, suggest bay-wide seasonal shifts in net community production (as inferred from dissolved oxygen) are in phase with simulated pCO_2 at the sea surface. Thus, it is possible that forcing on the CO_2 source/sink strength by biological production may be more important in parts of the bay's interior not sampled during the BaySys cruise.

Objective 2: The Bay's Carbon System into the Future

Numerical simulations using a biogeochemical model coupled to the NEMO framework for Hudson Bay (BLING V0+DIC) show that the low annual average atmospheric carbon sink in the bay is not expected to appreciably change before 2070 and that climate change impacts on the surface flux are more pronounced than those associated with regulation. The lack of organic sediments (Kuzyk et al., 2009) suggests the bay has not had a strong biological pump, a requisite (along with deep-water formation) for strong and sustained CO_2 uptake. Results from Section 3.3 confirm that Hudson Bay is an oligotrophic sea, and our simulations indicate that it will remain oligotrophic in the future.

The overall lack of change in our simulated net air-sea carbon fluxes is likely related to the global standoff between increasing atmospheric CO_2 concentration (driving increased uptake) and increasing seawater temperature (driving increased outgassing). Although the net annual average air-sea carbon flux is not expected to appreciably change, our simulations indicate that the total flux will be distributed differently through the year, which has implications for ecosystem processes, as well as potential carbon sequestration. Earlier sea ice break-up will contribute to earlier peak CO_2 uptake, but the simulations suggest that while uptake in the spring may increase, summertime uptake will likely not increase. The largest change in the surface CO_2 flux is expected to occur during the fall, and in this season the system is anticipated to toggle from a weak carbon sink to a strong source. This is likely the system's response to the combination of warming seawater, coupled with a reduction in autumn sea ice cover, that will allow surface waters to remain exposed to the atmosphere, as primary production declines with the end of summer and the ecosystem shifts to net respiration. The future role of biology on the long-term air-sea flux budget remains uncertain. Indications are that the terrestrial organic carbon load delivered by Arctic rivers will increase with river discharge (Amon et al., 2012). Ultimately, with low primary production in Hudson Bay, there is limited capacity for carbon burial to offset the effects of future increases in terrestrial organic carbon inputs, particularly if the addition of the organic material is nitrogen-poor, as is permafrost-bound peat. Thus, under future scenarios, the Hudson Bay system may accumulate inorganic carbon, including pCO_2 due to increasing atmospheric CO_2 concentrations and CO_2 production from the degradation of terrestrial organic material, beyond what can be offset by new production.

Collectively the accumulation of inorganic carbon in Hudson Bay would drive increasing CO_2 supersaturation and aragonite under-saturation, especially in parts of the bay with characteristically high meteoric water fractions, like southeast Hudson Bay. A reduction in seawater pH is forecast to accompany the projected increase in pCO_2 into the future. Bay-wide the surface waters are projected to remain saturated with respect to aragonite (i.e., $\Omega_{Ar}>1$) during all seasons. However, subsurface waters are already undersaturated with respect to aragonite, and the simulations predict that undersaturation to only increase through the middle of the century. This is consistent with our understanding of the contemporary system (e.g., Azetsu-Scott et al., 2014; Burt et al., 2016), with waters becoming progressively more corrosive to $CaCO_3$ minerals into the future. Work however remains to understand the seasonal and spatial trends in projected acidification in Hudson Bay, which may control its ultimate impacts on the ecosystem.

River regulation acts to flatten the annual hydrograph of river discharge, with water held back in reservoirs during the spring and summer and released in the winter to meet the heightened hydroelectric demands of that season (Section 3.2). A principal objective of this study was to assess the relative roles of regulation versus climate change in controlling the CO_2 source/sink status of Hudson Bay. We do know the riverine delivery of DOC, DIC, and TA to the bay is highly dynamic. We do not know if regulation has increased the flux of these dissolved constituents from the Nelson River, but we do know that it has affected the river's hydrograph, and thus should impact at least the timing of the lateral flux. The BaySys results show that the timing is important in terms of the fate of the terrigenous DOC (whether it is degraded within the watershed or river versus in the coastal waters near the river mouth). The river delivery of DOC in winter should be higher with regulation given its association with river discharge. In winter, following the suggestion of Kazmiruk et al. (2021), the riverine DOC will be better preserved en route to the bay relative to summer transport because of darkness that limits photodegradation and low temperatures that limit microbial degradation. Conversely, DOC should be degraded further upstream in the open water season, implying the residual DOC transported downstream may be less biodegradable than its winter counterpart. Thus, the high biodegradability of Hudson Bay riverine DOC in late winter, together with high concentrations and fluxes of riverine DOC implies that regulation should increase the DIC stock in coastal waters proximal to the river outlet through the mineralization of DOC, locally raising pCO_2 and decreasing aragonite saturation, a prediction supported by our simulations. Sipler et al. (2017a, 2017b) demonstrated that microbial communities in coastal waters respond strongly to terrestrial DOC delivery and depending on the nutrient ratios of the terrestrial material, may exacerbate nitrate limitation for phytoplankton.

The age and origin of carbon transported to the contemporary marine system are not known in any detail, much less how it will change in the future. The inevitability of increased delivery of old carbon, in response to a thawing of the permafrost-laden Hudson Bay Lowlands, raises questions about the composition and biodegradability of future loads of DOC and POC, and thus the impact of terrestrially-derived organic carbon on the marine carbon cycle is not certain. Super-imposed on climate change impacts on the 'land to sea' aquatic carbon continuum (e.g., Cole et al., 2007) is the poorly quantified variability in the properties of exported freshwater arising from future upstream land-and-water-use changes, including water impoundment for hydroelectric production (Deemer et al., 2016, Teodoru et al., 2012; Regnier et al., 2013). For example, Maavara et al. (2020) showed how dams impact the riverine nutrient ratios that are delivered to the coastal ocean because of the retention of phosphorous and silicon in reservoirs. The take-away message is that future states of the carbon system in Hudson Bay are subject to forcing that remains difficult to constrain. That said, our best tool to project the response of the bay's carbon system to changes induced by climate and regulation remains the application of ever-improving numerical models.

The BaySys biogeochemical simulations indicate that bay-wide, future changes in the CO_2 system of Hudson Bay, including air-sea exchange and acidification, will mainly be driven by climate change, but that river regulation has significant impacts, particularly for pH. In addition, regulation appears to decrease the air-sea carbon flux during seasons when uptake is expected and increase the flux during seasons when outgassing is expected. Thus overall, regulation serves to decrease the atmospheric CO_2 sink in Hudson Bay. The expected impact of regulation on the surface flux is projected to be largest in the summer, winter, and fall (in that order). We have not been able to definitively identify the mechanism by which regulation impacts the fluxes, but regulation does have a strong influence on surface seawater salinity and stratification (limiting the availability of nutrients for biological production outside of the winter season).

Our simulation results do not yet allow us to consider how impacts of the regulation vary spatially within the bay. Observations resulting from the BaySys field program highlight pronounced spatial patterns in the surface DIC flux and other carbon system parameters, and thus a regional assessment of future regulation impacts across the bay is warranted.

3.4.6 Gaps and Recommendations

BaySys Team 4 research has advanced our understanding of marine carbon cycling in Hudson Bay and allowed us to quantify the bay's status as a CO_2 sink, in addition to its current state of ocean acidification. By doing so we have exceeded the requirements set out by our first objective. An analysis of simulations of the inorganic carbon system of Hudson Bay using the biochemical model BLING V0+DIC coupled to the 3D ocean model NEMO has provided insight into future net bay-wide carbon exchange budgets to 2070, allowing us to tease out the relative contributions of climate change and regulation on the source/sink status of Hudson Bay. We have qualified the results based on our empirical understanding of the bay's carbon cycle. By doing so we have successfully addressed the second objective of this project. Thus, the deliverables set out by our objectives have been met.

The research reported here has also raised new questions on the bay's carbon cycle that will require ongoing analysis of existing data, the acquisition of new data, and refined tools to address important knowledge gaps. On-going and proposed research will contribute to understanding the bay's carbon system, including the long-term ramifications of water regulation on carbon cycling in the bay. A detailed gap assessment of the BaySys Team 4 program has focused attention on several key areas that remain impediments toward a fuller understanding of the contemporary and future carbon system across the HBC, and thus require further work. These include:

a) BaySys research has augmented our understanding of variations in the concentration of inorganic and organic carbon in Hudson Bay rivers, and results demonstrate that river impact on the bay's carbon system is a function of the inorganic and organic carbon load, its speciation, the degradability of organic carbon, timing of delivery, biogeochemical properties of the receiving system, and mixing. Fundamental differences in the carbon load, its speciation, and impact on the marine system have been observed among rivers draining Precambrian Shield and Hudson Plains. The temporal variability (both seasonal and inter-annual) in the biogeochemistry of major rivers entering Hudson Bay is under-sampled and we are without data from several large rivers entering the bay from eastern Hudson Bay and James Bay. Elsewhere in the Arctic temporal variation in river biogeochemistry has been documented (e.g., Holmes et al., 2012, 2018; Tank et al., 2012; Rosa et al., 2012) and seven of the 10 largest rivers entering the HBC do so through James Bay (Déry et al., 2005). These omissions constitute a significant gap in our understanding of river impact on the marine carbon system on local and regional spatial scales, and across temporal scales from months to years.

b) BaySys Team 4 research focused on the marine system, where river water was considered an input. Greater focus on the land-to-sea carbon continuum and the role of carbon processing in reservoirs, river sections, and lakes on the estuarine and marine carbon system is warranted. These aquatic nodes are biogeochemical engines contributing to the downstream transport of carbon and nutrients (timing, quantity, and quality) (Cole et al., 2007; Regnier et al., 2013, Maavara et al., 2020). Organic material produced in reservoirs on the lower Nelson River, and released from permafrost-laden peatlands may be contributing to the extraordinarily high biodegradability of DOC in Nelson River water – a hypothesis that needs to be verified. Hudson Bay Lowlands contains large inventories of organic material at risk from thaw and release into the aquatic network, and there is evidence that ancient carbon is already being mobilized as DOC in some Hudson Bay river basins (Godin et al., 2017). An examination of the land-to-sea carbon continuum in northern Manitoba additionally would provide a holistic assessment of the impact of hydroelectric reservoirs on the carbon cycle through space and time. Climate change and energy policy would benefit from resulting information.

c) Related to (b), the POC in the lower reaches of the Nelson River appears sourced primarily from the local material (i.e., soils introduced by riverbank erosion and suspended sediments and resuspension of river bed sediment; Stainton, 2018). However, we don't know with any confidence the source of the DOC delivered to the bay in the river water. It may be expected that DOC sources and composition vary seasonally, but these characteristics remain unassessed. The analysis of organic carbon and major nutrients in their various forms is warranted to understand carbon source pathways, transformation processes in the rivers, present, and future supply rates, and ultimately the impact on downstream carbon systems.

d) Observations indicate that OA is already a risk in Hudson Bay deep waters, and regionally in surface waters, particularly in southeastern Hudson Bay. Modelling suggests OA will increase in Hudson Bay. Time-series studies are required to follow its progress and ecosystem impacts. Emphasis needs to be placed on year-round monitoring.

e) BaySys science has clearly shown that the major impacts of river inflow on the marine carbon system are realized close to river mouths, where river water fractions are high. Research has highlighted opposing consequences of riverine carbon on the marine system, with the resulting dilution of TA and DIC in the marine system contributing to local (sometimes severe) undersaturation in CO_2 and degradation of organic carbon supporting CO_2 oversaturation, encouraging both CO_2 emissions and, in some cases, severe aragonite under-saturation. A host of factors should impact where the relative contributions of these opposing processes are strongest, including season, river discharge, estuarine residence time and mixing dictated by tides and wind, and the presence of water column stratification associated with the regional distribution of freshwater from rivers and sea ice melt. Direct sampling of DIC, TA, and OC in river-dominated estuarine and plume environments is needed to better understand exactly how river inputs alter the carbonate system parameters of Hudson Bay. This is especially important given that river impacts have been shown to differ geographically and are likely subject to modification by climate change and, perhaps more importantly, continued hydroelectric development in the region. Further use of incubation and benchtop light exposure experiments are required to explore space and time constraints on degradation rates of organic carbon. Estuaries should be targeted so that we understand the marine response to watersheds of different underlying geology and regulation (e.g., Nelson, La Grande, Great Whale).

f) Related to (e), numerical modelling is well suited to addressing multivariate complex process interactions such as those described in points above. High-resolution modelling will benefit from heightened monitoring and process studies and should be applied to estuarine zones of the Nelson River, in James Bay, and in southeastern Hudson Bay to explore space/time impacts of river and sea ice mixing on local to regional carbon cycling and ecosystems.

g) BaySys research confirmed that Hudson Bay is a low-level carbon sink, based largely on field data and the application of remote sensing using temperature and salinity as the main drivers of pCO_2 variability across Hudson Bay over the open water season. Current and future work is focusing on the synergistic use of remote sensing and model data, combined with machine learning techniques, to develop regional estimates of sea-air CO_2 fluxes, considering both thermodynamics and biology. The outcome will be regional carbon sink estimates, with uncertainties, over the periods of available satellite data (i.e., back at least as far as 2000).

h) BLING version 0 + DIC is a reduced complexity phosphorus-based biogeochemical model that only considers the pelagic (plankton within the water column) system and not the sympagic system associated with a sea ice cover. The preliminary assessment reported here suggests that the simulated carbon system parameters are believable, but a more comprehensive assessment of BLING v0+DIC's ability to replicate pH, in addition to pCO_2 and the surface flux of DIC in Hudson Bay is warranted (and pending), including and intercomparison of results between BLING Version 0 + DIC and the BioGeoChemical Ice Incorporated Model (BiGCIIM). We have the least confidence in the ability for BLING V0+DIC to tease out impacts of regulation during the winter and early in the spring season given that sympagic processes regulating both biology and the carbon system of under-ice waters are not explicitly represented in the model. Thus, the comparison of modelled output against the more comprehensive biogeochemical model is warranted to augment our understanding of future states of Bay's carbon system during the ice-covered seasons. A continued investment of resources toward biogeochemical modelling is warranted to verify the cumulative impact of terrestrial carbon and freshwater on OA, regional ecosystems, and carbon budgets, and assess the impact of change, including land/water use and climate, on future OA states, food webs, and carbon budgets.

3.4.7 References cited

The following is a list of publications produced and cited by Teams within the BaySys project.

Ahmed, M.M.M., Else, B.G.T., Butterworth, B., Capelle, D., Guéguen, C., Miller, L.A., Meilleur, C., and Papakyriakou, T. (2021). Widespread surface water pCO2 undersaturation during ice-melt season in an Arctic continental shelf sea (Hudson Bay, Canada), *Elementa: Science of the Anthropocene*, 9(1), 00130. https://doi.org/10.1525/elementa.2020.00130.

Ahmed, M.M.M., Else, B.G.T., Capelle, D., Miller, L.A., and Papakyriakou, T. (2020). Underestimation of surface pCO2 and air-sea CO2 fluxes due to freshwater stratification in an Arctic shelf sea, Hudson Bay. *Elementa: Science of the Anthropocene*, 8(1), 084. https://doi.org/10.1525/elementa.084.

Burt, W.J., Thomas, H., Miller, L.A., Granskog, M.A., Papakyriakou, T.N., Pengelly, L. (2016). Inorganic carbon cycling and biogeochemical processes in an Arctic inland sea (Hudson Bay). *Biogeosciences*, 13(16), 4659-4671.

Capelle, D. Kuzyk, Z.A., Papakyriakou, T., Gueguen, C., Miller, L., and R. Macdonald, (2020a). Effect of terrestrial organic matter on ocean acidification and CO2 flux in an Arctic shelf sea, *Progress in Oceanography*, 185(102319). 10.1016/j.pocean.2020.102319.

Capelle, D., Kamula, M., Kuzyk, Z.A., Ahmed, M., Else, B., Miller, L.A., and Papakyriakou, T. (2020b). Do run-off and sea ice melt/brine distributions drive seasonal CO2 flux and ocean acidification in Hudson Bay. Presentation at Arctic Change 2020, ArcticNet, 7-10 December, 2020, Virtual Conference.

Castro de la Guardia, L., Garcia- Quintana, Y., Claret, M., Hu, X., Galbraith, E. D., & Myers, P.G. (2019). Assessing the role of high-frequency winds and sea ice loss on Arctic phytoplankton blooms in an ice-ocean- biogeochemical model. *Journal of Geophysical Research: Biogeosciences*, 124, 2728–2750. https://doi.org/ 10.1029/2018JG004869

Déry, S.J., Stadnyk, T.A., MacDonald, M.K., Gauli-Sharma, B., (2016). Recent trends and variability in river discharge across northern Canada. *Hydrological Earth Systems Science*. 20, 4801–4818. https://doi.org/10.5194/hess-20-4801-2016

Déry, S.J., Stadnyk, T.A., MacDonald, M.K., Koenig, K.A., Guay, C. (2018). Flow alteration impacts on Hudson Bay river discharge, *Hydrological Processes*, 32, 3576-3587. 10.1002/hyp.13285.

Godin, P., Macdonald, R.W., Kuzyk, Z.A., Goñi, M.A., Stern, G.A., (2017). Organic matter compositions of rivers draining into Hudson Bay: Present-day trends and potential as recorders of future climate change. *Journal of Geophysical Research Biogeosciences*, 122, 1848–1869. https://doi.org/10.1002/2016JG003569

Guéguen, C., Mokhtar, M., Perroud, A., McCullough, G., Papakyriakou, T., (2016). Mixing and photoreactivity of dissolved organic matter in the Nelson/Hayes estuarine system (Hudson Bay, Canada). *Journal of Marine Systems*, 161, 42–48. https://doi.org/10.1016/j.jmarsys.2016.05.005

Huyghe, S., (in prep.). Surface sediment characteristics and recent sedimentary patterns in Hudson Bay. Thesis in preparation to Department of Geological Sciences, University of Manitoba.

IPCC, (2013). Climate Change 2013: The Physical Science Basis. Contribution of Working Group I to the Fifth Assessment Report of the Intergovernmental Panel on Climate Change [Stocker, T.F., D. Qin, G.-K.

Plattner, M. Tignor, S.K. Allen, J. Boschung, A. Nauels, Y. Xia, V. Bex and P.M. Midgley (eds.)]. Cambridge University Press, Cambridge, United Kingdom and New York, NY, USA, 1535 pp.

Islam, S. (2021). Composition and transformation of dissolved organic matter in Hudson Bay, Canada. PhD Thesis. Trent University, Environmental and Life Sciences Graduate Program, September, 2021, 185 pp.

Kazmiruk, Z., Capelle, D., Kamula, M., Rysgaard, S., Papakyriakou, T., and Kuzyk, ZZ.A. (2021). High biodegradability of riverine dissolved organic carbon in late winter in Hudson Bay, Canada, *Elementa: Science of the Anthropocene*, 9(1), 00123. https://doi.org/10.1525/elementa.2020.00123

Landy, J.C., Ehn, J.K., Babb, D.G., Thériault, N., Barber, D.G. (2017). Sea ice thickness in the Eastern Canadian Arctic: Hudson Bay Complex & Baffin Bay. *Remote Sensing and Environment,* 200, 281–294. 10.1016/j.rse.2017.08.019

Lukovich, J.V., Jafarikhasragh, S., Myers, P.G., Ridenour, N., Castro de la Guardia, L., Hu, X., Grivault, N., Marson, J.M., Pennelly, C., Stroeve, J.C., Sydor, K., Wong, K., Stadnyk, T.A., Barber, D.G. (2021a). Simulated relative climate change and regulation impacts on sea ice and oceanographic conditions in the Hudson Bay Complex. *Elementa: Science of the Anthropocene,* 9(1), 00127. https://doi.org/10.1525/elementa.2020.00127

Stainton, T. (2018). Sources and transport of particulate matter in the Nelson River system, Manitoba [M.Sc. thesis]. Winnipeg, Manitoba: Department of Geological Sciences, University of Manitoba: 154 (pages).

Other Works Cited

Abril G., Borges A.V. (2005). Carbon Dioxide and Methane Emissions from Estuaries. In: Tremblay A., Varfalvy L., Roehm C., Garneau M. (eds) *Greenhouse Gas Emissions — Fluxes and Processes*. Environmental Science. Springer, Berlin, Heidelberg. https://doi.org/10.1007/978-3-540-26643-3_8

AMAP, (2018). AMAP Assessment 2018: Arctic Ocean Acidification. Arctic Monitoring and Assessment Programme (AMAP), Tromso, Norway. vi+187pp

AMAP, (2017). Snow, water, ice and parmafrost in the Arctic (SWIPA) 2017, Arctic Monitoring and Assessment Programme (AMAP), Oslo, Norway. xiv + 269 pp.

AMAP, (2013). AMAP Assessment 2013: Arctic Ocean Acidification. Arctic Monitoring and Assessment Programme (AMAP), Oslo, Norway. viii + 99 pp.

Amon, R.M.W., Rinehart, A.J., Duan, S., Louchouarn, P., Prokushkin, A., Guggenberger, G., Bauch, D., Stedmon, C., Raymond, P.A., Holmes, R.M., McClelland, J.W., Peterson, B.J.,Walker, S.A.., Zhulidov, A.V. (2012). Dissolved organic matter sources in large Arctic rivers. *Geochimica et Cosmochimica Acta* 94, 217–237.

Anctil, F., and R. Couture, (1994). Cumulative impacts of hydroelectric development on the fresh water balance in Hudson Bay, Canadian Journal of Civil Engineering, ISSN 0315-1468; ; CODEN CJCEB8; 21(2), 297-306.

Anderson L.G., Falck, E., Jones, E.P., Jutterström, S., Swift, J.H. (2004). Enhanced uptake of atmospheric CO2 during freezing of seawater: A field study in Storfjorden, Svalbard. *Journal of Geophysical Research*, 109, C06004. 10.1029/2003JC002120.

Azetsu-Scott, K., Clarke, A., Falkner, K., Hamilton, J., Jones, E.P., Lee, C., Petrie, B., Prinsenberg, S., Starr, M., Yeats, P., (2010). Calcium carbonate saturation states in the waters of the Canadian Arctic Archipelago and the Labrador Sea. *Journal of Geophysical Research*, 115, C11021. https://doi.org/10.1029/2009JC005917.

Azetsu-Scott, K., Starr, M., Mei, Z-P., and Granskog, M. (2014). Low calcium carbonate saturation states in an Arctic inland sea having large and varying fluvial inputs: The Hudson Bay system. *Journal of Geophysical Research: (Oceans)*, 119, 6210-6220. 10.1002/2014JC009948

Bates, N., and Mathis, J. (2009). The Arctic Ocean marine carbon cycle: evaluation of air-sea CO_2 exchanges, ocean acidification impacts and potential feedbacks. *Biogeosciences*, *6*, 2433–2459.

Burgers, T., Tremblay, J.-É., Else, B.G.T., and Papakyriakou, T. (2020). Estimates of net community production from multiple approaches surrounding the spring ice-edge bloom in Baffin Bay. *Elementa: Science of the Anthropocene*, 8(1), 013. https://doi.org/10.1525/elementa.013.

Burgers T.M., Miller L.A., Thomas H., Else B.G.T., Gosselin M., Papakyriakou, T. (2017). Surface water pCO_2 variations and sea-air CO_2 fluxes during summer in the eastern Canadian Arctic. *Journal of Geophysical Research (Oceans)*, 122(12), 9663-9678. 10.1002/2017JC013250

Butterworth, B.J., and Miller, S.D. (2016). Air-sea exchange of carbon dioxide in the Southern Ocean and Antarctic marginal ice zone. *Geophysical Research Letters*, *43*, 7223–7230. 10.1002/2016GL069581.

Carmack, E.C., Yamamoto-Kawai, M., Haine, T.W.N., Bacon, S., Bluhm, B.A., Lique, C., Melling, H., Polyakov, I.V., Straneo, F., Timmermans, M.L., Williams, W.J., (2016). Freshwater and its role in the Arctic Marine System: Sources, disposition, storage, export, and physical and biogeochemical consequences in the Arctic and global oceans. *Journal of Geophysical Research Biogeosciences*, 121, 675–717. https://doi.org/10.1002/2015JG003140.

Ciais, P., Sabine, C., Bala, G., Bopp, L., Brovkin, V., Canadell, J., Chhabra, A., DeFries, R., Galloway, J., Heimann, M., Jones, C., Le Quéré, C., Myneny, R.B., Piao, S., Thornton, P., (2013). Carbon and Other Biogeochemical Cycles Chapter 6. Clim. Chang. 2013 Phys. Sci. Basis. Contrib. Work. Gr. I to Fifth Assess. Rep. Intergov. Panel Clim. Chang. 465–570. https://doi.org/10.1017/CBO9781107415324.014

Deal, C.J., N. Steiner, J. Christian, J.C. Kinney, K. Denman, S. Elliott, G. Gibson, M. Jin, D. Lavoie, S. Lee, W. Lee, W. Maslowski, J. Wang and E. Watanabe, (2014). Progress and challenges in biogeochemical modelling of the Pacific Arctic Region. In: Grebmeier, J.M. and W. Maslowski (Eds.). *The Pacific Arctic Region: Ecosystem Status and Trends in a Rapidly Changing Environment*. Springer Publishing, 2014.

Deemer, B.R., Harrison, J.A., Li, S. (2016). Greenhouse gas emissions from reservoir water surfaces: a new global synthesis. *Bioscience*, 66(11), 949–964. https://doi.org/10.1093/biosci/biw117.

Déry, S.J., Mlynowski, T.J., Hernández-Henríquez, M.A., Straneo, F. (2011). Interannual variability and interdecadal trends in Hudson Bay Streamflow. *Journal of Marine Systems*, 88, 341–351. https://doi.org/10.1016/j.jmarsys.2010.12.002.

Déry, S.J., Stieglitz, M., McKenna, E.C., and Wood, E.F. (2005). Characteristics and trends of river discharge into Hudson, James, and Ungava Bays, 1964–2000. *Journal of Climate*, 18, 2540–2557, 10.1175/JCLI3440.1.

DeVries, T., (2014). The oceanic anthropogenic CO2 sink: Storage, air-sea fluxes, and transports over the industrial era. *Global Biogeochemical Cycles*, 28, 631-647. //10.1002/2013GB004739.

Dickson, A.G., Sabine, C.L., & Christian, J.R. (Eds). (2007). *Guide to best practices for ocean CO2 measurements*, PICES Special Publication 3, Sidney, BC: North Pacific Marine Science Organization.

Doney, S.C., Fabry, V.J., Feely, R.A., Kleypas, J.A., (2009). Ocean Acidification: the Other CO2 Problem. *Annual Review of Marine Science,* 1, 169–192. https://doi.org/10.1146/annurev.marine.010908.163834.

Drake, T.W., Wickland, K.P., Spencer, R.G.M., McKnight, D.M., Striegl, R.G. (2015). Ancient low–molecularweight organic acids in permafrost fuel rapid carbon dioxide production upon thaw. *Environmental Sciences,* 112, 13946–13951.

Duarte, C.M., Hendriks, I.E., Moore, T.S., Olsen, Y.S., Steckbauer, A., Ramajo, L., Carstensen, J., Trotter, J.A., McCulloch, M., (2013). Is Ocean Acidification an Open-Ocean Syndrome? Understanding Anthropogenic Impacts on Seawater pH. *Estuaries and Coasts*, 36, 221–236. https://doi.org/10.1007/s12237-013-9594-3

Else, B.G.T., Papakyriakou, T.N., Galley, R. J., Mucci, A., Gosselin, M, Miller, L. A.., Shadwick, E. H., Thomas, H. (2012). Annual cycles of pCO2 in the southeastern Beaufort Sea: New understandings of air-sea CO2 exchange in arctic polynya regions. *Journal of Geophysical Research: Oceans*, 117(C9), C00G13. http://dx.doi.org/10.1029/2011jc007346.

Eastwood, R.A., Macdonald, R.W., Ehn, J.K., Heath, J., Arragutainaq, L., Myers, P.G., Barber, D.G., Kuzyk, Z.A. (2020). Role of river runoff and sea ice brine rejection in controlling stratification throughout winter in southeast Hudson Bay. *Estuaries and Coasts*, 43, 756–786. 10.1007/s12237-020-00698-0

Else, B.G.T., Papakyriakou, T., Granskog, M. A., Yackel, J.J. (2008a). Observations of sea surface fCO2 distributions and estimated air–sea CO2 fluxes in the Hudson Bay region (Canada) during the open water season. *Journal of Geophysical Research: Oceans*, 113(C8), C08026. http://dx.doi.org/10.1029/ 2007jc004389.

Else, B.G.T., Yackel, J.J.., Papakyriakou, T. (2008b). Application of satellite remote sensing techniques for estimating air-sea CO2 fluxes in Hudson Bay, Canada during the ice-free season. *Remote Sensing of Environment,* 112(9), 3550–3562. http://dx.doi.org/10.1016/j.rse.2008.04.013.

Else, B.G.T., Galley, R.J., Papakyriakou, T.N., Miller, L.A., Mucci, A., Barber, D., (2012). Sea surface pCO2 cycles and CO2 fluxes at landfast sea ice edges in Amundsen Gulf, Canada. *Journal of Geophysical Research,* 117(12), C09010. https://doi.org/10.1029/ 2012JC007901.

Environment Canada (1978). *Water Quality Data: Manitoba 1961–1976,* Inland Waters Dir., Ottawa.

Ferland, J., Gosselin, M., Starr, M., (2011). Environmental control of summer primary production in the Hudson Bay system: The role of stratification. *Journal of Marine Systems*, 88, 385–400. https://doi.org/10.1016/j.jmarsys.2011.03.015

Fransson, A., Chierici, M., Skjelvan, I., Olsen, A., Assmy, P., Peterson, A.K., Spreen, G., and Ward B. (2017). Effects of sea ice and biogeochemical processes and storms on under-ice water fCO_2 during the winter-spring transition in the high Arctic Ocean: Implications for sea-air CO_2 fluxes: UNDER-ICE WATER fCO_2, FLUX, PROCESSES. *Journal of Geophysical Research: Oceans*, 122(7), 5566–5587. 10.1002/2016JC012478.

Friedlingstein, P., M.W. Jones, M. O'Sullivan, and 73 others, (2019). Global carbon budget, ESSD, 11 (4), 1783-1838, https://doi.org/10.5194/essd-11-1783-2019

Galbraith, E.D., and A. C. Martiny, (2015). A simple nutrient-dependence mechanism for predicting the stoichiometry of marine ecosystems, PNAS, 112, 27, 8199-8204, www.pnas.org/cgi/doi/10.1073/pnas.1423917112

Galbraith E.D., Gnanadesikan, A., Dunne, J.P., and Hiscock, M.R. (2010). Regional impacts of iron-light colimitation in a global biogeochemical model. *Biogeosciences*, 7, 1043–1064. www.biogeosciences.net/7/1043/2010/

Geilfus, N-X, Galley, R, Crabeck, O, Papakyriakou, T, Landy, J, Tison, JL, Rysgaard, S. (2015). Inorganic carbon dynamics of melt-pond-covered first-year sea ice in the Canadian Arctic. *Biogeosciences*, 12(6), 2047–2061. http://dx.doi.org/10.5194/bg-12-2047-2015.

Godin, P., Macdonald, R.W., Kuzyk, Z.A., Goñi, M.A., Stern, G.A., (2017). Organic matter compositions of rivers draining into Hudson Bay: present-day trends and potential as recorders of future climate change. *Journal of Geophysical Research: Biogeosciences*, 122, 1848–1869. https://doi.org/10.1002/2016JG003569.

Gorham, E., (1991). Northern peatlands – the role in the carbon cycle and probable responses to climatic warming, *Ecological Applications*, 1(2), 182-195. 10.2307/1941811

Granskog, M.A., Kuzyk, Z.A., Azetsu-Scott, K., Macdonald, R.W. (2011). Distributions of runoff, sea ice melt and brine using δ18O and salinity data — A new view on freshwater cycling in Hudson Bay. *Journal of Marine Sciences*, 88, 362–374. https://doi.org/10.1016/j.jmarsys.2011.03.011

Granskog, M.A., Macdonald, R.W., Kuzyk, Z.A., Senneville, S., Mundy, C.-J., Barber, D.G., Stern, G.A., Saucier, F., (2009). Coastal conduit in southwestern Hudson Bay (Canada) in summer : Rapid transit of freshwater and significant loss of colored dissolved organic matter. *Journal of Geophysical Research*, 114, 1–15. https://doi.org/10.1029/2009JC005270

Granskog, M.A., Macdonald, R.W., Mundy, C.-J., Barber, D.G., (2007). Distribution, characteristics and potential impacts of chromophoric dissolved organic matter (CDOM) in Hudson Strait and Hudson Bay, Canada. *Continental Shelf Research*, 27, 2032–2050. https://doi.org/10.1016/j.csr.2007.05.001

Guéguen, C., Granskog, M.A., McCullough, G., Barber, D.G., (2011). Characterisation of colored dissolved organic matter in Hudson Bay and Hudson Strait using parallel factor analysis. *Journal of Marine Systems*, 88, 423–433. https://doi.org/10.1016/j.jmarsys.2010.12.001

Guéguen, C., Mokhtar, M., Perroud, A., McCullough, G., Papakyriakou, T., (2016). Mixing and photoreactivity of dissolved organic matter in the Nelson/Hayes estuarine system (Hudson Bay, Canada). *Journal of Marine Systems*, 161, 42–48. https://doi.org/10.1016/j.jmarsys.2016.05.005.

Hendriks, I., Duarte, C.M., and Álvarez, M. (2010). Vulnerability of marine biodiversity to ocean acidification: a meta-analysis. *Estuary, Coastal Shelf Science*, 86, 157-164. 10.1016/j.ecss.2009.11.022

Hochheim, K.P., Barber, D.G., (2010). Atmospheric forcing of sea ice in Hudson Bay during the fall period, 1980–2005. *Journal of Geophysical Research*, 115, C05009. https://doi.org/10.1029/2009JC005334

Hochheim, K.P., Barber, D.G., Barber, D.G., (2014). An Update on the Ice Climatology of the Hudson Bay System An Update on the Ice Climatology of the Hudson Bay System. *Arctic, Antarctic, Alpine Research*, 46, 66–83.

Holmes, R.M., McClelland, J.W., Peterson, B.J., Tank, S.E., Bulygina, E., Eglinton, T.I., Gordeev, V.V., Gurtovaya, T.Y., Raymond, P.A., Repeta, D.J., Staples, R., Striegl, R.G., Zhulidov, A.V., Zimov, S.A., (2012). Seasonal and annual fluxes of nutrients and organic matter from large rivers to the Arctic Ocean and surrounding seas. *Estuaries and Coasts*, 35, 369–382. https://doi.org/10.1007/s12237-011-9386-6.

Holmes, R.M., McClelland, J.W., Tank, S.E., Spencer, R.G.M., and Shiklomanov S.I. (2018). *Arctic Great Rivers Observatory*. Water Quality Dataset, Version 20200106. Available at https://www.arcticgreatrivers.org/data.

Key, R. M., Olsen, A., van Heuven, S., Lauvset, S. K., Velo, A., Lin, X., Hoppema, M. (2015). Global Ocean Data Analysis Project, Version 2 (GLODAPv2). ORNL/CDIAC- 162, NDP-093. Carbon Dioxide Information Analysis Center, Oak Ridge National Laboratory, US Dept. of Energy, Oak Ridge, Tennessee. 10.3334/CDIAC/OTG.NDP093_GLODAPv2, 2. https://doi.org/10.3334/CDIAC/OTG.NDP093_GLODAPv2

Kuzyk, Z.A., Goñi, M.A., Stern, G.A., Macdonald, R.W. (2008). Sources, pathways and sinks of particulate organic matter in Hudson Bay: Evidence from lignin distributions. *Marine Chemistry*, 112, 215–229. https://doi.org/10.1016/j.marchem.2008.08.001

Kuzyk, Z.A., Macdonald, R.W., Johannessen, S.C., Gobeil, C., Stern, G.A. (2009). Towards a sediment and organic carbon budget for Hudson Bay. *Marine Geology*, 264, 190–208. https://doi.org/10.1016/j.margeo.2009.05.006

Kuzyk, Z.A., Macdonald, R.W., Tremblay, J.É., Stern, G.A., (2010). Elemental and stable isotopic constraints on river influence and patterns of nitrogen cycling and biological productivity in Hudson Bay. *Continental Shelf Research*, 30, 163–176. https://doi.org/10.1016/j.csr.2009.10.014

Landy, J.C., Ehn, J.K., Babb, D.G., Theriault, N., Barber, D.G. (2017). Sea ice thickness in the Eastern Canadian Arctic: Hudson Bay Complex and Baffin Bay. *Remote Sensing of Environment*, 200, 281–294. http://dx.doi.org/10.1016/j.rse.2017.08.019.

Lansard, B.A., Mucci, A., Miller, L.A., Macdonald, R.W., Gratton, Y. (2012). Seasonal variability of water mass distribution in the southeastern Beaufort Sea determined by total alkalinity and delta O-18, *Journal of Geophysical Research: Oceans*, 117, C03003. 10.1029/2011JC007299

Lapierre, J-F., Guillemette, F., Berggren, M., Giorgio, P.A. (2013). Increases in terrestrially derived carbon stimulate organic carbon processing and CO2 emissions in boreal aquatic ecosystems. *Nature*, 4, 3972.

Lauvset, S.K., Key, R.M., Olsen, A., Heuven, S. Van, Velo, A., Lin, X., Jutterström, S. (2016). A new global interior ocean mapped climatology : the 1 ◦ × 1 ◦ GLODAP version 2. 325–340. https://doi.org/10.5194/essd-8-325-2016

Maavera, T., Akbarzadeh, Z., and Van Cappelen, P. (2020a). Global dam-driven changes to riverine N:P:Si ratios delivered to the coastal ocean, *Geophysical Research Letters*, 47, e2020GL088288.https://doi.org/10.1029/2020GL088288.

Maavera, T., Chen, Q., Van Meter, K., Brown, L.E., Zhang, J., Ni, J., and Zarfl, C. (2020b). River dam impacts on biogeochemical cycling. *Nature Reivews: Earth & Enviornment*, 1, 103-116, https://doi.org/10.1038/s43017-019-0019-0.

MacGilchrist GA, Garabato ACN, Tsubouchi T, Bacon S, Torres-Valdés S, Azetsu-Scott K. (2014). The Arctic Ocean carbon sink. *Deep Research Part I*, 86, 39–55. 10.1016/j.dsr.2014.01.002

Manizza, M., Follows, M.J., Dutkiewicz, S., Menemenlis, D., Hill, C.N., Key, R.M., (2013). Changes in the Arctic Ocean CO_2 sink (1996-2007): A regional model analysis. *Global Biogeochemistry: Cycles*, 27, 1108–1118. https://doi.org/10.1002/2012GB004491

Mann, P.J., Davydova, A., Zimov, N., Spencer, R.G.M., Davydov, S., Bulygina, E., Zimov, S., Holmes, R.M., (2012). Controls on the composition and lability of dissolved organic matter in Siberia's Kolyma River basin. *Journal of Geophysical Research: Biogeosciences*, 117, 1–15. https://doi.org/10.1029/2011JG001798.

Mathis, J.T., R.S. and 15 others (2012). Storm-induced upwelling of high pCO_2 waters onto the continental shelf of the western Arctic Ocean and implications for carbonate mineral saturation states. *Geophysical Research Letters*, 39, 10.1029/2012GL051574.

Meire, L., Søgaard, D.H., Mortensen, J., Meysman, F.J.R., Soetaert, K., Arendt, K.E., Juul-Pedersen, T., Blicher, M.E., and Rysgaard, S. (2015). Glacial meltwater and primary production are drivers of strong CO2 uptake in fjord and coastal waters adjacent to the Greenland Ice Sheet. *Biogeosciences*, 12, 2347–2363. 10.5194/bg-12-2347-2015

Meybeck, M., and Ragu, A. (1995). River discharges to the oceans: An assessment of suspended solids, major ions and nutrients, report, U. N. Envrionment Programme, Geneva, Switzerland.

Miller, L.A., Papakyriakou, T., Collins, R.E., Deming, J.W., Ehn, J.K., Macdonald, R.W., Mucci, A., Owens, O., Raudsepp, M., and Sutherland, N. (2011). Carbon dynamics in sea ice: A winter flux time series. *Journal of Geophysical Research: Oceans*, 116, 1-20. 10.1029/2009JC006058

Müller, O., Seuthe, L., Bratbak, G., Paulsen, M.L. (2018). Bacterial response to permafrost derived organic matter input in an Arctic Fjord. *Frontiers in Marine Science* 5, 263.

Mundy, C.J., Gosselin, M., Starr, M., Michel, C., (2010). Riverine export and the effects of circulation on dissolved organic carbon in the Hudson Bay system, Canada. *Liminomolgy and Oceanography*, 55, 315–323. https://doi.org/10.4319/lo.2010.55.1.0315

NASA (2019). Physical Oceanographic Distributed Active Archive Centrer, Jet Propulsion Laboratory, California Institute of Technology, https://podaac.jpl.nasa.gov/dataset/MODIS_AQUA_L3_SST_THERMAL_MONTHLY_4KM_DAYTIME_V2019.0).

Niemi, A., Bednaršek, N., Michel, C., Feely, R., Williams, W., Azetsu-Scott, K., Wulkusz, W., and Reist J.D. (2021). Biological impact of ocean acidification in the Canadian Arctic: Widespread severe pteropond shell dissolution in Amundsen Gulf. *Frontier Marine Sciences*, 8, 600184. 10.3389/fmars.2021.600184.

Olsen, A., Key, R.M., Heuven, S., Van, Lauvset, S.K., Velo, A., Lin, X., Jutterström, S. (2016). The Global Ocean Data Analysis Project version 2 (GLODAPv2) – an internally consistent data product for the world ocean. 297–323. https://doi.org/10.5194/essd-8-297-2016

Östlund, H.G., and Hut, G. (1984). Arctic Ocean water mass balance from isotope data, 89, NC4, 6373-6381. 10.1029/JC089iC04p06373

Pierrot D, Neill C, Sullivan K, Castle R, Wanninkhof R, Lüger H, Johannessen T, Olsen A, Feely RA, Cosca CE. (2009). Recommendations for autonomous underway pCO2 measuring systems and data-reduction routines. *Deep Research Part II*, 56, 512–522. 10.1016/j.dsr2.2008.12.005

Pierrot, D.E.L., and Wallace, D.W.R. (2006). MS Excel Program Developed for CO2 System Calculations. ORNL/CDIAC-105a. Carbon Dioxide Information Analysis Center, Oak Ridge National Laboratory, U.S. Department of Energy, Oak Ridge, Tennessee.

Prinsenberg, S.J. (1988). Ice-cover and ice-ridge contributions to the freshwater contents of Hudson Bay and Foxe Basin. *Arctic*, 41(1), 6– 11.

Prinsenberg, S.J. (1984). Freshwater contents and heat budgets of James Bay and Hudson Bay. *Continental Shelf Research*, 3(2) 191-200. 10.1016/0278-4343(84)90007-4

Regnier, P., Friedlingstein, P., Ciais, P. (2013). Anthropogenic perturbation of the carbon fluxes from land to ocean. *Nature Geoscience*, 6, 597-607.

Rivkin, R.B., and Legendre, L. (2001). Biogenic carbon cycling in the upper ocean: Effects of microbial respiration. *Science* 291, 2398–400.

Rosa, E., Gaillardet, J., Hillaire-Marcel, C., Hélie, J.-F., Richard, L.-F. (2012). Rock denudation rates and organic carbon exports along a latitudinal gradient in the Hudson, James, and Ungava bays watershed. *Canadian Journal of Earth Sciences*, 49, 742–757. https://doi.org/10.1139/e2012-021

Rysgaard, S., Glud, R.N., Sejr, M., Bendtsen, J., Christensen, P. (2007). Inorganic carbon transport during sea ice growth and decay: A carbon pump in polar seas. *Journal of Geophysical Research: Oceans*, 112(C3). http://dx.doi.org/10.1029/2006jc003572.

Semiletov, I., Pipko, I., Gustafsson, Ö., Anderson, L.G., Sergienko, V., Pugach, S., Dudarev, O., Charkin, A., Gukov, A., Bröder, L., Andersson, A., Spivak, E., and Shakhova, N. (2016). Acidificaiton of East Siberian Arctic Shelf waters through addition of freshwater and terrestrial carbon. *Nature Geoscience*, 10.1038/NEGO2695.

Shadwick, E.H., Thomas, H., Chierici, M., Else, B., Fransson, A., Michel, C., Miller, L.A., Mucci, A., Niemi, A., Papakyriakou, T.N., and Tremblay, J.-É. (2011). Seasonal variability of the inorganic carbon system in the Amundsen Gulf region of the Southeastern Beaufort Sea. *Limnology and Oceanography*, 56(1), 303-322.

Sibert, V., Zakardjian, B., Saucier, F., Gosselin, M., Starr, M., Senneville, S. (2010). Spatial and temporal variability of ice algal production in a 3D ice-ocean model of the Hudson Bay, Hudson Strait, and Foxe Basin system. *Polar Research*, 29(3), 353-378. 10.1111/j.1751-8369.2010.00184.x

Sibert, V., Zakardjian, B., Gosselin, M., Starr, M., Senneville, S., LeClainche, Y., (2011). 3D bio-physical model of the sympagic and planktonic productions in the Hudson Bay system. *Journal of Marine Systems*, 88, 401–422. https://doi.org/10.1016/j.jmarsys.2011.03.014

Sipler, R.E., Baer, S.E., Connelly, T.L., Frisher, M.E., Roberts, Q.N., Yager, P.L., and Bronk, D.A. (2017a). Chemical and photophysiological impact of terrestrially-derived dissolved organic matter on nitrate uptake in the coastal western Arctic. *Limnology and Oceanography*, 62, 1881-1894. 10.1002/lno.10541.

Sipler, R.E., Kellogg, C.T.E., Connelly, T.L., Frisher, M.E., Roberts, Q.N., Yager P.L., and Bronk, D.A. (2017b). Microbial community response to terrestrially derived dissolved organic matter in the coastal Arctic. *Frontiers in Microbiology*, 8, 1018. 10.3389/fmicb.2017.01018.

Spencer, R.G.M., Mann, P.J., Dittmar, T., Eglinton, T.I., McIntyre, C., Holmes, R.M., Zimov, N., A. Stubbins, (2015). Detecting the signature of permafrost thaw in Arctic rivers. *Geophysical Research Letters*, 42, 2830–2835.

Spreen, G, Kaleschke, L., and Heygster, G. (2008). Sea ice remote sensing using AMSR-E 89-GHz channels. *Journal of Geophysical Research: Oceans*, 113(C2), C02S03. http://dx.doi.org/10.1029/2005jc003384.

Stull, R.B. (1988). *An introduction to boundary layer meteorology*. Dordrecht, the Netherlands: Springer: 666. http://dx.doi.org/10.1007/978-94-009-3027-8_1.

Takahashi, T, Sutherland, S.C., Wanninkhof, R., Sweeney, C., Feely, R.A., Chipman, D.W., Hales, B., Friederich G., Chavez, F., Sabine, C. (2009). Climatological mean and decadal change in surface ocean pCO2, and net sea–air CO2 flux over the global oceans. *Deep Sea Research Part II: Topical Studies in Oceanography*, 56(8–10), 554–577. http://dx.doi.org/10.1016/s0967-0645(02)00003-6.

Takahashi, T., Olafsson, J., Goddard, J.G., Chipman, D.W., and Sutherland, S.C. (1993). Seasonal variation of CO_2 and nutrients in the high-latitude surface oceans: A comparative study. *Global Biogeochemical Cycles*, *7*(4), 843–878. 10.1029/93GB02263.

Tank S.E., Raymond P.A., Striegl R.G., McClelland J.W., Holmes R.M., Fiske G.J. and Peterson B.J. (2012). A land-to-ocean perspective on the magnitude, source and implication of DIC flux from major Arctic rivers to the Arctic Ocean. *Global Biogeochemical Cycles*, 26, GB4018

Teodoru, C., Bastien, J., Bonneville, M.C. (2012). The net carbon footprint of a newly created boreal hydroelectric reservoir. *Global Biogeochemical Cycles*, 26, GB2016. 10.1029/2011GB004187.

Vonk, J.E., Tank, S.E., Bowden, W.B., Laurion, I., Vincent, W.F., Alekseychik, P., Amyot, M., Billet, M.F., Canário, J., Cory, R.M., Deshpande, B.N., Helbig, M., Jammet, M., Karlsson, J., Larouche, J., MacMillan, G., Rautio, M., Walter Anthony, K.M., Wickland, K.P., (2015). Reviews and syntheses: effects of permafrost thaw on Arctic aquatic ecosystems. *Biogeosciences*, 12, 7129–7167. https://doi.org/10.5194/bg-12-7129-2015.

Wanninkhof, R. (2014). Relationship between wind speed and gas exchange over the ocean revisited, *Liminology Oceanographic Methods*, *12*, 351–362. 10.1029/92JC00188.

Weiss, R.F. (1974). Carbon dioxide in water and seawater: the solubility of a non-ideal gas. *Marine Chemistry, 2*(3), 203–215. 10.1016/0304-4203(74)90015-2.

Ward, C.P., and Cory, R.M. (2015). Chemical composition of dissolved organic matter draining permafrost soils. *Geochimica et Cosmochimica Acta*, 167, 63–79.

Weiss, R.F. (1974). Carbon dioxide in water and seawater: The solubility of a non-ideal gas. *Marine Chemistry*, 2(3), 203–215. http://dx.doi.org/10.1016/0304-4203(74)90015-2.

Weiss R.F. and Price, B.A. (1980). Nitrous oxide solubility in water and seawater. *Marine Chemistr*y, 8 (4), 347-359. https://doi.org/10.1016/0304-4203(80)90024-9.

Yager P.L., Wallace, D.W.R., Johnson, K.M., Smith Jr, W.O., Minnett, P.J., Deming, J.W. (1995). The Northeast Water Polynya as an atmospheric CO2 sink: A seasonal rectification hypothesis. *Journal of Geophysical Research*, 100(C3), 4389–98.

Yasunaka S, Siswanto E, Olsen A, Hoppema M, Watanabe E, Fransson A, Chierici M, Murata A, Lauvset SK, Wanninkhof R, et al. (2018). Arctic Ocean CO2 uptake: An improved multiyear estimate of the air-sea CO_2 flux incorporating chlorophyll a concentrations. *Biogeosciences*, 15(6), 1643–1661. 10.5194/bg-15-1643-2018

Zeebe, R.E., and Wolfe-Gladrow, D. (2001). CO2 in Seawater: Equilibrium, Kinetics, Isotopes. *Elsevier Oceanography Series*, 65, 360.

3.5 Contaminants (Team 5)

Team Member	Affiliation	Tasks contributed to			Role
Feiyue Wang	*a*	*5.1*	*5.2*	*5.3*	*Science Lead*
Allison Zacharias	*b*	*5.1*	*5.2*	*5.3*	*Hydro Lead*
Sarah Wakelin	*b*	*5.1*	*5.2*	*5.3*	*Hydro Lead*
Zou Zou Kuzyk	*a*	*5.1*	*5.2*	*5.3*	*Contributor*
David Lobb	*c*	*5.1*	*5.2*	*5.3*	*Contributor*
Philip Owens	*d*	*5.1*	*5.2*	*5.3*	*Contributor*
Ellen Pettigrew	*d*	*5.1*	*5.2*	*5.3*	*Contributor*
Robbie Macdonald	*e*	*5.1*	*5.2*	*5.3*	*Contributor*
Gary Stern	*a*	*5.1*	*5.2*	*5.3*	*Contributor*
Kathleen Munson	*a*	*5.1*	*5.2*	*5.3*	*Contributor*
Masoud Goharrokhi	*c*	*5.1*	*5.2*	*5.3*	*Contributor*
Tassia Stainton	*a*	*5.1*	*5.2*	*5.3*	*Contributor*
James Singer	*a*	*5.1*	*5.2*	*5.3*	*Contributor*
Samantha Huyghe	*a*	*5.1*	*5.2*	*5.3*	*Contributor*
Zakhar Kazmiruk	*a*	*5.1*	*5.2*	*5.3*	*Contributor*
Aaron Desilet	*c*	*5.1*	*5.2*	*5.3*	*Contributor*
Elise Kazmierczak	*a*	*5.1*	*5.2*	*5.3*	*Contributor*
Brendan Brooks	*a*	*5.1*	*5.2*	*5.3*	*Contributor*
Saad Hamdo	*a*	*5.1*	*5.2*	*5.3*	*Contributor*
Hoda Pahlavan	*c*	*5.1*	*5.2*	*5.3*	*Contributor*
Debbie Armstrong	*a*	*5.1*	*5.2*	*5.3*	*Technician*
Mary O'Brien	*e*	*5.1*	*5.2*	*5.3*	*Technician*
Michelle Kamula	*a*	*5.1*	*5.2*	*5.3*	*Technician*
Shiva Lashkari	*a*	*5.1*	*5.2*	*5.3*	*Technician*
Ainsleigh Loria	*a*	*5.1*	*5.2*	*5.3*	*Technician*
Jiang Liu	*a*	*5.1*	*5.2*	*5.3*	*Collaborator*
Zhiyuan (Jeff) Gao	*a*	*5.1*	*5.2*	*5.3*	*Collaborator*

a) Centre for Earth Observation Science, University of Manitoba, Winnipeg, Manitoba, Canada.
b) Manitoba Hydro, Winnipeg, Manitoba, Canada.
c) Department of Soil Science, University of Manitoba, Winnipeg, Manitoba, Canada.
d) University of Northern British Columbia, British Columbia, Canada.
e) Fisheries and Ocean Canada.

3.5.1 Introduction and Objective

The objective of Team 5 was to determine the relative impact of hydroelectric regulation and climate change on the cycling of mercury (Hg) in the Hudson Bay system including the lower Nelson River Basin (LNRB). As stated in the project proposal, Team 5 focuses on Hg because of the historical elevation in fish Hg concentrations following waterbody impoundment in the region, which brought in a large influx of freshly flooded, labile organic matter that fueled microbial methylation of inorganic Hg. Mercury is present in the environment in various chemical forms. Where appropriate, the main emphasis of Team 5 was methylmercury (MeHg), as MeHg is the bioaccumulating and biomagnifying form of Hg in both freshwater and marine food webs.

Previously published research, funded in part by ArcticNet and Manitoba Hydro, has measured various forms of Hg in Hudson Bay and its watershed: Total Hg (THg, the sum of all chemical forms of Hg) was measured throughout Hudson Bay and in many of the river outlets into the bay by researchers from the University of Manitoba (Hare et al., 2008, 2010). This work produced the first mass budget of total Hg in the system (Hare et al., 2008, 2010), which identified sediment resuspension within Hudson Bay (Hare et al., 2008; Kuzyk et al., 2009) as a previously unrecognized source of total Hg to the bay. However, the distribution of total Hg does not enable future projections of human exposure to Hg since humans are exposed to MeHg primarily through food web biomagnification.

Mercury speciation measurements, which included gaseous elemental Hg, dimethyl Hg, monomethyl Hg (the sum of the later two chemical forms of Hg are analytically defined MeHg in our studies), and total Hg were measured in Hudson Bay seawater from three depths per station by researchers from the University of Alberta (Kirk & St. Louis, 2009). However, the limited depth resolution precluded a full evaluation of sources, sinks, or internal cycling of MeHg in the bay.

Building on these previous studies, BaySys Team 5 focused on addressing major knowledge gaps of MeHg cycling in Hudson Bay and LNRB. Based on changing freshwater inputs into the bay from hydroelectric regulation and climate-induced changes in the bay watershed, we aimed to determine the past, current, and future sources and sinks of MeHg. We also investigated how organic matter, including resuspended sediment, controls MeHg production.

The hypotheses of BaySys Team 5 were focused on three known processes in MeHg production in similar freshwater and marine systems (Figure 3.5.1). These include 1) impoundment of rivers in boreal regions which is known to stimulate sediment production of MeHg and transfer it into the water column where it enters the food web (Hall et al., 2005; St. Louis et al., 2004); 2) Estuarine and marine sediments (Hammerschmidt & Fitzgerald, 2006), which could be a dominate MeHg source in shallow systems such as Hudson Bay; and 3) sub-surface seawater (Lehnherr et al., 2011; Wang et al., 2012, 2018), which can be elevated in MeHg due to processes that may be associated with the breakdown of organic matter (Sunderland et al., 2009; Wang et al., 2012).

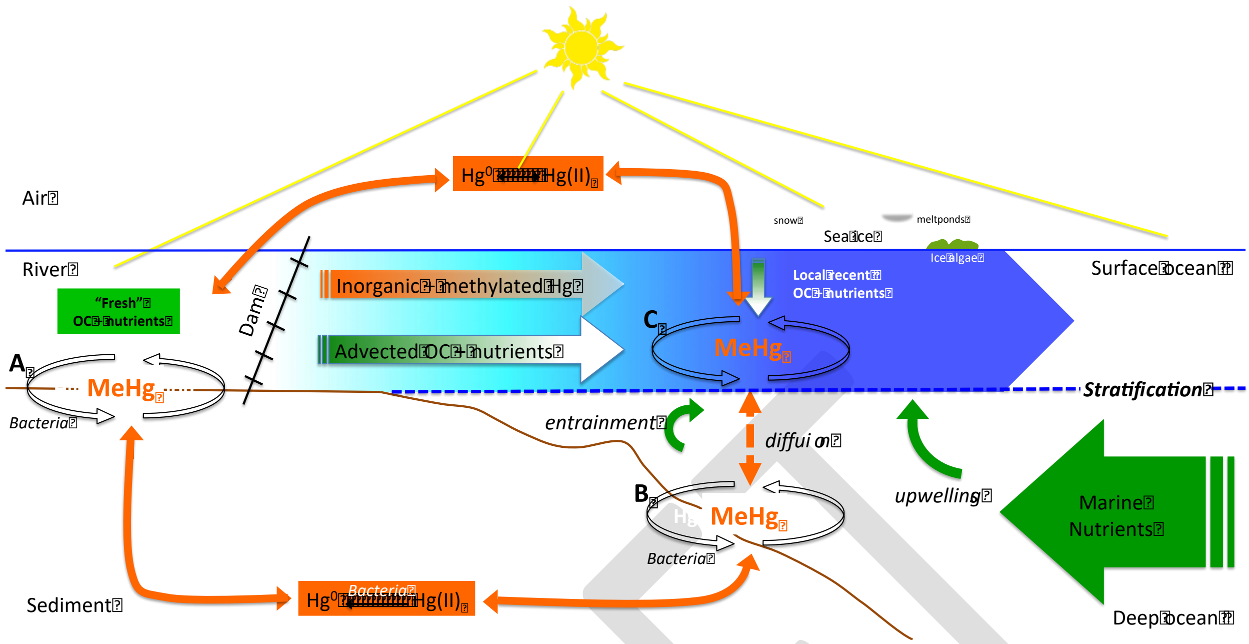

FIGURE 3.5.1 Schematic view of freshwater-marine coupling showing the production of methylmercury in hydroelectrically regulated water bodies (A), estuarine sediment (B), and sub-surface seawater (C). Hg: mercury; Hg^0: elemental mercury; Hg(II): divalent mercury; MeHg: methylmercury; OC: organic carbon.

Regardless of which of the above processes dominate MeHg production, results from previous studies suggest that Hg methylation and hence uptake into the food web is associated with organic matter cycling. Thus, Team 5's primary hypothesis (H5.1) posed that:

> **H5.1:** Organic matter is the primary control over Hg methylation in the water column and sediments.

To further investigate the role of organic matter in MeHg production specifically in regard to the Hudson Bay system, Team 5's second hypothesis (H5.2) posed that:

> **H5.2:** Suspended sediments in Hudson Bay have multiple sources (e.g., erosion and runoff from land surfaces within the watershed, erosion of the banks and beds of the rivers and estuaries of the bay, erosion of the bay's coastline, resuspension of sediments within the bay, as well as organic material produced within the bay), which affect their role in the transport and methylation of Hg and will respond differently to climate change.

The potential for links between organic matter cycling and MeHg production to influence human exposure to Hg served as the central focus of our final hypothesis (H5.3), which posed that:

> **H5.3:** Flooding and changing climate are playing an increasingly important role in Hg accumulation at the base of the Hudson Bay marine and coastal food webs.

3.5.2 Analysis and Methods

Team 5 research included both critical reviews of historical fish Hg data in the region, as well as obtaining new data from the BaySys field research program. The historical fish Hg data Team 5 reviewed include:

- Commercial and monitoring collection surveys;
- The Coordinated Aquatic Monitoring Program (CAMP) which is a joint program between Manitoba Hydro and the Government of Manitoba; and,
- Aquatic studies for Manitoba Hydro's Wuskwatim (constructed), Keeyask (under construction), and Conawapa (environmental assessment initiated but the project has been deferred) generating stations.

The BaySys field research campaigns Team 5 participated in include:

- Northern Manitoba/CAMP sampling campaigns 2016–2017 (winter and summer): Hg and organic and inorganic matter in water column and sediments;
- BaySys mooring program cruise 2016: organic and inorganic matter (no Hg due to lack of clean sampling capacity);
- Churchill River and mobile ice survey 2017: Hg, carbon sampling in collaboration with Team 4;
- Nelson Estuary landfast ice survey 2017: Hg, carbon sampling in collaboration with Team 4;
- BaySys mooring program cruise 2017: retrieval of sediment traps material for Hg and organic and inorganic matter analysis; and,
- BaySys bay-wide survey cruise 2018: Hg, organic and inorganic matter.

Total Hg and MeHg mass balance models are being constructed to determine the balance between sources and sinks within Hudson Bay as a reservoir by better constraining sources of MeHg to Hudson Bay and losses of MeHg from the bay. While the construction of the MeHg mass balance is the Task 5.3 deliverable, Tasks 5.1 and 5.2 inform our understanding of both the mass balance inputs and outputs as well as the internal MeHg processing within the bay that are essential for mass balance construction.

Between BaySys Teams 4 and 5, we are using the watershed and estuary campaigns to constrain the riverine inputs of total Hg and MeHg, organic and inorganic matter during winter (Churchill and Nanuk winter campaigns) and spring/summer (CAMP system sampling; 2016, 2017, and 2018 cruises) and previously unpublished work (A. Hare 2005–2010; G. McCullough 2005–2010; ArcticNet 2010). These seasonal campaign data are being evaluated to understand the inputs of Hg and organic and inorganic matter from rivers, through estuaries, and persistence into the bay.

We are also constraining the sediment burial of MeHg and organic matter from sediment cores collected during the bay-wide cruises (2016, 2018) and the sediment trap material (2017, 2018 cruises) as well as archived samples from James Bay and southwest Hudson Bay (Z. Z. Kuzyk).

Bay-wide cruise sediment core collection included both coastal and basin sites including offshore from Chesterfield Inlet and the Nelson River that can be used to estimate offshore transport and resuspension of riverine inputs.

The transport of Hg and MeHg across the river-estuary-marine gradient helps us characterize the major MeHg sources needed for the mass balance, while the sediment data allow us to evaluate the major MeHg sinks in the mass balance. Ongoing quantification of MeHg in zooplankton and benthic invertebrates will also help constrain the MeHg sinks in the mass balance and contribute directly to our evaluation of H5.3. The evaluation of the organic matter in sediment and sediment trap material will help revise the carbon mass balance for Hudson Bay (Kuzyk et al., 2009) in collaboration with Team 4 and addresses Task 5.2. The comparison between MeHg, both in magnitude and as the % of total Hg present, and inorganic and organic matter properties will address Task 5.1.

3.5.3 Results and Discussion

Team 5 presents the results of their analyses following three tasks that were established at the onset of the BaySys project and discusses them within the greater context of the Team's objectives, and the overarching project.

> ***Task 5.1: Relationship between Hg methylation and organic matter remineralization –*** to determine how Hg methylation responds to changes in organic matter remineralization.
>
> ***Task 5.2: Suspended sediment and organic matter fingerprinting –*** to assess the sources of organic matter and suspended sediment within the LNRB, its estuary, and Hudson Bay using traditional (surveys and budgets) and fingerprinting techniques.
>
> ***Task 5.3: Mass balance modelling of methyl Hg in Hudson Bay –*** to develop a MeHg mass budget for the Hudson Bay.

Relationship between mercury methylation and organic matter remineralization (Task 5.1)

The relationship between Hg methylation and organic matter remineralization was investigated at all the three potential MeHg "hotspots": rivers and lakes, estuaries, and Hudson Bay seawater (see Figure 3.5.1).

Rivers and Lakes

Past-, present-day, and future Hg methylation potentials were studied by a suite of techniques involving long-term fish Hg trend analysis and laboratory soil incubation experiments.

<u>Fish mercury trend analysis:</u> Long-term temporal trends (1972–2018) in fish muscle Hg concentrations were analyzed for 55 waterbodies that are ("on-system") or are not ("off-system") influenced by hydroelectric regulation (Figure 3.5.2) (Munson et al., in review). The data set examined includes a total of 34,617 individual muscle Hg measurements for Lake Whitefish, Northern Pike, and Walleye from historical and current monitoring programs, such as those from commercial and monitoring collection surveys, the CAMP program, and from aquatic studies as

part of the assessment of the Wuskwatim, Keeyask, and Conawapa (deferred) generating stations. Multiple linear regression models show a decreasing trend in fish Hg from the 36 on-system waterbodies between 1992–2018, confirming long-term recovery nearly 50 years following initial impoundment. A slightly decreasing trend is also detected in fish Hg from the 19 off-system waterbodies over the same period, consistent with declining atmospheric Hg emissions in the region.

Despite the general decreases, significant increases in fish Hg were observed intermittently over the past two decades in most of the on-system and off-system waterbodies subject to recent monitoring. Length-standardized fish Hg concentrations increased by up to 100 % in Northern Pike and up to 175% in Walleye between 2001–2010, reaching 0.79 μg g^{-1} in some of the water bodies over the most recent decade (2010–2018) (Figure 3.5.3). These recent increases in fish Hg appear to follow a similar pattern observed in recent decades from hydroelectric reservoirs in northern Québec, Canada (Bilodeau et al., 2017), and cannot be explained by atmospheric emissions which are generally decreasing in the region and North America. To investigate whether the observed secondary increases in fish Hg can be attributed to subsequent pulses in Hg methylation caused by dry/wet cycles following initial impoundment, we calculated monthly and annual water level anomalies based on the difference between measured values and mean historical water level data set values for off-system lakes and mean post-impoundment water level data set values for on-system waterbodies. Neither water level anomalies nor the surface area proxy indicated that water level was the primary control on fish Hg during long-term recovery from impoundment, perhaps due to the small water level anomalies in the on-system waterbodies compared to that off-system.

Instead, available water quality data indicated water chemistry effects on fish Hg. We found a significant negative relationship between fish Hg and surface water pH and total Kjeldahl nitrogen (TKN) (Figure 3.5.4) for both Northern Pike and Walleye for all waterbodies during years that spanned the ~2010 increases in fish Hg. The pH of lake water can influence Hg speciation and MeHg production, whereas the relationship between fish Hg and TKN suggests some trophic control over regional fish Hg concentrations. The lack of historical carbon or nitrogen isotope data prevented us from evaluating internal processes behind the fish Hg and TKN relationship, but it is known that invasive species such as rainbow smelt have been established in the Nelson River region water bodies since the 1990s, which could serve as a potential modulator of fish Hg, as has recently been suggested for Walleye in Lake Winnipeg (Jansen, 2021). Water quality changes in these water bodies are expected to accelerate, as the region's widespread distribution of continuous, discontinuous, and sporadic permafrost is particularly sensitive to a warming climate.

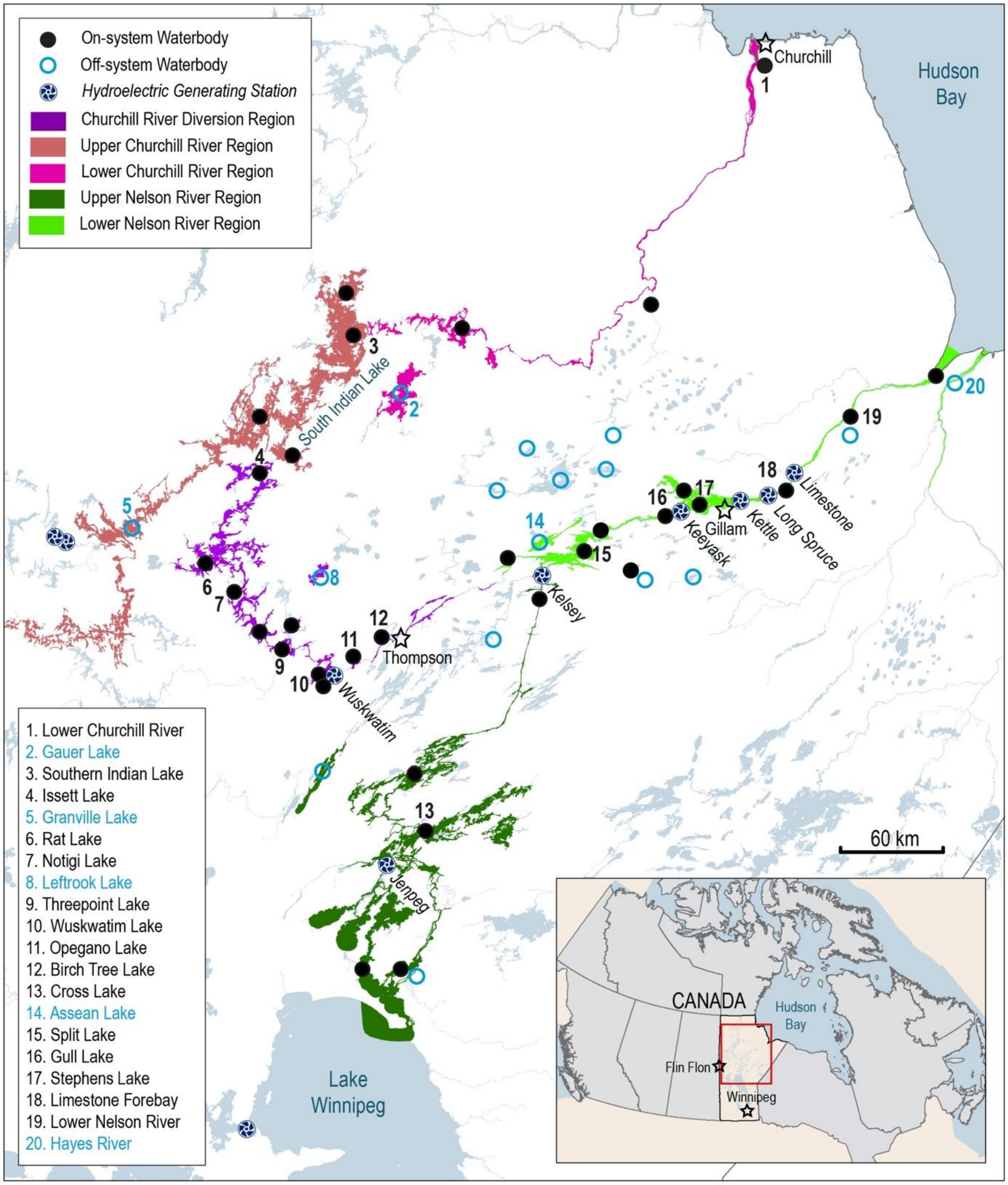

FIGURE 3.5.2 Map of the on-system (black circles) and off-system (blue circles) waterbodies in Northern Manitoba where temporal trends of fish mercury between 1972–2018 were analyzed. Those numbered are water bodies where fish mercury was monitored at least three times since 2000. The base map was created by Manitoba Hydro with data from Manitoba Hydro, the Government of Manitoba, and the Government of Canada (Munson et al., in review).

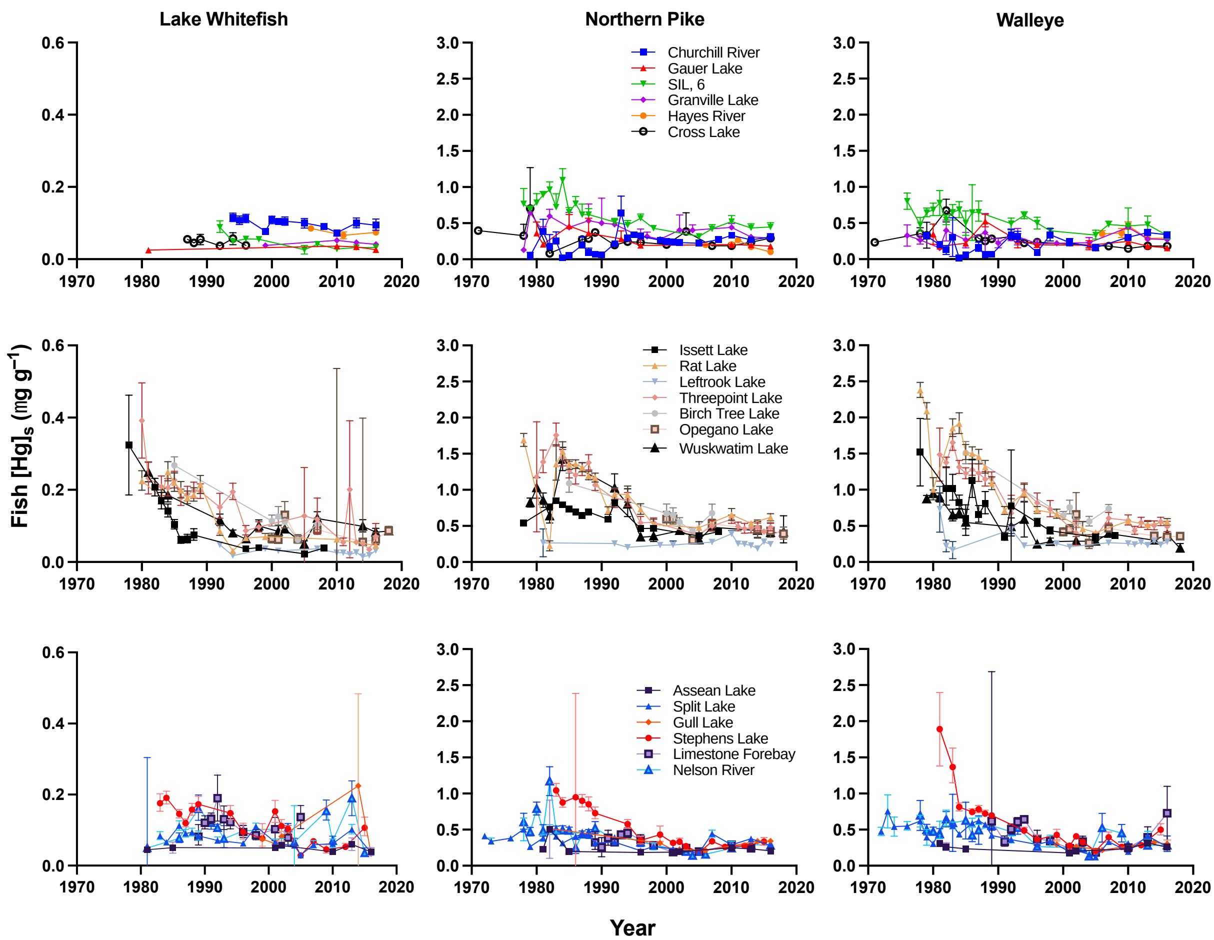

FIGURE 3.5.3 Time series of northern Manitoba length-standardized mean annual fish mercury concentrations ($[Hg]_s$) for Lake Whitefish (left panels), Northern Pike (center panels), and Walleye (right panels). The top panels are the Churchill River region as well as the Hayes River and Cross Lake. Middle panels are the water bodies in the Churchill River Diversion region. Bottom panels are water bodies in the Nelson River. Error bars represent 95 % confidence intervals around calculated mean (Munson et al., in review).

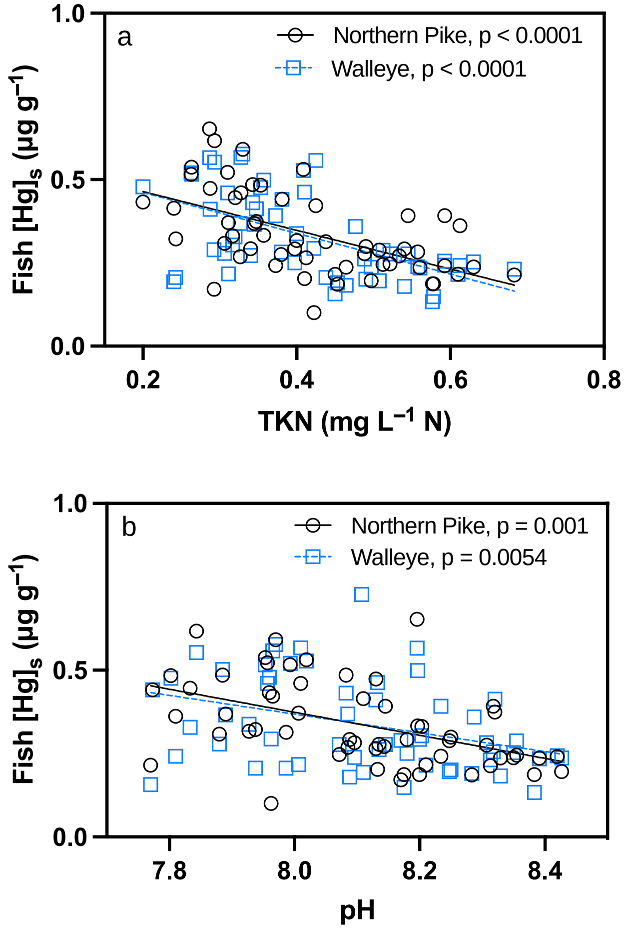

FIGURE 3.5.4 Least-squares regression of length-standardized mean fish mercury concentrations ($[Hg]_s$) for Northern Pike (open circles) and Walleye (open squares) against surface water a) total Kjeldahl nitrogen (TKN, n = 63), and b) pH (n = 64) between 2009–2016. Solid lines indicate linear regression for Northern Pike and dashed lines for Walleye (Munson et al., in review).

<u>Soil incubation study for future mercury methylation potential:</u> Samples from the BaySys/CAMP waterbody sampling between 2016-2017 were used to determine watershed links between Hg and organic matter and its influence on Hudson Bay. An incubation study was carried out with nearshore topsoils that have been periodically submerged in water and offshore topsoils that are 10–20 m farther inland (Singer, 2020). The soils were collected from two on-system lakes (Stephens Lake and Split Lake) and one off-system lake (Assean Lake). The soils were flooded in the laboratory with natural water from the LNRB and incubated for 196 hours to measure MeHg and associated variables in soil, porewater, and overlying water. MeHg production and transfer to overlying water were observed within days of flooding with soils from both on-system and off-system waterbodies, with the highest MeHg concentrations found in the flooded nearshore soil of Stephens Lake (Singer, 2020) (Figure 3.5.5). This suggests that ongoing water level fluctuations in the Nelson River System can change MeHg concentrations within the watershed, supporting **H5.1** within the Nelson River watershed.

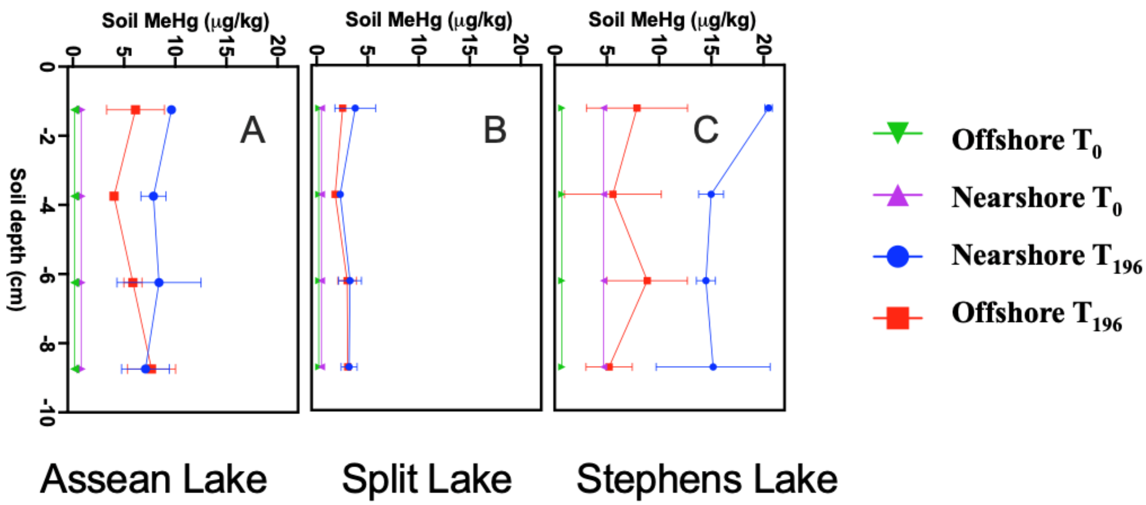

FIGURE 3.5.5 Vertical distribution profiles of methylmercury (MeHg) in the flooded soil from Assean, Split, and Stephens Lakes throughout the 196-hour flooding incubation (Singer, 2020). Initial concentrations (T_0) are uniform throughout the 10 cm depth of homogenized soil from both offshore (green triangles) and nearshore (purple triangles) samples. At the end of the incubation (T_{196}), offshore (red squares) MeHg were lower than nearshore (blue circles) samples. The error bars represent one standard deviation between duplicate experiments.

Estuaries

Estuaries may be sources or sinks for MeHg depending on its association with particulate matter and the fate of that material (degradation, deposition, or export). Despite local deposition of particulate-bound MeHg within the Nelson River system, MeHg associated with dissolved organic matter still can enter Hudson Bay. This could occur due to particulate matter degradation within the watershed. Extensive degradation of terrestrial particulate organic carbon may occur in estuaries receiving inputs from permafrost-dominated watersheds (Sánchez-García et al., 2011). Particulates derived from primary production in reservoirs (e.g., freshwater algae) also are labile and likely to decompose with increasing salinity. On the other hand, dissolved total Hg that is transported into the bay could be subject to methylation, forming MeHg in the water column or the sediments. Published multiyear data from the Nelson and Churchill Rivers (Kirk & St. Louis, 2009) supports high particulate matter association. Thus, if the particulate matter is not degraded in the lower river reaches or the estuary, deposition of MeHg within the watershed or nearshore in the estuary is a likely fate. Sites of rapid sedimentation where MeHg could be buried efficiently in the Nelson estuary have been documented (Duboc et al., 2017). However, an important process of sedimentation in these areas involves the rapid deposition of relatively coarse-grained sediments delivered by hyperpycnal flows associated with floods of the Nelson River. The hyperpycnal flows are believed to be caused by the ice-jam formation and have become less frequent after river regulation (Duboc et al., 2017). The size of the potential sediment sink for Hg in the Nelson estuary or western Hudson Bay, in general, is not yet clear because modern sites of sediment deposition are based on previous work (Kuzyk et al., 2009) and the newly collected sediment core data and sub-bottom data are still being analyzed (Huyghe, thesis in prep.). Resuspension during fall storms is a dominant process as evidenced by large accumulations of sediment during fall in the sediment traps that were deployed for an annual cycle at the Nelson estuary moorings.

Incubation of dissolved organic matter from the Nelson River System during the Nanuk winter campaign found a high % loss over 45 days (Kazmiruk, 2018) (Figure 3.5.6). The % loss of dissolved organic matter from the Nelson River System was in excess of 50 % and was greater than that of similar incubations of dissolved organic matter from the Hayes or Great Whale Rivers as well as higher than marine dissolved organic matter from the southwest or southeast Hudson Bay (Kazmiruk, 2018).

Sampling during Nanuk and Churchill estuary campaigns in 2017 and the bay-wide cruises between 2016-2018 suggests that Hg associated with dissolved, rather than particulate matter, can be converted to MeHg during the winter. However, there are no clear signs of offshore transport of MeHg. Although elevated wintertime remineralization of organic matter occurs in the Nelson River Estuary compared to Eastern Hudson Bay systems, there is no clear spatial variability of MeHg distributions in the bay to indicate that this remineralization results in MeHg loadings to the bay. Furthermore, the lack of spatial variability in zooplankton Hg suggests that the estuaries are not hotspots of MeHg entry into the Hudson Bay food web.

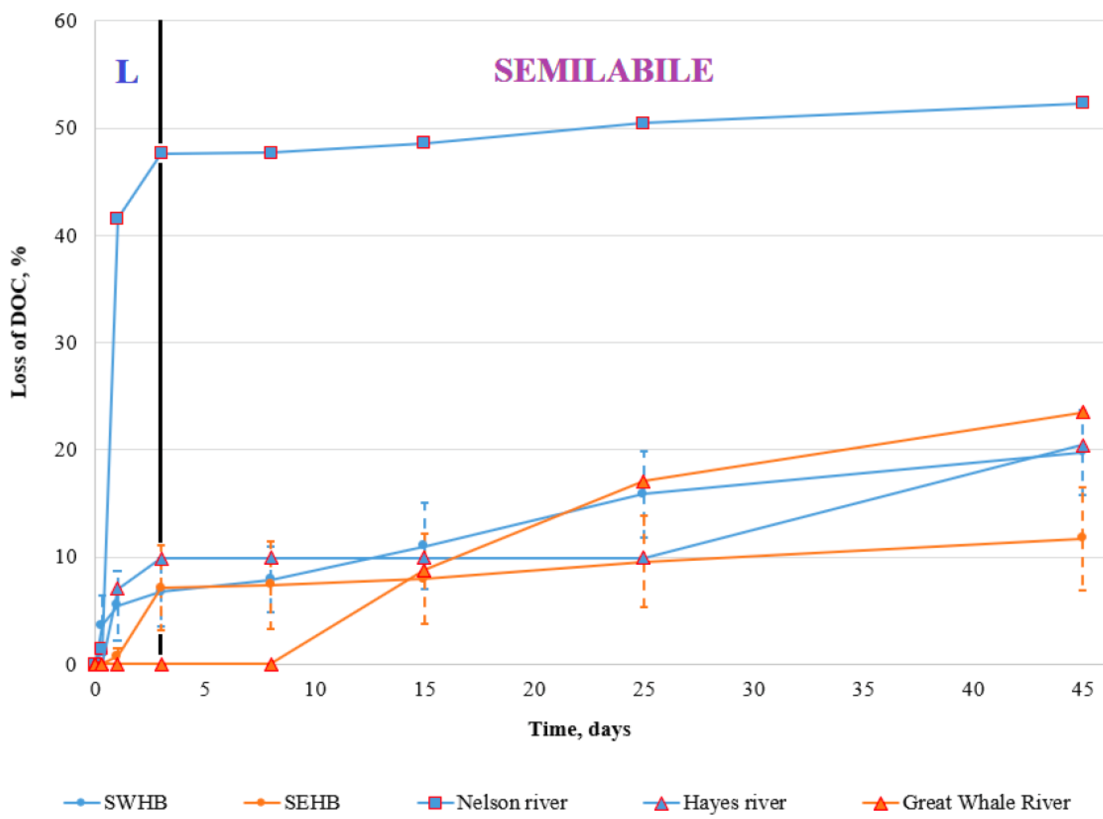

FIGURE 3.5.6 Microbial degradation of dissolved organic carbon (DOC) in Nelson, Hayes, and Great Whale River and the adjacent coastal waters of southwestern (SWHB) and southeastern (SEHB) Hudson Bay over 45-day incubation period presented Bay (Kazmiruk, 2018). The vertical bold line at 3 days separates labile (L) and semi-labile fractions of DOC.

Hudson Bay

Analysis to date suggests that the previous carbon budget (Kuzyk et al., 2009) may have underestimated the amount of post-deposition processing on sediments, due to widespread bioturbation, slumping, and resuspension. The distribution of total Hg and MeHg appears to be impacted by this processing, with focusing of Hg species offshore away from scoured shore sediments and away from river mouths.

During the bay-wide 2018 cruise, we found significant ($p < 0.0001$) negative relationships between MeHg and dissolved oxygen in the water column across all stations and sampling depth (Munson et al., in review). In contrast, we did not see a significant relationship between total Hg and dissolved oxygen. These relationships support **H5.1** and suggest that as dissolved organic matter is consumed and dissolved oxygen concentrations are drawn down, total Hg is converted into methyl Hg. The high wintertime loss of dissolved organic matter from the Nelson River System, when compared to the Great Whale or marine sites, indicates that MeHg could be produced from riverine total Hg even during relatively unproductive winter months. Although consistent with organic matter remineralization as the primary driver in MeHg production, the relationship between MeHg and dissolved oxygen does not distinguish between potential riverine and marine sources of MeHg. The breakdown of organic matter in the sediment and the breakdown of marine organic matter in the water column can also promote the creation of MeHg. Sediment core analysis is ongoing (delayed due to the COVID-19 pandemic).

Suspended Sediment and Organic Matter Fingerprinting (Task 5.2)

While the above soil incubation experiment demonstrated that MeHg can be produced and transferred into the water column following flooding of *in situ* soils, another component of the Hg and MeHg delivered by rivers to Hudson Bay is that associated with the river's suspended particulate load. We were thus interested in determining the provenance, organic composition, and Hg/MeHg content of the suspended particulates being transported within the Nelson River system. Previous work had shown evidence of bank erosion particularly of ice-bonded riverbanks along the Rat-Burntwood River/Churchill River Diversion corridor. We suspected that these processes would be the major sources of sediment (and thus total Hg) to the LNRB. The Upper Nelson River system could be expected to be another important source of suspended particulates to the Lower Nelson River system and hence Hudson Bay because of the well-known eutrophication and algal blooms in Lake Winnipeg.

Techniques for collecting fluvial fine-grained suspended sediment are evaluated. A commonly used time-integrated fine sediment sampler (TIFSS) is found to be a suitable sampler for the collection of a representative sample of sufficient mass for the investigation of the properties of fluvial suspended sediment (Goharrokhi et al., 2020; Goharrokhi et al., 2019). A high-flow-rate, sequential filtration is found to be a more portable and cost-effective system for collecting and concentrating fluvial suspended sediment. The techniques allow us to collect representative source materials in the Nelson River Basin/Hudson Bay for subsequent characterization and linkage with Hg and MeHg cycling.

Organic matter characterization (Stainton, 2019) and inorganic matter characterization (Masoud Goharrokhi, Ph.D. thesis, in prep) found that particulate material in the LNRB is local in origin from shoreline erosion, with little downstream transport of particulates from either the Rat-

Burntwood River system or Lake Winnipeg. Much of the particulate matter transported from upstream areas are removed (buried or transformed) in the reservoirs of Split Lake and Stephens Lake. The outflow from these lakes carries a dominant signal of algal-derived particulate organic matter. Local bank erosion downstream of each control structure adds again a signal of soil-derived organic matter. Thus, there is a sequence of particle and organic matter losses and additions as the Nelson River flows to Hudson Bay. We expect that these processes modulate the delivery of Hg and MeHg by rivers to the bay but at this point, we cannot quantify the effects nor generalize to other (unregulated) rivers. One expects that accelerated bank erosion in areas of permafrost thawing may represent an additional source of Hg to northern rivers compared to those draining watersheds without permafrost. Across eight rivers that were sampled during BaySys, Hg concentrations indeed showed an increasing trend northward along the west coast of Hudson Bay (Figure 3.5.7). The weaker latitudinal relationship for MeHg supports the notion that the cycling of MeHg is more complex than that of the inorganic forms.

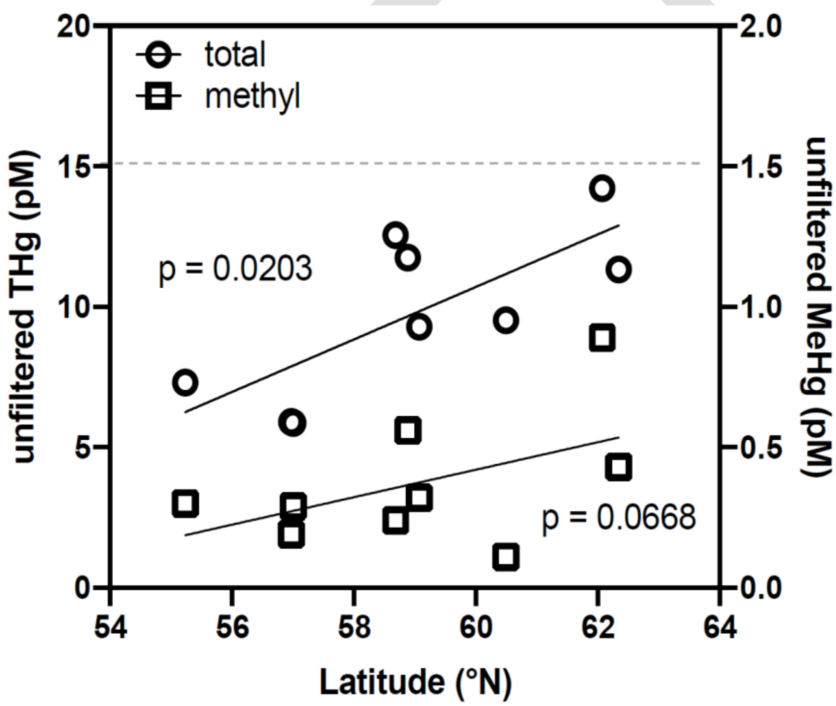

FIGURE 3.5.7 Latitudinal trends in total Hg (THg) and MeHg concentrations in river water for eight rivers sampled near their mouths along the western shore of Hudson Bay.

Winter estuarine dissolved organic matter consumption measured during the Nanuk and ArcticNet campaigns in James Bay suggests that annual losses of organic matter may exceed previous estimates that are largely limited to measurements in spring and summer (Kazmiruk, 2018). This could be especially relevant due to the alterations in wintertime discharge from the Nelson River due to regulation.

Surface sediments from cores subsamples collected from the bay and estuaries are currently being fingerprinted for compound-specific stable isotopes to determine relative contributions from terrestrial and marine sources. Additional characterization, including C/N ratios and carbon and nitrogen isotopes, are ongoing for multiple sections of cores. The sediment age dating model has identified regions of post-deposition processing, including bioturbation, sediment slumping, and sediment resuspension. Preliminary results suggest that the bay sediment is largely influenced by post-depositional processing that may, in turn, impact the distribution of methyl Hg in the sediment due to both transport and *in situ* production.

Mass balance modelling of methylmercury in Hudson Bay (Task 5.3)

Mass balance modelling of MeHg in Hudson Bay is ongoing as the analysis of some relevant samples is delayed due to the COVID-19 pandemic. Water column concentrations of total Hg and MeHg measured during the bay-wide cruise are similar to those measured in low-resolution data (Kirk et al., 2008) and lower than those indicated in the previous mass balance of total Hg in Hudson Bay (Hare et al., 2008). As a result, Hudson Bay is not a source of either total or MeHg to surrounding Arctic waters, as previously indicated (Hare et al., 2008). The relatively low Hg species concentrations have important consequences for the transfer of Hg in the food web. We measured low concentrations of Hg in lower levels of the Hudson Bay, consistent with previous data showing that while the food web of Hudson Bay bioaccumulates Hg in the food web, the concentrations are low relative to Pan-Arctic concentrations (Pomerleau et al., 2016). In contrast to **H5.3**, no clear spatial relationships indicate riverine or ice cover controls over Hg sources in the Hudson Bay food web. Although freshwater inputs from rivers and ice melt may control the timing of Hg entry into the Hudson Bay food web, we do not see evidence that either controls the magnitude.

Mass balance modelling of methylmercury in Hudson Bay follows a similar method used for the total Hg mass balance in the bay (Hare et al., 2008). Major sources and sinks considered include the atmosphere, rivers, coastal erosion, oceanic circulation, sedimentation, and biotic uptake. Atmospheric deposition of MeHg is assumed to be of minimal importance due to low concentrations of MeHg in the global atmosphere (Strode et al., 2007) and regional precipitations sources (Baya et al., 2015; Sanei et al., 2010). In addition to the detailed MeHg data on the Nelson River obtained as part of the CAMP, Nanuk, and bay-wide campaigns, the lower section of other major rivers (Churchill, Hayes, Winisk, and Povungnituk Rivers) was also sampled during the bay-wide Campaign via helicopter and boat in collaboration with Teams 3 and 4. The final mass budget is still being developed, but preliminary results show that the overall concentrations of both total Hg and MeHg in the bay are low and are reflected in the low concentrations in the base of the Hudson Bay marine food web.

3.5.4 Conclusions

The BaySys proposal required Team 5 to address three highly integrated objectives through a series of observational fieldwork and analysis. We conclude this chapter by summarizing the results from our BaySys investigations as they pertain to each stated objective.

Hypothesis 5.1: Organic matter is a primary control over Hg methylation in the water column and sediments.

The relationships between MeHg versus dissolved oxygen and nitrate indicators of organic carbon remineralization, and the fact that these are different from the relationships between total Hg and these indicators, support our hypothesis that organic matter controls Hg methylation. The assignment to the relative role of riverine, marine, or sediment sources of organic matter in MeHg production is pending as the MeHg mass budget has yet to be completed. Historically, impacts of hydroelectric regulation outweighed those of regional or global climatic changes on Hg cycling, as a large influx of freshly flooded, labile organic matter fuels microbial methylation of inorganic Hg. This is confirmed by the peak Hg concentrations in fish in the Churchill/Nelson River systems shortly after the initial impoundment. Presently, water level fluctuations from either hydroelectric regulation or climate change have the potential to induce Hg methylation in freshwater systems. However, from fish Hg concentrations, which serve as an integrated measure of Hg production, these fluctuations appear to be less important to MeHg production than overall water quality and trophic dynamics.

Hypothesis 5.2: The suspended sediments in Hudson Bay have multiple sources (e.g., erosion and runoff from land surfaces within the watershed, erosion of the banks and beds of the rivers and estuaries of the bay, erosion of the bay's coastline, resuspension of sediments within the bay, as well as organic material produced within the bay), which affect their role in the transport and methylation of Hg in Hudson Bay and will respond differently to climate change.

There is a sequence of suspended particulate matter and associated organic matter losses and additions as the Nelson River flows to Hudson Bay. Much of the suspended particulate matter transported from upstream areas in the Nelson River is removed (buried or transformed) in the reservoirs of Split Lake and Stephens Lake. The outflow from these lakes carries a dominant signal of algal-derived particulate organic matter. Local bank erosion downstream of each control structure adds again a signal of soil-derived organic matter. These processes likely modulate the delivery of Hg and MeHg by rivers to the bay. Accelerated bank erosion in areas of permafrost thawing may represent an additional source of Hg to northern rivers compared to those draining watersheds without permafrost, but its impact on the MeHg cycling appears to be more complex. Once arrived in Hudson Bay marine water, the extent of bulk organic matter remineralization, rather than organic matter source, appears to control MeHg concentrations. This suggests that only very large changes in organic matter content from hydroelectric regulation of freshwater inputs could outweigh climatic controls on MeHg production through water column stratification and oxygenation.

Hypothesis 5.3: Flooding and changing climate are playing an increasingly important role in Hg accumulation at the base of the Hudson Bay marine and coastal food webs.

Analysis of total and MeHg in both zooplankton and benthic organisms reveals little spatial variability across Hudson Bay, with no overall trend of higher Hg in biota near riverine inputs that would indicate rapid uptake of MeHg into the food web. The bioaccumulation of Hg in the Hudson Bay food web is not elevated relative to similar Arctic systems. Neither climate change nor hydroelectric regulation appears to have a direct role on Hg food web entry form available spatial data.

Summary: Differentiating the impact of hydroelectric regulation or climate change on Hg

Hydroelectric regulation in the Churchill/Nelson River watersheds was responsible for rapid MeHg production in the on-system waterbodies and accumulation in fish following the initial impoundment. Fish Hg concentrations have decreased since then toward the long-term recovery, with subsequent impoundment having a much lesser impact. Recent intermittent increases in fish Hg have been observed in many of the on-system, as well as off-system, water bodies, which appear to be driven primarily by climate-induced changes in water quality and trophic dynamics. At the present, there is no clear evidence that either hydroelectric regulation or climate change has had a significant impact on Hg accumulation at the base of the Hudson Bay marine and coastal food webs. This however could change in the future, as thawing of the widespread permafrost in the region accelerates and as more invasive species are introduced. Both of these processes affect Hg bioaccumulation through changes to water chemistry and trophic dynamics and have the potential to magnify the impact of both hydroelectric regulation and climate change on Hg accumulation in the Hudson Bay marine and coastal food webs.

3.5.5 Gaps and Recommendations

An incredible amount of data were collected as part of BaySys Team 5, such that it will require significant time beyond the funded BaySys project to utilize its full capacity and to understand all ramifications of the counter-opposing forces of water regulation and climate change. We have addressed the deliverables of our objectives and uncovered new processes which have bearing on the overarching objectives of BaySys. We conclude by summarizing these gaps and making recommendations for further work from the perspective of Team 5:

Gaps:

a) Mass budget of MeHg in the Hudson Bay system: A major gap in Team 5’s research is the delay associated with the development of the MeHg mass budget for the Hudson Bay system. COVID-19 resulted in restrictions including the complete shutdown of our analytical laboratories since March 2020. Several research personnel have since moved on and found employment elsewhere. As such, there are approximately 200 marine sediment samples have yet to be analyzed for MeHg and organic carbon, which delayed the development of the MeHg mass budget. As the pandemic-related restrictions are easing up, a new part-time technician has been hired to assist with the analysis. We expect to complete the sample analysis by December 2021 and publish the mass budget in 2022.

b) Peer-review publications: While Team 5 has resulted in several methodological papers published in peer-reviewed journals, much of the data interpretation and science deliverables remain to be published due to COVID-induced delays in student progress and the departure of several research personnel to new career opportunities. The PIs have committed to leading the manuscript writing process and we expect most of the manuscripts will be published in peer-reviewed journals in 2022.

c) Data gap from the eastern Hudson Bay: Another major gap is the lack of data from the eastern Hudson Bay which will affect the completeness of the MeHg mass budget. This gap is due to the ice conditions in 2018 that prevented the CCGS Amundsen-based bay-wide fieldwork in the eastern part of the bay.

d) Zooplankton data: The collection of zooplankton is limited by ice conditions that can interfere with net deployment at sea. As a result, the results of our food web analysis of Hg are biased towards regions of the bay where nets could be deployed. Our findings are therefore limited to regions without heavy ice cover.

Future Recommendations:

a) We recommend future follow-up studies to address questions on when and to which extent fish Hg concentrations in regulated water bodies will recover. While it is clear that fish Hg concentrations in regulated water bodies are decreasing toward long-term recovery, intermittently increases have been observed which will prolong the time toward recovery and potentially affect the new "baseline" concentrations at recovery. BaySys has identified that changes in water chemistry, rather than in atmospheric emissions or regional hydrology, as the most likely cause for post-impoundment fish Hg variability. We recommend future efforts be undertaken to identify what are these key changes in water chemistry including the downstream effect of Lake Winnipeg eutrophication, as well as in aquatic ecology (e.g., invasive species).

b) We recommend more parameters be included in the ongoing CAMP monitoring program. In addition to fish Hg concentrations, CAMP should also regularly measure parameters related to water chemistry and trophic dynamics to better interpret fish Hg trends. Among the top priority are total Hg and MeHg concentrations in lake water, dissolved and particular organic carbon, and stable isotopes of carbon and nitrogen in fish muscle.

c) Better characterization of sedimentation in the watershed: Increased riverbank destabilization and erosion were indicated by the characterization of changes in the source material of suspended organic matter along the length of the Burntwood-Nelson River system (Stainton, 2019). The sediment core collection was attempted in several water bodies, including Threepoint, Split, and Stephens Lakes, to determine the deposition of this material within the Hudson Bay watershed and its propensity for transfer to Hudson Bay itself. However, difficulties in sediment core collection and the quality of material for sediment dating and analysis prevent us from accounting for sedimentation within the watershed (Singer, 2020).

d) Better characterization of atmospheric Hg species: Although atmospheric deposition of MeHg is assumed to be minimal, the relative concentrations of dissolved monomethylmercury (MMHg) and gaseous dimethylmercury (DMHg) have been proposed as an important loss process for the Arctic and are subject to changes in ice cover (Soerensen et al., 2016). Without DMHg measurements, we rely on previous measurements, in different ice cover, to estimate DMHg evasion (Baya et al., 2015; Kirk et al., 2008).

3.5.6 References Cited

The following is a list of publications produced and cited by Teams within the BaySys project.

Goharrokhi, M., Lobb, D.A., Owens, P.N. (2020). Evaluation of high-flow rate continuous-flow centrifugation and filtration devices for sampling and concentrating fine-grained suspended sediment. *Hydrological Processes,* 34, 3882–3893.

Goharrokhi, M., Pahlavan, H., Lobb, D.A., Owens, P.N., Clark, S.P. (2019). Assessing issues associated with a time-integrated fluvial fine sediment sampler. *Hydrological Processes,* 33, 2048–2056.

Kazmiruk, Z. (2018). Potential for microbial degredationdegradation of terrestrial dissolved organic carbon in coastal Hudson Bay. Department of Environment and Geography. M.Sc. University of Manitoba, Winnipeg, MB, 2018.

Munson, K.M., Jansen, W.A., Stern, G., Wang, F. (in review). Intermittent increases in boreal lake fish mercury despite long-term recovery from hydroelectric regulation. *Environmental Science and Technology*.

Singer, J. (2020). Mercury Cycling in Hydroelectric Reservoirs of Northern Manitoba Decades After Impoundment. Department of Environment and Geography. M.Sc. University of Manitoba, Winnipeg, MB, 2020.

Stainton, T. (2019). An initial investigation into the sources and transport of particulate organic matter in the Nelson River System, Manitoba. Department of Geological Sciences. M.Sc. University of Manitoba, Winnipeg, MB, 2019.

Other Works Cited

Baya, P.A., Gosselin, M., Lehnherr, I., St. Louis, V.L., Hintelmann, H. (2015). Determination of monomethylmercury and dimethylmercury in the Arctic marine boundary layer. *Environmental Science and Technology,* 49, 223–232.

Bilodeau, F., Therrien, J., Schetange, R. (2017). Intensity and duration of effects of impoundment on mercury levels in fishes of hydroelectric reservoirs in northern Québec (Canada). *Inland Waters,* 7, 493–503.

Bodaly, R.A., Jansen, W.A., Majewski, A.R., Fudge, R.J.P., Strange, N.E., Derksen, A.J., Green, D.J. (2007). Postimpoundment time course of increased mercury concentrations in fish in hydroelectric reservoirs of northern Manitoba, Canada. *Archives of Environmental Contamination and Toxicology,* 53, 379–389.

Duboc, Q., St-Onge, G., Lajeunesse, P. (2017). Sediment records of the influence of river damming on the dynamics of the Nelson and Churchill Rivers, western Hudson Bay, Canada, during the last centuries. *Holocene,* 27, 712–725.

Hall, B.D., St. Louis, V.L., Rolfhus, K.R., Bodaly, R.A., Paterson, M.J. (2005). The impact of reservoir creation on the biogeochemical cycling of methyl and total mercury in boreal upland forests. *Ecosystems,* 8, 248–266.

Hammerschmidt, C.R., Fitzgerald, W.F. (2006). Photodecomposition of methylmercury in an arctic Alaskan lake. *Environmental science & technology*, 40, 1212-1216.

Hare, A., Stern, G.A., Macdonald, R.W., Kuzyk, Z.Z., Wang, F. (2008). Contemporary and preindustrial mass budgets of mercury in the Hudson Bay marine system: The role of sediment recycling. *Science Total Environment*, 406, 190.

Hare, A.A., Stern, G.A., Kuzyk, Z.Z., Macdonald, R.W., Johannessen, S.C., Wang, F. (2010). Natural and anthropogenic mercury distribution in marine sediments from Hudson Bay, Canada. *Environmental Science and Technology*, 44, 5805-5811.

Jansen, W. (2021). Mercury concentrations in commercial fish species from Lake Winnipeg, 1971–2019. *Journal of Great Lakes Research*, 47, 648–662.

Kirk, J.L., and St. Louis, V.L. (2009). Multiyear Total and Methyl Mercury Exports from Two Major Sub-Arctic Rivers Draining into Hudson Bay, Canada. *Environmental Science & Technology*, 43, 2254-2261.

Kirk, J.L., St. Louis, V.L., Hintelmann, H., Lehnherr, I., Else, B., Poissant, L. (2008). Methylated mercury species in marine waters of the Canadian high and sub Arctic. *Environmental Science & Technology*, 42, 8367-8373.

Kirk, J.L., St. Louis, V.L. (2009). Multiyear total and methyl mercury exports from two major sub-Arctic rivers draining into Hudson Bay, Canada. *Environmental Science & Technology*, 43, 2254-2261.

Kuzyk, Z.A., Macdonald, R.W., Johannessen, S., Gobeil, C., Stern, G. (2009). Towards a sediment and organic carbon budget for Hudson Bay. *Marine Geology*, 264, 190-208.

Lehnherr, I., St Louis, V.L., Hintelmann, H., Kirk, J.L. (2011). Methylation of inorganic mercury in polar marine waters. *Nature Geosciences*, 4, 298-302.

Pomerleau, C., Stern, G.A., Pućko, M., Foster, K.L., Macdonald, R.W., Fortier, L. (2016). Pan-Arctic concentrations of mercury and stable isotope ratios of carbon (δ(13)C) and nitrogen (δ(15)N) in marine zooplankton. *Science Total Environment*, 551–552, 92–100.

Sanei, H., Outridge, P.M., Goodarzi, F., Wang, F., Armstrong, D., Warren, K. (2010). Wet deposition mercury fluxes in the Canadian sub-Arctic and southern Alberta, measured using an automated precipitation collector adapted to cold regions. *Atmospheric Environment*, 44, 1672-1681.

Sánchez-García, L., Alling, V., Pugach, S., Vonk, J., van Dongen, B., Humborg, C., Dudarev, O., Semiletov, I., Gustafsson, Ö. (2011). Inventories and behavior of particulate organic carbon in the Laptev and East Siberian seas. *Global Biogeochemical Cycles*, 25(2), GB2007. 10.1029/2010GB003862.

Soerensen, A.L., Jacob, D.J., Schartup, A., Fisher, J.A., Lehnherr, I., St Louis, V.L., Jeroen, L-E., Sonke, J.E., Krabbenhoft, D.P., Sunderland, E.M. (2016). A mass budget for mercury and methylmercury in the Arctic Ocean. *Global Biogeochemical Cycles*, 30(4), 560–575.

St. Louis, V.L., Rudd, J.W.M., Kelly, C.A., Bodaly, R.A.D., Paterson, M.J., Beaty, K.G., Hesslein, R.H., Heyes, A., and Majewski, A.R. (2004). The rise and fall of mercury methylation in an experimental reservoir. *Environmental Science & Technology*, 38(5), 1348–1358.

Strode, S.A., Jaegle, L., Selin, N.E., Jacob, D.J., Park, R.J., Yantosca, R.M., Mason, R.P., Slemr, F. (2007). Air-sea exchange in the global mercury cycle. *Global Biogeochemical Cycles*, 21(1). GB1017. 10.1029/2006GB002766.

Sunderland, E.M., Krabbenhoft, D.P., Moreau, J.W., Strode, S.A., Landing, W.M. (2009). Mercury sources, distribution, and bioavailability in the North Pacific Ocean: Insights from data and models. *Global Biogeochemical Cycles*, 23, GB2010. 10.1029/2008GB003425.

Wang, F., Macdonald, R., Armstrong, D., Stern, G. (2012). Total and methylated mercury in the Beaufort Sea: The role of local and recent organic remineralization. *Environmental Science & Technology*, 46, 11821–11828.

Wang, K., Munson, K.M., Beaupre-Laperriere, A., Mucci, A., Macdonald, R.W., and Wang, F. (2018). Subsurface seawater methylmercury maximum explains biotic mercury concentrations in the Canadian Arctic. *Science Reports*, 8, 14465. 10.1038/s41598-018-32760-0.

3.6 Ocean Modelling (Team 6)

Team Member	Affiliation	Tasks Contributed To						Role
Paul G. Myers	a	6.1	6.2	6.3	6.4	6.5	6.6	Science Lead
Jennifer C. Lukovich	b	6.1	6.2	6.3	6.4	6.5	6.6	Science Lead
Kevin Sydor	c	6.1	6.2	6.3	6.4	6.5	6.6	Hydro Lead
Karen Wong	c	6.1	6.2	6.3	6.4	6.5	6.6	Hydro Lead
Natasha Ridenour	a	6.1	6.2	6.3	6.4	6.5	6.6	Contributor
Ran Tao	a	6.1	6.2	6.3	6.4	6.5	6.6	Contributor
Shabnam Jafarikhasragh	b	6.1	6.2	6.3	6.4	6.5	6.6	Contributor
Yiran Xu	a	6.1	6.2	6.3	6.4	6.5	6.6	Contributor
Yarisbel Garcia-Quintana	a	6.1	6.2	6.3	6.4	6.5	6.6	Contributor
Xianmin Hu	a	6.1	6.2	6.3	6.4	6.5	6.6	Contributor
Frédéric Dupont	d	6.1	6.2	6.3	6.4	6.5	6.6	Collaborator

a) Department of Earth and Atmospheric Sciences, University of Alberta, Edmonton, Alberta, Canada.
b) Centre for Earth Observation Science, University of Manitoba, Winnipeg, Manitoba, Canada
c) Manitoba Hydro, Winnipeg, Manitoba, Canada.
d) Environment Climate Change Canada.

3.6.1 Introduction and Objectives

Team 6 was to develop, run, evaluate and produce the modelling experiment outputs that would be used by BaySys Teams in investigating the relative impacts of climate change and regulation on freshwater-marine coupling within the Hudson Bay Complex (HBC), defined as Foxe Basin, Hudson Bay, James Bay, Hudson Strait, and Ungava Bay. Two key objectives from the original proposal were: To investigate the relative impacts of climate change and regulation of freshwater-marine coupling within the HBC from a modelling perspective using the Nucleus for European Modelling of the Ocean (NEMO) model and to provide an integrated observational-modelling freshwater/marine framework for model-data comparison on local (~ 20 - 100 km; estuary and coastal) and regional (~100 - 1000 km; bay-wide) scales.

In support of Team 1 hypotheses, a sea ice and oceanographic model was used to further study the effects of freshwater loading and ice cover on the circulation of Hudson Bay. This modelling perspective was based on the NEMO ocean general circulation model coupled to the LIM2 sea ice model. Central to Team 6 goals was the development of an integrated observational-modelling framework that provided insight on, and improved representation of, physical, biological, and biogeochemical processes in the Hudson Bay system. The modelling provided a framework and tools to simulate projected changes in marine state and dynamic variables and enabled the integration of observations and numerical analyses.

In winter 2015, based on comments from the original proposal review, Dr. Paul Myers from the University of Alberta was invited to join BaySys to add an ocean modeller to the Team. The group at the University of Alberta ran the NEMO model for several years prior and provided a much-needed ocean modelling expertise. For the BaySys project, the University of Alberta ran an Arctic NEMO configuration (Figure 3.6.1) to provide a local (20-100 km; estuary and coastal) and a regional (100-1000 km; bay-wide) perspective to look at the changes in freshwater marine coupling in response to a changing climate and regulated and naturalized regimes. The Arctic configuration further provided a link between Arctic and sub-Arctic domains to look at the tightly integrated nature of the high latitude climate system in the HBC.

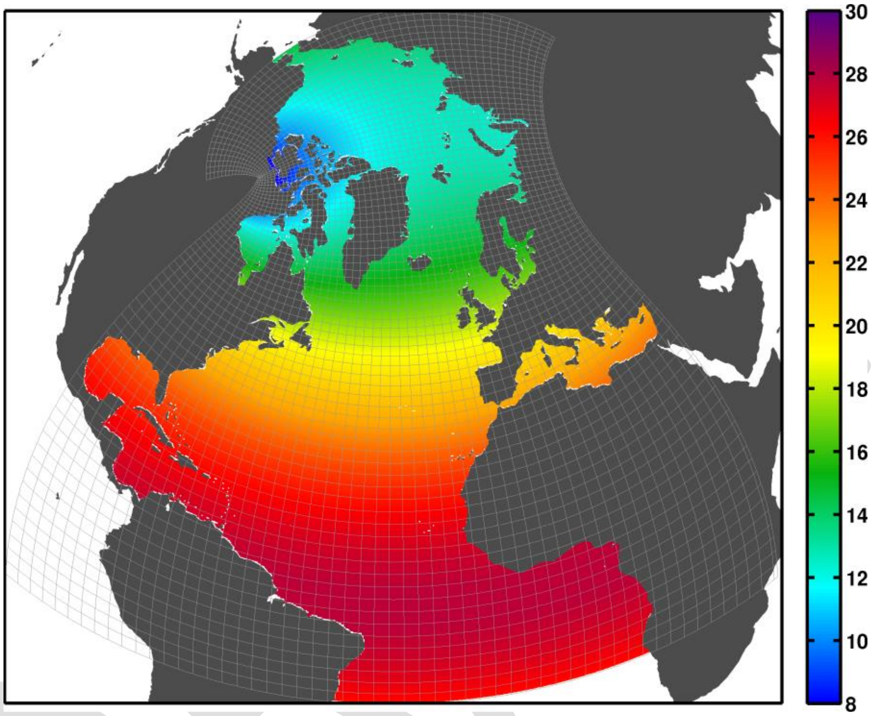

FIGURE 3.6.1 Arctic NEMO configuration

The pan-Arctic domain is essential in ensuring that the climate change signal (a hemispheric-scale phenomenon) within the HBC is adequately simulated and is reflected in our modelling. Previous studies (Ingram and Prinsenberg, 1998; Jones et al., 2003) have demonstrated that waters from the Canadian Arctic, Siberian Rivers, and Pacific Water (Bering Strait) all enter the HBC over timescales of 2 to 10 years. Given that Hudson Bay is filled with Arctic Waters, and climate change is expected to have the largest impacts at high latitude, understanding the response of the HBC to a changing climate requires inputs that represent how the Arctic is responding to the climate forcing, potentially modifying the exchange into the HBC. It is also important to note that given the timescale of the response, it is the overall changes to forcing and runoff from the Arctic that will be important, not short-term changes in river regulation in that region, as those effects will be integrated out over the transit times of the given waters to the HBC.

A set of five working tasks were established by Team 6 to ensure the Team, and overall project objectives could be addressed. These tasks are interrelated and were written to address task 1.5

originally included as part of Team 1. Tasks 6.1 to 6.5 are addressed in the methods and results sections below.

- 1.5) Coupled atmosphere/sea ice/ocean model
- 6.1) Preparation of Naturalized and Regulated Experiments (Historical and Future)
- 6.2) Ongoing Detailed Analysis of Naturalized Experiments
- 6.3) Ongoing Detailed Analysis of Regulated Experiments
- 6.4) Sensitivity Experiments (Input Data and Parameter) Run and Analysis
- 6.5) Dissemination of atmosphere/sea ice/ocean Model Outputs

3.6.2 Analysis and Methods

The model used for the BaySys project is the Nucleus for European Modelling of the Ocean (NEMO) numerical framework version 3.6 (Madec, G. & the NEMO Team, 2008). This model was coupled with the Louvain-la-Neuve sea ice model LIM2 (Fichefet & Morales Maqueda, 1997). With the need to consider the pan-Arctic domain, the configuration used is the Arctic and Northern Hemisphere Atlantic (ANHA), which uses a tri-polar grid, with open boundaries at Bering Strait and 20S. These boundaries are chosen to be far enough from the study region to limit the impact of far-field behavior on the HBC. Details on the data used at the boundaries, as well as sensitivity experiments to confirm their limited impact are discussed in the following subsections. A ¼ degree resolution (hereafter ANHA4) is used to balance the need to represent boundary currents and some mesoscale processes while also allowing multiple century-long integrations to be carried out while including passive tracers and biogeochemical model components. The ANHA4 configuration has a resolution of 10 - 16 km in the HBC (Figure 3.6.2). The configuration has 50 vertical geopotential z-levels, with the layer thickness smoothly increasing from 1.05 m at the surface, to 453.13 m in the last level. A partial step is also enabled to better resolve the bathymetry. No temperature or salinity restoring is applied, to avoid damping the runoff and climate signals we wish to study. Vertical mixing at subgrid scales is parameterized using a turbulent kinetic energy closure model (Madec et al., 2016). For lateral mixing, the model uses a biLaplacian operator with an eddy viscosity of 1.5 X 10^{11} m^4s^{-1}. Subgridscale tracer lateral diffusion is parameterized with an isopycnal Laplacian operator with an iso-neutral eddy diffusivity of 300 m^2s^{-1}. The model baroclinic timestep is 1080 s. Tidal forcing is included by specifying geopotential tidal forcing with 9 constituents in the momentum equations (K1, K2, M2, M4 N2, O1, P1, Q1, S2), as well as at the lateral open boundaries. The tidal constituents are taken from the Oregon State global tide prediction model TPX08 (Egbert and Erofeeva, 2002). The use of the tides means the experiments are run with NEMO v3.6's nonlinear free surface and variable volume formulations activated. Initial Conditions are from the Polar Hydrographic Climatology version 3.0 (PHC3.0; Steele et al. (2001)).

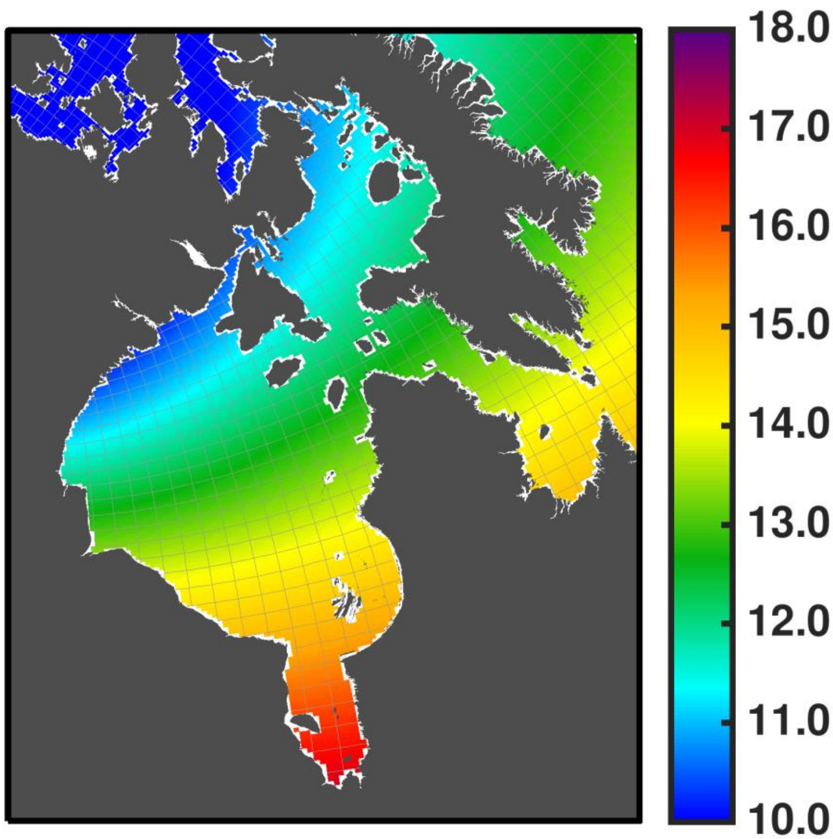

FIGURE 3.6.2 The ANHA 4 Configuration in the HBC. The colour scale shows the model grid resolution in km.

Climate Model Forcing

A five-member ensemble of CMIP5 model experiments was chosen to provide the atmospheric fields to drive the ocean/sea ice model. The members were chosen to bracket future changes in temperature and precipitation across the Hudson Bay domain, and thus maximize climatic variability (Braun et al., 2020). The ensemble size was limited to five because of the expense of running 100-year long experiments with NEMO. The choice of CMIP5 model experiment was also impacted by the need to provide the needed fields over the NEMO domain, as well as a desire to harmonize the forcing with that used by the freshwater runoff Team. Three general circulation models (GCM) were chosen:

- MIROC5 (Model for Interdisciplinary Research On Climate) was developed cooperatively by the Japanese research community for the IPCC 5th assessment (Watanabe et al., 2010) with resolution T85 for the atmosphere and the equivalent 1.4 degrees for the ocean except near the Equator (Watanabe et al., 2010),
- MRI-CGCM3 (Meteorological Research Institute Coupled General Circulation Model) was also developed in Japan for the 5th Assessment, with an atmospheric resolution of T159 and oceanic horizontal resolution of 1 degree in longitude and 0.5 in latitude (Yukimoto et al., 2012),

- GFDL-CM3 (Geophysical Fluid Dynamics Laboratory Community Model) was developed at the NOAA Geophysical Fluid Dynamics Laboratory with a cube-sphere grid, giving a C48 horizontal resolution (163 to 231 km grid size; (Donner et al., 2011)).

For both MIROC5 and MRI-CGCM3, two Representative Concentration Pathways (GCM-RCP), 4.5 and 8.5 were chosen. For the fifth member, a RCP4.5 experiment from GFDL-CM3 was used. Further details on the ensemble member selection are given in Stadnyk et al. (2019) and Braun et al. (2020).

To drive NEMO, the following fields were used from the GCM experiments: 3 hourly surface air temperature, atmospheric humidity, zonal and meridional surface winds, and radiation (shortwave and downwelling longwave). Six hourly surface atmospheric pressure was also needed for the biogeochemical modules discussed below. Temperature, precipitation, and wind were bias-corrected using Watch Forcing Data, ERA-Interim (or WFDEI), over the ocean domain, as discussed in Stadnyk et al. (2019) and Braun et al. (2020). Forcing fields were interpolated onto the NEMO model grid during the runs using NEMO's on-the-fly interpolation function (Madec, G. and the NEMO Team, 2008). The Coordinated Ocean-ice Reference Experiments bulk formulae were applied to compute fluxes of heat, water, and momentum (Large and Yeager, 2009) for each model timestep. Monthly averaged boundary conditions at the model open boundaries of Bering Strait and 20S were also taken from the output of the given CMIP5 experiment. An additional historical control experiment was run from 1980-2018 using ERA-Interim forcing (Dee et al., 2011) and historical runoff.

Runoff Forcing

Given the focus in BaySys on studying freshwater dynamics within the HBC, runoff forcing was an important aspect of the modelling experiments. Within the HBC, hydrological simulations were performed with a modified version of Arctic-HYPE (Arctic-HYdrological Predictions for the Environment; Andersson et al. (2015); Gelfan et al. (2017)), a hydrological model, which was improved and calibrated for the region (MacDonald et al., 2018). Arctic-HYPE was forced by the same bias-corrected atmospheric forcing sets as used to drive the NEMO simulations described above. Although MacDonald et al. (2018) used additional GCM simulations, they were not considered here. In all cases, monthly river discharge for the HBC was produced for each GCM/RCP pair, using the GCM's historical forcing simulation for 1981-2005 and the future simulation for 2006-2070. Two versions of Arctic-HYPE were run for each climate simulation, one naturalized scenario and one including river regulation (Stadnyk et al., 2021). As such, two sets of 90-year long hydrological discharge scenarios were produced to drive NEMO - naturalized and regulated, for each bias-corrected GCM/RCP pair. Additionally, historical WFDEI fields were used to produced naturalized and regulated runoff over 1980-2018 to drive a historical control simulation.

An additional set of Arctic-HYPE simulations were carried out (Stadnyk et al., 2020) for the Pan-Arctic domain, again driven by the same 5 bias-corrected GCM/RCP forcing sets for 1980-2070, plus the WFDEI historical forcing over 1980-2018. Given a lack of details on regulation of Russian rivers, only naturalized output was produced for the Pan-Arctic domain (Stadnyk et al., 2020). For both regions and all simulations, the HYPE output was then regridded from the river mouth positions onto the NEMO model grid using the approach discussed in Hu et al. (2018) and

Hayashida et al. (2019). Within the same river mouth polygons, enhanced vertical mixing of 2 X 10^{-3} m^2 s^{-1} was used through the first 30 m of the water column to prevent unrealistic low salinities in long narrow estuaries, such as the Ob.

For the rest of the model domain, river runoff was taken from the Canadian Centre for Climate Modelling and Analysis (CC-CMA) CanESM2 model (Arora et al., 2011), based on historical (1950-2005), RCP4.5 (2006-2070), and RCP8.5 (2006-2070) experiments and a variable velocity flow river routing algorithm (Arora & Boer, 1999).

Beyond river runoff, freshwater is also added into the high latitude ocean by discharge from the Greenland Ice Sheet. This discharge has two components. Liquid melt, including tundra discharge, is added to the model similarly to river runoff. Solid discharge or calving is included in the model through a Lagrangian iceberg module (Marson et al., 2018). This module includes the modification to apply ocean fields vertically through the thickness of the iceberg, as discussed in Marson et al. (2018).

For both liquid discharge and solid calving, we used fields from Lenaerts et al. (2015). As discussed in Gillard et al. (2020), for the historical period, the Greenland Ice Sheet solid ice discharge in Lenaerts et al. (2015) is constructed from remote sensing records for 2000-2012 (Ettema et al., 2014). Meanwhile, the liquid runoff portion of the Greenland Ice Sheet freshwater forcing originates from the runoff from Regional Atmospheric Climate Model version 2.1 (hereafter, RACMO2.1; van Meijgaard et al., 2008). RACMO2.1 has a spatial resolution of ~11 km, is forced by ERA-Interim fields at its lateral boundaries, has a Greenland Ice Sheet surface mass balance (van Angelen et al., 2014), and improvements for the climate over Greenland (Ettema et al., 2010). Runoff is given spatial variability by the subdivision into eight basins. The historical scenario calculates runoff based on RACMO2.1 (1960-2012) for each basin. For the meltwater calculations beyond 2012, the regional climate model is forced with an atmospheric circulation climate model HadGEM2-ES. Runoff is distributed evenly to the ocean grid points along each basin and assimilated into the coupled land-atmosphere ocean climate model Community Earth System Model (CESM, version 1.1.2). The CESM is used to simulate multiple scenarios, three of which have been used in this study: a historical (1850-2005) and two future climate scenarios (2006- 2200). Further details on how the RACMO fields are used in the NEMO model can be found in Gillard et al. (2020). Gillard et al. (2020) also show, over the 2004-2016 period, that the use of the RACMO fields in NEMO leads to comparable results over the sub-Polar North Atlantic Ocean when compared to the more observationally-based product of Bamber et al. (2012, 2018).

Biogeochemical Model Components

Previously, the ANHA4 configuration had been run coupled with the Biogeochemistry with Light Iron and Nutrient limitation and Gases (BLING) Version 0 (Galbraith et al., 2010). BLING version 0 is a reduced complexity biogeochemical model with four prognostic tracers: inorganic phosphate, dissolved organic phosphate, oxygen, and iron. It diagnoses chlorophyll-a (chl-a), phytoplankton production, and particle export considering light, macronutrient, and iron limitations as well as a temperature dependency. Using BLING as the choice for biogeochemical modelling has the benefit of lower computational demands, an advantage for running long simulations on high-resolution grids like ANHA4 (Castro de la Guardia, 2018). A detailed discussion of the setup and evaluation of ANHA4 and BLINGv0 can be found in Castro de la Guardia (2018); Castro de la Guardia et al. (2019). Despite having only four prognostic tracers, BLING can reproduce the basic bloom dynamics and magnitude within the HBC complex (Castro de la Guardia, 2018; Castro de la Guardia et al., 2019). Given the interest in the carbon system within BaySys, and the need to use BLING while the BioGeoChemical Ice Incorporated Model (BIGCIIM) was being coupled to NEMO (see below for further details), BLING was updated to the newer BLINGv0 + DIC version (Galbraith et al., 2015), which adds dissolved carbon and alkalinity as prognostic variables (and a suite of diagnosed quantities).

For BaySys, BLINGv0 + DIC was run coupled with NEMO for all 3 historical scenarios (MRI, MIROC, GFDL) over the historical period of 1980-2005 for both regulated and naturalized river runoff. For the future periods, various practical considerations limited the future experiments with BLING to just the RCP8.5 scenarios of MRI and MIROC. In each case, 2006-2070 was run for each forcing for both naturalized and regulated runoff.

Biological fields were initialized with both observed climatology and model output, as discussed below. Dissolved oxygen and inorganic phosphate fields were derived from observed climatologies from World Ocean Atlas 2012 version 2 (WOA13; Garcia et al., 2014). Dissolved iron and organic phosphate come from Geophysical Fluid Dynamics Laboratory (GFDL) Earth System Model version2 (ESM2M) coupled with BLING (Galbraith et al., 2015). The GFDL ESM2M simulation is a global configuration at 1-degree nominal resolution and geopotential vertical coordinates. The simulation has a 100-year spin-up period using year 1860 forcing and an atmospheric carbon dioxide partial pressure (pCO2) of 286 ppm. The initial conditions were built using the average of the last 20 years of the spin-up period.

The initial conditions of total alkalinity (Talk) and dissolved inorganic carbon (DIC) were derived from observed climatology from the mapped product of the Global Ocean Data Analysis Project version2 (Key et al., 2015; Lauvset et al., 2016; Oslen et al., 2016). These fields were remapped onto the ANHA4 grid with units of mol m-3. However, DIC initial conditions are normalized to the simulation start year (DIC_ic = DIC_GLODAPv2 – DIC_diff). The variable DIC_diff is the anthropogenic carbon using DeVries (2014) estimates, and it is calculated as the difference between DIC_DeVries(yri) and DIC_DeVries(current - year).

Open boundary conditions for all tracers in BLING (PO4, DOP, Fed, Talk, DIC, O2) and atmospheric pCO2 are derived from a yearly output of the Community Earth System Model version1 (CESM1) with biogeochemistry (BGC) simulations that were also part of the Coupled Model Intercomparison Project phase 5 (CMPI5). We used the CESM1-BGC output 1 of ensemble r1i1p1 of the pre-industrial control and twentieth-century experiments (RCP4.5 and RCP8.5; Lindsay et al. (2014)). Tracer data were extracted at 20 South (Far-field southern boundary of ANHA) in the Atlantic Ocean and Bering Strait, the boundaries of the ANHA4 configuration. A source of iron at the surface ocean was added following the relation between dust deposition and iron concentrations described in Galbraith et al. (2010). The climatological monthly dust deposition input at the surface of the ANHA4 domain was derived from the Global Ozone Chemistry Aerosol Radiation and Transport model (Ginoux et al., 2001).

One limitation of BLING is that it only considers the pelagic (plankton within the water column) system and Hudson Bay experiences seasonal ice cover. In terms of biogeochemistry, it is important to include/investigate the dynamics of both the sympagic (organisms associated with the sea ice) and the pelagic systems and their interactions. Additionally, the limiting nutrient in the Arctic and subarctic region is nitrogen (Tremblay & Gagnon, 2009; Tremblay et al., 2009). Due to the importance of these factors, it was planned to couple the BioGeoChemical Ice Incorporated Model (BiGCIIM), based on the original model of Sibert et al. (2010, 2011), to NEMOv3.6 and LIM2 for BaySys. The prognostic tracers within BiGCIIM are primary producers (micro-algae), which are split into ice-algae and a large and a small group of phytoplankton (diatoms and flagellates respectively), secondary consumers split into ice-fauna, mesozooplankton and microzooplankton, particulate organic matter, dissolved organic matter, Nitrate, ammonium, and a bottom storage compartment. Mass balance is maintained through rates connecting each prognostic tracer.

A simple carbon module was then added to BiGCIIM (Lavoie, pers. comm.). The carbon module calculates dissolved inorganic carbon (DIC) and total alkalinity (TALK) through the use of rates of respiration, production (uptake of carbon), and remineralisation based on the original nitrogen model and the exchange between the ocean surface and atmosphere and DIC inputted from the rivers. The initial conditions for BiGCIIM were created from observational data available from the World Ocean Atlas 2018 (Garcia et al., 2018). Observational data were interpolated over the ANHA4 domain. These fields were used to create the open boundary condition for the model domain.

The river nutrient inputs are more sensitive, and average nitrate, ammonium, particulate organic matter, dissolved organic matter, phosphate, dissolved inorganic carbon, and total alkalinity were obtained from the observations collected by the Arctic Great Rivers Observatory (Holliday et al., 2020) to produce boundary conditions at the scale of the whole domain. The average nutrient input is then applied over the whole domain and is multiplied by the discharge provided by the HYPE model regulated and unregulated runoff forcings.

Climate Experiment Setup

The BaySys NEMO experiments used to study the impacts of climate change and river regulation are summarized in the schematic in Figure 3.6.3. The historical period is defined as 1980 to 2005. Three pairs of experiments are run over 1980-2005, each pair having NEMO forced by the biased corrected atmospheric forcing associated with the historical control run of each GCM (MIROC5, MRICGCM3, and GFDL-CM3). Each pair then includes A-HYPE river runoff produced using the forcing from the given bias-corrected historical GCM simulation. Additionally, a pair of historical control experiments are run using ERA-Interim forcing, with naturalized and regulated A-HYPE river runoff driven by ERA-based WFDEI forcing. The historical experiment with naturalized and regulated river runoff was then extended to 2018 to allow direct comparison with the BaySys observations and mooring records, as summarized in the following section.

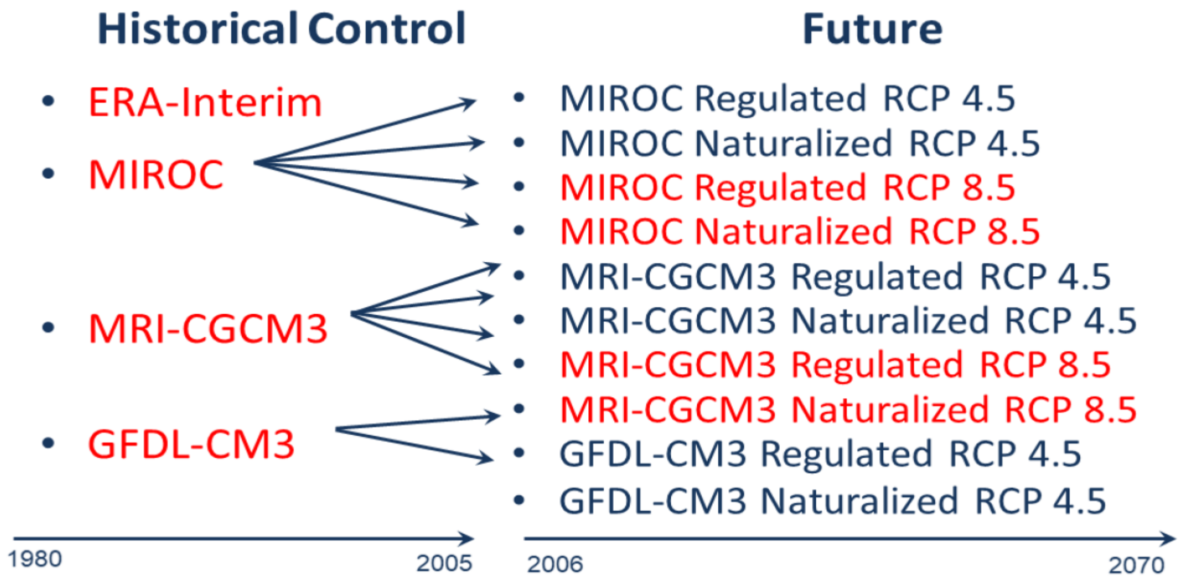

FIGURE 3.6.3 Summary of NEMO model experiments and the associated forcing products.

Each historical experiment was then continued from the start of 2006 to 2070 using the climate forcing from each GCM. For MIROC5 and MRI5-CGCM3, two RCP pairs (RCP4.5 and RCP8.5) were used. For GFDL-CM3, only RCP4.5 forcing was used. The result is a 10-member ensemble of NEMO experiments over 2006-2070, 5 members each with naturalized and regulated river runoff forcing from A-HYPE.

3.6.3 Results and Discussions

Team 6 presents the results of their analyses following six tasks that were established at the onset of the BaySys project and discusses them within the greater context of the Team's objectives, and overarching project.

> ***Task 1.5 Coupled atmosphere/sea ice/ocean model -*** In support of Team 1 hypotheses, sea ice and oceanographic models will be used to further study the effects of freshwater loading and ice cover on the circulation of Hudson Bay.

> ***Task 6.1 Evaluation and Historical Simulations –*** to assess initial regulation impacts, using numerical experiments to study freshwater/marine coupling in Hudson Bay for naturalized (regulation extracted from HYPE model) and regulated discharge data provided by Team 2 and COREv2/ERA-Interim atmospheric forcing from 1979-2009.

> ***Task 6.2 Climate change impacts for naturalized and regulated flow regimes in the HBC –*** to assess and distinguish impacts of climate- and regulation-induced change on Hudson Bay, running numerical experiments using historical (1979-2009) and projected (2010-2070) forcing,

including bias-corrected precipitation, winds, and temperature from the 4 CIMP5 scenarios decided upon by Team 2.

***Task 6.3 Sensitivity Experiments (Input Data and Parameter) Run and Analysis* –** to quantify the uncertainty associated with open boundary conditions and the use of multiple runoff scenarios for the NEMO model, Team 6 will conduct sensitivity analyses.

Coupled atmosphere/sea ice/ocean model (Task 1.5)

Kirillov et al. (2020) examined the sea ice at three Hudson Bay moorings as well as satellite and CIS data. Here we compare the historical control run against the observed ice fields for each of 2016-2017 and 2017-2018 (Figure 3.6.4). For the AN01 mooring, ice formation in the model starts at the same time as in the observations in Dec 2016. In both, there is a short period of rapid growth to about 0.5 m within a week or so. Then there is slow quasi-linear thermodynamic growth through the rest of winter, reaching 1.5 m by April. The model ice is on the thicker end of the observational spectrum and thicker than the empirical line but not unrealistically so. The ice distribution from the mooring is more variable and thinner in May, but not in the model, with the model ice beginning to thin in late May, with a slope consistent with observations, if a bit thicker. The CIS charts suggest thick first-year ice in July when the model still has about 0.7 m ice. The behavior is similar in 2017, with the model ice at the mooring location forming in November, as with the observations. The sea ice is thinner than in 2016-2017, only reaching about 1.2 m by late winter. The model sea ice is thicker than the main distribution but much closer to the empirical line this year. The model sea ice melts too slowly, with still 0.5 to 1.0 m ice remaining in June (with there is little in the observations), before disappearing in July.

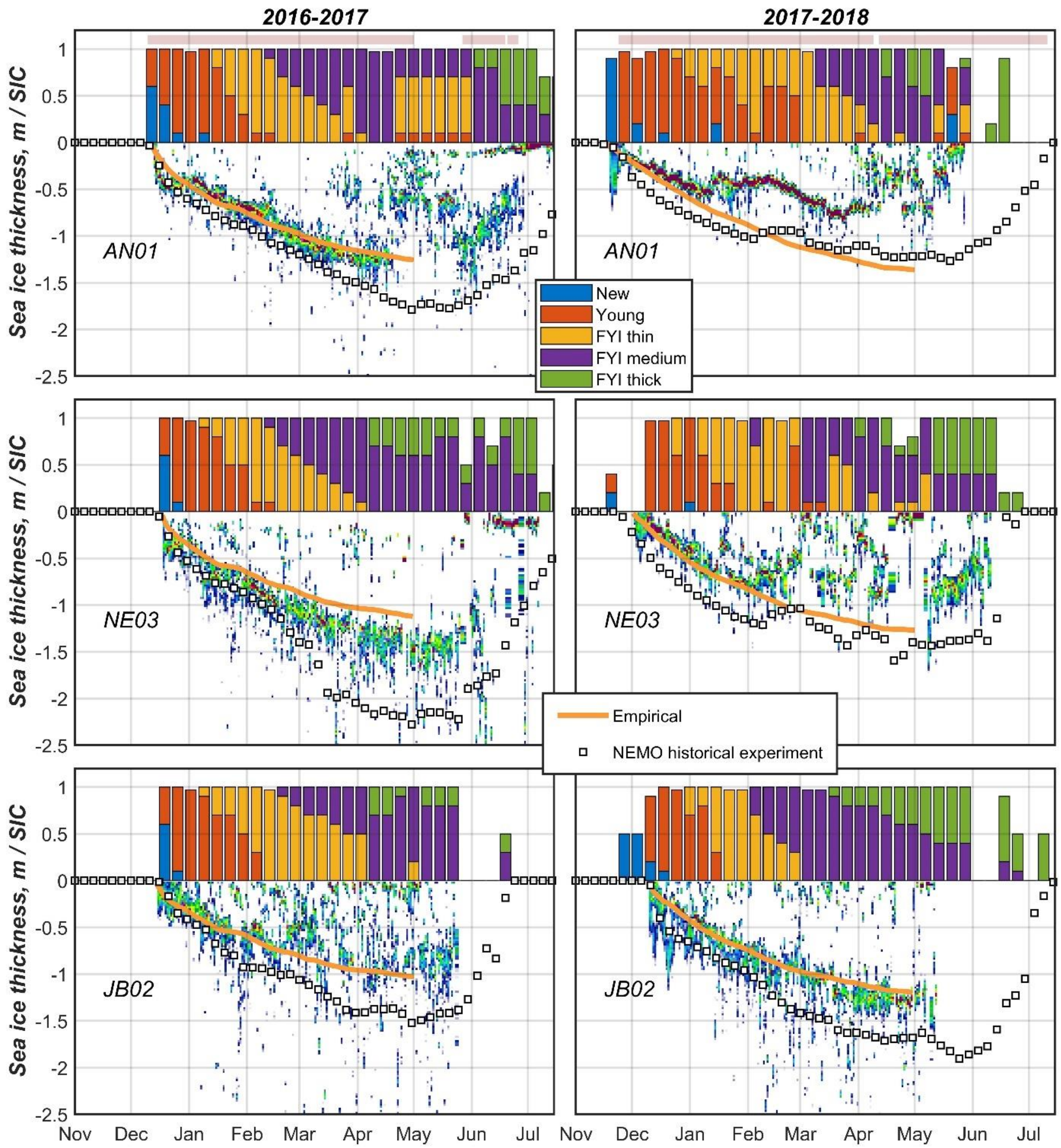

FIGURE 3.6.4 Evolution of sea ice thickness and ice types at AN01 (top), NE03 (middle), and JB02 (bottom) during winter 2017 and 2018. The measured sea ice thicknesses are shown as a percent occurrence, and those maxima (from green to red colors) correspond to the peak probability of daily sea ice thickness at 2cm bin spacing. Daily mean sea ice thickness estimated from empirical thermodynamic growth is shown with orange line. CIS data on partial concentration of different types of sea ice are shown with color bars (new < 10 cm, young ¡ 10-30 cm, FYI thin 30-70 cm, FYI medium 70-120 cm, and FYI thick > 120 cm). Availability of OSI405c ice drift data are shown with pink horizontal bars at the top of the figure. More detail in Kirillov et al. (2020).

The model versus mooring comparison is similar at NE03. In spring 2017, the model sea ice exceeds 2 m in thickness, with a greater discrepancy from observations, although some thick ice is in the observed distribution. Decay is faster in the model than at AN01 and the model sea ice disappears by early July, close to the observational timing. The sea ice fields in 2017-2018 also compare well, with the model at the upper end of the observed distribution and close to the empirical line. At this location, decay occurs at around the same time as observations for this year, with the ice being gone in June.

Behavior at JB02 is similar, with the model at the thicker end of the observational distribution, with the model sea ice a bit thicker than the empirical line. The model sea ice reaches 1.5 m by May, with a rapid decay in June, like in the observations, if a bit slower. The comparison is similar in 2017-2018, but with the model sea ice thickness within the thicker part of the observed distribution. But the model decay in June is much slower than the observations, with the model having 1 m sea ice going into July.

Jafarikhasragh et al. (2019) provided an assessment of simulated sea surface temperature (SST) sensitivity to atmospheric forcing and model resolution in the HBC. This study led to an improved understanding of bulk heat flux parameterizations in the NEMO model, and how the model produces heat fluxes and drives SST on a basin-wide scale, with implications for air-sea heat flux characterization.

Investigation of simulated thermodynamic and dynamic contributions to changes in sea ice thickness on seasonal timescales showed that thermodynamic processes govern sea ice thickness changes in the HBC (Jafarikhasragh et al., 2020). It was further demonstrated that surface energy rather than ocean heat flux contributes to thermodynamic changes, while wind stress is associated with dynamic ice thickness changes. In light of demonstrated correspondence between observed and simulated sea ice conditions, results from this analysis led to an improved understanding of processes governing changes in sea ice thickness on seasonal timescales in the HBC, with implications for prediction.

NEMO Baseline Comparisons

Here we compare the Arctic North Hemisphere Atlantic (ANHA) configuration with the ECCC Regional Ice-Ocean Prediction System (RIOPS). RIOPS is thus an operational regional ice-ocean prediction system. It is run at 1/12 of a degree, so with a horizontal resolution of 4-5km resolution in the Arctic (Figure 3.6.5). As an operational system, it includes full data assimilation and is used mainly for short-term sea ice forecasting. The product is publicly available at https://eccc-msc.github.io/open-data/msc-data/nwp_riops/readme_riops-datamart-alpha_en/. The RIOPS domain is similar to ANHA, having been extracted from a global ORCA12 grid and includes all of the Arctic Ocean as well as the North Atlantic from 27N. Unlike ANHA which uses the sea ice model LIM2, RIOPS uses CICE, which is a multi-category sea ice model with 10 ice thickness categories in each grid cell ([0 0.1 0.15 0.3 0.5 0.7 1.2 2 4 6+ m]). RIOPS is a follow-on to the Global Ice-Ocean Prediction System (GIOPS), which uses a multi-variate SEEK filter for data assimilation (Lellouche et al., 2012, Smith et al., 2015). The assimilation system assimilates sea level anomalies from satellite altimeters (AVISO), sea surface temperature (from both satellite and *in situ* observations), and subsurface temperature and salinity (from Argo, CTD, XBT, moorings, marine mammals). The RIOPS prediction system then has three components: RIPS 3DVar ice analysis, Pseudo-Analysis, and 48hr Forecasts. A 24h run from a previous restart is thus nudged to the GIOPS analysis using spectral nudging (Thompson et al., 2006).

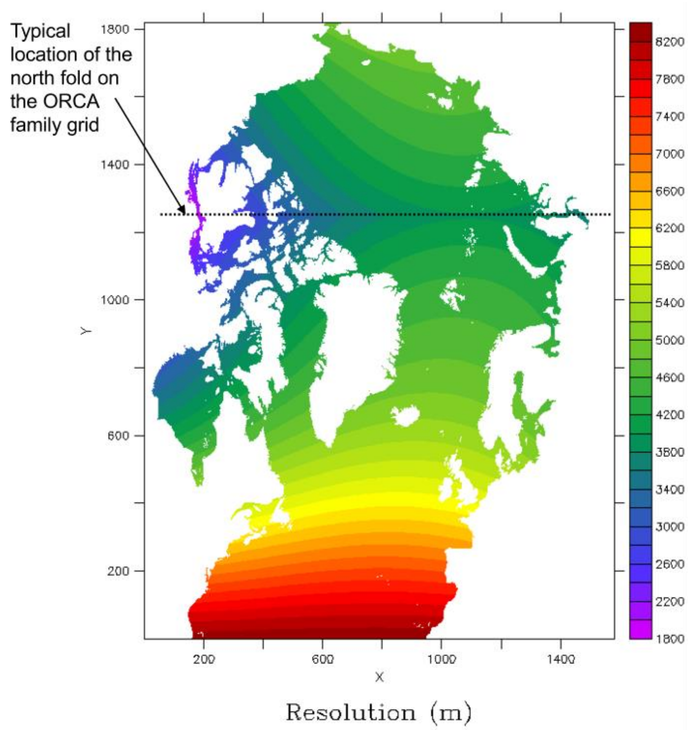

FIGURE 3.6.5 Domain Presentation: 1580x1817x50, 512 procs CREG12. Extracted from ORCA12 (1/12th degree resolution) with the north fold stitched back. Resolution is max. near the artificial pole over northern Canada at 1.8 km and min. along the Atlantic northern boundary (8.2km).

Given the different focus on the models (short term forecast vs long prognostic climate integrations), different sea ice models (single category LIM2 versus multi-category CICE), and the presence of data assimilation in RIOPS, it should not be expected that the specific details from the two outputs will agree on the grid-scale level. Yet, such a comparison is of interest as it can help show some of the strengths, as well as limitations, of prognostic modelling systems. Given the timing of this comparison (i.e., before the BaySys climate ensemble had been run), the ANHA experiments used for the comparison were the historical hindcast ANHA4 and ANHA12 experiments from Ridenour et al. (2019).

As part of this analysis, the first field considered was the sea surface temperature bias between RIOPS and ANHA for each month in 2017 and 2018 (see Appendix A-1). The SST bias between the two products goes to zero in winter when the bay is ice-covered. In general, the SSTs track during the open water period, with both products showing an SST peak in August. The largest bias of up to 1C is seen in Spring, leading to colder surface waters in the ANHA configuration. The freeze-up process is well-represented, with a small SST bias in Autumn. This result is sensitive to the atmospheric product used (as it controls the air-sea fluxes that set the surface temperature), as using CGRF forcing in ANHA12 (compared to ERA-Interim) led to reduced bias in Spring but a larger Autumn bias. Spatially, the SST bias is largest in NW Hudson Bay. The behavior for the bias is similar in both 2017 and 2018. The vertical temperature structure suggests an increasing bias with depth, with more heat penetrating through the top 50 m and 100 m in ANHA. In terms of Sea Surface Salinity (SSS), the version of RIOPS used here has a known major salt bias in the first half of the year, due to excessive ice formation incurred through its data assimilation (Frederic Dupont, personnel communication). The bias is very small in Summer and Autumn. The SSS's from ANHA are closer to those described in observational analyses (e.g., Ingram & Prinsenberg, 1998).

Sea ice bias can be seen in the formation and melt seasons (both products have the bay ice-covered in Winter and ice-free in Summer) (see Appendix A-3). ANHA has delayed ice formation in Autumn and slightly early melt in Spring. The sea ice in RIOPS is thickest in late Winter, exceeding 2m on a bay-wide average, compared to ~1.6m in ANHA. RIOPS, through the issue in the sea ice data assimilation, produces some unrealistic features like 10+ m seasonal sea ice in Foxe Basin. There is no significant bias in sea ice drift, with the 95% confidence interval of each product overlapping the other in most months. In general, the sea ice drift velocities are within 1-2 cm/s of the other product. The sea ice thickness distributions in both RIOPS and ANHA compare similarly to that from Cryosat (Landry et al., 2017), underestimating the thickest and thinnest thickness bins and overestimating the concentration in the bins around the median (see Appendix A-4). The ANHA sea ice fields compare more closely with the BaySys moorings (AN01, NE03, JB02), especially in 2017-2018.

Detailed Analysis of Naturalized & Regulated Experiments (Task 6.1/6.2)

The preparation of naturalized and regulated NEMO experiments for the historical and future scenarios was laid out in the Analysis Methods Section 3.6.2 of this chapter. To evaluate projected climate change and regulation impacts in the HBC, analysis was completed for historical (H; 1981 - 2010) and future (P; 2021-2050 and 2041-2070) naturalized (N) and regulated (R) experiments (Table 3.6.1) for the five-member CMIP5 ensemble. Specifically, climate change (CC), combined climate change and regulation (CCpR), historical regulated (Rh), and cumulative regulated (Rc) impacts are evaluated as follows:

$$CC = PN - HN;$$
$$CCpR = PR - HR;$$
$$Rh = HR - HN;$$
$$Rc = CCpR - CC,$$

where 'subtraction' indicates comparisons between relevant simulations to estimate relative impacts. It should be noted that whereas Rh, intended to identify the impacts of regulation uninfluenced by climate change, will be affected by differences in internal climate variability associated with naturalized and regulated simulations run separately, the cumulative regulation impacts Rc, intended to identify cumulative (historical and future) regulation impacts, is computed as the residual in the difference within (rather than between) each naturalized and regulated simulation and thus may be considered a more reliable estimate of regulation impacts. Percent relative climate change and regulation impacts are computed as $\left(CC/(|CC| + |Rc|)\right) \cdot 100$ and $\left(Rc/(|CC| + |Rc|)\right) \cdot 100$, respectively. Each is also multiplied by the sign of the change in CCpR to indicate whether the relative contribution from each reinforces or counteracts the projected combined climate change and regulation impacts.

TABLE 3.6.1 List of identifiers for each scenario analysis conducted.

Historical	H	Naturalized	N
Projected/future	P	Regulated	R

Traditional diagnostics including time-series and Hovmöller plots (contour plots as a function of latitude (longitude) and time) are used to provide a spatiotemporal characterization of monthly changes in oceanographic and sea ice variables in response to climate change and regulation. Also examined is the change in persistence or 'memory' of marine variables using a diagnostic known as the e-folding time spatial distribution (EFSD) used in past studies to evaluate changes in the Beaufort Sea marginal ice zone (Lukovich and Barber, 2005). This diagnostic is implemented by computing temporal autocorrelations of sea ice variable (SIC, SIT, u_{ice}, and v_{ice}) anomalies at each grid point and corresponding e-folding times of mean values for the 30-year (historical or future) interval considered, and mapping e-folding times in 'weeks' (5-day means based on NEMO output frequency) at each grid point to identify spatial distributions in timescales, and (near-shore and off-shore) changes in response to both regulation and climate, with implications for prediction and planning applications. Additional and more concise descriptions are provided below.

Temporal

1. Monthly time series for ensemble of CMIP5 simulations and uncertainty (standard deviation in CMIP5 ensemble)
2. Difference time series for
   a. Historic and future naturalized (CC)
   b. Naturalized and regulated historic (R)
   c. Historic and future regulated (CC+R/CCpR)
3. Percent climate change and regulation impacts for sea ice variables

Spatial

4. Hovmöller plots and differences between historic and future naturalized and regulated CMIP5 ensemble (with uncertainty based on standard deviation $\sigma_{HN,HR}$ and $\sigma_{PN,PR}$, respectively), with total uncertainty $\sigma_{tot} = \sqrt{\sigma_{HN,HR}{}^2 + \sigma_{PN,PR}{}^2}$
5. Hovmöller plots and differences between individual historic and future members of CMIP5 ensemble, with uncertainty based on spatial variability for each, and total uncertainty computed as in 4.

E-folding time spatial distribution (to monitor persistence)

6. Ensemble CMIP5 EFSD for December to April timeframe

   Difference EFSD ensemble maps for
   a. Historic and future naturalized (CC)
   b. Naturalized and regulated historic (R)
   c. Historic and future regulated (CC+R/CCpR)

Results from this comprehensive analysis can be found in detail in Lukovich et al. (2021) and suggest that regulation suppresses in winter months and reinforces/enhances in summer months climate change impacts on SST and sea ice state and dynamics. Specifically, in winter, regulation suppresses a projected 4×10^5 km^2 (~ 1×10^5 km^3) decrease in sea ice area (volume) due to climate change by ~30% throughout Hudson Bay, and weakens cyclonic circulation by ~50%, particularly in southwestern Hudson Bay; in summer, regulation suppresses a projected 2 – 3 °C increase in SST due to climate change. Results from this analysis further highlight bay-wide and regional reductions in sea ice concentration and thickness in the southwest and northeast Hudson Bay in response to a changing climate, east-west asymmetry in sea ice drift response in support of past studies, suppression of sea ice loss in central Hudson Bay and cyclonic circulation in winter in response to regulation and suggest amplification of regulation impacts offshore in a changing climate.

Sensitivity Experiments (Input Data and Parameter) run and Analysis (Task 6.3)

Existing NEMO configurations were used to carry out sensitivity experiments and begin to understand aspects of the circulation of the HBC. Some of these were carried out within the framework of BaySys, while others were not, but all still helped provide insight on the model and its functioning in the HBC. Ridenour et al. (2019) provided a look at present-day freshwater dynamics in the HBC, in addition to evaluating the sensitivity of the region to model resolution and runoff forcing. Using different estimates of runoff allowed this work to analyze the model sensitivity to the amount, and seasonality, of the runoff product. The main result was that the annually-averaged HBC freshwater budget is mainly a balance between river discharge and freshwater advected out of the region: The surface fluxes (ice melt and growth, and precipitation and evaporation) are the dominant term on seasonal time scales. Increased discharge in runoff datasets leads to stronger circulation patterns, while decreased discharge and seasonality throughout the year led to weaker circulation. Lower freshwater and volume exchange between sub-regions and between the HBC and North Atlantic were also due to decreased discharge and seasonality. Increased model resolution was able to reproduce freshwater contained in sea ice, however, there was generally little impact on fluxes through gates between different sub-basins. The one exception where small-scale processes were found to be important was between Southampton and Baffin Islands. Freshwater interior-boundary exchange was also impacted by higher model resolution via the Ekman and mean components of the flow. Overall, the results show far-field factors have little impact on Hudson Bay, which is driven by local (and Arctic) runoff and climate forcing.

Dissemination of atmospheric/sea ice/ocean model outputs

NEMO output was provided to each science Team at their request (Table 6.3.2), with specific post-processing to convert from NEMO netcdf formatting to formats more easily accessible by each user. Visualizations (ex. maps and graphs) were also provided upon request.

TABLE 6.3.2 List of NEMO outputs provided to researchers from several BaySys Teams.

Team	***Researcher***	***Purpose***
1	Greg McCullough	for freshwater budget studies
1	Sergei Kirillov	for model/mooring comparisons
1	Igor Dmitrenko	for vorticity input and circulation studies
2	Tricia Stadnyk	maps of Arctic freshwater content
3	Lucas Barbedo de Freitas	to assist with phytoplankton bloom studies
3	Janghan Lee	to assist with nutrient budget
3	Marie Pierrejean	for benthic ecology question
3	Sarah Schembri	to drive Ichthyop model
4	David Capelle	for input for carbon box model.

In addition to specific requests, model fields (ocean properties, circulation, Hudson Strait transports, etc.) were provided to several groups in both Team 1 and Team 3. Team 4 received a detailed subset of model fields (shelf, interior, above and below mixed layer) to help drive their carbon-system box model, while the biogeochemical BLING model output for comparison purposes was also being provided.

Through the completion of all of Team 6 tasks, important insights have become clear. Our temporal analysis including monthly time series showed that climate change impacts ascertained through comparison of historical (1981-2010) and future (2021-2050 and 2041-2070) naturalized simulations are evident in sea surface temperature increases of approximately 2 – 3 °C in summer, with values ranging from 1 to 3 degrees Celsius amongst the five CMIP5 simulations. They indicated decreases in sea ice area on the order of 4× 10^5 km2 and in sea ice volume of ~ 1 × 10^5 km3, in addition to enhanced meridional drift and cyclonic circulation in January, February, and to a lesser extent March. Results from our analysis also suggest that regulation suppresses in winter months and reinforces/enhances in summer months climate change impacts on SST and sea ice state and dynamics.

Lastly, although the ensemble mean of scenarios with naturalized river runoff suggests a slight freshening (~0.2 g/kg) of the bay (Garcia-Quintana et al., 2020), there is a large discrepancy between ensemble members, with some scenarios suggested a strong freshening, while others suggest little change or even a slight increase in upper ocean salinity. With regulated river runoff, the ensemble mean salinity reduction is slightly larger (~0.3 g/kg) with no scenarios suggesting an increase in the bay's salinity. The differences between the naturalized and regulated runs look to be related to the timing of the discharge and the residence time for freshwater in the basin. Years of strong discharge add more freshwater to the bay than can be exported through Hudson Strait, lowering the salinity, and increasing freshwater residence times, with the reverse occurring in years of weak discharge.

3.6.4 Conclusions

The BaySys proposal required Team 6 to address one overall objective that was designed to understand the relative impacts of regulation and climate change using ocean and atmospheric modelling in the HBC. We conclude this chapter by summarizing the results from our BaySys investigations as they pertain to the objective.

> ***Hypothesis 6.1*** Freshwater-marine coupling is expected to be influenced on local scales by regulation through changes in seasonality and timing of FW discharge that will influence upwelling, coastal/offshore interactions, mixing, formation of the seasonal ice zone, polynya formation, and timing and magnitude of density-driven currents, and on regional scales by climate change through bay-wide changes in sea ice state and dynamics, FW circulation, OSA interactions due to local and non-local oceanographic and atmospheric forcing.

The objective of Team 6 was to support the other BaySys Teams in investigating the relative impacts of climate change and regulation on freshwater-marine coupling within the HBC (Foxe Basin, Hudson Bay, James Bay, Hudson Strait). In support of Team 1 hypotheses, a sea ice and oceanographic model was used to further study the effects of freshwater loading and ice cover on the circulation of Hudson Bay. This modelling perspective is based on the Nucleus for European Modelling of the Ocean (NEMO) ocean general circulation model coupled to the LIM2 sea ice model. Central also to Team 6 goals is the development of an integrated observational-modelling framework that will provide insight on, and improved representation of, physical, biological, and biogeochemical processes in the Hudson Bay system. The modelling will provide a framework and tool with which to simulate projected changes in marine state and dynamic variables, while also enabling integration of observations and numerical analyses.

Team 6 thus focused on the application of a modelling framework for the BaySys project that will provide insight into the relative effects of climate change and hydroelectric regulation on physical and biogeochemical conditions in the Hudson Bay system. Thus, an existing NEMO modelling configuration, ANHA4, was selected to use in the BaySys project. The version of the ANHA NEMO configuration that existed at the start of the project was used in several initial studies, discussed in greater detail in section 2, that helped provide the framework for the developments needed to carry out the planned long BaySys climate change integrations. Development during the BaySys project including switching to the newer v3.6 of NEMO that allowed for the inclusion of explicit representation of the tides, for example. Significant effort was spent in incorporating runoff from the new and improved HYPE hydrological models (Stadnyk et al., 2020), as well as incorporating forcing from the bias-corrected versions of multiple CMIP5 models. Improvement also occurred in terms of the biogeochemical modules, with the inclusion of a carbon module as part of BLING, and the ongoing work developing and coupling BIGCCIM, with its sympagic as well as pelagic components. The switch to v3.6 of NEMO also enhanced the speed of the simulations through its inclusion of land masking (Madec, 2008). In the end, the NEMO ANHA4 configuration, in conjunction with the BLINGv0 + DIC model and 7 passive tracers, took only 18 hours of CPU time when run on 256 processors on the Compute Canada machine graham, to run 2 years of simulation. This thus made it possible to carry out the 10 near century-long integrations (5 with naturalized runoff and 5 with regulated runoff) central to the BaySys goal of studying the relative impacts of climate change and regulation. Yet, in terms of real-time, which admittedly depends on external factors like throughput on the Compute Canada systems, which is driven by allocation size, this meant about 3 to 4 months running time per experiment. This makes clear why the NEMO model ensembles have only 5 members for each runoff case, while the hydrological model used 19 (Stadnyk et al., 2021). A larger NEMO model ensemble would have been good but was not computationally practical. As part of any modelling study, the results need to be evaluated against observations and other models to understand its ability to properly simulate the real world and understand the limitations and weaknesses of the model. In general, since no model is good at representing all processes and all scales, such evaluation has to be carried out as part of the detailed analysis within individual studies. Thus, aspects of this work within BaySys are being carried out and reported in each of the modelling studies using NEMO output, some of which are highlighted below.

That said, some general overall big picture evaluation can and should be carried out. Section 3.6.3 is a comparison of the historical control run with the BaySys moorings, as well as a subset of other observations available within the bay. The historical control run is used for this evaluation given that it is based on realistic forcing from a reanalysis product (ERA-Interim) unlike the climate experiments, which are forced from given climate simulations that have their internal variability. As the general evaluation shows, in many ways, the model agrees well with the observations, especially when considering the inherent limitations of comparing point source measurements with model fields that are averaged over a grid cell. That said, there are discrepancies between model and observations, such as a too diffuse model thermocline, that need to be highlighted, and considered carefully when discussing model results and results concluded from them. In the end, Team 6 is satisfied with the model configuration that has been run for BaySys, and that overall, it does a good job of representing the main features of the circulation and hydrography of the HBC. Thus, the BaySys model experiments are an ideal base for beginning to understand freshwater-marine coupling and the relative role of climate change and regulation on the HBC.

Results using output from these experiments will appear in many studies, both in the BaySys project Special Feature in *Elementa: Science of the Anthropocene* and beyond. Dmitrenko et al. (2020) used the model output to help scale up mooring data to the bay scale to show that atmospheric vorticity sets the basin-scale circulation within Hudson Bay. Central to BaySys is the question of the relative role of climate change versus river regulation. This led to a suite of 3 core papers putting the present day in the context of the longer historical record (Lukovich et al., 2020a, 2020b) before using the long integrations to show that climate change impacts are evident in terms of sea surface temperature increases and sea ice decreases (Lukovich et al., 2020c). This last work (Lukovich et al., 2020c) also showed that regulation suppresses climate impacts in winter and reinforces them in summer.

As the large number of collaborators indicates, getting a suitable NEMO model configuration developed and running for the BaySys project was a major endeavour. A huge amount of development, testing, and evaluation occurred at intermediate stages that are not highlighted in any publication but were needed to produce the present product (See Phase 1 report - Ch.9). In the end, we feel such effort was well worth it, producing a tool that allows for the detailed study of the HBC, now and in the future, for many years to come. As part of this process, more experiments, and more years of simulation, of the oceanographic conditions with the HBC have been carried out compared to all the previous modelling studies combined.

Results from NEMO showed, 1) the temperature of the bay will warm over the next 50 years, with the bay annually-averaged warming between 2005 and 2070 being ~1.5C, averaged over the

5-member ensemble of climate simulations considered by BaySys for the numerical modelling. Changing from Naturalized to Regulated River Runoff has little impact on this warming. 2) Sea ice concentration and thickness in the bay will significantly decrease over the next 50 years, with the bay averaged reductions between 2005 and 2070 being ~20% in concentration and 0.15-0.2 m in thickness, averaged over the 5-member ensemble of climate simulations considered by BaySys for the numerical modelling. Changing from Naturalized to Regulated River Runoff has little impact on the annually averaged sea ice changes. 3) Although the ensemble mean of scenarios with naturalized river runoff suggests a slight freshening (~0.2 g/kg) of the bay, there is a large discrepancy between ensemble members, with some scenarios suggested a strong freshening, while others suggest little change or even a slight increase in upper ocean salinity. With regulated river runoff, the ensemble mean salinity reduction is slightly larger (~0.3 g/kg) with no scenarios suggesting an increase in the bay's salinity. The differences between the naturalized and regulated runs look to be related to the timing of the discharge and the residence time for freshwater in the basin.

Through the modelling exercises, BaySys determined that regulation suppresses in winter months and reinforces/enhances in summer months climate change impacts on SST and sea ice state and dynamics. Specifically, in winter, regulation suppresses a projected $4x10^5$ km^2 (~1x 10^5 km^3) decrease in sea ice area (volume) due to climate change by ~30% throughout Hudson Bay, and weakens cyclonic circulation by ~50%, particularly in southwestern Hudson Bay; in summer, regulation suppresses a projected 2 – 3 °C increase in SST due to climate change.

Results from BaySys further highlight bay-wide and regional reductions in sea ice concentration and thickness in the southwest and northeast Hudson Bay in response to a changing climate, east-west asymmetry in sea ice drift response in support of past studies, suppression of sea ice loss in central Hudson Bay and cyclonic circulation in winter in response to regulation and suggest amplification of regulation impacts offshore in a changing climate.

The innovation from BaySys modelling allowed us to segregate climate change from regulation because it was the first time an exercise to incorporate hydroelectric regulation, reservoirs and irrigation were undertaken on such a massive continental scale. This has truly revolutionized what we are capable of predicting in terms of hydrology and coupled ocean-terrestrial modelling.

3.6.5 Gaps and Recommendations

BaySys saw the development of a modelling system for the HBC, integrating hydrological, tidal, and atmospheric climate forcing data with numerical model development of the ocean, sea ice, and biogeochemical components of the system to carry out long term studies of marine freshwater coupling. This system was built to be sufficiently flexible that additional modules or drivers could be added for future studies, as well as regional nests for higher resolution localized studies.

a) Continuing work and development on the model and the modelling system is warranted to improve predictions of future conditions and consequences of regulation.

b) Gaining access to improved model bathymetry is likely to improve the representation of the circulation, as well as tidal amplitudes. Studies of the model vertical mixing scheme are likely needed to understand why the model thermocline is too diffuse, and thus improve representation of the upper ocean structure.

c) Switching to a more advanced sea ice model would potentially improve issues, especially in terms of breakup and freeze-up dates. Resolution could be enhanced (at the cost of significantly increased computational requirements) to look at the current structure and coastal processes in more detail.

d) Potentially the use of the AGRIF nesting tool may allow for detailed studies of given regions, such as estuaries. In the end, although comprehensive, the modelling in BaySys is just a start for understanding the circulation and hydrography, and their evolution in the HBC.

3.6.7 References Cited

The following is a list of publications produced and cited by Teams within the BaySys project.

Braun, M., Thiombiano, A., Vieira, M., Stadnyk, T.A. (2021). Representing climate evolution in ensembles of GCM simulations for the Hudson Bay System. *Elementa: Science of the Anthropocene*, 9(1), 00011. https://doi.org/10.1525/elementa.2021.00011

Dmitrenko, I., Myers, P.G., Kirillov, S.A., Babb, D.G., Volkov, D.L., Lukovich, J.V., Tao, R., Ehn, J.K., Sydor, K., Barber, D.G. (2020). Atmospheric vorticity controls bay-scale circulation in Hudson Bay, *Elementa: Science of the Anthropocene*, 8(1). https://doi.org/10.1525/elementa.049

Eastwood, R.A., Macdonald, R.W., Ehn, J.K., Heath, J., Arragurtainaq, L., Myers, P.G., Barber, D.G., Kuzyk, Z.A., (2020). Role of River Runoff and sea Ice Brine Rejection in Controlling Stratification Throughout Winter in Southeast Hudson Bay. *Estuaries and Coasts*, 43, 756-786. https://doi.org/10.1007/s12237-020-00698-0)

Hu, X., Sun, J., Chan, T., Myers, P.G. (2018). Thermodynamic and dynamic ice thickness contributions in the Canadian Arctic Archipelago in NEMO-LIM2 numerical simulations. *The Cryosphere*, 12, 1233–1247. 10.5194/tc-12-1233-2018.

Jafarikhasragh, S., Lukovich, J. V., Hu, X., Myers, P. G., Sydor, K., & Barber, D. G. (2019). Modelling Sea Surface Temperature (SST) in the Hudson Bay Complex Using Bulk Heat Flux Parameterization: Sensitivity to Atmospheric Forcing, and Model Resolution. *Atmosphere-Ocean*, 57(2), 120-133.

Jafarikhasragh, S., Lukovich, J., Hu, X., Myers, P., Sydor, K., et al. (2020). Hudson Bay Complex thermodynamic and dynamic sea ice thickness regimes from an ocean-ice model. *Journal of Geophysical Research*.

Kirillov, S., Babb, D.G., Dmitrenko, I., Landy, J., Lukovich, J., Ehn, J., Sydor, K., Barber, D., Stroeve, J. (2020). Atmospheric forcing drives the winter sea ice thickness asymmetry of Hudson Bay. *Journal of Geophysical Research: Oceans*, 125, e2019JC015756. https://doi.org/10.1029/2019JC015756

MacDonald, M.K., Stadnyk, T.A., Déry, S.J., Braun, M., Gustafsson, D., Isberg, K., Arheimer, B. (2018). Impacts of 1.5 and 2.0 degrees C warming on pan-Arctic river discharge into the Hudson Bay complex through 2070. *Geophysical Research Letters*, 45(15), 7561-7570.

McCullough, G.K., Kuzyk, Z.A., Ehn, J.K., Babb, D.G., Ridenour, N., Myers, P.G., Wong, K., Koenig, K., Sydor, K., Barber, D.G. (2019). Freshwater-Marine Interactions in the Greater Hudson Bay Marine Region. P. 155–197 in Z.A. Kuzyk and L.M. Candlish, ed., *From Science to Policy in the Greater Hudson Bay Marine Region: An Integrated Regional Impact Study (IRIS) of Climate Change and Modernization.* ArcticNet, Québec City, 424 pp.

Ridenour, N.A., Hu, X., Sydor, K., Myers, P.G., Barber, D.G. (2019). Revisiting the circulation of Hudson Bay: Evidence for a seasonal pattern. *Geophysical Research Letters*, 46. https://doi.org/10.1029/2019GL082344

Ridenour, N.A., Hu, X., Jafarikhasragh, S., Landy, J.C., Lukovich, J.V., Stadnyk, T.A., Sydor, K., Myers, P.G., Barber, D.G. (2019). Sensitivity of freshwater dynamics to ocean model resolution and river discharge forcing in the Hudson Bay Complex. *Journal of Marine Systems*, 196, 48-64.

Stadnyk, T.A., Tefs, A., Broesky, M., Déry, S.J., Myers, P.G., Ridenour, N.A., Vonderbank, L., Gustafsson, D. (2021). Changing freshwater contributions to the Arctic: a 90-year trend analysis (1981-2070). *Elementa: Science of the Anthropocene*, 9(1), 00098. https://doi.org/10.1525/elementa.2020.00098

Stadnyk, T.A., Déry, S.J., MacDonald, M.K., Koenig, K.A. (2019). Freshwater System. In Barber, D., Kuzyk, Z., Candlish, L. *An Integrated Regional Impact Assessment of Hudson Bay: Implications of a Changing Environment*. Québec City, QC, Canada.

Other Works Cited

Andersson, J., Pechlivanidis, I., Gustafsson, D., Donnelly, C., Arheimer, B. (2015). Key factors for improving large-scale hydrological model performance. *European Water*, 49, 77–88.

Arora, V., and Boer, G. (1999). A variable velocity flow routing algorithm for GCMs. *Journal of Geophysical Research*, 104. 30965–30979.

Arora V, Scinocca J, Boer G, Christian J, Denman K, Flato, G.M., Kharin, V.V., Lee, W.G., Merryfield, W.J. (2011). Carbon emission limits required to satisfy future representative concentration pathways of greenhouse gases. *Geophysical Research Letters*, 38(5). 10.1029/2010GL046270.

Bamber, J., Broeke, M.V.D., Ettema, Lenaerts, J., Rignot, E. (2012). Recent large increases in freshwater fluxes from Greenland into the North Atlantic. *Geophysical Research Letters*, 39. 10.1029/2012GL052552.

Bamber J, Tedstone A, King M, Howat I, Enderlin E, van den Broeke, M.R., Noel, B. (2018). Land ice freshwater budget of the arctic and north atlantic oceans: 1. data, methods, and results. *Geophysical Research Letters*, 123(3), 1827–1837. 10.1002/2017JC013605.

Castro de la Guardia, C., Myers, P., Derocher, A., Lunn, N., terwisscha van Scheltinga, A. (2017). Sea ice cylce in western Hudson Bay, Canada from a polar bear persepective. *Marine Ecology Progress Series*, 564, 225–233. 10.3354/meps11964.

Castro de la Guardia, L. (2018). Modelling the response of Arctic and Subarctic marine systems to climate warming. Ph.D. thesis, University of Alberta.

Castro de la Guardia, L., Derocher, A., Myers, P., Terwisscha van Scheltinga, A., Lunn, N. (2013). Future sea ice conditions in western Hudson Bay and consequences for polar bears in the 21st century. *Global Change Biology*, 1–13. 10.1111/gcb.12272.

Castro de la Guardia, L., Garcia-Quintana, Y., Claret, M., Hu, X., Galbraith, E. (2019). Winds and sea ice loss on Arctic phytoplankton blooms in an iceoceanbiogeochemical model. *JGR Biogeosciences*, 124, 2728–2750. 10.1029/2018JG004869.

Dee, D.P., Uppala, S.M., Simmons, A.J., Berrisford, P., Poli, P., Kobayashi, S., Andrae, U., Balmaseda, M.A., Balsamo, G., Bauer, D.P. and Bechtold, P. (2011). The ERA-Interim reanalysis: Configuration and performance of the data assimilation system. *Quarterly Journal of the royal meteorological society*, 137(656), 553-597.

Donner, L.J., Wyman, B.L., Hemler, R.S., Horowitz, L.W., Ming, Y., Zhao, M., Golaz, J.C., Ginoux, P., Lin, S.J., Schwarzkopf, M.D. and Austin, J., (2011). The dynamical core, physical parameterizations, and basic simulation characteristics of the atmospheric component AM3 of the GFDL global coupled model CM3. *Journal of Climate*, 24(13), 3484-3519.

Egbert, G., and Erofeeva, S. (2002). Efficient inverse modelling of barotropic ocean tides. *Journal of Atmospheric and Oceanic Technology*, 19, 183–204.

Enderlin, E. M., Howat, I. M., Jeong, S., Noh, M. J., Van Angelen, J. H., & Van Den Broeke, M. R. (2014). An improved mass budget for the Greenland ice sheet. *Geophysical Research Letters*, *41*(3), 866-872.

Ettema, J., Van den Broeke, M. R., Meijgaard, E. V., Van de Berg, W. J., Box, J. E., & Steffen, K. (2010). Climate of the Greenland ice sheet using a high-resolution climate model–Part 1: Evaluation. *The Cryosphere*, *4*(4), 511-527.

Fichefet, T., and Morales Maqueda, M.A. (1997). Sensitivity of a global sea ice model to the treatment of ice thermodynamics and dynamics. *Journal of Geophysical Research*, 102, 12609–12646.

Galbraith E.D., A. Gnanadesikan, J. P. Dunne, and M. R. Hiscock (2010). Regional impacts of iron-light colimitation in a global biogeochemical model. *Biogeosciences*, 7, 1043–1064. www.biogeosciences.net/7/1043/2010/

Galbraith, E.D., Dunne, J.P., Gnanadesikan, A., Slater, R.D., Sarmiento, J.L., Dufour, C.O., De Souza, G.F., Bianchi, D., Claret, M., Rodgers, K.B. and Marvasti, S.S., (2015). Complex functionality with minimal computation: Promise and pitfalls of reduced-tracer ocean biogeochemistry models. *Journal of Advances in Modeling Earth Systems*, *7*(4), 2012-2028.

Garcia H, Boyer T, Locarnini R, Mishonov A, Paver C, et al. (2018). World Ocean Atlas 2018 (pre-release): Product Documentation. A Mishonov Technical Ed, NOAA Atlas NESDIS.

Garcia HE, Locarnini RA, Boyer TP, Antonov JI, Baranova O, et al. (2014a). World Ocean Atlas 2013: Dissolved inorganic nutrients (phosphate, nitrate, silicate). S Levitus, Ed, A Mishonov Technical Ed, NOAA Atlas NESDIS 4: 25.

Garcia HE, Locarnini RA, Boyer TP, Antonov JI, Baranova O, et al. (2014b). World Ocean Atlas 2013: Dissolved oxygen, apparent oxgyen utilization, and oxygen saturation. S Levitus, Ed, A Mishonov Technical Ed, NOAA Atlas NESDIS 3: 27.

Gelfan, A., Gustafsson, D., Motovilov, Y., Arheimer, B., Kalugin, A., Krylenko, I. and Lavrenov, A., (2017). Climate change impact on the water regime of two great Arctic rivers: modeling and uncertainty issues. *Climatic change*, 141(3), 499-515.

Gillard, L., Marson, H., Johnson, H., Myers, P. (2020). The Fate of Greenlands Glacial Melt and Iceberg Discharge. Atmosphere-Ocean Submitted.

Hayashida, H., Christian, J.R., Holdsworth, A.M., Hu, X., Monahan, A.H., Mortenson, E., Myers, P.G., Riche, O.G., Sou, T. and Steiner, N.S., (2019). CSIB v1 (Canadian Sea-ice Biogeochemistry): a sea-ice biogeochemical model for the NEMO community ocean modelling framework. *Geoscientific Model Development*, *12*(5), 1965-1990.

Hochheim, K.P., Barber, D.G., (2010). Atmospheric forcing of sea ice in Hudson Bay during the fall period, 1980–2005. *Journal of Geophysical Research*, 115, C05009. https://doi.org/10.1029/2009JC005334

Hochheim, K., Lukovich, J., Barber, D. (2011). Atmospheric forcing of sea ice in Hudson Bay during the spring period, 1980-2005. *Journal of Marine Systems*, 88, 476–487.

Holliday, N.P., Bersch, M., Berx, B., Chafik, L., Cunningham, S., Florindo-López, C., Hátún, H., Johns, W., Josey, S.A., Larsen, K.M.H. and Mulet, S. (2020). Ocean circulation causes the largest freshening event for 120 years in eastern subpolar North Atlantic. *Nature communications*, *11*(1), 1-15.

Ingram, R.G., and Prinsenberg, S. (1998). *Coastal oceanography of Hudson Bay and surrounding eastern Canadian Arctic waters coastal segment*. in Robinson AR, Brink KH, eds., The Sea, Volume 11, pp. 835–861. John Wiley and sons, Inc.

Jones, E.P., Swift, J.H., Anderson, L.G., Lipizer, M., Civitarese, G., Falkner, K.K., Kattner, G. and McLaughlin, F. (2003). Tracing Pacific water in the North Atlantic ocean. *Journal of Geophysical Research: Oceans*, *108*(C4).

Large, W.G., and Yeager, S.G. (2009). The global climatology of an interannually varying air-sea flux data set. *Climatic Dynamics*, 33, 341–464. 10.1007/s00382-008-0441-3.

Lenaerts, J.T., Le Bars, D., Van Kampenhout, L., Vizcaino, M., Enderlin, E.M. and Van Den Broeke, M.R. (2015). Representing Greenland ice sheet freshwater fluxes in climate models. *Geophysical Research Letters*, *42*(15), 6373-6381.

Lindsay, K., Bonan, G.B., Doney, S.C., Hoffman, F.M., Lawrence, D.M., Long, M.C., Mahowald, N.M., Keith Moore, J., Randerson, J.T. and Thornton, P.E. (2014). Preindustrial-control and twentieth-century carbon cycle experiments with the Earth System Model CESM1 (BGC). *Journal of Climate*, *27*(24), 8981-9005.

Madec, G. (2008). NEMO ocean engine. Institut Pierre-Simon Palace (IPSL).

Madec, G. and the NEMO Team. (2008). NEMO ocean engine. Institut Pierre-Simon Palace (IPSL).

Marson, J., Myers, P., Hu, X., Le Sommer, L. (2018). Using vertically integrated ocean elds to characterize Greenland icebergs' distribution and lifetime. *Geophysical Research Letters*, 45, 4208–4217. 10.1029/2018GL077676.

Sibert, V., Zakardjian, B., Gosselin, M., Starr, M., Senneville, S., LeClainche, Y., (2011). 3D bio-physical model of the sympagic and planktonic productions in the Hudson Bay system *Journal of Marine Systems*, 88, 401–422. https://doi.org/10.1016/j.jmarsys.2011.03.014

Sibert, V., Zakardjian, B., Saucier, F., Gosselin, M., Starr, M., Senneville, S. (2010). Spatial and temporal variability of ice algal production in a 3D ice-ocean model of the Hudson Bay, Hudson Strait, and Foxe Basin system. *Polar Research*, 29(3), 353-378. 10.1111/j.1751-8369.2010.00184.x

Steele, M., Morley, R., Ermold, W. (2001). PHC: A global ocean hydrography with a high-quality Arctic Ocean. *Journal of Climate*, 14, 2079–2087.

Tao, R., & Myers, P. G. (2021). Modelling the advection of pollutants in the Hudson Bay complex. *Journal of Marine Systems*, *214*, 103474.

Tremblay, J., and Gagnon, J. (2009). The effects of irradiance and nutrient supply on the productivity of Arctic waters: a perspective on climate change. in Nihoul J, (eds) AK, eds., *Influence of Climate Change on the Changing Arctic and Sub-Arctic Conditions*, pp. 73–93. Springer Science and Business Media BV.

Tremblay, J. É., Raimbault, P., Garcia, N., Lansard, B., Babin, M., & Gagnon, J. (2014). Impact of river discharge, upwelling and vertical mixing on the nutrient loading and productivity of the Canadian Beaufort Shelf. *Biogeosciences*, *11*(17), 4853-4868.

van Angelen, J., van den Broeke, M., Wouters, B., Lenaerts, J. (2014). Contemporary (19602012) Evolution of the Climate and Surface Mass Balance of the Greenland Ice Sheet. *Survey Geophysical*, 35, 1155–1174.

van Meijgaard, E., Van Ulft, L. H., Van de Berg, W. J., Bosveld, F. C., Van den Hurk, B. J. J. M., Lenderink, G., & Siebesma, A. P. (2008). *The KNMI regional atmospheric climate model RACMO, version 2.1* (p. 43). De Bilt, Netherlands: KNMI.

Watanabe, M., Suzuki, T., O'ishi, R., Komuro, Y., Watanabe, S., Emori, S., Takemura, T., Chikira, M., Ogura, T., Sekiguchi, M. and Takata, K. (2010). Improved climate simulation by MIROC5: Mean states, variability, and climate sensitivity. *Journal of Climate*, *23*(23), 6312-6335.

Yukimoto, S., Adachi, Y., Hosaka, M., Sakami, T., Yoshimura, H., Hirabara, M., Tanaka, T.Y., Shindo, E., Tsujino, H., Deushi, M. and Mizuta, R., (2012). A new global climate model of the Meteorological Research Institute: MRI-CGCM3—Model description and basic performance—. *Journal of the Meteorological Society of Japan. Ser. II*, *90*, 23-64.

CHAPTER 4 INTEGRATION

The combined research efforts of the six project Teams represented an unprecedented effort to better understand the Hudson Bay Complex (HBC). To provide a scientific basis to separate climate change effects from those of regulation of freshwater, the unique role of rivers and estuaries in the HBC were examined. The project team's expertise in physical, biological, and biogeochemical conditions in the HBC allowed for a collaborative and innovative method to examine the HBC from the perspective of the different subsystems. The Teams applied a unifying, holistic Earth System Science vision, in which new knowledge from various scientific approaches (observation, experiment, and modelling), across multiple fields of study (physics, chemistry, geology, hydrology, biology) and spatial scales (watershed, river, estuary, coastal domain, offshore sea) were integrated to study the HBC as a system. At one end of the spectrum, the approaches included individual process studies (e.g., degradation of dissolved organic matter in the Nelson River estuary, wave impacts on sea ice); at the other end, it recognized interactions among the atmosphere, hydrosphere, litho/pedosphere and biosphere (e.g., influence of atmospheric circulation on freshwater export through Hudson Strait). Both types of studies add to our understanding of this system, and informed the central questions of the BaySys program – what are the relative contributions of regulation and climate change on freshwater-marine coupling in Hudson Bay? Furthermore, the integration of observation data and modelling was key to understanding the present-day processes and predicting future impacts of climate change and regulation impacts on the system. This Integration Chapter outlines and discusses how the studies of processes within various spheres and across multiple subsystems by BaySys are integrated into a study of the complex system of Hudson Bay and the question of its response to climate change and regulation.

Integrated BaySys project results are presented and discussed within a series of coupled systems, both at the spatio-temporal scales of riverine, estuarine, and coastal Regions of Freshwater Influence (ROFIs) and the larger scales of bay-wide processes. The results are presented in this way because interaction of forcings begins at the smaller spatio-temporal scales of the ROFIs, where the responses to individual and coupled forcings can initiate. Small scale processes feed up in scale affecting regions, and ultimately the bay, and beyond. For example, physical, chemical, and biological systems are altered by passage through natural and imposed hydrological regimes so that rivers provide an integrated signal from watersheds. This makes fluvial systems good indicators of the combined impacts of regulation, land use, and climate change in their watersheds, but it also means that the direct impacts of regulation are most readily distinguished within and in proximity to fluvial systems. At the larger, bay-wide scale, forcing from the various regions and spheres were found to interact in increasingly complex ways, making it more challenging to distinguish between the impacts of climate and regulation on the system. Moreover, the HBC is part of a global, interconnected ocean system that, on long time scales (years to decades or longer), will respond to the changes occurring in connected ocean areas (e.g., sea-level rise, Arctic Ocean warming, freshening, and nutrient levels). Regulation has a more direct impact than climate change on the short time scales (weeks, months), but longer-term, both regulation and climate change and their interaction (which can be either offsetting or additive) are more difficult to characterize. At every scale, Team members have responded to this complexity in order to analyse and highlight the significance and implications of their findings for the relative roles of climate change and river regulation on modifying the processes in question within each subsystem of the HBC (Figure 4.1).

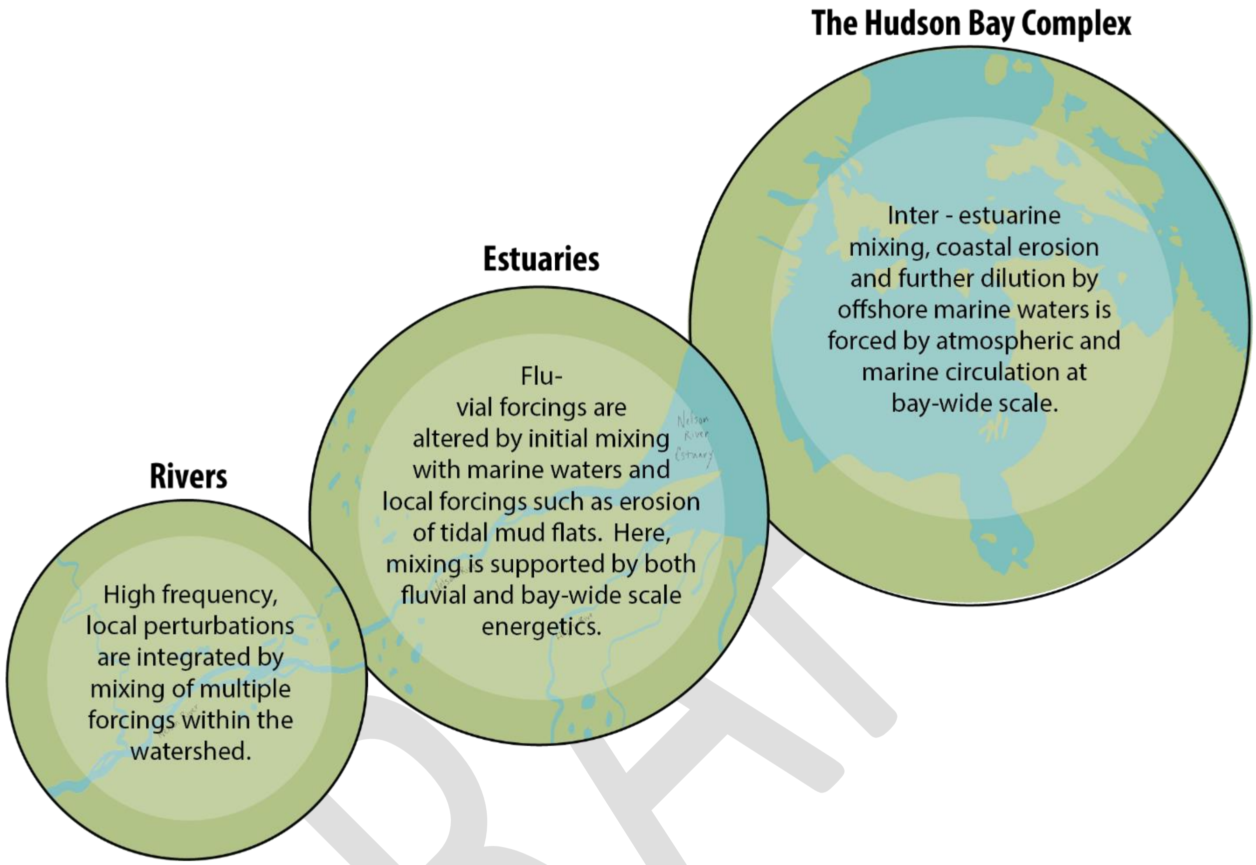

FIGURE 4.1 Schematic illustrating the various parts of the Hudson Bay System from the rivers to the estuaries, to the HBC as a whole. BaySys researchers have integrated and produced results at each level of this system.

4.1 Rivers

To understand the functioning of the freshwater-marine systems within the HBC, it is necessary to first discuss the project findings related to the numerous surrounding rivers contributing freshwater into the system. Some HBC rivers are well studied or regularly monitored; other rivers are poorly sampled and some, not at all. Almost all Teams utilized data from the rivers, including hydrometric and water quality data, geochemical tracers, and fish mercury data. Describing present-day hydrology for the entire drainage basin of Hudson Bay (HBDB), including ungauged portions, was thus an important foundation for the project, followed by modelling at the scale of the drainage basin to project how discharge would change under future climate scenarios. From a biogeochemical perspective, 17 individual rivers and lakes were sampled during the BaySys project; however, the Nelson and Churchill Rivers were extensively sampled throughout the multiple field campaigns, or as part of previous research programs (ie., CAMPS), and have provided some of the best evidence for addressing BaySys objectives.

Freshwater fluxes: past, present, and future

Over the entire Hudson Bay marine complex, river discharge has historically comprised about three-quarters of the net freshwater supply (McCullough et al., 2019). Present-day river discharge is partially constrained by a network of gauging stations although the number of stations within the HBDB decreased during recent decades and the northern parts of the HBDB including Nunavut and northern Quebec portions have few gauges. New hydrometric stations installed in nine rivers in eastern James Bay by Hydro Quebec and academic partners will help to improve the coverage in this area (de Melo et al., in prep).

Because of the vast size and heterogeneity of the drainage basin, the brevity of discharge records, and decadal climate variability that affects river discharge, there have been different temporal trends reported for river discharge in the HBDB. From 1964 to 2003, river discharge in 64 northern Canadian rivers including many in the HBC showed a decreasing trend with an overall decrease of about 10% over the four decades (Déry, 2005). Later works showed the rivers are behaving/responding differently and trends are reversing. Hence why taking such a long-term approach to trend analysis here is so important. As part of BaySys, Déry and coworkers (Déry et al., 2016) provided an updated analysis using data for 42 northern Canadian rivers (including data for >30 stations in the Hudson Bay basin) spanning 1964 to 2013 and found that river discharge significantly increased. An analysis for Hudson Bay rivers specifically showed there were at least two or three distinct temporal phases with a downward trend in discharge from the mid-1960s to the mid-1980s, followed by a period of relatively stable high flows in the mid-1980s and early 1990s, and then an upward trend in the more recent decades (Déry et al., 2011; Déry et al., 2016). The total annual river discharge into HBC has been in the order of 760 km^3/yr but the interannual variability is on average nearly 10% and there have been several exceptional years. A year of major oceanographic data collection in Hudson Bay was 2005, which was one of those exceptional years with record-high annual river discharge (438.8 $km^3\ yr^{-1}$) to western Hudson and James Bay (Déry et al., 2016). Different regions also show different temporal trends especially if the discharges are considered on a seasonal basis. Déry et al. (2016) described how east Hudson Bay and James Bay region had increasing annual flows and increasing winter flows due in part to the La Grande Rivière system. McCullough et al. (2019) reported that the diversion of the Caniapiscau River reduced discharge into Hudson Strait by 14% and increased flow into James Bay by 8% and that the winter portion of annual discharge into James Bay was increased from 12% to 31% by the operation of the La Grande Rivière hydroelectric complex. Although the seasonal shift due to Nelson River regulation was much smaller (from 26% of annual discharge before regulation to 31% after), diversions in both systems caused significant increases in discharge into their respective estuaries (McCullough et al., 2019).

For projecting future river discharge in BaySys, we used a continental-scale hydrological model (Hydrological Predictions for the Environment, HYPE), together with climate data from the Coupled Model Intercomparison Project (CMIP). The aim was to have river discharge projections both to study in their own right and to use as input to the Nucleus for European Modelling of the Ocean (NEMO) ice-ocean model. Both the hydrologic model and the NEMO ocean model are complex and computationally demanding. Thus, a necessary first step was to select a reduced number of CMIP climate data ensembles from the 54 different ensembles that were available. Ultimately, we selected two hierarchical, differently sized simulation ensembles were selected – one with five members and one with 19 members – to represent the climate evolution for the region. These two ensembles were rigorously compared using 10 extreme climate indicators and their changes for different spatial domains (the full study region and seven sub-regions), different time domains (annual and seasonal basis), and considering two future climate horizons. The results revealed that the smaller ensemble was sufficient to adequately reproduce the mean and spread in the indicators found for the larger ensemble (Braun et al., 2021).

Using the ensembles described above, Braun et al. (2021) determined that the atmosphere over the HBDB would warm at from 1.2 to 2.5 times the rate of global mean temperature, that is, in the event of 2°C global warming, annual temperatures would increase by about 3°C in the south to 5°C in the far north. This warming will reduce frost and icing days during the shoulder seasons (spring, fall) especially in the southern portion of the drainage basin. Total precipitation, as well as 5-day maxima, will increase by up to 10% in the future, with slightly higher average precipitation intensities. This affects dry spells, which the analysis projects to be slightly shorter in the future (Braun et al., 2021). Total precipitation is expected to increase throughout the HBDB, with larger increases in the eastern portion of the study region. This gradient is less pronounced for 5-day precipitation amounts (which can drive major discharge events), where increases are also projected for southern and eastern basins, particularly in summer and winter. Macdonald et al., (2018) predicted steady-state to modest (not statistically significant) increases in discharge from Nelson River discharge due to climate change through the next half-century. More generally, their predictions that discharge will increase, given a global warming increase of 1.5°C, range from “more likely than not” in the western HBDB to “virtually certain” in Foxe Basin, and that the magnitude and probability are both higher should warming increase by 2°C. However, under either scenario median increases are projected to be less than 10% except in Foxe Basin, where discharge may increase by more than 20% under 2°C global warming (Macdonald et al., 2018). Stadnyk et al. (2021) report all pan-Arctic river results under climate change scenarios run for BaySys.

Biogeochemical fluxes: past, present, and future

Riverine fluxes of nutrients and carbon are small when compared to the massive fluxes that occur within marine environments, due to advection and upwelling. For example, the estimated annual nitrate input of 2×10^{10} g N for the whole bay from rivers is more than an order of magnitude smaller than the estimated winter re-supply of nitrate from marine sources (124×10^{10} g N, assuming a total area of 5.48×10^5 km^2 for marine waters). Additionally, while the riverine fluxes of carbon in its various forms to the bay are large relative to other Arctic seas, collectively they only represent a small fraction of the carbon that is stored in the upper water column (~ 20 m) of the bay’s coastal corridor. For example, the annual flux of dissolved inorganic carbon (DIC) and alkalinity (TA) from all rivers entering the bay is larger than all but a few of the largest Arctic rivers, it constitutes less than 1% of the DIC and TA contained in the upper 20 m of the coastal sea. The exception is dissolved organic carbon (DOC), where the river influx annually represents ~ 8% of what is stored in the upper coastal sea. Thus, river water dilutes TA and DIC, while augmenting the availability of organic carbon in the marine system. Additionally, we confirmed that rivers in the southwest of Hudson Bay have much higher concentrations of DIC and TA than rivers draining Precambrian Shield. Sea ice melt typically has lower concentrations for both DIC and TA relative to the southwest rivers, but not necessarily relative to rivers that drain other parts of the bay's watershed. In the marine system, the run-off from the Precambrian Shield and sea ice melt will both cause severe undersaturation in the concentration of dissolved CO_2 (expressed as a CO_2 partial pressure; pCO_2) relative to atmospheric values on mixing with seawater, even if both the river water and seawater are saturated in CO_2. The main impacts of such dilution are highly localized, rapidly dissipating upon mixing with seawater. BaySys research has demonstrated that riverine fluxes of freshwater, heat, sediment, nutrients and carbon strongly affect other conditions (thermodynamic, biological, and biogeochemical) in estuaries and the riverine coastal domain in the bay (Ahmed et al., 2021; Capelle et al., 2020; Kazmiruk et al., 2021.

An important backdrop for understanding biogeochemical fluxes of Hudson Bay rivers and especially those draining the Hudson Bay Lowlands (formerly Tyrell Sea) is that on geologic time scales, the sedimentary system is adjusting to falling relative sea-level – due to postglacial isostatic rebound in Hudson Bay – in other words, in their lower reaches, the rivers are incising and eroding previously deposited sediments and transporting them into the bay. Current rates of land uplift are about 1 cm/yr in western and southern Hudson Bay (Tsuji et al., 2016; Sella et al., 2007; Simon et al., 2017). Sea-level rise associated with global warming has reached 0.36 cm/yr over the last two decades so that the level of Hudson Bay is currently falling at about 0.6 cm/yr relative to its shores. It is expected that sea-level rise associated with global warming may come to dominate sometime in the twenty-first century thus changing the fundamental controls onshore erosion and near-shore resuspension. Effects of isostatic adjustment are also important for processes being considered at the watershed scale. Faster rates of uplift in the northern vs. southern portion of the Nelson River watershed will tend to promote erosion on southern or western shores of lakes with outlets nearer the centre of uplift, which is the case with all of the larger lakes from Lake Winnipeg to Hudson Bay.

Past studies have assessed dissolved carbon (organic and inorganic; DOC & DIC) and nutrient fluxes from limited data sets mostly lacking the ice-covered season (Godin et al., 2017; Kuzyk et al., 2008a; Mundy et al., 2010; Burt et al., 2016; Rosa et al., 2012). Nutrient, carbon, and mercury concentrations were measured in several rivers as part of BaySys with some additional data obtained during winter for the Nelson, Hayes, and Churchill Rivers. Data from past monitoring programs, including on fish mercury concentrations, were also compiled, synthesized, and statistically analyzed. Overall, the rivers are important sources of nitrogen as well as silicon, although there are regional differences. The carbon fluxes vary regionally as well. Organic carbon tends to be high in both boreal (wetland dominated) and tundra rivers. The Nelson and the other rivers draining the Hudson Bay Lowlands of the Hudson Plains deliver an important alkalinity component, which has a buffering effect in relation to pH changes in the Nelson estuary and surrounding ROFI. As mentioned, freshwater is very low in alkalinity and DIC enters the bay from rivers draining the Precambrian Shield and to sea ice melt. The main impacts of such dilution are highly localized, rapidly dissipating upon mixing with seawater. Increasing river discharge together with warmer and wetter conditions that promote faster weathering and increased productivity in the watershed is expected to increase the fluxes of all these constituents.

Nelson River processes

The Nelson River was a focus for studies of biogeochemical fluxes and implications of regulation and climate change. Several research groups conducted field activities in the Nelson River watershed to obtain new water quality and soils data and also analyzed portions of historical data sets generated by past monitoring programs (such as the Coordinated Aquatic Monitoring Program (CAMP) and the earlier Federal Ecological Monitoring Project). The Teams focussed primarily on processes that mobilize and transport sediment, organic matter, and mercury from the watershed to the estuary and the bay. Many of these processes are sensitive to climate change (especially warming and runoff) and regulation (river discharge) and may interact with changes in runoff to modify fluxes of materials to the bay.

Goharrokhi et al. (2021) used new sediment core data from Lake Winnipeg to demonstrate that the lake efficiently traps sediments from the Saskatchewan, Red-Assiniboine, and Winnipeg River sub-catchments and erosion of its shores. The results imply that the main-stem Nelson River at its origin (as the natural outflow from Lake Winnipeg) carries a low load of mineral sediment. Results of Stainton et al. (in review) support this finding by showing that the lowest suspended sediment concentrations across the entire Nelson River system occur in the upper Nelson River between Lake Winnipeg and the Jenpeg Generating System. However, the suspended particulate matter in this area below Lake Winnipeg contains the highest proportion of organic carbon and nitrogen throughout the Nelson system, reflecting high autochthonous (algal) production in the lake and its export to the Nelson River system. Furthermore, a comparison of data spanning 30 years indicates an increase in the organic component over time associated with the eutrophication of Lake Winnipeg. As described in McCullough et al. (2012), higher runoff and more frequent flooding, which are associated with climate variability and/or change, have been a significant factor in the eutrophication of Lake Winnipeg, together with higher anthropogenic phosphorous loading onto the land. A previous study found that phosphorous levels in the Upper Nelson River increased immediately after Lake Winnipeg regulation but then stabilized as a new balance was reached between discharge and shoreline erosion (Rosenberg, 2005). These new findings suggest that elevated algal-derived suspended organic matter in the upper Nelson is an ongoing impact of changes in Lake Winnipeg. These results may be relevant in the context of mercury cycling, which is affected by organic matter and eutrophication in various ways (cf., Razavi et al., 2015).

Stainton et al. (in review) also characterized suspended particulate matter along the Rat-Burntwood River (RBR) system, which receives Churchill River diversion flows and is a major tributary of the Nelson River main stem at Thompson. The RBR contrasted sharply with the upper Nelson River in terms of water quality having high suspended sediment levels due to bank and shoreline erosion. Permafrost thaw appears to be an important factor in bank erosion and suspended sediment supply. Even without an increase in discharge, the warmer, wetter period during the 2000s was associated with higher suspended sediment levels than the late 1980s-early 1990s cooler, dryer period. Thus, the temporal trends run counter to predictions of increasing bank stabilization post-development. In the lower Nelson River system, below Split Lake, the new data indicate that relatively high suspended sediment concentrations are maintained by numerous local sources of sediment, which are again primarily associated with bank erosion. The organic component of the suspended sediment resembles soil organic matter in its nitrogen content except for reservoirs like Stephens Lake, where nitrogen-rich algal matter locally modifies the material. Impoundment has probably increased the retention time and reactions involving organic carbon, which will affect the carbon exports downstream and possibly to Hudson Bay. The large influx of freshly flooded organic carbon caused rapid increases in fish mercury following impoundment, although fish mercury has been gradually decreasing toward recovery since then. Colour and other inorganic tracers confirm the findings from the organic compositional data (both bulk proxies and biomarker data – Stainton et al., in review) about sources of particulate material being locally sourced along the lower Nelson River. Causes of bank erosion in the lower Nelson and sensitivity to warming (permafrost thaw) vs. fluctuations in discharge due to regulation should be evaluated in further work.

Newly collected sediment cores were used to compare sedimentation rates and mercury deposition in on-system lakes/reservoirs (Threepoint Lake and Stephens Lake) vs. natural off-system lakes (Leftrook Lake and Assean Lake) (Singer, 2019). Despite decreases in Hg emissions and atmospheric deposition since the 1990s, accumulation rates of total mercury in sediments remained high when compared with an earlier period (1960-1989). We attribute this to inputs of soil-associated mercury, which is supported by a positive association between sedimentation rates and total mercury accumulation rates. The relationship between accumulation rates of methylmercury and sedimentation rates was less straightforward. Although we would have expected an increase in methylation rates with increased algal productivity in the reservoirs, the increased sediment and soil organic matter (OM) flux could have a dilution effect on methylmercury concentrations, and soil-derived organic matter does not strongly stimulate bacterial methylation of mercury in sediments in the way that phytoplankton-derived organic matter does (Bravo et al., 2017). Climate-driven increases in productivity in the on-system lakes/reservoirs may lead to higher bacterial methylation rates in reservoir sediments but if fluxes of soil OM remain high (due to bank erosion, for example), the accumulation rates of methylmercury in sediments may remain low.

4.2 Estuaries

Hudson Bay estuaries are the next step in the system from which regulation and climate change impacts can be presented and discussed through an integrative approach. BaySys Teams worked together to understand the coupling and impacts of freshwater discharge entering the bay from the rivers. Although intermediate in scale between rivers and Hudson Bay itself, estuaries are nonetheless large, dynamic systems where discharge, tides, and storms interact at multiple frequencies, and where the spatial domain is elastic, depending not only on the interaction of these forces but on practical definitions of inner and outer boundaries (Abril & Borges, 2005). Here, on an intermediate, variable spatial scale, BaySys Teams examined impacts of climate change and regulation through the lens of freshwater-marine coupling, carbon biogeochemistry, algal communities, and primary production, and freshwater modelling.

The Nelson-Hayes Estuary is characterized by high river discharge, 103 and 20 km^3 y^{-1}, in the Nelson and Hayes Rivers, respectively, accounting for 17% of annual flow into Hudson and

James Bays (Stadnyk et al., 2019). River discharge encounters tides, with up to 5.6 m amplitudes, in the inner estuary (Wang et al., 2012) and wind-waves and storm swell off the bay (Figure 3.1.9). Taken together, these forces determine the spatial extent, volume, and residence time within which estuarine physical, chemical and biological processes occur. River and seawater mix through the entire water column at the river mouth; as the admixture flows seaward, it quickly forms into a shallow surface plume which transports fresh and entrained seawater and its dissolved and particulate load into Hudson Bay. The seaward extent of this plume varies with both river discharge and tide state (Basu et al., In prep.) while vertical stratification and surface salinity are affected by landfast ice cover and storms.

Nelson River discharge into the estuary has been altered by regulation and climate. Diversion of the majority of the flow of the Churchill River increased the Nelson's annual discharge by an average of 22% at the mouth. Since the 1960s, December to March discharge has increased much more, on the order of 70%, due to combined impacts of climate, storage, and diversion (McCullough et al., 2019). With Macdonald et al. (2018) predicting steady-state to modest (not statistically significant) further increases in discharge from Nelson River discharge due to climate change through the next half-century, one expects the plume size to increase proportionally (all else being equal). However, because the Nelson River plume is weakly stratified even during winter, small to moderate changes in its size is going to be less evident than, for example, the changes in the highly-stratified winter plume of the La Grande River, where the salinity of 5 isohaline has since 1976 expanded from about 200 km^3 to 1200 km^3 with increased winter river discharge (Ingram & Larouche, 1987; Messier, 1989; Peck et al., Submitted). Further increases of the present extent of the La Grande River core plume area appear to be limited by coastal geometry and the associated width of the landfast ice cover (Peck et al., Submitted).

Tides are dramatically altered by winter ice. Although at the bay-wide scale the amplitude is strongly damped by friction due to the ice cover, velocities in the inner estuary are increased, because local land-fast ice constricts flow at the river mouth (Wang et al., 2012). Mixing of river water and seawater thus occurs further up the Nelson River mouth during winter than summer, in contrast to the Churchill River, Great Whale River, and La Grande River estuaries (Ingram & Larouche, 1987; Messier et al., 1989; Kuzyk et al., 2008b). Wang et al., (2012) also showed that turbidity generated by turbulent river-tide interaction in the inner Nelson estuary is reduced in winter, presumably due to sealing of mud-flat sources by land-fast ice.

The Nelson estuary is directly exposed to intermittent storm winds off Hudson Bay. Dmitrenko et al. (2020) showed that northerly winds are associated with positive deviations in sea level height in the Nelson-Hayes Estuary. The significance of winds to fresh-water-salt-water mixing and biological processes in the inner estuary remains unquantified. In the outer estuary, Dmitrenko et al. (2020) demonstrated that atmospheric cyclones passing over the bay supported eastward circulation so that most Nelson-Hayes freshwater joins the conduit of freshwater along the southern coast of Hudson Bay, and ultimately, northward into and through Hudson Strait. Low concentrations of dissolved inorganic carbon and alkalinity constituents were observed to follow their low salinity source water from rivers and sea ice melt, pooling in the south and southeastern Hudson Bay based on data from several ship cruises, including the 2018 BaySys cruise. The pooling of freshwater in southeastern Hudson Bay, mostly from rivers, but also sea ice melt, results from this circulation pattern that leads to heightened regional sensitivity to ocean acidification. However, Dmitrenko et al. (2020) also pointed out that offshore Ekman transport generated by anticyclonic circulation can reduce or even reverse this prevailing flow, such that some freshwater passes out of the coastal conduit and into central Hudson Bay. Thus, storm frequency, timing, and intensity will cause variation in freshwater transport pathways from year to year, which means a single year's observations (cf., Granskog et al., 2011) may not be particularly representative of average conditions.

An earlier, ArcticNet-funded study of the Nelson estuary (Guéguen et al., 2016) concluded that during summer, terrestrially-derived coloured dissolved organic matter (CDOM) is a conservative tracer of river water within the spatio-temporal regime of the Nelson-Hayes plume. This result allowed Basu et al. (in prep.) to use remote sensing techniques to map river water influence seaward beyond the visible sediment plume. They demonstrated exponential decay of the freshwater plume, with 25% of the initial CDOM signal remaining as far as 150–200 km from the rivers' mouths and some remaining signal distinguishable as far as 400 km from the Nelson River mouth. The extent of the CDOM plume at any dilution increased with increasing river discharge and was greater during spring than neap tides. On the other hand, the correlation of suspended sediment concentration with discharge was not significant, presumably because the larger source of sediments was subaqueous coastal erosion (resuspension) rather than river transport.

Dalman et al. (in prep.) examined the influence of freshwater on ice algae and phytoplankton biomass and production in the Nelson and Churchill River estuaries from winter to early summer. There are very strong contrasts in the estuary form and function between the ice-covered and ice-free seasons that influence primary production. During the winter-spring transition, riverine input brought higher nutrient concentrations than marine waters but had a negative influence on algal biomass by decreasing habitat availability and increasing osmotic stress within low-salinity waters. During late spring-early summer after ice breakup, phytoplankton biomass followed a different spatial pattern from ice algae, with high chlorophyll-*a* concentrations yet low nutrients and high turbidity in the river due to an exported freshwater community that had depleted nutrients upstream, a minimum within the turbid mixing zone of the estuary, followed by a rapid increase towards the marine environment, where nutrients and light levels were more favourable. In conclusion, freshwater input had a significant impact on primary production both for ice algal and phytoplankton communities in the proximity of the southwest Hudson Bay estuaries. However, due to a lack of temporal resolution, the study was only able to elucidate some of the mechanisms at play. A more detailed spring-summer time series study is required to tease out the impact of freshwater on dynamics of primary production within the Nelson River estuary.

Jacquemot et al. (2021) found that distinct protist communities developed in each of the Churchill, Nelson-Hayes, and Great Whale estuaries. In the Nelson-Hayes estuary, which was sampled more intensively than the others, the authors suggested that the mixotroph and heterotroph-dominated community that inhabits the zone of maximum turbidity would be sensitive to changes in the extent and residence time of this zone. Considering the major role of resuspension in generating turbidity within this estuary, it seems likely that the balance between auto- and heterotrophs in the estuary depends on interaction between discharge, which together with tide determines plume extent, and sediment supply by local erosion, which is determined by discharge-tide interaction and winds. It will require modelling of both flow and sediment transport in the estuary to understand how this interaction may relate to regulation and climate change.

The degradation of dissolved organic carbon (DOC) delivered by the Nelson and Hayes Rivers to the estuary was explored using an incubation experiment approach and various DOC/DOM characterization techniques. Kazmiruk et al. (2021) assessed the biodegradability of DOC in both riverine and coastal (estuarine) waters in late winter using 45-day incubation experiments. The Nelson and Hayes were compared to the Great Whale River in southeast Hudson Bay. The results showed that 24–60% of the DOC in the rivers and on average 21% of the DOC in the immediate coastal waters was biodegradable. Differences in biodegradability appeared to depend on the properties of the rivers/watersheds and physical and biochemical processes in the aquatic environments. DOC biodegradability correlated strongly with DOC concentration, which was higher during winter than summer in all studied rivers and higher in the Nelson and Hayes rivers, draining the Hudson Bay Lowlands, than in most previously studied large rivers of the Arctic watershed. The Nelson River had the highest winter DOC concentrations and most degradable DOC during late winter. The high biodegradability of Hudson Bay riverine DOC in late winter and high concentrations and fluxes of riverine DOC at that time imply strong leverage for future increases in DOC fluxes to impact the carbon cycle of these coastal waters.

The photoreactivity of DOM was studied in Churchill and Nelson River waters and simulated estuary water (mixture of Churchill River and bay waters) using incubation experiments. The river water was highly photoreactive. Photodecay rates were negatively correlated with initial concentrations of CDOM (Islam and Guéguen, in review). Composition of the DOM was found to affect photodegradation with higher O/C ratios found in the photolabile pool compared to the photoproduced and photoresistant pools. The results suggest solar exposure can stimulate photo-oxidation of DOM and potentially enhance decarboxylation and the release of more CO, CO_2, and small carboxylic acids. For DOM in general, the photodegradation process was more important than microbial degradation in the river water but the reverse was true in the estuary and coastal waters, where microbial degradation dominated. For the light-absorbing fraction of DOM (CDOM), photodegradation was much more important in all settings.

The degradation of OM from light as well as microbial activity leads to a build-up of pCO_2 and associated implications for gas exchange and acidification, and some of the highest pCO_2 measurements in surface waters were observed in parts of the estuary and associated river plume. These areas actively outgassed CO_2 to the atmosphere. However, we also observed areas of low pCO_2 in surface waters within the estuary. Depending on the nutrient ratio of the OM, the build-up of pCO_2 and associated implications for gas exchange and acidification may be offset to some degree through the combination of new primary production made possible through the release of nutrients from remineralized organic material, and through the drop in pCO_2 brought about by the diluting effect of mixing sea- and river- waters. The relative contribution of these processes in moderating pCO_2 and other carbon variables has yet to be assessed for any of the large estuaries in Hudson Bay. The high degree of spatial variability in these variables observed for the Nelson Estuary underpins the complexity of this system in particular.

In summary, circulation and water residence time, forced by complex interactions of river discharge, tidal dynamics, and winds, acting within the constraints of morphometry and bed materials, create the particular nutrient and light environment that determines biological production and diversity in the Nelson-Hayes estuary. BaySys science has built on earlier studies of the physical and biogeochemical environment by ArcticNet researchers and Manitoba Hydro staff and contractors to improve our understanding of the biogeochemical processes that link this with biological processes in the estuary. Information from data collected in winter and during the ice-breakup seasons has been used to study the impact of seasonal ice on these processes, and to demonstrate for the first time that estuarine biological productivity peaks during the never-before studied spring ice breakup period. BaySys results show that variability in the estuarine light environment is not dependent directly on discharge. Rather, time-dependent variations in turbidity and hence light climate are largely determined by littoral erosion. Thus, trends in river discharge, whether due to regulation or climate change, may have little effect on turbidity and light-dependent biological processes (photosynthesis, photodegradation of DOM) in estuarine waters. Changes in nutrients and carbon delivered by the river will separately affect the biological and biogeochemical processes. On the other hand, BaySys results demonstrate the importance of seasonal ice cover to estuarine circulation and turbidity, so we expect reduced sea ice duration which will follow from predicted warming to cause concomitant shifts in biogeochemical processes through the 21st century. For instance, the ice-covered estuary is marked by lower salinity and turbidity and higher nutrient concentrations. DOM released by the river is more biodegradable than when the bay and estuary are ice-free, but photodegradation rates are reduced less in the lower light environment. Because photosynthesis is limited by low light, both for phytoplankton and ice algae, we expect that a higher fraction of terrestrial DOM, DIC, and nutrients are exported from the estuary to the offshore in winter than in summer.

During summer, photodegradation of DOM contributes nutrients and small organic compounds to the water column in addition to inorganic nutrients and DOC directly delivered by the river. BaySys results demonstrate that, in summer, river water, carrying dissolved nutrients, spread far beyond the turbid plume generated in the river mouth and from the littoral bed, so that in the outer estuary we expect that nutrients are largely consumed rather than exported further into the bay. POC that was delivered during the winter likely undergoes resuspension and lateral transport and conceivably would undergo some degradation and contribute additional nutrients and organic molecules that feed the microbial community. Longer open-water season will favour more photosynthesis over respiration (increasing CO_2 uptake potential), whereas increased terrestrial DOM and POM exports due to increased river discharge and greater release from watershed sources will favour respiration. Unfortunately, the NEMO model that supported integration of biogeochemical processes at a bay-wide scale, lacked sufficient resolution to support integration and prediction of biological and biogeochemical properties at the estuarine scale. A high-resolution physical and sediment model at the estuarine scale must be considered the basis of any future studies of the ecosystem that is the Nelson-Hayes estuary.

4.3 Coastal Regions

Transiting counter-clockwise around the bay's coastal corridor we observed in the northwest of the bay the seawater to be of high salinity and high in concentration of DIC and alkalinity, but largely undersaturated in pCO_2 relative to atmospheric values. The undersaturated pCO_2 observations were probably a result of ice melt dilution, and possibly biological productivity promoted by mixing with high-nutrient sub-surface waters in the polynya located in the northwest of the bay. The highest pCO_2 values on the other hand were mainly observed along the coast in southern Hudson Bay, in areas with warm water of low salinity close to the Churchill and Nelson Estuaries, and ice-covered waters in the bay's southeast.

South and east of the Nelson Estuary we observed an accumulation of meteoric water such that it extended across the upper 50 m of the water column along the bay's southern coast, with the highest fractional composition across the mouth of James Bay and south of the Belcher Islands (southeastern Hudson Bay). By comparison, the distribution of sea ice melt in surface waters was patchy. Large SIM fractions were observed offshore of the Nelson Estuary, and then again pooled across the mouth of James Bay and into southeastern Hudson Bay. Meteoric water however was by far the prominent freshwater source, reaching fractional compositions of 25% at the mouth of James Bay.

The lowest concentrations of alkalinity and DIC were observed in the upper water column in proximity to James Bay and southeast Hudson Bay. Both dissolved inorganic carbon and alkalinity were noticeably depressed in the upper 50 m of the water column at the mouth of James Bay and these waters were both low in pH and undersaturated in the calcium carbonate mineral aragonite, which collectively indicates the seawater was at a heightened state of ocean acidification. Upstream, the seawater was supersaturated in aragonite along the coastal corridor along the west coast and north of the Nelson River, but lower saturation states prevailed within 20 m of the surface from southeast Hudson Bay along the east coast to Hudson Strait.

The general trends observed in BaySys are in line with previous studies (e.g., Burt et al., 2016), and in particular, Azetsu-Scott et al. (2014) who reported aragonite undersaturation in southeastern Hudson Bay surface waters with high river-run-off fractions (>10%). Burt et al. (2016) speculated the pCO_2 undersaturation (together with low pH and aragonite undersaturation) in southeast Hudson Bay to result from the mineralization of accumulated organic material attributed to the large rivers in the bay's southwest and the bay's cyclonic coastal circulation. Ahmed et al. (2021), and before them Else et al. (2008a, 2008b) attributed high pCO_2 in coastal waters to the degradation of organic material. While more work is needed to attribute factors associated with low (and high pCO_2) from region to region, BaySys research has shown that bay-wide within the coastal corridor, the mineralization of organic carbon is a major contributor not only to elevated pCO_2, but also low pH and aragonite saturation state (Ω_{Ar}) (Capelle et al., 2020).

BaySys Teams made a novel contribution to the knowledge of freshwater production and sediment transport by sea ice development in southern Hudson Bay. Barber et al. (2021) reported on widespread accumulation of up to 18 m thick, very fresh deformed ice along the southern coast of Hudson Bay. This ice not only contributes disproportionately large volumes of freshwater to the coastal region; it also transports sediments entrained sediments from tidal flats out to many 10s of kilometres offshore. We estimated that 8×10^6 tonnes of fine to very coarse sediments were entrained in such ice in the spring of 2019. This deformed, muddy ice was associated with a region of low salinity, organic-rich waters, and would have significantly attenuated light required for in-ice and sub-ice primary production. Sediment released by sea ice was notable as far northwest as the AN01 mooring location, where the ADCP backscattering and sediment trap records showed evidence for the release of fine sediment, especially during the ice melt period (Petrusevich et al., 2020).

4.4 Bay-Wide

Observations

Because long time series of oceanographic variables are not available for the HBC, a lot of what we think we know about the oceanographic conditions comes from individual field campaigns. When comparing results from these campaigns, it has become increasingly evident that we need to keep in mind interannual variability in this system and that each new set of observations must be placed into some kind of longer-term context. Many parameters show wide interannual variability or even multiple 'modes' of variation (cf., Galbraith & Larouche, 2011).

Baseline evaluation of conditions in the HBC during the BaySys 2016-2018 field program timeframe was developed to provide an analytical framework and context for studies conducted by all BaySys Teams, while also highlighting extremes relative to the 1981-2010 climatology. Evaluation of atmospheric and river discharge conditions within the HBC showed that 2016 was characterized by unusually warm conditions (terrestrial and marine) throughout the annual cycle; 2017 by strong cyclone activity in February and high precipitation in January, October, and November; and 2018 by cold and windy conditions throughout the annual cycle (Lukovich et al., 2021a, 2021b). Evaluation of terrestrial conditions showed higher than normal land surface temperatures within the Hudson Bay freshwater watershed for all of the 2016-2018 period (excluding a colder than normal spell August to November 2018), particularly in January (2016 and 2017), higher than normal precipitation in October (2016 and 2017), and higher than normal terrestrial discharge to the HBC in March (2016 and 2017), with drier than average June through October (2016-2018) (Lukovich et al., 2021a, 2021b).

Evaluation of oceanographic and sea ice conditions (Lukovich et al., 2021b) showed high sea surface temperatures (SSTs) in northwestern Hudson Bay from May to July in 2016 to 2018 relative to the 1981-2010 climatology. SSTs were also warmer in 2016 and 2017 than in 2018 relative to the 1981-2010 climatology. Similarly, unusually low sea ice cover existed from August to December in 2016, July to September in 2017, while unusually high sea ice cover existed in January, February, and October of 2018. The ice-free season was approximately 20 days longer in 2016 than in 2018. Unusually high ice drift speeds occurred in April 2016 and 2017, and May 2018 and coincided with strong winds in 2016 and 2018, and following strong winds in March 2017. Strong meridional circulation was observed in spring in 2016, winter in 2017, while weak meridional circulation existed in 2018. In a case study of an extreme event, the blizzard from March 7 – 9, 2017 evaluated using Lagrangian dispersion statistics was shown to suppress sea ice deformation off the coast of Churchill (Lukovich et al., 2021b).

BaySys observations confirmed that the distribution of carbon system variables in the surface waters of Hudson Bay generally followed the distribution of salinity, consistent with previous observations (i.e., Burt et al., 2016; Azetsu-Scott et al., 2014). Potentially corrosive seawater was widely observed in deep waters and shoaled to within 25 m of the surface east of James Bay, consistent with observations from other studies (e.g., Burt et al., 2016; Azetsu-Scott et al., 2014). The pervasive and sometimes strong surface layer stability reported by Ahmed et al. (2020) that resulted from freshwater pooling at the surface facilitates the build-up of pCO_2 in deeper waters, contributing to observations of low pH and aragonite undersaturation. BaySys results (Capelle et al., 2020) indicated that much of the OC material degraded in the deep water and the bay's interior is of marine origin.

We determined that several processes influence the bay's CO_2 exchange budget with the atmosphere over a range of temporal and spatial scales. The total open water (May to October) CO_2 sink was estimated to be 7.2 TgC for Hudson Bay and Hudson Strait. At other times of the year, the bay loses CO_2 to the atmosphere, and thus we estimate the total annual uptake to be closer to about 6 TgC, establishing the bay as a weak to moderate CO_2 sink (Ahmed et al., 2021), comparable in size to other Arctic peripheral seas (e.g., Laptev and East Siberian Seas). With no evidence of an effective biological pump in the sediment record of the bay, likely, much of the carbon taken into the system (from rivers and gas exchange at the sea surface) is exported to Baffin Bay and the North Atlantic through Hudson Strait.

In terms of sea ice, it has been recognized for more than a decade that there is a significant difference in the sea ice regime between western and eastern Hudson Bay (Saucier et al., 2004; Joly et al., 2011; Hochheim & Barber, 2014; Landy et al., 2017). Asymmetries in sea ice thickness in western vs eastern Hudson Bay had been ascribed to the prevailing northwesterly winds which maintain a large latent heat polynya in NW Hudson Bay (Kivalliq Polynya; Bruneau et al., 2021) and cause dynamical thickening of drifting ice against the eastern coast (Landy et al., 2017). Different atmospheric forcing conditions during the ice growth (December–April) season were found to be key elements explaining the asymmetries, with strong westerly winds causing thicker ice in eastern Hudson Bay and consequently delaying spring breakup by 3-4 weeks in that area (Kirillov et al., 2020). Furthermore, years with strong northwesterly winds were characterized by a larger Kivalliq polynya and greater ice production.

Although ridging is known to be important in southern Hudson Bay and James Bay, heavily deformed and sediment-laden ice floes were encountered along the southwest Hudson Bay coast during the BaySys 2018 cruise. A survey of one of these floes revealed a maximum ridge height of 4.6 m and an average freeboard of 2.2 m, corresponding to an estimated total thickness of 18 m, which is a very thick piece of sea ice, particularly within the seasonal ice cover of Hudson Bay (Barber et al., 2021). Oxygen isotopic analysis ($\delta^{18}O$) revealed this ice had formed from marine waters, while the presence of both clay and boulders on the ice surface suggested sediment had been entrained through anchoring to the ocean floor and suspension freezing within frazil ice that forms within the coastal tidal flaw lead (Barber et al., 2021). Sediment-laden sea ice forms and is transported throughout winter but is not evident until spring when the snow melts and sediment concentrates at the melting ice surface. Analysis of satellite imagery reveals that over the past decade the areal extent of sediment-laden ice during June has varied from 47 and 118 km^2. Sediment-laden ice affects light transmission through the ice and therefore biological productivity, as well as representing a mechanism for redistributing sediment and contaminants from coastal areas to the offshore waters of Hudson Bay. Given that sediment-laden sea ice forms from marine waters within the tidal flats and tidal flaw leads throughout winter, it seems likely that alteration of the hydrograph to higher freshwater outflow during winter has little effect on this process. In terms of climate change, it is suggested that enhanced dynamics (weather, tide), longer open water season while the air temperature is below freezing, etc., could result in more sediment entrainment into the ice (Barber et al., 2021).

Modelling

In addition to the new observations from the BaySys cruises, NEMO was used during BaySys to study present-day freshwater dynamics associated with river runoff and sea ice melt (Ridenour et al., 2019a) as well as the bay's circulation (Ridenour et al., 2019b). The residence times varied from 32.2 years in Foxe Basin, 17.6 years in Hudson Bay, 21.5 years in James Bay, and 9.5 years in Hudson Strait. The estimates for Hudson Bay are somewhat longer than most previous estimates (Prinsenberg, 1986; St-Laurent et al., 2011; Pett & Roff, 1982) but consistent with proposals that river discharge can mix into the deep waters (Granskog et al., 2011). In terms of circulation, strong geostrophic, cyclonic flow was historically considered a defining feature of Hudson Bay, found and supported by numerous observational and modelling studies. However, other studies (Gagnon & Gough, 2005: St. Laurent et al., 2011) hinted that this circulation pattern may not be as stable as previously thought. Using NEMO, Ridenour et al. (2019b) showed the presence of weak anticyclonic flow in eastern Hudson Bay in summer. This finding was supported by satellite-based observations of absolute dynamic topography and geostrophic velocity. This flow, while geostrophic, is strongest through the center of the bay, and is induced by the spring freshet and strengthened by anticyclonic seasonal wind patterns (Ridenour et al., 2019b).

Biological System

Through an improved characterization of parameters describing the under-ice light field Matthes et al. (2021) produced the most accurate early spring primary production estimates to date, while also providing critical information for modelling studies examining scenarios of the future Arctic Ocean. These new parameters and associated measuring techniques were applied to obtain the first measurements of spring primary production in Hudson Bay in which 32% of annual microalgal biomass was determined to be produced during the sea ice melt period. Matthes et al. (2021) also reassessed annual production to be double that provided in historic estimates. However, nitrogen availability sets an upper cap on the carrying capacity of Hudson Bay in terms of primary production and upper trophic levels. Only 20% of the annual primary production is "new" or export production, which can support food webs and fisheries, for example. The new production supported by vertical replenishment of nitrate during winter amounts to only 13 g C m-2 on average, which is very low.

An interesting set of studies within BaySys informed us about the timing of biological production in the water column of Hudson Bay. In offshore waters, the timing was closely tied to sea ice melt/break up, thus early ice breakup triggers early phytoplankton bloom. Production had occurred under the ice in places, but bloom conditions are considered to require the greater light availability that follows ice melt. BaySys results also showed that a fall phytoplankton blooms occurred. Fall blooms may, in part, result from the advection of pigment-rich phytoplankton cells previously produced in the subsurface chlorophyll maximum. However, the fall blooms are potentially productive and characterized by a size structure and photo-acclimation state similar to those blooming at the ice edge earlier in summer (Barbedo et al., 2020). The fall bloom is important to characterize because it may come to play an increasingly important role in the future if fall freeze-up is increasingly delayed.

In terms of the benthic system, the study by Pierrejean et al. (2020) surveyed the epibenthic communities in Hudson Bay and Hudson Strait and explored their relationships with environmental variables, including mean annual primary production and particulate organic carbon in surface water, bottom oceanographic variables, and substrate type. Three communities were defined based on biomass and taxonomic composition. Ordination analyses showed them to be associated primarily with substrate type, salinity, and annual primary production. A first community, associated with coarse substrate, was distributed along the coastlines and near the river mouths. This community was characterized by the lowest density and taxonomic richness and the highest biomass of filter and suspension feeders. A second community, composed mostly of deposit feeders and small abundant epibenthic organisms, was associated with soft substrate and distributed in the deepest waters. A third community, associated with mixed substrate and mostly located near polynyas, was characterized by high diversity and biomass, with no dominant taxon. The overall analysis indicated that bottom salinity and surface-water particulate organic carbon content were the main environmental drivers of these epibenthic community patterns. In the face of climate change, projections of increased river inflow and a longer open water season for the Hudson Bay and Hudson Strait could have major impacts on these epibenthic communities, emphasizing a need to continually improve our ability to evaluate and predict shifts in epibenthic richness and distribution (Pierrejean et al., 2020).

Freshwater Forcing and Future Changes

As part of the BaySys project, Team 2 generated a 90-year timeseries of pan-Arctic discharge entering the Arctic basin using the far-field HYPE model and domain. Freshwater discharge to the Arctic basin was continuously modelled (daily timestep) across 23 million km2 from 1981 to 2070, including the five GCM-RCP climate simulations used to drive the NEMO model. In Stadnyk et al. (2021) collaboration, Team 2 provided Team 6 modellers these continuous input data, which was subsequently used to drive NEMO and assess the freshwater content of the Arctic basin. Key findings include:

1) freshwater discharge to the Arctic basin is expected to increase by ~22% in the 21st century – nearly double what has previously been reported in the literature as a result of including future timeseries,

2) both climate change and regulation are contributing to more uniform delivery of freshwater volume to the HBC domain throughout the year, reducing significantly previously observed seasonal cycles;

3) the amount, and potential impact of increasing terrestrial discharge into to the Arctic basin is more significant further than previous simulations (without dynamic discharge timeseries) have shown, highlighting the need to consider freshwater when assessing thermohaline-driven circulation (Stadnyk et al., 2021).

BaySys Team members also investigated relative contributions from climate change and river discharge regulation to changes in marine conditions in the HBC using a subset of five CMIP5 atmospheric forcing scenarios, HYPE discharge data both naturalized (natural, without anthropogenic intervention) and regulated (anthropogenically-controlled through diversions, dams, reservoirs), and NEMO ice-ocean model output for the 1981-2070 timeframe. Results from this analysis highlight bay-wide and regional reductions in sea ice concentration and thickness in southwest and northeast Hudson Bay in response to a changing climate, and east-west asymmetry in sea ice drift response in support of past studies. Whether regulation amplifies or suppresses the climate change signal depends on the variable and the time of the year. Specifically, regulation amplifies SSTs from April to August, suppresses sea ice loss by ~-30% in March, contributes to enhanced sea ice drift speed by ~30%, and reduces meridional circulation by ~20% in January due to enhanced zonal drift. Results further suggest amplification of regulation impacts offshore in a changing climate (Lukovich et al., 2021c).

NEMO runs under different RCP4.5 and RCP8.5 climate scenarios, with naturalized and regulated river runoff based on the same climate scenarios, also was used to model future freshwater dynamics in the HBC. Preliminary results show that the temperature of the HBC (Top 50 m) will warm over the next 50 years, with annual average warming of ~ 1.5°C between 2005 and 2070. Changing from Naturalized to regulated river runoff has little impact on this warming, as it is driven by the climate signal. At the same time, future scenarios show that sea ice concentration and thickness in the HBC will significantly decrease over the next 50 years, driven by climate change. HBC averaged reductions in sea ice between 2005 and 2070 will be ~ 20% in concentration and 0.15-0.2 m in thickness. Changing from naturalized to regulated river runoff had little impact on the annually averaged sea ice changes. Lastly, the HBC will freshen by 2070, with regulation playing a role through the changing both the time of the discharge and the freshwater residence time. With regulated river runoff, the ensemble mean salinity reduction is slightly larger (~ 0.3 g/kg). No scenarios suggesting an increase in the HBC's salinity. The differences between the naturalized and regulated runs appear to be related to the timing of the discharge and the residence time for freshwater in the basin. Years of strong discharge add more freshwater to the HBC than can be exported through Hudson Strait, lowering the salinity, and increasing freshwater residence times, with the reverse occurring in years of weak discharge (Garcia-Quintana et al., in prep). In a general sense, the results are similar to previous work in which a regional sea ice–ocean model was used to investigate the response of the HBC to a climate-warming scenario (mean air temperature change of 3.9°C) (Joly et al., 2010). Those simulations also showed earlier melt of sea ice and pronounced heating of the water column. One of the major accomplishments of BaySys project has been to bring together river regulation and climate change into a coordinated hydrological-ocean-sea modelling environment, forced with a common set of climate change general circulation model (GCM) scenarios. This innovation will be key to not only understanding current period processes but also being able to hindcast and forecast, to improve process understanding, and to better understand the relative contributions of regulation and climate change on freshwater-marine coupling in the HBC.

This novel modelling environment also allowed for the integration of a biogeochemical model into this coupled FW-marine system. The biogeochemical model BLING V0+DIC was coupled to the NEMO framework for Hudson Bay. Modelling confirms the bay to be a low-level carbon sink during modern times and that uptake rates are not expected to appreciably change before 2070, and that climate change impacts on the surface flux are more pronounced than those associated with regulation. The lack of organic sediments (Kuzyk et al., 2009) suggests the bay has not had a strong biological pump, a requisite (along with deep-water formation) for strong and sustained CO_2 uptake. Results from Section 3.3 of this report confirm that Hudson Bay is an oligotrophic sea, and our simulations indicate that it will remain oligotrophic in the future.

Although the net annual average air-sea carbon flux is not expected to appreciably change, our simulations indicate that the total flux will be distributed differently through the year, which has implications for ecosystem processes, as well as potential carbon sequestration. Earlier sea ice break-up will contribute to earlier peak CO_2 uptake, but the simulations suggest that while uptake in the spring may increase, summertime uptake will likely not increase. The largest change in the surface CO_2 flux is expected to occur during the fall, and in this season the system is anticipated to toggle from a weak carbon sink to a strong source.

In general, the impact of regulation in future simulations is to reduce the absorption of atmospheric carbon into Hudson Bay, decreasing spring and summer uptake and increasing fall and winter release. In future scenarios, regulation is associated with marginally lower surface pH than in the naturalized scenarios in all months, with the largest impacts of regulation evident in the summertime. Despite changes in pH in deeper water also mainly attributable to climate, regulation is projected to have a stronger influence than we observed for surface waters.

If the terrestrial organic carbon load delivered by Arctic rivers will increase with river discharge as expected (e.g., Amon et al., 2012), under future scenarios, the Hudson Bay system may accumulate inorganic carbon, including pCO_2 due to increasing atmospheric CO_2 concentrations and CO_2 production from the degradation of terrestrial organic material. We expect the build-up of pCO_2 will not be offset by biological production. Collectively the accumulation of inorganic carbon in Hudson Bay would drive increasing CO_2 supersaturation and aragonite under-saturation, especially in parts of the bay with characteristically high meteoric water fractions, like southeast Hudson Bay. A reduction in seawater pH is forecast to accompany the projected increase in pCO_2 into the future. Bay-wide, the surface waters are projected to remain saturated with respect to aragonite during all seasons. However, subsurface waters are already undersaturated with respect to aragonite, and the simulations predict that undersaturation to only increase through the middle of the century. Work however remains to understand the seasonal and spatial trends in projected acidification in Hudson Bay, which may control its ultimate impacts on the ecosystem.

We have not been able to definitively identify the mechanism by which regulation impacts the fluxes, but regulation does have a strong influence on surface seawater salinity and stratification (limiting the availability of nutrients for biological production outside of the winter season). River regulation acts to flatten the annual hydrograph of river discharge, with water held back in reservoirs during the spring and summer and released in the winter to meet the heightened hydroelectric demands of that season. Thus, while we don't know how regulation affects the concentration of carbon constituents from the Nelson River, we do know that regulation will impact at least the timing of the lateral carbon flux. The BaySys results show that the timing is important in terms of the fate of the terrigenous DOC (whether it is degraded within the watershed or river versus in the coastal waters near the river mouth). The river delivery of DOC in winter should be higher with regulation given its association with river discharge. In winter, following the suggestion of Kazmiruk et al. (2021), the riverine DOC will be better preserved on route to the bay relative to summer transport because of darkness that limits photodegradation and low temperatures that limit microbial degradation. Conversely, DOC should be degraded further upstream in the open water season, implying the residual DOC transported downstream may be less biodegradable than its winter counterpart. Thus, the high biodegradability of Nelson River DOC in late winter, together with high concentrations and fluxes of riverine DOC implies that regulation should increase the DIC stock in coastal waters proximal to the river outlet through the mineralization of DOC, locally raising pCO_2 and decreasing aragonite saturation, a prediction supported by our simulations. Thus, conceptually the projected response of the carbon system to regulation appears valid. Our simulation results do not yet allow us to consider how impacts of the regulation vary spatially within the bay. Observations resulting from the BaySys field program highlight pronounced spatial patterns in the surface DIC flux and other carbon system parameters, and thus a regional assessment of future regulation impacts across the bay is warranted.

The integration of results to provide a scientific basis separating climate change effects from those of regulation of freshwater within the HBC was an integral scientific deliverable of the BaySys project. The combined efforts presented within this chapter demonstrate the successes of this unprecedented and innovative endeavour by allowing for a more holistic system study to take place. Addressing the BaySys objective through a series of coupled systems across multiple fields of study and spatial/temporal scales encouraged BaySys Teams to not only identify, but to examine the interactions between their Teams' process studies (as seen throughout Chapter 3), and the larger interconnected systems within which all these processes occur. The BaySys project demonstrated that the integration of both observational data and modelling was key to understanding the present-day processes and in turn using it as a baseline in helping to calculate the future impacts of climate change and regulation on each system. Overall, this Integration Chapter should help encourage future researchers of the HBC system to adopt and refine this observation/modelling approach; improving our holistic understanding of the HBC processes and improving climate and ecosystem projections.

4.5 References Cited

Ahmed, M.M.M., Else, B.G.T., Butterworth, B., Capelle, D., Guéguen, C., Miller, L.A., Meilleur, C., and Papakyriakou, T. (2021). Widespread surface water pCO2 undersaturation during ice-melt season in an Arctic continental shelf sea (Hudson Bay, Canada), *Elementa: Science of the Anthropocene*, 9(1), 00130. https://doi.org/10.1525/elementa.2020.00130.

Ahmed, M.M.M., Else, B.G.T., Capelle, D., Miller, L.A., and Papakyriakou, T. (2020). Underestimation of surface pCO2 and air-sea CO2 fluxes due to freshwater stratification in an Arctic shelf sea, Hudson Bay. *Elementa: Science of the Anthropocene*, 8(1), 084. https://doi.org/10.1525/elementa.084.

Amon, R.M.W., Rinehart, A.J., Duan, S., Louchouarn, P., Prokushkin, A., Guggenberger, G., Bauch, D., Stedmon, C., Raymond, P.A., Holmes, R.M., McClelland, J.W., Peterson, B.J.,Walker, S.A.., Zhulidov, A.V. (2012). Dissolved organic matter sources in large Arctic rivers. *Geochimica et Cosmochimica Acta*, 94, 217–237.

Azetsu-Scott, K., Starr, M., Mei, Z-P., and Granskog, M. (2014). Low calcium carbonate saturation states in an Arctic inland sea having large and varying fluvial inputs: The Hudson Bay system. *Journal of Geophysical Research: (Oceans)*, 119, 6210-6220. 10.1002/2014JC009948

Barbedo, L., S. Bélanger, J.-É. Tremblay (2020). Climate control of sea ice edge phytoplankton blooms in the Hudson Bay system. *Elementa: Science of the Anthropocene*, 8(1), 039. https://doi.org/10.1525/elementa.039

Barber D.G., M.L. Harasyn, D.G. Babb, D. Capelle, G. McCullough, L.A. Dalman, L.C. Matthes, J.K. Ehn, S. Kirillov, A. Basu, M. Fayak, S. Schembri, T. Papkyriakou, M.M.M. Ahmed, B. Else, C. Guéguen, C. Meilleur, I. Dmitrenko, C.J. Mundy, Z. Kuzyk, S. Rysgaard, J. Stroeve, and K. Sydor. (2021). Sediment-laden sea ice in southern Hudson Bay: Entrainment, transport, and biogeochemical significance. *Elementa: Science of the Anthropocene*, 9(1), 00108. https://doi.org/10.1525/elementa.2020.00108

Basu, A., G. K. McCullough, D. G. Barber, K. Sydor, A. Mukhopadhyay, D. Doxaran, S. Bélanger, and J. K. Ehn, (in prep.). Characterizing the Nelson/Hayes River plume extent in Hudson Bay using remotely sensed CDOM and suspended sediment data. *Elementa: Science of the Anthropocene*. manuscript in preparation.

Braun, M., Thiombiano, A., Vieira, M., Stadnyk, T.A. (2021). Representing climate evolution in ensembles of GCM simulations for the Hudson Bay System. *Elementa: Science of the Anthropocene*, 9(1), 00011. https://doi.org/10.1525/elementa.2021.00011

Bravo, A.G., Bouchet, S., Tolu, J., Björn, E., Mateos-Rivera, A., & Bertilsson, S. (2017). Molecular composition of organic matter controls methylmercury formation in boreal lakes. *Nature Communications*, 8(1), 1-9.

Bruneau, J., Babb, D., Chan, W., Kirillov, S., Ehn, J., Hanesiak, J., Barber, D.G. (2021). The ice factory of Hudson Bay: Spatiotemporal variability of the Kivalliq Polynya. *Elementa: Science of the Anthropocene*, 9(1), 00168. https://doi.org/10.1525/elementa.2020.00168

Burt, W.J., Thomas, H., Miller, L.A., Granskog, M.A., Papakyriakou, T.N., Pengelly, L. (2016). Inorganic carbon cycling and biogeochemical processes in an Arctic inland sea (Hudson Bay) *Biogeosciences*, 13(16), 4659-4671.

Capelle, D. Kuzyk, Z.A., Papakyriakou, T., Gueguen, C., Miller, L., and R. Macdonald, (2020). Effect of terrestrial organic matter on ocean acidification and CO2 flux in an Arctic shelf sea, Prog. Phys. Oceanogr., 185, 102319. 10.1016/j.pocean.2020.102319.

Dalman et al., (in review). Microalgal response to a seasonal freshwater input in southwestern Hudson Bay.

Déry, S.J., Stadnyk, T.A., MacDonald, M.K., Gauli-Sharma, B. (2016). Recent trends and variability in river discharge across northern Canada. *Hydrology and Earth System Sciences*, 20(12), 4801-4818. https://doi.org/10.5194/hess-20-4801-2016

Déry, S.J., Mlynowski, T.J., Hernandez-Henriquez, M.A., Straneo, F. (2011). Interannual variability and interdecadal trends in Hudson Bay streamflow. *Journal of Marine Systems*, 88(3), 341-351.

Déry, S.J., Stieglitz, M., McKenna, E.C., Wood, E.F. (2005). Characteristics and trends of river discharge into Hudson, James, and Ungava Bays, 1964-2000. *Journal of Climate*, 18, 2540-2557.

Dmitrenko, I.A., P.G. Myers, S.A. Kirillov, D.G. Babb, D.L. Volkov, J.V. Lukovich, R. Tao, J.K. Ehn, K. Sydor, and D.G. Barber. (2020). Atmospheric vorticity sets the basin-scale circulation in Hudson Bay. *Elementa: Science of the Anthropocene*, 8(1), 049. https://doi.org/10.1525/elementa.049

Else, B.G.T, Papakyriakou, T., Granskog, M. A., Yackel, J.J. (2008a). Observations of sea surface fCO2 distributions and estimated air–sea CO2 fluxes in the Hudson Bay region (Canada) during the open water season. *Journal of Geophysical Research: Oceans*, 113(C8), C08026. http://dx.doi.org/10.1029/2007jc004389.

Else, B.G.T., Yackel, J.J., Papakyriakou, T. (2008b). Application of satellite remote sensing techniques for estimating air-sea CO2 fluxes in Hudson Bay, Canada during the ice-free season. *Remote Sensing of Environment*, 112(9), 3550–3562. http://dx.doi.org/10.1016/j.rse.2008.04.013.

Gagnon, A.S., and Gough, W.A. (2005). Climate change scenarios for the Hudson Bay region: an intermodel comparison. *Climatic Change*, 69(2), 269-297.

Galbraith, P.S., and Larouche, P. (2011). Reprint of "Sea-surface temperature in Hudson Bay and Hudson Strait in relation to air temperature and ice cover breakup, 1985–2009". *Journal of Marine Systems*, 88(3), 463-475.

Godin, P., Macdonald, R. W., Kuzyk, Z. Z. A., Goñi, M. A., & Stern, G. A. (2017). Organic matter compositions of rivers draining into Hudson Bay: Present-day trends and potential as recorders of future climate change. *Journal of Geophysical Research: Biogeosciences*, 122(7), 1848-1869.

Goharrokhi, M., McCullough, G.K., Owens, P.N., Lobb, D.A. (2021). Sedimentation dynamics within a large shallow lake and its role in sediment transport in a continental-sale watershed. *Journal of Great Lakes Research*, 47(3), 725-740. https://doi.org/10.1016/j.jglr.2021.03.022

Granskog, M.A., Kuzyk, Z.A., Azetsu-Scott, K., Macdonald, R.W. (2011). Distributions of runoff, sea ice melt and brine using δ18O and salinity data: A new view on freshwater cycling in Hudson Bay. *Journal of Marine Systems*, 88(3), 362-374.

Guéguen, C., Mokhtar, M., Perroud, A., McCullough, G., Papakyriakou, T., (2016). Mixing and photoreactivity of dissolved organic matter in the Nelson/Hayes estuarine system (Hudson Bay, Canada). *Journal of Marine Systems*, 161, 42–48. https://doi.org/10.1016/j.jmarsys.2016.05.005

Hochheim, K.P., and Barber, D.G. (2014). An update on the ice climatology of the Hudson Bay system. *Arctic, Antarctic, and Alpine Research*, 46(1), 66-83.

Ingram, R.G., and P. Larouche (1987). Variability of an under-ice river plume in Hudson Bay. *Journal of Geophysical Research*, 92(C9), 9541-9547.

Islam, S., and Guéguen, C. (in review). Photochemical and microbial transformations of dissolved organic matter in Hudson Bay.

Jacquemot, L., D. Kalenitchenko, L.C. Matthes, A. Vigneron, C.J. Mundy, J-E. Tremblay, and C. Lovejoy (2021). Corrigendum: Protist communities along freshwater–marine transition zones in Hudson Bay (Canada). *Elementa: Science of the Anthropocene*, 9(1), 00111. https://doi.org/10.1525/elementa.2021.00111

Joly, S., Senneville, S., Caya, D., Saucier, F. (2011). Sensitivity of Hudson Bay sea ice 912 and ocean climate to atmospheric temperature forcing. *Climate Dynamics*, 36, 1835–1849. 10.1007/s00382-009-0731-4.

Kazmiruk, Z.V., Capelle, D., Kamula, C.M., Rysgaard, S., Papakyriakou, T., and Kuzyk, Z.A. (2021). High biodegradability of riverine dissolved organic carbon in late winter in Hudson Bay, Canada. *Elementa: Science of the Anthropocene* 9(1), 00123. https://doi.org/10.1525/elementa.2020.00123

Kirillov, S., Babb, D., Dmitrenko, I., Landy, J., Lukovich, J., Ehn, J., Sydor, K., Barber, D., Stroeve, J. (2020). Atmospheric forcing drives the winter sea ice thickness asymmetry of Hudson Bay. *Journal of Geophysical Research: Oceans*, 125 e2019JC015756. https://doi.org/10.1029/2019JC015756

Kuzyk, Z. Z. A., Macdonald, R. W., Johannessen, S. C., Gobeil, C., & Stern, G. A. (2009). Towards a sediment and organic carbon budget for Hudson Bay. *Marine Geology*, 264(3-4), 190-208.

Kuzyk, Z. Z. A., Goñi, M. A., Stern, G. A., & Macdonald, R. W. (2008a). Sources, pathways and sinks of particulate organic matter in Hudson Bay: Evidence from lignin distributions. *Marine Chemistry*, 112(3-4), 215-229.

Kuzyk, Z. A., Macdonald, R. W., Granskog, M. A., Scharien, R. K., Galley, R. J., Michel, C., Barber, D.G., & Stern, G. (2008b). Sea ice, hydrological, and biological processes in the Churchill River estuary region, Hudson Bay. *Estuarine, Coastal and Shelf Science*, 77(3), 369-384.

Landy, J.C., J.K. Ehn, D.G. Babb, N. Theriault, D.G. Barber (2017). Sea ice thickness in the Eastern Canadian Arctic: Hudson Bay Complex and Baffin Bay. *Remote Sensing of the Environment*, 200 281-294. 10.106/j.rse.2017.08.019

Lukovich, JV, Jafarikhasragh, S, Myers, PG, Ridenour, N, Castro de la Guardia, L, Hu, X, Grivault, N, Marson, JM, Pennelly, C, Stroeve, JC, Sydor, K, Wong, K, Stadnyk, TA, Barber, DG. (2021a). Simulated relative climate change and regulation impacts on sea ice and oceanographic conditions in the Hudson Bay Complex. *Elementa: Science of the Anthropocene*, 9(1):00127. https://doi.org/10.1525/elementa.2020.00127

Lukovich, J.V., Tefs, A., Jafarikhasragh, S., Pennelly, C., Kirillov, S., Myers, P.G., Stadnyk, T.A., Sydor, K., Wong, K., Stroeve, J., Barber, D.G. (2021b). A baseline evaluation of atmospheric and river discharge conditions in the Hudson Bay Complex during 2016-2018. *Elementa: Science of the Anthropocene*, *9(1), 00126.* https://doi.org/10.1525/elementa.2020.00126

Lukovich, JV, Jafarikhasragh, S, Tefs, A, Myers, PG, Sydor, M, Wong, K, Stroeve, JC, Stadnyk, TA, Babb, D, Barber, DG. (2021c). A baseline evaluation of oceanographic and sea ice conditions in the Hudson Bay Complex during 2016-2018. *Elementa: Science of the Anthropocene*, 9(1), 00128. https://doi.org/10.1525/elementa.2020.00128

Macdonald, M., Stadnyk, T.A., Déry, S.J., Koenig, K. (2018). Impacts of 1.5°C and 2.0°C warming on pan-Arctic river discharge in the Hudson Bay Complex through 2070. *Geophysics Research Letters*, 45(15), 7561-7570.

Matthes, L.C., Ehn, J.K., Dalman, L. A., Babb, D.G., Peeken, I., Harasyn, M., Kiriliov, S., Lee, J., Bélanger, S., Tremblay, J.-É., Barber, D.G. and Mundy, C.J. (2021). Environmental drivers of spring primary production in Hudson Bay. *Elementa: Science of the Anthropocene*, 9(1), 00160. https://doi.org/10.1525/elementa.2020.00160

McCullough, G.K., Kuzyk, Z.A., Ehn, J.K., Babb, D.G., Ridenour, N., Myers, P.G., Wong, K., Koenig, K., Sydor, K., Barber, D.G. (2019). Freshwater-Marine Interactions in the Greater Hudson Bay Marine Region. P. 155–197 in Z.A. Kuzyk and L.M. Candlish, ed., *From Science to Policy in the Greater Hudson Bay Marine Region: An Integrated Regional Impact Study (IRIS) of Climate Change and Modernization.* ArcticNet, Québec City, 424 pp.

McCullough, G.K., Page, S.J., Hesslein, R.H., Stainton, M.P., Kling, H.J., Salki, A.G., & Barber, D.G. (2012). Hydrological forcing of a recent trophic surge in Lake Winnipeg. *Journal of Great Lakes Research*, 38, 95-105.

Messier, D., S. Lepage, and S. Margerie (1989). Influence du couvert de glace sur l'étendue du panache de La Grande Rivière (baie James). *Arctic*, 42(3), 278–284.

Mundy, C.J., Gosselin, M., Starr, M., & Michel, C. (2010). Riverine export and the effects of circulation on dissolved organic carbon in the Hudson Bay system, Canada. *Limnology and Oceanography*, 315-323.

Pett, R.J., & Roff, J.C. (1982). Some observations and deductions concerning the deep waters of Hudson Bay. *Naturaliste Canadien*, 109, 767-774.

Pierrejean, M., Babb, D.G., Maps F., Nozais C. & P. Archambault (2020). Spatial distribution of epifaunal communities in the Hudson Bay system. *Elementa Science of the Anthropocene*, 8(1). doi.org/10.1525/elementa.00044

Prinsenberg, S. J. (1986). The circulation pattern and current structure of Hudson Bay. *Elsevier oceanography series*, 44, 187-204.

Razavi, N. R., Qu, M., Chen, D., Zhong, Y., Ren, W., Wang, Y., & Campbell, L. M. (2015). Effect of eutrophication on mercury (Hg) dynamics in subtropical reservoirs from a high Hg deposition ecoregion. *Limnology and Oceanography*, 60(2), 386-401.

Ridenour N., X.Hu, S. Jafarikhasragh, J.C.Landy, J.V. Lukovich, T.A. Stadnyk, K. Sydor, P.G. Myers, D.G. Barber (2019a), Sensitivity of freshwater dynamics to ocean model resolution and river discharge forcing the Hudson Bay Complex, *Journal of Marine Systems*, 196, 48-64, https://doi.org/10.1016/j.jmarsys.2019.04.002

Ridenour, N.A., X. Hu, K. Sydor, P.G. Myers, D.G. Barber. (2019b). Revisiting the circulation of Hudson Bay: Evidence for a seasonal pattern. *Geophysical Research Letters*, 46. https://doi.org/10.1029/2019GL082344

Rosa, E., Gaillardet, J., Hillaire-Marcel, C., Hélie, J. F., & Richard, L. F. (2012). Rock denudation rates and organic carbon exports along a latitudinal gradient in the Hudson, James, and Ungava bays watershed. *Canadian Journal of Earth Sciences*, 49(6), 742-757.

Saucier, F., Senneville, S., Prinsenberg, S., Roy, F., Smith, G., et al. (2004). Modelling the 982 sea ice-ocean seasonal cycle in Hudson Bay, Foxe Basin and Hudson Strait, 983 Canada. *Climate Dynamics*, 23, 303–326. 10.1007/s00382-004-0445-6.

Sella, G. F., Stein, S., Dixon, T. H., Craymer, M., James, T. S., Mazzotti, S., & Dokka, R. K. (2007). Observation of glacial isostatic adjustment in “stable” North America with GPS. *Geophysical Research Letters*, 34(2).

Simon, K. M., Riva, R. E. M., Kleinherenbrink, M., & Tangdamrongsub, N. (2017). A data-driven model for constraint of present-day glacial isostatic adjustment in North America. *Earth and Planetary Science Letters*, 474, 322-333.

Singer, J. (2020). Mercury cycling in hydroelectric reservoirs of northern Manitoba decades after impoundment. (Master’s thesis). University of Manitoba, Winnipeg, Canada. https://mspace.lib.umanitoba.ca/handle/1993/34506

Stadnyk, T.A., Tefs, A., Broesky, M., Déry, S.J., Myers, P.G., Ridenour, N.A., Vonderbank, L., Gustafsson, D. (2021). Changing freshwater contributions to the Arctic: a 90-year trend analysis (1981-2070). *Elementa: Science of the Anthropocene*, 9(1), 00098. https://doi.org/10.1525/elementa.2020.00098

Stadnyk, T.A., Déry, S.J., MacDonald, M.K., Koenig, K.A. (2019). Freshwater System. In Barber, D., Kuzyk, Z., Candlish, L. *An Integrated Regional Impact Assessment of Hudson Bay: Implications of a Changing Environment*. Québec City, QC, Canada.

Stainton et al. (in review). Sources and characteristics of particulate matter in the Nelson River system.

St-Laurent, P., Straneo, F., Dumais, J. F., & Barber, D. G. (2011). What is the fate of the river waters of Hudson Bay?. *Journal of Marine Systems*, 88(3), 352-361.

Tsuji, L. J., Daradich, A., Gomez, N., Hay, C., & Mitrovica, J. X. (2016). Sea level change in the western James Bay region of subarctic Ontario: Emergent land and implications for Treaty No. 9. *Arctic*, 99-107.

Wang, R., G.K. McCullough, G.G. Gunn, K.P. Hochheim, A. Dorostkar, K. Sydor, D.G. Barber. (2012). An observational study of ice effects on Nelson River estuarine variability, Hudson Bay, Canada. *Continental Shelf Research*, 47, 68–77.

CHAPTER 5 GAPS, FUTURE WORK, AND RECOMMENDATIONS

BaySys focused on the determination of the relative contributions of water regulation and that of climate change on freshwater-marine coupling in Hudson Bay. As with all research projects the initial tasks and deliverables evolved throughout the project both due to incoming data, new knowledge, and changes in the practical aspects of sampling. As noted in Chapter 3, the BaySys Central Team monitored the progress of each research Team's task list to ensure that all objectives and deliverables were tracked through to project completion. Deliverables have all been specified within the Team project summaries, and objectives that were either not met or will require analysis beyond the end of funding (December 2021) have been identified as **research gaps** (hereinafter gaps). With such an extensive project, complications arose, delays occurred, and unintended complexities impacted a small number of deliverables that will be presented in this chapter. It is important to note that the BaySys project fieldwork and analysis proceeded through several delays due to unforeseen weather and sea ice conditions, HQP turnover and emergencies, and most impactfully the global COVID-19 pandemic which shut down most university labs. All these circumstances impacted our researcher's ability to fulfill some project tasks. Along with an explanation of each research gap, we discuss the implications to the overall project objectives and deliverables that these gaps pose.

With extensive data collection and analysis, it was apparent that certain results and lines of evidence would lead to new research questions as the project progressed. Recommendations for future work are presented in this chapter along with brief discussions of how this research could further improve our understanding of the Hudson Bay Complex (HBC). New research questions arising from the BaySys project will ultimately lead to future project proposals and future collaborations between scientists, industry partners, and communities around the region.

5.1 Research Gaps

5.1.1 Fieldwork and Data Collection

The BaySys project produced the largest bay-wide sampling campaign in the Hudson Bay. Despite the efforts and planning put into each of the seven field campaigns, some gaps still exist from the observational field record, specifically the sample size from eastern Hudson Bay's coastal and river regions. During the 2018 BaySys bay-wide field campaign, the CCGS Amundsen could not reach the eastern parts of the bay as planned in early June due to timing and the thickness of sea ice present in the region. This led to a very small sample size from eastern Hudson Bay, including its rivers during the second leg of the field campaign (see Phase 1 report for more details). Tasks associated with the fieldwork and data collection were not heavily impacted by this, although additional sampling from along the eastern Hudson Bay coast and rivers would help to provide more detail for the overall bay-wide system. Without these larger sample sizes, estimates of primary production, carbon, and importantly the mercury budget must be considered as provisional in this region due to the limited sampling coverage in the eastern portion of the bay. The same limitation applies to estimates of pre-bloom nutrient levels, which were established more than a year prior to the main 2018 spring/summer expedition. As research continues to focus on the HBC and its underlying freshwater and marine systems, these gaps will be filled in over time and will be available to be compared to and expanded upon from the established BaySys datasets.

5.1.2 Data Analysis and Results (Tasks 1.4; 4.4; 5.2; 5.3)

Task 1.4 Remote Sensing - To conduct a Bay-wide survey of the timing (weekly time scale) of sea ice formation and decay (5 km spatial resolution) by analysis of remotely sensed data following Hochheim and Barber (2014).

Task 4.4 Remote Sensing – to ensure that regional trends may be assessed relative to observed variation in atmospheric, hydrologic, and oceanic drivers and provide an independent satellite-based assessment of total DOC photo mineralization across the bay to assess the regional and Bay-wide influence of photochemical processing of organic matter on pCO2.

Task 5.2: Suspended sediment and organic matter fingerprinting – to assess the sources of organic matter and suspended sediment within the LNRB, its estuary, and Hudson Bay using traditional (surveys and budgets) and fingerprinting techniques.

Task 5.3: Mass balance modelling of methyl Hg in Hudson Bay – to develop a MeHg mass budget for the Hudson Bay.

Following 2 years of extensive data collection, analysis progressed in several labs across Canada as part of the BaySys project. While significant progress was made by all Teams resulting in numerous peer-reviewed publications, conference presentations/posters, and providing their ability to address almost all Team and project objectives, some delays occurred throughout the project impacting the research gaps listed below.

For the Marine and Climate Systems research team, data analysis proceeded without significant delay. All tasks were completed (between Team 1 and Team 6), however, within the analysis of remote sensing data (Task 1.4), CDOM and O^{18} data were completed from the coastal portions of the bay, but the offshore analysis component was not yet available nor included in this report. This is in part due to lab access during the pandemic, and the availability of the graduate student who had been working on it during a family emergency. These analyses remain ongoing and will be provided as an addendum to this final report for the BaySys project. Furthermore, the major portion of the O^{18} data set associated with freshwater partitioning into ice melt and river water sources was accomplished and published as a part of Ahmed et al. (2020).

Concerning Task 4.4 from the Carbon Team, the open-water fluxes for the fall season have been completed through satellite-derived average seawater temperature and modelled monthly average wind speeds. This contributed to the Team objectives and helped to address their hypotheses as discussed in Chapter 3.4, however, a second facet of the remote sensing results remain under development within an active Post Doctoral project. This portion of the remote sensing analysis will focus on the synergistic use of remote sensing and model data, combined with machine learning techniques, to develop regional estimates of sea-air CO_2 fluxes, considering both thermodynamics and biology. The outcome will be regional carbon sink estimates, with uncertainties, over the periods of available satellite data (i.e., back at least as far as 2000). It is expected to be complete by Spring 2022.

The Contaminants research Team is in the unfortunate position to have had multiple research gaps arise from delays in data analysis and of which specifically impact the completion of their Team's project tasks and objectives. A major gap in Team 5's research is the delay associated with the development of the MeHg mass budget for the Hudson Bay system (Task 5.2 and Task 5.3). COVID-19 resulted in restrictions including the complete shutdown of our analytical laboratories since March 2020. Several research personnel have since moved on and found employment elsewhere. As such, approximately 200 marine sediment samples have yet to be analyzed for MeHg and organic carbon, which delayed the development of the MeHg mass budget. As the pandemic-related restrictions are easing up, a new part-time technician has been hired to assist with the analysis. We expect to complete the sample analysis by December 2021 and publish the mass budget in 2022. Once peer-reviewed, this MeHg mass budget will be added as an addendum to the BaySys project report to fulfill the Team 5 objectives. With all this noted, due to the sensitivity of these results, it should still be emphasized that with the lack of data from the eastern portion of the bay, we cannot be as confident in the results as we intended, and further investigation will need to occur in the future to complement and strengthen these results.

5.1.3 Modelling (Task 3.4; 4.5)

Task 3.4 Biogeochemical modelling - coupled 3D ecosystem model to predict plausible changes in the timing and magnitude of primary and secondary production associated with the sea ice and within the water column of Hudson Bay, in response to climate change and freshwater inputs.

Task 4.5 Biogeochemical Modelling - coupled 3D ecosystem model to distinguish effects of climate variability from hydroelectric regime forcing on the bay's carbon system parameters, and net CO2 exchange budgets.

Regarding the modelling components of the project, there have been delays in the development of complex biogeochemical modelling (BiGCIIM) tied to Nucleus for European Modelling of the Ocean (NEMO). This complex modelling component was in development by one of the project's Ph.D. students for several years. Although it was not completed in time for this report, the biogeochemical model BLING was used instead (see sections 3.4 and 3.6). The development and refinement of BiGCIIM have since been completed and will be run and analyzed following the end of the BaySys project. Results from the BiGCIIM analysis will ultimately be provided to Manitoba Hydro and updated in this report as an addendum following the project's end date.

The delay in the completion of BiGCIIM impact the outcome of some Team's tasks, specifically tasks 3.4 and 4.5, differently as they are related directly to the completion of the BIGCIIM biogeochemical model. For Team 3, the completion of task 3.4 which will include the output and analysis from the BIGCIIM model, will be completed following the end of the project and added as an amendment to this report in Spring 2022. Team 4, however, decided to use the existing

BLING biogeochemical output, already tied to NEMO, as an interim step to address their current objectives. They have provided an in-depth analysis using the BLING model but will also include additional studies comparing their results to those using BiGCIIM following the completion of the project. In addition, Team 4 has included a box model analysis as one component of their modelling task.

Lastly, it is important to note that because of delays in running the BIGCIIM model, it was decided that the NEMO model coupled with BLING was going to be run again only with RCP8.5 so that Team 4 could use those output to complete their Team tasks.
As a whole, the research gaps were minor as the project came to an end, and it is important to note that research using BaySys data will continue for years to come as new insights derived from analysing these data will serve to further enhance our understanding of the relative contributions of water regulation and climate change on freshwater-marine coupling in Hudson Bay.

5.2 Future Work and Recommendations

5.2.1 Bay-wide and Coastal Research

The multi-disciplinary research approach of the BaySys project has inevitably led to several novel inquiries and research ideas extending beyond the original proposal. If this program were to continue, it would be worth some time to focus on new mooring observational programs on the surface layer (~25-30 m-thick layer) to collect in-situ observations from the bay. This could include a very simple mooring configuration with 4 to 5 CT sensors, 1 ADCP, and a single acoustic release, in addition to any other biochemical sensors needed for primary analysis, and possibly automated water samplers to derive a time series from. It would be beneficial to incorporate the near-surface scope through a large array of near-coastal moorings to capture the seasonal transformations associated with vertical mixing of freshwater in these regions. Such mooring observations of the near-surface layer were unsuccessfully attempted during BaySys using long instrumented pipes that were designed to withstand impacts with sea ice. However, in some cases, the deployment of these pipes was not successful, while in other cases the pipes were lost likely because the weak link that was added to the line was too weak to withstand high dynamic events. Moreover, with improved AUV technology and preliminary drone studies conducted during the BaySys campaign (see Harasyn et al., 2019, 2020), it could be recommended to use new gliders carrying sensors to collect data on near-surface waters in Hudson Bay.

The HBC would be an ideal region for using AUVs during the open water season, and possibly beneath sea ice as the ice-avoidance technology evolves. The newly completed Churchill Marine Observatory (CMO) research facility, located in Churchill, Manitoba, is well suited to launch and recover glider drones or other AUVs. During the ice-covered period, ice-tethered moorings could be deployed to capture this lacking component of the BaySys datasets (near-surface layer). These moorings could be designed so that they would drop to the seafloor when the ice melts, such that they could then be recovered with the William Kennedy research vessel, also based out of Churchill. In addition, this kind of study would extend within the western polynya during the winter months, as based on the results from BaySys, the west coast polynya is a region now known to host large biological activity in terms of high production, and ventilation, etc. and would be important to focus more on that polynya. Understanding the surface mixing layer in more detail throughout the year would complement the results of the BaySys project, specifically through the mooring program data.

For all the years of work in Nelson and Hayes estuaries (including the BaySys project), a complete optical dataset with all IOPs, AOPs, and optically active substances measured coincidently, has not been collected and there are currently no complementary measurements that coincide in time with satellite overpasses. Following BaySys, it would be important to develop an efficient field program using again, the William Kennedy and its zodiacs, to capture sediment dynamics in the estuary and on mudflats, and to provide a more detailed validation of the satellite algorithms. Such research would help improve the coastal model (Delft3D) to include sediment dynamics, which would allow the study of the effect of winds, storms, waves, tides, runoff levels, and possibly even ice.

5.2.2 Modelling

HYPE freshwater discharge simulations were extended from the end of the baseline period (2010) through to the end of the observation period for BaySys (end of 2018) to allow driving NEMO during this period with reanalysis (not projected GCM) forcing. The gap-filled, extended-to-the-outlet discharge record generated by Team 2, however, ends in 2016 and has not been updated to present. This means these extended HYPE simulations cannot, at the moment, be validated against observed discharge for accuracy. We recommend that the gap-filled discharge record be extended until the end of 2018 to allow for this validation in the future. Regarding the NEMO output, modules for multi-category sea ice LIM3 should be added into future studies, along with an improved representation of bathymetry, and tidal forcing in future models of the bay.

Further modelling efforts are essential for understanding freshwater residence time in the bay and its outflow to the Labrador Sea depending on wind forcing. A focus on the climatic forcing of the Hudson Bay circulation and freshwater cycle using NEMO simulations back to the 1950s would be important for future studies. Beyond this, modelling would be further improved with greater spatial resolution, and high-resolution nesting in important, high-interest areas, including within the Nelson River Estuary. A sensitivity study on mixing processes, diffusivity, and representation of the thermocline should be a larger part of future studies.

The dynamic linkage between climate, hydrology, and ocean circulation is critical research needed to better understand the positive feedback mechanisms acting to exasperate global climate change. BaySys research has uncovered that freshwater discharge can influence ocean circulation and sea ice processes to a significant extent – now, more than ever, it is important to further explore the dynamics of these relationships. Similarly, it is critical to understand the extreme future projections within the context of our past. Though BaySys made an effort to look at pre-regulation periods, it would be prudent to extend the record further back in time using pre-industrial control runs from GCMs to establish an even longer pre-regulation time series from which we can explore changes in climate and freshwater extremes. This is particularly important to study in the context of impacts on ocean circulation and the formation of AMOC. Finally, we have seen evidence within BaySys that thermally-driven processes are important for the ecosystem, nutrients, and ocean circulation patterns. It is an expectation that under climate change that there will be an even greater difference in the temperature of freshwater discharge versus the colder, saline ocean water. It would be interesting to examine the dynamic impacts of freshwater discharge and its temperature under climate change scenarios, which was not done under BaySys.

Biogeochemical modelling needs to be embedded within the future modelling strategies discussed above. The preliminary assessment of BLING V0 +DIC indicates that overall, regulation serves to increase the bay's susceptibility to ocean acidification and decrease the bay's uptake of atmospheric CO_2, with the largest changes observed in the spring, fall, and winter seasons. Additional work is required to examine projected spatial trends for CO_2 exchange dynamics, pH, and Ω_{Ar} regional OA risk in surface waters of Hudson Bay. Our model lacks the spatial resolution to resolve the intricacy of biogeochemical processes in complex mixing systems, like estuaries and adjacent coastal seas. The carbon dynamics in sea ice is not represented in BLING v0+DIC, and thus in this study sea ice existed as an impermeable slab from the perspective of the carbon system. The biogeochemical model, BiGCIIM, alternatively, integrates to some degree sea ice biological and carbon systems with those of the underlying seawater. Our best tool to project the response of the bay's carbon system to changes induced by climate and regulation remains the application of ever-improving numerical models. Thus, a continued investment of resources toward biogeochemical modelling is warranted to verify the cumulative impact of terrestrial carbon and freshwater on OA, regional ecosystems, and carbon budgets, and assess the impact of change, including land/water use and climate, on future OA states, food webs, and carbon budgets.

5.2.3 Lakes and Watershed Studies

The focus of BaySys (apart from Teams 2 and 5) was within the marine-dominated parts of the bay. What stands out for future endeavours is the need for a stronger focus on the watershed while maintaining a connection to the bay. The river work for most of the BaySys Teams consisted of one-off spot samples at the zero-salinity mark during the 2018 Amundsen campaign and a geographically limited winter program at the terminus of the Nelson and Hayes rivers. A focus on the lakes, but also an examination of the contribution of other nodes along the interconnected aquatic network connecting the Manitoba Great Lakes (MBGL) to the bay via the Nelson and Churchill River systems would be essential in future programs. The MBGL lakes, notably Lake Winnipeg, are important nodes from many perspectives. A big part of the local watershed to the bay is peatland, largely wetland, with some areas underlain by discontinuous or continuous permafrost, which accounts for several concerns from a climate change perspective. That said, the area is also used for a large part of Manitoba Hydro's production. The role of impoundment, for hydroelectric production, on estuarine and coastal marine processes remains unassessed. The particulate and dissolved load of the wetlands and small rivers feeding the

Nelson and Churchill contain surprisingly high concentrations of nutrients and organic matter with high seasonal variability, that depending on the quantity and composition of the material making it to the bay, will have a strong bearing on the estuarine and coastal system biological and biogeochemical dynamics in the southwest and southeastern Hudson Bay. The nodes themselves are under-studied biogeochemical engines, and with the additions of existing greenhouse gas (GHG) research on Lake Winnipeg and the Lower Nelson River (already funded by Manitoba Hydro), the William Kennedy research vessel and CMO research facility, this type of work can be feasible in the near future. Climate change and energy policy would benefit from the resulting information.

With further respect to the freshwater flow into the bay, and a study of the greater watershed area, under continued permafrost thaw and changes in thermokarst, slumping or formation of thermokarst lakes, a question that comes up is how these processes affect the delivery of freshwater to the bay. In addition, there should be an effort focused on resilience as a key part of future work concerning the bay. Studies that focus on impacts of changing climate, including extreme events on infrastructure (i.e., ice storms have led to increased outages, with negative impacts on remote communities) as well as food security for nearby and surrounding communities. This may be something that is conducted through a partnership between the network of SIKU and the Sea Ice Prediction Network (SIPN) and integrating it with both the sea ice forecasting efforts from the University of Manitoba and the flood forecasting system of Manitoba Hydro.

Viewing the watershed to the bay as a continuum and studying it in terms of freshwater, carbon, and mercury sources and transports, including the lakes/reservoirs as big reactors where liquid water gets transformed to ice (and back again), and carbon and mercury transform inorganic and organic forms can be a primary focus moving forward. Freeze-up progresses quite differently because of the reservoirs and based on BaySys results, it is known that winter water quality (DOC) is unusual compared to summer samples. In addition, the Nelson River watershed is a place within which research can be used to better understand the “browning of boreal rivers”, which is a phenomenon happening all around the world.

The scientific Team leads, along with BaySys collaborators have developed a natural extension to the results of BaySys known as BaySys-Freshwater that will be pursued following the conclusion of the current project. This future project will be coordinated around a single research question: What are the relative contributions of climate change and water regulation to modifying the transport and fate of carbon across the freshwater-marine continuum of the Nelson River system? The focus on carbon would logically extend to other nutrients such as phosphorous and nitrogen that are coupled with carbon in its biogeochemical cycling, and the emphasis would be on how the properties of the Nelson River outflow into the Nelson River Estuary are affected by processes in the watershed including regulation, land-use change, and climate change. The work would focus geographically along a corridor starting at the Upper Manitoba Great Lakes and ending in the Nelson River Estuary and include a combination of *in situ* sampling, automated sampling, remote sensing, and modelling.

5.2.4 Climate Change vs. Regulation vs. Land Use

Expanding on BaySys, an area of research that could intersect is the effects of land-use change vs climate change vs regulation on material fluxes from headwaters to the bay. For example, we do not understand how the sequestration of particle-borne nutrients, carbon, and contaminants (buried, adsorbed, or incorporated into algae) will respond to increased residence time in reservoirs vs impact of climate-induced changes in hydrology on same residence times. A subset of these processes would reduce the regional greenhouse gas (GHG) footprint, while counter-acting these processes would be the build-up and outgas of GHGs, like CO_2 and methane (CH_4) that result from degradation pathways of organic material. An added level of complexity is associated with the possible impact of climate change on crops, treatments, and tillage, hence on nutrient, carbon, and contaminant export through interaction with changing hydrology, changing reservoir operation, and hence on nutrient, carbon, and contamination flow to Hudson Bay. This type of future work could include a better understanding of the impact of diversion (including non-hydro diversion e.g., Assiniboine through Manitoba) on nutrient and contaminant fluxes vs impact of climate change on the frequency, and scale of such diversions. Lastly, this type of study extends our understanding of the impacts of climate change and regulation on the bay through the impact of warming on productivity leading to increased carbon or nitrogen fixation and sequestration, leading to new questions surrounding how these interact with changing hydrology and residence times, and how it influences in-lake and in-reservoir sequestration vs export and delivery to Hudson Bay. Also, this raises further questions of the impact of increased productivity on the scavenging and sedimentation of contaminants and carbon, with the latter possibly initiating important feedbacks on GHG emission totals.

Finally, one of the fundamental underlying assumptions within BaySys was that future regulation was held constant based on historic practices. It would be interesting to explore dynamic regulation using optimization models that would dynamically alter regulation rules based on future climate conditions and freshwater supply.

5.3 References Cited

Ahmed, M.M.M., Else, B.G.T., Capelle, D., Miller, L.A., and Papakyriakou, T. (2020). Underestimation of surface pCO2 and air-sea CO2 fluxes due to freshwater stratification in an Arctic shelf sea, Hudson Bay. *Elementa: Science of the Anthropocene*, 8(1), 084. https://doi.org/10.1525/elementa.084.

Harasyn, M.L., Isleifson, D., Chan, W., Barber, D.G., (2020). Multi-scale observations of the co-evolution of sea ice thermophysical properties and microwave brightness temperatures during the summer melt period in Hudson Bay. *Elementa: Science of the Anthropocene*, 8(1), 16. http://doi.org/10.1525/elementa.412

Harasyn, M.L., Isleifson, D., Barber, D.G. (2019). The influence of surface sediment presence on observed passive microwave brightness temperatures of first year sea ice during the summer melt period. *Canadian Journal of Remote Sensing*, 23(1), 1–17. 10.1080/07038992.2019.1625759

Hochheim, K. P. and D. G. Barber (2014). An update on the ice climatology of the Hudson Bay System. *Arctic, Antarctic, and Alpine Research*, 46(1), 66–83.

CHAPTER 6 CONCLUSIONS

The BaySys project examined the influence of freshwater on Hudson Bay marine and coastal systems. Our objective was to provide a scientific basis to separate climate change effects from those of hydroelectric regulation of freshwater on physical, biological, and biogeochemical coupling in the Hudson Bay Complex (HBC). BaySys researchers conducted the first bay-wide survey with detailed observations of freshwater-marine interactions at periods throughout the annual cycle and during the critical spring bloom. We developed a complex modelling system for the HBC, integrating hydrological, tidal, and atmospheric climate forcing data with numerical model development of the ocean, sea ice, and biogeochemical components of the system to carry out long-term studies of freshwater-marine coupling. The overarching vision of BaySys was one of the unique aspects of the study. Not only were relative contributions of water regulation and climate change being assessed in the present, but also in the past (with the Churchill River Diversion), and importantly into the future (through the climate change projections). A key feature of BaySys was how we treated the entire hydroclimate system and the resulting freshwater-marine coupling within the context of a ‘system’. In this chapter we summarize the key results of the BaySys project from the perspective of the individual Teams (Team Conclusions) then conclude on the issues that cross-cut these themes (Cross-Cutting Conclusions), providing new insights into how the HBC operates as a system.

6.1 Team Conclusions

Team 1 results show that ocean circulation, momentum forcing of winds on the surface, tides, and importantly, interaction with shallow exposed coastal shorelines, all play a role in the freshwater-marine coupling of the HBC. To no surprise, the formation and persistence of sea ice strongly modulated air-sea interactions, tidal forcing as well as how terrestrial freshwater debouches into HBC. For example, Andrews et al. (2018) reported statistically significant trends in both earlier ice break-up and delayed freeze-up across the HBC resulting in the lengthening of the open water season by almost 1 day per year on average for the 1980-2014 period. Galbraith & Larouche (2011) associated this decline in sea ice persistence with a consistent increase in sea surface temperatures across the HBC. However, recent Team 1 results showed that changing wind patterns over 2008-2018, leading up to the BaySys field experiments, resulted in an enhanced drift of sea ice towards the east, and consequently earlier ice break-up and polynya formation along the western side of HBC and delayed ice break-up in the eastern side (Landy et al., 2017; Kirillov et al., 2020; Bruneau et al., 2021; Ehn et al., in prep.). Consequently, this decade saw a spatially varying trend in sea-surface temperature (SST) across the HBC associated with sea ice persistence patterns. However, despite this varying pattern over the 2008-18 decade, a longer trend analysis covering 1982-2020 continued to show statistically significant declines in sea ice duration and increases in the open water SST. Comparisons of BaySys AN01 mooring observations over 2016-2018 with the only previous one-year-long record in 1981-1982 by Prinsenberg (1977) showed that significant increases in freshwater content and water column stratification have occurred throughout sea ice decline. However, trend analysis and attribution of freshening of the water column is not possible due to the lack of field data and therefore, need to rely on numerical simulation.

Thus, BaySys marine and climate system studies concluded that climate change is the main driver of the reduction in sea ice, as well as the increase in SST. Nucleus for European Modelling of the Ocean (NEMO) modelling experiments comparing regulated versus non-regulated scenarios indicated that, in summer, the effects of regulation, while relatively smaller, suppresses the SST increase. However, in winter, the effects of regulation opposed the climate change signal. Thus, scenarios with regulation are predicted to lose slightly less ice in March than they might otherwise if no regulation was present in HBC. The causes for the freshening of the water column are not as easy to attribute to climate change or regulation. The reduction in salinity follows Arctic-wide trends, also seen in Labrador Sea, however, wintertime release of river discharge may also result in riverine freshwater being more readily entrained in offshore and deep waters of Hudson Bay (e.g., Eastwood et al., 2020).

Climatic variations, like the increasing air temperature or precipitation changes, also impact the landfast ice cycle by affecting the timing of freeze-up and break-up, and ice thickness through both thermodynamic and mechanical growth. Trends in landfast ice duration roughly follow that of the offshore sea ice patterns (Gupta et al., in review). A reduction in the landfast ice duration means a longer open water condition prevalent in the coastal zone. This has implications on coastal erosion and sediment resuspension from the seafloor, and on how terrestrial freshwater enters and disperses into the marine environment. A surprising finding from the BaySys winter campaign was the extent to which tidal amplitudes and currents suppressed a storm-driven increase in the landfast ice extent. With the widening of the landfast ice fringe by a few kilometers, the tidal amplitudes near the coast decreased from about 3 m to 1 m in a matter of a day.

Heavily deformed areas of sediment-laden sea ice were observed in southern Hudson Bay for the first time during the BaySys 2018 cruise. Although initially thought to be freshwater ice, it was subsequently determined that this ice was a unique form of multiyear-like sea ice type that was much thicker than the surrounding seasonal sea ice, impeding the CCGS Amundsen’s traverse through southern Hudson Bay. Using a mix of *in situ* and remotely sensed datasets, the formation of this ice type was linked to frazil ice that forms from marine waters and entrains sediment from coastal areas in the dynamic tidal flaw lead system. Deformed sediment-laden ice may either be entrained in the landfast sea ice or enter the mobile ice pack and be advected around the southern end of the bay (i.e., from the Nelson Estuary towards James Bay). Sediment-laden ice was also observed further westward in Hudson Bay, affecting the late-spring sediment trap samples at mooring AN01 located 100 nm north-northwest off Churchill, and in Foxe Basin.

Sea ice melt supplies twice as much seasonal freshwater as does fluvial discharge to Hudson Bay itself, but neither source is evenly distributed. Three-quarters (75%) of the fluvial supply enters along the southwest coast (Nelson River, in particular) or flows into Hudson Bay via James Bay. The climate gradient ensures that the thickest sea ice is generated in northern Hudson Bay, but southward and eastward transport of sea ice causes most ice melt to collect in the central to south-eastern half of the bay. Consequently, the freshwater inventory in Hudson Bay ranges from as little as 1.0 m in the northwest to 8–10 m in the southeast near the Belcher Islands.

The residence time of riverine water in Hudson Bay can be expected to be affected both by regulation and by climate change, with important implications for water column stability and thus primary production and support of the Hudson Bay ecosystem. This is also seen as consistent with what the NEMO model showed. During an anticyclonic wind forcing (i.e., storm), the background geostrophic cyclonic circulation in Hudson Bay was found to slow down or even reverse. This effect would likely result, in the absence of a change in the sea ice melt/growth flux, in a reduction of the freshwater transport in Hudson Bay and to Hudson Strait, and therefore an increase in the riverine water residence time in HBC. That said we also expect enhanced sea ice melt could increase the speed of the surface flow, and thus reduce overall riverine freshwater residence time. Thus, the long-term trends in regional wind forcing, which have been seen to affect sea ice drift patterns, may also modify the pace of riverine freshwater removal from the Hudson Bay as well as stratification and vertical mixing in some regions, although the rate of these changes and their geography can only be estimated with numerical simulations. The combination of field observations and numerical modelling was seen as the only viable way to assess the impacts of climate change at the HBC-wide scale. Future research, combining observations and modelling, will focus on better understanding freshwater transport within and in/out of HBC, and its role in the global climate system.

Team 2 results show that freshwater quantity is an important component when it comes to freshwater-marine coupling in the HBC. Most importantly, this work has resulted in the first-ever coupling of a dynamic runoff product across a pan-Arctic domain to an ocean circulation model. This allows the BaySys Team to assess the role that freshwater variability has on ocean circulation and sea ice process, as well as contaminant, biogeochemical, and ecosystem processes.

We have used these models to show that freshwater runoff into the Arctic region and Hudson Bay is increasing over the historic record and is anticipated to continue to increase into the future. Discharge will peak earlier and higher than previously observed, particularly at higher latitudes. This is the result of a ubiquitous warming trend, with more warming at higher latitudes, and a shift toward more precipitation in the winter months and hotter, drier summer conditions. Though climate change is imposing changes on the hydrograph, from an intra-annual perspective, it is regulation that has resulted in more drastic changes to the hydrograph in terms of hydropeaking signatures, and a general flattening trend relative to rivers with little to no regulation.

There is considerable uncertainty identified in our modelling, imposed most significantly by the input data used to drive the models, but also as a result of the model structure (choice of hydrologic model). Input data uncertainty can be mitigated to some extent by taking an ensemble approach to simulation, selecting, and using multiple input datasets to drive the hydrologic models and averaging their output. Uncertainties are shown to be larger during wetter periods relative to drier periods. Though not yet complete, it is important to propagate uncertainty through to the NEMO model to evaluate the impact uncertainty in freshwater contributions have on the changes in sea ice and ocean circulation processes.

The effects of climate change are seen not only in the changing magnitude and timing of flood peaks but also increased spatial variability. Modelled predictions for the La Grande Rivière Complex (LGRC) (and much of the James Bay and Eastern Hudson Bay drainage) generally show agreement in the direction and magnitude of changes. This is contrasted in the Nelson Churchill River Basin (NCRB), which as a water-limited basin sees greater disagreement between ensemble members with dominantly increasing precipitation or evapotranspiration. This results in the NCRB showing large inter-annual variability in discharge and in ensemble agreement, where the LGRC has larger intra-annual variability of ensemble agreement.

Through joint Ouranos, HYPE, and NEMO experiments, BaySys was able to conclude that the sequencing and timing of the freshwater input into the bay is at least as important as the total long-term freshwater input. Experiments forced with basically the same long-term average runoff ended up with significantly different freshwater budgets, including lower salinities in the regulated scenarios. The differences between the naturalized and regulated runs look to be related to the timing of the discharge and the residence time for freshwater in the basin. Additionally, years of strong discharge add more freshwater to the bay than can be exported through Hudson Strait, increasing freshwater residence times, and lowering salinity, with the reverse occurring in years of weak discharge. Therefore, the sequencing and timing of the freshwater input are at least as important as the total long-term freshwater input.

The work presented by Team 2 has offered an expansive study of the hydrologic impacts of climate change and regulation. We examined changes to modelled flow, but across numerous elements of the hydrologic cycle as well as presenting an in-depth look at modelled agreement, sensitivity, and multi-model uncertainty. The oceanographic and biogeochemical effects of the varying timescale and magnitude of modelled ensemble discharge and agreement between these two large, regulated watersheds as well as changes to the remaining Hudson Bay Drainage Basin will offer novel insight into Hudson Bay across numerous disciplines.

Team 3 results reaffirm those of previous studies in showing that primary production, on average, is low with respect to other areas of the Arctic and sub-Arctic (Tremblay et al., 2019). This situation occurs even though ice thickness and the duration of the ice-covered period of the year are relatively low in the bay, which favors light penetration and should promote primary production (PP). However, this advantage in light penetration is counteracted by the strong freshwater stratification that rivers impart to the upper water column. This stratification curtails the upward re-supply of nutrients during winter, which ultimately limits the ability of ice algae and phytoplankton to accumulate biomass. This nutrient supply is enhanced in the northwestern polynya, where the wind patterns linked to the North Atlantic Oscillation reduce the ice cover and enhance vertical mixing in some years. The resulting early-onset and intensification of primary production in this sector of Hudson Bay quickly starts the feeding period for the food web and contributes to make the area a hotspot of marine wildlife. Given the otherwise low levels of productivity in the bay, the supply of river nutrients in estuaries provides a crucial source of nutrients to nearshore areas. In this regard, the wide-ranging concentrations of nutrients observed across rivers were primarily attributed to differences in their natural setting, with no visible effect of regulation. However, regulation increased the relative contribution of winter to the annual nutrient transport into the bay. Because winter nutrient transport occurs during a period of relatively low productivity in estuaries, the nutrients presumably propagate further offshore than they otherwise would, which sets the stage for a relatively wide and intense spring bloom in those areas.

Estuarine transition zones were characterized by a diversity of productivity levels and microbial communities that occupied the distinct niches created by varied combinations of runoff, nutrient concentrations/ratios, and tidal forcings during early spring/summer. For the Nelson Estuary, in particular, local phytoplankton production was controlled by the spatial transition from light limitation in turbid river waters to nutrient limitation in marine waters. Low salinities near the mouth of estuaries also had an adverse impact on the primary production of ice algae during winter/spring. By affecting river discharge, its partitioning between seasons, and the stability of the salt transition zone, regulation and future changes in precipitation can therefore influence the structure and productivity of local plankton communities.

With the exception of the northwestern polynya, where all components of the lower food web were enhanced, spatial patterns epibenthic communities were opposite to those that would be expected from the distribution of primary production. Despite the relatively low levels of algal productivity offshore, the diversity and biomass of epibenthos were generally similar to those observed in other Arctic regions. Moreover, the coastal waters subjected to the influence of rivers and nutrient inputs harbored the lowest epibenthic density, biomass, and richness, presumably due to a negative impact of sediment loading. Enhanced winter discharge for regulated rivers has the potential to exacerbate this negative impact by covering the organisms with sediment before they can gain access to fresh food in the spring/summer.

In the HBC, Arctic cod hatch relatively early in comparison with other seasonally ice-covered regions. The earliest hatchers in the bay can be traced back to coastal waters that are exposed to relatively warm water during winter, which supports the so-called ‘freshwater refuge’ hypothesis whereby warmer temperatures allow for a higher growth rate and longer feeding season for the fish that hatch there. This enhancement may be particularly crucial for the survival of Arctic cod in Hudson Bay given the relatively low levels of PP and zooplankton biomass we observed. In this context, the relatively high winter discharge observed in regulated rivers may prove beneficial for the success of Arctic cod, provided that the fish do not hatch so early as to lack food.

Finally, the work of Team 3 has provided a large number of insights into the ecological functioning of Hudson Bay, showing that the biological carrying capacity of marine waters is relatively low. In such a setting, the input of rivers nutrients into the coastal zone and the enhanced vertical replenishment of nutrients in the Kivalliq polynya are particularly crucial in supplying grazers and upper trophic levels with food in those key areas. For the polynya, inter-annual variations in productivity levels are controlled primarily by long-range climatic forcings. While no effect of regulation on in-river nutrient concentrations was detected, regulation potentially impacts the food web through the seasonal shift in river discharge, which affects the timing and propagation of nutrient transports as well as the input of sediment and organic matter that affects water transparency and the benthic habitat. By favoring early hatching, the enhanced delivery of relatively warm waters during winter months in regulated rivers possibly has a positive effect on the growth and survival of Arctic cod larvae.

Team 4 results indicate that Hudson Bay is a moderate CO_2 sink over the open water season, taking in approximately 7.2 TgC. We estimate the annual total uptake to be somewhere closer to 6 TgC after considering CO_2 emissions in the late fall and winter. Observations highlight pronounced variation in variables that make up the bay's carbon system. Inorganic carbon was much higher in areas dominated by high salinity water from the Arctic Basin, while the concentration of inorganic carbon is much lower in areas of low salinity because of high fractional compositions of river water and/or sea ice melt. The carbon chemistry of rivers entering Hudson Bay differed depending on the underlying geology of the drainage basin, with those rivers draining the Hudson Plains in the southwest and south delivering water with a high concentration of dissolved inorganic carbon (DIC), organic carbon (DOC), and alkalinity (TA), while rivers draining Precambrian Shield had low concentrations of DIC, TA, and DOC. Sea ice melt also is low in alkalinity and dissolved carbon. Despite these differences, all rivers (and sea ice melt) dilute the marine store of DIC and TA in the bay, while augmenting (as in the case with rivers) the bay's concentration of DOC. The impact of diluting TA and DIC acts to depress pCO_2, while the degradation of DOC through microbial and photochemical processes increases pCO_2. These counter-acting processes both strongly impact the marine carbon cycle in proximity to river mouths. Additionally, lowering the alkalinity causes seawater to be more poorly buffered against a drop in pH with increasing pCO_2, thus elevating the risk of ocean acidification. BaySys results show that the DOC from the southwest rivers, and in particular from the Nelson River has very high concentrations of DOC that is highly susceptible to degradation, locally driving pCO_2 supersaturation that underpins CO_2 outgassing, while also locally elevating the state of ocean acidification. BaySys research identifies degradation of DOC to be a major factor in elevating pCO_2 and susceptibility to ocean acidification in bay-wide coastal waters.

The future CO_2 source/sink status of Hudson Bay depends on the relative balance of several processes. Increasing atmospheric CO_2 concentration will encourage uptake while the degradation of higher river loads of organic carbon, in conjunction with seawater having a lower solubility to CO_2 because of warming, will encourage CO_2 emissions. A longer ice-free season should allow for earlier peak CO_2 uptake at the height of spring/summer biological production, but elevated rates of uptake should not be expected in the open water season because of nutrient limitations. Biogeochemical modelling suggests that on average, and over an annual cycle, the future flux of CO_2 is not expected to appreciably change, and hence the processes that would encourage greater uptake will be approximately balanced by those processes favouring emissions. Seasonally, however, pronounced changes in the bay's source/sink status are expected, with greater uptake in the spring and higher emissions in the fall and winter. In all future scenarios, Hudson Bay will accumulate inorganic carbon due to increasing atmospheric CO_2 concentrations *and* increased CO_2 production from terrestrial organic carbon degradation beyond what can be offset by biological production, leading to escalating states of ocean acidification, particularly in deep water. Regionally, the impact may be most strongly felt in the southeast, where characteristically the proportion of sea ice melt and river water is greatest.

If the water flow through Hudson Strait and Foxe Basin into Hudson Bay is considered, the annual additions of runoff and ice melt/brine from the Arctic basin could more strongly influence the change in CO_2 flux and acidification in Hudson Bay than terrestrial organic matter delivery, with local exceptions, including areas in proximity to river plumes and estuary waters. Thus, future warming and freshening in upstream areas of the Arctic Ocean may significantly affect the carbon cycle in Hudson Bay even more than changes in the watershed that lead to enhanced carbon transfers.

Biogeochemical modelling suggests that future changes in the bay-wide source/sink status will mainly be attributable to climate change, however, regulation will significantly impact seasonal CO_2 uptake, in addition to seawater pH. Additional work is required to better understand the four-season impact of river regulation on the downstream river flux of carbon and its various forms and its impact regionally on the bay's carbon cycle, both under contemporary and future hydrologic and climatic regimes.

Team 5 examined processes that affect mercury (Hg) load, fate, and effects within the HBC. The Team analyzed historical fish mercury data between 1972–2018 from 55 waterbodies that are ("on-system") or are not ("off-system") influenced by hydroelectric regulation in the Nelson River, Churchill River, and Churchill River Diversion regions. The results show that fish mercury from on-system waterbodies continues to decrease toward recovery from hydroelectric regulation nearly 50 years following initial impoundment in the region. Despite the general decreases, significant increases in fish mercury were observed intermittently, especially over the past two decades in most of the on-system and off-system waterbodies. Length-standardized fish Hg concentrations increased by up to 100 % in Northern Pike and up to 175% in Walleye between 2001–2010, reaching 0.79 $\mu g\ g^{-1}$ in some of the water bodies over the most recent decade (2010–2018). The analysis shows that these intermittent fish Hg increases cannot be explained by atmospheric emissions or regional hydrology, and that future fish Hg concentrations in the region are likely to be affected by climate-induced changes in water chemistry and trophic dynamics. Laboratory incubation studies show that mercury methylation potential remains high in the water fluctuation zone of these water bodies, and its sensitivity to a changing climate will likely control the long-term variability of fish Hg.

Development of a mass budget of methylmercury in the HBC is ongoing, due to delays caused by the pandemic, and the lack of data from the eastern part of the bay. The results so far suggest the contribution of riverine methylmercury from the Nelson River system to the Hudson Bay marine system is small. At the present, there is no clear evidence that either hydroelectric regulation or climate change has had a significant impact on Hg accumulation at the base of the Hudson Bay marine and coastal food webs. This however could change in the future, as thawing of the widespread permafrost in the region accelerates and as more invasive species are introduced. Both of these processes affect Hg bioaccumulation through changes to water chemistry and trophic dynamics and have the potential to magnify the impact of both hydroelectric regulation and climate change on Hg accumulation in the Hudson Bay marine and coastal food webs.

Team 6 developed a modelling system for the HBC, integrating hydrological, tidal, and atmospheric climate forcing data with numerical model development of the ocean, sea ice, and biogeochemical components of the system to carry out long-term studies of marine freshwater coupling. The system was built, upon the NEMO framework, to be sufficiently flexible that additional modules or drivers could be added for future studies, as well as regional nests for higher resolution localized studies.

Results from NEMO showed, the temperature of the bay will warm over the next 50 years, with the bay annually-averaged warming between 2005 and 2070 being ~1.5 °C, averaged over the 5-member ensemble of climate simulations considered by BaySys for the numerical modelling. Changing from Naturalized to Regulated River Runoff has little impact on this warming. Sea ice concentration and thickness in the bay will significantly decrease over the next 50 years, with the bay averaged reductions between 2005 and 2070 being ~20% in concentration and 0.15-0.2 m in thickness, averaged over the 5-member ensemble of climate simulations considered by BaySys for the numerical modelling. Changing from Naturalized to Regulated River Runoff has little impact on the annually averaged sea ice changes. Although the ensemble mean of scenarios with naturalized river runoff suggests a slight freshening (~0.2 g/kg) of the bay, there is a large discrepancy between ensemble members, with some scenarios suggested a strong freshening, while others suggest little change or even a slight increase in upper ocean salinity. With regulated river runoff, the ensemble mean salinity reduction is slightly larger (~0.3 g/kg) with no scenarios suggesting an increase in the bay's salinity. The differences between the naturalized and regulated runs look to be related to the timing of the discharge and the residence time for freshwater in the basin.

Through the modelling exercises, BaySys determined that regulation suppresses in winter months and reinforces/enhances in summer months the climate change impacts on SST and sea ice state and dynamics. Specifically, in winter, regulation suppresses a projected 4×10^5 km^2 (~1x 10^5 km^3) decrease in sea ice area (volume) due to climate change by ~30% throughout Hudson Bay, and weakens cyclonic circulation by ~50%, particularly in southwestern Hudson Bay, and in summer, regulation suppresses a projected 2 – 3 °C increase in SST due to climate change.

The innovation from BaySys modelling allowed us to segregate climate change from regulation because it was the first time an exercise to incorporate hydroelectric regulation, reservoirs and irrigation were undertaken on such a massive continental scale. This has truly revolutionized what we can predict in terms of hydrology and coupled ocean-terrestrial modelling.

6.2 Cross-Cutting Conclusions

BaySys measurements, coincident in space and time, are a unique contribution to our understanding of freshwater-marine coupling in the HBC. Measurements within the watershed, in estuaries, and the bay, all contributed to a better understanding of the physical processes for sediment transport, river discharge, and the sequencing and timing of freshwater inputs to the bay, and the impacts of this freshwater on marine processes at different times throughout the annual cycle. In complementary studies, BaySys research for the first time quantified the effect of Lake Winnipeg (Manitoba Hydro's largest reservoir) in intercepting 89% of sediment transported from the upper Nelson watershed and demonstrated that particulate carbon transported in the lower Nelson River derives from local sources. BaySys watershed modelers predicted that CO2-driven warming will cause increased river discharges throughout the HBC watershed, but least in the Nelson watershed, and that this would occur mostly as snowmelt runoff. The results also indicated that summer discharge may decrease (HYPE model results) with implications related to future reservoir operation.

Through BaySys we calculated a net CO_2 uptake of 21±8 mmol CO_2 m^{-2} day^{-1} (13.5±5 TgC) during the spring and early summer seasons of 2018. Combining this result with previously determined CO_2 uptake rates for late summer and fall seasons, we estimate the annual CO_2 uptake of Hudson Bay during the open water season to be 12 TgC yr^{-1}. Thus, Hudson Bay is a contemporary carbon sink over the ice-free season. The results of BaySys however suggest that the Hudson Bay carbon sink will be smaller on an annual basis, or even be a CO_2 source, largely because of extensive remineralization of terrigenous DOC throughout the winter season.

BaySys experiments and observations also confirmed that Nelson and Churchill River DOC is highly degradable. Riverine particulate OC is likely also degradable in part based on its composition; however, it represents only a small fraction of the DOC.

Water potentially corrosive to calcifying organisms is widespread in deep waters but also was observed near to the surface in proximity to James Bay. Potentially corrosive water shoals to within ~ 25 m of the surface east of James Bay, whereas near-surface waters in western and southwestern Hudson Bay, including the Nelson outlet, are less prone to acidification.

BaySys provided the first-ever late spring measurements of offshore waters in west-central Hudson Bay. The timing of the main pulse of production was confirmed to be controlled by light availability with polynya waters supporting earlier commencement of the springtime bloom. Nutrient availability was greatest closer to the west coast where the winter polynya presence likely drives deep mixing. A surprising feature of the bay was the presence of a sub-ice suspended algal bloom (Matthes et al., 2021). The extensiveness of such a bloom has only been observed under the central Arctic multiyear sea ice pack and therefore represents a previously unknown contribution to primary production under first-year sea ice and at a much lower latitude than previously observed.

New assessments of open-water primary production by remote sensing showed that productivity in the marginal ice zone of offshore waters is strongly linked to large-scale climate forcing through its impact on ice dynamics and vertical nutrient supply. Negative phases of the Arctic Oscillation (and of the North Atlantic Oscillation) are associated with elevated phytoplankton biomasses in the upper water column. Locally, rivers have a negative influence on ice algal and pelagic primary production via freshwater impacts on sea ice structure, turbidity from riverine dissolved and particulate matter and late spring-summer depleted nutrient concentrations.

Rivers deliver nutrients during winter, but the bay-wide impact of these deliveries is small. At a more local scale, the winter nutrient supply pre-conditions primary production in affected nearshore areas. While no evidence currently indicates regulated rivers differ from unregulated ones in regard to nutrient compositions and concentrations, enhanced winter discharge may lead to a wider dispersal of river nutrients away from the mouth of regulated rivers.

BaySys research spurred innovative ideas that contributed to Manitoba Hydro's vision of leadership in energy reliability and environmental stewardship. The modelling and observational work from BaySys showed the relative importance of the timing, magnitude, and relative changes in the hydrological cycle and their downstream impacts on the marine system. The datasets and knowledge, provided by BaySys, contribute to environmental assessments, climate change impacts and adaptation studies, refining compliance standards with respect to environmental monitoring, and define mitigation and adaptive follow-up programs. Collaboration on climate and watershed modelling has also benefited Manitoba Hydro from an energy supply and risk perspective.

Information collected and models developed under BaySys enhanced Manitoba Hydro's understanding of the impacts of the Churchill River Diversion & Lake Winnipeg Regulation projects compared to the impacts of other factors such as climate change. This research informed climate change studies on the variability of water supply and related risks to energy production, and mercury cycling and accumulation in fish, as related to the effects of Manitoba Hydro operations which ultimately drain into Hudson Bay. This research ultimately helped inform Manitoba Hydro's understanding of its carbon footprint, complement carbon cycling, and reservoir greenhouse gas (GHG) studies. It supported Manitoba Hydro's efforts to advocate for policies that recognize hydropower as a low carbon emitter and will comply with any future GHG reporting requirements, or public inquiries. Information from the BaySys research project also enhanced Manitoba Hydro's goals of sustainable development, proactively protecting the environment, and methods for adapting to climate change. The collaborative research program provided data that can be used to refine environmental impact assessment predictions and address regulatory compliance requirements such as potential mitigation measures or follow-up programs related to existing operations, license renewals, and future developments.

6.3 References Cited

Andrews, J.A., Babb, D.G., Barber, D.G. (2018). Climate change and sea ice: shipping in Hudson Bay, James Bay, Hudson Strait, and Foxe Basin (1980-2016). *Elementa: Science of the Anthropocene*, 6, 19. 10.1525/elementa.281

Bruneau, J., Babb, D.G., Chan, W., Kirillov, S., Ehn, J.K., Hanesiak, J., Barber, D.G., (2021). The ice factory of Hudson Bay: Spatio-temporal variability of the polynya in northwestern Hudson Bay. *Elementa: Science of the Anthropocene*, 9(1), 00168. https://doi.org/10.1525/elementa.2020.00168

Eastwood, R.A., Macdonald, R.W., Ehn, J.K., Heath, J., Arragurtainaq, L., Myers, P.G., Barber, D.G., Kuzyk, Z.A., (2020). Role of River Runoff and sea Ice Brine Rejection in Controlling Stratification Throughout Winter in Southeast Hudson Bay. *Estuaries and Coasts*, 43, 756-786. https://doi.org/10.1007/s12237-020-00698-0)

Ehn, J.K., Mukhopadhyay, A., Kirillov, S., Gupta, K., Babb, D.G., Sydor, K., Barber, D.G. (in prep.). Sea Surface Temperature patterns and trends in relation to seasonal sea ice persistence in the Hudson Bay Complex, 2008-2018. *Elementa: Science of the Anthropocene*, manuscript in preparation.

Galbraith, P. S., & Larouche, P. (2011). Reprint of "Sea-surface temperature in Hudson Bay and Hudson Strait in relation to air temperature and ice cover breakup, 1985–2009". *Journal of Marine Systems*, 88(3), 463-475.

Gupta, K., Mukopadhyay, A., Babb, D.G., Barber, D.G., Ehn, J.K. (submitted). Landfast sea ice in Hudson Bay and James Bay: Annual cycle, variability and trends, 2000-2019. *Elementa: Science of the Anthropocene*, manuscript submitted.

Kirillov, S., Babb, D.G., Dmitrenko, I., Landy, J., Lukovich, J., Ehn, J., Sydor, K., Barber, D., Stroeve, J. (2020). Atmospheric forcing drives the winter sea ice thickness asymmetry of Hudson Bay. *Journal of Geophysical Research: Oceans*, 125, e2019JC015756. https://doi.org/10.1029/2019JC015756

Landy, J.C., Ehn, J.K., Babb, D.G., Theriault, N., Barber, D.G. (2017). Sea ice thickness in the Eastern Canadian Arctic: Hudson Bay Complex and Baffin Bay. *Remote Sensing of the Environment*, 200, 281-294. 10.106/j.rse.2017.08.019

Matthes, L.C., Ehn, J.K., Dalman, L. A., Babb, D.G., Peeken, I., Harasyn, M., Kiriliov, S., Lee, J., Bélanger, S., Tremblay, J.-É., Barber, D.G. and Mundy, C.J. (2021). Environmental drivers of spring primary production in Hudson Bay. *Elementa: Science of the Anthropocene*, 9(1), 00160. https://doi.org/10.1525/elementa.2020.00160

Prinsenberg, S. J. (1977). Freshwater Budget of Hudson Bay. Canada Department of Fisheries and Oceans Manuscript Report Series No. 5.

Tremblay, J-É., Lee, J., Gosselin, M., & Bélanger, S. (2019). Nutrient Dynamics and Marine Biological Productivity in the Greater Hudson Bay Marine Region. In: Kuzyk, Z., Candlish, L. (Ed.), *From Science to Policy in the Greater Hudson Bay Marine Region: An Integrated Regional Impact Study (IRIS) of Climate Change and Modernization* (225-243). ArcticNet, Quebec, Canada.